Cranfield UNIVERSITY

Susan Ann Servais

Physical modelling of low-cost modifications to the Crump weir in order to improve fish passage: Development of favourable swimming conditions and investigation of the hydrometric effect

Engineering Systems Department

PhD Thesis

Cranfield University
Shrivenham

Cranfield UNIVERSITY

Engineering Systems Department

PhD Thesis

Academic Year 2005/06

Susan Ann Servais

Physical modelling of low-cost modifications to the Crump weir in order to improve fish passage: Development of favourable swimming conditions and investigation of the hydrometric effect

Supervisor
Dr David G. Rhodes

June 2006

Cranfield University
Shrivenham

Abstract

More than 350 Crump-type weirs (which are triangular in profile) form part of the Environment Agency's hydrometric network in rivers across England and Wales. These weirs operate as effective measurement structures and are useful over a large flow range. However, they also act as barriers that impede the passage of many species of coarse fish within their natural habitat.

The primary aim of this research project was to recommend modifications to Crump weirs in order to improve fish passage, while still allowing the weirs to fulfill their hydrometric purpose in a reliable way. It was an additional requirement that any proposed solution(s) be both practical and achievable at low-cost. This is in contrast to conventional fish pass solutions, that tend to be expensive, are generally not hydrometrically rated, and most of which were not designed with coarse fish in mind.

The method used was a model study conducted in the laboratory, which allowed for a great number of layouts to be trialled. Laboratory research combined with fish swimming data provides a basis for projecting successful fish ascents. Brimpton weir on the River Enborne was chosen as a suitable reference on which to base laboratory model tests.

The preferred arrangement (termed a 'rotated-V' layout) was found to be a series of baffles located on the downstream slope of the Crump weir. These baffles effectively act as weirs at low flows and roughness elements at high flows. Each baffle has a slot which helps to form a path of ascent for fish. The baffle closest to the crest was set at the same height as the crest, as this led to optimum low velocities in the slots on the downstream slope.

Extensive testing revealed that the proposed solution results in a change in a weir's hydrometric characteristics. However, it was demonstrated that the deviation of the coefficient of discharge is predictable. Therefore, it allows for reliable flow measurement to be achieved (subject to a standardised calibration trial using volumetric flow measurement techniques). In addition, a detailed measurement and analysis of water velocities within the recommended solution strongly suggest that it substantially improves on the fish passage capability of a Crump weir.

Acknowledgements

To my supervisor, David Rhodes. Thank you for providing the environment and encouragement to enable me to do this PhD. Thank you for all the many hours you helped in the laboratory and for the suggestions and support for writing the research papers as well as the guidelines for the Environment Agency.

To the Engineering Physical Science and Research Council and to the Environment Agency of England and Wales for providing funding. Special mention goes to Greg Armstrong (National Fish Pass Officer), and the rest of the Low Cost Solutions for Crump Weirs Board who provided input, comments and suggestions along the way.

To the staff in the workshops (both in AL3 as well as the wood workshop) for assisting with manufacture of the model and the occasional borrowing of tools. Also to Craig Tucker for his practical help.

To my fellow PhD candidates in Heaviside lab for your input, lunches and general perseverance. A special thanks to Suresh for all the laughs, coffee and being my computer consultant and friend, and Darina, for your friendship, inspiration and motivation.

To my friends, both in South Africa as well as in the UK, many thanks for your support, prayers and encouragement.

To my siblings, Paul, Angela, Michael and Christopher for your input and ribaldry, and especially my brother Paul for your proof-reading assistance. Mom and Dad this short thank you does not do justice to all your help, guidance and enthusiastic support (financial, emotional and not to forget baby-sitting duties) over the years.

To my nine-month old daughter Rebecca Servais, for being a very tolerant and happy baby!

To my husband, Marc Servais - for your love, support, encouragement, generosity in helping me (especially with computer programming), laughs, tennis, and sharing post-graduate (PhD) studies with me. It has certainly had its moments! Now I know a bit more about content-based motion compensation, and find myself looking at video images far more critically. I know you enjoyed learning about fish and sometimes helping out in the laboratory playing with the LEGO® bricks, water and electronic equipment!

Contents

List of Tables

List of Figures

Notation and Glossary

A. Latin names of fish

Common name	Latin name
Barbel	*Barbus barbus*
Bream	*Abramis brama*
Brown trout	*Salmo trutta*
Chub	*Leuciscus cephalus*
Dace	*Leuciscus leuciscus*
Eels/Elver	*Anguilla anguilla*
Grayling	*Thymallus thymallus*
Roach	*Rutilus rutilus*
Smelt	*Osmerus eperlanus*

B. Acronyms

Acronym	Full title
CFD	Computational fluid dynamics
EPSRC	Engineering and Physical Sciences Research Council
FCA	Fish Cross-sectional Area
ICOLD	International Commission on Large Dams
OD	Outside diameter of a pipe
PT-ST	Pitot tube - static tube
RA	Representative area
VPM	Velocity propeller meter

C. Notation

C.1. General notation

Symbol	Unit	Description
A	m^2	Area of the approach channel (i.e. upstream of weir)
b	m	Breadth of weir
β	ratio	Diameter ratio: $\beta = d/D$ [Equation 3–3]
C	non-dim.	Discharge coefficient [Equation 3–3] $C = 0.5959 + 0.0312\beta^{2.1} - 0.1840\beta^{8} + 0.0029\beta^{2.5}(10^6/Re_D)^{0.75} \ldots$

Symbol	Unit	Description
		$+ 0.039L_1\beta^4/(1-\beta^4) - 0.0337L_2\beta^3$
C_d	non-dim.	Coefficient of discharge
C_v	non-dim.	Coefficient allowing for approach velocity $(H/h)^{3/2}$
d	m	Internal orifice diameter [Equation 3–3]
d	m	Height of baffle: Figure 3–30
D	m	Upstream internal pipe diameter: $D = 0.15037$m [Equation 3–3]
Δ	m	Difference between the highest point of the baffle and the weir crest level (see section 5.1.2)
E	non-dim.	Velocity of approach factor: $E = \frac{1}{\sqrt{1-\beta^4}}$ [Equation 3–3]
f	non-dim.	Drowned flow reduction factor used in non-modular flow (for modular flow $f = 1$)
Fr	non-dim.	Froude Number
F	non-dim	Fineness ratio of a fish (in fish exclusion formula)
g	ms^{-2}	Acceleration due to gravity ($g = 9.80665\ \mathrm{ms}^{-2}$)
H	m	Total (energy) head
h	m	Measured head (use of subscripts 1 and 2 denotes position)
l	m	Distance from crest to centre of baffle on the crest: Figure 3–30
$[L]$		Dimension abbreviation for SI unit of length.
L	cm	Standard length of a fish, from the snout to the caudal peduncle
L	m	Relative pressure tapping spacing as applied in Equation 3–3
L_1	m	For upstream pressure tapping $L_1 = 1$
L_2	m	For downstream pressure tapping $L_2 = 0.47$
M	mm	Free gap between bars (in fish exclusion formula)
p	Pa or Nm^{-2}	Differential pressure (static) across the orifice plate [Equation 3–3]
p	m	Vertical height of the weir from the base to the crest
p_{ref}	Nm^{-2}	Standard atmosphere $p_{ref} = 101325N/m^2$
Q	$\mathrm{m}^3\mathrm{s}^{-1}$	Discharge over the weir (also ls^{-1})
ν	$\mathrm{m}^2\mathrm{s}^{-1}$	Kinematic viscosity of water
R	m	Wetted perimeter (for a rectangular channel or slot, $R = by/(b+2y)$
$Re_{channel}$	non-dim	Channel Reynolds number where $Re_{channel} = VR/\mu$
Re_D	non-dim.	Pipe Reynolds Number where $Re_D = UD/\mu$ [Equation 3–3]
$[T]$		Dimension abbreviation for SI unit of time.
U	ms^{-1}	Mean axial velocity of the water in the pipe [Equation 3–3]
v	ms^{-1}	Velocity of flow
X_c		Percentage uncertainty in C_dC_vf (BS3680 1986)
y	m	Depth of flow

C.2. Subscripts

Subscript	Use
1	H_1 or h_1 upstream head
2	H_2 or h_2 downstream head
m	Model (used as a subscript e.g. $\mathrm{L_m}, \mathrm{v_m}$)
p	Prototype (used as a subscript e.g. L_p, v_p)

C.3. Axis definitions as used in the laboratory

Axis	Position
h	localised axis parallel to weir
w	localised axis normal to weir
x	horizontal
y	vertical
x'	parallel to the weir
y'	normal to the weir

D. Engineering technical terms

afflux The increase in water depth upstream of a weir caused by the installation of that weir (Chadwick and Morfett 1994).

head In this text, normally referred to as the difference in water elevation between the crest of the Crump weir and the free surface level (upstream of the crest).

modular flow The condition when upstream water level is unaffected by downstream flow conditions.

non-modular flow The condition when downstream flow influences the upstream water level (and the weir can be said to be submerged).

Pitot-static tube Instrumentation consisting of two concentric tubes with a 90° bend, where the inner Pitot tube measures the stagnation pressure ($\frac{p_{static}}{\rho g} + \frac{v^2}{2g}$) and the outer tube the static pressure head ($\frac{p_{static}}{\rho g}$). As the differential reading is equal to the velocity head ($\frac{v^2}{2g}$), velocity at a given point can be calculated.

separation bubble or pocket The separated region of flow immediately downstream of the weir crest. The separation streamline acts as a boundary between separated flow below and unseparated flow above; the highest point on this streamline acts effectively as the relocated weir crest.

stratification Stratification refers to the process whereby two or more horizontal water layers occur in a reservoir, and each layer shows unique characteristics (e.g. temperature, density etc.) (Horton 2002).

streamline A line drawn parallel to the direction of flow in a given instant of time (Horton 2002).

tailwater Used to describe the water level immediately downstream of the weir.

vernier A type of scale which allows for fractional measurements e.g. 21.56 mm.

E. Biological terms

anaerobic environment An environment where there is no free oxygen.

aerobic environment An environment where oxygen is freely available.

anadromous Life cycle of reproduction in freshwater, feeding and growth at sea

benthic bottom swimming fish

catadromous Life cycle of reproduction at sea, feeding and growth in freshwater

caudal peduncle The standard length of a fish is measured from the snout to the 'caudal peduncle', or the centre of v-section in the tail of a fish.

diadromous Life cycles split between freshwater and marine environments (split into catadromous and anadromous)

eutrophication The process where water is over-enriched by nutrients, mainly nitrogen and phosphorous, thereby causing degradation in water quality owing to excessive plant growth and oxygen depletion (Horton 2002).

habitat Environment or surroundings where a plant / animal naturally lives or grows, which includes physical factors (temperature, moisture, light) and biological factors (food, predators) (Horton 2002)

limnophilic lake-loving or calm water fish

meteorology The study of atmospheric conditions in order to forecast weather (Oxford University Press 2003).

rheophilic current-loving fish

piscivorous Fish-eating predators, including both fish and birds species.

1. Introduction

"So-this-is-a-River"
"THE River," corrected the Rat.
"And you really live by the river? What a jolly life!"
"By it and with it and on it and in it," said the Rat. "It's brother and sister to me, and aunts, and company, and food and drink, and (naturally) washing. It's my world, and I don't want any other. What it hasn't got is not worth having, and what it doesn't know is not worth knowing. Lord! the times we've had together..."

The Wind in the Willows
KENNETH GRAHAME

1.1. Background

Water has and will always play an integral part in man's existence. History teaches one, that many wars were fought over the control of water supplies. Civilisations have prospered or failed, depending on their management or mismanagement of their water supplies and water resources.

Through the centuries, man's understanding of how to manage his environment has continuously changed because of his increased scientific knowledge and the rapid development of technology.

The Industrial Revolution led to mass production and mass urbanisation all of which had catastrophic effects on the natural environment e.g. as water mills were constructed to harvest energy, so these water wheels in turn effectively blocked off the free movement of fish.

As modern man has become more inventive, his demand for more energy to drive city life and industry, has increased. The end result has been a vast generation of waste, which is polluting the air, land, rivers and oceans.

Water pollution has been prominent among the threats to fish life, particularly in inland waters. Mankind has always had a keen interest in the well-being of fish stocks as a primary food source. This water pollution threat was centred in Western Europe and North America during the latter half of the 20th Century. Massive capital investment programs were implemented in water pollution control works.

However, with the development of hydrometric works and impoundment for water resources purposes, further barriers were introduced to fish movement, which have come to replace the pollution hazard as a threat to fish habitat.

As with any construction, impacts on the environment, can be negative or positive. For example, in the United Kingdom, typical structures included impoundment for water supplies, provisions for river crossings, water mills for power generation, navigation and flood defence (Environment Agency 1997b).

During the 20th Century - the Water Resources Act of 1963 (HMSO 1963) established the new River Authorities. Under Section 15 of the act, remits included a duty to assess water resources and the implementation of hydrometric schemes, including river flow gauging. Unfortunately, these hydrometric schemes have had a negative impact on 'fish passage' (i.e. the ability of fish to move freely up and down a river / water way / stream for the purposes of feeding and spawning).

Interest in fish passage was traditionally associated with the (commercial) viability of salmon, trout and eels. For decades, salmonid-specific requirements have driven fish passage research and field trials, and there is a wealth of information and design methodologies with regards to field-proven fish passage successes, especially in Europe and North America (e.g. Fort and Brayshaw 1961; Beach 1984; Clay 1995; ICOLD 1999; Katopodis 2005 etc.) Typical solutions are normally expensive, purpose-built structures either within or circumventing an existing structure or impediment.

In 1995, the Environment Agency of England and Wales, inherited over 1000 gauging stations, although a more recent count showed a total of approximately 1800 gauging weir sites (Armstrong 2000). There are 376 Crump-type structures within the Environment Agency's hydrometric network (Environment Agency 2001a), of which approximately a third are thought to be detrimental to fish passage (Environment Agency 1997b). In addition, there are many more triangular profile weirs. A Crump weir is a triangular profile weir with a 1:2 upstream slope and a 1:5 downstream slope, originally developed by Crump (1952) at the Hydraulics Research station. These weirs are effective measurement structures useful over a large flow range with small afflux (i.e. small increase in water level relative to increase in discharge) and suitable for use in modular (discharge related to upstream water level only) or non-modular flow conditions (discharge is affected by both upstream and downstream water levels). By design, super-critical flow forms on the downstream slope of an unmodified Crump weir, with the result that water depths are shallow and velocities are high. Scientific evidence for a select number of gauging weirs shows their detrimental effect on coarse fish (Pinniger 1998; Lucas and Frear 1995).

Towards the end of the 20th Century, guidance with regards to fish passage requirements began to emerge for both new structures and existing structures targeted for retrofitted solutions (e.g. Beach 1984; Carling and Dobson 1992; Christensen 1993; Clay 1995; Walters 1996a,b; Environment Agency 1997b). The Flat-V weir at Hurn, on the Moors River in Dorset, is an example of modifications to an existing structure. A number of solutions were investigated before a baffled solution, known as the Hurn-type baffle system (Armstrong *et al.* 2004), was trialled in the laboratory prior to being installed on site. Although anecdotal evidence (Armstrong *et al.* 2002) suggests that this fish pass is successful to some degree, conclusive results have yet to be published.

During the first few years of the 21st Century, research has been focussed on in-

corporating fish migration needs within the design of flow measurement structures, with the intention of maintaining existing levels of accuracy, culminating in a report by White *et al.* (2005b). One of the outcomes of this study is a proposed draft standard for fish passes at gauging stations.

Low-cost solutions are an alternative to traditional fish pass solutions as retrofitting the existing structures without costly structural modifications would be beneficial. Proposed solutions should be acceptable both hydrometrically and environmentally.

Past interest in fish passage focussed on the salmon and trout upstream migrations, which were important for commercial reasons. However, current environmental interest has increased awareness in river systems and habitat vitality, which includes concern over the impact of structures on fish movement for less (commercially) valuable coarse fish species. A study initiated by the Environment Agency has lead to the creation of a fish swimming speed database, Swimit[1]

Therefore the 'scene was set' for a laboratory-based research project into low-cost modifications to the Crump weir. Modifications comprising downstream baffles were physically modelled, in LEGO® bricks[2] initially and perspex ultimately, in a research project aimed at improving fish passage by developing favourable swimming conditions based on the burst speed data provided by the Swimit database (Environment Agency 2001b, 2003). In addition, the hydrometric effect as a result of the placement of baffles on the downstream slope was investigated. Modular and non-modular conditions at the unmodified Crump weir were compared, with single baffle, double baffle and the preferred fish pass arrangement (constructed in perspex).

This research project was carried out at Cranfield University, Shrivenham Campus, with joint funding from the Engineering and Physical Sciences Research Council (EPSRC) and the Environment Agency of England and Wales.

1.2. Project aims and scope

1.2.1. Project aims

The aims of this research project into low-cost modifications for improving fish passage at a Crump weir were two-fold:

- To make use of physical modelling for the development of one or more low-cost modification(s) to Crump-type weirs, in order to facilitate fish passage. A model of an existing weir (i.e. Brimpton weir) was used as the starting point.
- To investigate the effect of those modifications on the hydrometric function.

[1]Note that although Swimit versions 1.11 and 2.0 have been used throughout this thesis, the latest version, Swimit version 3.2 (Environment Agency 2005) supercedes all previous versions (Clifton-Dey 2006). Details of any analysis using subsequent version(s) of Swimit will be made available at the author's website Servais (2006).

[2]Note that as LEGO is a brand name, the registered trademark ® is included in the text. Subsequent references require capitalisation, e.g. 'LEGO bricks' (LEGO company 2006).

Firstly, a physical model of the low-flow section of the compound Crump at Brimpton on the River Enborne (Thames catchment) was used. Once an acceptable site-specific solution had been found, its applicability to a variety of sites was then investigated. The outcome was intended to be widely applicable to Crump-type weirs, either as a standard physical design or as a set of design rules.

1.2.2. Project scope

The project aims (above) and scope (below) have been developed and extended from the aims and objectives statements in the original EPSRC Case for Support (Rhodes 2001), the Memorandum of Understanding between the Environment Agency and Cranfield University (Brown 2001), the Experimental and Analytical Programme (Rhodes 2002) and the MPhil to PhD transfer report (Servais 2003).

- To test a variety of modifications using an existing 1:5 scale model of the low-flow section of Brimpton weir.
- To retard and significantly deepen the super-critical sheet flow on the downstream face of the Crump weir by using appropriate baffle arrangements, with the aim of providing suitable velocities and flow depths for a variety of fish species and sizes. A particular arrangement was assessed by reference to the hydraulic measurements at model scale and the fish swimming data for the five species available during the initial testing phase (Environment Agency 2001b).
- To generalise the solutions based on the outcome of the tests on the Brimpton weir model. Time constraints were acknowledged and it was hoped that the most promising solution would be applied in the field. Unfortunately this was not possible in the time available.
- To determine the effect of downstream modifications upon the hydrometric function over the whole flow range (i.e. for modular, and non-modular flow). The implications for gauging accuracy and reliability needed to be identified and if possible, quantified where structures are used for hydrometric purposes.
- Structural modifications were required to be self-cleansing, thereby preventing the entrapment of debris. Similarly, siltification was to be avoided as far as possible. Furthermore, changing physical variables including slope, baffle dimensions and depth were to be included in the guidelines. However, the size of the baffles and their spacing is actually fish-dependent, and the effect of slope-change was investigated to a limited extent by using a downstream slope of 1:4.55 (compared to the standard Crump gradient of 1:5).

1.3. Structure of the thesis

The rest of the report is briefly described below in order to explain its structure and content. The different chapters are presented, and where applicable, comments and constraints are pointed out.

Chapter 2: Review of the literature The subject areas of this thesis encompass both coarse fish behaviour (swimming capabilities and migration motivations) and civil engineering hydraulics with an emphasis on the Crump weir, with the common link of fish pass design. This chapter is divided into three sections presenting the relevant aspects from each of these disciplines.

Chapter 3: Equipment and Experimental Procedure Firstly details of the model Crump weir are provided. Secondly, the experimental equipment and calibration procedures are described, and finally the experimental methodology used throughout is presented. The experimental methodology is divided into two sections: (i) fish pass modification and (ii) hydrometric effect. Each of these two sections includes specific experiment procedures.

Chapter 4: Experiments on fish pass modifications The chapter is split into two main sections. Firstly, a multiplicity of baffle arrangements using LEGO is presented. Trials were initially conducted for the 90 percentile low-flow rate. A chosen layout was then further refined over the whole flow range. The second section presents and analyses the results from a detailed investigation into the chosen baffle arrangements using Perspex baffles. The in-depth analysis includes free surface flow measurements along the path of ascent (i.e. slots in the baffles), a flow visualisation presentation, the velocity measurement distributions in these slots at four different flow rates, and finally a debris analysis.

Chapter 5: Experiments on the hydrometric effect This chapter presents and discusses the results and analysis for both the modular and non-modular flow experiments. The modular flow investigated the effects of the following: an unmodified Crump weir, the location of the single baffle and a comparison with HR Wallingford data (White *et al.* 2005e), double baffle and the fish pass modifications. The non-modular flow experiments dealt with the unmodified weir, the effect of a single baffle and the effect of the chosen fish pass.

Chapter 6: Conclusions and Recommendations The final conclusions are presented and recommendations for future research are made.

Appendix A This appendix includes additional fish burst swimming speed graphs not included within the section on fish swimming speeds (i.e. section 2.1.3) in Chapter 2.

Appendix B: C programs Provides an overview of (most) of the C programs written and used by the author in the hydraulics laboratory specifically for this project. Typical pseudocode (i.e an algorithm showing the programming steps) is presented as an example of the type of logic and modular development of the program available in the project 'toolkit'.

Appendix C: Calibration Data and Equipment Layout Provides additional information on various items of equipment used, and calibration techniques and graphs which are not included in the main text, and are useful for reference purposes.

Appendix D: Trial baffle arrangements (LEGO bricks) This appendix serves as the project record for all of the LEGO trials and is divided into two sections: (i) experiments conducted at the 90 percentile low-flow, and (ii) experiments conducted over the whole flow range during the refinement process of the chosen layout.

Appendix E: Selected fish pass constructed from Perspex This serves as the project record for those results not included in Chapter 4. Although only one preferred baffle layout was trialled, two options were available with regards to the baffle closest to the crest. The results are thus split according to the first baffle height as well as the four flow rates tested. An additional consideration was the effect of the downstream slope on the velocities and free surface flow. Thus these results include additional results from a 1:4.55 trial in addition to the complete 1:5 downstream slope sets trialled. In the interests of generalisation, reference is made to 'flow rate per unit width'.

Appendix F: Video footage from the perspex fish pass trials This appendix contains a description of video footage taken during the research process, which also serves as an index for the DVD attached to this report. The footage is divided into two types: (i) Footage was taken for use with the image processing package, DigImage. Although not useful in gaining a knowledge of velocities on the downstream slope of the perspex fish pass, this proved useful for flow visualisation, and is considered to be part of the program record. (ii) Footage taken during debris testing trials.

Appendix G: Experiments on the hydrometric effect Additional graphs not included in the main text which form part of the project record are included in this appendix. In addition, three examples of the cross-checking techniques applied to the pressure transducers used in measuring head and discharge values are provided for information purposes.

Appendix H: List of Publications Provides a list of all of the papers published during the course of this research.

2. Theoretical Background and Literature Review

This research encompasses information obtained from the disciplines of fish behaviour and civil engineering hydraulics. Consequently, this literature review has been divided into three sections:

- coarse fish and their associated characteristics and behaviour, including research into swimming capabilities
- weirs and their directly relevant hydraulics, with an emphasis on triangular/Crump weirs
- fish passes including fish-pass hydraulics.

2.1. An introduction to coarse fish and factors affecting fish passage

Recent interest in coarse fish has led to research into their swimming capabilities, legislation has been updated and existing fish pass guidelines have been revised. This section summarises some of the key aspects which need to be considered when researching and designing fish-related structures.

2.1.1. Historical interest in coarse fish

Although most of the research and construction of fish pass structures have been been designed with the commercial species (i.e. salmon, trout and eels) in mind, consideration is now given to coarse fish species. Investigations into fish behaviour[1], and fish swimming capabilities (section 2.1.3) have generated a useful database of information which has been incorporated into the current research project.

[1]Fish behaviour is an extremely complex subject and is considered to be beyond the scope of this thesis. Only those factors and constraints relevant to Crump-type weirs and their immediate vicinity will be expanded upon in this document.

Integration of disciplines

In the last decade the fields of water engineering and fish behaviour have moved closer together, with both disciplines making an effort to coordinate research and field applications, e.g. ICOLD (1999), on the interaction between fish and dams, which is designed to facilitate communication between engineers, biologists and environmental specialists. Critical issues explored in this ICOLD text have been developed in section 2.1.2 and comment is made on factors beneficial to fish which can be influenced or changed at a Crump weir.

Katopodis (2005) recommends a systematic approach or 'toolkit' (i.e. number of methods) which encompasses the fish passage, ecological flow management regimes and fish habitat requirements. In addition, an overview of existing thinking and methods, the need for integrated research and development and recommendations for future research are provided as part of the development of this toolkit. The toolkit is categorised as follows: fish migrations and hydrology; fish behaviour and hydraulics; swimming performance and hydrodynamics; fish pass and fish screen hydraulics; ecological flow management; and research, test facilities and instrumentation.

The Environment Agency has commissioned a number of research projects related to fish swimming performances and fish movement in rivers. One such study included the impact of gauging weir structures upon coarse fish and their spawning migrations (Pinniger 1998), which identified Brimpton weir, located on the River Enborne in the Thames catchment, as being a problem for certain coarse fish species. The Agency's Thames Region conducted a strategic overview of their impounding structures (Environment Agency 1997b). Turnpenny *et al.* (1999) provided guidelines on the construction of gauging weirs in addition to identifying potential environmental impacts of gauging weirs.

In the past, the lack of relevant data on non-commercial fish (such as swimming performance) has presented problems in the design, maintenance and monitoring of fish passes. One of the aims of the current research has been to establish a relationship between the fish data now available and the hydraulic parameters associated with a modified Crump weir.

More recent studies considered the design of flow measurement structures with the stated aim of not compromising flow data accuracy whilst aiding fish migration (White *et al.* 2005b) and included the following themes:

- The effect of combined uncertainties at standard flow measurement structures was analysed in a desk study.
- The problems of trash at fish passes was reviewed with an emphasis on minimising trash.
- Hydraulic calibration of a Larinier fish pass was conducted at laboratory scale.
- A laboratory study was conducted into the fundamental requirements governing the arrangements of baffles nearest to the crest on the downstream slope of a triangular profile measuring weir.

- A Larinier fish pass with a submerged orifice upstream intake was tested as part of a combined fish pass - gauging structure.
- Recommendations were made for further research opportunities.

One of the outcomes of that research project was a new draft standard. This standard is currently entitled: 'Draft standard - Fishpasses at flow gauging structures' (White *et al.* 2005a).

2.1.2. Factors affecting fish, with emphasis on the freshwater environment

Fish have specific habitat and food requirements and there are a number of factors that influence the presence or absence of various fish species. These include water quality, temperature, velocity and depth. Additional considerations are likely to be species-specific. Although not exhaustive, the interrelationship of factors affecting fish life as described in ICOLD (1999) are illustrated in Table 2–1[2]. These factors are directly relevant to a riverine environment, but are not exclusive to that.

Table 2–1: Interdependent factors affecting fish life

Factors which cannot (easily) be influenced or changed
Water quality
Need to migrate
Availability of food
Water temperature
Factors more easily influenced or changed
Speed of the current
Depth of the water
Nature of the river bottom or banks
River regime

Certain factors, either from an engineering perspective or as a result of natural forces, have been identified as not being easy to control or change. More easily controllable factors are identified and are also briefly discussed below. Depending on the location and type of river, the time of year and fish species, etc., these factors will have different levels of importance.

FACTORS WHICH CANNOT (EASILY) BE INFLUENCED OR CHANGED

Water quality

Water quality is of vital importance when considering the sustainability of fish life. Table 2–2 illustrates the various chemical, physical and biological factors which influence water quality, either individually or in any combination (ICOLD 1999).

[2]The factors which can be influenced or changed in the context of this study have been added by the author.

Table 2–2: Water quality factors affecting fish life

Type of characteristic	**Characteristic**
Chemical	Dissolved oxygen content Sodium chloride content Phosphates and nitrates in the water PH/alkalinity
Physical	Amount of suspended matter
Biological	Wealth of plant and animal life

Dissolved oxygen content is perhaps the most important chemical factor, and its absence or excess has different impacts on fish life. It should be noted that different fish species have different tolerance levels. The phosphate and nitrate content is important as its absence leads to a shortage of food, whereas an overabundance results in eutrophication. This is the process where water is over-enriched by nutrients, mainly nitrogen and phosphorous, thereby causing degradation in water quality owing to excessive plant growth (in which algal blooms are symptomatic) and oxygen depletion (Horton 2002). Resultant low dissolved oxygen and excessive PH are detrimental to fish in general.

Suspended matter, especially sediment, affects the turbidity of the water and light penetration and in addition may even cause damage to gills. Land use and the management of effluents discharged into river systems contribute significantly to controlling river quality (ICOLD 1999). When considering implementing a fish pass, the existing water quality is one of the factors which needs to be taken into account. Sources of pollution might be better targeted before a fish pass is even considered.

Need to Migrate

Fish migrate for three principal reasons: reproduction (spawning), feeding and refuge (Lucas and Baras 2001). Annual migrations of commercial fish, both freshwater and saltwater, have for a long time been the focus of industrial research. Legislation and the construction of fish passes are a direct result of the desire to maintain the status quo and continued supply of this resource.

Fish migrations occur within and between different habitats – the terms given in Table 2–3 are dependent on the life-cycle of fish, with reference to their migration requirements (Lucas and Baras 2001; Porcher and Travade 2002).

Table 2–3: Definition of migration terminology

Term	**Definition**
Oceanodromous	Entire life-cycle completed within a marine environment
Potamodromous	Entire life-cycle completed within freshwater
Diadromous	Life cycles split between freshwater and marine evironments (split into catadromous and anadromous)
Anadromous	Reproduction in freshwater, feeding and growth at sea
Catadromous	Reproduction at sea, feeding and growth in freshwater

The fish for which the vast majority of fish ladders have been designed, are trout and salmon, both of which are anadromous. Eelways provide for the catadromous elvers and eels.

In general the coarse river fish do not migrate over such vast distances, although migrations do occur on a local scale. For example, recent studies by the Centre for Ecology and Hydrology using radio-tracking techniques have shown that an individual pike will migrate distances of the order of kilometres (Masters *et al.* 2002), and the same pike was found to return to a particular location after such migrations (Beaumont *et al.* 1986). This research has shown that fish migrate locally far more than was originally believed and exemplifies the need for modifications to an obstruction such as that created by a Crump weir.

Fish respond to a variety of stimuli (Table 2–4), some internal or instinctive, others externally applied, or frequently a combination of both acting together. It is therefore important that the external stimuli that promote migration are not significantly modified by engineering works, and that the latter are designed to mimic naturally occurring conditions as far as possible. For example, spring floods might be the principal spawning stimulus for a certain species of fish. The absence of such floods owing to the presence of a dam would cause the spawning to be delayed.

It is also worth noting that although local fish need to be taken into account, often the biomass of migrating fish far exceeds that of the resident population (ICOLD 1999).

Availability of food

The availability of food is dependent on the presence of phosphorus and nitrogen, the water quality and the nature of the river banks and bed (ICOLD 1999). As an example, a simple food pyramid is shown in Figure 2–1 which includes plankton for the base source or producer and pike as the apex predator. In between, insects, vegetation, algae, and other fish in varying combinations would need to be available in suitable numbers to provide a sustainable and balanced ecosystem. The other factors indicated in Table 2–4 also play a major role in the continuing balance of this simple pyramid.

Table 2–4: Stimuli for migration

Type of factor	**Factor**
Internal	Genetic and growth phase
	Hunger and metabolic balance
	Homing
Internal/external	Individual differences
External	Predator avoidance
	Light
	Temperature
	Hydrology and meteorology
	Water Quality
	Food availability

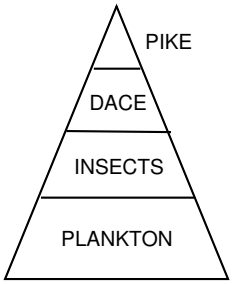

Figure 2–1: Diagram showing a typical simple food pyramid

The immediate availability of food is not necessarily an issue. The anadromous Atlantic salmon return to freshwater for spawning, at which point they no longer feed. It is therefore the energy reserves that a fish has stored and the 'overall cost' to that fish of proceeding up a river to a desired spawning habitat which needs to be taken into consideration (Larinier 2002b; Katopodis 2005).

Water temperature

Water temperature upstream of the point of interest and heat exchange with the atmosphere (through radiation and evaporation) both affect water temperature (in a specific location), which in turn influences the presence of different species of fish according to their favoured living conditions. Water temperature also has an important influence upon fish swimming speeds and endurance (section 2.1.3). However under field conditions, temperature is not subject to engineered control.

In large reservoirs temperature stratification can create problems, especially when outlets occur at different levels, whereas in rivers mixing of most water layers would normally occur naturally.

Where water temperature is not available for a specific site, data provided from a similar site could be used as an initial guide. Assuming temperature data is collected over time, assumptions would need to be verified and any design adjustments made if possible.

FACTORS MORE EASILY INFLUENCED OR CHANGED

Current speed / Water depth

Sensitivity to calm or flowing water depends upon the species of fish. Lake-loving or calm water fish are known as limnophilic and current-loving or river fish as rheophilic (Lucas and Baras 2001). The construction of any river barrier such as a weir changes the river characteristics and therefore affects the distribution of fish species.

In the UK there are many existing structures in the waterways that directly affect water depth, current speeds and water quality. Often the operating procedures also have a direct impact on all these factors, and are often designed according to specific legal requirements, for example those defining the extraction and return of water to a river system.

The localised effect of a structure on water depth and current speed also needs to be taken into account. With reference to an unmodified Crump weir, the shallow super-critical sheet flow that forms on the downstream slope can be prohibitive for most coarse fish species. One third of Crump weirs in England and Wales have been identified as being specifically problematic for fish (Environment Agency 1997b): hence the initiation of this research project.

River regime

River regime can be defined as "the distribution of flow over time" (ICOLD 1999). In this section the focus is on the impact of dams upon river engineering, and especially their effects upon fisheries.

The damming of rivers always affects fish in some way. For example, creation of a large stagnant body of water results in an increase in population of those fish favouring such conditions. Impacts are felt at the first impoundment, and then during the different seasons of the year, when stratification of the water in terms of temperature and water quality may be experienced. The availability of preferred spawning areas for certain fish species is greatly influenced by variations in habitat, such as changes in the growth of bank vegetation, reeds, water weeds, etc. New reservoirs are often stocked with fish, and the introduction of new species may drastically affect existing populations. The barrier effect of the dam or weir is also an obvious factor influencing fish passage.

Completion of a new dam, changes to the flow regime, water quality, current speed, and water levels all affect the fish population downstream (ICOLD 1999). Although the general water quality will not normally be significantly influenced by the positioning of a small weir, local variations in water quality, depth and velocity will be

affected. The presence of a structure can also pose problems to downstream fish migration. Specific zones as identified by Travade (2002), include the still water zone upstream of the impoundment, the spillway itself with direct or indirect mortality of fish passing over the structure, the presence of hydraulic turbines, and a potential increase in the suitable habitat required by piscivorous species.

2.1.3. Fish swimming speeds

The relationship between maximum swimming speed, fish length and water temperature is well established for salmonids, and Beach (1984) and Larinier (2002c) showed that for an increasing water temperature (from 2 °C to 25 °C), maximum swimming speeds also increased, while endurance (i.e. ability of fish to swim at the maximum swimming speed) decreased. One of the limitations of these graphs was the basic assumption that fish of the same size had the same swimming capabilities.

More recently, the Environment Agency has sponsored research and development into investigating the swimming speeds of British fish. Completion of phase one resulted in an Excel program, Swimit (Environment Agency 2001b), which combined with two technical reports (Clough and Turnpenny 2001; Turnpenny *et al.* 2001) provides information on the swimming speeds and endurances of five species of fish as well as a description of the techniques associated with obtaining them. Phase two extended the study, and the Excel spreadsheet has now been updated to include information from both projects (Environment Agency 2001b, 2003) for nine species (i.e. eight fish species and eel/elver).

Theoretical background

The findings from the literature review completed by Turnpenny *et al.* (2001) are briefly summarised below:

Swimming muscles: Fish use their muscles to swim, and different muscle types are required in aerobic and anaerobic environments, namely red muscle and white muscle respectively.

Red muscles contract only in the presence of oxygen and are used to maintain position in the flow, for migration and for ascent of low-flow velocity barriers. In an anaerobic environment the white muscles obtain energy from the conversion of glycogen into lactic acid. When its supply runs out, the glycogen needs to be replenished, which can only be done in an aerobic environment. White muscle is used for the burst speeds, which are normally required to escape predators and for ascending high flow velocity barriers (Wardle 1977, 1980, cited by Clough and Turnpenny 2001). Some species make use of a third muscle type, pink muscle, which is considered to occur between red and white muscle activity.

As indicated, muscle usage is associated with swimming speed, which can be categorised into cruising, sustained and burst speeds. Table 2–5 indicates the

various divisions in swimming speeds defined by Turnpenny *et al.* (2001), the analogy of a runner (Ayers 2002), and the muscles involved. After extreme exertion, such as leaping up a fish ladder, a fish would need to rest in order to replenish its glycogen, similar to a runner resting after the final sprint at the end of a race.

Table 2–5: Fish swimming speeds

Speed	**Maintenance time**	**Human analogy**	**Muscle**
Sustained	$>$ 200 min	Marathon	red
Prolonged	from 20 s to 200 min	800m	red/white
Burst	$\leq$ 20 s	100m	white

Power and drag: Fish are exposed to the same friction forces as any moving object within water, namely skin frictional drag associated with viscous shear stresses and form drag associated with pressure differences due to flow separation which are applied to the frontal area (Turnpenny *et al.* 2001).

Swimming uphill: Although the weight of a submerged fish in water is less than it would be in air, a gravitational force must still be overcome by the fish when ascending. If the fish is partially exposed, the work required to raise the fish increases correspondingly. (Formulae are given by Turnpenny *et al.* (2001).

Wave drag: The theory of wave drag provides an insight into the relationship between energy consumption and swimming depth. It shows that the closer a fish is to the surface, the greater the energy consumed by the production of surface waves. Minimum drag has been shown to be achieved when the immersion depth of the centre of gravity of the fish is approximately three times the diameter of the fish. Maximum drag occurring just below the water surface is approximately five times the minimum drag. A fish breaking the surface experiences approximately three times the minimum drag when its body is half exposed (Hertel 1969 cited by Clough and Turnpenny 2001).

Power availability: Propulsion is created by the lateral movement of the body surface and caudal fin, and power is supplied by the swimming muscles. A formula is given by Clough and Turnpenny (2001).

Fish swimming speed data from recent research

As indicated previously, phase one and phase two of the recent research and development into fish swimming speeds resulted in the compilation of the Swimit Excel spreadsheet (Environment Agency 2003), which allows the user to estimate both the sustained and the burst swimming speeds and estimated endurance times for nine

species namely: barbel, bream, brown trout, chub, dace, eels and elver, grayling, roach and smelt (Latin names in glossary). These species are considered representative of a broad range of fish, as well as being the dominant species in the English and Welsh river systems. This spreadsheet also allows the user to specify the percentage of population (i.e. 50 percentile or 90 percentile) for the required speeds.

The burst swimming speed information from the Swimit database is compared to the water velocities and is used as a design criterion in this research project. For each fish species and with increasing fish size, there is a change in the burst speed, which is also water temperature dependent over the temperature range (over the range of 10 to 15 °C, Environment Agency 2001b, 2003). Dace, brown trout and smelt show the typical trends based on the median burst swimming speeds (see Figures 2–2, 2–3 and 2–4 respectively):

Trend 1 (dace): Burst swimming speeds increasing with increasing fish size and water temperature (For roach, chub and barbel, see Figure A–1).

Trend 2 (brown trout): Burst swimming speeds increasing with increasing fish size but decreasing with increasing water temperature (For grayling, bream, elvers and eels, see Figure A–2).

Trend 3 (smelt): Burst swimming speeds increasing and then decreasing with fish size, and decreasing with increasing water temperature.

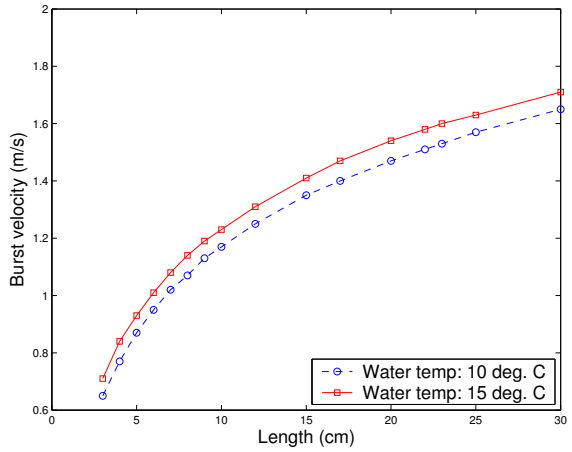

Figure 2–2: Dace, Trend 1: Fish size, temperature and swimming speeds

An additional consideration is whether any compensation would need to be made to the burst fish swimming speed as a result of the steep slope (e.g. such as the 20% gradient of the downstream slope of the Crump weir). Comments from Clough, as reported by Turnpenny (2003), suggested that it was probable that decreased water depths and the higher velocities associated with steeper slopes were more likely to be problematic rather than a gravitational effect (i.e. fish swimming against gravity). The assumption is that as long as a fish was fully submerged (i.e. by three times the body depth), the standard burst swimming speed data should be sufficient.

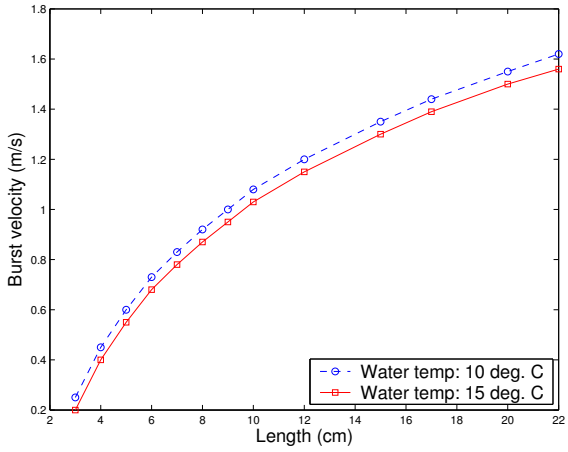

Figure 2–3: Brown trout, Trend 2: Fish size, temperature and swimming speeds

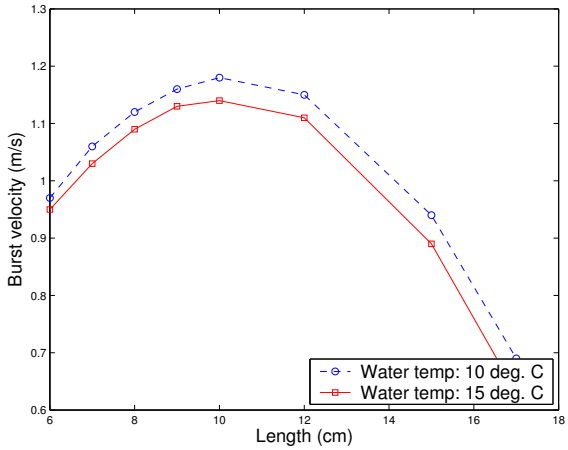

Figure 2–4: Smelt, Trend 3: Fish size, temperature and swimming speeds

2.2. Crump/triangular weirs and relevant hydraulics

Weirs are primarily used for one of four functions, namely, management of water levels, flow measurement, for environmental reasons or for channel stabilisation (Rickard *et al.* 2003). An active research and development area is that of flow measurement which takes into account accurate flow measurement capabilities of gauging structures whilst designed to aid or improve fish migration (Walters 1996a,b; Turnpenny *et al.* 1999; Sarker *et al.* 2001; Environment Agency 2001a; White *et al.* 2005b). In this section, one specific type of measuring weir, namely a Crump-type weir is considered.

2.2.1. Flow measurement requirements

As required by the Water Resources Act (HMSO 1963), water resources had to be assessed and hydrometric schemes implemented. Flow measurement is essential to the assessment of water resources. The Strategic Overview of Impounding Structures (Environment Agency 1997b) found that measurement is generally achieved by installing a gauging station at a strategic point. This normally takes the form of an impounding structure such as a gauging weir or non-impounding method such as electromagnetic or ultrasonic flow meters.

Gauging weirs work on the principle that a weir installation in a river results in an increase in water level (known as afflux) which can be measured. For each type of gauging weir a standard discharge equation allows for the calculation of discharge Q from a measurable head h (i.e. difference in upstream water level to crest elevation). These weirs need to be constructed and maintained within specification so as to ensure strict confidence level requirements are met.

A triangular profile weir, capable of accurate flow measurement applicable over a wide modular range, and providing predictable performance under submerged conditions was developed at the Hydraulics Research Station (Crump 1952). The standard 1:2 upstream and 1:5 downstream slopes of this type of weir as proposed at that time is now commonly referred to as a Crump weir.

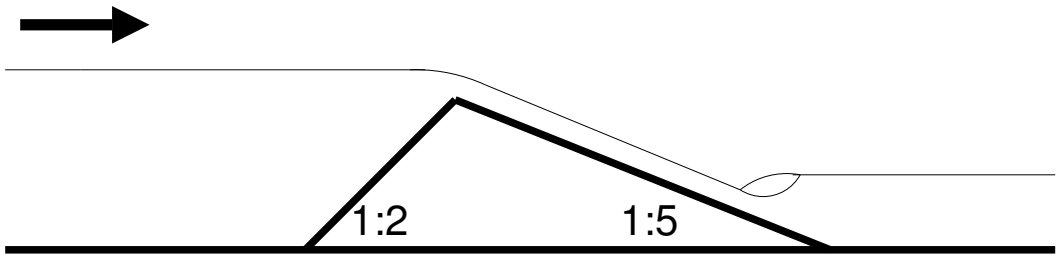

Figure 2–5: Schematic diagram of a Crump weir

Figure 2–5 shows a schematic diagram of a Crump weir which can be described as follows: In the deep water upstream of the crest, the flow regime is subcritical. On approaching the crest, the 1:2 upstream face reduces the cross-sectional area

thereby causing an increase in water velocity represented by converging streamlines. Downstream of the crest, flow is super-critical, potential energy is converted to kinetic energy on the 1:5 downstream face, water accelerates under gravity and water depth decreases until the formation of the hydraulic jump at the foot of the weir. The tailwater conditions are normally designed so that this jump will occur on the downstream face of the weir, thus preventing erosion problems further downstream. This is also in line with existing Environment Agency guidelines on Crump weir construction which are intended to promote fish migration at Crump weirs (see section 2.3.5 and Figure 2–18).

There are 376 Crump-type weirs (Environment Agency 2001a) in the Hydrometric Network of England and Wales, with approximately a third of these having been identified as being problematic in terms of fish passage (Environment Agency 1997b). The output of these gauging stations is logged in the National River Flow Archive which provides a database of daily and monthly flow data for use in research and national monitoring programmes.

2.2.2. Crump weir specifications

Guidelines pertaining to the minimum upstream gauged head (h_1), height of weir (p), breadth of weir (b) and combinations of these factors, as defined in Figure 2–6, are provided in the British Standard (BS3680 1986). Truncation (see Figure 2–6) of the weir is permissible within the requirements of the standard. Specifications include details of upstream and downstream stilling-wells and crest pressure tappings.

The specifications for the design, installation, maintenance, discharge characteristics and flow measurement uncertainties of an unmodified (i.e. standard) Crump weir are given by the British Standards Institution (BS3680 1986). The application of the gauging function of the weir is further divided into modular and non-modular flow:

Modular, unsubmerged or free flow is the flow condition when the upstream water level is unaffected by downstream flow conditions. The difference in elevation (h_1 in Figure 2–6) between the upstream water level and the weir crest level, the breadth of the weir (b), coefficients of discharge (C_d) and approach velocity (C_v), in addition to the gravity constant (g) are all included in Equation 2–1 defining modular flow. Modular flow is assured when $H_2/H_1 \leq 0.75$ (Herschy *et al.* 1977), where $H = h + v^2/2g$.

$$Q = (2/3)^{3/2} C_d C_v \sqrt{g} b h_1^{3/2} \tag{2–1}$$

The approach velocity coefficient (C_v) is defined as $C_v = (H_1/h_1)^{1.5}$. The discharge coefficient (C_d) is almost independent of the head (h_1) and C_d can be considered to be 1.163 when $h_1 \geq 0.1$ m. The exception is for low heads when fluid properties affect C_d. In this case, $C_d = 1.163(1 - (0.003/h_1))^{1.5}$.

The British Standard states that the upstream water level may be measured by a number of techniques, namely hook-, point-, staff- or recording gauge.

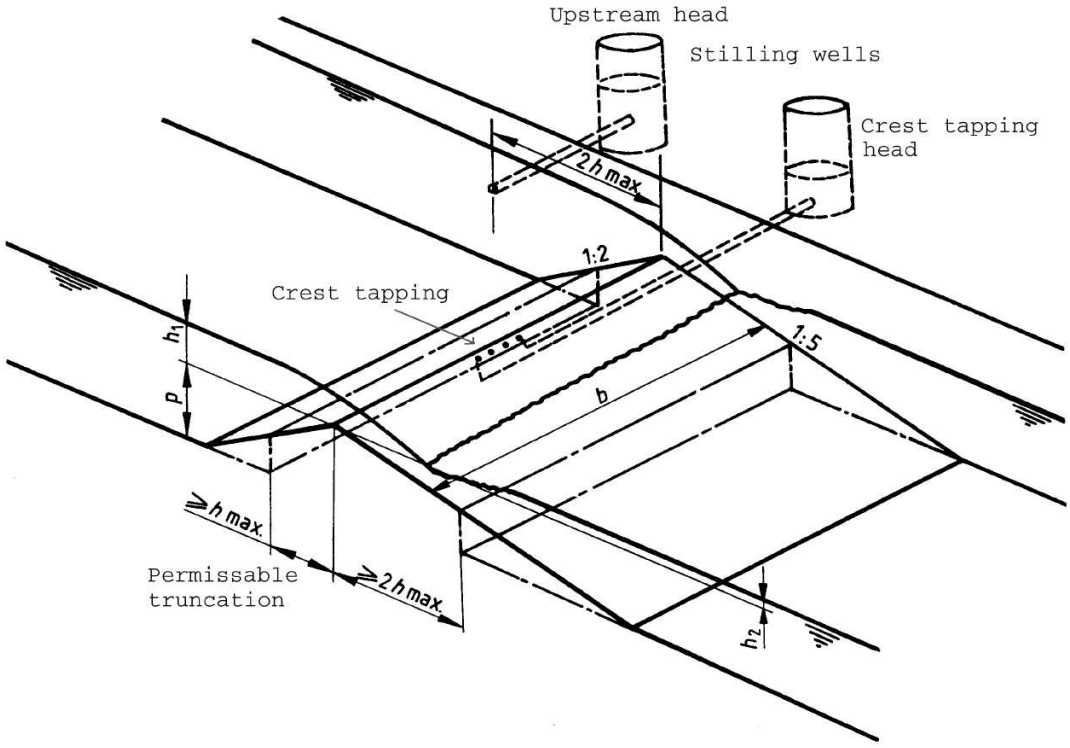

Figure 2–6: General layout of a typical Crump weir (BS3680 1986)

The effects of free surface fluctuations are reduced by the use of a separate stilling-well, which is connected to the flow through a pipe or slot large enough to give a short response time. The weir crest level is predetermined by the use of land surveying techniques, and it is normally the difference between the upstream water level and weir crest level that is recorded.

Non-modular or submerged flow arises when downstream flow influences the upstream water level. For non-modular flow, the non-dimensional drowned flow reduction factor, f, is applied to Equation 2–1, and results in Equation 2–2.

$$Q = (2/3)^{3/2} C_d C_v f \sqrt{g} b h_1^{3/2} \tag{2–2}$$

Non-modular flow can be determined using two methods, (a) either by measuring the difference in head between the upstream stilling-well and that of the crest tappings, or (b) by measuring the difference between the head in the upstream stilling-well and that in a downstream stilling-well connected to the tailwater. This latter method is not normally recommended as small errors in the head difference measurement may result in large errors in the calculation of the discharge, Q. (Herschy *et al.* 1977).

Accuracy and uncertainty

As described in the British Standard (BS3680 1986), measurement accuracy at a Crump weir is a combination of three factors: (i) head measurement accuracy, (ii) the physical installation of the weir (i.e. the as-built measurements as compared to the standard specifications) and (iii) the application of the coefficients in discharge calculations.

Both random and systematic uncertainty need to be taken into consideration when calculating uncertainties in flow measurement, which are expected to lie within the 95% confidence intervals (BS3680 1986). Systematic error relating to the coefficient of discharge for a Crump weir built within the British Standard guideline requirements can be calculated using Equation 2–3 and random error has been given as $X'_C = \pm 0.5\%$ (BS3680 1986). Worked examples for calculating uncertainty are given in the British Standard.

$$X''_c = \pm\left(\frac{10C_v}{f} - 9\right) \tag{2–3}$$

2.2.3. Compound Crump weirs

In order to achieve accurate gauging over a large stage-discharge range, it is common practice to combine weirs of different elevations in one structure. Figure 2–7 illustrates the combination of two Crump weirs, resulting in a low-flow crest and high-flow crest. For low-flows, discharge is measured using only the low crest, whereas for higher flow rates, flow measurement is a combination of the discharge over both crests. Numerous examples of compound gauging weirs are available in the field, and are not limited to the use of Crump weirs. Most of the Environment Agency's Crump weirs are combination Crumps, or combinations with other gauging methods (for example, Flat V weirs).

2.2.4. Laboratory modelling

Table 2–6[3], provides a brief definition of the three types of similarity (i.e. geometric, kinematic and dynamic) which are normally considered in a hydraulics laboratory.

Froude number dependence

In free surface flows, the Froude number is a relevant non-dimensional group and may be the dominant influence on aspects of the flow physics. The velocity of the model in relation to that of the prototype is obtained using identical Froude numbers for the model and the prototype. The result is shown in Equation 2–4.

[3]After Hamill (2001), Lomax and Saul (1979) and Smith (2002).

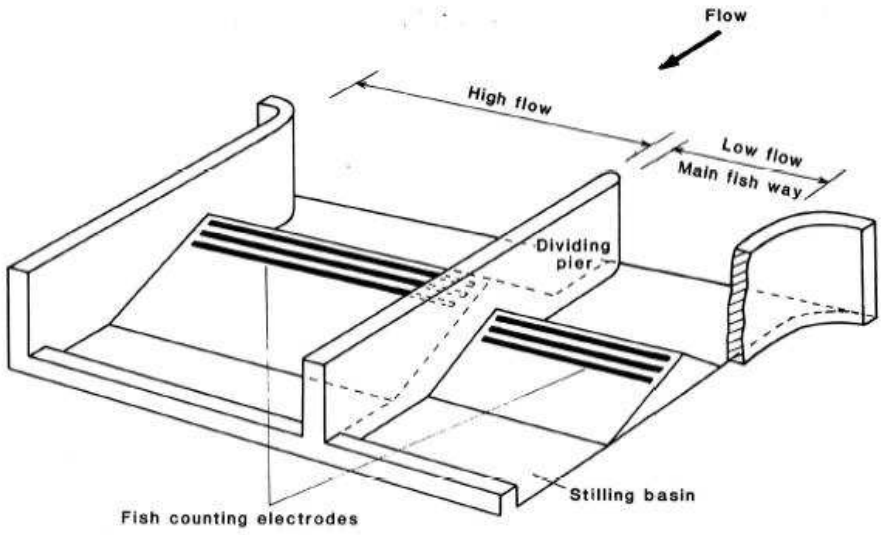

Figure 2–7: Compound Crump (Beach 1984)

Table 2–6: Hydraulic similarity

Type	**Defining characteristic**
Geometric	Shape: All significant features of the prototype are reproduced in the model. Scale factor is the ratio of the model quantity L_m to the prototype quantity L_p: $\lambda_L = \frac{L_m}{L_p}$
Kinematic	Motion: Velocities and accelerations are reproduced to scale in the model (both include a model: prototype time dimension ratio, T) and thus identical flow patterns are achieved. Velocity ratio: $\frac{v_m}{v_p} = \lambda_L \left(\frac{T_p}{T_m}\right)$ Acceleration ratio: $\frac{a_m}{a_p} = \lambda_L \left(\frac{{T_p}^2}{{T_m}^2}\right)$
Dynamic	Forces: At similar points, all forces are reproduced to scale in the model. Froude Number, $Fr = \frac{v}{\sqrt{gL}}$ representing $\frac{inertia\ forces}{gravity\ forces}$ Reynolds Number, $Re = \frac{\rho v L}{\mu}$ representing $\frac{inertia\ forces}{viscous\ forces}$

$$\begin{aligned} Fr_m &= Fr_p \\ \frac{v_m}{\sqrt{gL_m}} &= \frac{v_p}{\sqrt{gL_p}} \\ \frac{v_m}{v_p} &= \frac{\sqrt{gL_m}}{\sqrt{gL_p}} \\ &= \sqrt{\frac{L_m}{L_p}} \end{aligned} \tag{2–4}$$

The continuity equation ($Q = vA$) is similarly manipulated in order to obtain the flow relationship between the model and the prototype as illustrated in Equation 2–5. (From Equation 2–4 representing the velocity relationship, the length scale L, is equivalent to the measured head h.)

$$\begin{aligned} \frac{Q_m}{Q_p} &= \frac{v_m A_m}{v_p A_p} \\ &= \sqrt{\frac{h_m}{h_p}}\,\frac{A_m}{A_p} \\ &= \sqrt{\frac{h_m}{h_p}}\,\frac{b_m h_m}{b_p h_p} \\ &= \left(\frac{b_m}{b_p}\right)\left(\frac{h_m}{h_p}\right)^{1.5} \end{aligned} \tag{2–5}$$

Reynolds number dependence

As Reynolds number and Froude number similarity cannot be achieved simultaneously, a check needs to be made on the Reynolds number over the range of flows under consideration. Large scale-effects are generally avoided when flow conditions are turbulent, i.e. Re $>$ 2000 for open channel flows (Chadwick and Morfett 1994; Hamill 2001). The Reynolds number is calculated as for an open channel, which makes use the hydraulic radius, R. (Equation 2–6).

$$Re_{channel} = \rho R V/\mu \tag{2–6}$$

2.3. Fish passes and relevant hydraulics

The history of the fish pass dates back around 300 years in Europe, but it was only in the latter part of the 19th century and in the early 20th century that significant improvements were made. For example, legislation requiring the provision of some sort of salmon pass or ladder was included in the Salmon Fisheries (Scotland) Act of 1868. This included guidelines relating to the size and geometry of such passes (Salmon Advisory Committee 1997). In many cases, legislation has been and still is one of the driving forces behind the provision of fish passes.

Over the past century the development of fish passes has been interwoven with advances in the fields of hydraulics and fish biology, as well as pressures to preserve fish stocks and the growth in environmental awareness. Some of the more prominent approaches, with the researchers and their achievements, are described by Clay (1995). Denil, whose name was given to a specific type of fish pass (described in section 2.3.1) was one of the first to base fish pass designs on a scientific approach. The breadth of this field of study is illustrated by the fact that energy dissipation, the mechanics of fish swimming, fish attraction mechanisms, the monitoring of fish passes, and fish stress and other subject areas have all been emphasised at different times and in varying levels of detail. Clay also provides an overview of the current use of fish passes around the world and reports that international experiences are wide and varying, being especially influenced by the level of technology, available funds, and dependence on commercial fishing.

In this context, the terms fishway, fish ladder and fish pass tend to be synonymous, with the first term being generally applied in the U.S.A and the others in Europe. Clay (1995) defines a fishway as:

> "...essentially a water passage around or through an obstruction, designed to dissipate the energy in the water in such a manner as to enable fish to ascend without undue stress."

The Environment Agency recently produced guidance notes (Armstrong *et al.* 2004) which extends this definition as follows:

> "Any form of conduit, channel, lift, other device or structure which facilitates the free passage of migrating fish over, through or around any dam or other obstruction, whether natural or man-made, in either an upstream or a downstream direction."

2.3.1. Conventional fish passes

Many different fish passes have been described and depicted in numerous texts (including Beach 1984; Clay 1995; Salmon Advisory Committee 1997; ICOLD 1999; Larinier *et al.* 2002; Larinier 2002a; Travade and Larinier 2002 and Armstrong *et al.* 2004). The National Fish Pass Manual (Armstrong *et al.* 2004) provides design details for all the fish passes currently used within the Environment Agency.

Armstrong *et al.* (2004) categorised the fish passes as follows: pool passes, baffle fishways, easements, culverts and other river crossings, tidal flap gates and eels passes. The purpose of this section is to give a broad overview of most of these categories of fish passes, and an indication as to which types were found suitable for coarse fish. A general description and in some cases accompanying diagrams of each of the major types, is given below.

Pool passes

Pool passes, which are normally located on one or both sides of a structure within a river channel, are one of the commonest and oldest types of fish pass in use. The basic design is analogous to that of a staircase, and consists of a stepped channel forming pools of calmer/deeper water in which fish can rest. Figure 2–8 shows an example of a portion of a typical pool and traverse pass. This type of pass is normally fairly low maintenance, can accommodate change of direction easily and frequently and be integrated into a wide variety of structures. The channel normally has a shallower gradient than the rest of the weir or dam. This design type has also been used to surmount natural obstructions.

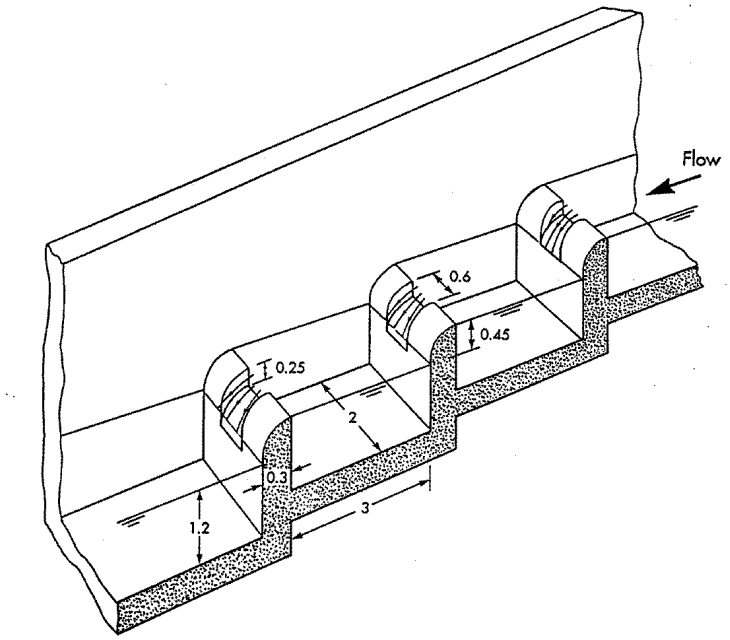

Figure 2–8: A typical pool and traverse pass (Carling and Dobson 1992; Salmon Advisory Committee 1997)

Flow patterns and the drops between the pools are of importance and have been the subject of various studies. Figure 2–9 (Larinier *et al.* 2002) differentiates between *plunging* and *streaming* flow. For the former, the water plunges towards the floor of the pool, and dissipation of energy is effected by turbulent mixing. In the latter case, energy is dissipated in the downstream pool by the formation of large circulation eddies. The recommendation is that pool passes are designed to operate either

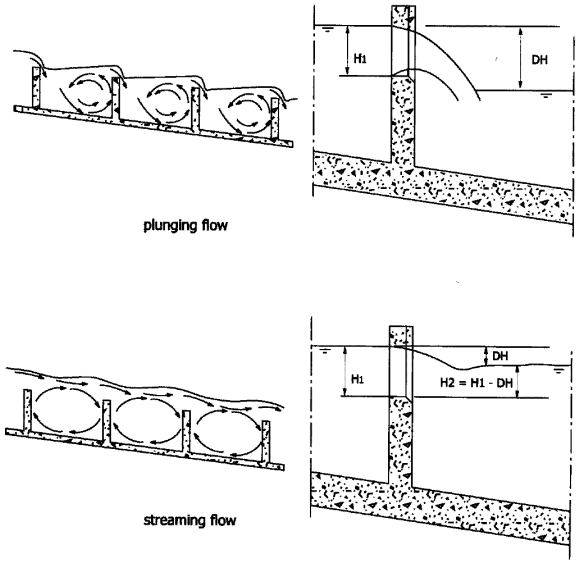

Figure 2–9: Stream flow patterns (streaming or plunging flow) (Larinier *et al.* 2002)

within one or the other flow type. For example, shad prefer to travel in shoals, and for them passes with plunging flows should be avoided.

There are many variations on the basic pool pass, and these include the use of notches (rectangular, triangular) and/or orifices in the weir walls. Table 2–7 provides a summary of the most common pool passes. These passes operate well with design slope of $<$ 10 % (except the 'V' notch weir which requires a slope of $<$ 5 %).

Table 2–7: Pool passes: list of common types and associated fish species applications (summarised from Armstrong *et al.* 2004)

Description	**Suitable species**
⋆ pool & traverse	plunging flow: high performance coarse fish streaming flow: high & low performance coarse fish (shad require streaming flow)
⋆ vertical (pool &) slot	high & low performance coarse fish, eel specific: barbel
⋆ pool & orifice	high & low performance coarse fish (incl. grayling, roach & perch, not shad or pike)
'V' notch weirs	high & low performance coarse fish low head loss ($<$ 0.25 m), all surface swim species
deep notch & submerged orifice	high & low performance coarse fish
ice harbour	no data
pool&chute	no data
⋆ fish locks	high & low performance coarse fish
fish lifts	high performance coarse fish

⋆ discussed in text

Since all of these passes were designed specifically for salmon (and/or trout), they are not necessarily applicable to other species[4]. The high performance (chub or barbel), low performance coarse fish species (most cyprinids) and eels which can generally be accommodated have been included in this table (as adapted from Armstrong *et al.* 2004). The '$\star$' in this table indicates those passes which have been described further in this text.

A good example of a type of fish pass designed specifically for salmon is the vertical slot type designed initially for the Hell's Gate rapids on the Frasier River in Canada (Clay 1995). Figure 2–10 illustrates the different flow patterns resulting from single and double jets, both of which provide resting areas for migrating fish. Additional factors considered during research trials at this fish pass type included turbidity of water, time of day, and lighting conditions.

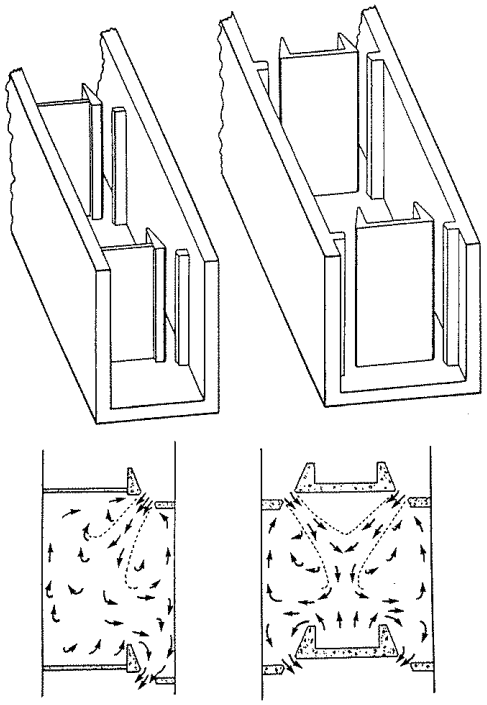

Figure 2–10: Vertical slot (single and double jet) (Andrew 1990 cited by Carling and Dobson 1992; Salmon Advisory Committee 1997)

Pool and orifice passes are normally used in combination with other types of passes, and provide a useful mechanism for controlling head, as well as an alternate pathway.

Figure 2–11 illustrates a typical fish lock. The lock consists of a high level chamber, with an upstream automatic sluice gate, and a low level chamber with an automatic sluice gate at exit. The two chambers are connected by an inclined conduit. With the downstream gate open and the upstream gate controlling the current through the lock, the fish are guided to the lock entrance by a small fish pass or other attraction method. After a prescribed duration, the attraction phase is terminated by closing

[4]Armstrong *et al.* (2004) included the suitability of these passes for salmon, high performance coarse, low performance coarse fish, *alosa alosa* and eels

the downstream gates. The inclined conduit then fills and the fish progress up the incline, attracted in that direction by the current. An attraction flow at the exit of the upper chamber encourages the fish to leave the lock and enter the headpond and the final phase commences. During this phase, the high level chamber needs to be emptied. This is achieved using a bypass, with the flow controlled such that low velocities are produced. This type of pass works well where there are high dams and a reasonably large number of fish, such as during peak migration periods. Generally, cycle duration takes between one and four hours.

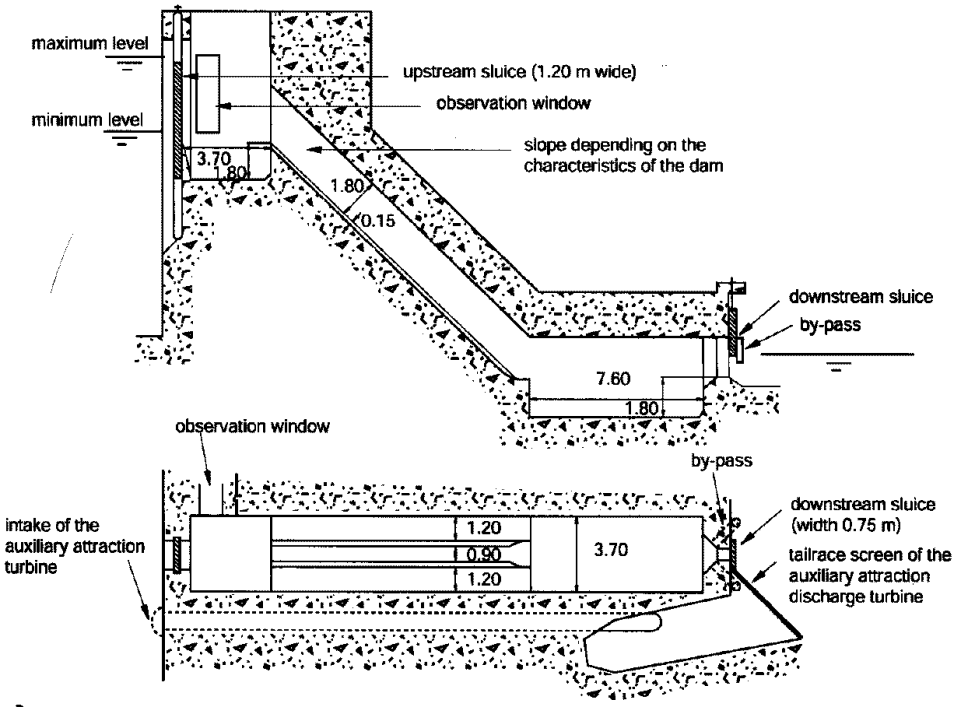

Figure 2–11: Typical Fish Lock (Travade and Larinier 2002)

Baffle fishways

Similar to pool passes in that these passes are normally built within or adjacent to a river structure, these passes are designed to operate on steeper gradients (generally suitable up to 20%) than the pool passes.

In essence, a baffle fishway is comprised of a dedicated channel with custom-built, normally steel baffles fitted at a closer distance together than the weirs customarily used at a pool pass solution. These elements are specifically designed to develop helical currents within the channel, thereby dissipating energy along the whole section of the fish pass. These passes tend to be species specific (which needs to be considered during the design period), as the energy dissipation needs to be in line with the swimming ability of the fish. In the same way that a flight of stairs has a landing, baffle passes can be installed in 'flights' with resting pools in between. In order to pass fish effectively, fish need to be able to pass up a flight either to

the top of the structure or to a resting pool (which depends on the total height to be passed). As indicated in Table 2–8 , baffle fishways can be divided into three categories according to the physical position of these baffles.

Table 2–8: Baffle passes: list of common types and associated fish species applications (summarised from Armstrong *et al.* 2004)

Description	**Suitable species**
Side & bottom baffle passes	
⋆ - *Plane baffle Denils*	high & low performance coarse species
- *Fatou Denils*	no data
- *Alaskan 'A' Denils*	high & low performance coarse species
Bottom baffle passes	
⋆ - *Super-active baffle (Larinier) pass*	high & low performance coarse species
- *Chevron baffles*	not suitable
Side baffle passes	
- *Chevron side baffles*	not suitable

⋆ discussed in text

As baffle fishways are located within a channel, it is possible to specify both a 'biological' (i.e. according species and size specific requirements) and an 'hydraulic' operating range.

The formation of helical currents occurs between a minimum and maximum flow rate. Below the minimum flow, baffle fishways operate as a mini-pool, whereas above the maximum flow rate at which helical currents form, supercritical flow is characteristic and energy is not dissipated sufficiently (Larinier 2002a).

Figure 2–12 shows a 3-D schematic of a Denil pass. In addition, the baffle detail depicts the wall and floor nature of the baffles, which in a plane baffle Denil are orientated at a 45° angle to the floor (see the longitudinal section), with a 10% to 20% channel slope. Disadvantages of the baffle fishways include difficult construction owing to intricate design, potential maintenance problem, and the limited flow range at which a particular pass can operate. If space allows, a battery of passes designed for different flow rates can accommodate a larger range of flows.

Super-active baffle or Larinier passes (Figure 2–13) have been widely used in France and are becoming increasing popular in the UK. The herringbone pattern used for the baffles positioned on the bottom of the dedicated fish channel are characteristic of this type of pass. Flow rate relationships for this type of fish pass are well-documented (Larinier 2002a). Recent laboratory research (White *et al.* 2005d) has been carried out to calibrate this type of pass to hydrometric standards, for use alone or as part of a flow measurement system. Additional studies considering the combination of a Crump and Larinier solution are discussed in section 2.3.4.

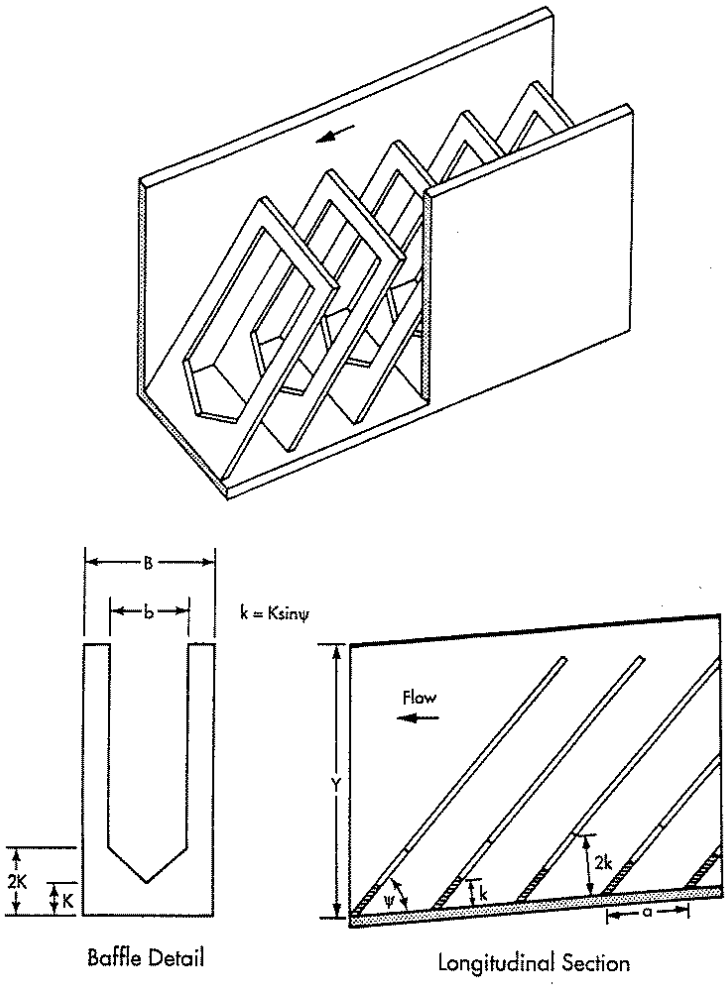

Figure 2–12: Denil pass (Carling and Dobson 1992)

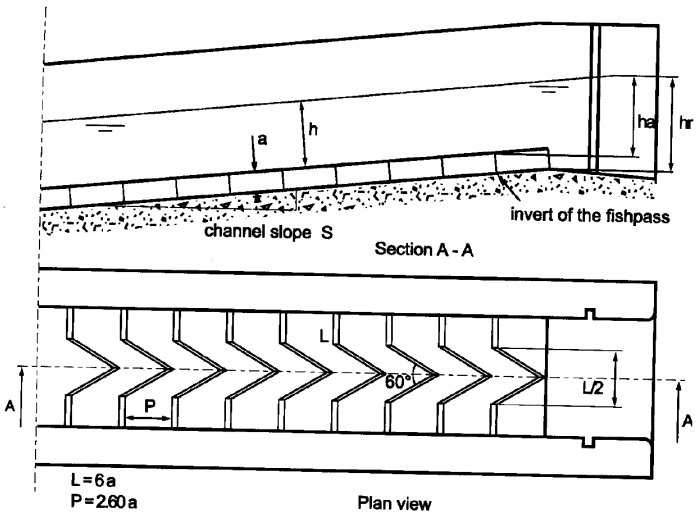

Figure 2–13: Super-active baffle (Larinier) pass (Larinier 2002a)

Easements

While new structures are required to follow a set process which would include more stringent fish pass requirements (Armstrong *et al.* 2004), fish passage at existing structures is often accommodated using easements. Table 2–9 presents the easement categories as identified by Armstrong *et al.* (2004). Modifications made to the downstream face of the weir would fall under the easement category.

Table 2–9: Easement categories and associated fish species applications (summarised from Armstrong *et al.* 2004)

Description	**Suitable species**
⋆ Notches and gaps	not normally used independently
⋆ Baulks	some coarse species depending on design
⋆ Baffle systems	e.g. Hurn weir (specifically for dace)
Preliminary weirs	Site specific
Modifications to the natural bed	Site specific
Rock ramps	Site specific
Sweeps	Site specific
Artificial river systems	Site specific

⋆ discussed in text

A simple form of modification might include notches (or slots) which could be added to a downstream weir face. An example of this type of approach is the dished channel (Figure 2–14) which consists of a shallow trough on the downstream face of the weir. One of the disadvantages of this type of pass, is that the integrity of the structure might be compromised (Fort and Brayshaw 1961). Gaps may be used for narrow crested, vertical weirs and may take the form of a gap from the crest to the base of the weir. The size of the gap is normally determined by fish species requirements. In both cases, the type of flow (i.e. streaming or plunging) needs to be taken into account as this is indicative of the species suitability. These are often used in combination with other easement methods.

The diagonal baulk (Figure 2–15) fish pass is constructed using a diagonal beam on the downstream face of the weir, with a notch at the top of the spillway, creating a shallow gradient channel. An enhancing beam at the crest is also in place which effectively guides water through the notch. A baulk can be added to the downstream slope of a triangular profile weir with ease and would not normally cause structural problems (Fort and Brayshaw 1961). The length and angle of the baulk are critical to successful fish passage.

An example of a baffle system is that of Hurn weir, further discussed in section 2.3.4.

Culverts

Fish passage through culverts, under bridges, and at fords can also be problematic, and highlights the need to ensure connectivity of an entire water reach to ensure

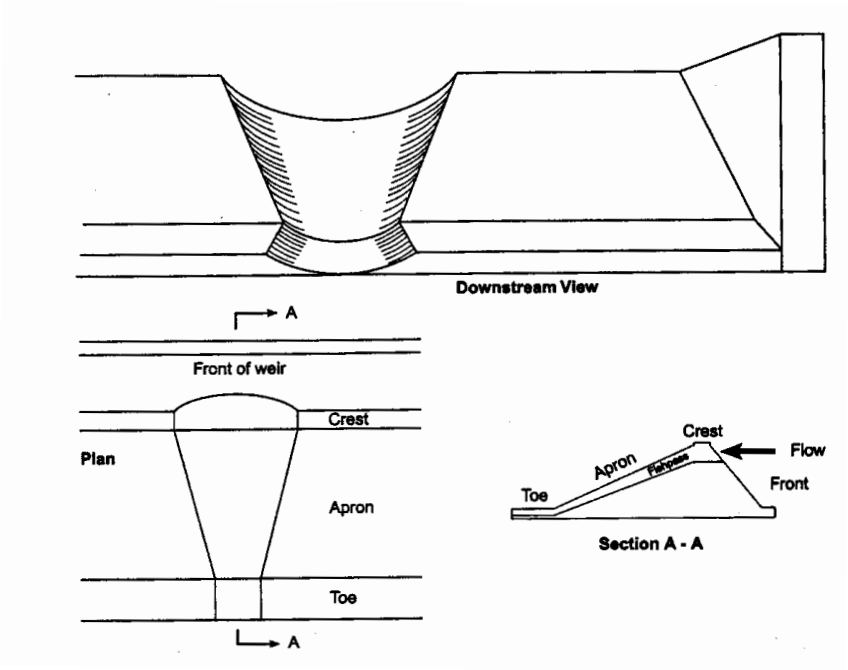

Figure 2–14: Dished channel (Salmon Advisory Committee 1997)

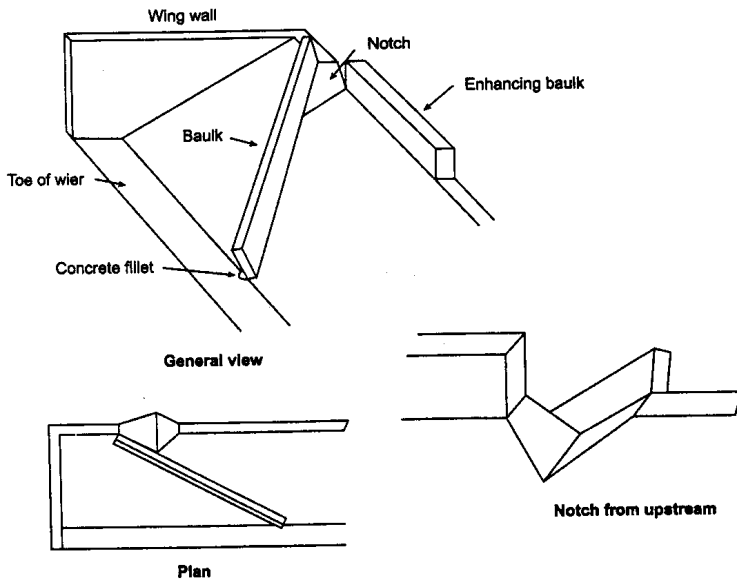

(a) Baulk

Figure 2–15: Baulk (Salmon Advisory Committee 1997)

retainment of viable habitat within a system. Culvert-related fish passage problems and solutions (which include the use of baffles) are not further explored within the context of this research as the problems are normally specifically related to the very low gradients encountered.

Eel passes

Specifically designed for eels, this type is normally a shute which has a roughened surface (concrete or bristles) that provides friction for the eels' locomotion. Overheating of the eels caused by exposure to air and sun, and the increased risk of predation can cause problems.

Removal of structure

One solution to a fish passage problem is the removal of the obstruction, in order to allow fish to pass unhindered upstream. However, this type of approach would need to take into account the uses of the structure under consideration.

2.3.2. Fish pass design criteria

The literature describing common design practices, as well as common design-specific criteria is relatively extensive and well-documented. The following topics provide an overview of typical design criteria for a specific fish pass which need to be taken into account.

Target species The target species for which the fish pass is being designed must be identified. The fish species for this research project are those identified by the Swimit (Environment Agency 2001b, 2003) spreadsheet, namely barbel, bream, brown trout, chub, dace, eels and elver, grayling, roach and smelt.

Operation period The operation requirements for the fish pass in terms of time of year and the flow rates are also important. Table 2–10, as reproduced from the National Fish Pass Manual (Environment Agency 1997b and updated by Armstrong *et al.* 2004), provides guidance periods with the proviso that site specific information be sought from the relevant specialists.

Table 2–10: Suggested fish pass operational periods

Type	**Periods (Inclusive)**
Salmon	April - November
Trout	October - November
Coarse Fish	March - June
Elvers	May - July

Hydrology Site specific flow data should be obtained as a pre-requisite to designing a successful fish pass. Such data should include the mean daily flow for the period of operation of the fish pass (Turnpenny *et al.* 1999).

As fish swimming performance is water temperature related, this needs to be taken into consideration.

Choice of fish pass design An inappropriate choice of fish pass, given the particular environment and application, and/or the inadequate dimensioning of that structure (Larinier 2002c) would both lead to malfunctioning.

Entrance and exit conditions The entrance to a fish pass is considered to be at the downstream end of the pass, with the exit upstream. Entrance and exit flow velocities need to be within the swimming capabilities of target fish species.

Debris / trash accumulation The prevention of debris entrapment needs to be specifically considered. White *et al.* (2005c) report that a number of devices are employed at fish passes, and these include screens, fixed deflectors and floating booms. They further recommend that as Crump weirs are considered to be at a higher risk for trash accumulation (low head with horizontal crest), an upstream deflector and/or trap be considered, with the aim of preventing trash from reaching the crest and thus changing the flow calibration. An additional consideration is the use of remote surveillance.

Location and attractivity Field experience has shown that if fish cannot find the pass entrance (which is at the downstream end of the fish passage), it will not fulfil the intended design application. Larinier (2002c) reported that lack of attractiveness is one of the main causes of fish pass malfunction. The location of a fish pass is associated with three factors, namely the position of the pass itself (i.e. close to the river banks is preferable to the centre of the river), the position of the fish pass entrance, and the size of the entrance.

Assuming site suitability, the advantages for having a fish pass on the side of the river include fish behaviour patterns (fish tend to swim along the sides), monitoring and maintenance of the pass (Armstrong *et al.* 2004).

Armstrong *et al.* (2004) recommends that the entrance position be located as close to the downstream side of the obstruction as possible, as constrained by the specific discharge characteristics of a structure.

The entrance width is small in proportion to the structure and therefore attention needs to be paid to the design of the flow that will act as a stimulus (in the form of an entrance jet) allowing fish to be attracted to the fish pass (Larinier 2002c). Bates (2000) reported that the depth to which the entrance jet will penetrate is a function of the momentum, alignment and shape of the jet.

Protection It is not enough to consider the barrier of the structure itself in terms of fish passage. Problems are encountered at offtake structures as well as hydroelectric applications where high fish mortality rates are encountered. These are normally associated with mechanical devices such as turbines and pumps. Fish protection can be divided into a number of categories when considering hydroelectric applications (Stone and Webster Engineering Corp. (1996) as cited in Clay (1995); Travade (2002)).

Behavioural barriers try to make use of natural stimuli in attracting or repelling fish. As these are not physical barriers, minimal maintenance is re-

quired, although effectiveness in the field has often not reached the expectations aroused from controlled conditions. These types include air bubbles, light, water jet curtains, hanging chains, electricity and hydrodynamic louvers.

Physical barriers such as screens are designed to prevent fish from swimming through them. Fish species, size, swimming abilities, and hydraulics all need to be taken into account in a screen installment design so as to ensure effective screening. Disadvantages include high maintenance costs.

Retrofitting has been necessary as many dams and hydroelectric schemes were built before fish requirements were taken into account. Screens and/or trash racks can be used to divert fish from dangerous or impassable areas to a purpose-built bypass which can accommodate the fish. The effectiveness of a bypass is normally dependent on the location as well as entrance conditions.

Fish-collection devices In the case of high dams, it is often necessary to capture and transport fish.

Predator protection A decision must be taken on whether protection from predators and any undesirable downstream migrators, such as lamprey, might be required (ICOLD 1999).

Operation and maintenance As with any water resource, the continued functioning and life of any structure requires the successful operation, and implied maintenance of that structure. This includes appropriate funding and the allocation of staff who are responsible for the fish pass. Fish passage malfunction is also caused by the inadequate maintenance of working parts (Larinier 2002c).

Monitoring Quantitative methods in monitoring fish migration have been extensively researched. Methods include mechanical, electrical, visual, mark recapture, catch data, and full river trapping. The success of any fish pass can only be determined by the successful migration, in both upstream and downstream direction, of the species attempting to use it. Normally a statistical analysis of attempts and the determination of the success/failure rate would enable the responsible person to reach a conclusion. Because of the large variety of techniques available for use, the assessment method chosen should be the one which provides the required and/or best information within the available budget. Table 2–11 presents a summary of the main techniques adopted by Lucas and Baras (2001).

During the design phase of a fish pass, it is useful to consult the specialists responsible for monitoring the fish population. In this way, assessment techniques can be accommodated during the design phase.

Design standards Guidance on the construction of gauging weirs, as initially formulated by the Thames Region in their Strategic Overview of Impounding Structures (Environment Agency 1997b), is provided in Armstrong *et al.* (2004).

Table 2–11: Fish population assessment techniques (Lucas and Baras 2001)

Impact	**Technique**
Capture Independent Technique	Visual Observation
	Electric Currents
	Hydroacoustics
Capture Dependent Technique	Variations in density (catch analysis)
	Marks and tags

A draft standard for 'Fishpasses at flow gauging stations' has been published in White *et al.* (2005a). The aspects impacting directly on this research project are dealt with in section 2.3.5.

Legislation Although the precise legislative requirements are beyond the scope of this study, no design guidance is complete without taking current legislation requirements and the project cycle practices on-board. Armstrong *et al.* (2004) provides a useful resource in this regard, and attention is drawn to the fact that in England and Wales, any modifications or new designs for fish passage need to be directed through the National Fish Passage Panel (NFPP) in order to comply and follow the approval process. As various planning permissions, and Health and Safety requirements need to be taken into account, consultation with the NFPP is beneficial from the project initiation.

As this research is aimed at low-cost modifications to triangular profile weirs, it is likely that the works may not fall within the scope of the formal authorisation process, but would still be required to conform to any requirements within existing legislation. The Environment Agency, which is the statutory body, recommends that NFPP be informed of any works so that authorisation status can be determined, best practice and design guidance can be given and their fish pass database can be updated appropriately.

2.3.3. Fish pass trials: field or laboratory?

Model testing is a well-established means of trialling a variety of design parameters for hydraulic structures, and there are accepted methods and procedures to ensure accurate scaling between the model and the prototype (e.g. Froude number and Reynolds number similarity are discussed in sections 2.2.4 and 3.1.4).

Although fish pass efficiency trials have been conducted using live fish in a laboratory situation, a number of difficulties present themselves. Experiments using fish were conducted by White and Hartley (1970) at two triangular profile flat-V weirs, the results of which present some of the problems associated with using fish in laboratory trials. Notwithstanding problems associated with obtaining, keeping and using fish and any associated welfare issues, fish species, type and size all need to be considered. In addition to fish behaviourial aspects which might influence results,

fish in themselves are not scalable, and juvenile fish do not necessarily have the same capabilities as the adults.

Another approach is to test the hydraulic parameters within a hydraulics laboratory while performing fish passage trials using live fish in a suitable field laboratory.

Guiny *et al.* (2005) effectively used this approach as part of a controlled experimental program to determine the hydraulic and biological aspects of fish passes with reference to Atlantic salmon. The passing efficiencies of three of typical types of passes were tested using juvenile Atlantic salmon (parr). This study considered both the hydraulic as well as the biological factors relating to a fish pass by using two experimental flumes. Head loss, velocity patterns and turbulence structures were measured in a simplified, laboratory model in a flume which was identically dimensioned to the flume used to test the preferred routes. The model represented a simplified fish pass of two pools, divided by a cross-wall. The cross-wall was constructed such that it represented a weir, orifice, or vertical slot-type fish pass as well as several combinations thereof. Differences between the fish passes were found to be independent of the downstream entrance condition flow velocities, although flow characteristics and fish pass efficiency were found to be correlated. A slot-only based pass was more efficient than the orifice or weir pass, whereas an orifice combined with a weir pass resulted in increased efficiencies over a wider flow range. Behaviour strategies in relation to energy expenditure and cover requirements were also considered. Overall, the study provided guidance for Atlantic salmon parr and related fish passage design, and it was anticipated that with further testing, the guidance would be applicable to adult salmon.

2.3.4. Fish passage research at triangular profile gauging weirs

Designing for fish passage at gauging stations while maintaining the integrity and accuracy of the structure is a challenge. Existing hydrometric structures have been found to be detrimental to fish passage and current practice includes retro-fitting existing structures in an effort to remedy known problem sites (Beach 1984; Walters 1996a,b; Environment Agency 1997a,b; Pinniger 1998; Turnpenny *et al.* 1999; Environment Agency 2001a; White *et al.* 2005b).

The Hurn-type baffle system used at a Flat-V gauging weir, laboratory testing on a Crump (Brimpton) weir and recent research into using a Crump-Larinier combination are discussed below.

The Hurn-type baffle system

A recent example of modifying an existing structure is that of the Hurn weir on the Moors River in Dorset (Walters 1996a,b; Environment Agency 1997a). This is a Flat-V gauging weir[5] which has been retro-fitted in an attempt to improve fish passage for a smaller coarse fish species, namely dace. The National Rivers Authority

[5]A Flat-V weir has a 1:2 upstream, 1:5 downstream longitudinal profile, with a 1:10 to 1:40 cross-slopes.

initially installed a Denil type fish pass on the centreline of the weir which proved to be unsuccessful in passing dace through the weir.

In 1995, Exeter University, School of Engineering, changed the fish pass type to an easement method that used a 1:13 scale hydraulic model to test a series of baffles on the downstream slope of the weir. The arrangement was designed to improve the depth and velocity requirements (designed for a burst speed of 1.5 ms^{-1}), measure the velocities and determine the use of the baffles for gauging purposes (Walters 1996a). A mixture of slots and grooves located in the baffles were found experimentally (Walters 1996b) and this arrangement was then installed using baffles made of recycled plastic, in the field at a cost of £8000 (Environment Agency 1997a), not including research and development costs. Figure 2–16 shows the Hurn weir in operation.

Figure 2–16: Photograph of Hurn weir (February 2002, flow rate unknown)

Initial trials showed dace making use of the structure, but these were not finalised, nor has pass efficiency been determined (Armstrong *et al.* 2004). The easements used at Hurn have come to be known as the Hurn-type baffle system (Armstrong *et al.* 2004).

Laboratory testing on a Crump weir at Shrivenham (Sarker 2000)

As part of a research project into CFD applications for modelling local features in a river, Sarker (2000) attempted to numerically model (using commercial software) the free surface flow over a multiple baffle arrangement, modifying the downstream apron of a Crump weir with a view to improving fish passage.

A numerical and physical model based on the low-flow section of the compound Crump weir located at Brimpton, on the River Enborne in the Thames catchment

was used to predict the free surface profile for the 95 percentile low-flow. Thin steel plates were used to model baffles (at a 1:5 scale) parallel to the weir crest, which were installed at 30, 60 and 120 mm centre-to-centre. The 60 mm spacing was found to be optimal, and further investigations were pursued using vertical slots on the side of the flume, of 12, 22 and 32 mm width respectively. Water depth, and not water velocity, was primarily used to compare the effect of the baffles, with the focus of the project being on the comparison between the numerical and physical models. The 1:5 Brimpton model and baffle spacing of 60 mm was used as a starting point for the research described in this document.

Crump and Larinier combination (White *et al.* 2005d,f)

Recent research at HR Wallingford includes two studies on the use of a Larinier fish pass, as part of the Environment Agency research into flow measurement structure design with the stated aims of improving fish passage without compromising flow data accuracy (White *et al.* 2005d,f). The draft guidelines state that an uncertainty of less than 2% at the 95% confidence interval would be typically expected for the determined coefficient of discharge White *et al.* (2005a).

The first laboratory investigation, as reported by White *et al.* (2005d), was to provide an accurate hydrometric calibration for the Larinier fish pass. In this test, a Crump weir and a Larinier fish pass were set in series. Calibration tests for modular flow on the Larinier fish pass found that there are three distinct phases, with an associated effect on the coefficient of discharge. Three-dimensional flow occurs first, with spilling until the upstream baffle is completely over-topped, and is reflected in a rising coefficient of discharge. Each baffle effectively acts as a weir at this point. As flow continues to increase, the three-dimensional flow changes to two-dimensional flow (forward and vertical), and is characterised by a falling coefficient of discharge. Quasi two-dimensional flow occurs in the third phase where the baffles are effectively acting as bed roughness elements, and results in a constant coefficient of discharge. Modular limit tests were also conducted. Recommendations included setting the crest level of the gauging structure so that fish would be able to surmount both structures, while ensuring modular flow conditions and therefore gauging accuracy. A sufficient resting area between the fish pass and the weir providing a low velocity area would also be required.

In the second investigation, White *et al.* (2005f) made use of the results from the gauging conditions and the effect on the coefficient of discharge for the modular flow rates (reported above). The Larinier fish pass was set parallel to a flow measurement structure, and made use of a submerged orifice upstream intake for fish exit. Testing was conducted to provide information on flow conditions upstream, downstream, within the fish pass and within the stilling basin of the measuring weir. Variations on the design were also tested, and minor modifications were made where necessary to entrance and exit conditions. A planned output (see section 2.3.5) was to provide a first draft on a combined fish pass-gauging weir standard, and this investigation was used to confirm the proposed design parameters for this draft.

HR Wallingford study on the near-crest arrangements of baffles on downstream slope of the Crump weir (White *et al.* 2005e)

The Hurn-type baffles were considered promising as an inexpensive fish passage approach but were problematic in that the presence of the baffles changed the hydrometric performance. Therefore, an investigation into the near-crest arrangements of baffles on the downstream slope of the Crump weir was instituted. This formed part of the research into flow measurement structure design with the stated aims of improving fish passage without compromising flow data accuracy (White *et al.* 2005b).

Four single baffles were placed on the downstream slope of the test Crump. The baffles tested were 40 mm, 30 mm, 20 mm and 10 mm high and placed at distances of 250 mm and/or 125 mm from the crest (measured from the crest to the upstream face of the baffle). The baffle shapes themselves were based on the Hurn-type baffles. The width and radius of each baffle was related to the total baffle height. Thus for a baffle height of T, the width was set to $2T/3$ weir baffle and the top radius was thus $T/3$.

For the scenarios tested, a maximum of 7% deviation to the basic Crump weir coefficient of discharge was recorded. The minimum design distance of the baffle closest to the crest was then recommended such that there would only be a 1% reduction in the coefficient of discharge for the basic Crump weir (i.e. a 'no-effect' criterion) (White *et al.* 2005e).

The effects of a single baffle were tested, and the presence of a second baffle or a series of baffles downstream of the crest was not considered, presumably because the first baffle was to be placed sufficiently far downstream so as to cause a 1% reduction on the coefficient of discharge.

2.3.5. Existing fish passage guidelines relating to Crump weirs

Guidance relating to unmodified Crump weirs

Early guidance regarding fish passage at a Crump weir was based on the swimming abilities of migratory fish, specifically salmon and trout. Figure 2–17 illustrates the water velocities versus gauged head on a typical Crump weir. The maximum allowable velocity recommended by Beach (1984) was 3.5 ms^{-1}. This was based on a salmon of 0.54 m body length at 10 °C for a swimming duration of 1.5 minutes (in the z-direction as shown in the inset in Figure 2–17). Further requirements imposed conditions upon the height of the weir p and upon the tail-water immediately downstream of the weir apron. Sufficient energy dissipation needed to be catered for during the stilling basin design so as to ensure that the super-critical and highly turbulent flow was not continued downstream.

Armstrong *et al.* (2004) reported that there was no reference to minimum water depths in Beach (1984), and that the recommended swimming speeds were 'extremely challenging' for coarse fish. Figures 2–2 to 2–4 (page 16) and A–1 to A–2

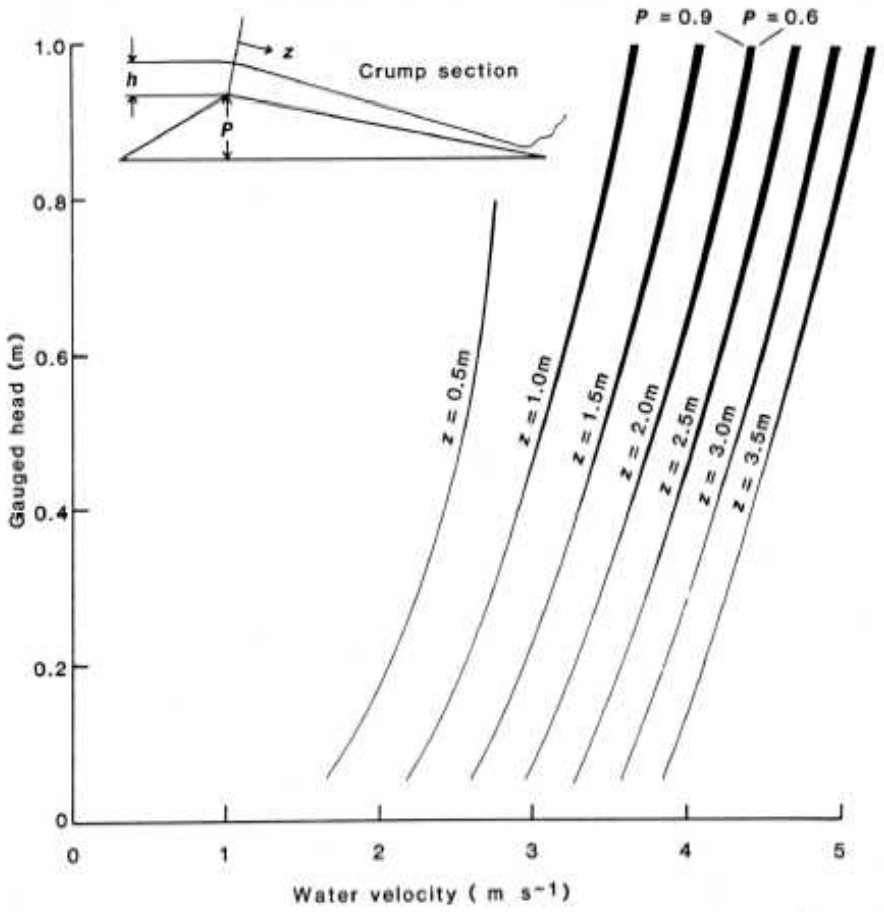

Figure 2–17: Velocities on downstream slope of the Crump weir (Beach 1984)

(page 230) show the mean burst speed velocities associated with each species and fish size and for two temperatures (compiled using the Swimit results, Environment Agency 2001b, 2003). These burst speed velocities show that although Beach's recommendations allow the passage of migratory fish (i.e. salmon and sea trout), the resulting velocity conditions exceed the swimming abilities of most coarse fish.

Together with the recommended construction guidelines for new Crump and Flat-V weirs (repeated verbatim in Figure 2–18), updated operational conditions when fish passes should be swimmable by the targeted fish, as given in Table 2–10, were recommended by Armstrong *et al.* (2004).

1. The maximum difference in level between crest level and the downstream tail water level is to be not greater than 0.5m for Crump weirs and 0.3m for Flat V's.
2. The maximum velocity should be no more than 3.5ms^{-1} on the downstream face of the weir immediately upstream of the hydraulic jump.
3. The mean approach velocity in the stilling basin must be no more than 0.7ms^{-1} for migratory salmonids (including trout) or 0.3ms^{-1} for coarse fish.
4. The stilling basin should have a minimum depth of 300mm below tail bed level[1].
5. The hydraulic jump is to form on the face of the weir, not in the stilling basin.
6. It is desirable to truncate the downstream face of the weir. Where it is truncated the toe of the weir must be drowned, and the hydraulic jump must form up-stream of the truncation.
7. The tail stilling basin must be a minimum of 3.0m in length downstream of any truncation, or of the bottom of the weir slope.
8. The designer must produce the necessary calculations[2] to show that the requirements above are met, and these should be included in the Environmental Impact Assessment that is carried out for the site[3].
9. Where particular design features other than those above need to be included to accommodate fish passage, consultation with the National Fish Passage Panel will be required.

Notes:

[1] explanatory diagrams can be provided if required.

[2] see Herschy, R.W, White, W.R, & Whitehead, E,. 'The Design of Crump Weirs', Technical Memorandum No 8, February 1977, Department of the Environment, Water Data Unit Report, ISBN 0 904871 08 8. Page 43.

[3] via the National or Area Environmental Assessment Staff as appropriate.

Figure 2–18: Recommended construction guidelines for gauging weirs (Armstrong *et al.* 2004)

Draft standard for 'Fishpasses at flow gauging structures'

One of the outcomes of the current research into flow measurement structure design which was aiming to improving fish passage without compromising flow data accuracy is a new draft standard. This standard is currently entitled: 'Draft standard - Fishpasses at flow gauging structures' (White *et al.* 2005a).

This document firstly lists existing British and International Standards relating to flow measurement structure design as normative references. The common elements from these different documents are presented as one summary and provide guidance on site selection, installation conditions, guidance on the approach channel, downstream channel conditions, comments on the gauging structure, fish pass structure, maintenance requirements and the head measurements. Further details are then provided on the basic parameters of the fish pass design. These include guidance on maximum water velocities, location and attraction flows, and downstream entry and upstream exit conditions. Only the super-active Larinier fish pass is dealt with

in the section on fish pass performance, as this is the only fish pass for which the hydrometric testing is considered sufficient. The coefficient of discharge for the rated Larinier fish pass is required to have an uncertainty of (typically) less than 2% at the 95% confidence interval. The intention is that this section would be expanded upon in the future. The computation of discharge for modular and non-modular flow conditions and a section of computation of uncertainty of measurement, with a worked example complete the draft standard.

Guidelines on positioning baffle(s)

As discussed in section 2.3.4, HR Wallingford have considered the effect of the first baffle on the coefficient of discharge from the perspective that the discharge should not be allowed more than a 1% reduction from the existing standard. Their approach has been to consider the position of the first baffle such that the baffle does not interfere with the separation bubble downstream of the crest.

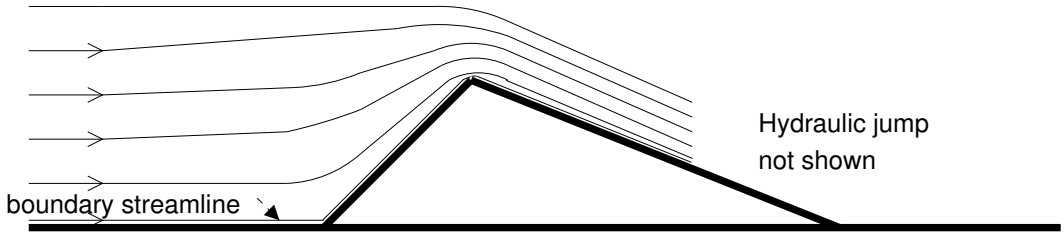

(a) Typical streamlines for an ideal fluid

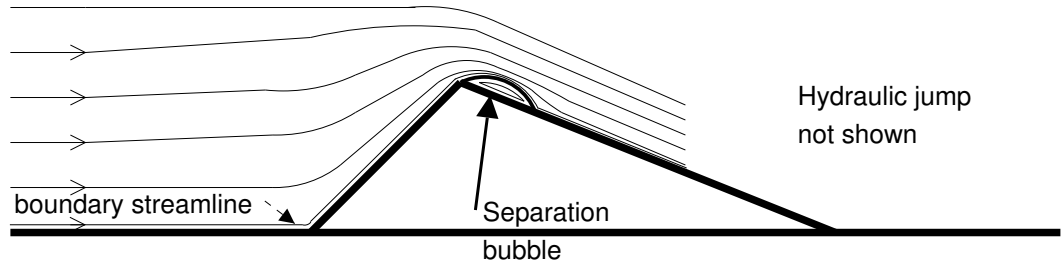

(b) Typical streamlines for a real fluid showing the formation of the separation bubble

Figure 2–19: Theoretical diagrams showing ideal and real streamlines at the crest of the Crump weir

Streamline flow and the development of the separation bubble at the crest of the Crump weir affects the coefficient of discharge. For an ideal fluid, the boundary streamline would follow the surface of the weir, as shown in Figure 2–19(a). In a real fluid with viscosity, the boundary streamline detaches from the weir surface, and the area immediately downstream of the crest experiences substantial energy losses, and this is represented by an area of eddying flow in the boundary layer. The streamline reattaches to the weir surface a short distance downstream of the crest, having created a small self-contained region commonly called the separation bubble or pocket (Figure 2–19(b)). The separation streamline between the separated and unseparated flows effectively acts as a boundary between the two flow regions, and in essence has the effect of redefining the weir geometry. Thus the weir crest has

been effectively relocated at the highest point of the separation bubble. The size of this separation bubble increases with increasing the head on the weir.

The presence of a baffle interferes with the formation of a separation bubble immediately downstream of the weir crest. The baffle effectively distorts the geometry of the separation streamline, and thus causes a deviation of the coefficient of discharge. At a high enough flow, the separation bubble becomes large enough to encompass the baffle (as shown in Figure 2–20).

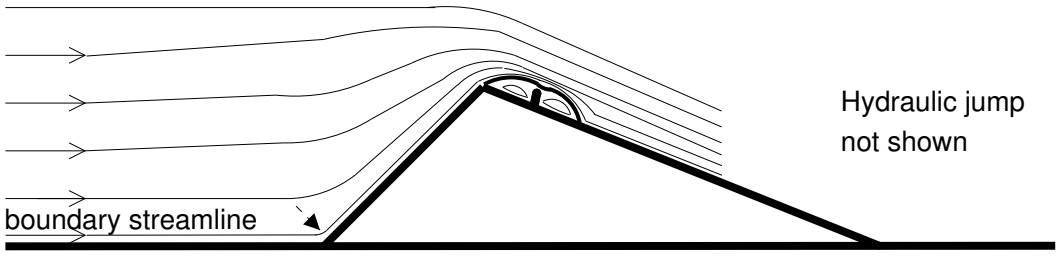

Figure 2–20: Theoretical diagram showing the possible effect of a single baffle on streamlines at the crest of the Crump weir

2.4. Summary

This chapter introduced relevant background information pertaining to the disciplines of fish behaviour and civil engineering hydraulics. Firstly, aspects with regards to fish and fish behaviour were discussed, with emphasis placed on the data available from recent research into fish swimming speeds. This swimming speed data will be used within the context of this thesis as a means of initially assessing the applicability of a multiplicity of fish passages modelled during the research project and subsequently, as input in a method predicting fish pass efficiency for the preferred fish pass. Next, Crump weirs and flow measurement principals were introduced. The concepts of modular and non-modular flow were presented and laboratory modelling requirements were discussed. The literature review was rounded off with an overview of conventional fish passes, fish pass design criteria, recent fish passage research at triangular profile gauging weirs, and existing guidelines relating to Crump weirs.

3. Equipment and Experimental Procedure

For this study into an adaption of the downstream slope of the Crump weir for suitable fish passage conditions, laboratory modelling has been favoured over computational fluid dynamics, because highly unsteady turbulent, free surface flow, over multiple baffles would have

(a) been computationally very time consuming for each geometry and flow rate

(b) not been as convincing as a physical model; doubts about the faithfulness of the model in reproducing the flow phenomena would have persisted.

In order to carry out the trials, the model low-flow section of a compound Crump weir (Brimpton on the River Enborne) was available from a previous project and was re-installed in the testing flume. This chapter describes the experimental approach taken for this project, and has been divided into four sections:

- Model of the Crump weir
- Experimental equipment and calibration procedures
- Experimental methodology: Fish pass modifications
- Experimental methodology: Hydrometric effect

Figure 3–1 provides an overview of the various classes of experiments conducted during this research project. The experiment classes were not necessarily carried out in the order suggested by this diagram, but have been grouped logically in order to ease the presentation of the results.

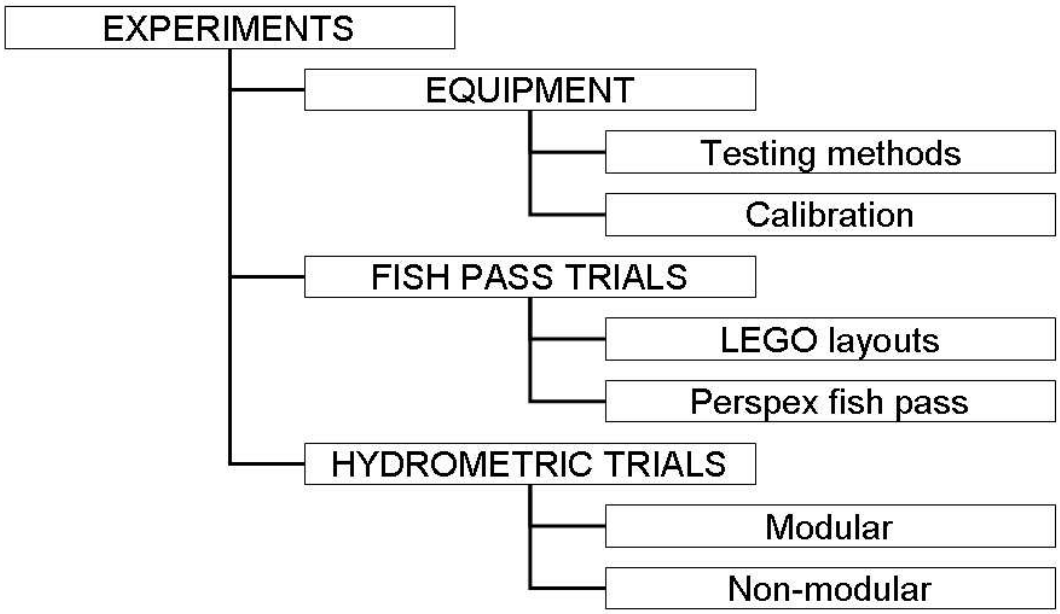

Figure 3–1: Schematic diagram of experiment classes

3.1. Model of the Crump weir

3.1.1. Laboratory modelling vs computational fluid dynamics

Sarker (2000) attempted to numerically model (using commercial software) the free surface flow over a multiple baffle arrangement, modifying the downstream apron of a Crump weir. The computer storage requirements were massive and a fully converged solution was not obtained for the single flow attempted. Thus for the current research project the decision to use laboratory modelling over CFD determined that a far greater number of layouts could be considered in a short period of time. In addition, no time was expended on the calibration of a numerical model.

3.1.2. Development of the physical model

The existing Brimpton weir model fabricated for Sarker (2000) was used as a starting point into the investigation of low-cost modifications to the Crump weir. This model is based on the low-flow section of the compound Crump weir located at Brimpton, on the River Enborne in the Thames catchment. The site was previously identified by Pinniger (1998), and considered by the Environment Agency to be a suitable example on which to continue to base a model (Armstrong 2000). Figures 3–2 and 3–3 show the original construction drawings for the cross-section and low-flow longitudinal section of the Brimpton weir used as a basis for the construction of the model (Sarker 2000).

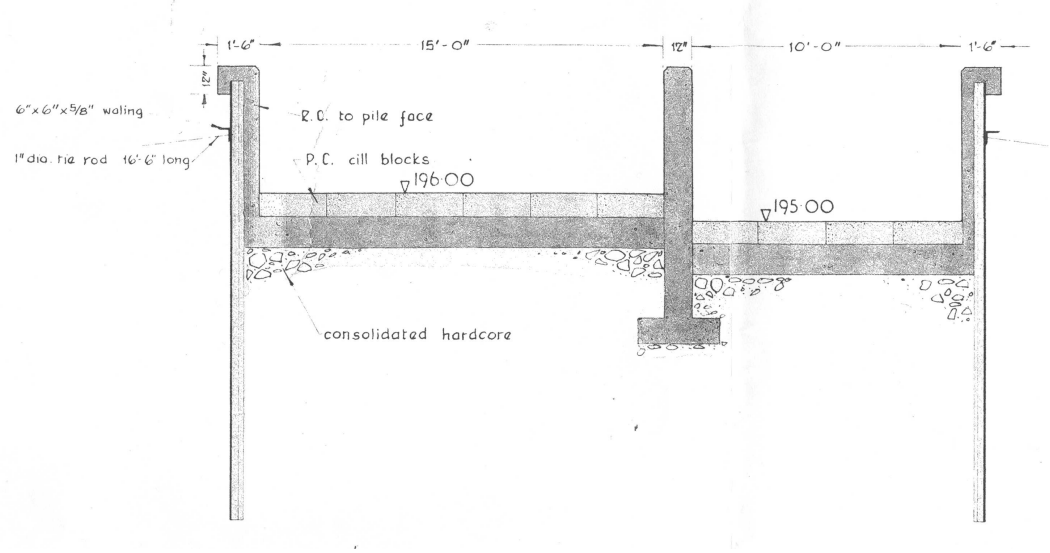

Figure 3–2: Brimpton weir: Cross-section (adapted from the original Environment Agency (1966) construction drawing)

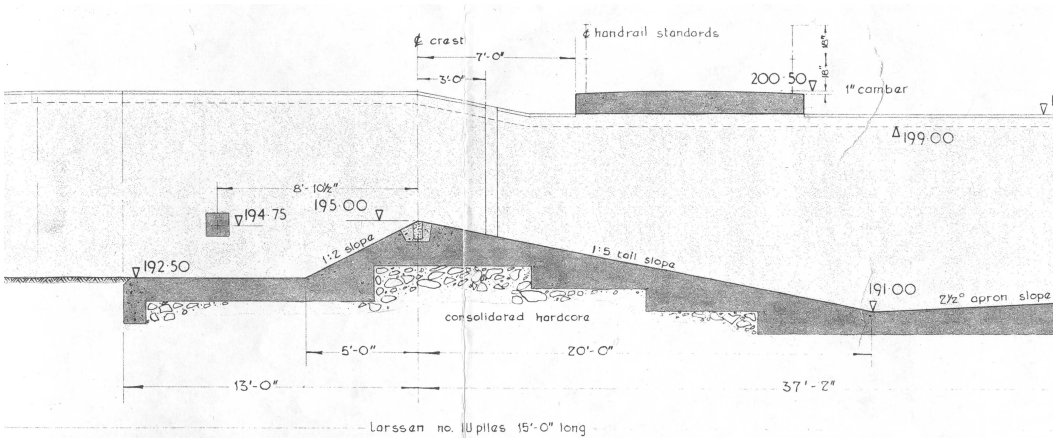

Figure 3–3: Brimpton weir: Low-flow longitudinal section (adapted from the original Environment Agency (1966) construction drawing)

3.1.3. Installation of the model

The Brimpton model was installed in a 0.613 m wide x 0.585 m deep x 8.262 m long flume (Figure 3–4). Water was recirculated through the closed system by a variable speed centrifugal pump, with a nominal capacity of 60 ls^{-1}. The pump discharged into a 150 mm diameter delivery main in which a flow straightener was installed 22 pipe diameters upstream of the orifice plate used for flow measurement. The delivery main discharged via a contraction of rectangular cross-sections into the inlet chamber where it emerged as a free surface flow and then out through a honeycomb flow straightener and into a contracting section. These measures were taken to achieve a fairly uniform cross-sectional velocity distribution.

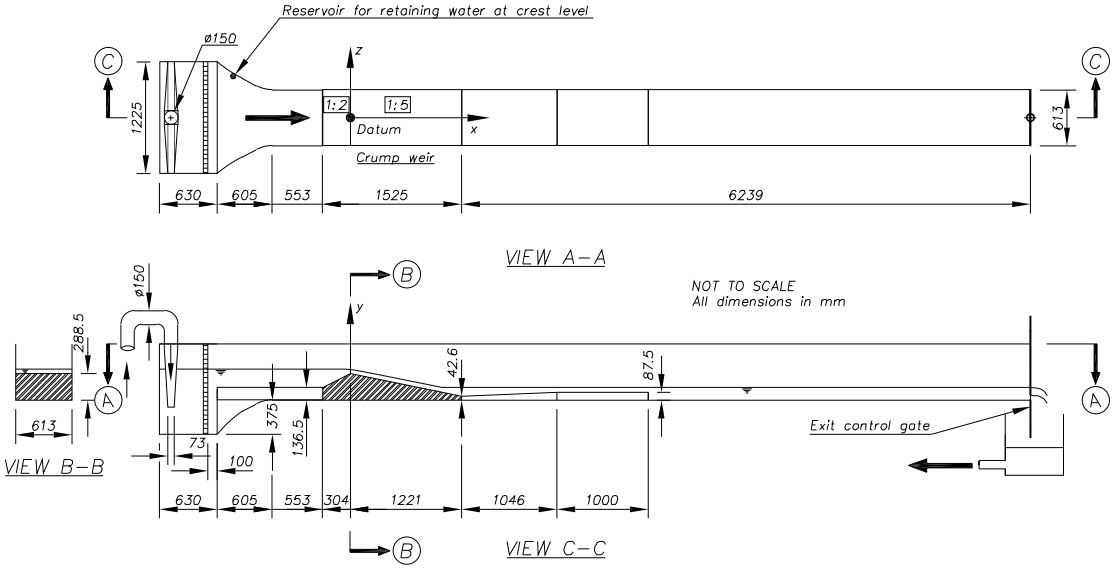

Figure 3–4: Schematic layout of flume

A reference level reservoir for retaining water at weir crest level, was located just downstream of the honeycomb as shown in Figure 3–4. Six static pressure tappings[1] were located in the floor, three each side of the channel axis, at a dimension upstream from the crest corresponding to the well tapping into the stilling well at Brimpton. A similar set of six crest tappings were located in accordance with the British Standard (BS3680 1986) and a further set of six tappings in the floor downstream of the weir, corresponding to the downstream stilling well at Brimpton.

Figure 3–5 shows an annotated photograph of the flume with the delivery main in the foreground, including the positioning of the pump, orifice plate and direction of flow within pipework. The positioning of the traverse gear frame (see section 3.2) above the Crump weir was such that the maximum possible measurement range was utilised. Flow depth was controlled by a full-width adjustable tail gate, which discharged into the sump located upstream of the pump. The tailgate was normally set such that the hydraulic jump occurred well below the downstream end of the Crump, as shown in the photograph.

3.1.4. Dimensional analysis

General similarity theory was introduced in section 2.2.4. The application of similarity concepts, and the decision to use a model based on the Froude number rather than the Reynolds number is discussed with reference to the 1:5 Brimpton scale model:

Froude number similarity Given that the laboratory flume was nominally two

[1]Throughout this report, the term *static pressure tappings* is used interchangeably with *pressure tappings*

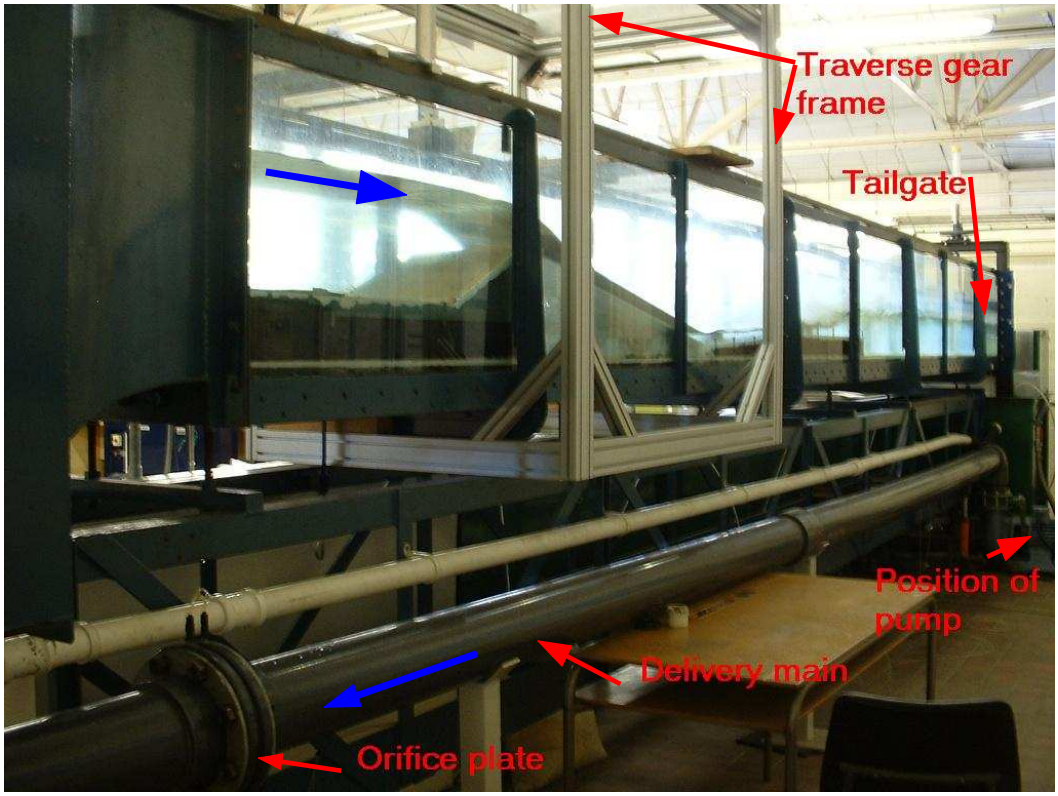

Figure 3–5: Photo of flume from the upstream side of the Crump weir, showing positioning of the traverse gear, pump, delivery main, orifice plate and tailgate.

feet wide and that the low-flow section of the Brimpton weir was ten feet wide, these dimensions were compatible with a practically sized model of the low-flow section at a scale of 1:5 (i.e. $L_m = 1 : L_p = 5$) and this is the scale factor that was adopted for the Brimpton model. Employing identical Froude numbers, the model and prototype velocities were related as shown in Equation 2–4. For the Brimpton weir that gave the following result (Equation 3–1):

$$\frac{v_m}{v_p} \approx 0.4472 \tag{3–1}$$

From the continuity equation ($Q = vA$):

$$\begin{aligned} \frac{Q_m}{Q_p} &= \left(\frac{24.2}{120}\right)\left(\frac{1}{5}\right)^{1.5} \\ &\approx 0.01804 \end{aligned} \tag{3–2}$$

The crest length for the prototype was 120 inches (i.e. 3046 mm) and therefore the crest length of the 1:5 scale should have been 24 inches (i.e. 609.6 mm). However, the actual installed crest length was 24.2 inches (i.e. 614.6 mm) (as has been taken into account in Equation 3–2).

Reynolds number verification One of the limitations of using hydraulic similarity is that it is not possible to achieve Reynolds number and Froude number similarity simultaneously. As viscous forces are usually small and the Reynolds number is generally large for open channel flow, for this type of application models are usually designed using Froude number similarity. Once the velocity distributions associated with the chosen low-cost fish passage had been captured, the Reynolds numbers were assessed at each slot using equation 2–6 (section 2.2.4) which verified this underlying assumption (see section 4.2.4).

Air entrainment

Air entrainment is known to be present at super-critical flows at field scale. For example, a site visit to see the use of baffles on the Hurn weir (Armstrong *et al.* 2002) included a brief discussion on air entrainment present at field scale that was not documented or predicted from the 1:13 scale model study. The effect of air entrainment on the 1:5 Brimpton model is unknown, and this is one of the areas that would need to be addressed in field scale trials.

3.1.5. Flow rate relationships

Available orifice plates and associated flow rate relationships

Four orifice plates with static pressure tappings located at distances D and D/2 upstream and downstream respectively were available for flow measurement. Table 3–1 indicates the diameters and the calculated maximum flow rates (BS1042 1992) for each one, based on the maximum head difference of 4 m which could measured by the manometer. The choice of orifice plate for a specific experiment was dictated by the flow range required. For example, for the lower flow rates, more accurate measurements were achieved using the smaller orifice plates.

Table 3–1: Orifice plate data

Diameter (mm)	Calculated maximum flow rates (ls^{-1})
109.91	60.0
61.95	16.3
37.90	6.0
30.45	3.87

Obtaining the discharge Q in the pipeline required the measurement of the head across the orifice plate and using Equation 3–3 given in BS1042 (1992). (Definitions of the terms used in this equation are given in the Glossary.)

$$Q = CE\left(\frac{\pi}{4}\right)d^2\sqrt{2gp} \tag{3–3}$$

3.1.6. Capturing and recording water levels

An important part of the experimental process included capturing data relating to water levels at strategic points. Both the static pressure tappings and the reservoir used to capture the crest water level (the latter depicted in Figure 3–4) are discussed below.

Pressure tappings: The methods used to measure water levels in the field, as prescribed in the British Standard (BS3680 1986), have been presented in section 2.2.2. The same specifications were applied in the model, but using static pressure tappings instead. The static pressure tappings for the upstream, downstream and crest positions were located in transverse rows of six, three on each side of the channel centreline, as shown schematically in Figure 3–6(a). Each tapping was created by drilling a 2 mm hole through the wood into which were glued short lengths of 11 gauge ($\approx$ 3 mm OD) stainless steel tube, shown in Figure 3–6(b). The tubes were connected to 4 mm OD nylon hoses by means of silicone tubing and Legris pneumatic fittings.

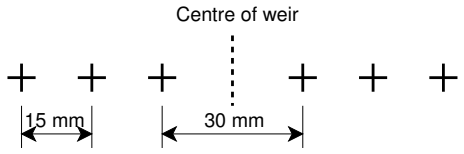

(a) Plan view: Schematic arrangement of the six 2 mm tappings

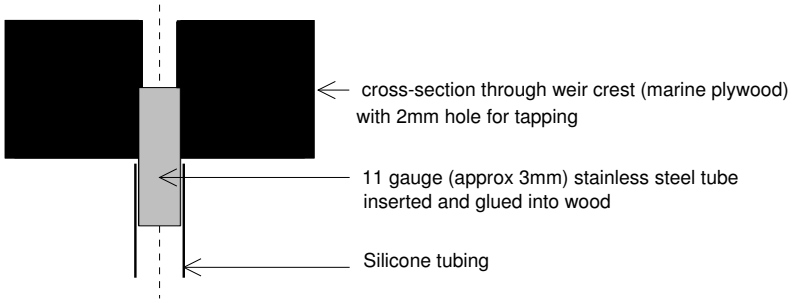

(b) Cross-section: Details of connection arrangements for a single 2 mm tapping

Figure 3–6: Detail of pressure tapping layout at model scale

In measuring the upstream water level relative to the weir crest level at laboratory scale, a high degree of precision was required. For the model, upstream static pressure tappings located in the floor were used rather then the wall tapping and stilling well at field scale. The static pressure tappings were located 540 mm upstream of the crest, one fifth of the dimension at field scale. The crest pressure tappings were located 4 mm downstream of the crest in line with the British Standard (BS3680 1986). The downstream stilling well position was also replaced by downstream static pressure tappings at a distance of 2340 mm from the crest scaled on the Brimpton weir downstream stilling well location.

Figure 3–7 shows the use of Legris tubing connecting the pressure tappings on the underside of the model, upstream of the crest and at the crest. For problem identification, each tube was numbered, and the position recorded. In addition, the upstream static pressure tappings were connected with white tubing, while the crest pressure tappings connected with red tubing. A similar tubing arrangement was made for the downstream static pressure tappings. The tubing was bundled together and conducted over the side of the flume in a manner which least disturbed the flow. Each set of six was connected to a manifold which delivered an average pressure to the transducer, i.e. there were three manifolds connected to the pressure transducer with isolating ball valves. Appendix C.1.1 outlines the process that was followed in order to prime the hoses connected to the pressure tappings.

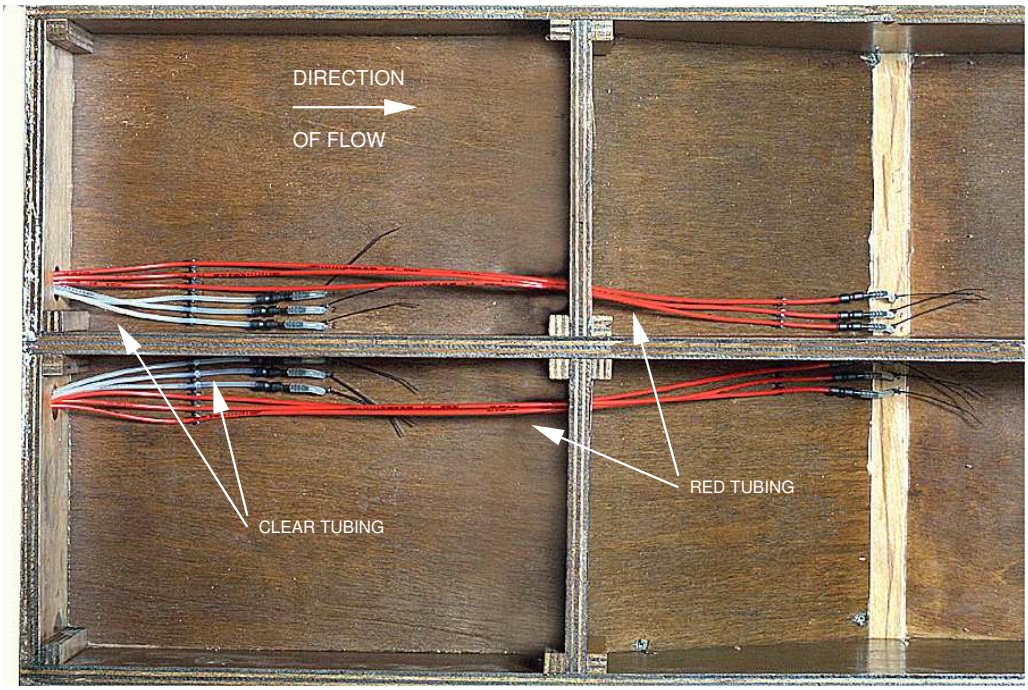

Figure 3–7: Underside of model: crest and upstream pressure tappings

The pressure transducer output a D.C. voltage on a 0-10V scale, which was correlated with the pressure during the calibration process. Where possible, pressure transducer readings were verified by measuring the difference between the static head upstream of the weir and weir crest level, using a pointer gauge with vernier[2].

Reservoir used to record crest water level Identifying and preserving the exact crest level as reference was an important part of obtaining head measurements for modular and non-modular flows. Figure 3–8 illustrates the reservoir which was designed in order to retain a water level identical to that of the crest level.

[2]The use of the pointer gauge with the vernier has been referred to as the 'pointer gauge method' in this text.

The reservoir was connected to the flume water by means of a short length of 6 mm OD nylon line via an isolating ball valve. The method used to eye in the water level is described in Appendix C.1.2. Once the reservoir had been filled to crest level, the ball valve was snapped shut. The reservoir was connected to the low-pressure port of the pressure transducer. Appendix C.1.1 outlines the process used in priming the tubing leading from this reservoir.

The reservoir was originally situated on the centreline of the flume, upstream of the weir and near to the entrance to the contraction. The effect of the reservoir placement on the velocity profile was investigated. The velocity profile across the width of the channel was measured at the position of the upstream static pressure tappings. This was performed twice: with and without the reservoir in place. The largest orifice plate was used and the pump was operated at maximum speed. Since only very small variations in the velocity profile were recorded, it was concluded that the presence of the reservoir did not significantly influence the velocity distribution. After a time, it proved necessary to move the reservoir to the current position on the left-hand side of the flume (as shown in Figure 3–4) as it had been fixed to the wooden floor which lifted. The reservoir was then fixed to the side of the flume so that floor movement would not affect the preserved initial water level.

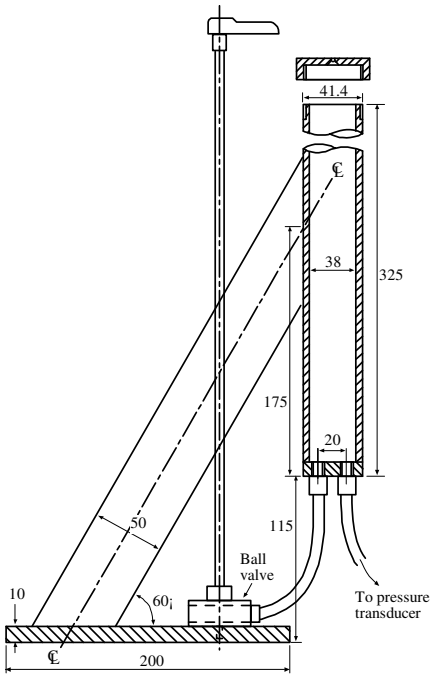

Figure 3–8: Upstream reservoir

3.2. Experimental equipment and calibration procedures

This section provides details of the experimental equipment and the techniques and instrumentation used in data collection. The 3-axis computer controlled traverse

gear system, which provides an accurate method of positioning instrumentation within a three-dimensional space, and the data acquisition techniques (including the instrumentation installed on the traverse gear) are described. The various items of equipment and their associated calibration techniques are introduced.

3.2.1. Traverse gear

The instrument positioning system consists of a 3-axis computer controlled traverse gear (Time and Precision Ltd.) with a resolution of 1/4000 mm in the x, y and z directions.

The software required to drive any instrumentation attached to the traverse gear to a specific location and then collect data was written as a suite of C programs. An example of such a procedure is that of the main batch file and associated program for the traverse gear (f_batTG.bat) which allowed the user to choose to move, with or without logging data at the position. Appendix B provides an overview of the programs written for the project. Many of these programs make use of the functions that drive the traverse gear. Some of them were extended to allow for the automatic traversal of any particular probe, which proved invaluable in allowing for substantial data collection during long experiments (especially those experiments associated with velocity distribution.)

For coordination between data sets from different experiments, a panel pin was inserted at the centre of the weir crest and x_0, y_0 and z_0 reference co-ordinates were located by eyeing-in the centre of the probe under consideration.

A limitation of the traverse gear system, used to drive the instrumentation to required measurement positions, was that it was out of range of the downstream end of the weir. The positioning of the laboratory model coincided with one of the braces for the flume, which prevented the traverse gear framework from being shifted incrementally.

3.2.2. Data acquisition techniques

As described in the manual (Advantech 1994), the 12-bit PCL818HG LabCard, henceforth referred to as the LabCard, is a multifunction data acquisition card with high performance and high gain capabilities. This equipment was originally designed for use in DOS-mode.

Figure 3–9 shows a simple layout of the PCLD-8115 Wiring Terminal Board associated with the LabCard. It has eight channels available for differential analog inputs. The required channel or channels are user-defined. The custom-written C programs prompted the user for input, as well as providing a reminder to make sure that the equipment was connected to the appropriate channel selected according to the required gain[3].

[3]Gain refers to the amplification factor. In standard mode with a gain of one, the LabCard converts an incoming voltage on a 0-10V range. When the input range is significantly different, e.g. on a 0-1V range, there is provision to apply a gain that amplifies the incoming signal so as to exploit the full resolution of the LabCard.

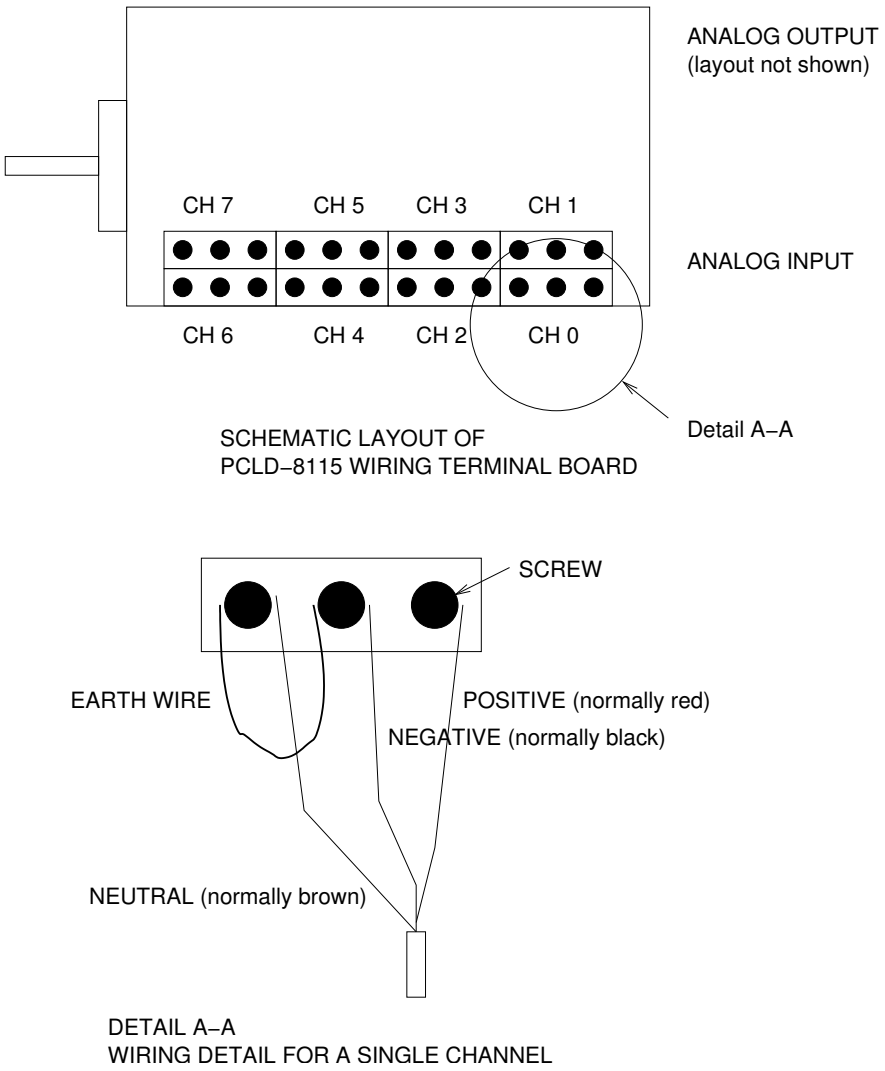

Figure 3–9: Schematic layout of PCLD-8115 wiring terminal board

For this project the LabCard was used to convert an analog input signal to digital format, which is referred to simply as A/D conversion. The driver was a *Terminate and Stay Resident* program that needed to be loaded before the application was started and good practice required the release of the driver after the application was finished.

The software which drove the LabCard was simplified by the use of a parameter table and a number of standard function calls. The program language/compiler used for this project was Borland Turbo C/C++. The standard parameter table for the LabCard had 55 adjustable parameters, and allowed the user to specify the different functionalities. Table 3–2 shows only those parameters which were redefined at different stages within the programs used for this project[4]. Table 3–3 shows the Gain Table used by the program when setting the appropriate gain for the pressure transducer (described next) and wave probe (section 3.2.3). Appendix B

[4]Sample frequency was set at 200 samples per minute for this project. Changes to source code of param[5], param[6] and param[14] are required to change the frequency.

describes the concepts used in designing the suite of C programs which make use of this hardware.

Table 3–2: Table of parameters which can be redefined during program operation

Parameter Type	Specific Number(s)	Application
Start channel	param[15]	Choice of channel
Stop channel	param[16]	Choice of channel
Gain	param[17]	Set the Gain either to a specific value or use the predefined gain table

Table 3–3: Gain table

Channel No.	Gain code	Voltage Range	Applicable Instrument
0	4	0V to 10V	20 mb Pressure Transducer
1	1	-5V to 5V	Wave Probe
2	4	0V to 10V	400 mb Pressure Transducer
3	6	0V to 0.1V	Velocity Propeller Meter

Use and calibration of pressure transducers

Four[5] Druck Ltd LPM 5480 pressure transducers were available, with ranges 0.5 mb, 5 mb, 20 mb and 400 mb. The output of each transducer was 0-10V DC. The transducer sensed differential pressure by means of a low displacement membrane. Movement of this membrane was measured by an eddy current detector, and the 0-10 V DC output was then read by the A/D converter described earlier.

Linear regression analysis was performed on the data collected during the pressure transducer calibration tests and as an example, the relationship between voltage and pressure for the 20 mb transducer is represented graphically in Figure 3–10. Table 3–4 provides the regression equations for all of the available pressure transducers.

Appendix C.1.3 describes the method which was followed when priming a pressure transducer and Appendix C.4 details the pressure transducer calibration procedure followed.

3.2.3. Water depth determination using wave probes

The wave probe monitor was supplied by HR Wallingford, and three small wave probes were fabricated in addition to the larger probe provided with the monitor. Each probe consists of a pair of parallel stainless steel wires, the dimensions of

[5]Although calibrated, and used initially, the 0.5 mb, 5 mb were found to be outside of the range required for most of the experimental work associated with this research project.

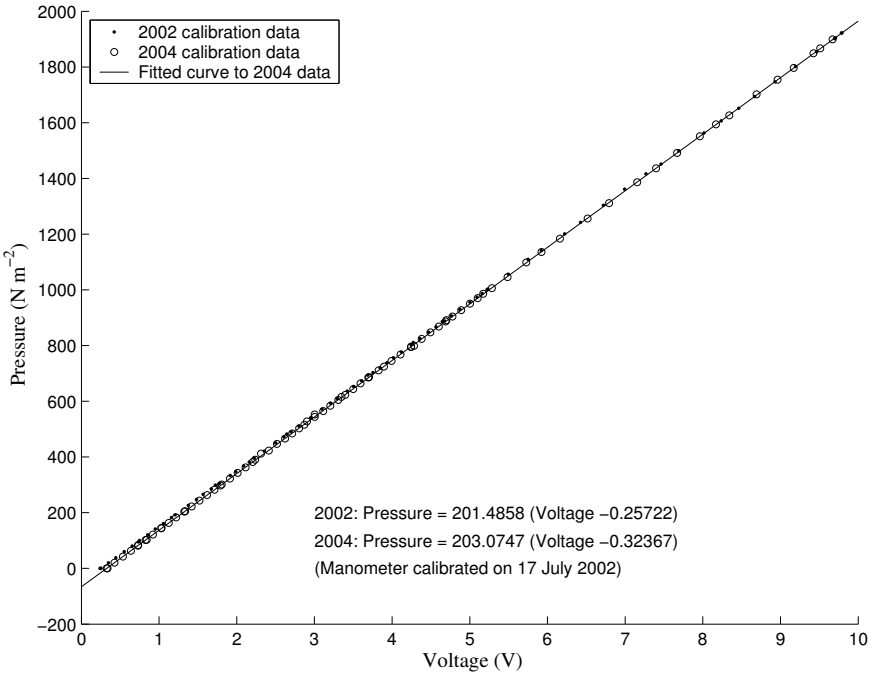

Figure 3–10: 20 mb Pressure transducer

Table 3–4: Relationship between voltage and pressure

Pressure Transducer	Equation
0.5 mb	Pressure $= 5.6285 \times (\text{Voltage} - 0.18078)$
5 mb	Pressure $= 50.4425 \times (\text{Voltage} - 0.25402)$
20 mb	Pressure $= 201.4858 \times (\text{Voltage} - 0.25722)$ (original calibration)
20 mb	Pressure $= 203.0747 \times (\text{Voltage} - 0.32367)$ (re-calibrated 22 April 2004)
400 mb	Pressure $= 4009.2028 \times (\text{Voltage} - 0.20942)$

which are given in Table 3–5. The wave probes replaced the traditional pointer gauge method (section 3.1.6) for measuring free-surface profiles and was used in combination with the 3-axis computer controlled traverse gear.

The wave probes used in testing consisted of a pair of parallel stainless steel wires and operated according to the following principle: As a wave probe was immersed further and further into the water, so the flow of current between the two wires increased proportionally[6]. Thus by measuring the voltage[7] between the two wires, it was possible to determine the depth of the probe and calculate a regression equation for use with a specific test, an example of which is shown in Figure 3–11. Because

[6]This is because a greater volume of water (between the two wires) was available to act as a conductor.

[7]According to Ohm's Law, voltage is directly proportional to current.

Table 3–5: Dimensions of the wave probes

OD ϕ (mm) of tubing	Distance f (mm) between tubes (centre-to-centre)
large probe	14
1.100	2.3
0.895	1.9
0.810	1.8

water temperature and conductivity varies over time, good practice required that the probe be calibrated over the required depth range (HR Wallingford 2002) before and after use on a given day. Appendix C.2 describes the conclusions drawn from initial calibration tests carried out, as well as the calibration procedures and setup requirements when using a wave probe.

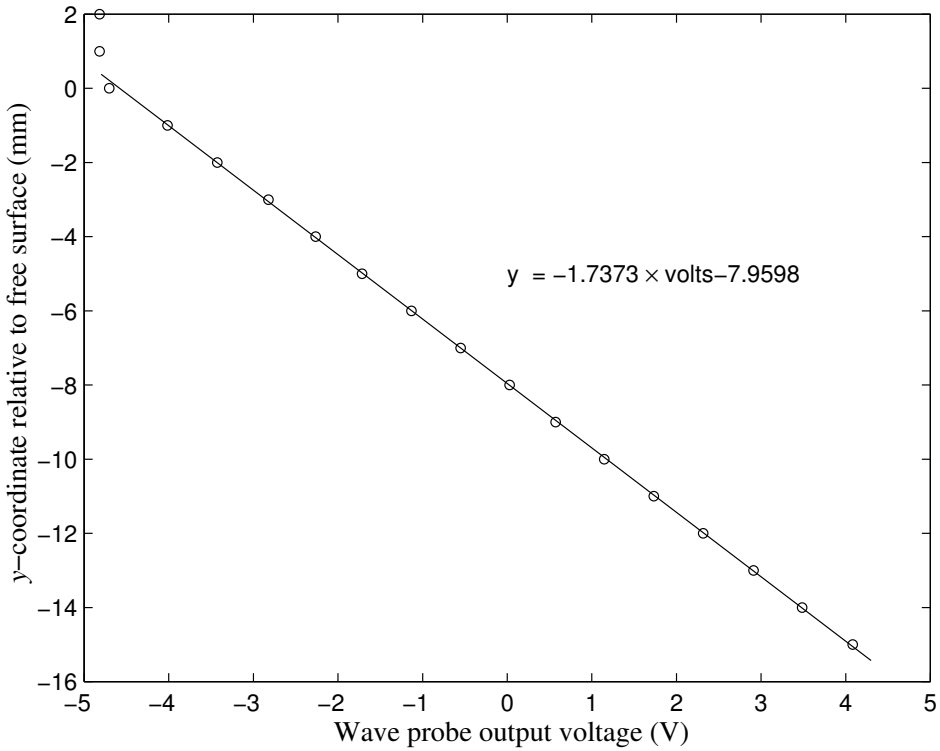

Figure 3–11: Typical wave probe calibration results showing equation from regression analysis

Figure 3–12 shows the fabrication details of the 0.81 mm OD wave probe, which was typical of the design. Each of the probes consisted of two parallel stainless steel tubes which were 270 mm long. At the top end of the wave probe, each tube was electrically connected to a cable with a 4 mm socket. The two tubes, shrink-wrapped for electrical insulation, were encased in a 5 mm OD stainless steel sheath. At the lower end, the pair of tubes protruded by 50 mm. The exposed portion acted as the

sensor which was immersed during measurement. As a precaution against surface tension effects, the minimum distance between the two tubes was set to greater than a single tube diameter, in order to prevent droplets from spanning the gap.

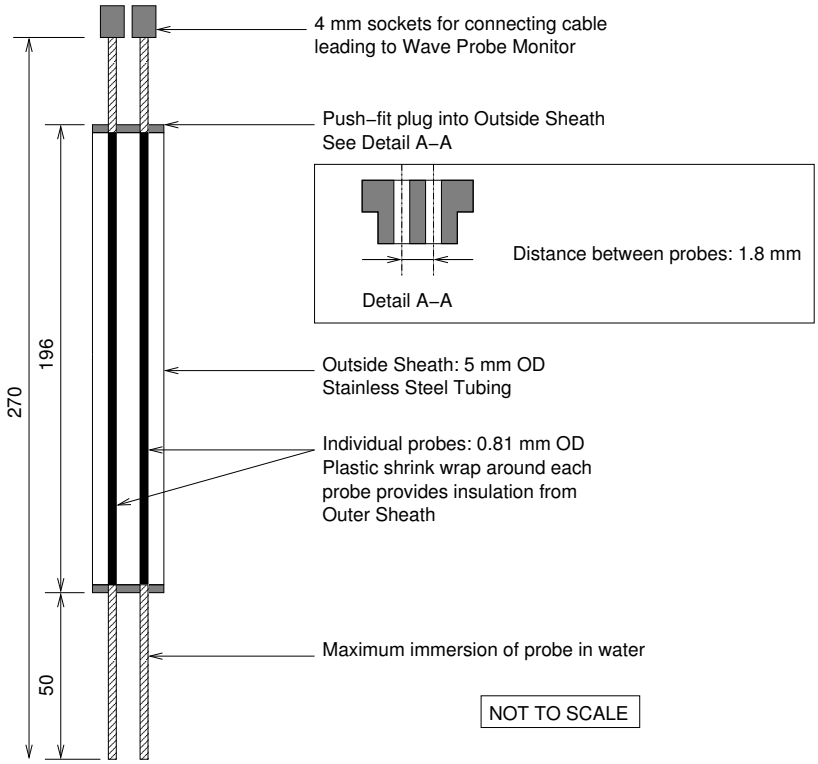

Figure 3–12: General arrangement of wave probe with 0.81 mm OD tubes

The probe provided by HR Wallingford was similar in design but larger. The two parallel stainless steel rods were 192 mm long, with a distance of 14 mm centre-to-centre. It was found during use of the probes that the larger probe was generally more accurate over the whole discharge range, as for the smaller probes higher flow velocities caused an elevation of the free surface that spanned across the smaller probe gap. The photograph in Figure 3–13 shows one of the smaller wave probes and the large wave probe, both compared with a 150 mm stainless steel ruler.

As reported by Servais (2003), the 1.10 mm OD miniaturised wave probe was tested on the unmodified Crump weir where minimal free surface fluctuations provided optimal conditions for comparison with the pointer gauge method. The wave probe and pointer gauge were separately clamped into the traverse gear and driven to successive positions to measure the free surface profile along the centreline of the weir. Measurements were made from 75 mm upstream of the weir crest to 150 mm downstream, and the flow rate was set to 3.77 ls^{-1} corresponding to the 90 percentile low-flow (Q90) at Brimpton weir.

To assess the consistency of the wave probe method, the free surface profile was measured at two depths of immersion for comparison. The depths were chosen so as to register approximately -4 V and -0.25 V respectively on a hand-held voltmeter.

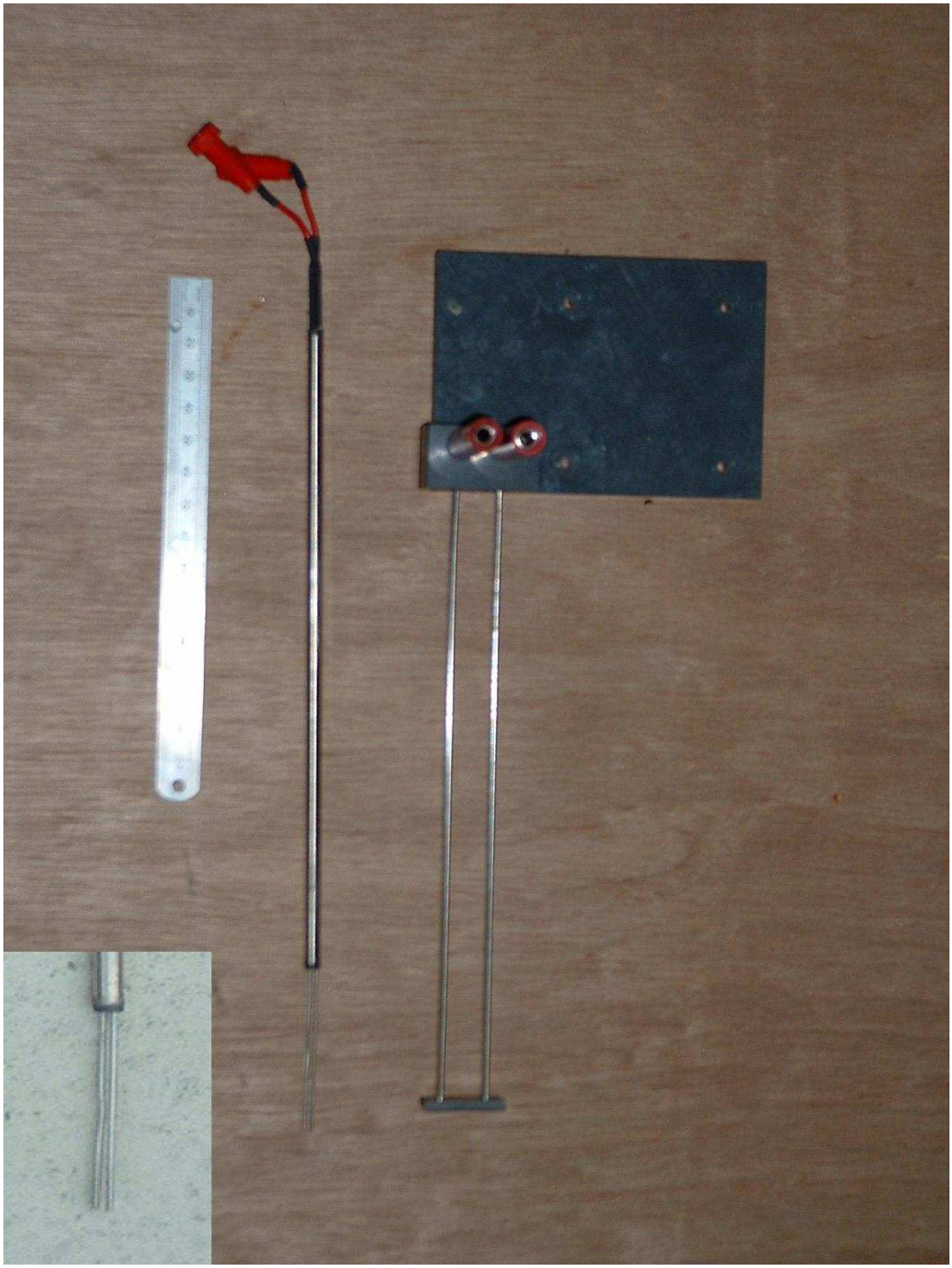

Figure 3–13: Small and large wave probes

Figure 3–14 shows the resulting free surface profile measured using the different techniques.

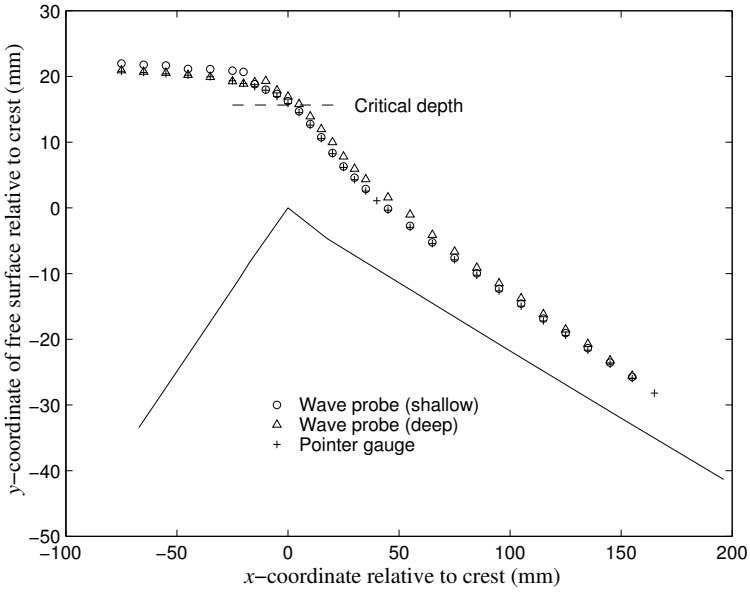

Figure 3–14: Comparison of the free surface profile (using the pointer gauge and 1.10 mmOD wave probe)

The shallow wave probe readings were close to the pointer gauge results throughout the super-critical region, but overestimated the water level in the sub-critical region (maximum difference of $\approx 8\%$). The deep wave probe measurements produced significant shock waves in the super-critical region, and in addition, a small jet of water was driven up between the two wires, causing an elevated ridge of water in the location of the probe. Thus the free surface profile was overestimated in the super-critical region. Good agreement was found between the deep wave probe measurements and the pointer gauge for the sub-critical regions.

Use of the miniature wave probes proved problematic during free surface measurements for the selected fish pass arrangement in which the baffles were constructed with perspex (reported in section 4.2). These problems were linked to the higher flow rates under investigation (corresponding to 50, 30 and 10 percentile low-flows), where the shock wave and elevated ridge of water in the location of the probe were both observed. In order to circumvent this problem, the large wave probe was used and that proved successful. It was found that by setting the wave probe datum at -27.5 mm (i.e. below the water surface), and ensuring that the wave probe was operated within a revised calibration depth range of 0 mm to 50 mm below the water surface, good results were obtained for fluctuating free surfaces. The use of the wave probe was considered to be a more accurate method than the pointer gauge for recording the time-averaged position of a highly unsteady free surface and had the advantage of logging data electronically.

3.2.4. Velocity investigations

Four different methods for velocity measurement were used. Table 3–6 provides an overview of the methods and their application.

Table 3–6: Instrumentation used during Velocity Investigations

Instrumentation	**Application**	**Comment**
Velocity propeller meter (VPM)	Spot measurements	Approximate, for comparison
Pitot tube - static tube (PT-ST) combinations		
1) plane parallel to apron	Velocity distr. above baffles, parallel to crest	More accurate detailed distribution
2) plane perpendicular to apron	Velocity distr. in slots	More accurate detailed distribution
DigImage (PTV)	Velocity distr. in slots	Unsuccessful
Acoustic Doppler velocimetry (ADV)	Velocity distr. in slots	Unsuccessful

Velocity propeller meter (VPM)

The velocity propeller meter, with an internal diameter of 10 mm proved valuable in quickly obtaining spot measurements in the multiplicity of baffle arrangements. One of the inherent advantages exploited by its use was the ability to move the instrument into and out of the water, as opposed to the PT-ST arrangement which had to be kept submerged.

This instrument was calibrated in March 2003 against the Pitot tube - static tube (PT-ST) combination, set parallel to the apron floor and described later, and the voltage output of the VPM was directly proportional to the velocity of the water. The VPM was initially calibrated from a 0.01 - 0.09 V range, which corresponded to 0.2 to 1.9 ms^{-1} (Figure 3–15). Although the VPM was not considered to be as accurate as the PT-ST combinations, it allowed a very quick and effective means of comparison of the spot velocities between one LEGO baffle arrangement and the next. Its use allowed for a greater number of LEGO layouts to be screened than would have been possible using the PT-ST arrangement. In May 2003 it became necessary to recalibrate the instrument after a hair was found to be wrapped around the shaft. At that stage it was not possible in the available time to calibrate the instrument over the same range used previously (Figure 3–15) and the new range (in terms of accuracy) was 0.01 - 0.065 V, which corresponded to 0.2 to 1.2 ms^{-1} (Figure 3–15). As the maximum velocity criterion for fish swimming speeds was shown to be 0.51 ms^{-1} at field scale, this reduction in range was not considered to be significant for the screening process used. The calibration equation was written into the C code so that velocities were also printed to screen, thus allowing for the immediate comparison of velocities during the experimental process.

Pitot tube - static tube (PT-ST) combinations

A 2.05 mm OD Pitot-static tube, specifically fabricated to give a high resolution velocity head measurement in very shallow water depths, had been used by Egonjic (2000). However, Egonjic reported that the small diameter and correspondingly

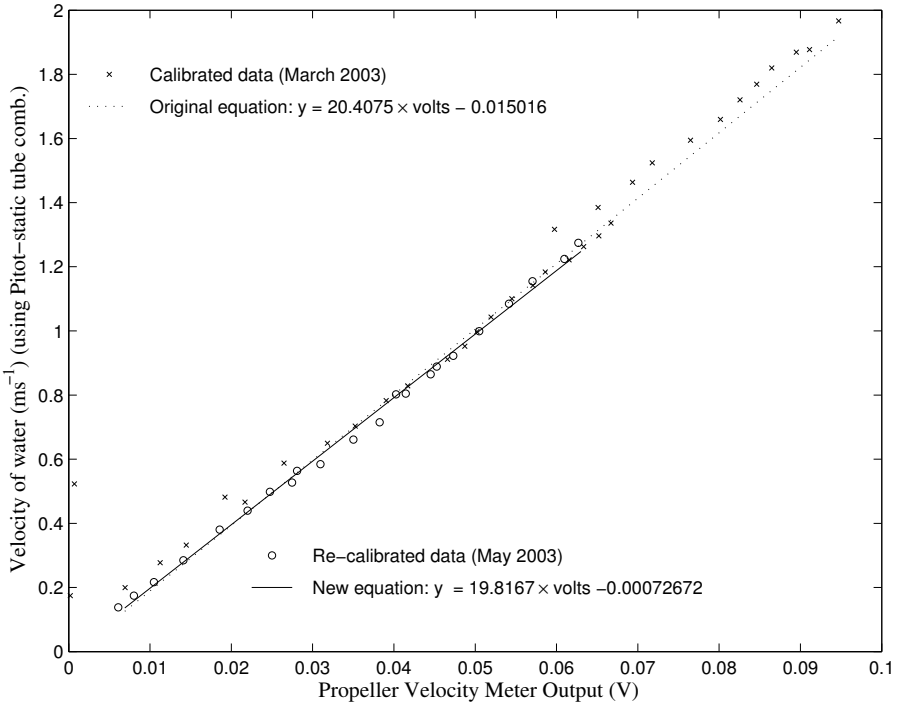

Figure 3–15: Velocity Propeller Meter calibration curve

small orifices and conduits in the Pitot-static tube had resulted in unacceptably long delay periods required for the probe/pressure transducer combinations to reach equilibrium after a change of differential pressure. The problem had been solved at the same scale (as the 2.05 mm OD Pitot-static tube) by using separate parallel Pitot tube - static tube probes with a lateral displacement of 25 mm (Egonjic 2000). This combination, referred to as the PT-ST combination, was used in the present project.

The PT-ST combination had been devised in-house during Egonjic's experimental phase and consisted of two parallel tubes, each with an outside diameter of 2.05 mm. The tubes were mounted in parallel such that the stagnation point of the Pitot tube was in line with the static pressure tappings as shown in Figure 3–16. This combination, setup with the tubes parallel to the apron slope, was used for measuring 2-d flows invariant across the width of the weir (i.e. in the z-direction).

Figure 3–17(a) illustrates the practical implications of using the PT-ST arrangement parallel to the apron floor. The velocity distribution shown by way of example in Figure 3–17(b) was therefore incomplete. As it was not possible to measure the velocity head in both corners using a single setup, repetition of the experiment with the Pitot tube and static tube switched around was required. An inherent disadvantage to such a solution was that it was a time-consuming process to reset the experiment, with a long lead time needed for re-priming of the pressure transducer and moving the (primed) PT-ST probes to the exact position required.

As an alternative, a PT-ST arrangement was configured for use within a plane normal to the apron floor. On a practical note this resulted in the static tube being fixed above the Pitot tube, 12.5 mm centre-to-centre, (as in Figure 3–18(a)) so that

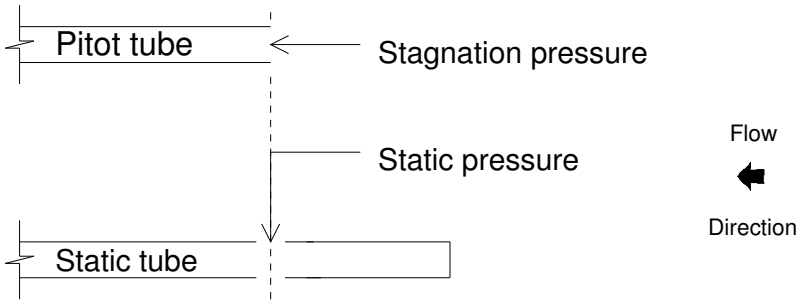

Figure 3–16: Alignment of the tips of the Pitot tube and the static tube in the Pitot tube - static tube combinations (not to scale)

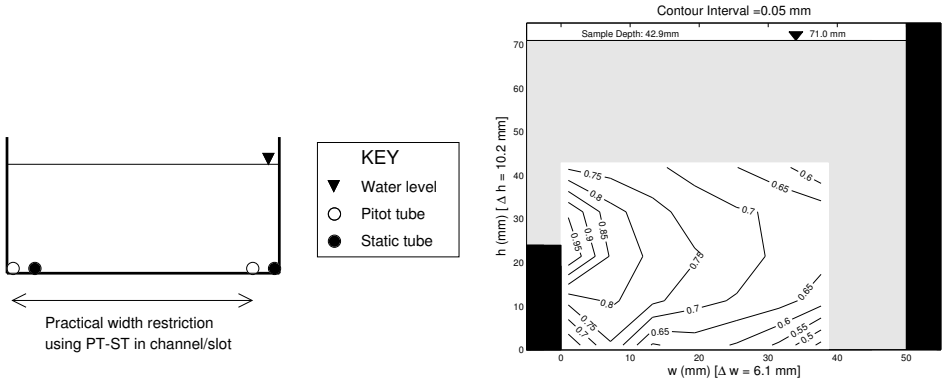

(a) Position of a parallel PT-ST arrangement within a slot

(b) Velocity distribution for a PT-ST parallel to apron slope

Figure 3–17: Application of the PT-ST combination parallel to apron slope

the whole width of a slot could be measured without switching the probes around. Figure 3–18(b) shows the resulting velocity distribution for the same conditions as used in Figure 3–17(b). Although the contours do not match up exactly (as a result of the different orientations of the Pitot tube to static tube), the velocity distribution plots are considered to be acceptable for the purpose of comparing water velocities to fish swimming speeds as used in section 4.2.4.

DigImage (particle tracking velocimetry)

DigImage[8] is an image processing package using particle tracking which was available from a previous project (Egonjic 2000). It was originally envisaged (Rhodes 2001, 2002) that it would be possible to use it for the detailed analysis of flows for the preferred fish passage arrangement.

The preferred fish pass was fabricated out of perspex (described in section 3.3), and the necessary equipment was setup and used to record video images to be used in the

[8]As a method for analysing fluid flows, DigImage was developed by DAMTEC Technologies at the Department of Applied Mathematics and Theoretical Physics, Cambridge University (Egonjic 2000).

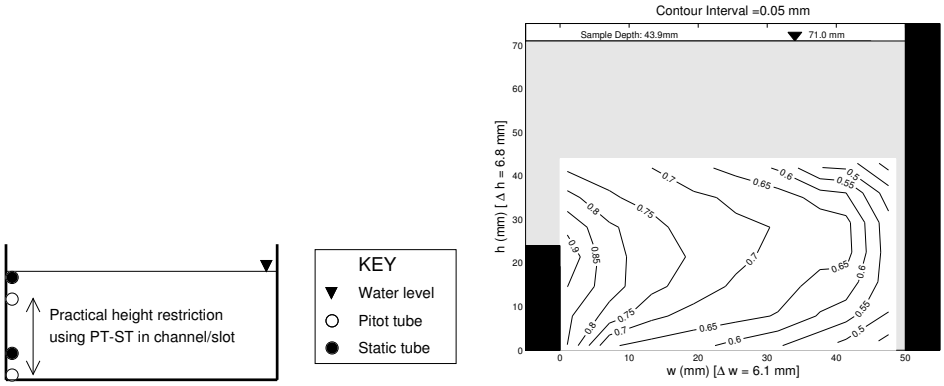

(a) Position of a PT-ST arrangement, positioned in the vertical plane, within a slot

(b) Velocity distribution for a PT-ST, positioned in the vertical plane, within a slot

Figure 3–18: Application of a PT-ST arrangement, positioned in the vertical plane, within a slot

anticipated flow analysis. However, it was found that the velocities within the slots of the fish pass were too high for successful tracking of the particles between four successive frames, as required for a successful analysis. In addition, flow between the slots was highly three dimensional, which also contributed to the difficulties experienced obtaining a viable data set. Consequently, the analysis part of the image processing package was not useable and particle tracking velocimetry using DigImage was eventually abandoned in favour of the simpler Pitot tube - static tube combination described above.

As the use of DigImage in this research project was not successful, the background concepts, relevant image processing theory, computer modelling techniques and physical experimental setup requirements have not been further described within this report. However, although DigImage was consequently not used for the intended velocity measurements, the video footage was useful for flow visualisation purposes. Footage taken of both the plan view and cross-sectional view of the preferred fish passage as constructed in perspex has been described in section 4.2.3. In addition, this footage has been attached to this thesis as part of the full laboratory record, and Appendix F includes a description of the recorded time periods and associated experiments.

Acoustic Doppler velocimetry (ADV)

Towards the end of the project, the opportunity arose to borrow an acoustic-Doppler instrument on a trial basis from OSIL Ltd. The intention was to try and use the instrument to obtain velocity distribution data in between the baffles of the preferred baffle arrangement which had been constructed out of perspex at that stage. The footage intended for the DigImage analysis, used in a flow visualisation exercise described in section 4.2.3, demonstrated that flow in the regions between the baffles was turbulent and exhibited eddying flow structures. Consequently the VPM and PT-ST arrangement were not suitable for use in these regions.

A standard 3D 16 Hz MicroADV instrument (see Figure 3–19 below) was trialled on the downstream slope of the weir, with the preferred perspex fish pass baffle arrangement (see section 4.2) in place.

Figure 3–19: Sontek 16 MHz MicroADV

The downward-looking 3-dimensional microADV required a theoretical minimum water depth of $\approx$ 50 mm in which to operate (Williams *et al.* 2005). After setting up the equipment it was found that the maximum flow depth that could be measured was insufficient for meaningful data sampling. With the maximum flow rate through the flume (similar to that shown in Figure 4–41) and higher than the 10 percentile low-flow, the depth of flow on the downstream slope was approximately 100 mm, which allowed velocity measurements no further than approximately 5 mm from the bed. In addition, air entrainment was aggravated by the probe, which in turn caused the transmitter/receiver heads to be submerged. As the depth of the slot was 40 mm, it was decided not to pursue the investigation.

3.3. Experimental methodology: Fish pass modifications

The investigations into the fish pass modifications has been divided into two main categories. Firstly, LEGO was used to model a number of potential layouts and then secondly, a preferred layout was fabricated out of perspex (allowing for two different heights of the baffle closest to the crest). Figure 3–20 shows a diagrammatic overview of the fish pass modification experiments. The experiment methodologies are further discussed in the text below.

A multiplicity of baffle arrangements was tested using LEGO bricks to quickly fabricate the different geometries. The baffle arrangements were assessed using the criteria of water depth (a quick visual reference) and spot measurements of velocity

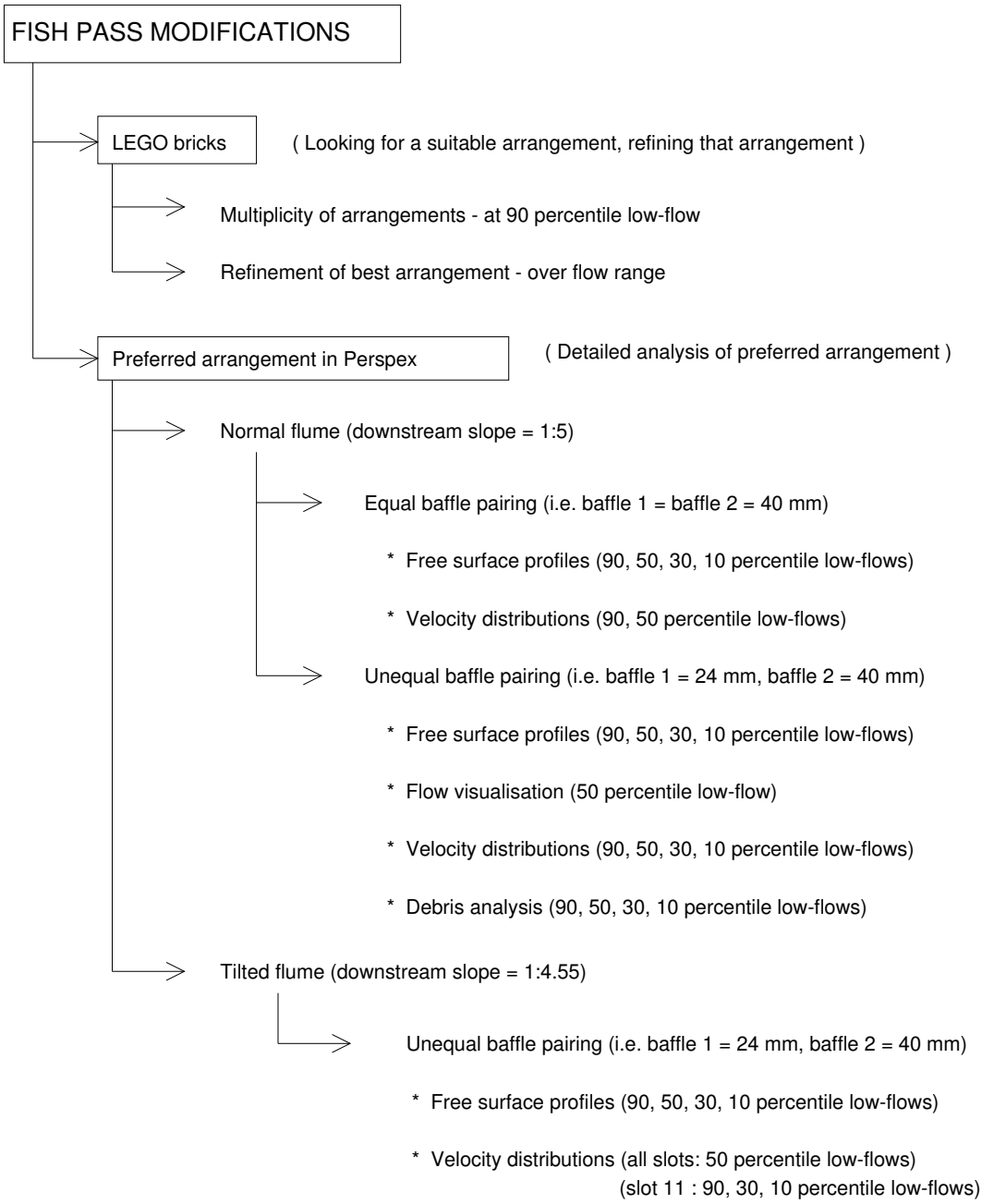

Figure 3–20: Diagrammatic overview of the fish pass modification experiments

in the baffle slots. For the critical assessment, the flow rate was set to the equivalent of the 90 percentile low-flow at Brimpton (Q90), given by the Environment Agency as the lower threshold above which the weir should allow fish passage. The next step was to refine the chosen arrangement over a large flow range. The experimental procedure used for both stages is described in section 3.3.1.

The most favourable solution developed using LEGO was then fabricated in perspex. Detailed investigations at 90, 50, 30 and 10 percentile low-flows were carried out including velocity distributions in the slots, free surface profiles along the anticipated fish pathways, stage-discharge analysis and the effect of debris on the baffles.

In addition the flume was tilted in order to investigate the effect of a non-standard slope, steeper than 1:5, on the apron of the triangular profile weir, and the measurements of velocity distribution and free surface profile were compared with the unmodified Crump weir. However, the maximum slope available in the flume[9] had a minimal effect on the slope of the apron, increasing it to only 1:4.55, and therefore the measurements differed little from those on the unmodified Crump weir. The experimental procedure is described in section 3.3.2.

Both the LEGO and the perspex velocity results were compared to the burst speed swimming data available from the Swimit Excel spreadsheets (Environment Agency 2001b, 2003). However as the data was not used in the same way, the techniques employed have been described in section 3.3.1 and section 3.3.2 respectively.

3.3.1. Testing baffle arrangements using LEGO

The trial of many baffle arrangements was facilitated by constructing the baffles from LEGO bricks in units of two, three or four bricks high (see Table 3–7). Table 3–7 presents data from typical LEGO bricks and the associated parameters:

Table 3–7: Appropriate LEGO dimensions

Description	**Dimension** (mm)
Base plate	
Thickness of base	1.1
Snap-to-fit coupling / protrusion	1.9
Baffle: two layers of bricks	
Height (including 1.9 mm protrusion)	20.2
Breadth	15.8
Width	613
Baffle: three layers of bricks	
Height (including 1.9 mm protrusion)	30.6
Breadth	15.8
Width	613
Baffle: four layers of bricks	
Height (including 1.9 mm protrusion)	40.4
Breadth	15.8
Width	613

[9]The maximum slope was constrained by the physical arrangements of the flume. Two hydraulic jacks positioned at the end of the flume to provide the greatest moment, were used to change the angle of the flume. These were set to their minimum height. Additional considerations included the rotational strain placed on the flume which was not intended in its original design.

The following method describes the general setup and equipment used during the LEGO investigations (both for the 90 percentile low-flow screening process and for the wider flow range tests for the layout chosen for refinement):

- The LEGO bricks were installed on the downstream slope of the weir. Each LEGO layout was recorded and is presented for record purposes in Appendix D.
- The Velocity Propeller Meter (VPM) (section 3.2.4) was clamped into the 3-axis traverse gear and the base of the VPM was 'eyed-in' to the panel pin located at the centre of the crest. This provided a practical means of locating the coordinate (0,0,0) which was used as a constant origin for all of the experiments.
- For the 90 percentile low-flow the 61.95 mm orifice plate was used. The 109.91 mm orifice plate was used for the 50, 30 and 10 percentile low-flows.
- Velocities were recorded using the VPM at key points on the fish pathway. Generally, measurements were taken in the centre of the slots or where the velocity was at a maximum for that key point. Key points were any points considered to be of importance, either in terms of velocity, or in terms of position and were used in the screening process between the various LEGO layouts. Experimentation showed that maximum velocities in the baffle slots were likely to occur just above the apron floor. In some cases, additional measurements were taken between baffles in regions of lower velocity.

Presentation methods used for velocity comparisons and fish passage potential

The spot velocities measured are presented in a diagram showing the cross-section of the model weir, and accompany the record of each unique layout in Appendix D.

Model water velocities were adjusted to field scale and then compared with fish swimming speeds. The Swimit program (Environment Agency 2001b) showed that, for the five species[10] under investigation, at 10 °C for fish 10 cm in size and larger, the burst swimming speed was roughly ≥ 1.1 ms^{-1} at field scale (i.e. 0.51 ms^{-1} at model scale).

A reasonable estimate of the fish swimming distance (D) achievable at burst speed is the difference between the burst speed(V) and the water velocity (U) multiplied by a time period of 20 s (Larinier 2002), giving: $D = (V - U)T$.

Assuming a swimming path of 6.1 m, corresponding to the length of the downstream apron of Brimpton weir, a table of likely successful/failed ascents was compiled. These tables have not been included in this report as plotting the maximum velocity criterion of 0.51 ms^{-1} on each velocity distribution has allowed the success/failure of a particular layout to be visually assessed instead (Appendix D).

[10]At the time of these trials the results from Phase 2 (Environment Agency 2003) were not available.

3.3.2. Perspex fish pass experiments

Figure 3–21 shows the perspex fish pass model which was based on the preferred LEGO solution. As the effect of the first baffle would need to be investigated more fully, the installation of the perspex fish pass was initially designed to be flexible around the size and placement of the first baffle. Table 3–8 shows the model scale and corresponding field scale parameters required for the two scenarios which were tested. Two perspex spacer sections were constructed for placement between the crest and the first baffle. The rest of the pass was fabricated out of perspex, with clear perspex baffles fixed on a 10.5 mm black perspex base. A machined brass section (not shown) was manufactured and laid on the existing crest, increasing the crest height in line with the perspex base.

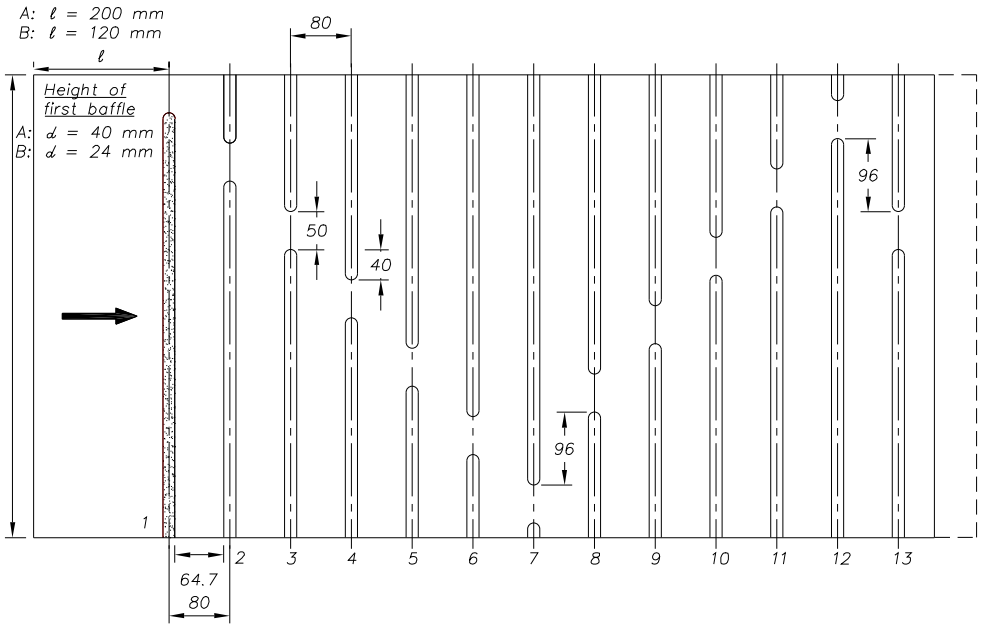

Figure 3–21: Perspex layout showing dimensions for both the equal and unequal baffle pairing (not to scale)

Table 3–8: Perspex baffle experiments: First baffle parameters

Layout Description	**Model scale**		**Field scale**	
	Baffle height (d)	Distance (l)	Baffle height (d)	Distance (l)
A. Equal baffle pairing	40	200	200	1000
B. Unequal baffle pairing	24	120	120	600

Two wooden baffles of identical width to the perspex baffles were fabricated such that the first baffle height could be changed between experiments. Both of these baffles were designed to have a baffle height (d) over distance of baffle from crest to centre (l) ratio of (d/l =) 0.2. In both cases, these parameters caused the first and second baffles to be level with the crest. Scenario A is used to describe the first

case, equal baffle pairing, where the first baffle was equal in height to the second baffle. Scenario B, unequal baffle pairing, refers to the second case, where the first baffle was smaller than the second baffle (see Table 3–8).

The practical implications of having different first baffle sizes was that the first baffle was positioned further down the slope for the equal baffle pairing, than for the unequal baffle pairing. The total number of baffles tested on the downstream slope was thus 13 for each scenario. Baffles are numbered from the crest down to the apron, thus Baffle 1 is closest to the crest and Baffle 13 is furthermost from the crest. This convention has been decided upon so that when baffles are added or subtracted to the downstream apron, the relative position of Baffle 1 remains constant.

The majority of the baffles were constructed out of perspex.

The following method describes the general setup for the free surface profile investigations:

- Either the equal baffle pairing or the unequal baffle pairing perspex fish passage arrangement was installed in the flume.
- The wave probe instrumentation was clamped in place, normal to the apron slope, and 'eyed-in' at the origin using the traverse gear equipment. This procedure was preferably carried out in a dry flume to prevent error-of-parallax problems. The tailgate was then raised and the flume filled with water in preparation for priming the pressure transducers. The wave probe was then moved to a position above the water level surface in preparation for calibration procedures. As the wave probe could not be driven to a depth greater than the calibration depth[11] used for these experiments (50 mm), specific care and attention to the order of events needed to be taken.
- The 400 mb pressure transducer was set up across the orifice plate. The relevant setup procedures (described in Appendix C) were completed. After priming, the pressure transducer was left to warm up for an hour which was found by experimentation to be a reasonable time period for the pressure transducer to reach equilibrium (as well as give any air trapped under the weir time to be displaced and the water surface to settle in preparation for attaining crest level). Datum sampling then commenced at zero differential pressure.
- The water was circulated through the flume with the tailgate raised, before being allowed to settle before calibration of the wave probe commenced, as described in Appendix C.2.
- The tailgate was lowered and the water level dropped before the wave probe was then driven back to the point of origin.

[11]Experimentation showed that when the wave probe was submerged deeper than the depth for which it was specifically calibrated on a particular occasion, a datum-shift was observed.

- The C-program used during the free surface flow experiments was started, so that the position of the origin was captured. The wave probe was then moved to a position sufficiently out of the way before the pump was switched on to achieve the required flow rate.
- Atmospheric temperature and water temperature were taken at the start and end of an experiment and on an hourly basis.
- The flow rate was captured at the beginning and at the end of the free surface flow experiment.
- The free surface flow experiment required the user to drive the probe to each desired point of measurement. The results, which were in the form of voltages correlating to the depth of the wave probe, were logged to an output file.

The following method describes the general setup for the velocity distribution investigations:

- Either the equal baffle pairing or the unequal baffle pairing perspex fish passage arrangement was installed in the flume.
- The appropriate Pitot tube - static tube (PT-ST) arrangement, positioned in the vertical plane (see Figure 3–18) was clamped in place, normal to the apron slope, and 'eyed-in' at the origin using the traverse gear equipment. This procedure was preferably carried out in a dry flume to prevent error-of-parallax problems. The tailgate was then raised and the flume filled with water in preparation for priming the pressure transducers.
- The 400 mb pressure transducer was set-up across the orifice plate, and 20 mb transducer was connected to the PT-ST in place. Priming procedures (and other relevant laboratory procedures as described in Appendix C) were completed. After priming, the pressure transducers were left to warm up for an hour which was found by experimentation to be a reasonable time period for both of the pressure transducers time to reach equilibrium (as well as give any air trapped under the weir time to be displaced and the water surface to settle in preparation for attaining crest level). Datum sampling then commenced at zero differential pressure.
- The required flow rate was set running before lowering the tailgate, thereby ensuring that the PT-ST remained under water at all times.
- The C-programs used during the velocity distribution experiments had been semi-automated. This allowed the user to drive the PT-ST instrumentation to the required pre-determined starting position in the centre of a slot whilst ensuring that the ends of the tubes remained submersed at all times. Once at the correct position, the user started the automated sampling process within the slot. Controlled by the program, the PT-ST was driven to each sample point, where a pause time of 60 seconds (determined experimentally as adequate for equilibrium to have been reached) was implemented before a 60

second sampling time-period commenced. Samples were taken in a grid-like fashion (see Figure 3–25(a)) at user-defined intervals. As it was important to ensure that the PT-ST tubes remained under water, the sample depth was chosen so that a water depth of at least 20 - 25 mm was maintained above the highest point of the probe. Because the depth of the majority of the baffles was 40 mm this implied that for some flow rates it was not possible to obtain a velocity distribution throughout the slot depths.

- Atmospheric temperature and water temperature were taken at the start and end of an experiment and on an hourly basis.

Choice of flow regimes

The following four hydrologically significant flow rates were considered to be significant with regards to fish passage at Brimpton weir (Armstrong 2002a, 2003a):

Q90 The 90 percentile low-flow was considered to be the worst case.

Q50 and Q30 It was considered important to provide for fish passage during the periods of April to July (see Table 2–10), which are typically represented by the Q50 and Q30 percentile low-flow scenarios. Q30 is considered to be representative of the Spring flows.

Q10 For a significantly wet summer, the 10 percentile low-flow was included.

Although Brimpton weir is a compound weir, only the low-flow crest was installed in the laboratory. In the field the higher flows would be carried by the whole compound weir, while lower flows would be carried by the low-flow weir alone. It was therefore necessary to determine the corresponding head required to represent the compound weir and calculate a laboratory flow rate which would represent each of the four flow rates considered to be significant. In Figure 3–22, the Brimpton compound weir stage-discharge curve and that of the low-flow weir alone have been plotted at model scale, with the 10, 30, 50 and 90-percentile low-flows indicated at the same stage on each curve. The required model flow rates were taken from the low-flow curve and applied in the laboratory test programme.

Column 2 in Table 3–9 presents field scale flow data for Brimpton weir. The corresponding model scale flow rates have been adjusted according to the head over the weir for a single crest. These are depicted graphically in Figure 3–22 and listed in Column 3 (of the table). In order to generalise the results, this data has been re-calculated as a 'flow rate per unit width' value at field scale (Column 4). Although throughout this thesis the results have been analysed with specific reference to Brimpton weir and the 90, 50, 30 and 10 percentile low-flows, for general application to other weirs, this flow rate per unit width is of more relevance and interest.

Brimpton weir flow-duration data for April to June as depicted in Figure 3–23 was adapted from the mean monthly flow and mean daily flow records (1968 - 1990/1991

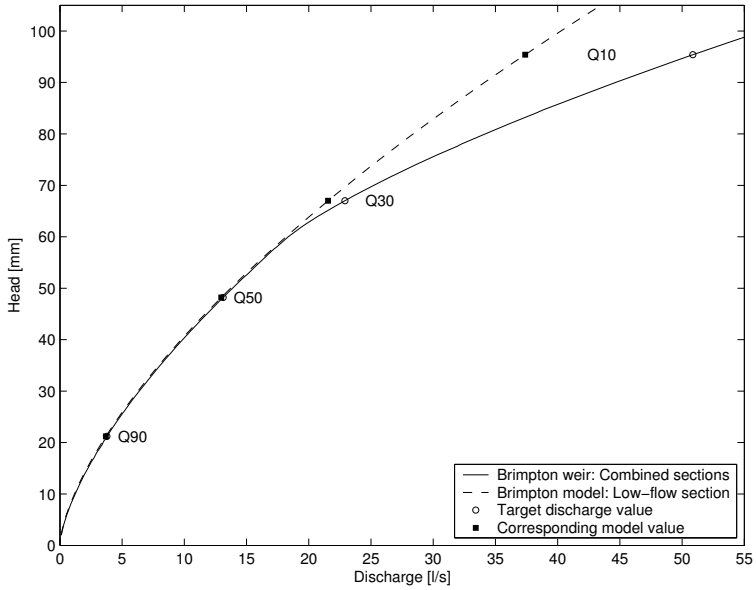

Figure 3–22: Brimpton model: Stage-discharge curve (at model scale)

Table 3–9: Brimpton data: Significant Brimpton field flow rates, adjusted corresponding flow rates for the low-flow model and generalised flow rates per unit width

Percentile low flow	Brimpton weir		General field application
	Field (m^3s^{-1})	Model (ls^{-1})	Flow rate/ unit width ($m^3s^{-1}/m = m^2s^{-1}$)
Q90	0.209	3.77	0.067
Q50	0.727	13.11	0.236
Q30	1.27	21.55	0.392
Q10	2.82	37.39	0.680

and 1991/1992 to 2002 respectively) (Rhodes and Servais 2006). These months were chosen as they fall within the March to June operational period suggested by the Environment Agency for when a fish pass would typically need to be operative (Armstrong *et al.* 2004). The yearly percentile low-flow data is also plotted on this figure. The fish pass arrangements have been tested over a flow range from 90 to 10 percentile low-flow, which covers 80% of the time for the yearly flow data. This is comparable to the April to June data where the 92.1 to 7.5 percentile values cover 84.6% of the time (Rhodes and Servais 2006). The flow-duration data for Brimpton weir was provided by the Environment Agency hydrology section (2002).

Temperature data

As the fish swimming speeds are linked to water temperature, the site specific water temperature needed to be taken into account. As temperature records for Brimpton weir were unavailable, the Fisheries Advisory Officer for England and Wales recommended and provided the Lower River Kennet data set (Figure 3–24) as being

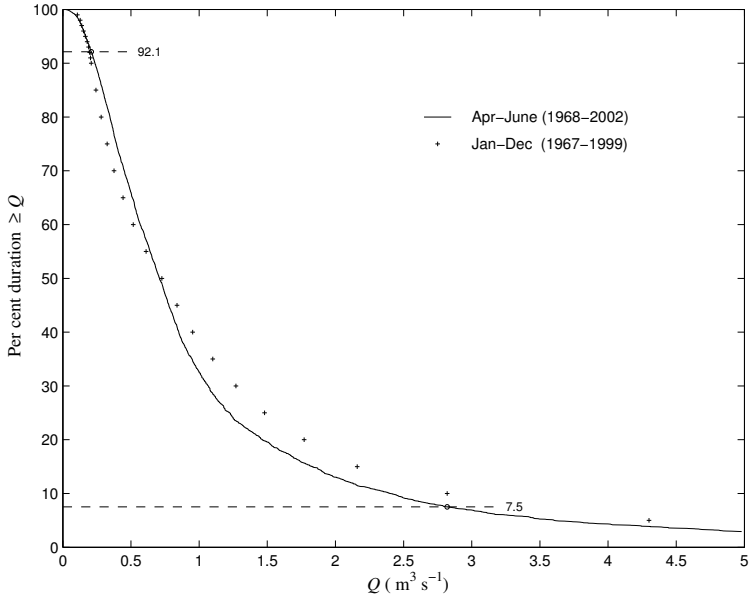

Figure 3–23: Brimpton model: Flow-duration data

typical and therefore useful as baseline data (Armstrong 2003b). The Kennet is situated near Reading, and is less than 50 miles away, with a similar geographical and atmospheric environment. For demonstration purposes, in this analysis, a temperature of 15 °C has been assumed, which would be equivalent to an average temperature for May and June.

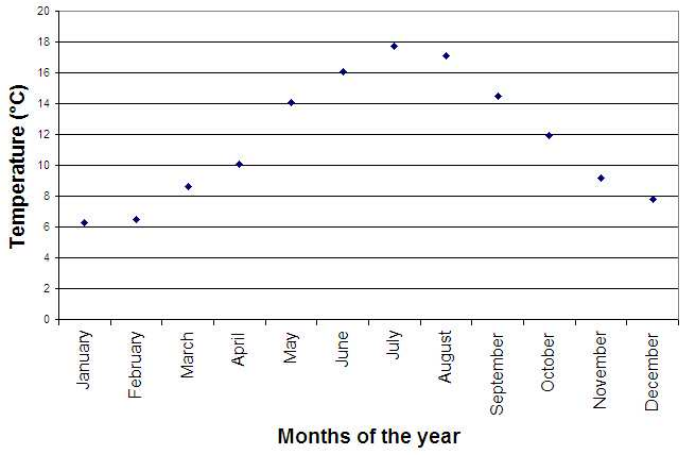

Figure 3–24: Typical baseline water temperatures (Lower River Kennet, Armstrong 2003b)

Presentation methods used for velocity distribution analysis and fish passage potential

The results from the velocity distribution experiments[12] have been differentiated firstly according to the height of the first and second baffle (i.e. equal or unequal baffle pairing), and secondly with regards to the gradient of the downstream slope (i.e. 1:5 compared to 1:4.55). The velocity distribution results are then linked to a fish passage efficiency matrix method. This method was developed to determine the fish passage potential for each slot as well as the cumulative effect along the path of ascent for each of the flow rates.

The description of the methods used to present the velocity distribution results are separated into two themes, namely:

a) presentation of velocity distribution results

b) developing a fish passage efficiency matrix

a) Presentation of velocity distribution results The water velocities in each slot, in a plane (y') normal to the downstream apron, were measured using the PT-ST equipment (configured for plane normal to the apron floor) described in section 3.2.3 and shown in Figure 3–18. The measurements taken in Slot 8 for the unequal baffle pairing, with a 50 percentile low-flow rate, a 1:5 downstream slope are used by way of example.

Figures 3–25(a) and (c) illustrate the grid pattern and show the sample points used for the 49 velocity measurements (7×7) normal to the downstream slope. In order to simplify the plotting of the velocity distributions which have been plotted as contour lines, all results have been plotted on a localised 'wh-axis' which is also defined on this figure. In this specific example, the general x′y′ axis as defined in Figure 4–4 at model scale, is mapped such that ($x = 665.900, y = -138.050, z = -141.875$) which is equivalent to the localised axis ($x = 665.900, w = 0, h = 0$). This localised axis is included on the figure to draw attention to the fact that the axis is set, and the velocity distributions are drawn, from the perspective of a fish swimming in the upstream direction: i.e. from the downstream side looking upwards towards the crest. The distance between the sample points (in this example) was 7.99 mm at model scale (40 mm at field scale), along the w-axis, represented by Δw, and 5.1 mm at model scale (25.5 mm at field scale), along the h-axis, represented by Δh. In addition, the water level data measured using the wave probe has been added to the slot at model scale, and scaled up to the field scale value for field scale.

Figure 3–25(b) shows the contour-plot velocity distribution in the slot at Baffle 8 at model scale, and Figure 3–25(d) shows the same example at field scale[13]. For comparative purposes, the model scale contour interval was set at

[12]The 84 velocity distribution results represent 29 laboratory testing days in total.

[13]For ease of reference, the comparative Δw and Δh have been included on the velocity distribution plots.

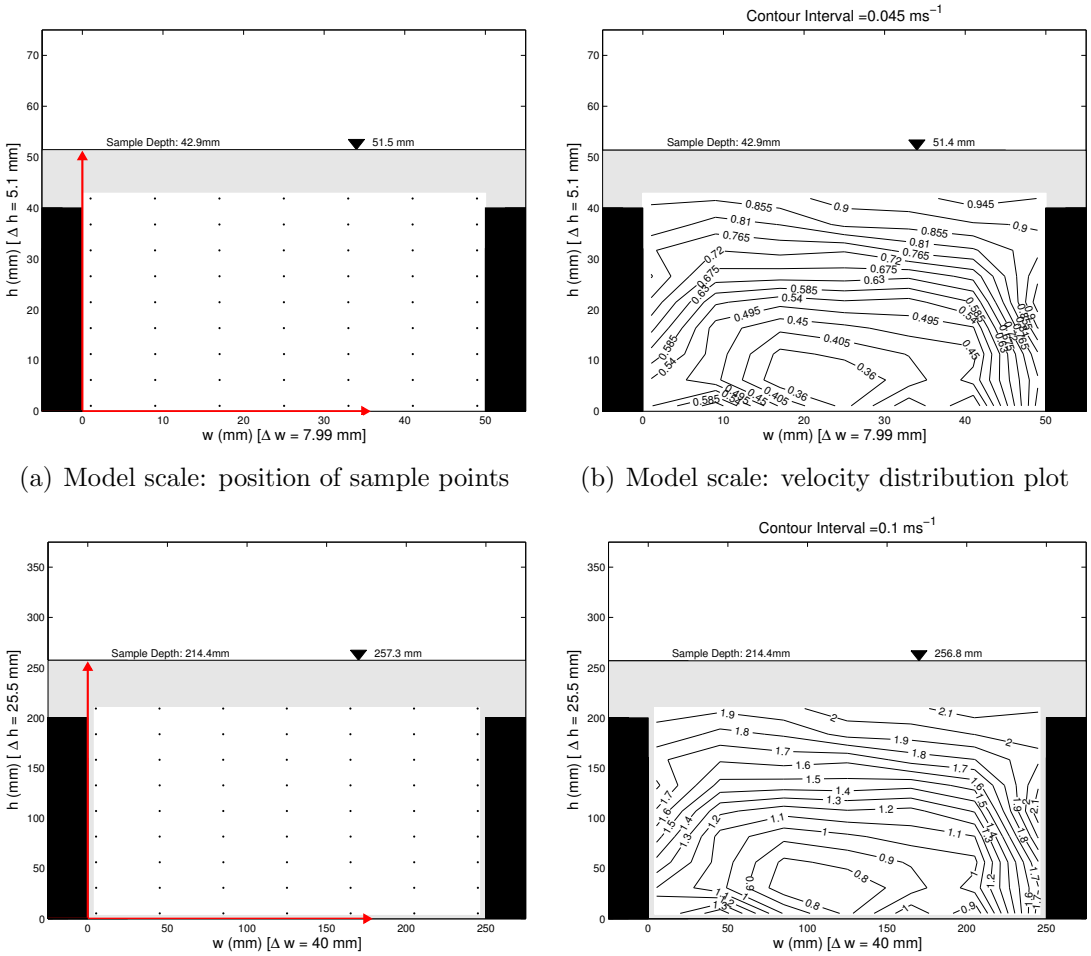

(a) Model scale: position of sample points

(b) Model scale: velocity distribution plot

(c) Field scale: position of sample points

(d) Field scale: velocity distribution plot

Figure 3–25: Cross-section of typical slot: Position of sample points and contour-plot velocity distribution at model scale and field scale (for the unequal baffle pairing at slot 8, 1:5, gradient and 50 percentile low-flow)

0.045 ms^{-1} which is approximately equivalent to a field scale contour interval of 0.1 ms^{-1}.

b) Developing a fish passage efficiency matrix As fish are not in themselves scalable, the velocity data sets recorded at model scale were scaled up to field scale for the development of a fish passage efficiency matrix. The criterion used requires that fish burst swimming speeds are greater than or equal to that of the water velocity for a given fish cross-sectional area (in terms of species, size and length).

This novel matrix method was developed to provide a quick means of assessing the theoretical success rate of a fish attempting to pass through a slot. Although there were nine fish species identified in the Swimit Excel spreadsheet (Environment Agency 2001b, 2003) which was used to populate the fish swimming data set, there are ten fish categories[14] identified in the fish matrix.

[14]The *anguilla anguilla* species (i.e. elvers and eels) are split into two categories to cater for

The general approach of the fish pass efficiency matrix method was to compare fish burst swimming speeds for a cross-sectional area as required by a fish (based on species and length), to the area available (using the velocity distribution data as measured for a specific slot) where velocities were less than the burst swimming speed. The following points describe the general method[15] employed (in a Matlab function) for populating the fish matrix:

i The velocity distribution data set for the target slot was reviewed, with each data point being associated with a measured water velocity (see Figure 3–25).

ii A 'fish exclusion formula' (Equation 3–4), as proposed by Turnpenny (1981, 1989) and represented in Armstrong *et al.* (2004), intended for excluding fish from intakes was considered as a reasonable starting point for determining a cross-sectional swimming area required by an average fish.

$$M = \frac{L}{0.209L + 0.656 + 1.2F} \tag{3–4}$$

This equation provides a means of calculating the free gap M (in cm) required in a mesh or bar screen to exclude a fish of length L (from snout to caudal peduncle in cm). An additional variable F, known as the 'fineness ratio' and given in Table 3–10[16] caters for the variable length:width ratio of fish. Figure 3–26 shows the relationship for each fish type.

This free gap or aperture is designed to exclude the smallest fish (Solomon 1992) of a species population (of a particular length). Figure 3–27(a) and (b) shows the aperture for a typical bar screen and square mesh respectively. However, what was needed for the analysis was a fish cross-sectional area, FCA, representing most of the fish of a particular species for a particular length. The free gap M has therefore been used as a basis for the calculation of a theoretical cross-sectional area for each unique species and length. This cross-sectional area is assumed to be representative of most, if not all, of a species population for a particular length. In Equation 3–5, M is assumed to be the radius, and each fish is assumed, for current purposes, to be circular in cross-section.

$$FCA = \pi M^2 \tag{3–5}$$

It is acknowledged that this method does not take into account the fact that fish shapes tend to be biased to the vertical rather then to the horizontal. As the area of lower velocity in the slots tends to be more biased to the horizontal (see Figure 3–25(d) as an example), using a circle of radius M is intended to ameliorate this to some degree.

their substantially different swimming capabilities.

[15]Suggestions and comments from Armstrong (2006) on preliminary results have been incorporated in this method.

[16]Note: The fineness ratios for grayling, barbel and smelt were not available. The worst case scenario (bream, $F = 2.99$, which is a deep bodied fish (Solomon 1992)) has therefore been used for present purposes.

Table 3–10: Fineness ratios for a range of freshwater fish (Note: Fineness ratios provided by Armstrong (2006))

Species	**Fineness ratio** F
Roach	3.51
Dace	4.83
Chub	4.39
Brown trout	4.37
Grayling*	2.99
Bream	2.99
Barbel*	2.99
Smelt*	2.99
Elvers	16
Eel	16

*F set equivalent to Bream

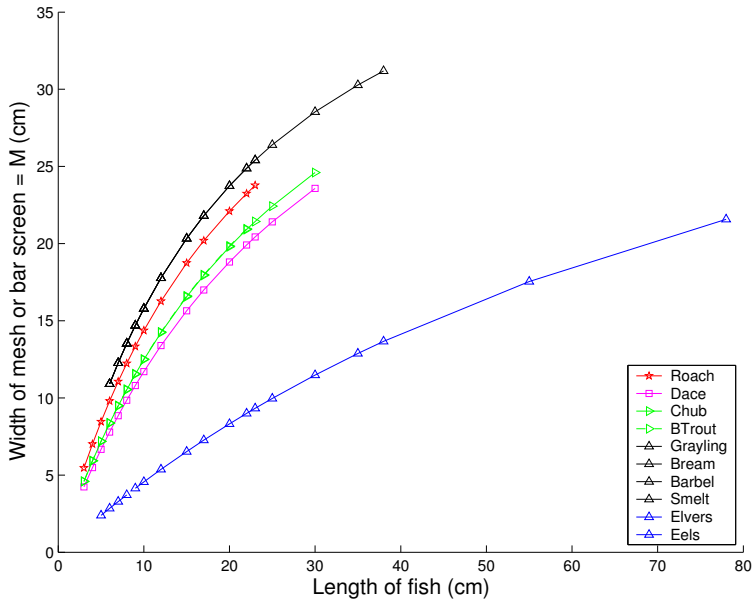

Figure 3–26: Mesh sizes according to fish species and length using the Turnpenny (1989) fish exclusion formula

Figure 3–28 shows fish length plotted against the cross-sectional area calculated in Equation 3–5. This cross-sectional information was added to a Matlab fish statistics 'lookup table' created from the Swimit Excel spreadsheets (Environment Agency 2003) with information pertaining to the fish species, size, and predicted mean burst speeds (for water temperatures of 10 °C and 15 °C respectively).

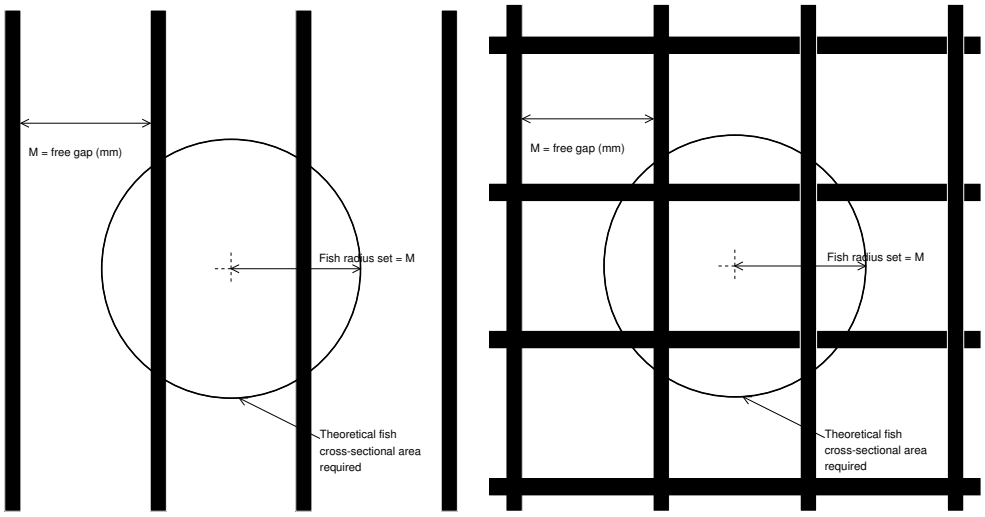

(a) Bar screen and outlined area of theoretical fish

(b) Fixed mesh of theoretical fish

Figure 3–27: Schematic diagrams of a bar screen and a fixed mess, with the cross-sectional area based on a fish of radius set equal to M

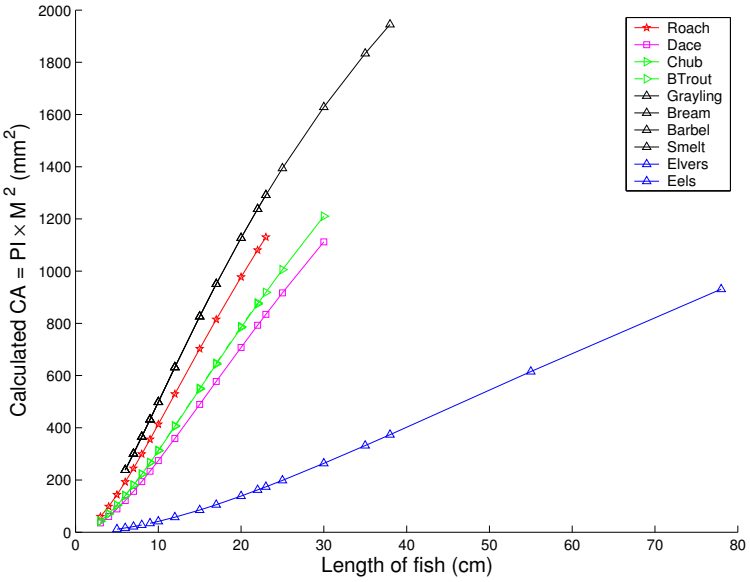

Figure 3–28: Calculated cross-sectional area according to fish species and length based on the free gap (πM^2)

iii For each fish (and fish length), the predicted mean burst speed was compared with the measured water velocity (as for each data point identified in (i) above). If the water velocity was less than the burst speed, this data point was deemed acceptable. A representative area (RA) was obtained by dividing the number of 'acceptable data points' with the 'total data points' and then multiplying that by the 'sample area' (where the velocity distribution has been measured).

$$\text{RA} = \frac{\text{acceptable data points}}{\text{total data points}} \times \text{sample area} \qquad (3\text{–}6)$$

iv If the cross-sectional area (FCA) required by the fish in (ii) was less than the representative area calculated in (iii), the slot was deemed passable for that specific fish (of specified length and at a particular water temperature).

v The data set was then plotted up in a matrix format, whereby the theoretical success of a fish (of specified length and at a particular water temperature) could be identified at a glance. The fish species are plotted on the x-axis, and the fish lengths along the y-axis. Each block is either black, shaded or white, each colour signifying a different outcome:

black	= pass (FCA required $<$ RA available)
shaded	= fail (FCA required $\geq$ RA available)
white	= no fish data available or not applicable (N/A)

The use of FCA $<$ RA implies that the burst speed velocity exceeds the water velocity. The fish pass efficiency matrix can be used to represent either a single slot or the total fish pass.

vi The velocity distribution example presented in Figure 3–25 has been redrawn (with 0.1 ms^{-1} contour intervals and a 'traffic light' colour system) in Figure 3–29(a) with the accompanying fish pass efficiency matrix in Figure 3–29(b).

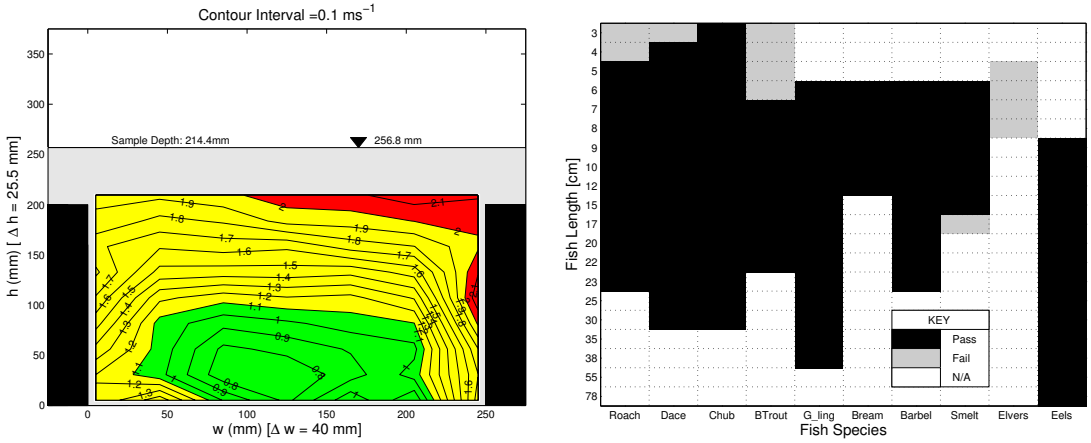

(a) Velocity distribution with traffic light system

(b) Fish pass efficiency matrix

Figure 3–29: Velocity distribution and associated fish pass matrix (for the unequal baffle pairing at Slot 8, 1:5, gradient and 50 percentile low-flow)

The green, yellow and red colours have been added to the velocity distribution to aid in visual identification of fish pass efficiency. Green represents those velocities less than 0.5 ms^{-1} (1.1 ms^{-1} at field scale), which was the maximum velocity criterion[17] used in the LEGO fish pass experiments. The field-scale range, in yellow, between 1.1 ms^{-1} and 2 ms^{-1}

[17]The 0.5 ms^{-1} model scale, and 1.1 ms^{-1} field scale velocity was based on the burst swimming speeds for roach, dace, chub and brown trout greater than 10 cm in length.

was arbitrarily identified as an intermediate velocity range. Trial and error also showed that this range was a fair indicator of a 'pass' prediction for fish smaller than 10 cm in length on the fish pass efficiency matrix. The red signifies velocities greater than 2 ms^{-1} at field scale. A mostly red velocity distribution was deemed to be unsuitable for successful fish passage. This colour coding will be used to describe the typical contour shapes found during the velocity distribution experiments.

From the fish efficiency matrix used in this example, roach between 5 cm and 23 cm in length and all of the chub under consideration would theoretically be able to pass through slot 8, whilst the velocities are too high for the elvers.

The stage-discharge analysis and the effect of varying d/l is dealt with in full in section 5.1.5.

3.4. Experimental methodology: Hydrometric effect

In order to determine the effect of the placement of the first baffle downstream of the Crump, a series of 'total head-discharge' experiments were carried out. The 'no-baffle' situation acted as a control, compared to a series of geometrically similar single baffles placed at seven unique positions downstream of the crest. The results were plotted non-dimensionally. White *et al.* (2005e) at HR Wallingford had also instituted a series of similar experiments using slightly different baffle shapes, but over a larger flow range (see section 2.3.4). Together both sets of results have provided a comprehensive set of non-dimensional curves.

More importantly, by comparing the non-dimensional perspex fish pass 'total head-discharge' results with the associated first baffle arrangement, it was found that a single baffle could not be used to determine the effect on the "total head-discharge' curve when a series of baffles was placed downstream. Therefore further investigations were conducted on various double baffle arrangements.

Non-modular flow was tested by raising the tailgate for a specific discharge. Once again the 'no-baffle' scenario was used as a control. A single baffle situation was investigated by raising the tailgate in small increments between recording water levels using the 20 mb pressure transducer. The perspex fish pass was not designed with non-modular flow experiments in mind, and as such the crest tappings in the model weir were unsuitable for use[18].

3.4.1. Modular flow

A total head-discharge experiment was firstly conducted for the Crump weir without baffles. A set of differently sized (but geometrically similar) baffles, ranging between

[18]During installation of the perspex fish passage, a machined brass section was used to achieve a good finish on the crest. This section was laid directly over the existing crest pressure tappings and suitable provision for the extension of these tappings was not found possible at the time.

20 mm and 60 mm in height, was fabricated in order to test for geometric similarity. Figure 3–30 depicts the general layout used for all these experiments. In each case, the baffle height is represented as d, with the baffle located at a distance of l from the crest to the centre of the baffle. The baffles were constructed such that the baffle radius was equal to $d/5$.

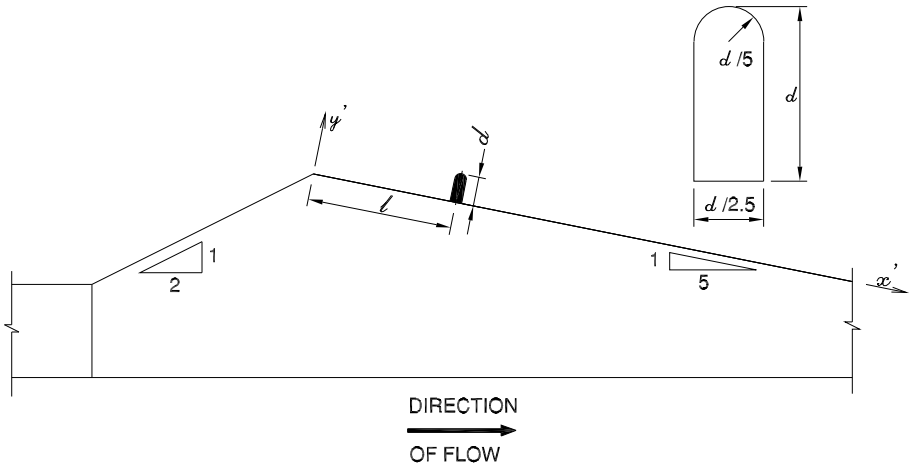

Figure 3–30: Longitudinal section of weir showing position of baffle

For sensitive measurement over the full range of modular flow, both the 109.91 mm and 61.95 mm orifice plates were used. The actual procedure is summarised as follows.

- The 400 mb pressure transducer was set up across the orifice plate, and the 20 mb pressure transducer was connected as shown in Figure 3–31. The relevant setup procedures (described in Appendix C) were completed. After priming, the pressure transducers were left to warm up for an hour which was found by experimentation to be a reasonable time period for both of the pressure transducers to reach equilibrium (as well as give any air trapped under the weir time to be displaced and the water surface to settle in preparation for attaining crest level). Datum sampling then commenced at zero differential pressure.

- With the water level in the flume initially above crest level, the tailgate was lowered so that crest water level would be captured in the upstream reservoir, and the pointer gauge was also set to zero to provide for checks upon the 20 mb pressure transducer.

- The experiment was started with a low head on the weir, and the supply pump speed was then incrementally increased over the experiment duration. The experimental procedure included a 5 minute pause between changes to the flow rate and reading the 400 mb pressure transducer, thus ensuring that equilibrium storage had been achieved in the system.

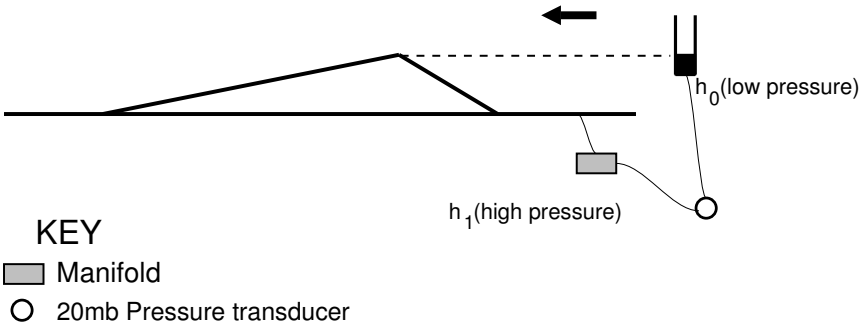

Figure 3–31: Layout of upstream static pressure tappings for modular flow experiments

- As described previously, the discharge Q was calculated from the differential pressure across the orifice plate using the equations in (BS1042 1992). The 400 mb pressure transducer was used to record this differential pressure across the orifice plate, and in most cases this was cross-checked[19] against the 4 m manometer.
- The 20 mb pressure transducer was used to measure the differential pressure between the upstream pressure tapping and the reservoir representing weir crest level, and was cross-checked against the pointer gauge reading.
- Water temperature and atmospheric pressure were routinely measured at the beginning and end of each experiment session and at hourly intervals in between. These measurements were included in the calculations for density and dynamic viscosity.

3.4.2. Non-modular flow

During the fabrication of the weir, three sets of pressure tappings were installed according to the specifications laid out in BS3680 (1986) and discussed in section 3.1.5. The following diagram (3–32) illustrates the arrangement used during the non-modular flow experiments.

For a normal Crump weir, non-modular flow has been shown to occur when $H_2 \leq 0.75H_1$ or when $h_p \leq 0.24H_1$ (BS3680 1986; Herschy *et al.* 1977) (see section 2.2.2 for definition of H). The modular discharge flow equation is adapted to provide for non-modular flow by the inclusion of f, the non-dimensional drowned flow reduction factor (see Equation 2–2 in Section 2.2.2).

As described previously, the discharge Q was measured by the 109.91 mm orifice plate throughout, using the 400 mb pressure transducer for the differential pressure, cross-checked against the 4 m manometer. The 20 mb pressure transducer was used to measure all three static pressures h_1, h_2 and h_p relative to weir crest represented by h_0. The actual procedure is summarised as follows:

[19]Figures G–3 to G–5 show typical results from this validation exercise.

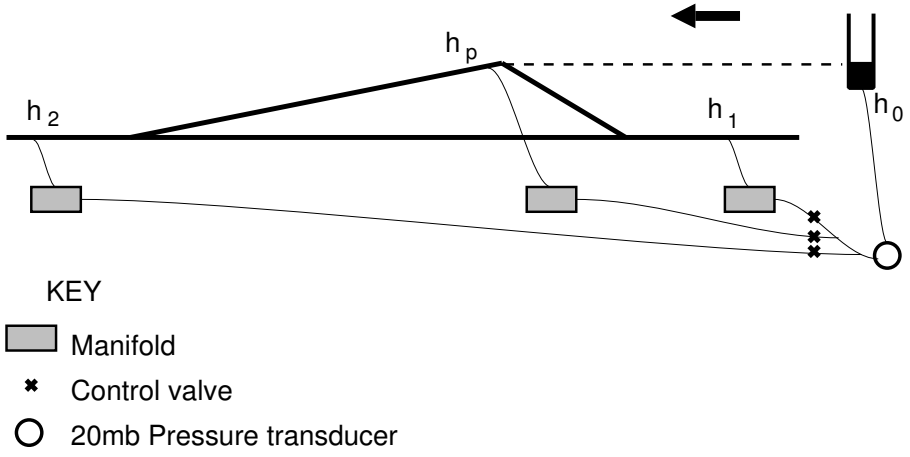

Figure 3–32: Layout of pressure tappings for non-modular flow experiments

- The 400 mb pressure transducer was set up across the orifice plate, and the 20 mb pressure transducer was connected as shown in Figure 3–32. Careful attention was paid to the bleeding process to ensure that no air was present in the system. After priming, the pressure transducers were left to warm up for an hour (for the reasons described in the modular flow experiment) before the datum sampling commenced at zero differential pressure.

- Crest water level was captured in the upstream reservoir, and the pointer gauge was also set to zero to enable validation of the 20 mb pressure transducer.

- The experimental flow rate was established. It should be noted that raising the tailgate caused the flow rate to decrease over the course of the experiment. The ideal situation would have been to re-establish the experimental flow rate at start conditions as closely as possible. However, this was soon found to be unworkable in being extremely time-consuming. As the final outcome of the experiments was to plot non-dimensional curves, it was therefore considered to be an unnecessary use of the available time.

- The tailgate was raised until downstream water levels were approximately 65% of upstream water levels.

- Experimental procedure included waiting five minutes between making any changes to the flow rate and recording data from the 400 mb pressure transducer, which was considered sufficient to ensure that equilibrium had been achieved in the system.

- Water temperature and atmospheric pressure were routinely measured at the beginning and end of the session and at hourly intervals in between.

- A five minute waiting time was maintained between raising the tailgate and sampling the 400 mb pressure transducer attached to the orifice plate. This reading provided the data required in order to determine the flow rate Q (as defined in section 3.1.5).

- As the upstream head, downstream head and where possible the crest head tappings were all measured with the 20 mb pressure transducer, a series of valves were installed to allow for the isolation of the line in question (see Figure 3–32). A delay of two minutes was instituted between opening/closing the respective valves before sampling from the pressure tappings in question.

3.5. Summary

This chapter has been divided into four sections. Firstly, an overview of the laboratory model, including installation, dimensional analysis, flow rate relationships and methods of capturing and recording water levels were presented. Next, details were provided on the experimental equipment used and associated calibration procedures. The setup and use of the traverse gear for measurement instrumentation, data acquisition techniques, wave probes for water depth measurements and velocity investigations were explored. As the nature of the experiments was two-fold (i.e. to find a suitable fish pass, and to determine the effect there-of on the hydrometric effect), experimental methodologies was split into two main sections, namely that of fish pass modifications and the hydrometric effect. The section on fish pass modifications was subdivided into the initial testing phase using LEGO bricks, followed by more detailed investigations into the preferred fish pass layout fabricated from perspex. The experimental methodology considering the hydrometric effect was also split into modular and non-modular flow categories. Both of these methodologies include an overview of the techniques and equipment used. Thus this chapter provides detailed background information for the presentation of the experimental results, analysis and discussion presented in the following two chapters.

4. Experiments on fish pass modifications

All of the laboratory tests were conducted on a 1:5 scale model of the low-flow section of the Brimpton weir. Firstly a multiplicity of baffle arrangements were trialled using LEGO, exploiting the quick-fit characteristics of the bricks. Initial testing was carried out at the 90 percentile low-flow, with the first baffle being located at a minimum distance downstream in an effort to preserve modular flow (although this was not actually achieved). Once an effective layout was identified, this was fine-tuned and tested over the whole flow range. Further analytical and experimental work was carried out on a perspex model of the preferred layout which was laid on top of the existing wooden section. This chapter has been divided according to the two main experimental phases:

- Testing a multiplicity of baffle arrangements using LEGO
- Investigations into the preferred baffle arrangements using Perspex baffles

Although the results in this chapter have been analysed with specific reference to Brimpton weir, the 'flow rates per unit width' as given in Table 3–9 provides details for generalisation of these results.

4.1. Testing a multiplicity of baffle arrangements using LEGO

A detailed description of the experimental procedures used in trialling the LEGO layouts has been presented in section 3.3.

4.1.1. Categorisation of baffle arrangements

The various baffle arrangements have been divided into categories, depending on their layout and operation. Figures 4–1 to 4–3 show the plan view in a plane parallel to the apron and represent typical layouts for each of the following main categories:

- Category 1: Centre Channel arrangement
- Category 2: Baulk arrangement

- Category 3: Diagonal arrangement
- Category 4: Rotated-V (with and without an additional narrow channel)
- Category 5: Side Channel arrangement

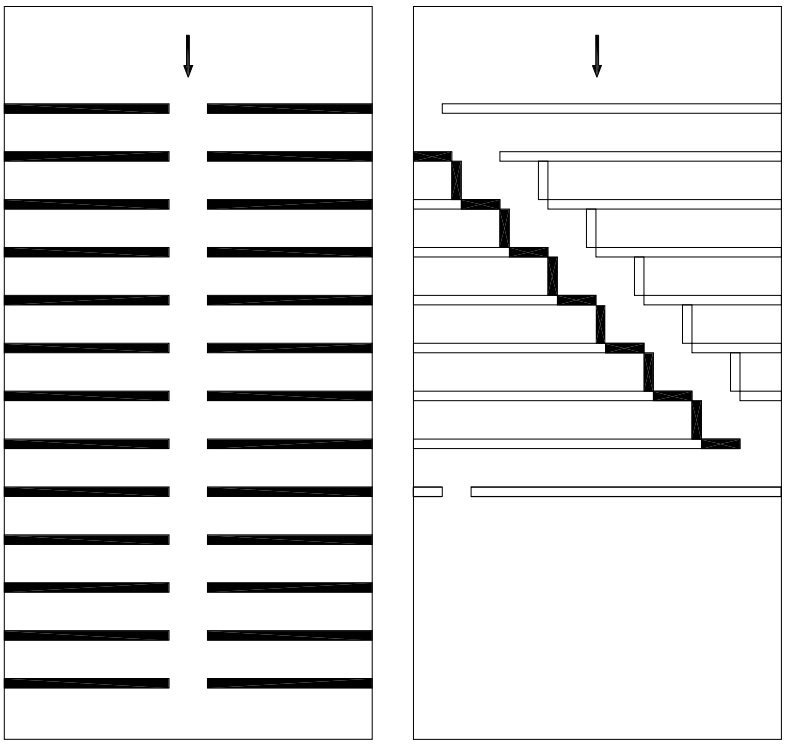

(a) Centre channel (b) Baulk

Figure 4–1: Typical layouts tested at the 90 percentile low-flow: Centre Channel and Baulk

The following parameters have been considered in the design of the layouts:

Baffle dimensions The number of LEGO bricks determines the height of each baffle whereas baffle width was fixed (see Table 3–7).

Slot width The slot width (labelled on Figure 4–2) refers to the gap in a baffle through which fish are expected to swim. In all cases the slot extends to the full height of a particular baffle.

Overlap This refers to the alignment of the slots (labelled on Figure 4–2), and is a function of the slot size and the angle of the pattern.

Baffle spacing The distance between two rows of baffles (i.e. from LEGO face-to-face, not centre-to-centre, labelled on Figure 4–2).

During this experimental phase, the 90 percentile low-flow was used as a basis from which to compare the velocities and flow depth. The following analysis will show that the rotated-V category was found to have the most development potential, which was subsequently investigated over a larger flow range (section 4.1.4).

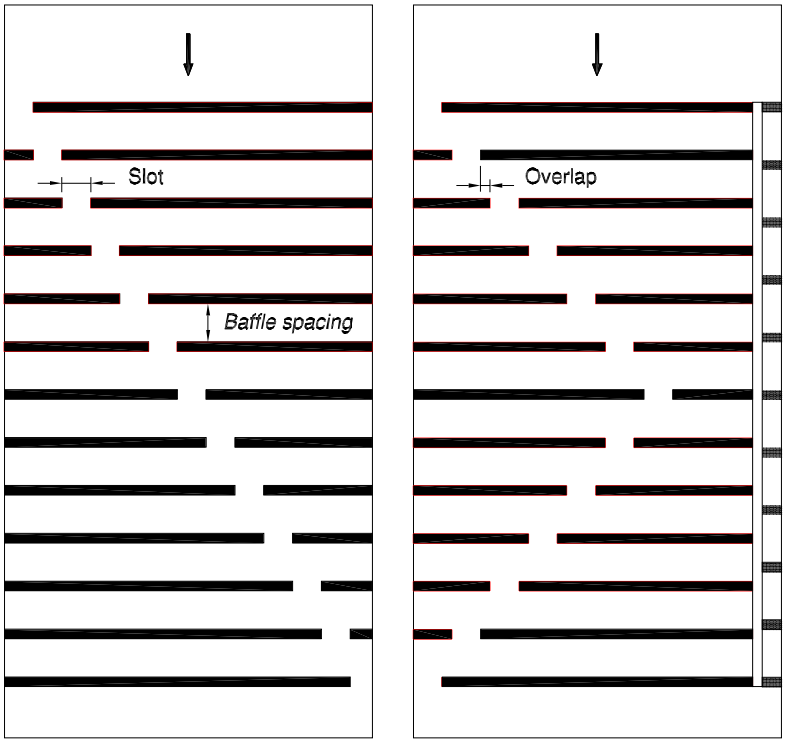

(a) Diagonal (b) Rotated-V

Figure 4–2: Typical layouts tested at the 90 percentile low-flow: Diagonal and Rotated-V with narrow channel

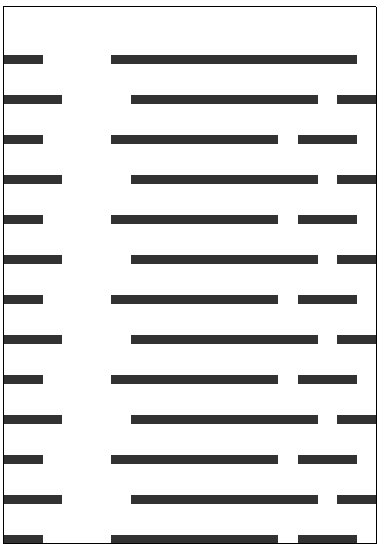

Figure 4–3: Typical layouts tested at the 90 percentile low-flow: Side gaps

Table 4–1: 90 percentile low-flow: Experiment data records

Experiment Number	**Baffle spacing** (mm)	**Slot** (mm)	**Overlap** (mm)	**Narrow channel** (mm)
Category 1: Centre Channel (see Figure D–2)				
Baffle layout 1	64	64	0	
Category 2: Baulk (see Figure D–3)				
Baffle layout 3	64	48	48	
Category 3: Diagonal (see Figures D–4 to D–14)				
Baffle layout 5	64	32	0	
LEGO layout 1.1	64	48	0	
Baffle layout 6	64	32	32	
LEGO layout 1.5	80	48	16	
LEGO layout 1.7	96	48	16	
LEGO layout 1.8	112	48	32	
LEGO layout 1.9	128	48	32	
LEGO layout 1.9(2)	128	48	40	
LEGO layout 1.4	144	48	48	
LEGO layout 1.10	144	48	40	
LEGO layout 1.6	176	48	64	
Category 4: Rotated-V (see Figures D–15 to D–17)				
Baffle layout 2	64	32	32	
Baffle layout 4	64	48	16	
LEGO layout 1.14	64	48	32	
Category 4: Rotated-V with Narrow Channel (see Figures D–18 to D–28)				
LEGO layout 2.1	64	48	32	32
LEGO layout 2.2	64	48	32	48
LEGO layout 1.16	64	48	40	64
LEGO layout 1.15	64	48	32	96
LEGO layout 1.17	64	48	40	80
LEGO layout 1.19	64	48	40	64
LEGO layout 1.18	64	48	40	80
LEGO layout 2.5	64	48	16	80
LEGO layout 2.6	64	48	16	80 (1st baffle higher)
LEGO layout 2.7	64	48	16	64
Category 5: Side gaps (see Figures D–29 to D–33)				
LEGO layout 2.3	64	32	32	
LEGO layout 5.1	64	32	32	
LEGO layout 5.2	64	32	32	
LEGO layout 5.3	64	48	48	
LEGO layout 5.4	64	48	48	

4.1.2. Progression of the testing programme

All of the experiments[1] conducted at the 90-percentile low-flow are recorded in Table 4–1 (see page 90), together with the baffle spacing[2], slot and overlap measurements.

The purpose of this section is to provide an insight into the progression of the experiments used to select an appropriate layout for further investigation. All results are presented and analysed in depth in section 4.1.3.

The Centre Channel arrangement depicted in Figure 4–1(a) was the starting point for the investigation into suitable LEGO layouts. Although water depths proved satisfactory, water velocities in the fish pathway down the centre downstream slope were above the maximum fish swimming speed threshold used to select an appropriate arrangement. In order to reduce the velocities, Diagonal arrangements as represented by Figure 4–2(a) were investigated. Three parameters were considered, namely (i) baffle spacing, (ii) slot width and (iii) overlap (i.e. stagger). The minimum face-to-face baffle spacing recommended by Armstrong (2002b) was ultimately adopted as a wider spacing resulted in super-critical flow between the baffles. It was found that a combination of bigger slots and larger overlaps reduced velocities to acceptable levels. Because of the narrow aspect ratio (width:length) of the Brimpton weir, it was necessary to change the direction of the fish path of ascent halfway up the fish pass. This resulted in the Rotated-V arrangements (see Figure 4–2(b)). Further refinements included adjustments to the overlap and entrance/exit positions of the slots as well as investigations into a narrow channel on the side of the weir. Two other configurations were investigated in the same time period as the Diagonal and Rotated-V experiments, namely the Baulk arrangement (Figure 4–1(b)) and the Side gaps arrangement (Figure 4–3). Because of unsatisfactory velocity measurements in the former, as well as concerns over large circulation eddies downstream of the Crump weir in the latter, these arrangements were not explored in further detail.

4.1.3. Presentation and analysis of results: multiplicity of layouts at the 90 percentile low-flow

The results are presented and discussed for each of the categories identified in Table 4–1. Where possible, preference has been given to a logical presentation of these results rather than to the original order and categorisation of the experiments. In addition, the entire set of the plan layouts and accompanying cross-sections showing recorded spot velocities are presented in Appendix D.

For the LEGO experiments, the position of the upstream face of the first baffle was set as shown in Table 4–2 (see discussion on the centre channel for this decision).

[1] Thirty-three layouts were trialled at the 90 percentile low-flow rate in twenty laboratory testing days over a period of approximately three months

[2] For this data set, the baffle spacing represents the distance from the downstream face of one baffle to the upstream face of the next (initially recorded as the number of LEGO studs for ease of reference during experiment set-up.)

Table 4–2: Location of first baffle as used in the LEGO experiments

Description	**Model scale** (mm)	**Field scale** (mm)
Crest to upstream face of 1st baffle	172	860
Crest to centre of 1st baffle	177.7	≈ 884

It would be normal as a design aspect of a Crump weir to have the hydraulic jump positioned on the downstream slope. However, for these experiments it was kept away from the apron where possible, while still preventing damage to the glass floor of the flume. This was done in the interests of a more general solution (rather than being only specific to Brimpton weir). Therefore the hydraulic jump and consequently the tailwater levels were kept as low as was practically possible in order that the head difference between the upstream and downstream water levels was maximised.

Category 1: Centre Channel arrangement

The centre channel arrangement was investigated in depth in order to test the various instrumentation and experimental procedures. This was a time-consuming process which included both the hands-on learning required to operate the equipment, debugging and general time taken to setup and use both the Pitot-static tube combination and wave probe equipment.

Layout of arrangement The centre channel layout (Servais *et al.* 2003; Servais 2003) in Figure 4–4 is a variant on that tested by Sarker *et al.* (2001) who reported that a 60 mm spacing between baffles maximised flow thickness. The baffles used were 30.4 mm high and 1.1 mm thick with the first baffle placed 170 mm from the crest and 32 mm slots down each side-wall of the flume. Those parameters were adapted for use with the LEGO, and because the brick locations on the LEGO board were limited to discrete steps, the distance from the crest to the centre of the first baffle became approximately 177 mm, allowing the upstream face of the baffle to be as close to 170 mm as possible. This also had the effect of setting the first baffle at approximately the same height as the crest. Thus in practical terms, the position of the upstream face was a summation of the distance (76 mm) from the crest to the edge of the LEGO base and the distance (96 mm or 12 studs) from the edge of the LEGO base to the upstream face of the baffle, giving 172 mm in total. This distance from the crest to the upstream baffle face was used for all of the LEGO layout sections reported in section 4.1.3.

Also, the baffle spacing of 60 mm became 64 mm face-to-face and 76.5 mm centre-to-centre with the LEGO thickness taken into account. Sarker (2000) reported that at the 95 percentile low-flow, the presence of the baffle did not alter modular flow conditions. The flow rate for the centre channel experiment was set to the 90 percentile low-flow of 3.77 ls^{-1}.

For ease of reference the following coordinate system is used in Figure 4–4 and throughout this thesis: A panel pin is used to mark the origins of two sets of axes (which share the same origin). The primary set of axes, (x, y, z), are orientated such that x is horizontal, y is vertical and z is used for width dimensions. The secondary set of axes, (x', y') are aligned so as to describe events either parallel (x') or normal (y') to the 1:5 downstream slope of the weir.

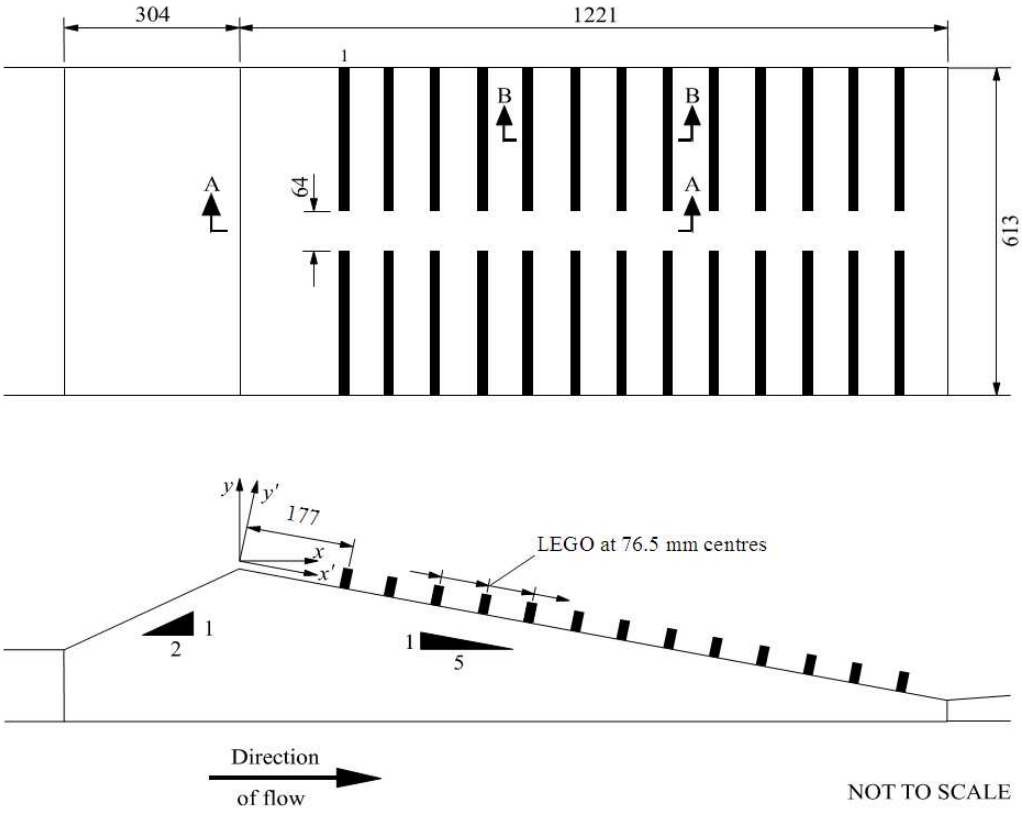

Figure 4–4: Centre Channel: Baffle arrangement on downstream face (all dimensions in mm)

Velocity distributions The parallel-mounted Pitot tube and static pressure tube combination (mounted in a plane parallel to the apron as described in section 3.2.4) was used for measuring streamwise velocity distributions on the downstream face of the weir.

The streamwise velocity distribution (Figure 4–5(a)) was measured at a series of y'-coordinates in the slot at the intersection of the centreline of the weir and the central plane of the fifth row of baffles. The maximum water velocity was found to be slightly greater than 1.1 ms^{-1} at model scale, which is equivalent to approximately 2.5 ms^{-1} at field scale. The position of this maximum was approximately 17 mm above the apron floor on the y' axis (i.e. 85 mm at field scale). The decrease in velocity towards the bed of the weir is the likely result of bed shear. The decrease in the upper portion of the velocity distribution might

be attributed to either the lateral shear-layer effect caused by the presence of the baffles, or to turbulence driven secondary currents.

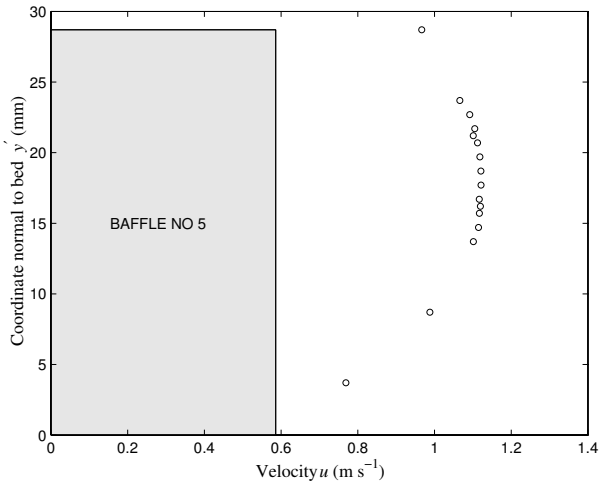

(a) Velocity distribution normal to the bed slope (in the gap in the 5th baffle row)

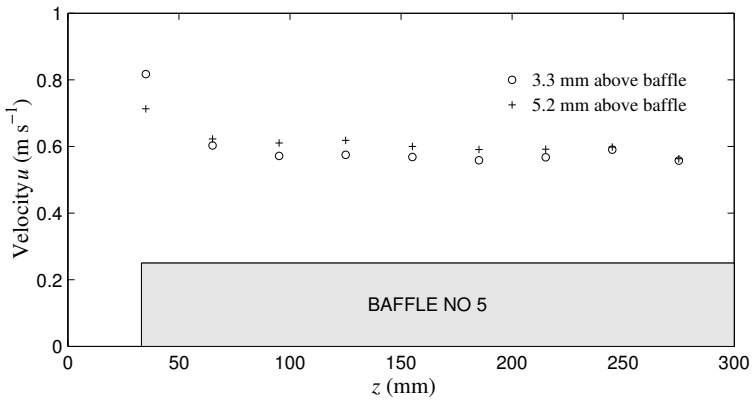

(b) The velocity distribution across the top of the fifth baffle

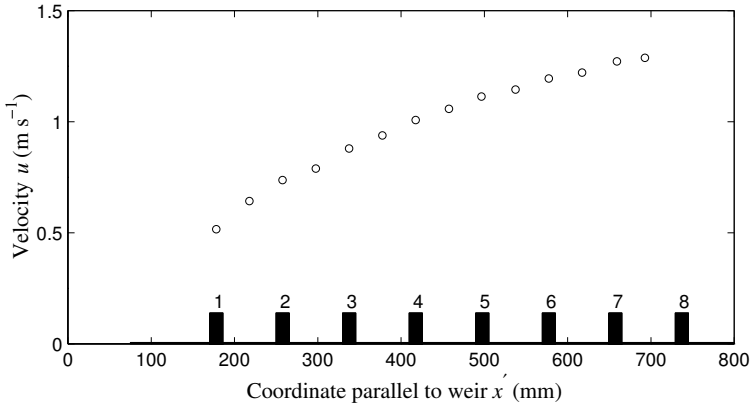

(c) Velocity distribution down the centre of the channel (i.e. Section A-A as shown on Figure 4–4)

Figure 4–5: Centre Channel: Velocity distributions

In addition to determining the velocity distribution normal to the weir face in the slot in the fifth baffle, measurements were taken across the top of the

fifth baffle. Figure 4–5(b) shows that the average velocity across the top of this baffle was about 0.6 ms^{-1} (equivalent to 1.3 ms^{-1} at field scale).

After determining the position of maximum velocity in the centre of the gap in the fifth row of baffles, the distribution of maximum velocity down the centre of the weir (Section A-A in Figure 4–4) was measured at 17 mm perpendicular to the apron floor. The results of these measurements are presented in Figure 4–5(c) which shows that the velocity increases with the x' coordinate down the length of the weir. The average velocity between baffles six and eight was recorded as 1.3 ms^{-1}, which translates to a field scale velocity of 2.9 ms^{-1}. Baffle 8 was the limit of travel for the traverse gear for that arrangement[3], though velocities continued to increase further down the slope.

It was as a result of the time-consuming nature[4] of the Pitot-static tube combination that the velocity propeller meter (VPM)[5] was brought into use. This allowed flow velocities to be measured very quickly and easily down the flow path, with the aim of achieving flow velocities less than the maximum fish swimming speed in order for a fish of a certain size to progress in the upstream direction.

Water depth measurements The second parameter considered during this phase of testing was that of water depth. The 1.10 mm OD wave probe was clamped to the traverse gear and the centre of the wave probe was then located at the same reference point (i.e. the origin marked by the panel pin) as that used for the Pitot-tube combination.

Free surface profiles were measured in two locations. Figures 4–6(a) and 4–6(b) show the results from over the top of the baffles, and through the centre of the baffle slots (Sections B-B and A-A respectively, as shown in Figure 4–4). The free surface profiles in Figure 4–6(b), with and without the baffles, demonstrate the favourable change in the water depth for fish passage created by the baffles.

At this point it was recognised that by placing baffles on the downstream slope of the weir, flow was inevitably thickened. Thus in terms of fish passage requirements, as long as flow depth was at least approximately equal to the height of three LEGO bricks, this was deemed sufficient for the sifting process.

Comparison with fish swimming speeds Figures 4–7 and 4–8 show a plan layout normal to the apron and a longitudinal cross-section of the weir. The plan view gives numerical values of the spot velocities, taken at 17 mm perpendicular to the apron at model scale, and boxed converted to field scale. The primary y-axis (drawn at crest on the cross-section in Figure 4–8) represents

[3]The traverse gear equipment was repositioned after this experiment was completed in order to rectify this shortcoming.

[4]The time required was determined by the initial priming time, the need to keep the Pitot-static tube combination under water to maintain that priming whilst moving between slots, and a 60 second sampling time.

[5]As previously acknowledged, the Pitot-static tube combination is more accurate, but the VPM was extremely effective when used comparatively between different LEGO combinations.

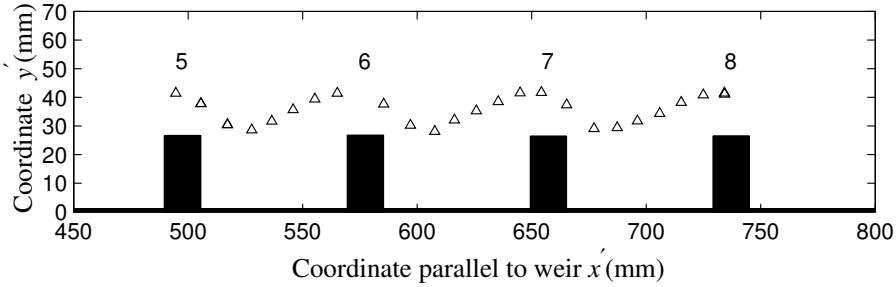

(a) Free surface profile over the top of the baffles 5 to 8 (i.e. Section B-B from Figure 4–4)

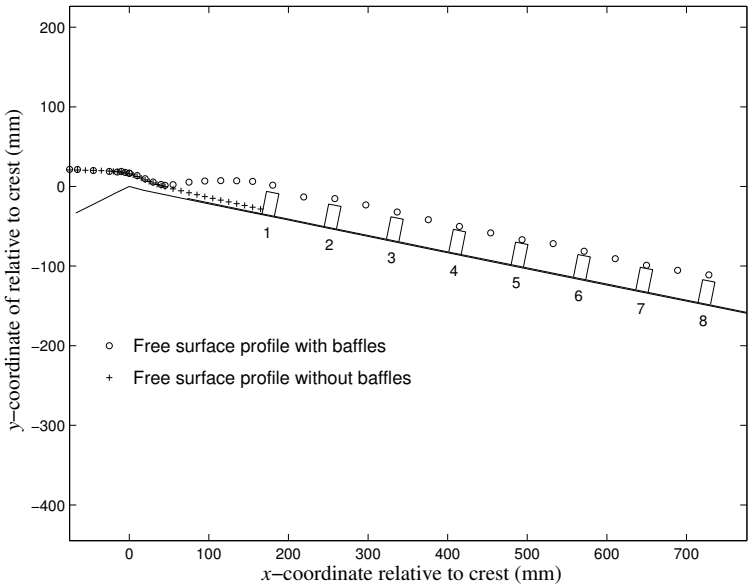

(b) Free surface profile down the centre of the channel (i.e. Section A-A from Figure 4–4)

Figure 4–6: Centre Channel: Free surface profiles

the baffles on the downstream slope of the weir, while the secondary y-axis provides the corresponding spot velocity values. Such diagrams provided a quick method for recording and comparing the multiplicity of LEGO baffle layouts trialled. The burst swimming speed of 0.51 ms^{-1} at model scale (1.1 ms^{-1} at field scale), used as a maximum velocity criterion for successful baffle layouts, was plotted on the cross-section. This maximum velocity criterion was derived from the Swimit results (Figures A–1 and A–2), as this criterion is well above the maximum burst speed which the fish under investigation (greater than 10 cm) are capable of swimming. As already mentioned and shown in Figure 4–8, the velocities down the centre of the channel were well in excess of this.

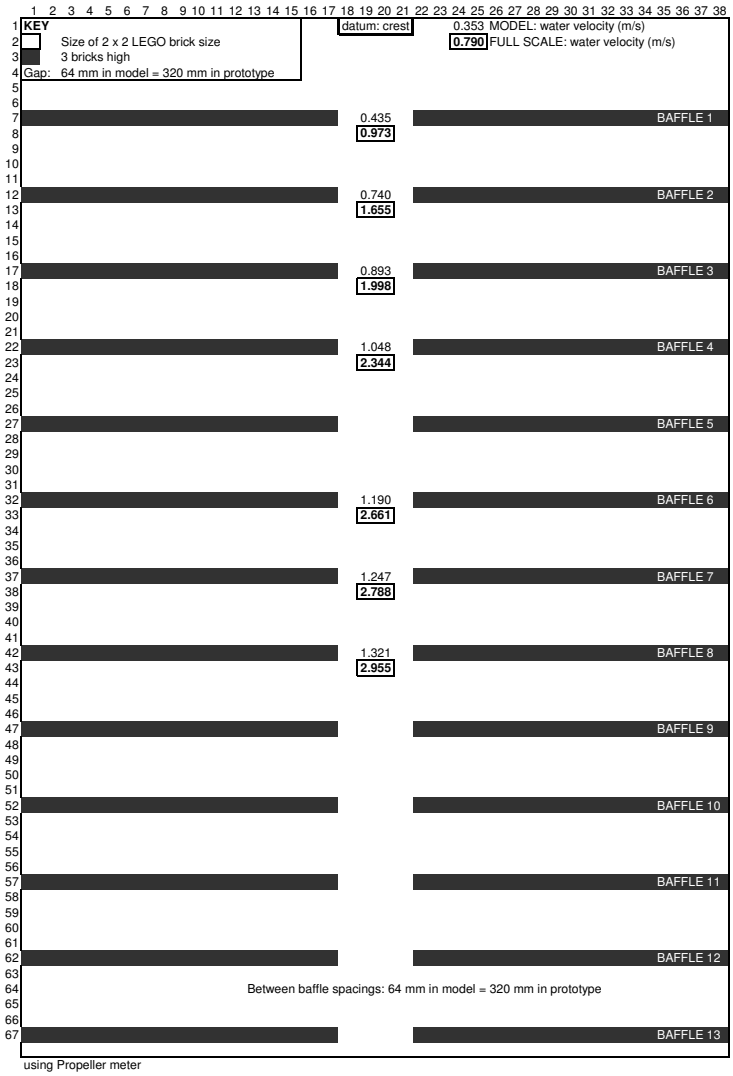

Figure 4–7: Centre Channel: Plan of Baffle Layout 1

Therefore, although the centre channel proved a useful starting point in the experimental procedures and recording methods to be followed throughout the LEGO trials, the velocity conditions were found to be unsuitable for the fish species of interest.

Discussion on flow patterns The main mechanisms identified in influencing the flow patterns associated with the centre channel are as follows:

- Upstream of the crest, flow was sub-critical and the presence of the first baffle influenced the separation bubble.(See sections 2.3.5, 5.1.2 and 5.1.4 for further discussion regarding streamlines on unmodified and modified Crump weirs).
- Increasing velocities were observed through the slots down the centre of the weir, which was jet-like in nature.
- The flow patterns observed in the baffled portion of the weir was indicative of the streaming flow (as in Figure 2–9) associated with the pool and

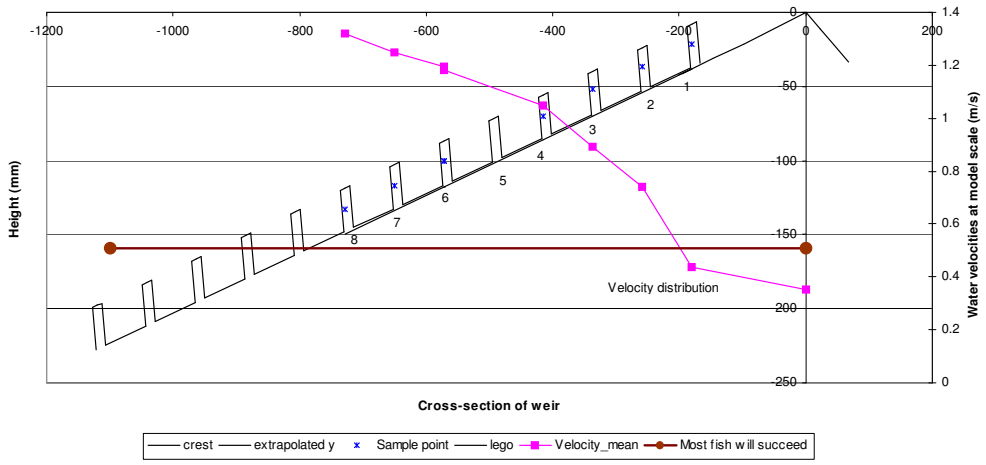

Figure 4–8: Centre Channel: Cross-section of Baffle Layout 1

weir type of fish pass.

In addition to inherent fixed dimensions of the LEGO base board, the increased roughness caused by the LEGO snap-to-fit studs was difficult to quantify and probably resulted in flow-thickening. During the LEGO trials this was not considered to be problematic as the intention was to construct the favoured solution from perspex in order to eliminate this problem.

Category 2: Baulk arrangement

Although LEGO proved to be a useful tool, it was restrictive in that the bricks had to be arranged in discrete locations determined by the LEGO base sheet with its rectangular grid of stud fixings. Thus although the layout tested in Figure 4–9 was guided by the baulk arrangement shown in Figure 2–15, with LEGO it was not possible to replicate the exact arrangement nor include a notch in the weir crest. The function of the first baffle parallel to the crest was similar to that of the enhancing baulk located on the crest, the purpose being to collect water and provide for adequate flow depth through the first slot. In the LEGO arrangement, additional baffles were located downstream of the first baffle in order to prevent the formation of super-critical flow. Figure 4–10 shows that between Baffle 3 and Baffle 6 the flow velocity was above the burst swimming speed criterion, and consequently an investigation of the baulk was not pursued.

Category 3: Diagonal arrangement

The results from the centre channel experiment showed that although baffles on the downstream slope of the weir thickened the flow, having a straight path parallel to the axis of the weir through the centre of the baffles did not provide the required

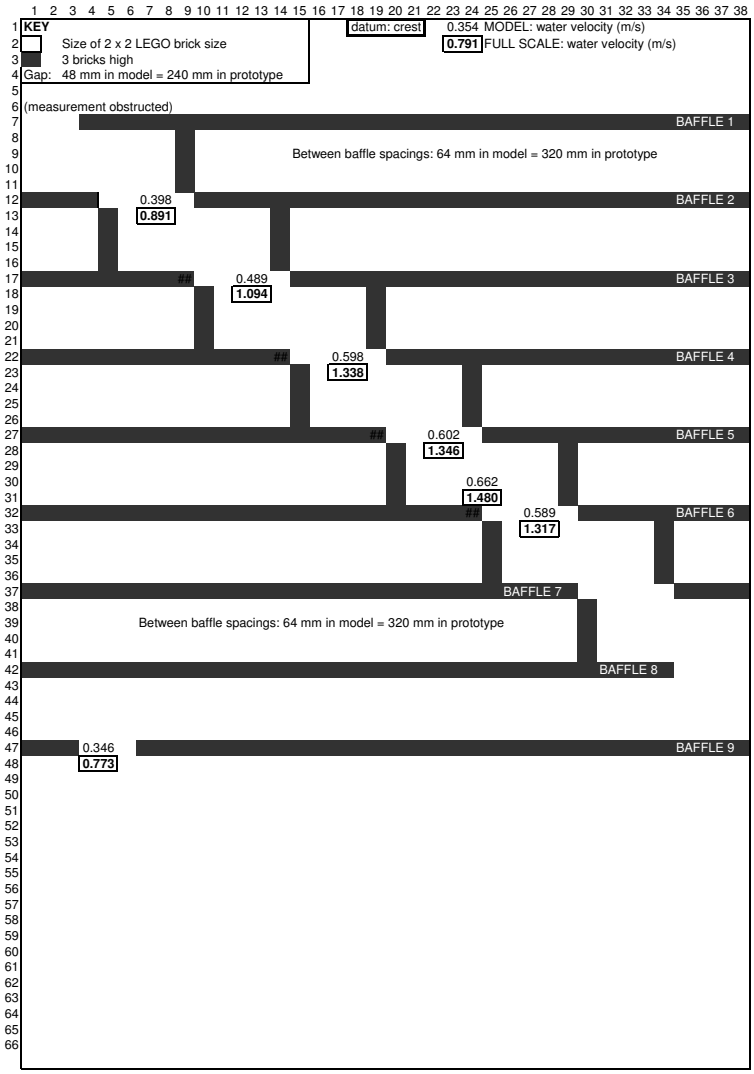

Figure 4–9: Baulk: Plan of Baffle layout 3

retardation of water velocity. It was therefore decided to experiment with slot size, baffle spacing and alignment (i.e.overlap).

The plan layouts and velocities of the diagonal[6] arrangements (from three[7] of the eleven layouts trialled) are shown in Figure 4–11. The diagonal layout velocities recorded at Baffle 8 (at model scale) varied between 0.52 ms^{-1} and 0.73 ms^{-1} which were approximately half the centre channel velocity of 1.32 ms^{-1} measured at the corresponding baffle position using the VPM.

From the eleven unique diagonal arrangements trialled (see Figures D–4 to D–28) the following trends were observed:

Overlap The higher velocities recorded for the diagonal layout corresponded with

[6]This type of layout is referred to as 'diagonal' in this document. and 'oblique' channel in the proposed Guidelines (Rhodes and Servais 2006).

[7]The experiment naming convention was changed from 'Baffle layout' to 'LEGO layout' during these trials. See AppendixD for detailed Figures D–4 to D–6.

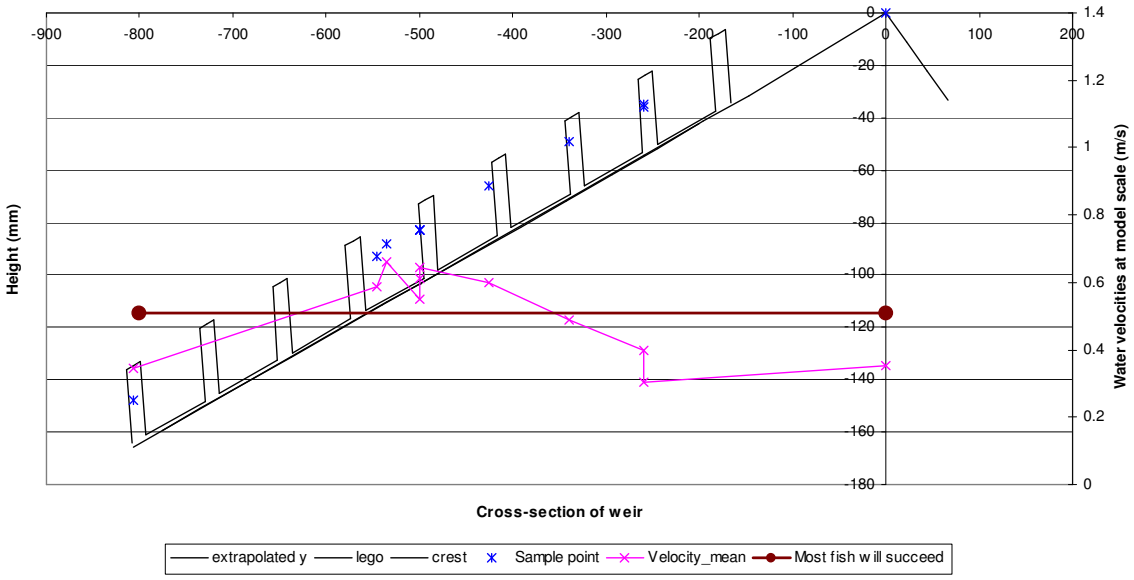

Figure 4–10: Baulk: Cross-section of Baffle layout 3 (Spot velocities taken at 17 mm perpendicular to apron, at model scale)

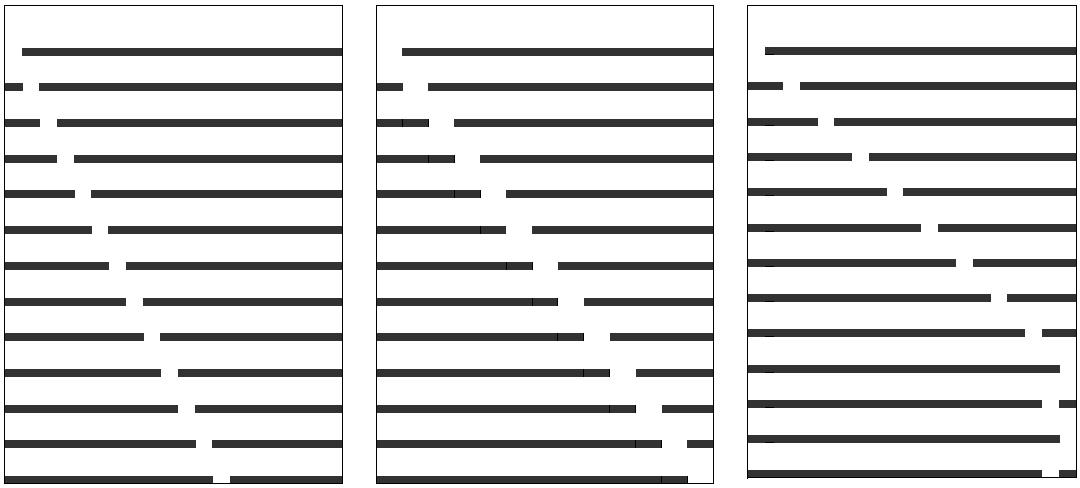

(a) Plan of Baffle layout 5 (Slot: 32 mm Overlap: 0 mm)

(b) Plan of LEGO layout 1.1 (Slot: 48 mm Overlap: 0 mm)

(c) Plan of Baffle layout 6 (Slot: 32 mm Overlap: 32 mm)

Figure 4–11: Diagonal layouts: Plan views showing effect of overlap (Baffle spacing: 64 mm)

the steeper path of ascent (i.e. effectively zero overlap). Velocities were significantly reduced by increasing this overlap and creating a shallower path of ascent.

Slot size An increase in the slot size resulted in a decrease in the velocities. A consequence of the Brimpton model, with its apron of narrow aspect ratio (width:length), was that a path of ascent of shallow gradient could reach the side-wall part-way along the apron. The 'rotated-V layouts' (discussed later) are a direct result of such cases. In Figure 4–35 for example, the path of ascent

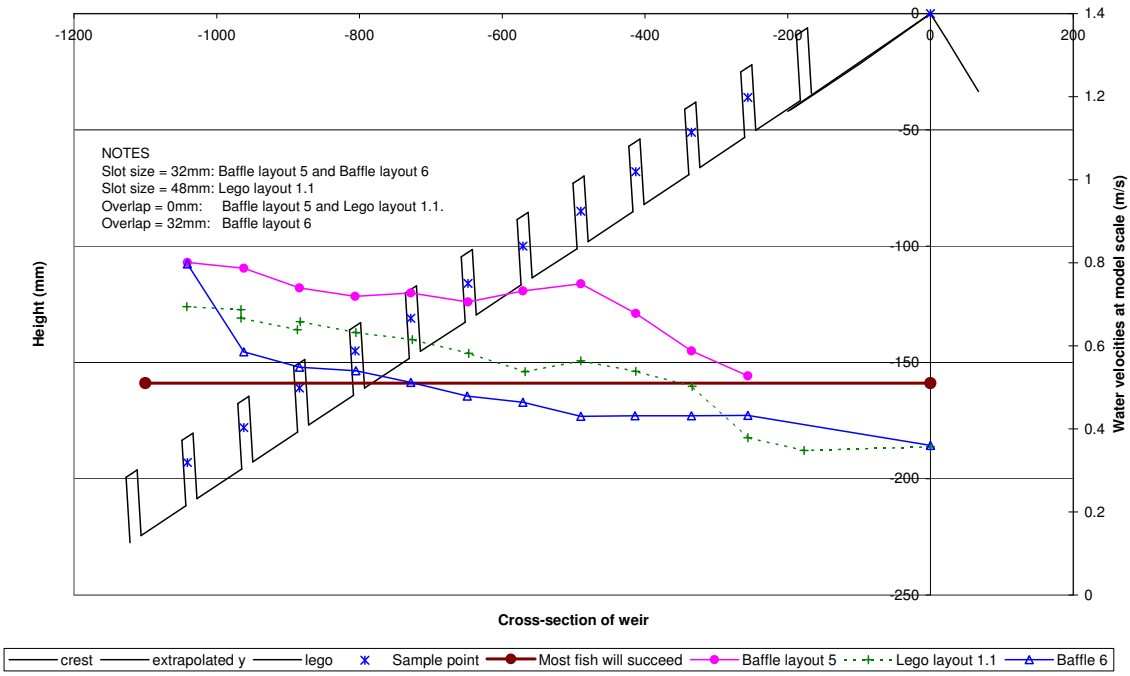

(a) Cross-section: comparison of spot velocities with a) varying overlap or b) slot size

Figure 4–12: Diagonal layouts: Cross-section showing comparison of spot velocities with a) varying overlap or b) slot size (Baffle spacing: 64 mm)

was reflected about the side-wall so as to increase the path length down the full extent of the weir.

Baffle spacing Instead of reflecting the path of ascent about the side-wall, the baffle spacing was increased at the same time as increasing the slot size. This also effectively decreased the number of baffles on the downstream slope.

With an increasing baffle spacing (face-to-face) for distances greater than 80 mm, the formation of an hydraulic jump, of increasing significance with associated super-critical flow, with higher velocities and a corresponding reduction in flow thickness, was observed between baffles. As the velocities in the slots were not as sensitive to the increase in spacing, experiment measurement practices played an important role in order that the effect of baffle spacing on the maximum velocity criterion for the whole fish path was not overlooked. As a result of these trials it was decided to use the minimum recommended face-to-face baffle spacing (Armstrong 2002b) of 60 mm at model scale (300 mm at field scale) and this corresponded to a LEGO spacing of 64 mm at model scale (or 320 mm at field scale).

Category 4: Rotated-V arrangements

As shown above, overlap and slot size are considered to be the two key elements in achieving velocities below the maximum velocity criterion on the downstream slope. The narrow aspect ratio (width: length) of the Brimpton weir apron limited the size

of the overlap on the downstream slope and was one of the reasons that a change in direction was introduced. A second consideration was the increase of velocity down the path of ascent, as observed during the diagonal experiments discussed above.

For the rotated-V variations, a 64 mm (320 mm field scale) baffle spacing and 48 mm (240 mm field scale) slot width were, with one exception[8], maintained as constant. These were fixed in line with the suggested baffle spacing and slot sizing criteria as provided by Armstrong (2002b).

During the design and experiment implementation, rotated-V variations were grouped into two types (See Table 4–1 for the design parameters):

- Rotated-V
- Rotated-V with narrow channel

Although these groupings seemed logical in terms of setup and testing, they have in retrospect made the presentation and analysis of the results more complicated if they are maintained as is. Instead, the results from these experiments will be presented and discussed in terms of the main channel and the narrow channel respectively. The velocity distribution cross-sectional diagrams and accompanying plan diagrams are presented in their entirety in Appendix D.

Main channel In total, five unique main channel layouts were tested, three of which were of the main channel only (Figure 4–13). The other four[9] included the narrow channel (Figure 4–14). The results are analysed under the following theme headings:

a) with and without the narrow channel
b) depth of spot velocity measurements
c) effect of slot size
d) angle of path of ascent (effect of overlap)
e) position of fish entrance/exit

For ease of reference, the list of unique layouts as well as the experiments, using the original experiment name and be it with or without the narrow channel, are listed here:

Arrangement 1 Baffle layout 2

Arrangement 2 Baffle layout 4, LEGO layout 2.5, LEGO layout 2.7

Arrangement 3 LEGO layout 1.14, LEGO layout 1.15, LEGO layout 2.1, LEGO layout 2.2

Arrangement 4 LEGO layout 2.6

Arrangement 5 LEGO layout 1.16, LEGO layout 1.17, LEGO layout 1.18, LEGO layout 1.19

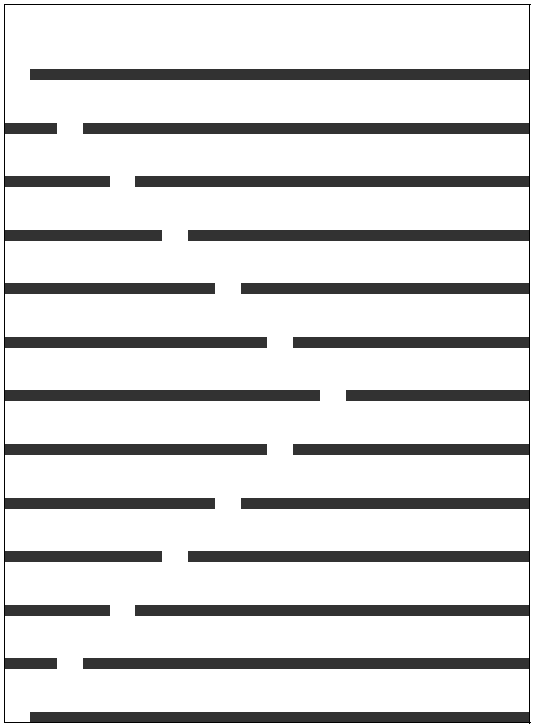

(a) Arrangement 1: Baffle layout 2 (Overlap = 32 mm, Slot width = 32 mm)

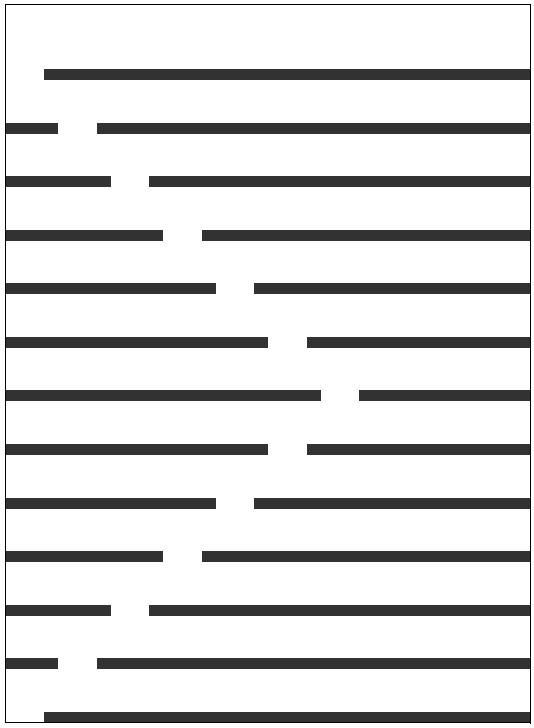

(b) Arrangement 2: Baffle layout 4 (Overlap = 16 mm, Slot width = 48 mm)

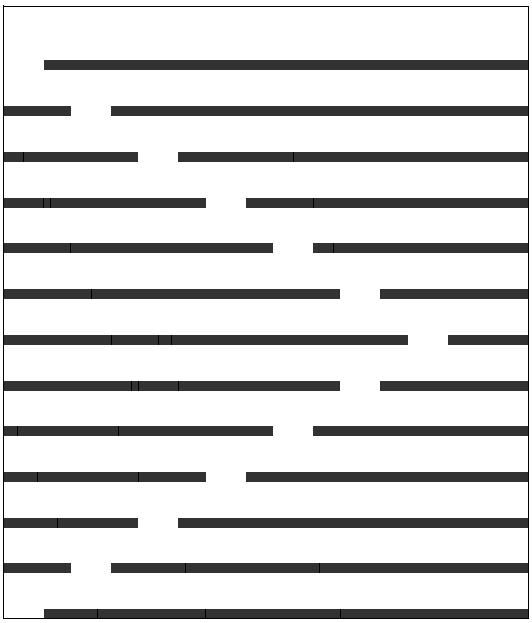

(c) Arrangement 3: LEGO layout 1.14 (Overlap = 32 mm, Slot width = 48 mm)

Figure 4–13: Rotated-V: Plan layouts with the main channel only

[8]For Baffle layout 2 (Figure D–15) the slot width was 32 mm at model scale and 160 mm at field scale.

[9]LEGO layouts 1.15 and 2.6 are also included in this figure, but for reference purposes as the main channel layout is identical to LEGO layout 1.14 and Baffle layout 4 respectively)

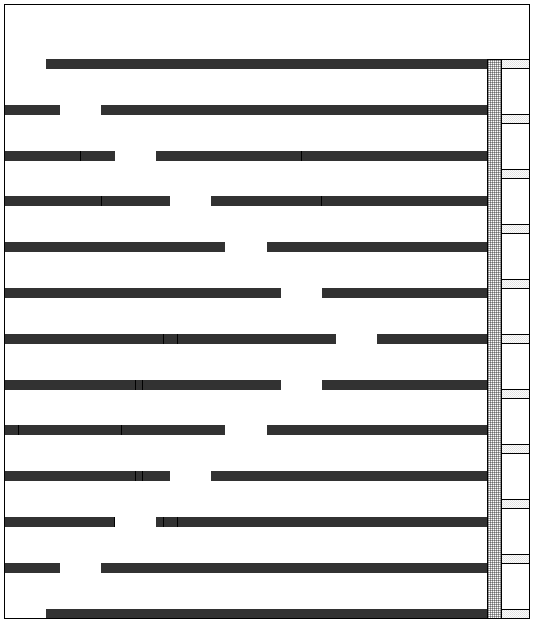

(a) Arrangement 2: LEGO layout 2.5 (Overlap = 16 mm), identical to Baffle layout 4)

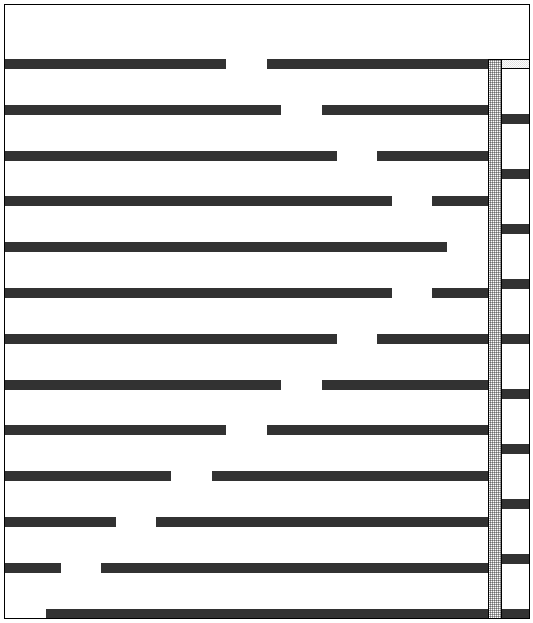

(b) Arrangement 4: LEGO layout 2.6 (Overlap = 16 mm)

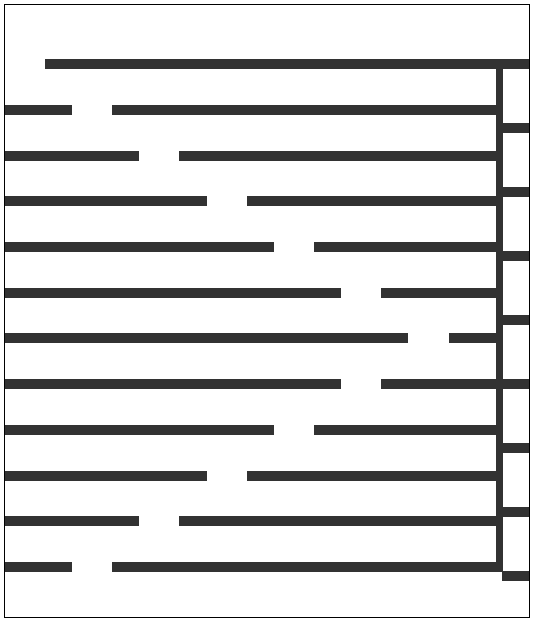

(c) Arrangement 3: LEGO layout 1.15 (Overlap = 32 mm, identical to LEGO layout 1.14)

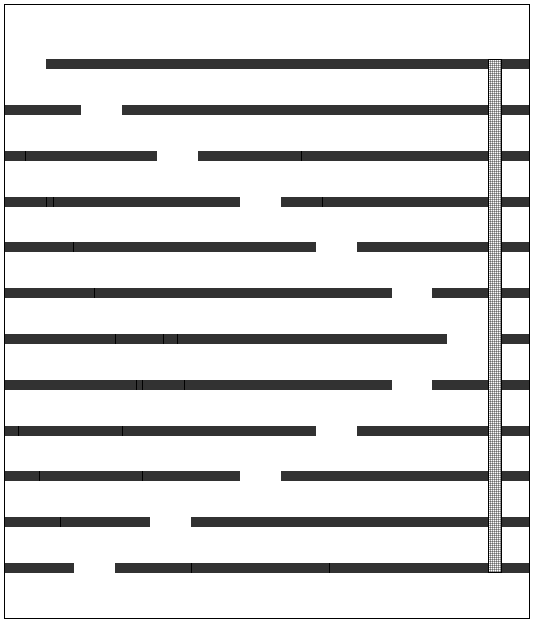

(d) Arrangement 5: LEGO layout 1.16 (Overlap = 40 mm)

Figure 4–14: Rotated-V: Plan layouts with both main and narrow channels

a) With and without the narrow channel As a time and resource saving measure, it was desirable to be able to use the LEGO to make changes to either the main and/or narrow channel. Therefore LEGO layout 1.14 (main channel only) was compared to LEGO layout 1.15 (i.e. identical main channel with the addition of a narrow channel occupying approximately 7% of the main channel) so that the effect of these changes on the spot velocities measured could be assessed.

A cross-sectional comparison of the spot velocities was carried out (see Figure 4–15) at identical coordinates within each slot for both of the chosen layouts. As the measured velocities showed on average a difference of approximately 3% with the introduction of the narrow channel, it was concluded that within the accuracies achieved during the LEGO testing period, it would be possible to simultaneously investigate various main layouts and narrow layouts in the flume.

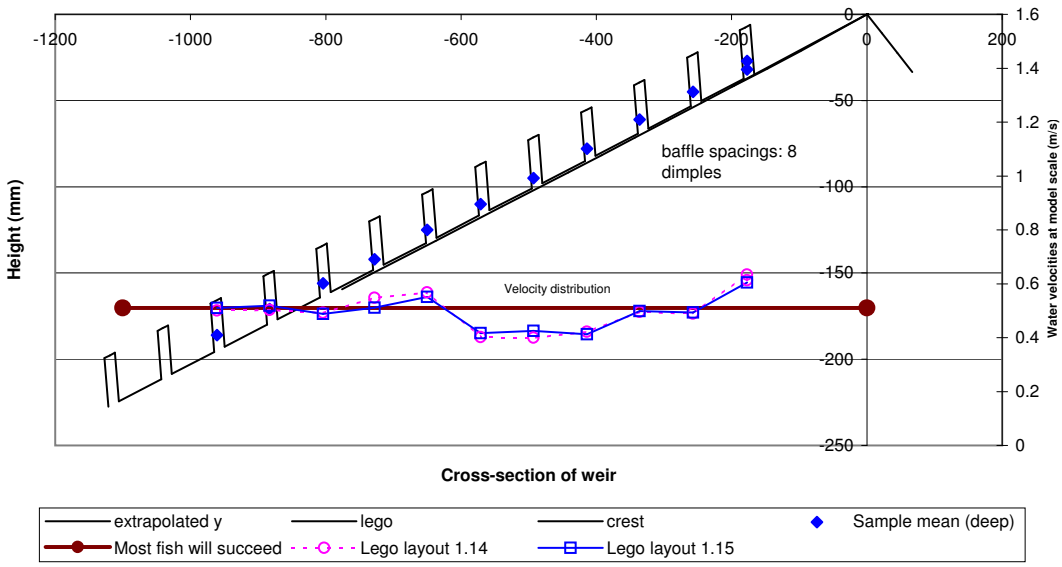

Figure 4–15: Rotated-V: Comparison of spot velocities in an identical main channel, with and without the narrow channel (i.e. for Arrangement 3)

b) Depth of spot velocity measurements An additional consideration was the physical depth of the spot velocities. From the centre channel experiments, the local maximum in a velocity distribution perpendicular to the bed slope in the slot at Baffle 5 was found to occur at approximately 17 mm (Figure 4–5), and it was erroneously assumed that this would also be the case for the diagonal and rotated-V layouts.

Halfway through the rotated-V experiments it was found that the maximum velocities were approximately 7 mm from the bed slope. Figure 4–16 shows the results from a typical rotated-V layout (i.e. Arrangement 3: LEGO layout 1.14 in Figure 4–13) which was used as a testbed to compare the effect of depth on the velocities recorded. In this diagram, 'shallow' implies that the velocity propeller meter (VPM) was at a shallow depth (i.e.17 mm perpendicular to the apron) fairly close to the water surface, while 'deep' (i.e.7 mm perpendicular to the apron) measurements were taken close to the apron floor. The maximum velocities in the slots for the rotated-V layouts were found to be at the 'deep' level rather than the 'shallow' level as had been the case for the centre channel results.

Since the use of the LEGO was primarily as a comparative tool, and because of time constraints it was decided not to repeat all of the experiments (i.e. diagonal and rotated-V layouts) completed up to that date.

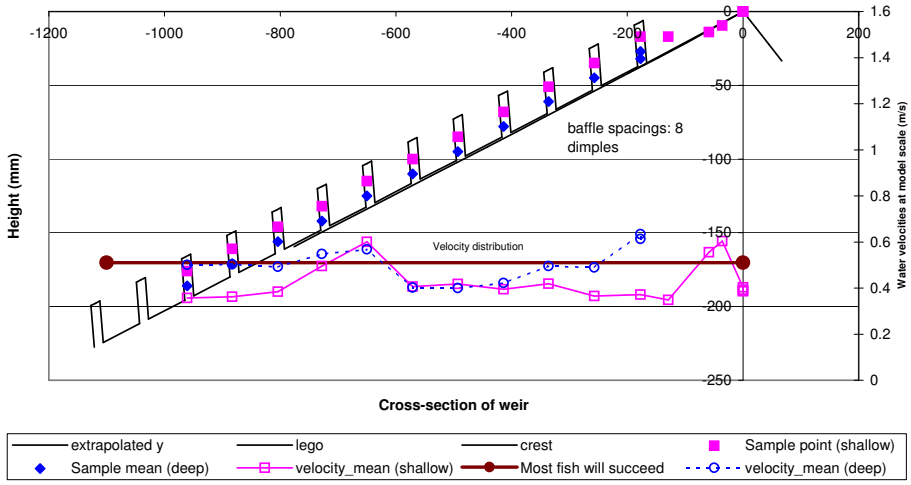

Figure 4–16: Rotated-V: Effect of depth of VPM during spot velocity measurements (using Arrangement 3: LEGO layout 1.14)

The diagonal experiments were all completed at the 'shallow' depth, while the rotated-V experiments have been analysed such that similar spot velocity depths are compared to each other.

c) Effect of slot size The diagonal arrangement trials (Figure 4–12) demonstrated a relationship between slot size and spot velocities. It was observed that increasing the slot size (for a constant overlap) resulted in a decrease in spot velocities down the slope. The purpose of this experiment was to verify if this trend continued.

Figure 4–17 shows the results from Arrangement 1: Baffle layout 2, with a slot size of 32 mm model scale (160 mm at field scale) and Arrangement 2: Baffle layout 4, with a slot size of 48 mm (240 mm at field scale). For each corresponding baffle position on the downstream slope, the larger slot size has a lower spot velocity, which was lower than the maximum velocity criterion in each case. However, these results do not reflect the anticipated higher velocities measured at a 'deep' level closer to the apron floor (see point b) above.

In addition to the reduced velocities achieved by pursuing a larger slot size, Armstrong (2002b) recommended that the minimum free gap in a baffle (i.e. slot size), be at least 200 mm (field scale) to accommodate large adult coarse fish, adult trout and small sea trout. This corresponds to 40 mm at model scale, and therefore the slot size of 48 mm satisfies this criterion.

d) Angle of path of ascent (effect of overlap) Figures 4–18 and 4–19 are summarised by Table 4–3 below, which illustrates that the choice of measurement depth (i.e. 'shallow' or 'deep') plays an important role when comparing slot velocities.

When the overlap distance increases and the path of ascent becomes shallower, velocities measured at the 'shallow' depth increase slightly, whereas those measured at the 'deep' position decrease slightly.

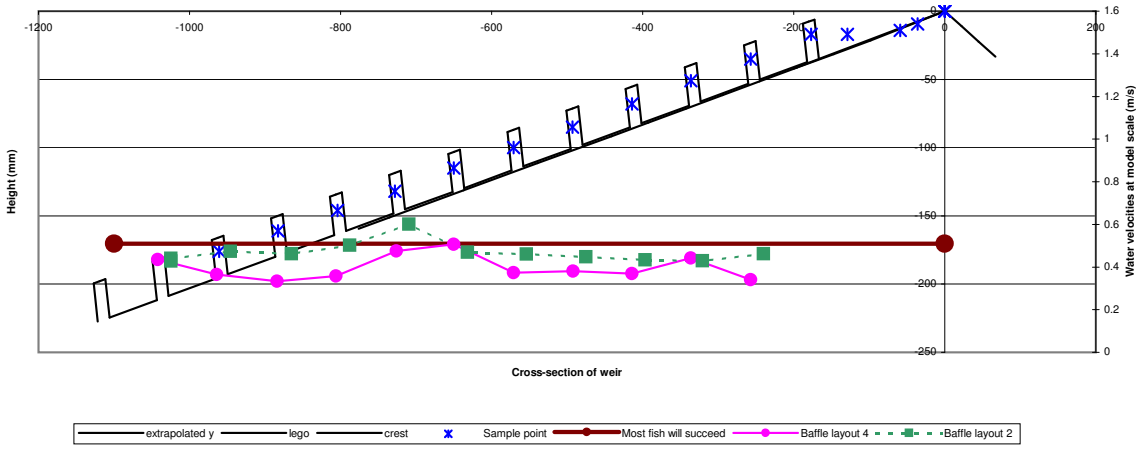

Figure 4–17: Rotated-V: Cross-sectional velocities showing effect of slot size (Arrangement 1: Baffle layout 2 = 32 mm and Arrangement 2: Baffle layout 4 = 48 mm) [Shallow VPM]

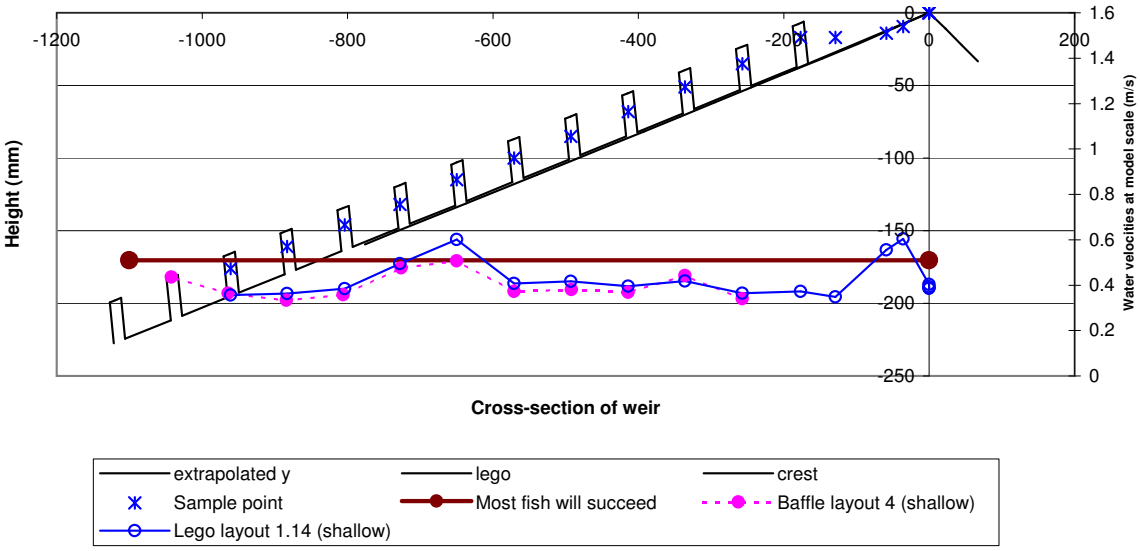

Figure 4–18: Rotated-V: Cross-sectional velocities showing the effect of overlap (Arrangement 2: Baffle layout 4 = 16 mm and Arrangement 3: LEGO layout 1.14 = 32 mm) [Shallow VPM]

Arrangement 5, which represents the largest overlap and the shallowest path of ascent, showed the most promising arrangement as all of the spot velocities measured (i.e. 'deep' level measurements) were below the maximum velocity criterion.

As part of the coarse filtering process used to find a suitable fish passage arrangement as modelled with the LEGO, only the spot velocities in the centre of a slot were routinely measured for the diagonal and rotated-V arrangements. Throughout the testing process, various spot velocities were measured between baffles and to the sides of a slot. As detailed

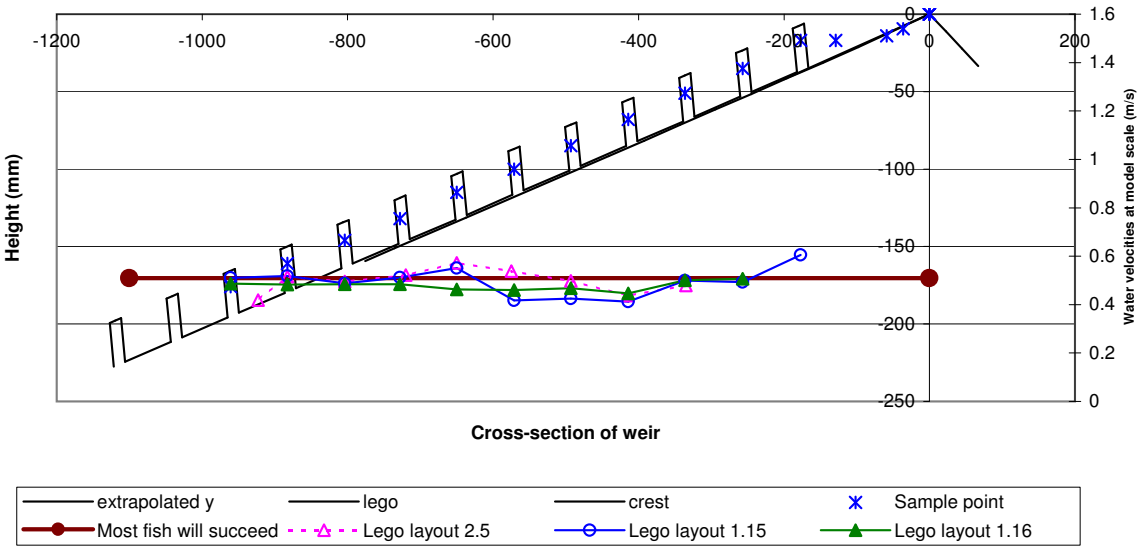

Figure 4–19: Rotated-V: Cross-sectional velocities showing the effect of overlap (Arrangement 2: LEGO layout 2.5 = 16 mm,Arrangement 3: LEGO layout 1.15 = 32 mm and Arrangement 5: LEGO layout 1.16 = 40 mm) [Deep VPM]

Table 4–3: Rotated-V: Effect of overlap as influenced by measurement depth

Arrangement	**Overlap Distance** (mm)	**Velocity comparison**
Depth of measurement: 'shallow'		
Arrangement 2	16	slightly lower on average
Arrangement 3	32	slightly higher on average
Depth of measurement: 'deep'		
Arrangement 2	16	slightly higher than larger overlaps
Arrangement 3	32	slightly lower than smallest overlap
Arrangement 5	40	slightly lower than smallest overlap

velocity distributions for the perspex fish ladder are reported on in section 4.2, these velocities are not reported on in this thesis, although they were included in decision making used during the sifting process used for selecting a suitable fish passage arrangement.

e) Position of entrance/exit Experts generally agree that the location of the entrance and exit of a fish pass is paramount for the success rate of that pass (Clay 1995, Larinier 2002c and Armstrong *et al.* 2004). When considering a single Crump weir on a river, fish would theoretically be able to find the entrance[10] by virtue of typical behaviour where they swim up

[10]The entrance is defined as the downstream approach and the exit is the point where the fish are able to enter into the impoundment. For the Crump weir this implies that the entrance is on the downstream face with the first baffle at the bottom, and the exit is at the top of the crest with

to the toe of a structure and then up and down along the bottom looking for an entrance. The rotated-V layouts have generally been designed such that the first slot of the fish pass would be located at a side wall, although the changing tailwater levels as determined by the discharge, would effectively determine which slot would be the effective bottom of the fish pass. For the compound Crump situation, the fish pass would probably be located on the lowest weir. Thus the position of the entrance slot and corresponding direction of the path of ascent, would then need to be assessed so as to create maximum opportunities for fish to find the entrance slot.

Arrangement 4: LEGO layout 2.6 was the only trial with the exit slot located in the centre of the weir although the entrance slot was located at the side wall of Baffle 13. The parameters of this design effectively changed the location of the reflection slot for the path of ascent from Baffle 7 to Baffle 5. All of the other rotated-V layouts had both the entrance slot (in Baffle 13) and the exit slot (in Baffle 1) located at the side wall, and reflection at Baffle 7. Figure 4–20 shows the results from this trial.

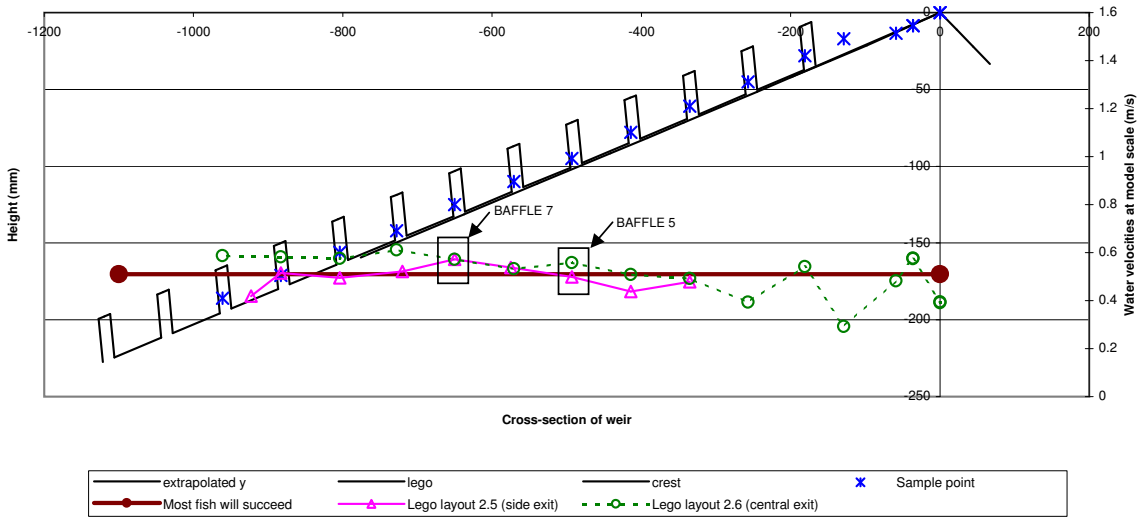

Figure 4–20: Rotated-V: Cross-sectional velocities for choice of fish ladder exit (Arrangement 3 vs Arrangement 4) [Deep VPM]

Firstly, in accordance with the geometric design, a local spot velocity maximum occurred at the reflection baffle (i.e. Baffle 5) for Arrangement 4, and at the reflection baffle (i.e. Baffle 7) for Arrangement 3. Secondly, the velocities recorded downstream of the reflection baffle for Arrangement 4 were greater than the maximum velocity criterion. Because of the greater number of baffles between the entrance (Baffle 13) and this reflection point, these velocities showed a steady increase along the downstream slope.

the last baffle at the top. However, for ease of reference, the baffles have been numbered from the top of the crest.

Using these parameters described above, it was concluded that Arrangement 2 (LEGO layout 2.5) and Arrangement 5 (LEGO layout 1.16) were found to have potential and these were both tested over the wider flow range (section 4.1.4).

Narrow channel The basic pool and weir concepts were used as a starting point for the narrow channel. This was intended as a very low velocity route for the small coarse fish. Armstrong (2002b) recommended that a minimum gap of 150 mm (i.e. 30 mm at model scale) be provided for adult coarse fish, juvenile trout and salmonids, and this was used as a guideline for the channel width. The narrow channel was built to a width of four LEGO studs, which equated to 32 mm at model scale or 160 mm at field scale. A dividing wall between the main channel and narrow channel was constructed of LEGO bricks and was initially one stud (8 mm model scale, 40 mm field scale),and later enlarged to two studs wide[11](16 mm model scale, 80 mm field scale).

Table 4–1 (on page 91) lists the face-to-face baffle distances used for the ten narrow channel experiments. For record purposes, the full set of results from these experiments are given in Figures D–18 to D–28.

For comparative purposes, the plan views for six of these arrangements are shown in Figure 4–21 and the cross-sectional velocities are presented in Figure 4–23. The plan views show the increase in the face-to-face baffle distance (i.e. between Figure 4–21(a) to (e)), with an increase from 32 mm to 96 mm. The height of the baffles was constant at three bricks high.

During these experiments, tracings[12] were made of the flow depths and position of the VPM in the narrow channel. The segment between baffles 2 and 5 for LEGO layout 2.6 as shown in Figure 4–22 is an example of one of these tracings. This figure also highlights the problem of sufficient measurement depth as encountered when measuring velocities in the shallow flow.

In Figure 4–23, an increase in baffle spacing results in a decrease of the cross-sectional spot velocities observed. For clarity and ease of comparison, only maximum velocities measured at or between each baffle are shown in this graph,and the baffles have not been included. For the smallest spacing, most of the flow passed over the top of the baffles, which effectively acted as roughness elements. As the baffle spacing increased from 48 mm to 80 mm, the large circulation eddies typical of streaming flow changed to the weiring flow patterns associated with plunging flow (as depicted in Figure 2–9 and observed in the laboratory as shown in Figure 4–22).

The effect of increasing baffle height for constant baffle spacing was explored for both a 64 mm and an 80 mm baffle spacing, as shown in Figures 4–24 and 4–25 respectively. The baffles used in LEGO layout 1.16 (64 mm spacing) and LEGO layout 1.17 (80 mm spacing) were three bricks high, with the velocities generally at the maximum velocity criterion level. Next, the first baffle was increased to four bricks high while keeping the rest at three bricks.

[11]This dividing wall width was increased because more LEGO bricks, two studs in width, were purchased and it was easier to construct.

[12]As the use of the narrow channel proved inefficient for the higher flow rates, these tracings have not been included in this thesis.

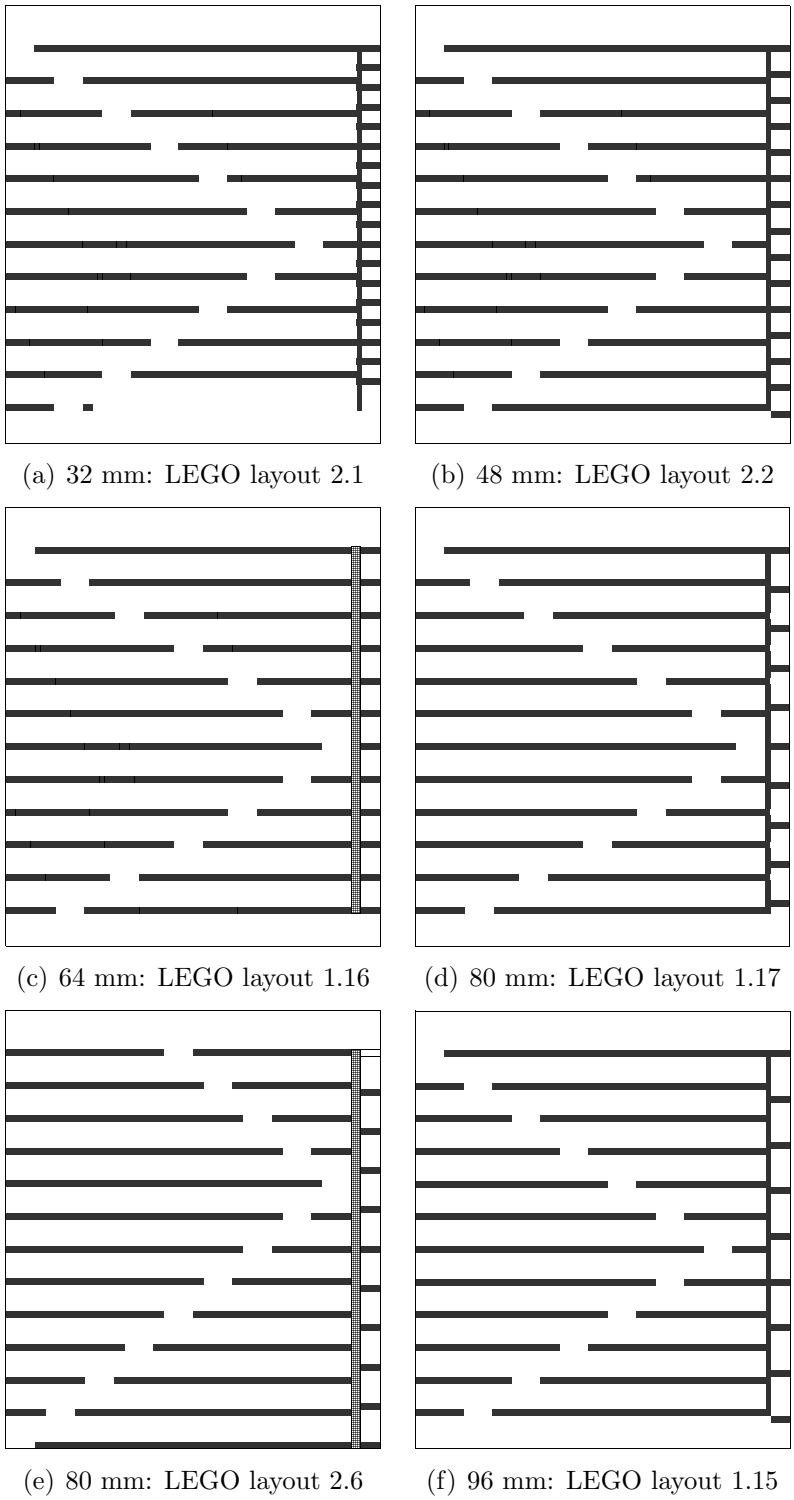

(a) 32 mm: LEGO layout 2.1

(b) 48 mm: LEGO layout 2.2

(c) 64 mm: LEGO layout 1.16

(d) 80 mm: LEGO layout 1.17

(e) 80 mm: LEGO layout 2.6

(f) 96 mm: LEGO layout 1.15

Figure 4–21: Rotated-V: Narrow channel plan views showing increasing baffle spacing

The velocities recorded at Baffle 1 were less than for the constant three brick high baffles. On average, the results for LEGO layout 1.19 (64 mm spacing) and LEGO layout 1.18 (80 mm spacing) showed improvement but the best

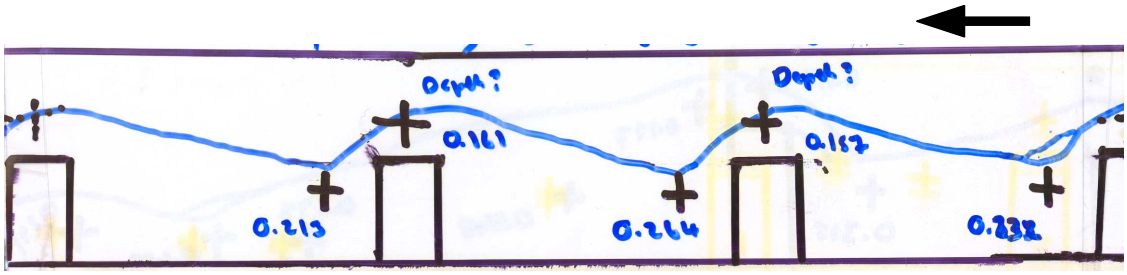

Figure 4–22: Rotated-V: Segment from the velocity and water depth record measured in the narrow channel (LEGO Layout 2.6, baffles 2 to 5)

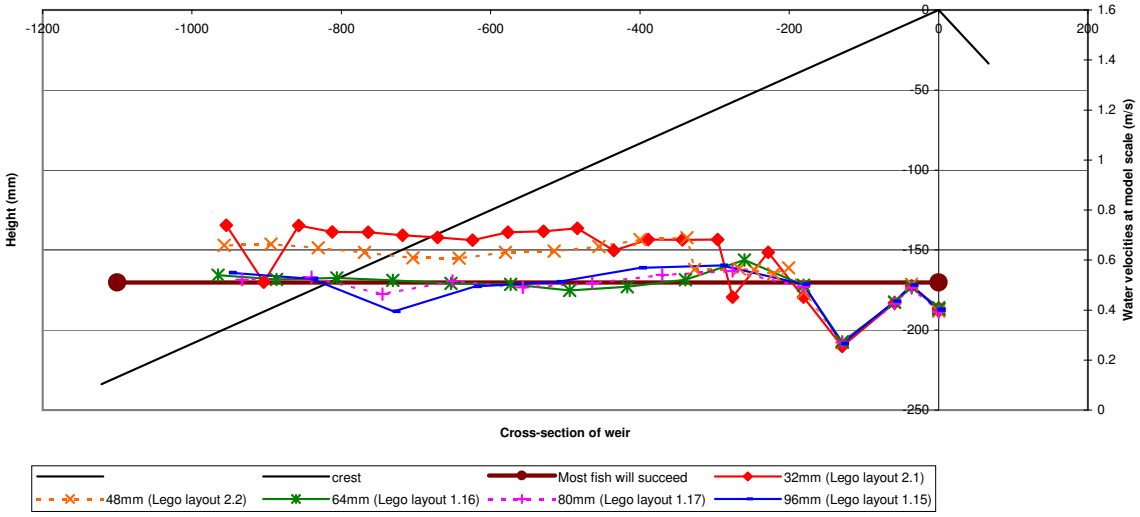

Figure 4–23: Rotated-V: Cross-sectional velocities from all baffle distances in the narrow channel (baffles not shown)

results were obtained by increasing all of the baffles in the narrow channel to four bricks high (i.e. LEGO layouts 2.5 and 2.7).

The improvement between the 'all three bricks' and and the 'all four bricks' high baffles for the 64 mm baffle spacing was in the order of 53%. Similarly, the improvement shown for the 80 mm baffle spacing was 60%. Thus for both spacings, an increase in the baffle height reduced measured velocities in the narrow channel. The underlying reason for this was that the flow rate through the narrow channel had effectively been reduced.

With regards to the narrow channel layout at the 90 percentile low-flow rate, the best arrangement was found to the 80 mm face-to-face four LEGO brick high arrangement.

Category 5: Side gaps

Three slightly different layouts were tested under this category, the typical elements of which are represented by Figure 4–3. In this approach, an open channel, similar

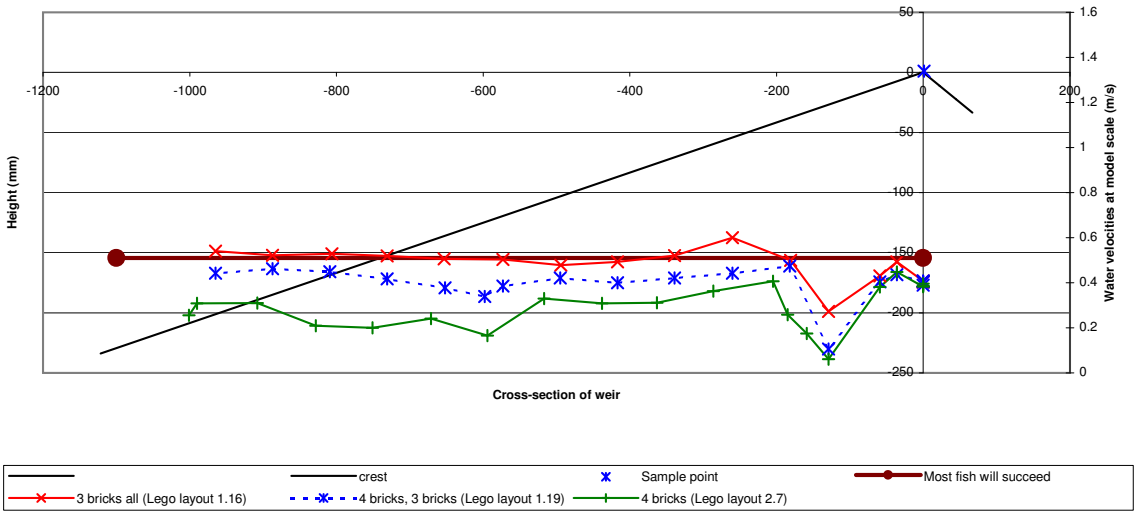

Figure 4–24: Rotated-V: Cross-sectional velocities from 64 mm baffle distances in the narrow channel (baffles not shown)

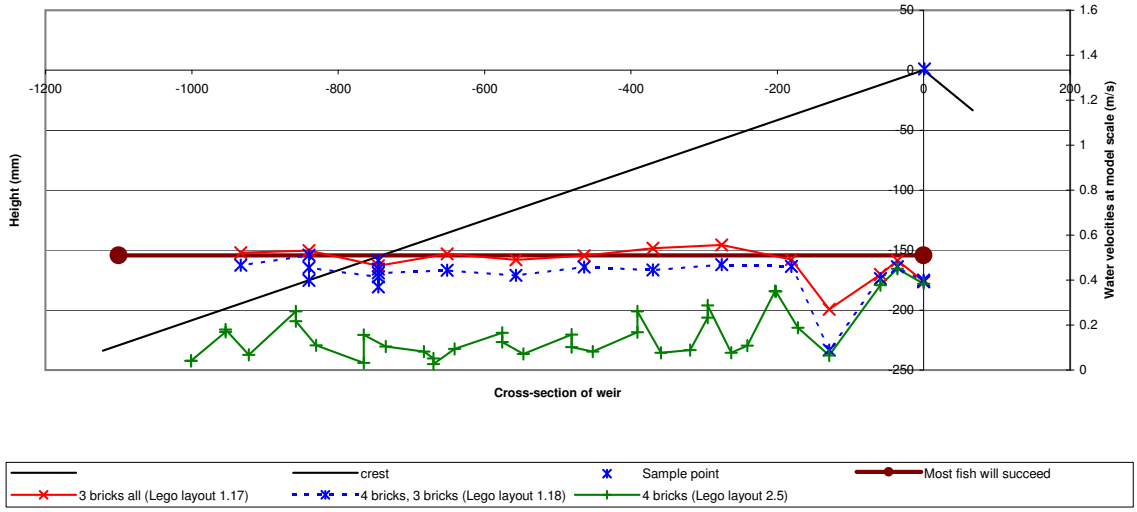

Figure 4–25: Rotated-V: Cross-sectional velocities from 80mm baffle distances in the narrow channel (baffles not shown)

in size to that of the centre channel, was located near one of the side walls. On the other side, a series of staggered slots were located which were intended to be the path of ascent for fish.

Although the velocities in these slots on the side of the weir were fairly low, flow down the open channel portion was extremely high. This resulted in large circulation eddies downstream of the last baffle, creating an erosion risk as well as potential difficulties for fish trying to ascend the weir. As the rotated-V arrangements had provided promising results resulted in more even downstream flow patterns, the side gaps arrangements were not taken further. Figures D–29 to D–33 present the results as part of the record of experiments.

4.1.4. Presentation and analysis of results: refinement of rotated-V arrangement over a larger flow range

Two of the LEGO layouts were chosen from the 90 percentile low-flow experiments to assess the LEGO fish passage performance over a wider flow range. The key flow rates identified for Brimpton weir were the 50 and 30 percentile low-flow (section 3.3.2). Where time and orifice-plate arrangements allowed, extra flow rates (i.e. 10, 25, 60, 70 percentile low-flows) were tested. The experiments[13] carried out during the refinement for the rotated-V layouts are recorded in Table 4–4.

Table 4–4: Rotated-V arrangements over larger flow range: Experiment data records

Exp. No. (LEGO layout)	**Baffle height** (no. of LEGO bricks)	**Baffle spacing** (mm)	**Slot** (mm)	**Overlap** (mm)	**Flow rate** (Percentile low-flow)
Rotated-V and Narrow channel					
6.1	3, 4 narrow	64	48	16	Q25, Q30, Q50
6.2	3, 4 narrow	64	48	40	Q30, Q50
6.3	4 (1st = 3) , 4	64	48	40	Q25, Q30
Rotated-V					
6.4	4 (1st = 2)	64	48	40	Q30, Q50, Q60 and Q70, Q90
6.4(2)	4, additional = 1, 1st =2	64	48	40	Q30, Q50, Q60 and Q70, Q90
6.5	4, 1st = 2	80	48	40	Q30, Q50

The selected layouts were Arrangement 2 (LEGO layout 2.5) and Arrangement 5 (LEGO layout 1.16), which were used as templates for LEGO layout 6.1 and 6.2 respectively although with one major difference. During the setup of these two experiments, the first baffle was placed further downstream then had been the position used throughout the 90 percentile low-flow experiment series (i.e. 236 mm instead of 172 mm from crest to the first baffle upstream face). The purpose for this change was to try to limit the effect of the baffles with regards to non-modular flow.

Although described in the text below, the easiest method of comparison between these different layouts is visually given in Figure 4–26 (as the eye is sensitive to the change in pattern).

The following analysis considers the narrow channel and the main channel cases separately.

Narrow channel As shown in the plan views[14] in Figure 4–26, the LEGO layouts 6.1, 6.2 and 6.3 included the narrow channel. For the narrow channel, the baffle

[13]These tests represent ten laboratory testing days.

[14]As with the 90 percentile low-flow tests, the complete plan and cross-sectional views for the flow range tests are presented in Appendix D.

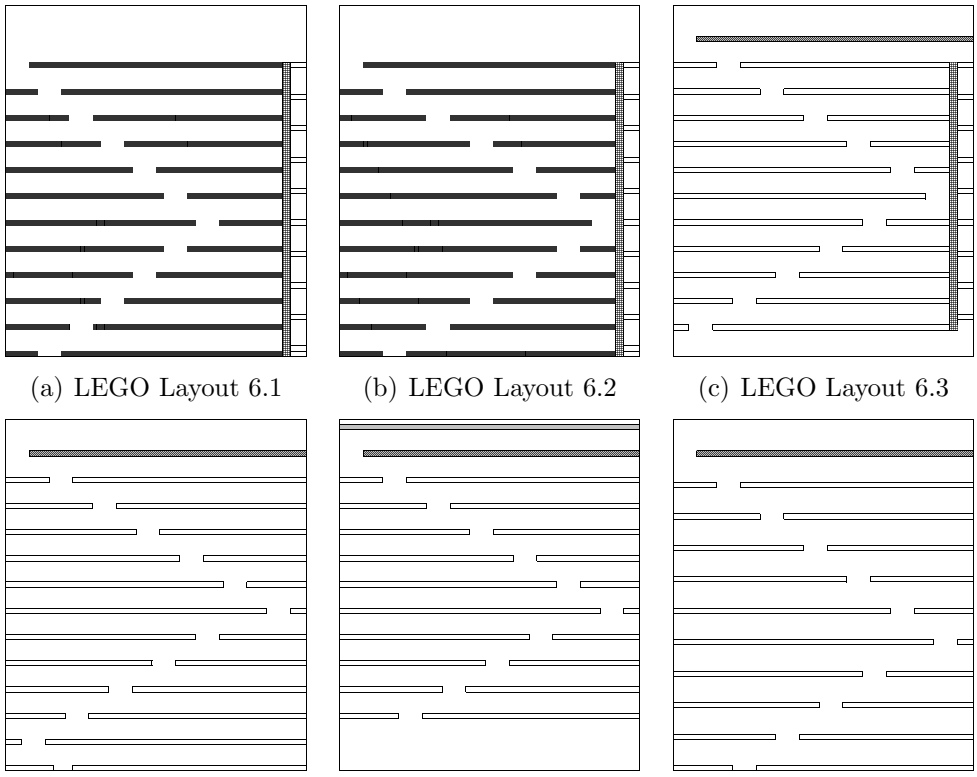

(a) LEGO Layout 6.1 (b) LEGO Layout 6.2 (c) LEGO Layout 6.3

(d) LEGO Layout 6.4 (e) LEGO Layout 6.4(2) (f) LEGO Layout 6.5

Figure 4–26: Range of flows: Rotated-V plan layouts

heights were set to four LEGO bricks[15]. This narrow channel was found to be very effective at the 90 percentile low-flow range and had provided velocities below the maximum velocity criterion.

Figure 4–27 shows the spot velocities measured in the narrow channel for LEGO layout 6.1, where for the 50, 30 and 25 percentile low-flow rates[16], these were found to be well beyond the maximum velocity criterion. (See Figures D–35 and D–36 for LEGO layouts 6.2 and 6.3 results.) Consequently, it was decided to remove the narrow channel as it provided no benefit to lowering the velocities for the higher flow rates.

Main channel For the 90 percentile low-flow rate experiments, all the baffles had been set to a height of three LEGO bricks. However, for the higher flow ranges, velocities in excess of the maximum velocity criterion were observed at all points except for at slot 2. Figure 4–28 shows the spot velocities from the 50, 30 and 25 percentile flows for LEGO layout 6.1.

In LEGO layout 6.2 (Figure 4–29), the path of ascent had been made shallower by increasing the size of the overlap from 16 mm to 40 mm, effectively reducing the velocities. However, as approximately 40% of the spot velocities from the 50 percentile and 30 percentile flow rates still exceeded the maximum

[15]Refer to Table 3–7 for model and field heights of the baffles.

[16]In order to complete the maximum number of experiments, these flow rates represent the range available using the 109.91 mm orifice plate.

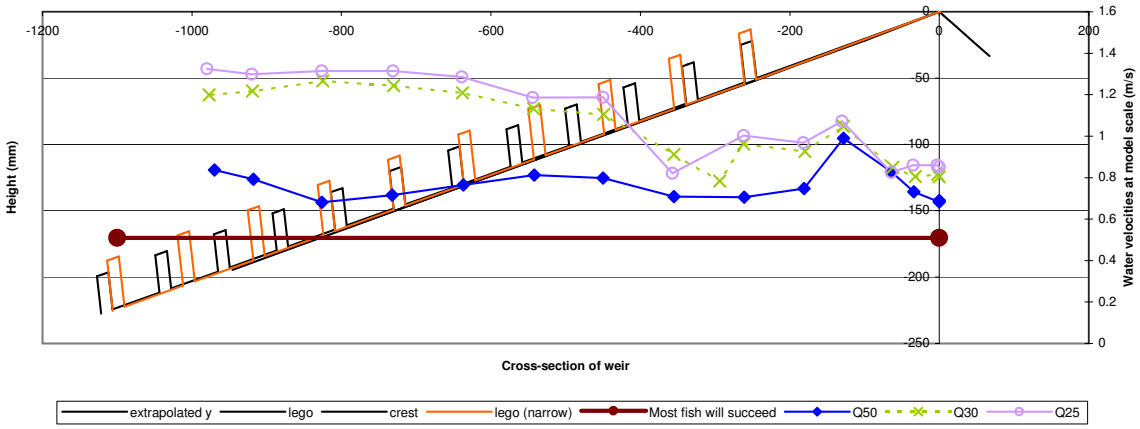

Figure 4–27: Range of flows: Typical velocities recorded in the narrow channel (as for LEGO layout 6.1)

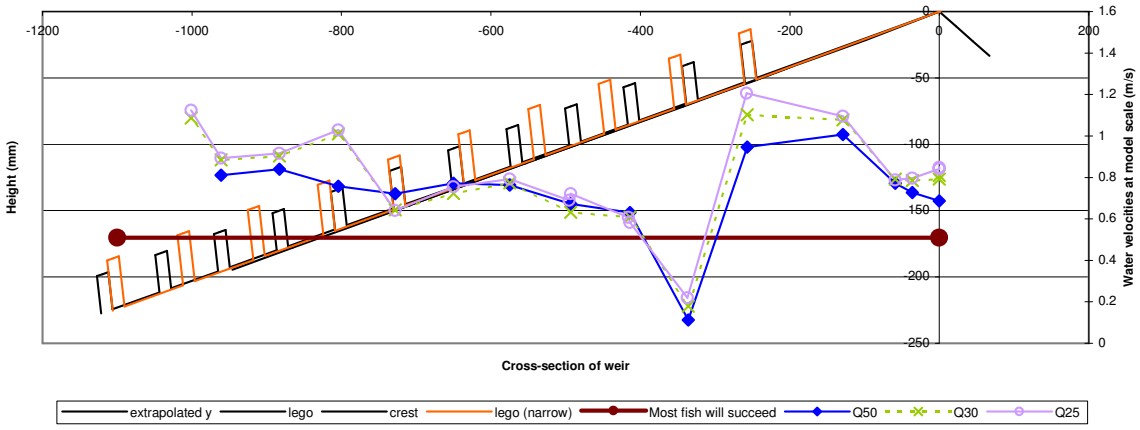

Figure 4–28: Range of flows: LEGO layout 6.1 (i.e. main channel baffles were three LEGO bricks high with a steep path of ascent)

velocity criterion, it was evident that a different approach would be needed. An additional concern was that the spot velocities measured upstream of slot 1 were well in excess of the maximum velocity criterion.

Three approaches were considered and adapted in order to reduce the velocities.

Firstly, a smaller baffle upstream of the first baffle (for LEGO layout 6.2) was introduced[17]. Figure 4–30 shows the results from the trial for a one brick or two brick high first LEGO baffle. Although still higher than the maximum velocity criterion, the addition of the two brick high first baffle reduced the spot velocities.

The second approach was to increase the main channel baffle heights from three LEGO bricks to four LEGO bricks.

[17]As a point of interest, this new baffle was introduced at the same position as all of the first baffles in the layouts tested for the 90 percentile low-flow range.

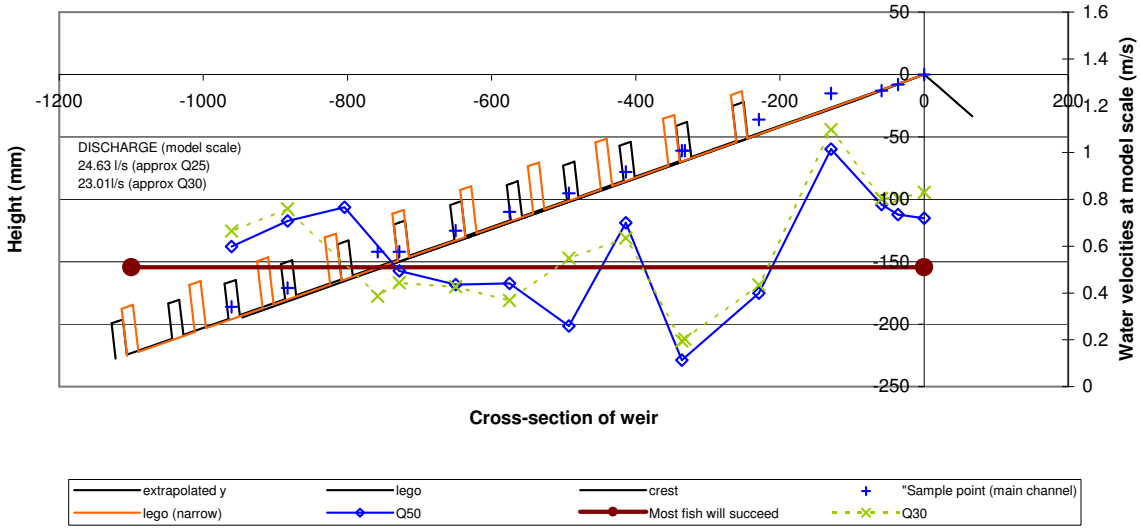

Figure 4–29: Range of flows: LEGO layout 6.2 (i.e. main channel baffles were three LEGO bricks high with a shallow path of ascent)

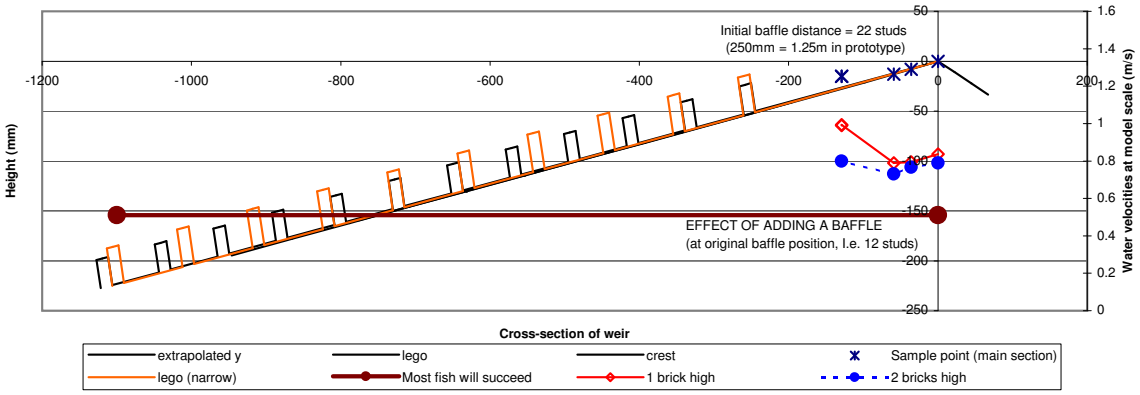

Figure 4–30: Range of flows: LEGO layout 6.2: considering size of first baffle (i.e. main channel baffles were three LEGO bricks high with a shallow path of ascent)

Thirdly, with the original alignment of slot 6 and 8, slot 8 was directly beneath slot 6. This resulted in a transfer of momentum being carried over in slot 8 with associated higher velocities. For example, in Figure 4–29 the model scale velocity in slot 6 was 0.44 ms^{-1} compared with 0.77 ms^{-1} in slot 8 at the 50 percentile low-flow. This represents a 43% increase in velocity for the aligned slots.

LEGO layout 6.3 (Figure 4–31) was thus a combination of these three approaches, where the first baffle was set to three LEGO bricks high, the rest of the baffles were set to four LEGO bricks high, and slot 8 was not aligned with slot 6. The results from this test were encouraging in that the majority of the spot velocities were below that of the maximum velocity criterion for this layout. With regards to the spot velocities, for a 50 percentile low flow, the velocities in slot 6 and slot 8 were 0.36 ms^{-1} and 0.49 ms^{-1} respectively,

representing a 26% increase for aligned slots. Thus the percentage increase was less and the velocities were below the maximum velocity criterion.

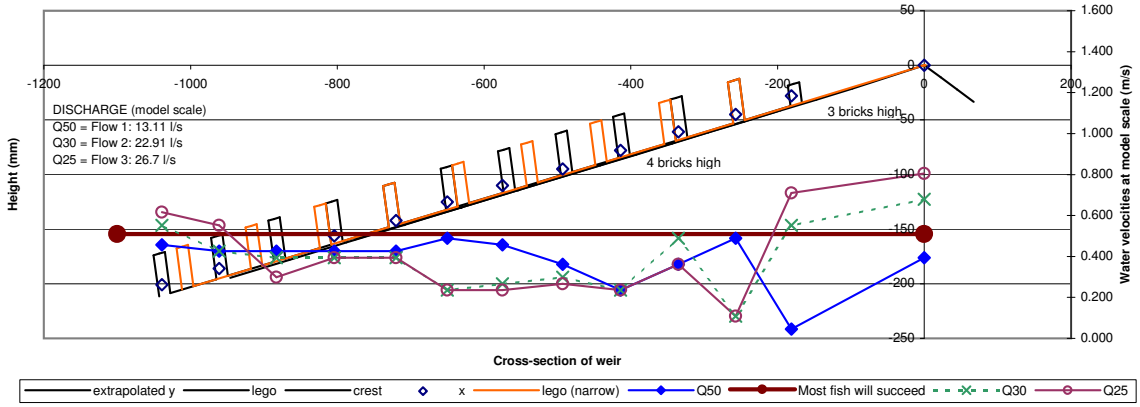

Figure 4–31: Range of flows: LEGO layout 6.3 (i.e. main channel baffles were four LEGO bricks high with a shallow path of ascent)

As indicated previously, the narrow channel was ineffective over the wider flow range and was thus removed at this point. The new layout, with the first baffle set to two LEGO bricks high, was renamed LEGO layout 6.4 (Figure 4–32).

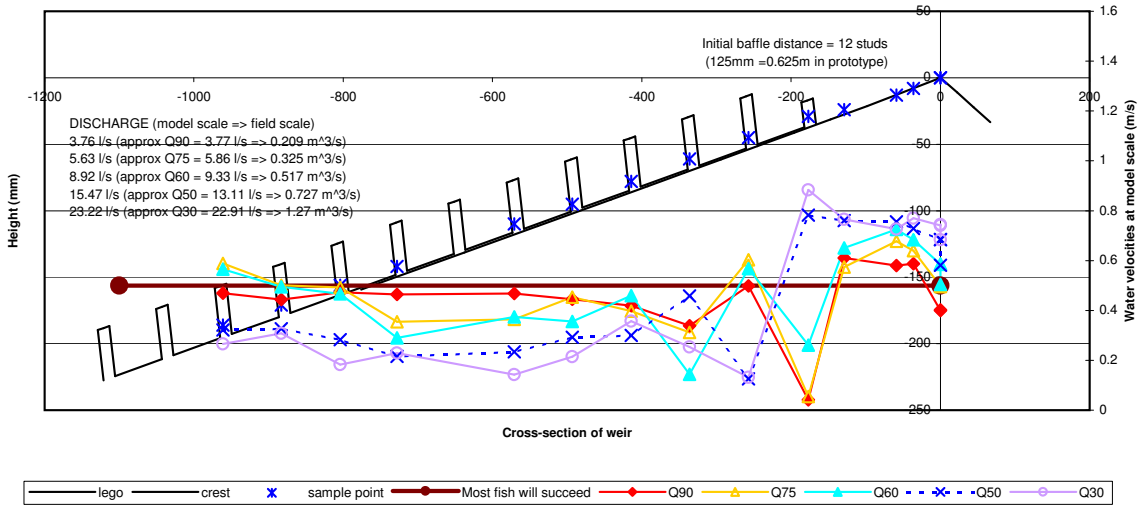

Figure 4–32: Range of flows: LEGO layout 6.4 (i.e. main channel baffles were four LEGO bricks high, first baffle was two bricks high, with a shallow path of ascent)

Additional velocities over the top of the baffles were sampled for LEGO layout 6.4 (see Figure 4–33). The maximum velocity recorded, at model scale, was 1.46 ms^{-1}, representing a field scale value of 3.26 ms^{-1} over the top of baffle 10 for the 30 percentile low-flow. The head on the model weir was 71.6 mm representing 358 mm at field scale, while the position of baffle 10 was at 883 mm at model scale or 4.415 m at field scale. These results compare favourably with the Beach (1984) velocity guidelines for salmon as shown in Figure 2–17. As

an example, for an unmodified weir with a head of approximately 0.35 m, and at a position of 3.5 m downstream of the crest, the expected velocities at that point are in the order of 4.25 ms^{-1}. Although these values are not directly comparable, as the presence of the baffles influences the head on the weir, the predicted velocities for the baffle layout are lower further down the apron.

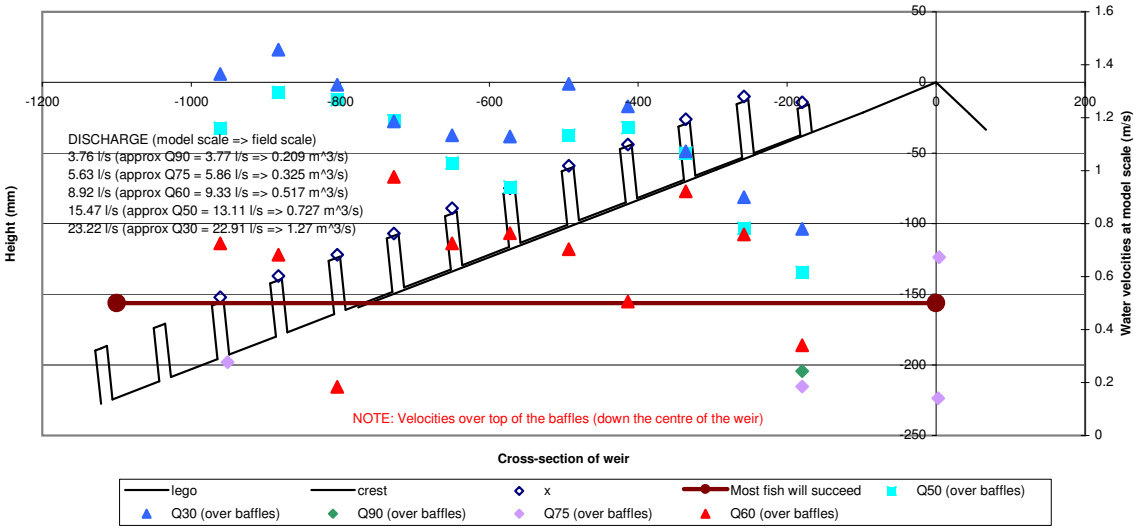

Figure 4–33: Range of flows: LEGO layout 6.4: velocities over top of baffles down centre of weir (i.e. main channel baffles were four LEGO bricks high, with an 80mm baffle spacing, and with a shallow path of ascent)

During the 90 percentile low-flow tests, baffle spacing was one of the parameters investigated and it was concluded at that point that a baffle spacing (face-to-face) of 64 mm was optimal. LEGO layout 6.5 was designed with an 80 mm baffle spacing to determine if this still held true for the wider flow range under investigation. As shown in Figure 4–34, the spot velocities in slots 4 to 6 (i.e. between -400 and -800 mm on the x-axis at model scale) were higher than the maximum velocity criterion at the 50 and 30 percentile low-flow rates. Thus in comparison, the 64 mm baffle spacing (used in LEGO layout 6.4) was lower. As this baffle spacing complied with baffle sizing guideline (Armstrong 2002b) described above, this spacing was maintained in the more detailed analysis described in section 4.2.

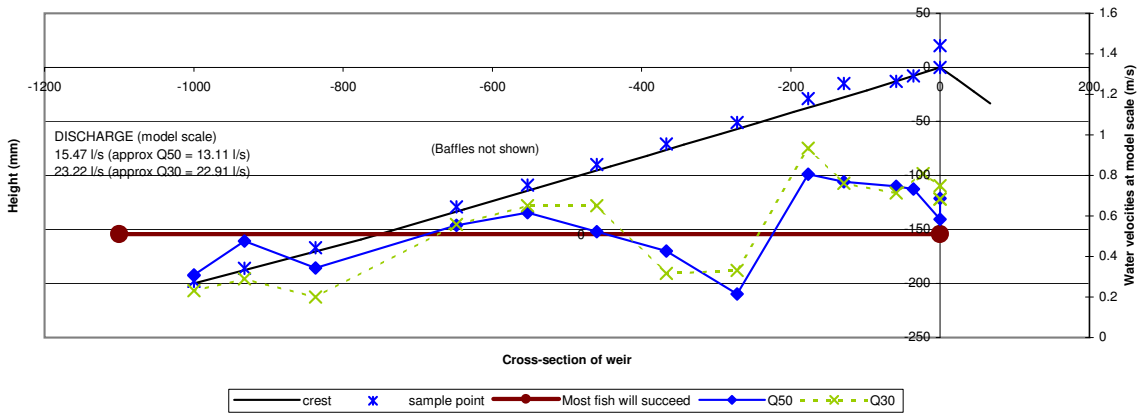

Figure 4–34: Range of flows: LEGO layout 6.5 (i.e. main channel baffles were four LEGO bricks high with a shallow path of ascent)

4.1.5. Preferred arrangement based on LEGO trials

Figure 4–35 shows a schematic diagram of the preferred layout based on LEGO layout 6.4. This layout was used as a starting point for the perspex baffles discussed next.

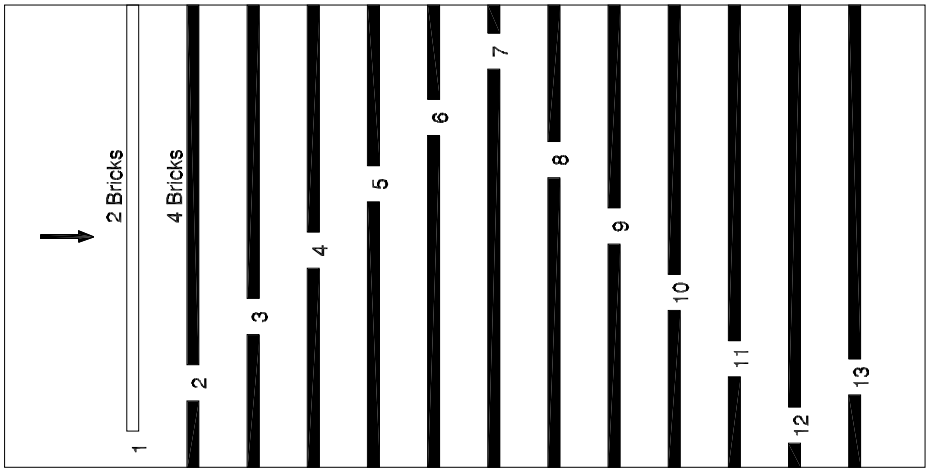

Figure 4–35: Preferred layout identified using LEGO over wider flow range, based on LEGO layout 6.4 (Overlap = 40 mm, slot width = 48 mm, baffle spacing = 64 mm)

4.2. Perspex fish pass experiments

As the preferred fish pass arrangement, LEGO layout 6.4 was selected as the main pattern for further trialling. A detailed description of the model (Figure 3–21) and the experimental procedures for the perspex fish pass trials have been presented in section 3.3.

4.2.1. Order of presentation of results

One of the primary goals of this research project was to be in a position to compile a set of guidelines for the modification of a Crump weir to improve fish passage. With this in mind, the main focus of the perspex fish passage experiments was to perform a detailed analysis of the flow conditions found on the downstream slope of a modified Crump weir, and therefore predict the suitability of these modifications for potential fish passage. The Swimit Excel spreadsheet (Environment Agency 2001b, 2003) provided the burst swimming speeds of coarse fish based on the species, size and water temperature required as input for a fish pass efficiency matrix method used to determine this potential.

As described in section 3.3, the perspex fish pass was fabricated to test two scenarios, A and B. When the first baffle and second baffle are equal in height (i.e. both 40 mm at model scale and 200 mm at field scale), this has been referred to as the 'equal baffle pairing' or Scenario A. Scenario B, also called 'unequal baffle pairing', refers to the arrangement where the first baffle is smaller than the rest of the baffles (i.e. 24 mm compared to 40 mm at model scale and 120 mm compared to 200 mm at field scale).

Table 4–5 provides an overview of the parameters and the flow rates at which they were tested during the perspex fish pass trials.

Table 4–5: Perspex fish pass trials: overview of experiments

Trial	**Normal flume**		**Tilted flume**
	Equal	Unequal	Unequal
Free surface profiles	90, 50, 30, 10	90, 50, 30, 10	90, 50, 30, 10
Flow visualisation		50	
Velocity distribution	90, 50	90, 50, 30, 10	50 slot 11: 90, 30, 10
Debris analysis	no	yes	no

Key : 90, 50, 30 and 10 = percentile low-flow rates

In this thesis the results have been presented with specific reference to the Brimpton weir hydrology (see section 3.3.2). However, in drawing up the guidelines (Rhodes and Servais 2006) these results need to be presented in terms of the 'flow rate per unit width' which allows for a more general application. Table 3–9 in section 3.3.2

provides the Brimpton data in terms of model flow, field flow and the generalised flow rate per unit width. The contour-plot velocity distribution diagrams presented in Appendix E also includes this information.

In this section on the perspex fish passage experiments, the results have been presented in the following fashion: Model scale free surface profiles are given and discussed (section 4.2.2), followed by a flow visualisation analysis (section 4.2.3). The velocity distributions are presented and discussed at field scale, for ease of comparison with the fish swimming data (section 4.2.4). As a specific case study, the 50 percentile low-flow (unequal baffle pairing, normal flume) was selected and the velocity distribution and accompanying fish pass efficiency matrices for the each slot in the fish pass are given and analysed. Because the velocity distribution measurements were extensive, only the problem slot velocity distributions, associated matrices for the rest of the flow rates, as well as typical distribution trends, have been presented in the main body of this thesis. The majority of the results have been presented in Appendix E as part of the full laboratory record. Finally, the results from the debris analysis trials are given and analysed (section 4.2.5).

4.2.2. Free surface profiles

The free surface profile measurements were taken at regular intervals along the path of ascent in the x-axis direction and in the centre of each slot (Figure 4–36). This plan diagram is not to scale and is thus representative of both the equal and unequal baffle pairing. The free surface flow profiles are plotted on Figure 4–37 at model scale. The discussion and analysis is presented under the following themes:

a) use of wave probe technology

b) unequal baffle pairing

c) equal baffle pairing

d) swimming depth criterion

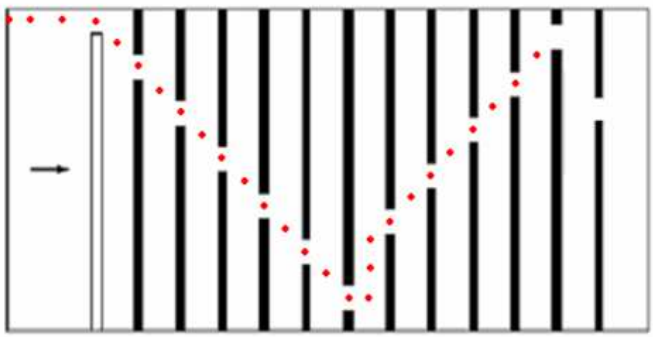

Figure 4–36: Typical path of wave probe data set

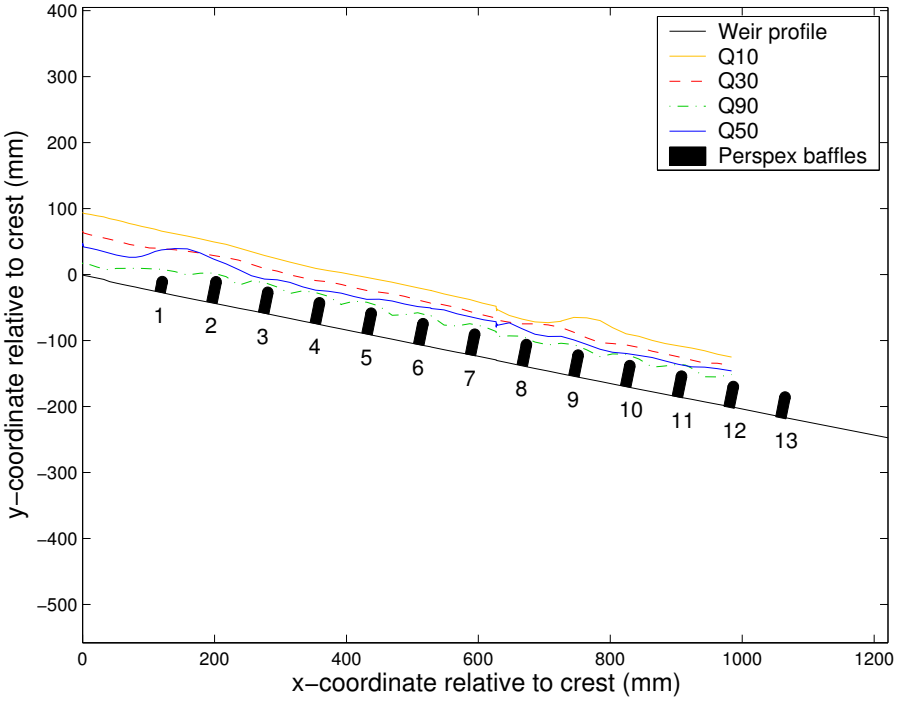

(a) Unequal baffle pairing (24 mm and 40 mm)

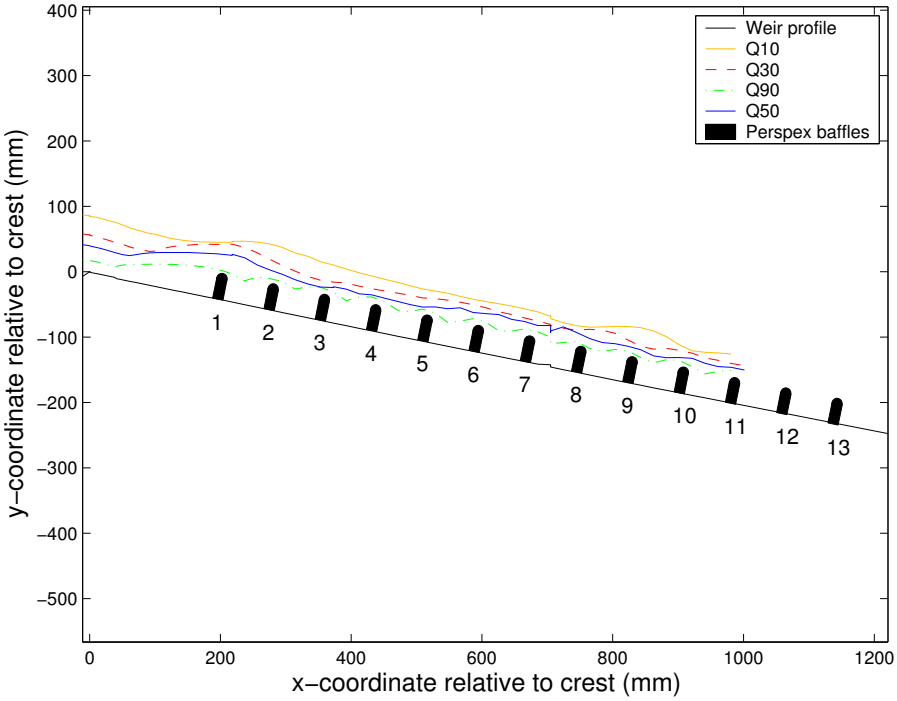

(b) Equal baffle pairing (40 mm and 40 mm)

Figure 4–37: Comparison of free surface profiles

a) Use of wave probe technology The free surface profile measurements were taken using the wave probe technique described in section 3.2.4. This method was fast and easy to use, and provided an accurate and repeatable method for recording free surface profiles.

The free surface profiles were measured ±1000mm from the crest, which was the limit of travel for the traverse gear. The tailgate was kept down as far as practical such that these profiles were not affected by the tailwater levels caused by this gate.

b) Unequal baffle pairing Figure 4–37(a) reflects the scenario where the first baffle is smaller than than the second baffle. The 90 percentile low-flow data illustrates the weiring action between baffles typical of plunging flow as observed for this flow rate. The effect of the first baffle is visibly evident for the 90 and the 50 percentile low-flow rates, while less of an impact is observed near the crest for the 30 and 10 percentile low-flows. At the 10 percentile low-flow profile, the free surface appears to be roughly parallel to the apron floor until between 600 mm and 800 mm, where a small standing wave is observed.

Digital photographs (Figures 4–38 to 4–41) taken while the flow was seeded[18] for the DigImage analysis trials provide a visual record of the free surface profile, from baffles 8 to 12, for each flow rate. The DigImage footage and the video footage taken for the purposes of the debris analysis provided an alternative means for keeping a record of typical free surface phenomena observed. Appendix F gives a summary of the footage contained in the DVD included at the back of this report. Further comment with regards to flow visualisation has been made in section 4.2.3).

The wave fronts observed on the downstream side of the apron tended to occur at a constant position relative to a specific slot location for a given flow rate. Figure 4–38 for the 90 percentile low-flow provides a clear illustration of the position of the wave fronts.

d) Equal baffle pairing In Figure 4–37(b), very similar free surface profile shapes, when compared to the unequal baffle pairing, occur for each corresponding flow rate. There were differences with regards to the location of the wave crests in terms of distance down the apron. However, this difference can probably be ascribed to the fact that the baffles themselves are further downstream in the equal baffle pairing. For the 10 percentile low-flow for example, the free surface appears to be roughly parallel to the apron until between 700 mm and 900 mm, where a small standing wave is observed. For both the equal and unequal baffle pairings, this small standing wave occurs at Baffle 9 in each case.

Swimming depth criterion Downstream of the first baffle position, both the equal and the unequal baffle pairings resulted in thickened flow exceeding the requirements from Armstrong (2002b) (i.e. 200 mm at field scale or 40 mm at model scale for adult coarse fish and juvenile trout and salmonids). At the 90 percentile low-flow rate, the flow upstream of the first baffle was deeper than for the unmodified weir, but still less than the minimum requirements. However, it is unlikely to be the water depth which would be the prohibiting factor at this point, as the section upstream of the first baffle is where the

[18]Seeding is the process whereby the pliolite (resin) used for particle tracking is introduced into the flume using a funnel upstream of the flume flow straighteners.

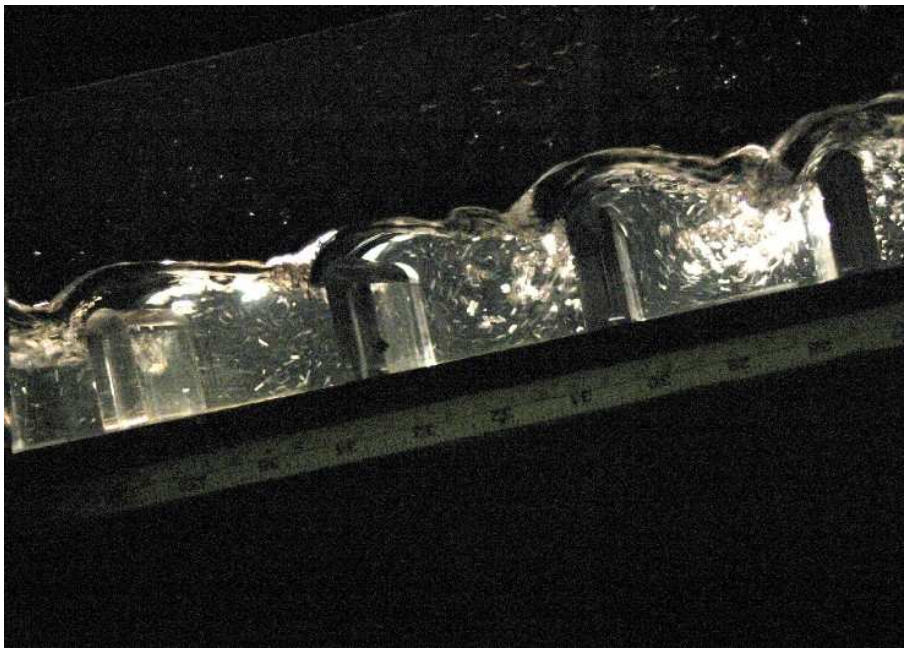

Figure 4–38: Free surface profile: unequal baffle pairing at the 90 percentile low-flow rate (baffles 8 to 12)

Figure 4–39: Free surface profile: unequal baffle pairing at the 50 percentile low-flow rate (baffles 8 to 12)

highest velocities are found. For the higher flow rates, this flow depth was thickened.

Change of downstream, gradient Because the weir, the traverse gear and measurement systems were integrated onto the flume frame, they were tilted as

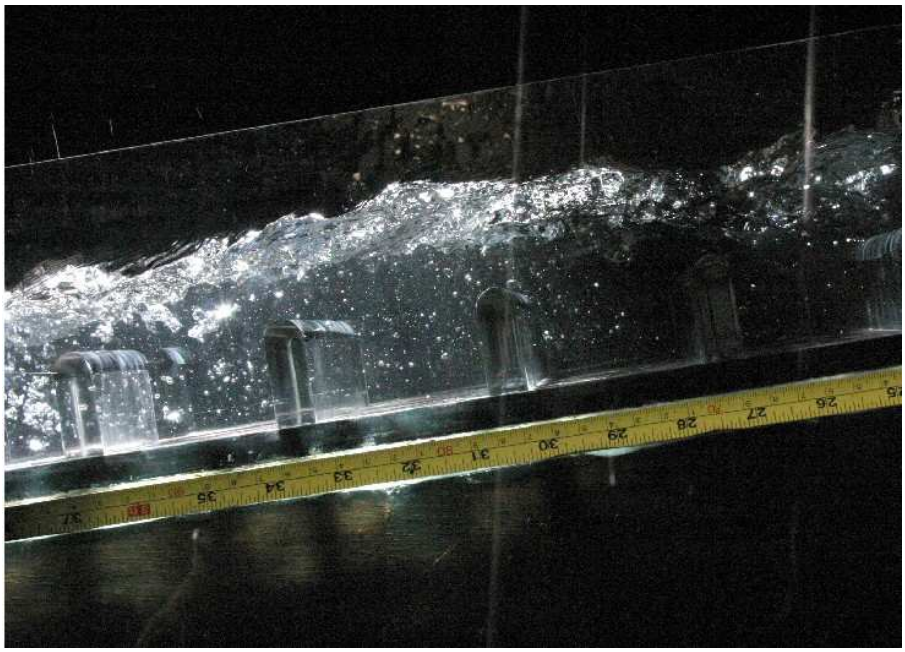

Figure 4–40: Free surface profile: unequal baffle pairing at the 30 percentile low-flow rate (baffles 8 to 12)

Figure 4–41: Free surface profile: unequal baffle pairing at the 10 percentile low-flow rate (baffles 8 to 12)

a unit to the maximum possible rotation of the flume in order to represent a non-standard slope of 1:4.55. This had the additional benefit of allowing the existing equipment and C-programs to be used directly.

Figure 4–42 shows the free surface profiles from both the normal and the

tilted flume positions plotted on the same axis[19] for the four flow rates under consideration. Attention is drawn to the fact that this is a distorted axes system, since if the axes are drawn equally (as those in Figures 4–37(a) and (b)) the difference in free surface levels is not clear (i.e. x increments are not equal to the y increments). For ease of reference, the position of the baffles has been indicated.

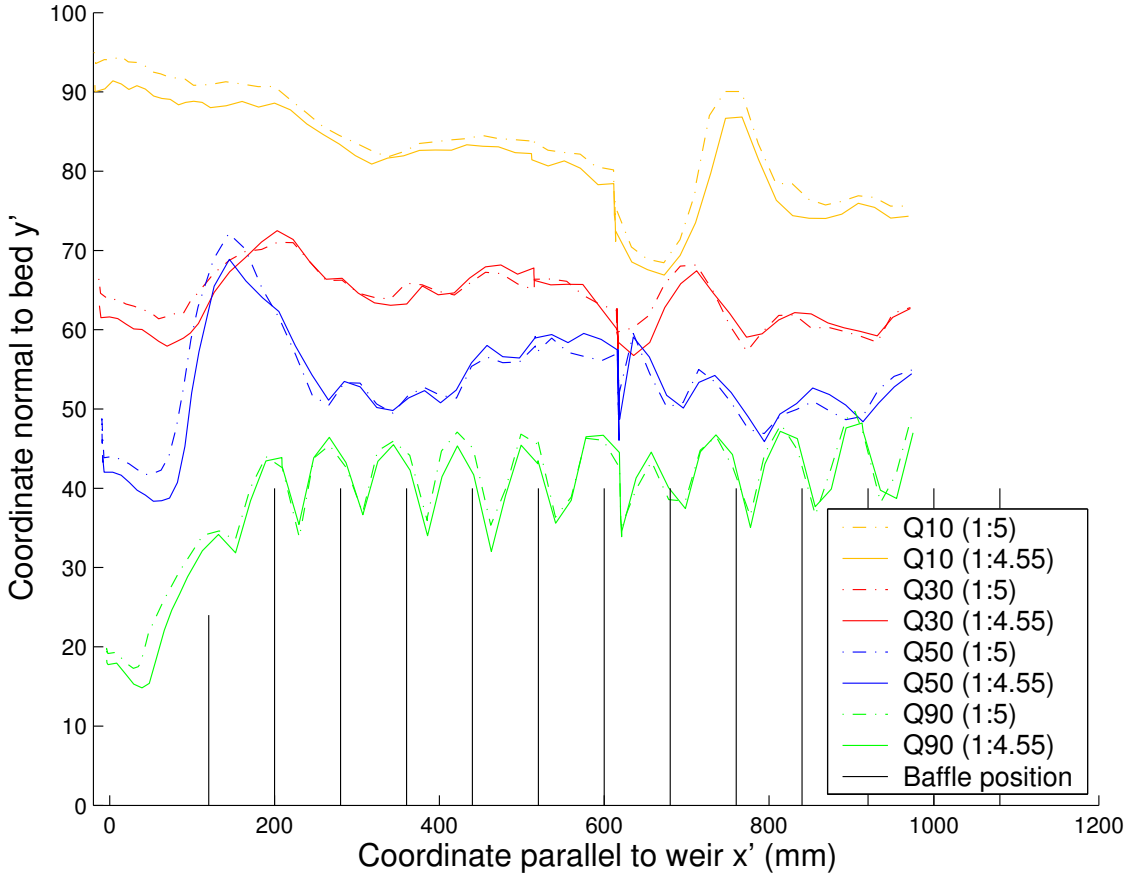

Figure 4–42: Free surface profiles: Effect of downstream slope, gradient change (1:4.55 vs 1:5)

For all four flow rates, the free surface profile is shallower upstream of the first baffle for the steeper slope (i.e. tilted flume) condition. The maximum deviation occurs upstream of the first baffle for 90, 30 and 10 percentile low-flows. For the 90 percentile low-flow rate, there is ± 30% difference, and as the flow rate increases, so this deviation decreases, from ± 17% for 50 percentile low-flow to ± 6.5% for the 30 percentile low flow. For the 10 percentile low-flow rate, two local maxima of ± 4% occur: the first is upstream of the first baffle and the second is above Baffle 9.

Therefore, except for the 90 percentile low-flow, from a fish swimming depth point of view, the increase in downstream slope still falls well within the sug-

[19]In both cases, the x coordinates are plotted parallel to the weir (x') and the y coordinates are plotted normal to the bed slope (y').

gested guidelines of 40 mm model scale (200 mm field scale) for coarse fish and juvenile salmon (Armstrong 2002b).

4.2.3. Flow visualisation results (using DigImage)

At the outset of this research project it was envisaged that the available DigImage, particle tracking software and accompanying hardware, would be useful in capturing velocity data (Rhodes 2001). For this reason, the preferred fish pass was prefabricated with black perspex base and clear baffles to allow for the required background finish. The base thus provided a dark background for contrast, whilst the baffles were constructed of clear perspex so that particles could still be followed in cross-section.

The equal and unequal baffle pairings were to have been tested using the DigImage setup. The unequal baffle pairing was initially installed and various attempts were made to capture useful video footage required for the particle tracking analysis process[20].

A number of problems were encountered with the DigImage system. Firstly, flow downstream of the third baffle resulted in a highly agitated flow surface which effectively precluded particle tracking downstream of this area because of surface water reflections. Secondly, there was a great deal of air entrainment, and the resultant small bubbles were not dissimilar to the seeding particles. Thirdly, although footage was captured upstream of the first three baffles, the velocities were still quite high. The analysis required particles to be matched and tracked through four successive frames but at best tracking was only achieved between two frames. In addition, the velocities encountered on the downstream slope proved to be higher than DigImage was capable of handling. Flow was also highly turbulent, and the particles moved swiftly in and out of the light sheet, further complicating an already difficult matching process.

A positive outcome of the DigImage experiments was that video footage suitable for flow visualisation was captured. Appendix F provides a key to the footage included in the DVD attached to this report. Although both the 70 percentile and 50 percentile low-flow rates were filmed, useful footage was determined amongst other things by surface water reflection, the number of particles visible within the flow, and lighting conditions. Only the 50 percentile data provided useful results:

Plan view Footage was captured for the plan view, where the light beam was set parallel to the apron and located from baffles 1 to 3. Figure 4–43 shows the resultant sketch[21]. Jet flow structures were visible in each of the slots, whilst turbulent flow eddies were visible between baffles. This footage proved the potential for the use of the PT-ST arrangements for velocity measurements in the slots and over the top of the baffles where streamlines were most likely to

[20]The setup of the equipment, CCTV camera, installation of the perspex baffles, light sheet etc. (i.e. excluding the analysis attempts) took two people ten laboratory days.

[21]The sketch maintains the direction of flow from the video footage, which shows the flow from right to left. The crest of the weir is thus on the right hand side.

be parallel. Slot placement had a direct impact on the flow patterns observed in between those baffles immediately downstream of each slot.

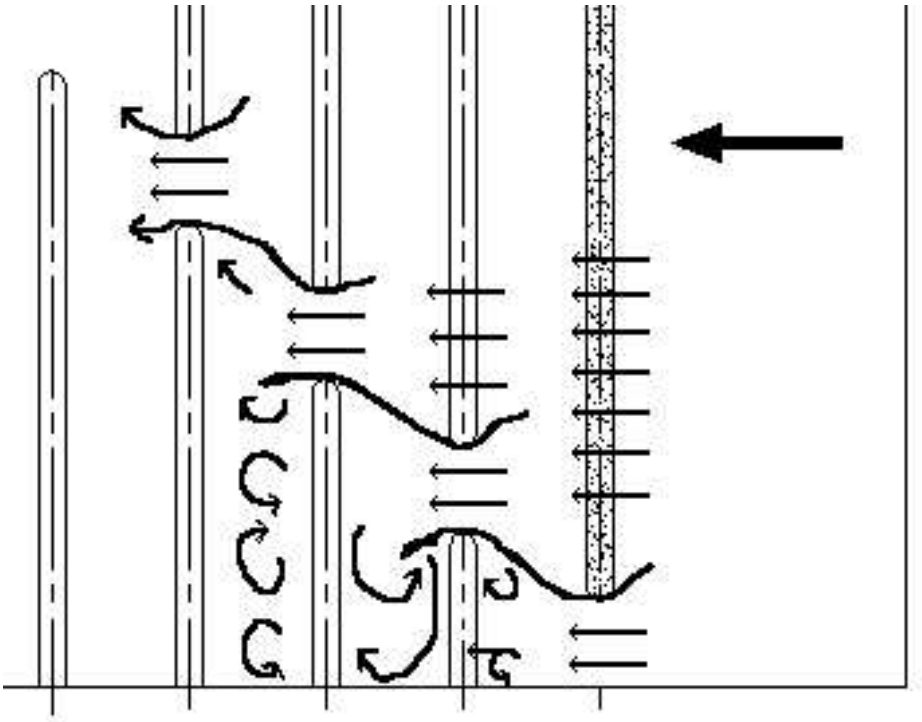

Figure 4–43: Flow visualisation sketch: Plan view from DigImage, for the unequal baffle pairing at a 50 percentile low-flow (Baffles 1 to 5)

Section The video footage, normal to the apron, was captured from the crest to Baffle 2 (light directed through Slot 1), and from Baffles 1 to 3 (light directed through Slot 2). Figure 4–44 shows a digital photograph taken during the former setup (i.e. from the crest to Baffle 3, light through Slot 2), with the flow visualisation arrows superimposed, as observed from the video.

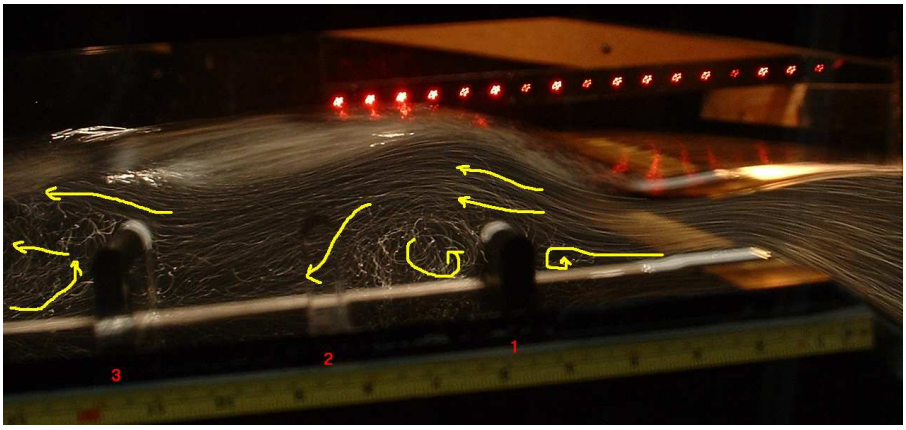

Figure 4–44: Flow visualisation sketch: Cross-sectional view of the unequal baffle pairing at a 50 percentile low-flow (Baffles 1 to 3)

Streamline flow occurred over the crest until the first baffle was reached, whereupon small rotational eddies were observed. The effect of the light sheet positioned at Slot 2 was to highlight flow patterns upstream of the first baffle where flow was impeded by the presence of that baffle. Rotational flow, typical of streaming flow mechanisms was observed upstream of that first baffle. Flow between Baffles 1 and 2, and upstream of Slot 2 showed streamline flow between the baffles, leading into jet flow through Slot 1, as indicated by the position of the light sheet.

4.2.4. Velocity distribution results and analysis of fish passage potential

The methodology behind the presentation of the velocity distribution results as well as the establishment of a fish passage efficiency matrix for predicting successful fish passage has been given in section 3.3.2. Table 4–5 (section 4.2.1) summarises the flow rates used.

As part of the detailed analysis of the flow phenomena, slot velocities were recorded in such a manner as to obtain velocity distributions useful in assessing the passing capability of each slot of the rotated-V fish pass, and therefore the fish pass in its entirety. In order to be effective, the fish pass needed to be passable at each slot individually, as well as collectively and in addition to the entrance and exit conditions of the fish pass.

The entrance (i.e. downstream conditions) has not been measured, as these conditions are tailwater dependent. Velocities in the slots at the downstream end of the apron are affected by the position of the hydraulic jump. Because the tailwater levels were purposely kept low so as to ensure general applicability of the results, velocities were not related to field scale values and consequently not of interest. Under normal operating conditions of a Crump weir, an hydraulic jump is generally designed to occur on the downstream slope of the weir. Thus the velocities at Brimpton specifically would be less than the more severe conditions observed in the laboratory. For general purposes, it is assumed that the fish which would benefit from the fish pass would be capable of reaching the downstream end of the apron (i.e. the fish pass entrance position). It is also assumed that the addition of the baffles on the downstream apron would not cause downstream velocities to become more adverse than if the fish pass was not installed.

Exit velocities (i.e. at the crest of the weir) have been measured and the velocity diagrams are accompanied by a cross-section marking the position of the measurements that are included in the analysis. For the preferred fish passage experiments, d/l was set equal to 0.2 which implies that the baffle height was set at the same level as the crest. This level ensured that velocity reduction in the slots was reduced as far as possible without raising the crest unduly (i.e. by making the baffle higher than the existing crest). By placing the first baffle such that $d/l = 0.2$, both the water depth and the velocity distributions were found to be the most challenging conditions encountered by the fish rather than conditions further down the slope. Although the fish pass arrangement has been designed with the maximum burst speeds in mind, fish are considered to be able to attain instantaneous speeds that are higher than burst speed velocities for very short periods of time (Armstrong

2003a, 2006). It is expected that fish would be able to exploit these speeds in order to surmount the final distance between the first baffle and the crest.

Table 4–6 lists those slots included and analysed within the main body of this report. In this table, 'equal' refers to the 'equal baffle pairing', where the first baffle height was set equal to the rest of the baffles. In the same manner, 'unequal' refers to the 'unequal baffle pairing', where the first baffle height was smaller than the rest of the baffles. For experiment record purposes the majority of the field-scale contour-plot velocity distributions and the accompanying fish passage efficiency matrices are presented in Appendix E. Since fish swimming speeds and water temperature are related, two fish pass efficiency matrices were calculated in each case although only 15 °C tables have been presented in the body of the thesis.

Table 4–6: Perspex fish passage trials: problem slots

Percentile	**Normal flume**		**Tilted flume**
low-flow	Equal	Unequal	Unequal
90	1	OK	OK (Slot 11)
50	6, 8	3, 6, 7	3, 7
30	N/A	OK	OK (Slot 11)
10	N/A	OK	OK (Slot 11)

see Case Studies F and G for problematic slots

see Appendix E for satisfactory results

Selected results from these experiments, which represent the general trends, are presented as the following case studies:

Case Study A Reynolds number verification

Case Study B Comparing a depth-averaged velocity mean with a contour-plot velocity distribution in a slot as a means of determining a predicted fish passage efficiency matrix

Case Study C Slot by slot contour-plot velocity results for the unequal baffle pairing arrangement (1:5 downstream slope, 50 percentile low-flow)

Case Study D Height of first baffle

Case Study E Velocities measured over the tops of the baffles

Case Study F Worst performing slots over experiment flow range (for 1:5 gradient)

Case Study G Effect of changing the downstream slope from 1:5 to 1:4.55

Case Study A: Reynolds number verification

As discussed in section 3.1.4, the Reynolds numbers were assessed to check that sufficiently large channel Reynolds numbers (i.e. > 2000) were obtained at model scale.

Relevant model scale slot statistics are provided in Table 4–7, with the addition of the water depth levels which give an indication of the actual water depth as opposed to the sample depth considered. Model scale Reynolds numbers were calculated using a slot depth-averaged velocity mean and the hydraulic radius (based on the sample depth). The field scale mean velocity is used in Case Study B.

The smallest (depth-averaged velocity and water depth at model scale) Reynolds number from the velocity distribution range of experiments[22] was produced at slot 1 of the unequal baffle pairing, with a downstream slope of 1:5, and at a 50 percentile low-flow. The Reynolds number was 4160, which compared to a calculated field scale Reynolds number of 48210.

Table 4–7: Unequal baffle pairing, Q50, Reynolds number, normal

	Model scale					Field scale
Slot No.	Water depth mm	Sample depth mm	Hydraulic radius mm	Mean velocity ms^{-1}	Reynolds No.	Mean velocity ms^{-1}
1	63.09	36.85	13.86	0.55	7571	1.23
2	64.83	36.85	14.52	0.63	9199	1.41
3	51.14	21.70	11.39	0.80	9246	1.80
4	50.26	21.70	11.39	0.78	8948	1.73
5	53.28	26.60	12.61	0.80	9415	1.78
6	57.08	26.61	12.61	0.76	9327	1.70
7	56.23	26.61	12.61	0.71	8703	1.59
8	51.36	41.31	15.17	0.66	9690	1.47
9	51.23	24.59	12.14	0.65	7979	1.45
10	49.68	24.59	12.14	0.77	9551	1.73
11	48.83	24.59	12.14	0.75	9189	1.67
12	NaN	31.51	13.61	0.73	10185	1.64

The flow physics were dominated by the free surface effect and therefore Froude number scaling was employed in the physical modelling of velocities and flow rates. As shown in Table 4–7, Reynolds numbers were high enough to represent fully turbulent flow, in which Reynolds number effects on scaling up would be of secondary importance.

[22]This was the smallest Reynolds number recorded for all of the slot-based velocity distribution experiments conducted on the preferred fish passage fabricated from perspex.

Case Study B: Comparing the mean velocity for a slot with the contour-plot velocity distribution

Table 4–7 includes the mean slot velocity at field scale for the unequal baffle pairing, for a 1:5 downstream slope and a 50 percentile low-flow. Slots 1 to 3 are considered for this case study.

One method of determining the suitability of flow within a slot for fish passage is to calculate the mean velocity (Armstrong 2006). This is then compared to the burst speed for the fish under consideration and used in drawing up a fish passage efficiency matrix. This technique for determining the success/failure of a specific fish has been described in section 4.2.4.

For comparative purposes with the (field scale) contour-plot velocity distributions used in this report, the (field scale) mean velocities, water depth and sample depth have been recorded on a cross-section through each slot in Figures 4–45(a) to 4–47(a).

Figures 4–45(b) to 4–47(b) show the accompanying fish pass efficiency matrices as calculated using the mean velocities for each slot and assuming a 15 °C water temperature. As described in section 4.2.4, in order to record a pass (black square) on the fish pass efficiency matrix, the following inequality is required: $FCA < RA$[23].

Figures 4–45(c) to 4–47(c) show the contour-plot velocity distribution at each slot, whilst Figures 4–45(d) to 4–47(d) show the fish pass efficiency matrices calculated using the measured velocities (converted to field scale). The flow phenomena observed are at each slot are described in Case Study C.

For the purposes of this case study, it is the comparison between the the fish pass efficiency matrices using the two different velocity approaches which is important. Thus the exact details of which fish are predicted to pass or fail are not relevant.

In all three slots, the fish pass efficiency matrices (graphs labelled (b)) calculated using the mean velocities predicted that fewer fish would be successful at a particular slot than would be the case using the more detailed contour-plot velocity distributions (graphs labelled (d)). The difference between the two methods is a result of the fact that the mean velocity method does not make provision for the possibilities of fish to exploit lower micro-velocity areas.

When compared to all of the experiments conducted, Slot 3 (Figure 4–47), at 50 percentile low-flow, for the 1:5 downstream slope and for the unequal baffle pairing showed the worst performance in terms of predicted fish passage. This slot is an example where the sample depth was shallow when compared to the measured water depth (137.9 mm compared to 285.7 mm at field scale). Retrospectively, this particular slot and flow rate should have had a deeper sample depth. However as the method used in analysing the velocity distribution had not been derived at that point in the experimental phase, this short-coming was not picked up at the time.

[23] FCA = 'fish cross-sectional area' based on fish length, and RA = 'representative area' where water velocity was less then burst speed. For the mean velocity method, the RA was taken to be the slot width × sample height.

The main reason for the shallow sample depth was the need for the Pitot tube - static -tube (PT-ST) arrangement to be submersed at all times, and sufficient care was taken to achieve this goal. (At times this procedure was in conflict with the goal of measuring velocities from the bed to the top of the baffle since the selected measurement depth was dependent upon the physical water level (flow dependent), any fluctuations and a possible perceived effect of air entrainment upon the instrumentation.)

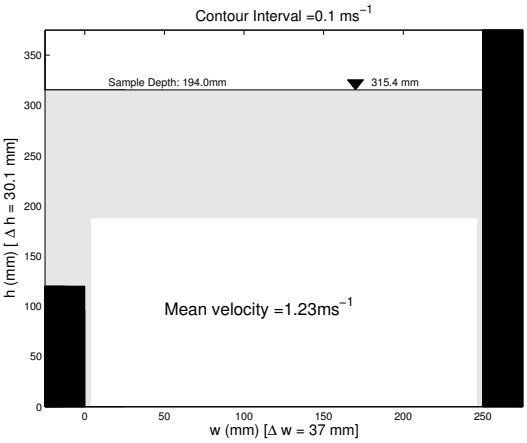

(a) Mean velocity

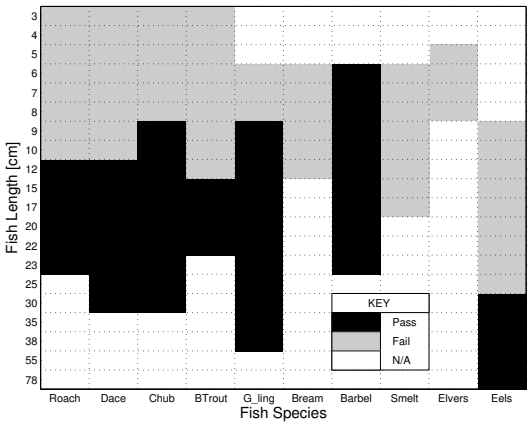

(b) Fish pass efficiency matrix (using mean velocities)

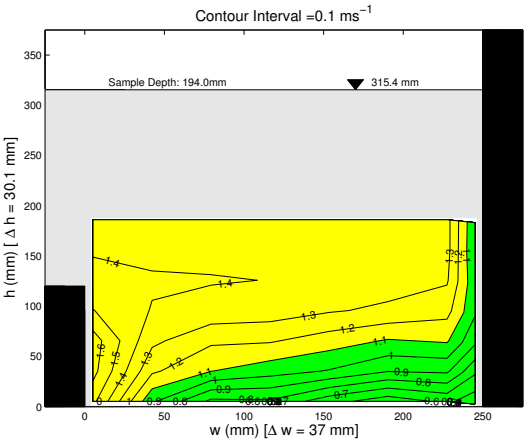

(c) Contour-plot velocity distribution

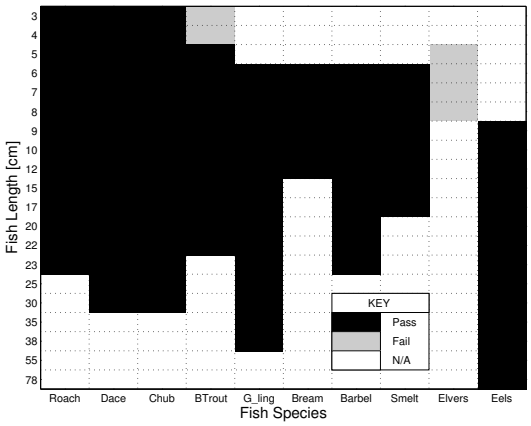

(d) Fish pass efficiency matrix (using measured velocities)

Figure 4–45: Comparison of mean velocity and contour-plot velocity distribution fish passage efficiency matrices (Slot 1)

Because the fish pass efficiency matrix method is based on the burst swimming speeds from the Swimit database (Environment Agency 2001b, 2003) and compared to laboratory measurements scaled up to field scale, this prediction method still needs to be verified in a field trial. As it does not take the instantaneous speeds[24] into account, more fish then predicted should theoretically be able to pass. As

[24]Instantaneous speeds are those speeds attained by fish which are higher than burst speeds but can only be sustained for very short periods of time. Burst speeds are always measured over a 20 second time period.

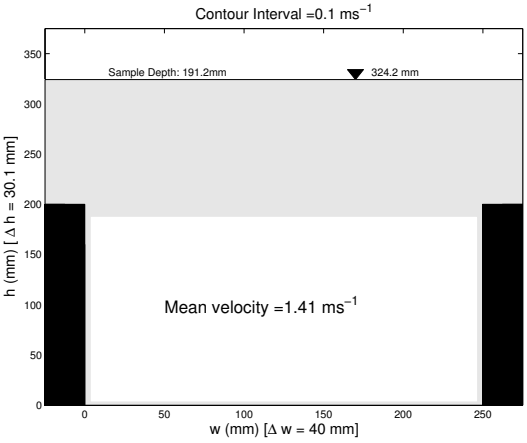

(a) Mean velocity

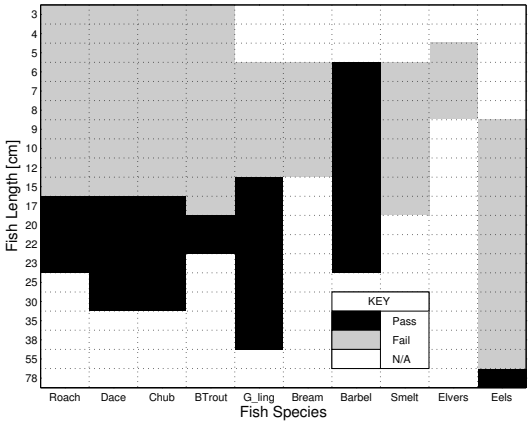

(b) Fish pass efficiency matrix (using mean velocities)

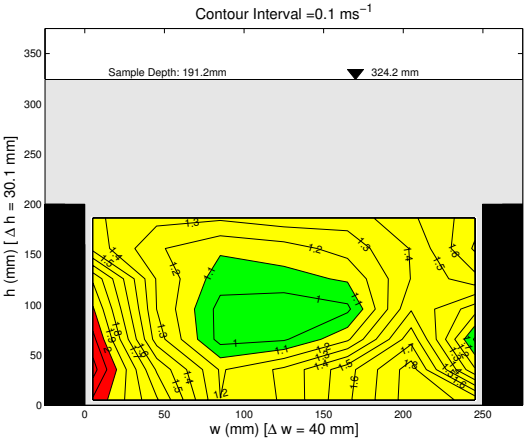

(c) Contour-plot velocity distribution

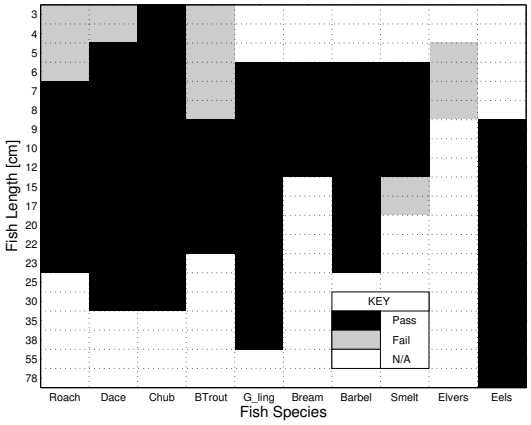

(d) Fish pass efficiency matrix (using measured velocities)

Figure 4–46: Comparison of mean velocity and contour-plot velocity distribution fish passage efficiency matrices (Slot 2)

this matrix is being used as a design tool, this shortcoming is seen as being on the conservative side.

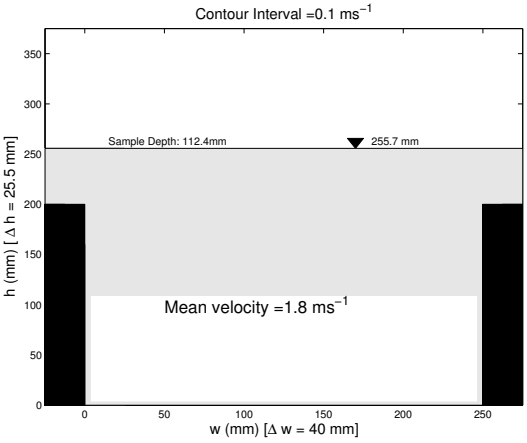

(a) Mean velocity

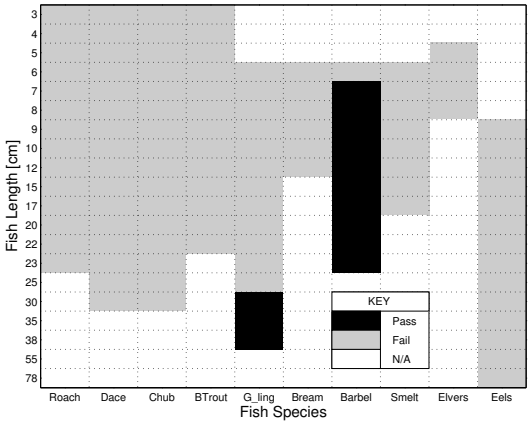

(b) Fish pass efficiency matrix (using mean velocities)

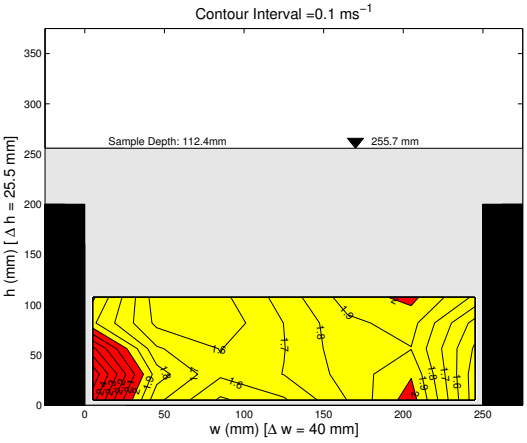

(c) Contour-plot velocity distribution

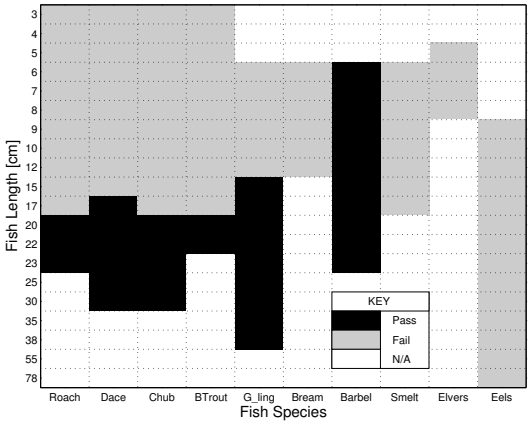

(d) Fish pass efficiency matrix (using measured velocities)

Figure 4–47: Comparison of mean velocity and contour-plot velocity fish passage efficiency matrices (Slot 3)

Case Study C: Slot by slot contour-plot velocity results and associated fish passage efficiency matrix for the unequal baffle pairing arrangement (1:5 downstream slope, 50 percentile low-flow)

The slot-specific contour-plot velocity distributions are presented at field scale because fish pass efficiency matrices were based on the fish burst speed swimming capabilities which were compared to the field scale velocities at each slot.

In this investigation the velocity distributions were restricted to two dimensions. Although the flow down the fish passage was three-dimensional, other than the qualitative flow visualisation process already described in section 4.2.3, the data sampling methods using the available instrumentation (i.e. PT-ST arrangements) was restricted to two-dimensional streamline flow. Turbulence and eddying flow structures were observed between the baffles during the flow visualisation process, further restricting velocity measurement possibilities. The flow visualisation plan view (for Baffles 1 to 5) and cross-sectional view (from the crest to Baffle 3) of the

flow structures observed have been presented in Figure 4–43 and 4–44 respectively.

Figures 4–48 and 4–49 show the contour-plot velocity distributions from Slot 1 to 12 at field scale. These plots are redrawn in Appendix E together with the accompanying fish pass efficiency matrices as part of the full project record. The worst slots (i.e. Slots 3, 6 and 7) are discussed as part of Case Study F.

Slot 1 The first baffle was 120 mm in height, while the water depth at this slot was 315.4 mm which allowed the velocity distribution depth to be sampled at 194 mm.

As would be expected because of the positioning of Slot 1 just downstream of the crest and against the side wall of the flume, lower velocities were recorded against the wall of the flume (i.e. $w \geq 240$ mm) and towards the bed (i.e. $h \leq 50$ mm), which can partly be attributed to the shear stresses associated with boundary layer flow. In the velocity distribution, where velocities were 1.1 ms^{-1} or under (depicted in green) is just less than 50% of the sampled area. Consequently the predicted fish pass efficiency matrix for this slot, as shown in Figure 4–45(d) shows that the majority of fish under consideration would be capable of passing this point. The exceptions are elvers and brown trout between 3 and 4 cm in length.

From the flow visualisation, jet flow was observed at plan view, while at Slot 1, a plunging flow regime appeared to predominate.

Slot 2 The flow depth was 324.2 mm and the sample depth was 119.2 mm. From the velocity distribution measurements (and verified in the flow visualisation footage in Figure 4–43) it was evident that this slot was characterised by the presence of a low velocity jet flow structure, ≤ 1.1 ms^{-1}, which occurred approximately in the centre of the slot. The area covered by velocities ≤ 1.1 ms^{-1} is smaller than that found at Slot 1. The highest velocities for Slot 2 occurred for $w < 20$ mm, and as indicated by the red on the velocity distribution graph, were above 2 ms^{-1}. The fish pass efficiency matrix (Figure 4–46(d)) predicts that these velocities are within the capabilities the following fish species and sizes: roach ≥ 7 cm , dace ≥ 5 cm, all of the chub, brown trout ≥ 9 cm , all of the grayling, bream and barbel, smelt ≤ 12 cm, and eels. None of the elvers are theoretically capable of passing through this slot.

Slot 3 - 6 One of the drawbacks of using the PT-ST probes was the need to ensure that they remained primed throughout the experiment. Although the free surface profile was fairly deep, this was not so easy to see during the experiment[25]. Because a series of slots were measured during one experiment session, it was essential to keep the PT-ST probe below the free surface. The sample depth for these experiments was not deep enough, and as a result some of the worst results in terms of the fish pass efficiency matrices have been recorded for this specific flow rate. Time constraints prevented these slots from being re-trialled.

[25]The free surface profile experiments were also completed after the velocity distribution experiments

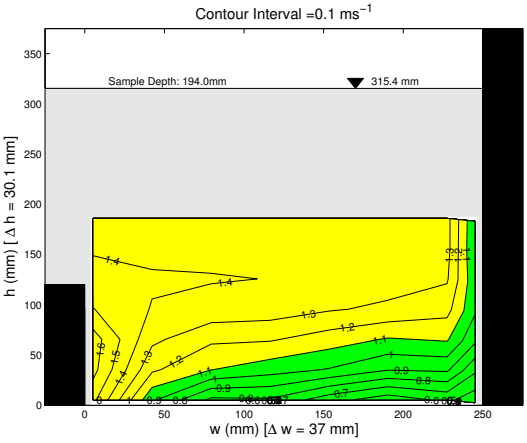

(a) Velocity Distribution: Slot 1

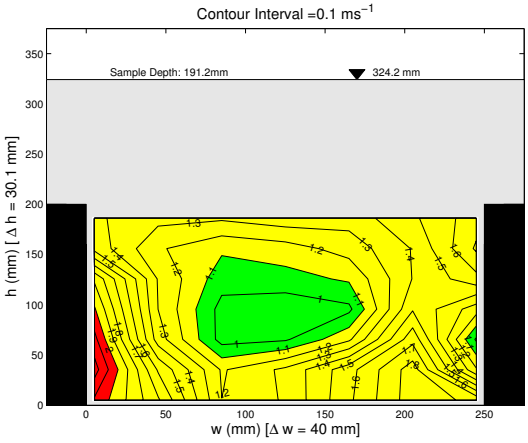

(b) Velocity Distribution: Slot 2

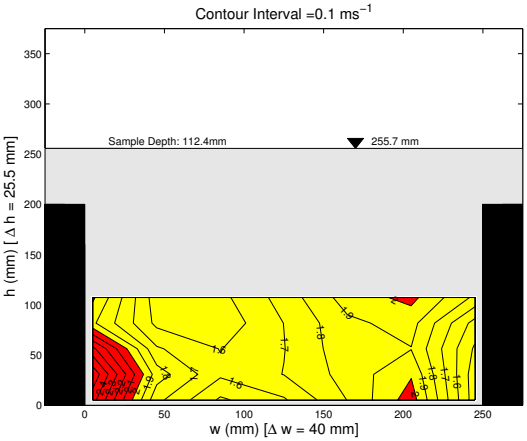

(c) Velocity Distribution: Slot 3

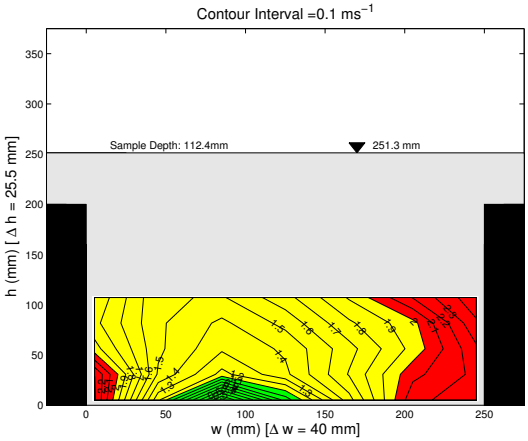

(d) Velocity Distribution: Slot 4

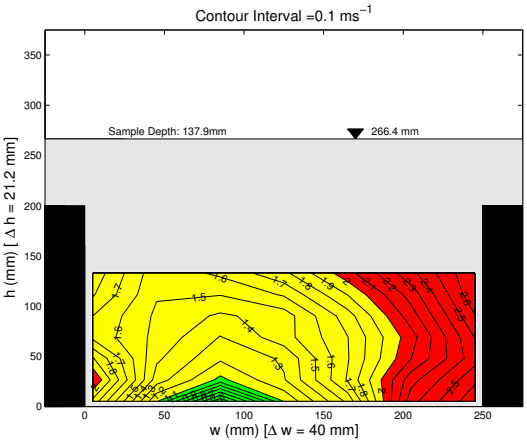

(e) Velocity Distribution: Slot 5

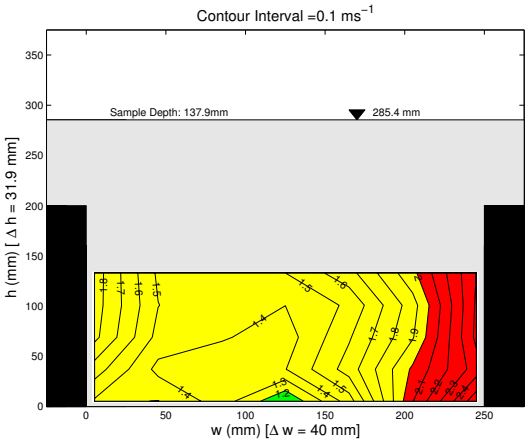

(f) Velocity Distribution: Slot 6

Figure 4–48: Unequal baffle pairing: Q50, gradient 1:5, 15 °C, Slot 1 to 6

As can be see from the lack of green, the velocities recorded in Slot 3 were higher than the 1.1 ms^{-1} criterion, and consequently the fish pass efficiency matrix (Figure 4–47(d)) predicts fewer fish capable of passing through this slot. The physical positioning of the slots in relation to each other, as caused by

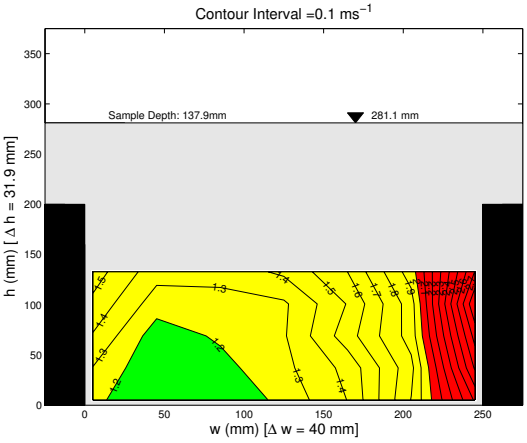

(a) Velocity Distribution: Slot 7

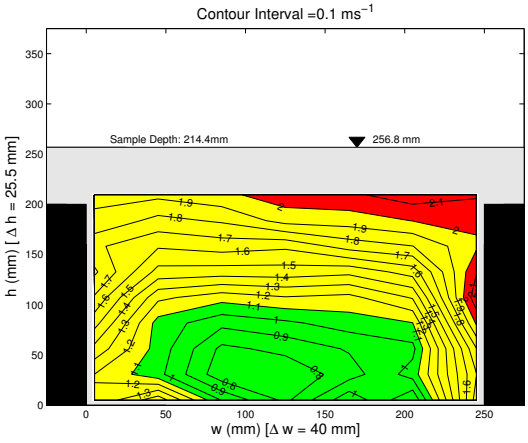

(b) Velocity Distribution: Slot 8

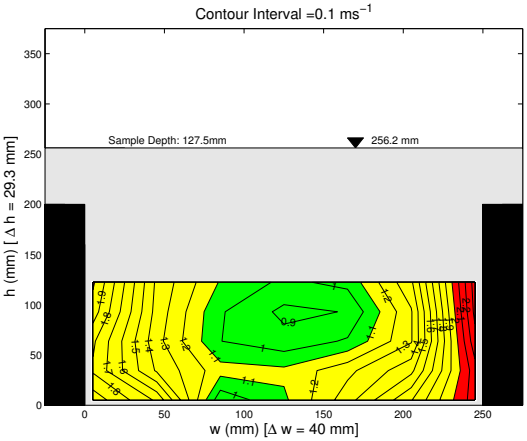

(c) Velocity Distribution: Slot 9

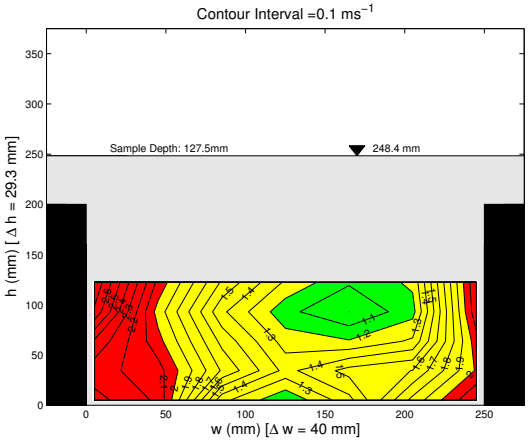

(d) Velocity Distribution: Slot 10

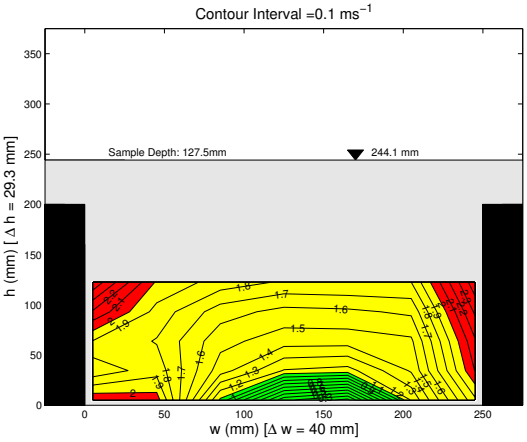

(e) Velocity Distribution: Slot 11

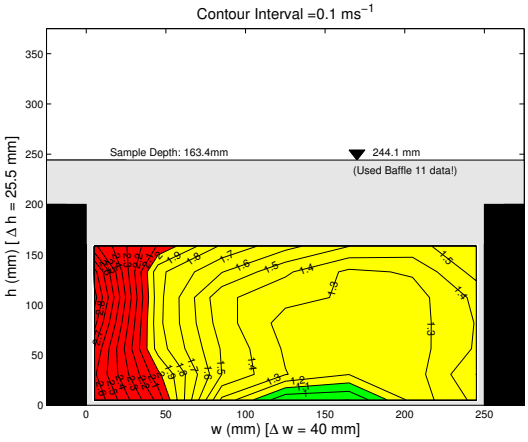

(f) Velocity Distribution: Slot 12

Figure 4–49: Unequal baffle pairing: Q50, gradient 1:5, 15 °C, Slot 7 to 12

staggering the slots is reflected in the contour shapes. The region of maximum velocity (i.e. in red) in Slot 3 occurs closest to $w < 40$ mm, which shows an increase in area when compared to Slot 2. This core region of higher velocity shifts sides between Slots 3 and 4. From Slot 4 to Slot 6, it occurs in that

part of the slot where 200 mm $< w <$ 250 mm. A region of lower velocity, coloured green, was observed as jet flow in Figure 4–43 and has been described in more detail in section 4.2.3. Predicted success or failure on the fish pass efficiency matrix is directly linked (i.e. fish cross-sectional area compared to area of lower velocity) to the size of this region of lower velocity. The use of the traffic light colouring system also provides a means of visually assessing potential success/failure of a particular slot.

Slot 7 - 12 These slots all show a region of lower flow velocity (in green), caused by the jet impinging on the baffle directly below the slot in each case. The horizontal positioning of the low-velocity area on the bed floor seen at Slots 7 and 8[26], became detached for Slots 9 and 10, before becoming reattached for Slots 11 and 12. The implications of this are that a smaller fish exploiting the lower velocity regions would theoretically need to move away from the bed floor at the relevant slots.

An additional consideration was the effect of the overlap on the velocity regions. The position of this low-velocity jet, as well as the high velocity region (in red) were both affected by the change in direction of the path of ascent (i.e. at Slot 7).

Flow through the slots was observed to have a three dimensional flow structure. In general, flow through a slot was observed to be jet-like, and generally impinged on the baffle immediately below it providing a mechanism for the dissipation of energy. An area of higher velocity occurred at either one or both sides of each slot.

Figure 4–50 shows two velocity profiles both recorded upstream of baffle 1 on the axis of Slot 1, the first measured at the crest and the second downstream of the crest. In both cases, the recorded velocities were higher than the 1.1 ms^{-1} maximum velocity threshold applied during the LEGO experiments. A contour-plot velocity distribution diagram and the associated fish pass efficiency matrix have not been completed for the sample positions upstream of the first baffle, as this analysis technique had not been devised during the experimental procedure. However, the mean velocities were calculated, and it would thus be possible to compare these velocities to the burst swimming speed of the fish (in a similar fashion to Case 2 above).

[26]The sample depth in Slot 8 was much higher than the rest as it was measured at the end of an experiment session and it was therefore not important if the probes were exposed to air at the end of the session.

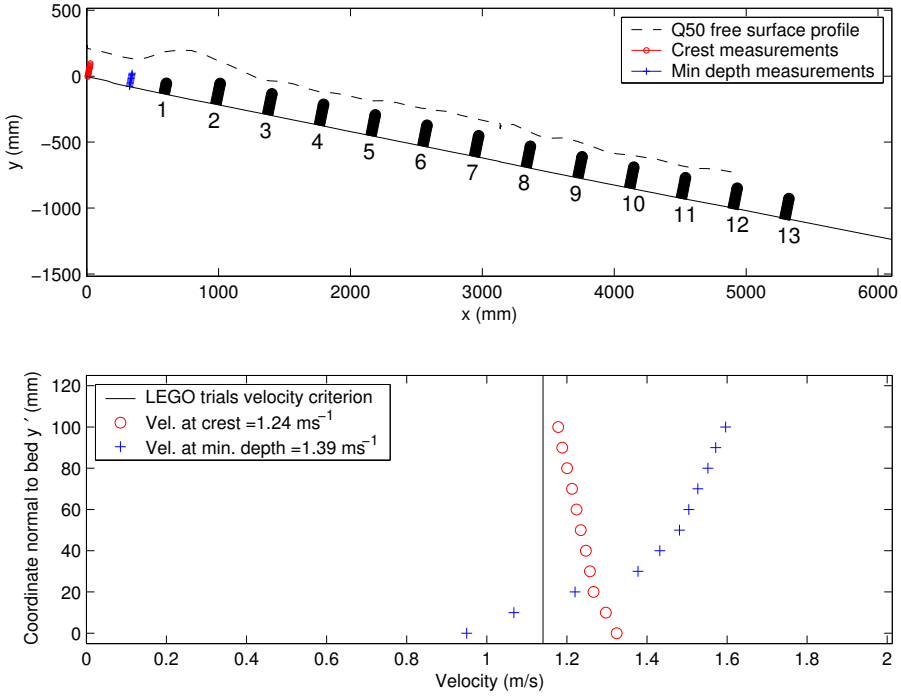

(a) Q50_p24

Figure 4–50: Velocities upstream of first baffle for the unequal baffle pairing at a 50 percentile low-flow, normal flume

Case Study D: Height of first baffle

The most demanding criterion in terms of velocity for the preferred fish pass was from the first baffle to the crest for both the equal and the unequal baffle pairing.

Since the unequal baffle pairing seemed to show the most potential from the LEGO trials and from a preliminary analysis of the perspex results, this was the arrangement for which most of the velocity trials were performed.

As an initial estimate of performance, both the mean velocities and the water depths recorded at each slot are plotted on Figures 4–51 and 4–52 respectively, with the 90 percentile low-flow data plotted on graph (a) and the 50 percentile low-flow data plotted on graph (b). In terms of the mean velocities, the unequal baffle pairing provides more favourable velocities over the baffle range, whereas the equal baffle pairing provides a slightly deeper water level at each corresponding baffle.

Figures 4–50 and 4–53 show that in terms of velocities upstream of the first baffle, both scenarios are more or less equally demanding for the 50 percentile low-flow. Fish would need to swim at a speed higher than the maximum burst speed criterion, which from anecdotal evidence should be achievable. This particular aspect needs careful attention during field trials.

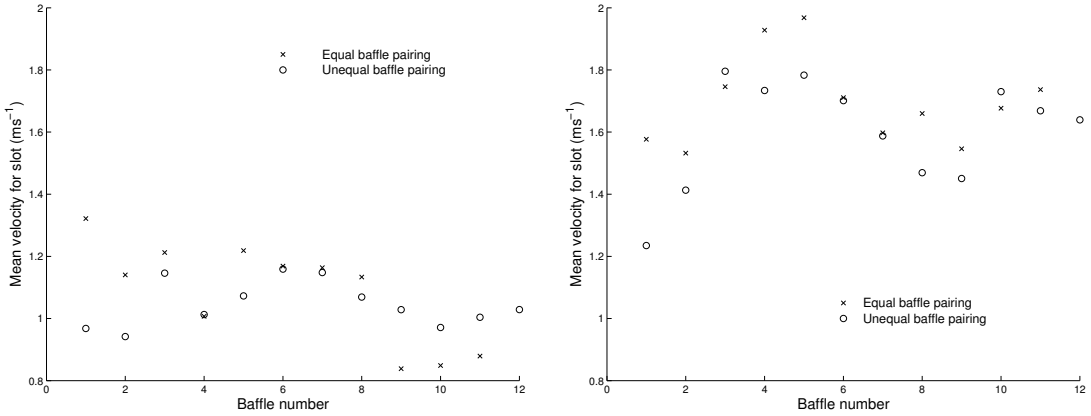

(a) Q90 (b) Q50

Figure 4–51: Comparison of mean velocities

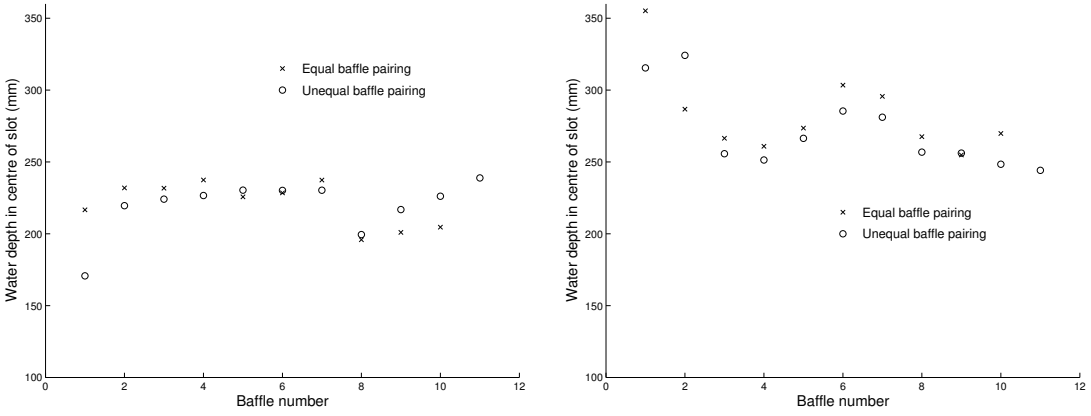

(a) Q90 (b) Q50

Figure 4–52: Comparison of water depths

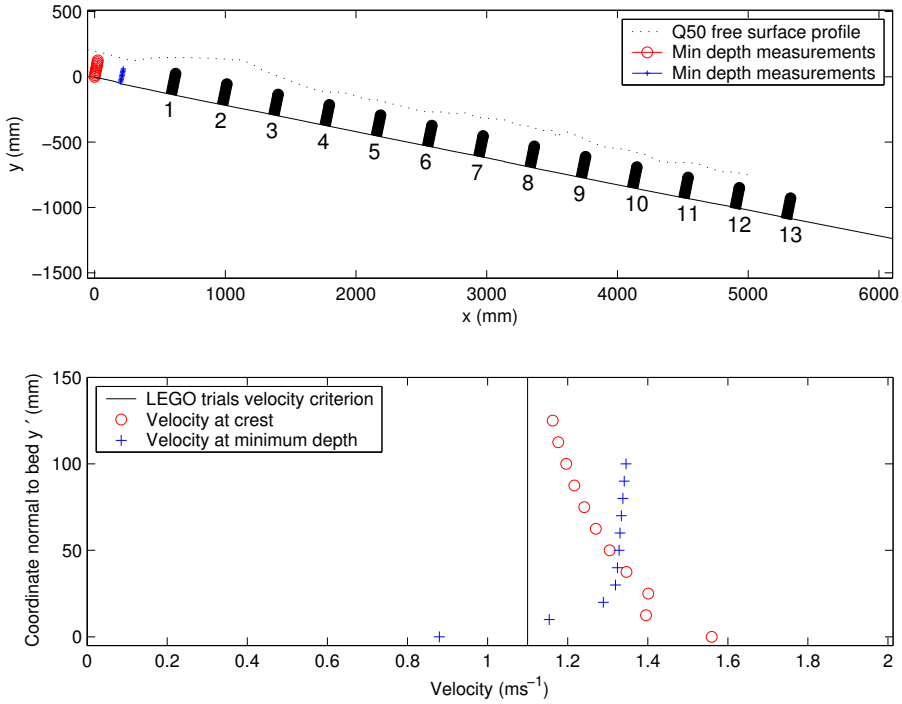

Figure 4–53: Velocities upstream of first baffle for the equal baffle pairing at a 50 percentile low-flow, normal flume

Case Study E: Velocities measured over the tops of the baffles

A complete analysis of the velocities recorded over the tops of the baffles was not performed mainly as a result of the requirement to keep the PT-ST probes completely submerged and primed during an experiment. This was found to be challenging with regards to water depth for the low flows. Some of the baffles at the higher flow ranges exhibited air entrainment, which was not a suitable environment for velocity measurements using this type of probe.

For the lower flow rates, any bigger fish swimming over the top of the baffles might not be submerged as a result of shallow water depths. Therefore the assumption (see section 2.1.3) that the maximum burst speed velocities determined in the Swimit study (Environment Agency 2001b, 2003) would be applicable for a fish swimming up a slope when it is submerged at least three times its own body depth (Turnpenny 2003) is invalid. Although no specific comment is made with regards to fish species and lengths which might exploit area over the tops of the baffles, the traffic-light system provides a visual guide to the expected velocities.

Five contour-plot velocity profiles were performed for the unequal baffle pairing, with a 1:5 downstream slope. Baffles 2 and 11 were considered for the 90 percentile and 50 percentile low-flow scenarios, whereas only Baffle 11 was trialled for the 10 percentile low-flow. Owing to the instrumentation setup, only $\frac{2}{3}$ of the width of the weir could be measured at any one time and because this was equivalent to approximately 2 m at field scale and a good representative portion, the instrumentation was not 'turned around' in order to measure the remaining portion.

For the 90 percentile low-flow scenario in Figures 4–54 and 4–55, the water level was fairly shallow, which would presumably prove difficult for any large fish choosing to swim over the tops of the baffles. The water depth over the top of Baffle 11 would scale up to roughly 50 mm, while a depth of 25 mm (approximately) was available over Baffle 2. The water velocities measured were mainly within the 1.1 ms^{-1} to 2 ms^{-1} range. This compares favourably with the recommendation from Beach (1984) that velocities on the downstream slope of the Crump weir should not be in excess of 3.5 ms^{-1} for salmon.

The water level observed at Baffle 2 (Figure 4–56) was higher than that at Baffle 11 (Figure 4–57) for the 50 percentile low-flow scenario. As with the 90 percentile low-flow experiment, the water velocities at Baffle 2 fell within the 'yellow' range of the contour-plot velocity distribution. However, at Baffle 11, acceleration of the water over the top of the baffles would account for the increase in velocity, with the majority of the contour-plot velocity distribution showing red (i.e. > 2 ms^{-1}).

The water depth for the 10 percentile low-flow over Baffle 11 (Figure 4–58) was approximately 200 mm deep (i.e. similar to the baffle height). A jet appeared to have become well established over the centre of the baffles, with maximum velocities in the order of 4.3 ms^{-1}. However, velocities closer to the side wall were well within the 3.5 ms^{-1} range suggested by Beach (1984) and would probably provide a useful path for the larger coarse fish and salmon.

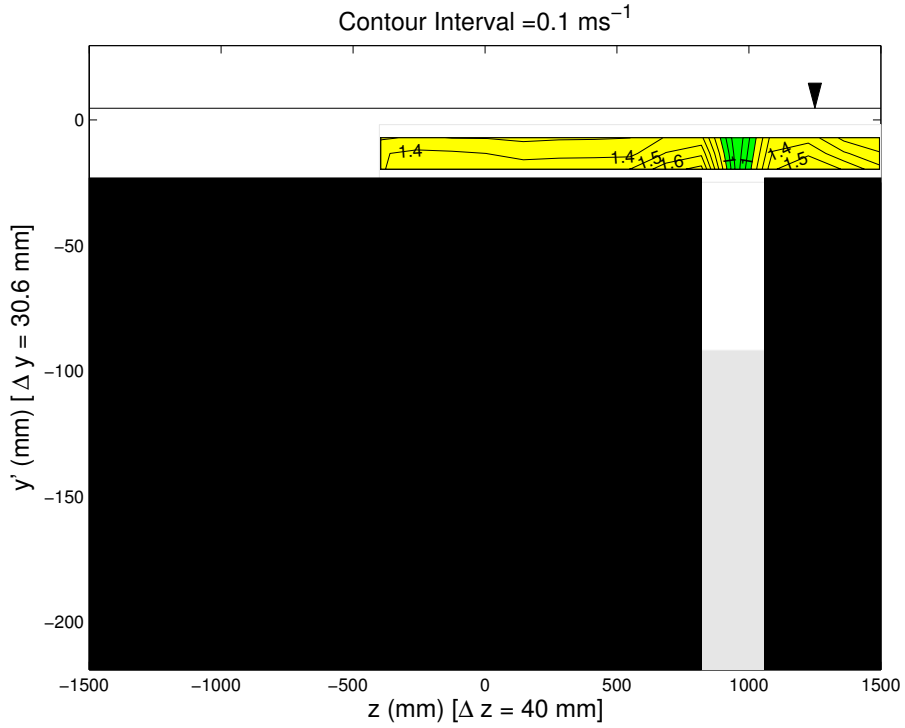

Figure 4–54: Top of Baffle 2: Unequal baffle pairing: Q90, gradient 1:5, 15° C

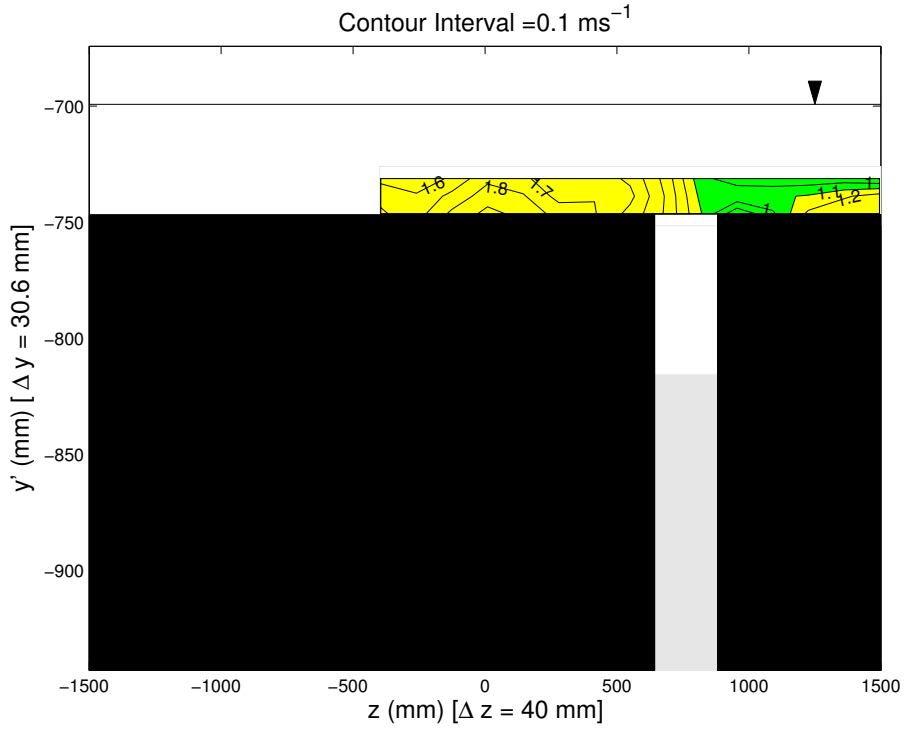

Figure 4–55: Top of Baffle 11: Unequal baffle pairing: Q90, gradient 1:5, 15° C

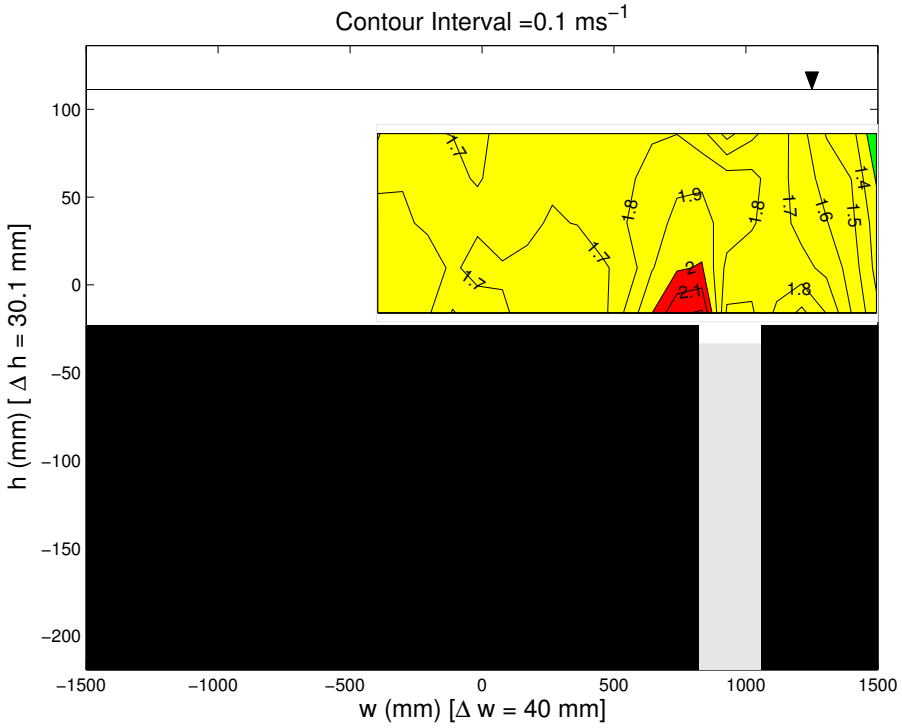

Figure 4–56: Top of Baffle 2: Unequal baffle pairing: Q50, gradient 1:5, 15° C

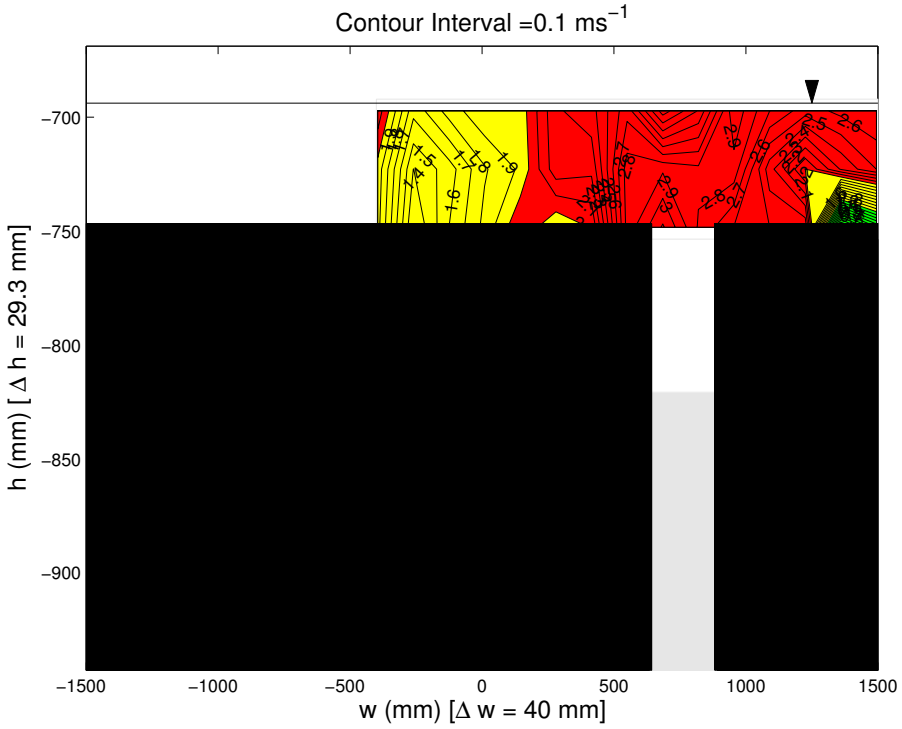

Figure 4–57: Top of Baffle 11: Unequal baffle pairing: Q50, gradient 1:5, 15 ° C

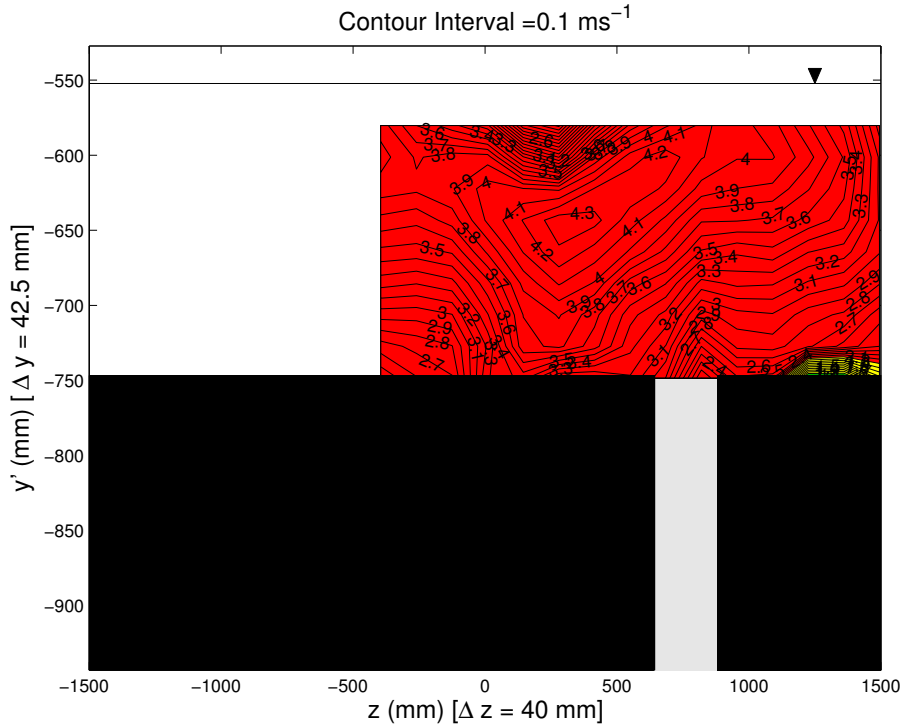

Figure 4–58: Top of Baffle 11: Unequal baffle pairing: Q10, gradient 1:5, 15° C

Case Study F: Worst performing slots over experiment flow range (for 1:5 gradient)

As it is considered to be the worst case, as well as identifying all the typical velocity distributions observed for the different scenarios, the complete set of results for the 50 percentile low-flow rate (with the unequal baffle pairing and at a 1:5 downstream slope) have been presented as Case Study B and C in this text. The accompanying fish matrices are presented alongside the velocity distribution in Figures E–21 to E–24. This study also provides a platform for identifying common flow patterns found during the perspex fish pass experiments.

The fish pass efficiency matrices have been set up for both 10 ° C and 15 ° C water temperatures, as illustrated in Figure 4–59. However, only the latter water temperature is considered for analysis in this thesis (see section 3.3.2). By using the Swimit spreadsheet (Environment Agency 2001b, 2003) these data sets can easily be extended for a wider temperature range.

The overall fish pass efficiency matrix, Figure 4–59(b), for the 50 percentile low-flow rate, unequal baffle pairing at a 1:5 downstream slope at a 15 ° C, indicates that this pass should be effective (within the limitations of the cross-sectional area assumptions) for roach, chub, and brown trout $\geq$ 20cm, dace $\geq$ 17cm, grayling $\geq$ 15cm and all the barbel. The efficiency matrix for Slots 1 to 12 is only as good as the worst case (or cases). For this example, the worst fish pass efficiency matrix was at Slot 3, while Slots 6 and 7 are also predicted to be problematic for a number of fish $>$ 10cm. In this analysis, the smelt success rate has not been used in this 'rule of thumb' measure, as increasing fish size has been shown to be accompanied by a decrease in swimming capabilities (as shown in Figure 2–4).

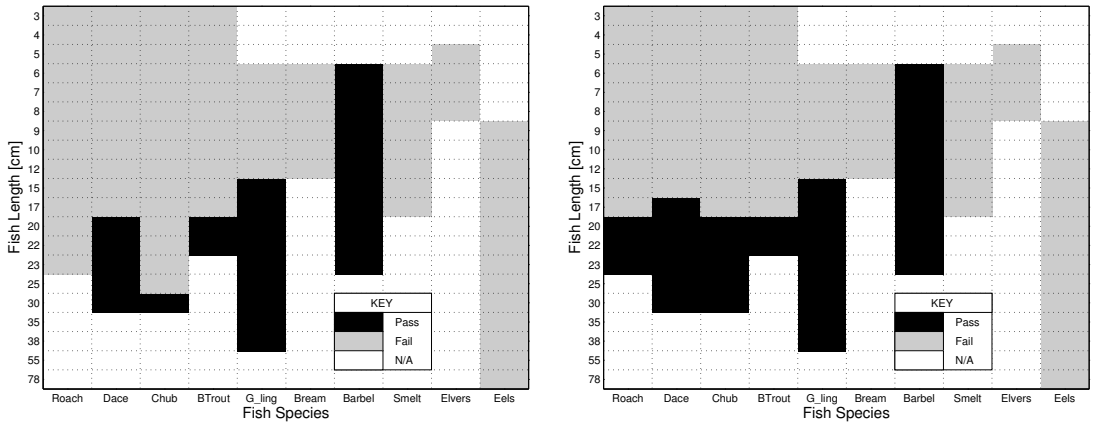

(a) 10° C

(b) 15° C

Figure 4–59: Unequal baffle pairing: Q50, gradient 1:5, 10° C and 15° C, Slot 1 to 12

The three worst slots for the 50 percentile low-flow rate, for the unequal baffle pairing and a 1:5 downstream slope are presented in Figure 4–60.

In Figure 4–61, for the 90 percentile low-flow rate, for the equal baffle pairing and a 1:5 downstream slope, the velocity measurements did not include the whole width

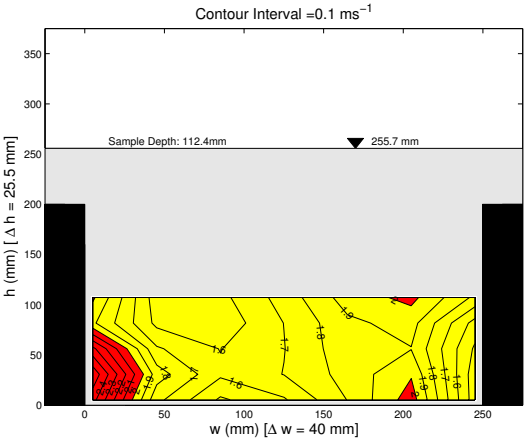

(a) Velocity Distribution: Slot 3

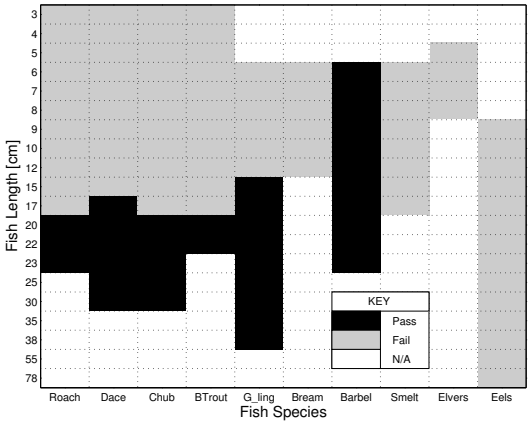

(b) Fish pass efficiency matrix: Slot 3

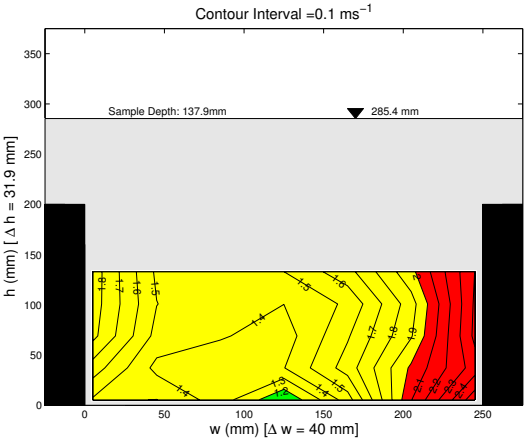

(c) Velocity Distribution: Slot 6

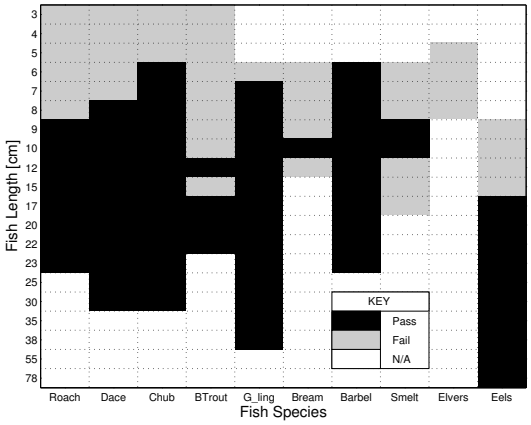

(d) Fish pass efficiency matrix: Slot 6

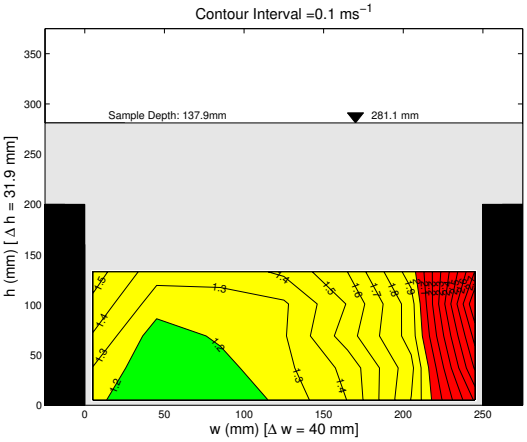

(e) Velocity Distribution: Slot 7

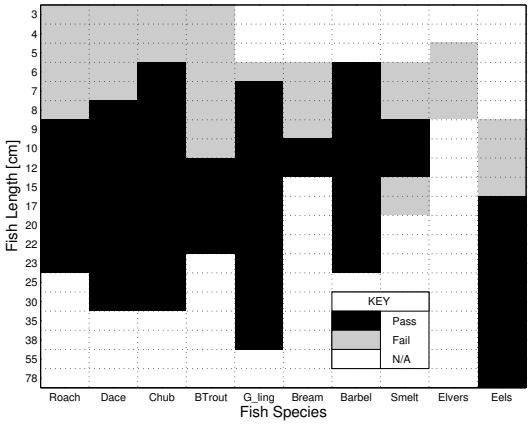

(f) Fish pass efficiency matrix: Slot 7

Figure 4–60: Unequal baffle pairing: Q50, gradient 1:5, 15° C, Slots 3, 6 and 7

of the slot. This was an experimental oversight, and as a result, the accompanying fish pass efficiency matrix indicates that the slot is less effective than what is most likely to be the case.

Figure 4–62 shows the results for the 50 percentile low-flow rate, equal baffle pairing

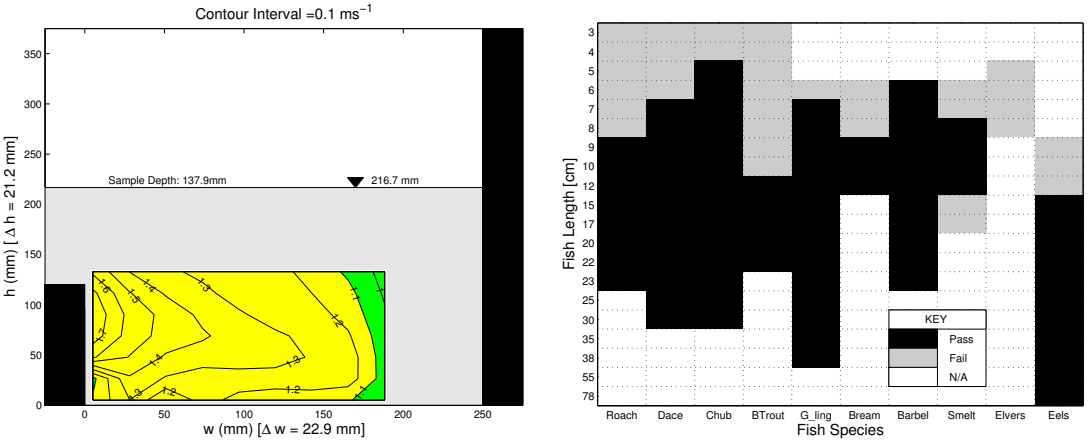

(a) Velocity Distribution: Slot 1

(b) Fish pass efficiency matrix: Slot 1

Figure 4–61: Equal baffle pairing: Q90, gradient 1:5, 15° C, Slot 1

and a 1:5 downstream slope. A comparison between the equal and the unequal baffle pairing layouts shows that in both cases Slot 6 appears to be one of the most challenging slots for the smaller fish.

Further analysis of the exact fish species which would theoretically be able to pass through the slots is not considered at this point. The following general comments are made with regards to the contour-plot velocity distributions and accompanying fish pass efficiency matrices:

- The fish pass efficiency matrices are limited by the depth of measurement, and for some of the slots (e.g. Figure 4–61) the matrix is affected by a small/narrow sample depth measurement. These experiments were time-consuming and it was not considered necessary during the experimentation procedure to repeat those which seemed to provide a fair indication of the velocity distribution. It is only with the application of the fish pass efficiency matrix method that such short-comings cause certain slots to be (perhaps unnecessarily) 'flagged'.

- The method used to determine each fish cross-sectional area needs further refinement. For the purposes of this thesis, where fineness ratios were not available, some of the species have been assumed to be equal in depth to the bream, which is a deep-bodied fish.

- A field scale study would be needed to assess the accuracy of the fish pass efficiency matrix method and thus further detailed analysis of some 'theoretical' pass or fail method is not warranted at this point.

- The percentile low-flow rates used in this thesis have also been converted to a more general 'flow rates per unit width'. The four flow rates used and presented in Appendix E are also given in terms of the flow rate per unit width values which form part of the general guidelines regarding the application of the rotated-V baffles (Rhodes and Servais 2006).

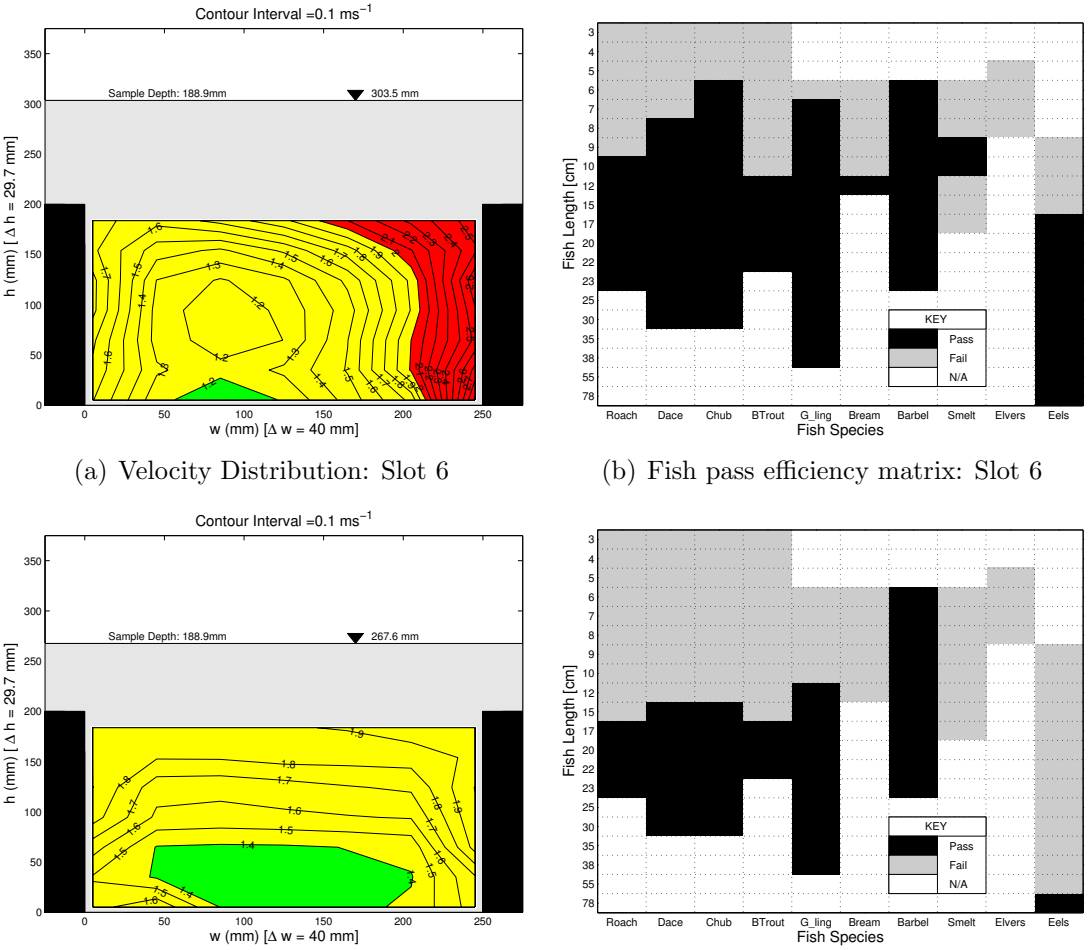

(a) Velocity Distribution: Slot 6

(b) Fish pass efficiency matrix: Slot 6

(c) Velocity Distribution: Slot 8

(d) Fish pass efficiency matrix: Slot 8

Figure 4–62: Equal baffle pairing: Q50, gradient 1:5, 15° C, Slot 6 and 8

Case Study G: Effect of changing the downstream slope from 1:5 to 1:4.55

One of the aims of the research project was to study the effect of a slope change on the fish pass. One means of changing the slope was to tilt the flume with the installed model as a unit (as described in section 3.3) using existing jacks under the flume. The maximum achievable slope using this method was 1:4.55. At the outset of the project it had been anticipated that a new wooden section would be installed allowing for the testing of a shallower gradient. However, as a more detailed investigation into the effect a baffle or baffles on the downstream slope was undertaken (see Chapter 5) this was curtailed.

Figures 4–63(a) and (b) show the contour-plot velocity distribution and associated fish pass efficiency matrix for the 1:5 gradient. These are then compared to Figures 4–63(c) and (d) which show the same diagrams for a 1:4.55 slope. Similarly, Figure 4–64 represents the results from Slot 7.

In both cases the velocities recorded for the steeper gradient were higher, as is visually represented by the 'traffic light' system. A slot-by-slot comparison for each of the measurements comparing the 1:5 to the 1:4.55 flume show that a similar outcome

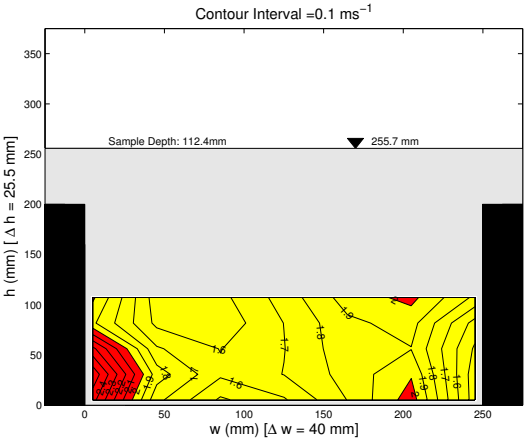

(a) Velocity Distribution: Gradient 1:5

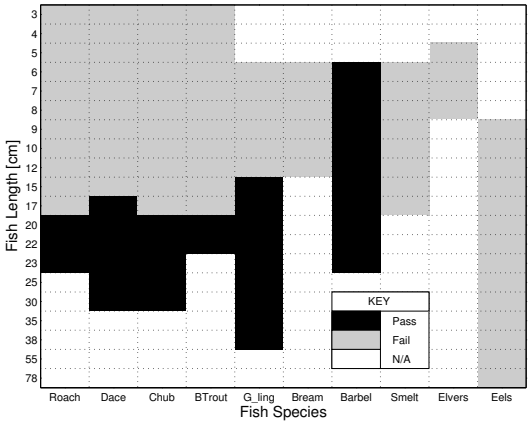

(b) Fish pass efficiency matrix: Gradient 1:5

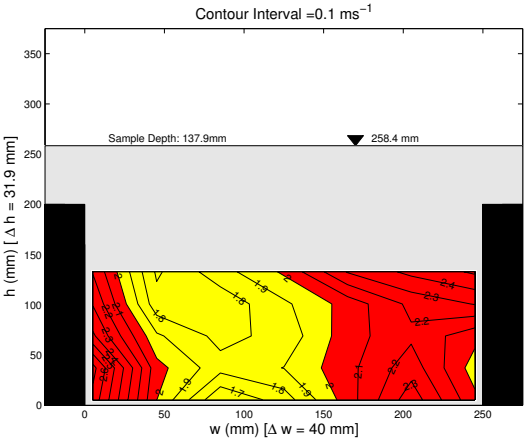

(c) Velocity Distribution: Gradient 1:4.55

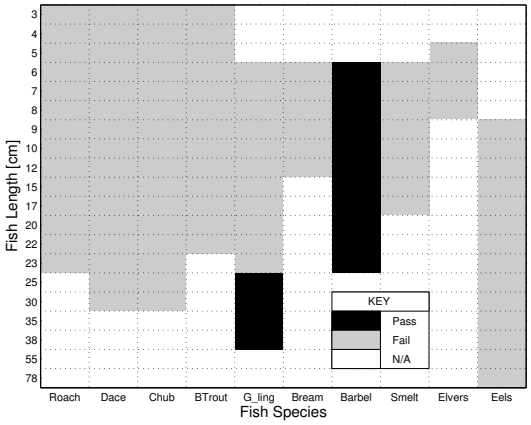

(d) Fish pass efficiency matrix: Gradient 1:4.55

Figure 4–63: Unequal baffle pairing: Q50, gradient 1:5 compared to 1:4.55, 15° C, Slot 3

is observed for the 50 percentile low-flow. Slots 3 and 7 were the worst performing slots for the 1:4.55 experiment, which with the exception of Slot 6 (see Table 4–6) correlates to the 1:5 experiment set. Both sets of results are fully presented in Appendix E.

For the 10, 30 and 90 percentile low-flows, only Slot 11 was tested for the 1:4.55 downstream slope. As this slot is not typically problematic, it was not possible to draw direct conclusions with regard to each of the specific flow rates. It is postulated however, that the preferred fish pass would go someway to alleviating fish passage problems for a slope steeper than 1:5, but the quantification thereof still needs to be determined. As the model was chiefly constructed out of perspex, it would be possible to test the same model in any flume, laid on a new weir[27].

[27]The existing wooden weir has come to an end of its useful design life as it has now warped, and part of the wood is rotten.

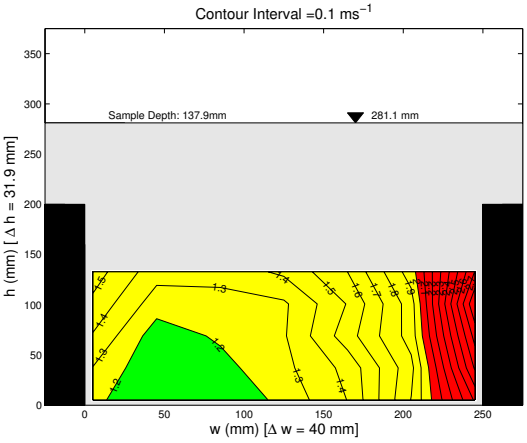

(a) Velocity Distribution: Gradient 1:5

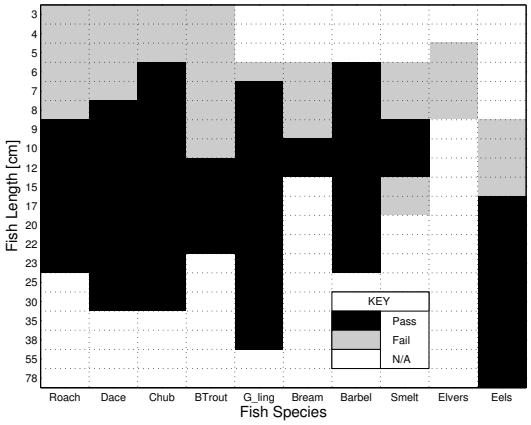

(b) Fish pass efficiency matrix: Gradient 1:5

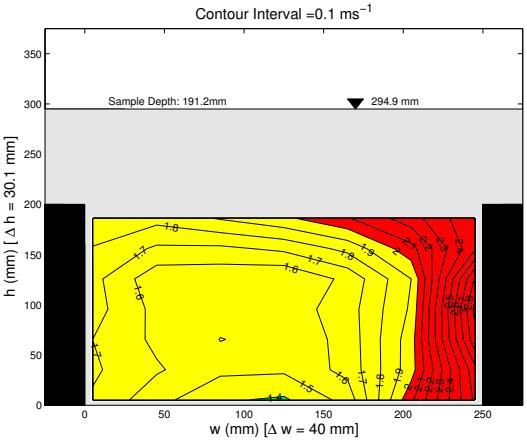

(c) Velocity Distribution: Gradient 1:4.55

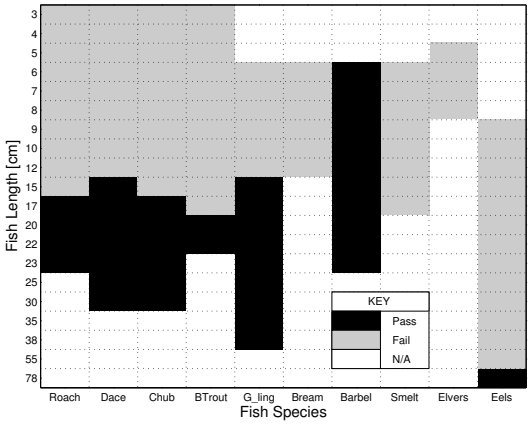

(d) Fish pass efficiency matrix: Gradient 1:4.55

Figure 4–64: Unequal baffle pairing: Q50, gradient 1:5 compared to 1:4.55, 15° C, Slot 7

4.2.5. Debris trials results and analysis

Debris/trash analysis

As structural modifications on the Crump weir were required to be self-cleansing, thereby preventing debris entrapment, three different materials were used in a direct study on the effects of debris. Procedures and comments on observations noted during the debris trials are presented in Tables 4–8 to 4–11 and the results from each flow rate are discussed separately for each debris type.

Dowels The dowels, representing logs, were soaked overnight before experiments commenced. For each flow rate 30 separate dowelling rods (i.e. two examples of each length and diameter) were introduced upstream of the weir. Extra care was required at the 90 percentile low-flow such that the longest sections were introduced into the flow up to a minute after the shortest lengths so as to prevent a log-jam upstream of the crest. Such precautions were not necessary for the other three flow rates. In the tables below, the dowels are identified (i)

by diameter, namely 6 mm, 15 mm and 20 mm (representing 30 mm, 75 mm and 100 mm at field scale) and (ii) by lengths, namely 36 mm (A), 72 mm (B), 143 mm (C), 287.5 mm (D) and 575 mm (E) (180 mm, 360 mm, 715 mm, 1437.5 mm and 2875 mm at field scale). For each experiment there were two rods of the same diameter and length. Figure 4–65 shows samples of 3 lengths of each diameter compared with a 150 mm steel rule. This was repeated ten times for each flow rate.

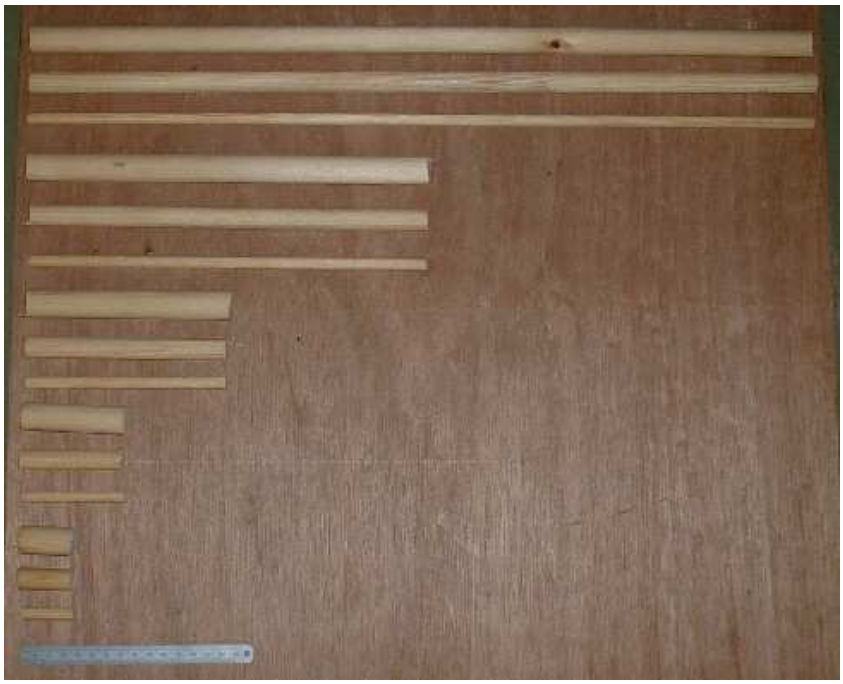

Figure 4–65: Debris: Photograph of the one of each length:diameter dowelling rod used

The majority of the baffles 72 mm (360 mm) and smaller (i.e. dowel types A and B) successfully passed downstream at the 90 percentile low-flow (Table 4–8). Approximately half of the C type dowelling was successful, whereas the majority of types D and E (i.e. > 1.5 m) failed or jammed to reach the bottom of the downstream apron.

For increasing flow rate, corresponding to the decreasing low-flow percentiles (i.e. 50, 30 and 10 percentiles), the number of dowels passing increased to 100%.

Three typical failure mechanisms included a short dowel across a slot (Figure 4–66(a)), a long dowel jamming itself down the path of ascent between the slots (Figure 4–66(b)) and a medium dowel lying over the top of an upstream baffle and butting diagonally downwards onto the upstream face of the baffle immediately downstream (Figure 4–66(c)).

Plastic bags For each flow rate, three identical bags were completely filled with water and introduced upstream of the weir. This was repeated five times which

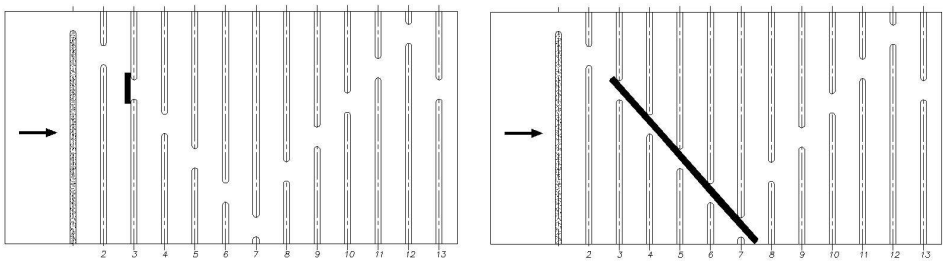

(a) Short dowel across slot opening (b) Long dowel stuck down path of ascent

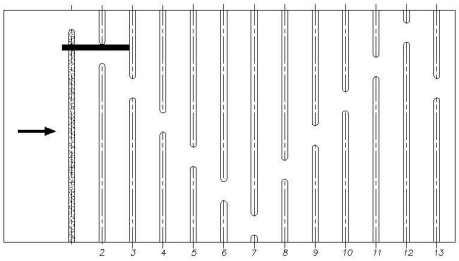

(c) Medium dowel over top of upstream baffle and butted up against the next baffle

Figure 4–66: Debris testing: Typical failure methods of the dowelling rods

provided sufficient evidence for cause of failure. Care was taken to displace the air as far as possible before release. The bags used were typical sandwich bags ($8\frac{1}{2}$ inches by $7\frac{1}{4}$ inches) representing plastic rubbish bags which might be introduced in a river.

For the 90 percentile low-flow (Table 4–8), on average one out of the three bags passed downstream. The mechanisms whereby the bags got stuck differed and included the location of the bag moving over the top of the baffle, and the alignment of the bag opening to the direction of flow. Thus bags were observed to 'creep' down the crest during alternatively filling and emptying, or 'stick' when a bag filled with water and settled between baffles. All of the bags passed down the crest at the 50 percentile and 10 percentile low-flow rates (Tables 4–9 and 4–11), whereas two got stuck during the 30 percentile low-flow (Table 4–10). The first stuck on the crest and the second wrapped itself around the slot edge on the eleventh baffle down the crest, thus effectively creating a blockage in the fish pass. Plastic bags effectively blocking the fish pass or influencing effective gauging are therefore much more likely to be a problem at low-flows than at high flows.

Twigs The twigs, representing branches, were soaked overnight before experiments commenced. Five different twigs were used in each case. For the 90 percentile low-flow, the twigs were introduced one after another and generally caused log-jam at the crest. When a single twig was introduced, at the 90 percentile low-flow, on no occasion did it pass over the weir. Subsequently the experimental procedure was modified, so that for the 50, 30 and 10 percentile low-flows, twigs were introduced individually and progress noted. This was repeated ten times for each flow rate.

The twigs used have been identified visually in the following photographs in Figure 4–67 and compared with a 150 mm steel rule.

(a) Twig A (max stem diameter = 7 mm, main stem and second stem length = 310 mm)

(b) Twig B (max stem diameter = 6 mm, main stem length = 390 mm)

(c) Twig C (max stem diameter = 9 mm, main stem length = 330 mm)

(d) Twig D (max stem diameter = 7 mm, main stem length = 320 mm)

(e) Twig E (max stem diameter = 6 mm, main stem length = 390 mm)

Figure 4–67: Photographs of twigs compared with a 150 mm steel rule

For the 90 percentile low-flow (Table 4–8) all of the twigs failed to pass down the model fish pass. The twigs either stuck on the crest or on the first few baffles downstream of the crest. In some cases the twigs were lodged in such a manner that the fish pass would still have been likely to be operable. In the field, however, for a Crump weir in use as a gauging structure, this would be likely to affect the head measurement. The twigs represented branches larger

than 1.5 m long, and the 90 percentile flow in the river would need to be sufficient to carry the branch to the crest of the Crump weir in the first place.

For the higher flow rates (Tables 4–9 to 4–11), the success rate of a twig passing over the baffled weir depended on a number of aspects: (a) The flow rate (the larger the flow rate the greater the success rate), (b) the number of stemmed junctions on the twig and their angles with the main stem of the twig, (c) and on the angle between the main stem and the weir crest. In the latter case, main stems aligned with the primary flow direction and normal to the crest, with stemmed junctions directed upstream, passed over more easily .

Aspect (b) implies that the orientation of the twigs with few/no stemmed junctions was important. With the majority of the stems pointed out of water, the success rate was higher. Twigs C, D and E were of this shape. If their orientation was such that the majority of the stems were in the water, these twigs were more likely to get stuck, especially at low flow rates. An increase in flow rate directly increased the chance of success.

It was not possible to complete a trial on sedimentation given the constraints[28] of the flume. However, the particles used in the DigImage analysis were introduced into the flume. It was observed that the particles were more likely to settle out in the impoundment region upstream of the crest. Very few of the pliolite particles used for the particle tracking process settled between the baffles, and thus for a low sediment load, sedimentation of the modified Crump is unlikely to be a problem.

[28]Provision and funding for this type of trial were not included in the original case for support (Rhodes 2001). No facilities were available for the addition, removal or calibration of sedimentation.

Table 4–8: Debris trials: 90 percentile low-flow

Run no.	**Dowels**						**Plastic bags**	**Twigs**				
	(2 of each length & diameter)						(3 bags tested)	(1 of each shape)				
	Diameter	A	B	C	D	E		a	b	c	d	e
1	6 mm	2	1	0	0	0	2 pass	0	0	0	0	0
	15 mm	2	2	0	0	0	*1 stuck at crest*					
	20 mm	2	1	0	0	0						
2	6 mm	2	2	1	0	0	0 pass	0	0	0	0	0
	15 mm	2	2	0	0	0	*1 stuck at crest*					
	20 mm	2	1	1	0	0	2 *on weir (3/4 way down)*					
3	6 mm	2	2	1	0	0	1 pass	0	0	0	0	0
	15 mm	2	2	0	0	0	*1 stuck at crest*					
	20 mm	2	2	2	0	0	*2 on weir (3/4 way down)*					
4	6 mm	2	1	2	1	0	1 pass	0	0	0	0	0
	15 mm	1	1	1	0	0	*2 stuck on weir*					
	20 mm	2	1	0	0	0	*(betw. 1st and 3rd baffle)*					
5	6 mm	2	2	2	1	0	1 pass	0	0	0	0	0
	15 mm	2	2	2	0	0	*2 stuck on weir*					
	20 mm	2	2	0	0	0	*(at 1st baffle)*					
6	6 mm	2	2	2	0	0		0	0	0	0	0
	15 mm	2	1	2	0	0						
	20 mm	2	1	2	0	0						
7	6 mm	2	2	2	0	0		0	0	0	0	0
	15 mm	1	2	0	0	0						
	20 mm	2	2	0	0	0						
8	6 mm	2	2	2	0	0		0	0	0	0	0
	15 mm	2	2	2	0	0						
	20 mm	2	2	2	0	0						
9	6 mm	2	2	2	0	0		0	0	0	0	0
	15 mm	2	2	2	0	0						
	20 mm	2	1	2	0	0						
10	6 mm	2	2	2	0	0		0	0	0	0	0
	15 mm	2	2	1	0	0						
	20 mm	2	2	2	0	0						

Key : 1 or 2 = pass 0 = fail

Table 4–9: Debris trials: 50 percentile low-flow

Run no.	**Dowels**						**Plastic bags**	**Twigs**				
	(2 of each length & diameter)						(3 bags tested)	(1 of each shape)				
	Diameter	A	B	C	D	E		a	b	c	d	e
1	6 mm	2	2	2	2	2	3/3 pass	0	1	1	0	0
	15 mm	2	2	2	2	2						
	20 mm	2	2	2	2	2						
2	6 mm	2	2	2	2	2	3/3 pass	0	0	0	0	0
	15 mm	2	2	2	2	2						
	20 mm	2	1	2	2	2						
3	6 mm	2	2	2	2	2	3/3 pass	0	1	1	1	0
	15 mm	2	1	2	2	2						
	20 mm	1	2	2	2	2						
4	6 mm	2	2	2	2	2	3/3 pass	0	1	0	0	0
	15 mm	2	2	2	2	2						
	20 mm	2	2	2	2	2						
5	6 mm	2	2	2	2	2	3/3 pass	0	0	1	0	0
	15 mm	2	2	2	2	2						
	20 mm	2	2	2	2	2						
6	6 mm	2	2	2	2	2		0	1	1	1	0
	15 mm	2	2	2	1	2						
	20 mm	2	2	2	2	2						
7	6 mm	2	2	2	1	2		0	1	0	1	0
	15 mm	2	2	2	2	2						
	20 mm	2	2	1	2	2						
8	6 mm	2	2	2	2	2		0	1	1	0	0
	15 mm	2	2	2	2	2						
	20 mm	2	2	2	2	2						
9	6 mm	2	2	2	2	2		0	0	0	1	0
	15 mm	2	2	2	2	2						
	20 mm	2	2	2	1	2						
10	6 mm	2	2	2	2	2		0	0	1	0	0
	15 mm	2	2	2	2	2						
	20 mm	2	2	2	2	2						

Key : 1 or 2 = pass 0 = fail

Table 4–10: Debris trials: 30 percentile low-flow

Run no.	**Dowels**	**Plastic bags**	**Twigs**
	(2 of each length & diameter)	(3 bags tested)	(1 of each shape)
	A B C D E		a b c d e
1	All pass	2/3 pass *1 on crest*	1 1 1 1 1
2	All pass	3/3 pass	0 0 0 0 1
3	All pass	2/3 pass *1/3 at Baffle 11 wrapped around slot edge*	1 0 0 0 0
4	All pass	3/3 pass	0 1 1 1 1
5	All pass	3/3 pass	1 1 0 1 0
6	All pass		0 1 1 0 0
7	All pass *except* *20* mm *D on u/s wall*		1 1 0 1 0
8	All pass		1 0 1 1 0
9	All pass		0 1 1 1 1
10	All pass *except the* *6* mm *B on u/s wall*		1 1 0 1 0

Key : 1 = pass 0 = fail

Table 4–11: Debris trials: 10 percentile low-flow

Run no.	**Dowels**	**Plastic bags**	**Twigs**
	(2 of each length & diameter)	(3 bags tested)	(1 of each shape)
	A B C D E		a b c d e
1	All pass	3/3 pass	1 1 1 1 1
2	All pass	3/3 pass	1 1 1 1 0
3	All pass	3/3 pass	1 1 1 1 0
4	All pass	3/3 pass	1 1 0 1 1
5	All pass	3/3 pass	1 1 0 1 1
6	All pass		1 1 0 1 1
7	All pass		1 1 1 1 1
8	All pass		1 1 1 1 0
9	All pass		1 1 1 1 1
10	All pass		1 0 1 1 0

Key : 1 = pass 0 = fail

4.3. Conclusions

This chapter is split into two main sections: (i) testing a multiplicity of baffle arrangements using LEGO, and (ii) detailed investigations of the preferred layout with the baffles fabricated from perspex.

Initially, the LEGO bricks were used to test a multiplicity of layouts for the 90 percentile low-flow range (i.e. corresponding to a flow rate per unit width of 0.067 m^2s^{-1}). Five categories were tested, and using the criterion that a layout was to be capable of passing the majority of five species of fish greater than 10cm in length (identified in the first Swimit trial, Environment Agency 2001b), a rotated-V with narrow channel layout was chosen for further refinement over a larger flow range. Final adjustments to this layout included the removal of the narrow channel, an increase in baffle height, and ensuring that slots were unaligned about the x-axis (i.e. before and after the point of inflection).

This preferred arrangement was then prefabricated in perspex. While keeping the first baffle level with the crest, provision was made for testing two different first baffle heights. These were referred to as the 'equal baffle pairing' (i.e. first baffle equal in height to the rest) and the 'unequal baffle pairing' (i.e. first baffle smaller than the rest of the baffles). A detailed analysis of the flow conditions on the downstream slope of the weir was then carried out for both scenarios. These included using a wave probe to locate free surface profiles and a Pitot tube - static tube (PT-ST) combination to perform a slot-based, contour-plot velocity distribution analysis accompanied by a fish pass efficiency matrix over a range of flows. The equipment initially intended for three-dimensional flow analysis, particle tracking using DigImage, was not suitable for the high velocity scenarios encountered. However, the video footage proved useful for flow visualisation and the camera installation was also used to record a debris trial.

In terms of depth of flow, fish swimming conditions benefitted from the use of baffles on the downstream slope of the weir. Assuming that an hydraulic jump is designed to occur on the downstream face of the weir, water depth is thickened at all flow rates from the position of the first baffle to the hydraulic jump. Together with the velocity results, the most challenging section of the weir would thus be between the crest and the first baffle. Although the fish pass arrangement has been designed with the maximum burst speeds in mind, fish are considered to be able to attain instantaneous speeds that are higher than burst speed velocities for very short periods of time (Armstrong 2003a, 2006). It is expected that fish would be able to exploit these speeds, enabling them to surmount the final stretch between the first baffle and the crest. The slots were staggered so that the jet from each slot would impinge directly on the baffle below. Slot size and baffle spacing were both chosen using the coarse fish guidelines provided by Armstrong (2002b). Baffle spacing was further selected to ensure that velocities downstream of each baffle slot were kept less than the velocities within the slots, and the baffle height was increased to cause the baffles to act as roughness elements for the higher flow rates.

Contour-plot velocity distributions were presented for a range of flow rates (i.e. corresponding to generalised flow rates per unit width of 0.067 m^2s^{-1},0.236 m^2s^{-1},

0.392 m^2s^{-1} and 0.680 m^2s^{-1}), both for the equal and unequal baffle pairing arrangements. In addition, the effects of a steeper downstream slope were investigated for the unequal baffle pairing. As part of a novel approach to determining the effectiveness of the fish pass, a fish pass efficiency matrix method was developed and applied to each slot individually and to the fish pass as a whole. This matrix provided an indication as to the predicted pass / fail rate of each fish species and length, using an area-based comparison between fish burst swimming speed and the water velocity. The overall results of the fish pass prediction matrices for the four flow rates tested showed that the use of the low-cost modifications to create a fish pass (using both the equal and unequal baffle pairings) at either the 1:5 or 1:4.55 gradient proved effective to a large degrees. Field tests are needed to verify the validity of these predictions.

Although results in the thesis are generally referred to in terms of Brimpton weir, they have also been generalised for the guidelines required by the Environment Agency (Rhodes and Servais 2006) by calculating the flow rate as a 'flow rate per unit width'.

5. Experiments on the hydrometric effect

The unmodified Crump weir provides reliable flow measurement with the advantage of a small increase in the water depth upstream of the weir (i.e. afflux) at high discharge events. In this project, baffles have been added to the downstream slope in order to improve conditions for fish passage, and the purpose of the experiments discussed in this chapter was to investigate the effect of such baffles upon the total head-discharge relationship.

Although the laboratory work was carried out on a scale model[1] of Brimpton weir (River Enborne, Thames catchment), the adopted fish pass solution is intended to be of general application to Crump weirs at field-scale. Crest pressure tappings are absent from the existing Brimpton weir, which utilises a downstream stilling well for measurement under non-modular flow conditions (Everard 2002; Power 2002). However, for breadth of application, the laboratory model incorporated both a downstream stilling well (in the form of pressure tappings) and crest pressure tappings.

This chapter has been divided into modular flow and non-modular flow. These concepts have been defined in section 2.2.2.

Modular flow: The modular flow experiments fall into the following categories:

Unmodified Crump weir (without baffles) The unmodified Crump weir (i.e. without baffles) was examined in order to compare the laboratory model results with the British Standard (BS1042 1992).

Single baffle The motivation for conducting single baffle experiments was based on the premise that it was the first baffle located downstream from the crest which dominated the hydrometric effect. Therefore a number of baffles of different heights (but geometrically scaled) were fabricated in order to explore the relationship. HR Wallingford (White *et al.* 2005e) had also conducted a number of experiments with similar baffles over a wider flow range, with the added requirement that minimum change was allowable in the total head-discharge relationship . The Cranfield and HR Wallingford data sets have been combined in order to expand the non-dimensional total head-discharge curves. After the fabrication of the preferred fish pass in perspex, a preliminary total head-discharge curve showed that the single baffle data would not be sufficient in estimating the hydrometric effect of a multi-baffled solution.

[1] All data in this chapter is quoted at laboratory scale.

Double baffles A small number of double baffle experiments were conducted to allow for comparison with the single baffle and the preferred (perspex) fish pass layout total head-discharge curves.

Fish pass The preferred fish pass layout described in section 3.3.2 included a first baffle of 24 mm set equal to crest height, with the remaining baffles sized to 40 mm. Additional total head-discharge data for a 40 mm first baffle have been included in Appendix G. (In Chapter 4, the layout with the smaller first baffle has been referred to as the unequal baffle pairing while the layout with the first and second baffles equal was designated the equal baffle pairing.)

Non-modular flow: Unmodified Crump weirs provide for accurate measurement by the combination of a drowned flow reduction factor (f) with the standard equation for modular flow. A series of experiments was initiated in order to determine the change under non-modular conditions. These experiments included the unmodified Crump without baffles, with a single baffle, and the preferred (perspex) fish pass arrangement.

5.1. Modular flow experiments

One of the project objectives was to ascertain the effect of downstream modifications upon the hydrometric function over the whole flow range - both for modular and non-modular flow. This section describes and analyses the modular flow experiments and includes the experiments that were conducted on the standard weir, weir with a single baffle, double baffles and for the preferred fish pass arrangement (i.e. including the equal and unequal baffle pairings). In addition, a comparison is made between these results and those obtained by HR Wallingford (White *et al.* 2005e).

The results of the experiments are discussed and analysed under the following topics:

- Unmodified Crump weir (i.e. no baffles scenario)
- Single baffle experiments
- Comparison of the single baffle experiments with the HR Wallingford results
- Double baffle experiments
- Preferred fish pass arrangement

5.1.1. Unmodified Crump weir (without baffles)

Two sets of total head-discharge experiments are illustrated in Figure 5–1.

(a) Early measurements (12/11/02) using a 4 m water manometer to obtain the differential pressures across the orifice plate (Rhodes and Servais 2003).

(b) Later measurements (03/02/04), using a 400 mb pressure transducer, sampled at 200 Hz and averaged over a minute, to obtain the differential pressures.

Fluctuating water levels in the 4 m manometer (caused by an unsteady pressure differential) resulted in human error being introduced in Method (a). This error was associated with reading the manometer by eye, and the problem was overcome by using Method (b). Also, in the latter[2] total head-discharge measurements, a higher water level was deliberately maintained in the flume exit sump to which the recirculating pump suction main was connected. (It was thought that at high flows the deviation of the total head-discharge measurements from the British Standard curve might be the result of air entrainment into the pump when the sump was drawn down.) The combination of the pressure transducer and modified sump water level gave an improved fit between the data and the British Standard equation, represented by a significant reduction in the mean square residual (MSR[3]) from 0.298 to 0.015 and illustrated by Figure 5–2. For medium to high heads, Figure 5–2 shows that the earlier measurements introduced a nearly constant percentage error whereas the later measurements gave a diminishing trend in percentage error with increasing head.

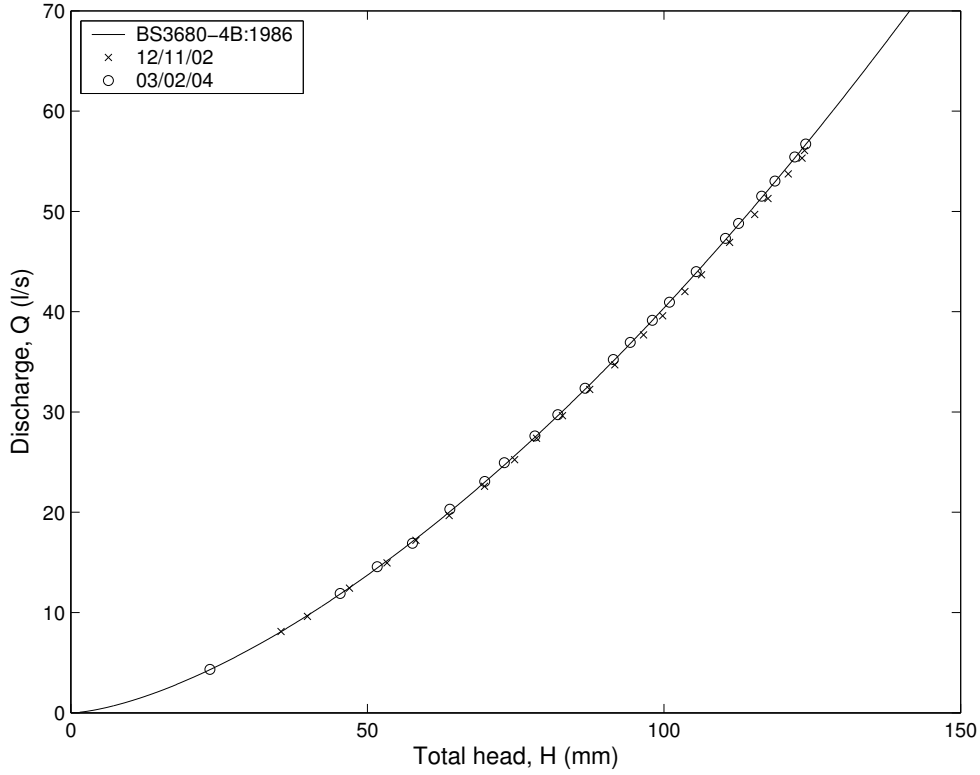

Figure 5–1: Total head-discharge experiments for the standard Crump weir

In conclusion, the installation and experimental techniques associated with using this model provide results which are sufficiently close to the British Standard re-

[2]The total head-discharge experiments for the standard Crump weir represent nine laboratory testing days.

[3]The MSR is the mean of the squared difference between the measured discharge and the corresponding British Standard discharge (for the same total head values).

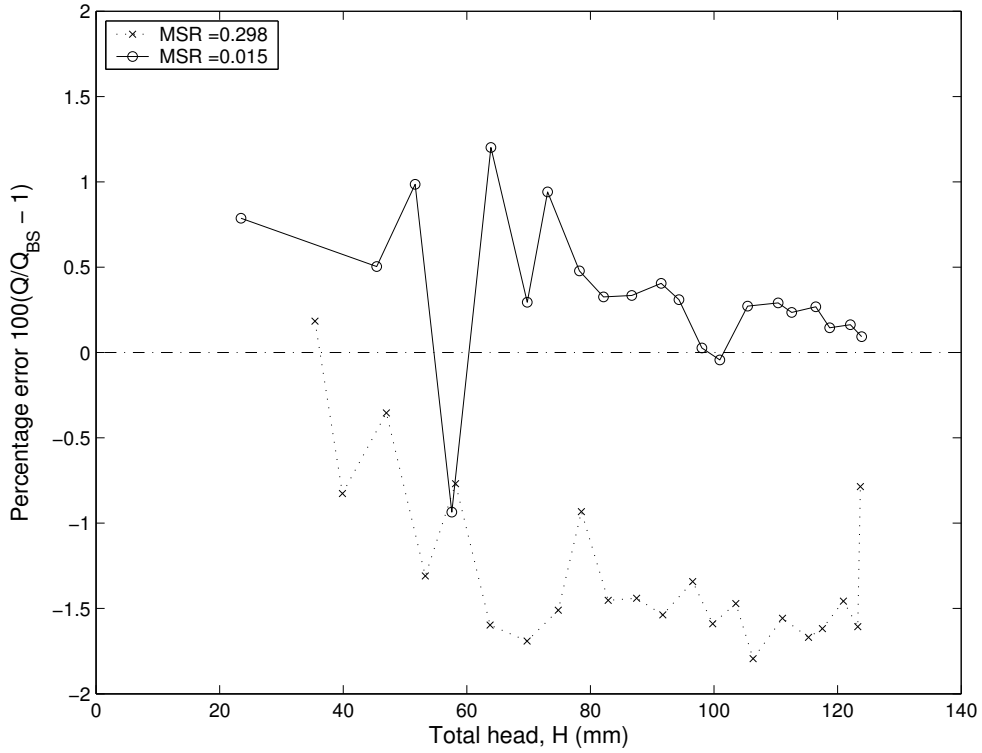

Figure 5–2: Total head vs Percentage error comparing the measured discharge vs British Standard

sults[4]. The results from the experiment dated 3 February 2004 have thus been used henceforth in any comparisons to laboratory data as being representative of British Standard discharge values for this particular Crump weir.

5.1.2. Single baffle experiments

Single baffles with geometrically similar cross-sectional geometries were installed as shown in Figure 3–30 for a wide range of prescribed d/l ratios. Each value of d/l defined a set of geometrically similar baffle arrangements, each having an effect on fish swimming conditions opposite to its impact upon the hydrometry. Generally, high values of d/l were expected to produce beneficial conditions for fish passage but to have a detrimental effect on the total head-discharge relationship, measured in terms of departure from British Standard conditions. By using more than one baffle size for the same d/l, the geometrical similarity of each baffle arrangement was confirmed.

Most experiments were conducted for $d/l = 0.2$ as velocity measurements done during fish passage trials indicated that in order to achieve fish passage for the majority of fish, it would be necessary to limit the velocity on the downstream slope of the Crump weir to 0.51 ms^{-1} at model scale. By ensuring that $d/l = 0.2$ and with baffles at a distance of 64 mm as shown in the LEGO trial arrangements

[4]A smaller orifice plate provided better accuracy for the lower end of the discharge curve, and for later total head-discharge curves, two orifice plates were used.

(see section 4.1.3), velocity maxima occurred upstream of the first baffle, rather than further down the slope. Nominally a $d/l = 0.2$ placed the baffle crest at the same level as the weir crest (actually, the highest point of the baffle was elevated slightly above the weir crest). That ratio was ultimately adopted in the multiple baffle preferred fish pass solution, even though a significant hydrometric effect was observed as is shown later in this section.

The higher $d/l = 0.24$ was designed to show clearly the effect of having the baffle crest significantly higher than the weir crest. The lower ratios, $d/l = 0.183$ to 0.067 were chosen to illustrate the trend of diminishing hydrometric effect (upon the weir discharge coefficient), culminating in an imperceptible effect at the lowest value of d/l.

Based on the premise that the first baffle located downstream from the crest would dominate the hydrometric effect, it was intended that whichever ratio was adopted in the multiple baffled fish pass solution, the results of these single baffle experiments would be useful in predicting the discharge coefficient of the baffled weir. That premise was shown to be in error by some later total head-discharge measurements with two baffles (double baffle experiments) and the multiple baffle arrangement.

For each d/l, the results are presented in a series of graphs showing:

- the geometry, using the 40 mm baffle for ease of comparison, and giving the elevation Δ of the highest point of the baffle above crest level for every baffle height (e.g. Figure 5–3).
- the total head-discharge relationships for the various baffle sizes used, in comparison with that for the British Standard without baffles (e.g. Figure 5–4).
- the total head-discharge data plotted non-dimensionally (e.g. Figure 5–5). The ordinate is the ratio of the measured discharge with the baffle to the British Standard discharge without any baffle, at the same total head (i.e. Q/Q_{BS} or Cd/Cd_{BS}). The abscissa is the ratio of total head to baffle height (H_1/d).

Table 5–1 below shows all the single baffle experiments[5].

The experimental results are discussed and graphs displayed for each individual ratio. Finally, all the data sets are plotted on the same set of axes for further comparison and analysis. The effect of the baffle on the separation bubble is then discussed.

d/l = 0.24

For each d/l there is a unique value of Δ/d, where Δ is defined as the difference between the highest point of the baffle and weir crest level. The highest point is

[5]These single baffle experiments which were generally conducted using two different orifice plates (required to achieve the full flow range at an acceptable level of accuracy), represent 23 days in the laboratory.

Table 5–1: List of single baffle experiments (in the modular flow range)

d/l **ratio**	**Baffle sizes**	
	109.91 mm **orifice plate**	**61.95** mm **orifice plate**
0.24	40	40
0.2	20 30 40 50 60	40 60
0.183	20 40	40 60
0.167	20 40	40 60
0.133	20 40	20 40 60
0.1	20 40	20 60
0.067	20 40	20 40 60

not actually in the centre of the baffle, but is found a little way upstream. For $d/l = 0.24$, $\Delta/d = 0.171$ as shown in Figure 5–3 and, for the 40 mm baffle under consideration, $\Delta = 6.8$ mm. The implication is that weir crest has effectively been moved downstream to the highest point on the baffle.

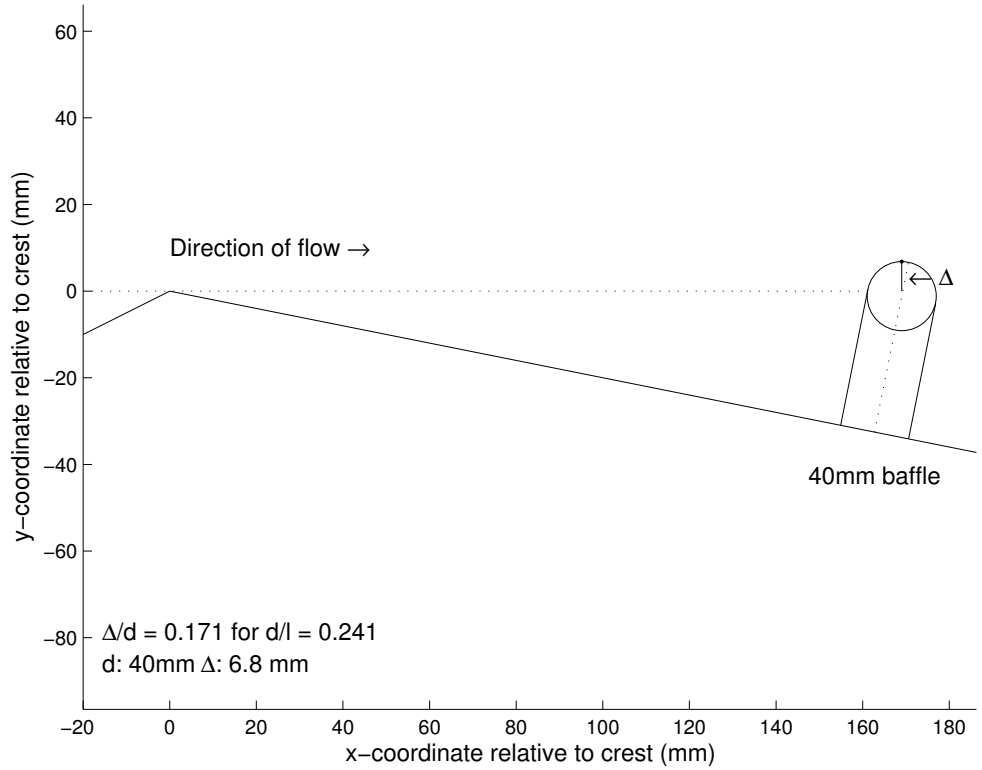

Figure 5–3: Placement of baffle for $d/l = 0.24$

Figure 5–4 shows the total head-discharge curve for the $d/l = 0.24$ layout. The experimental data illustrates that the positioning of the baffle higher than the weir crest results in a significant deviation, ranging from 50% at the lowest total head to 6% at best as shown and discussed with reference to Figure 5–4, from the British standard curve. For all of the d/l ratios, the corresponding discharge measured at a

particular total head is always less than the discharge calculated using the British Standard equation (Eq. 2–1, Sect. 2.2.2). Therefore, if the standard equation is used when a baffle is present, the discharge will always be overestimated to some degree.

For this particular experiment, only the 40 mm baffle was used, and therefore the resulting data forms a single curve. As all of the other d/l ratios consisted of at least two baffle sizes, multiple total head-discharge curves result in more cases. Therefore for clarity, the $d/l = 0.24$ total head-discharge curve is described in more detail and compared with the non-dimensionalised relationship plotted in Figure 5–5. Similar trends in the total head-discharge curves can be observed for the rest of the d/l ratios, although they tend not to be as pronounced and will not be discussed in the same detail. In general the non-dimensional total head-discharge relationships are of most interest, and these are discussed in more depth.

For $d/l = 0.24$, in Figure 5–4 the data lies in two distinct regions, one each side of the data point of $H_1 = 69.44$ mm and $Q = 20.77$ $l\text{s}^{-1}$. To the left of this point the data is right-shifted from the British Standard curve, the gap reduces with increasing H_1 and Q, reaching a minimum of $H_1 = 69.44$ mm and $Q = 20.77$ $l\text{s}^{-1}$. To the right of that point, the data gradually diverges from the British Standard curve.

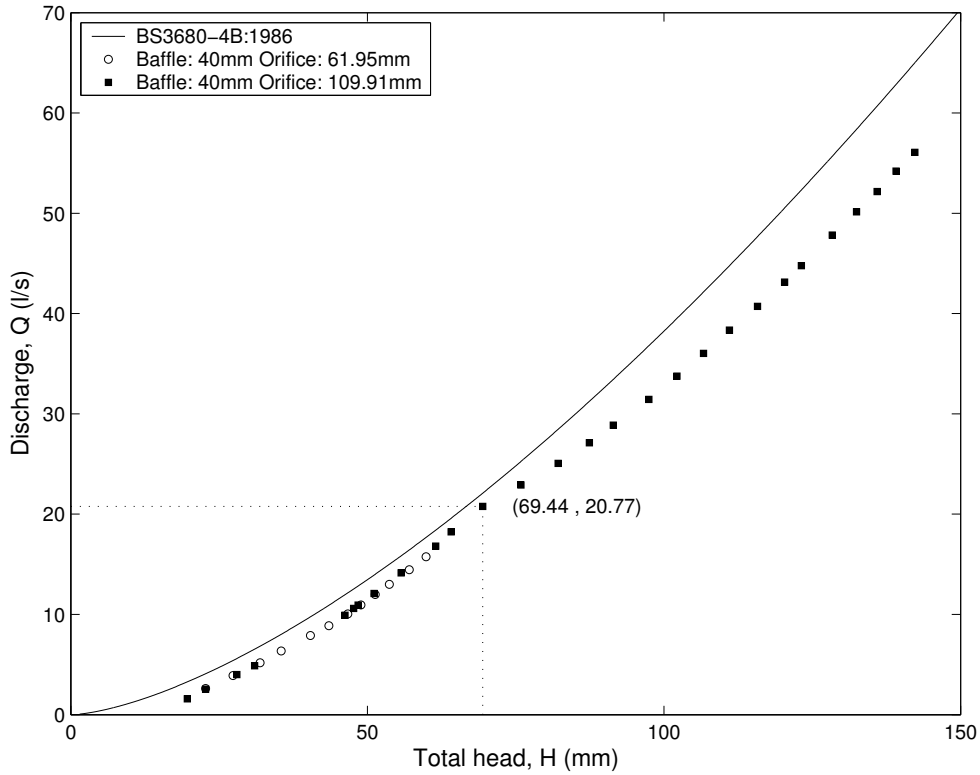

Figure 5–4: Total head-discharge curves with single baffle, $d/l = 0.24$

In Figure 5–5 the data rises steeply to a peak, falls away to a minimum level of $Q/Q_{BS} \approx 0.85$ and then rises very slightly to the limit of the data. The peak occurs where $H_1/d = 1.74$ and the factor $C_d/C_{d_{BS}}$ (and identical to Q/Q_{BS}) $= 0.94$ and corresponds directly with the division (i.e. $H_1 = 69.44$ mm and $Q = 20.77$ $l\text{s}^{-1}$) noted in Figure 5–4. Without the single baffle, $C_d/C_{d_{BS}} = 1$.

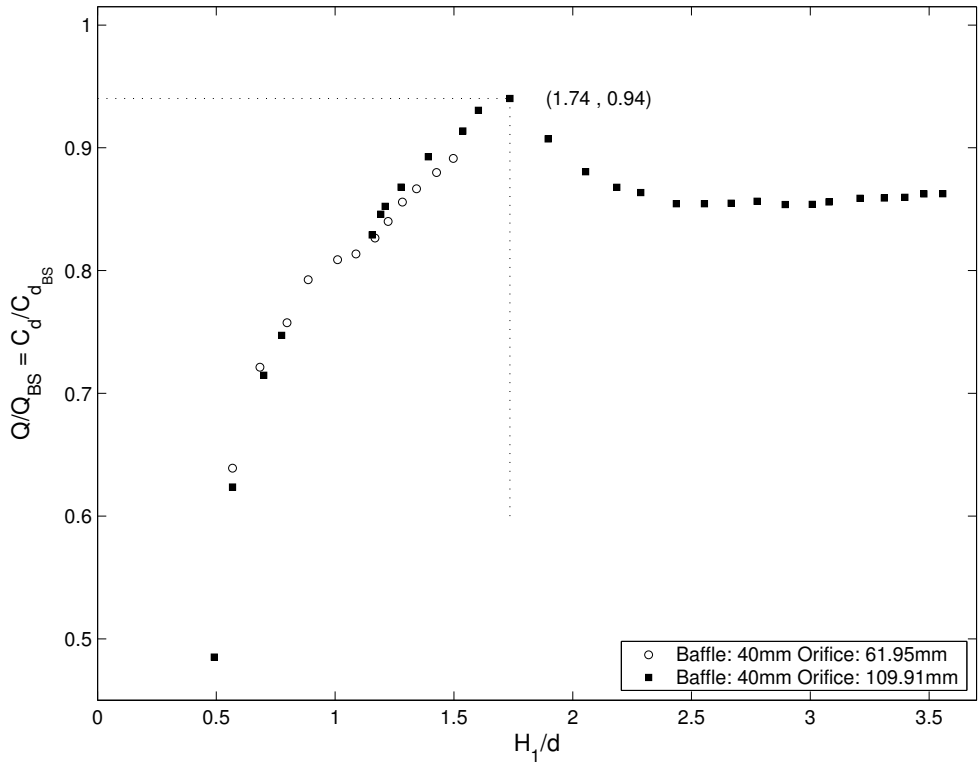

Figure 5–5: Non-dimensional total head-discharge relationships with single baffle, $d/l = 0.24$

For small values of H_1/d, the impact on $C_d/C_{d_{BS}}$ results in the greatest deviation from the British Standard. This implies that if the British Standard equation were directly applied for very low head values, the real discharge could be 50% less than the calculated discharge of that head, thus causing inflated discharge values. It is postulated that the deviation from the British Standard to the left of the peak of H_1/d is as a result of the transfer of control from the weir crest to the top of the baffle. The shape of the curve to the right of $H_1/d = 1.74$ is probably caused by the effects of the separation bubble (described in section 2.3.5).

Figure 5–5 has been replotted as Figure 5–6 using the same axes as those used for all of the non-dimensional graphs. The choice of axis dimensions is important in order to prevent the reader from gaining an inaccurate perception of the relationships between the different data sets. In this case, as only the 40 mm baffle was used in this experiment, the limit of the data was $H_1/d \approx 3.6$, whereas by using the 20 mm baffles for the rest of the experiments the data was extended to $H_1/d \approx 7$.

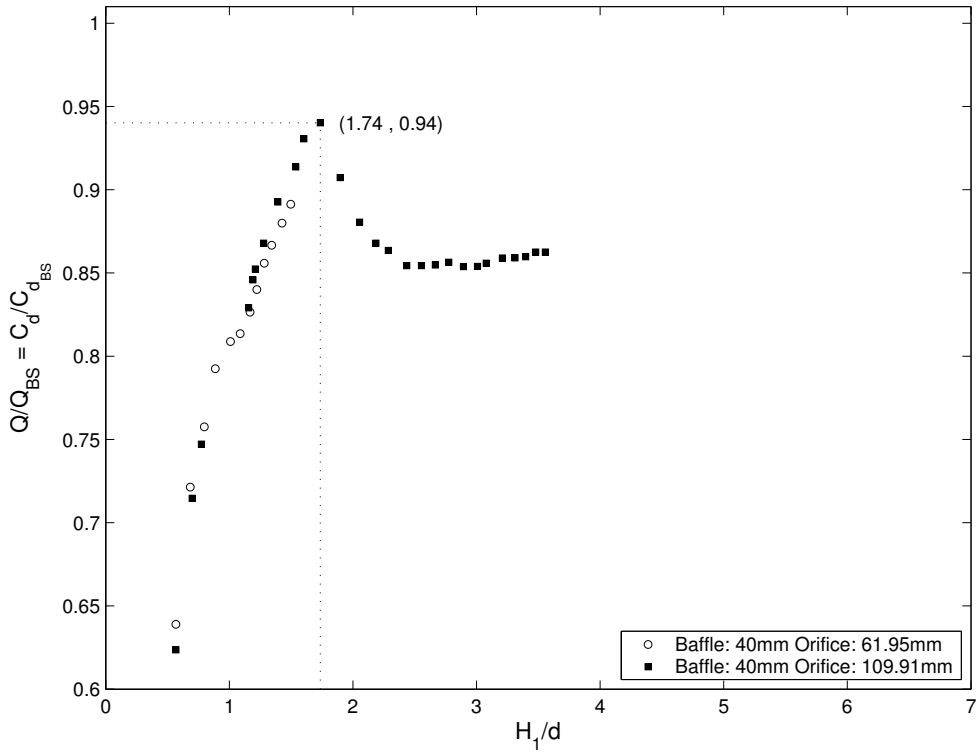

Figure 5–6: Standardised plot: Non-dimensional total head-discharge relationships with single baffle, $d/l = 0.24$

d/l = 0.2

The initial experimental results for the $d/l = 0.2$ experiments were reported by Rhodes and Servais (2004).

Figure 5–7 illustrates that for $d/l = 0.2$, the highest point of the baffle is slightly above the weir crest for all four baffle sizes tested. For example, $\Delta = 0.23$ mm for the 60 mm baffle resulting in the relationship of $\Delta/d = 3.88 \times 10^{-3}$. A positive Δ implies that the weir crest can considered to be drowned at zero and low-flow conditions.

All of the experimental data for the five baffle heights tested are shown in Figure 5–8, where the measurements increasingly depart from the British Standard curve for increasing head on the weir and decreasing baffle size.

The non-dimensional total head-discharge graph (Figure 5–9) is more informative as virtually all of the data collapses onto a single curve. This curve shows a somewhat similar shape to that represented in Figure 5–6, but as is to be expected with the lowering of the baffle in relation to the crest, departure from the British Standard factor of $C_d/C_{d_{BS}} = 1$ is far less extreme. The data to the left of the peak rises steeply to begin with, and then flattens out before rising again to the peak at $H_1/d = 1.68$ and $C_d/C_{d_{BS}} = 0.98$ for the 20 mm and 40 mm baffles. The 60 mm baffle has a slightly different shape in that the data comes to an initial peak, dips again and then peaks at $H_1/d = 1.68$. The reason for this discrepancy in the data is not clear. It is important to note that this shape is also observed in the double

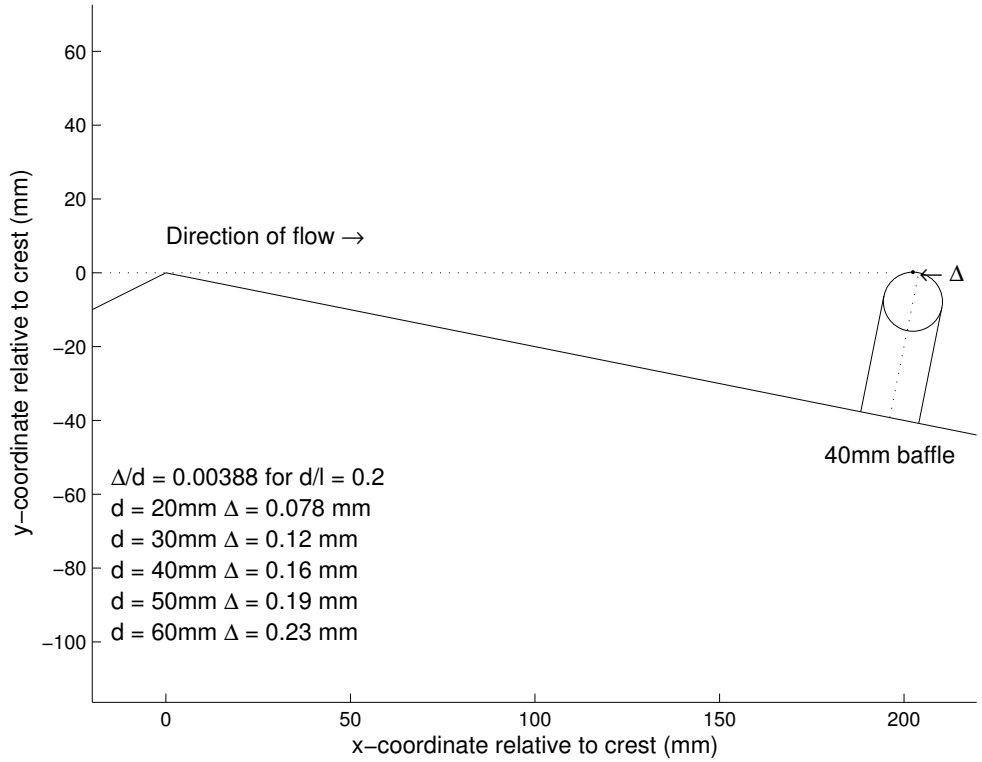

Figure 5–7: Placement of baffle for $d/l = 0.2$

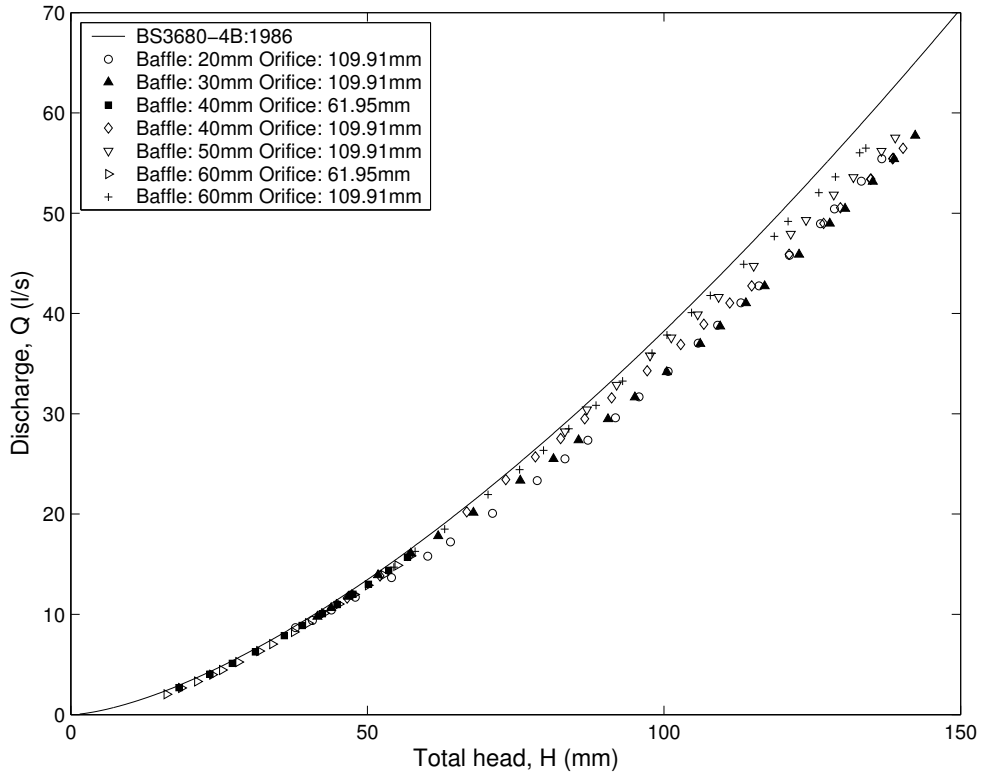

Figure 5–8: Total head-discharge curves with single baffle, $d/l = 0.2$

baffle experiments reported in section 5.1.4. To the right of the peak, the data falls away more gradually than the $d/l = 0.24$ data set until reaching a local minimum of approximately 0.87, before rising again to the end of the data set.

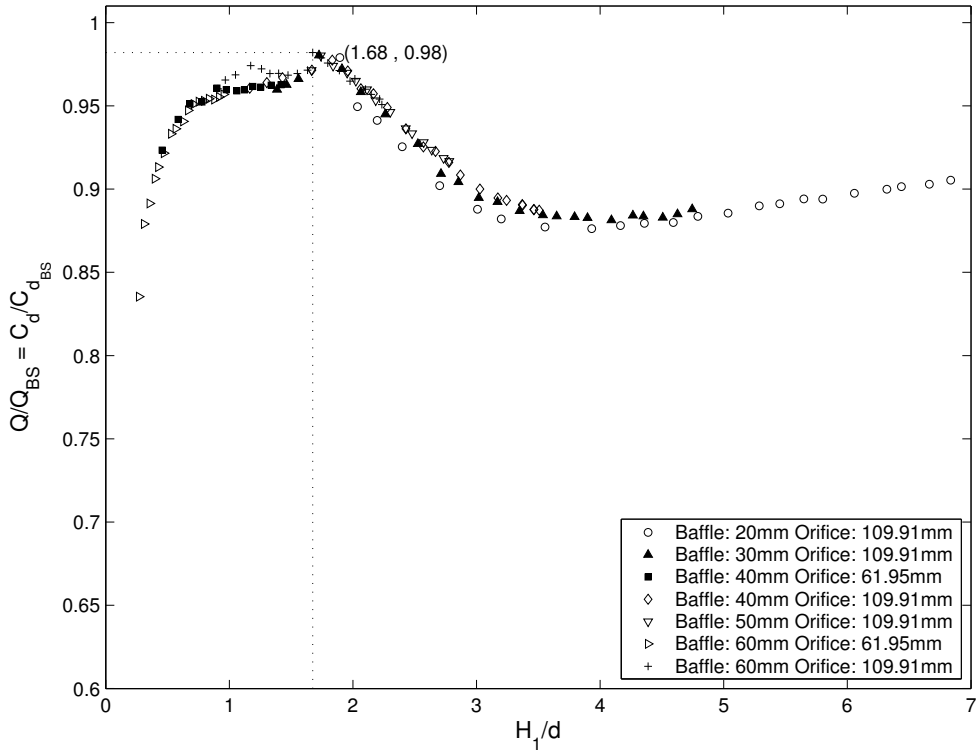

Figure 5–9: Non-dimensional total head-discharge relationships with single baffle, $d/l = 0.2$

Examination of the curve to the right of the peak shows that there is a slight upward shift in the data as the baffle size increases. Experience showed that the smaller the baffle, the more difficult to locate the baffle exactly parallel to the crest (in plan), normal to the crest (in cross-section) and at exactly the correct distance. In general placement accuracy was assessed to be ± 0.5 mm in either direction, resulting in a systematic error being introduced. An additional complication was that in order to complete all the experiments in as short a time period as possible, it proved necessary to keep the orifice plate in place and change the baffles. It is recognised that it would have introduced less error had it been possible to complete each total head-discharge experiment for a single installation of each baffle size. Changing the orifice plate would have required assistance not available during that testing period, and more importantly, would have introduced far more unproductive setup time periods when considering the time needed to prime and warm-up the pressure transducers.

The presence of the baffle interferes with the formation of a separation bubble immediately downstream of the weir crest. The baffle effectively distorts the geometry of the separation streamline, and thus causes the observed deviation (of the measured discharge from the British Standard) for the higher H_1/d values to the right of the peak (i.e. $H_1/d >= 1.68$). From this point, the baffle increasingly interferes

with the separated flow region until a minimum value of $C_d/C_{d_{BS}} \approx 0.87$ is reached, whereupon the separation bubble has become large enough to encompass the baffle (as shown in Figure 2–20). This effect diminishes at the higher values of H_1/d. The effect of the separation bubble is present throughout the range of d/l, and further comment on the mechanisms is continued later in the discussion of the combined data sets.

d/l = 0.183

Figure 5–10 illustrates that for $d/l = 0.183$, the highest point of the baffle is below the weir crest for all of the baffle sizes. For example, $\Delta = -5.23$ mm for the 60 mm baffle resulting in the relationship of $\Delta/d = -8.72 \times 10^{-2}$.

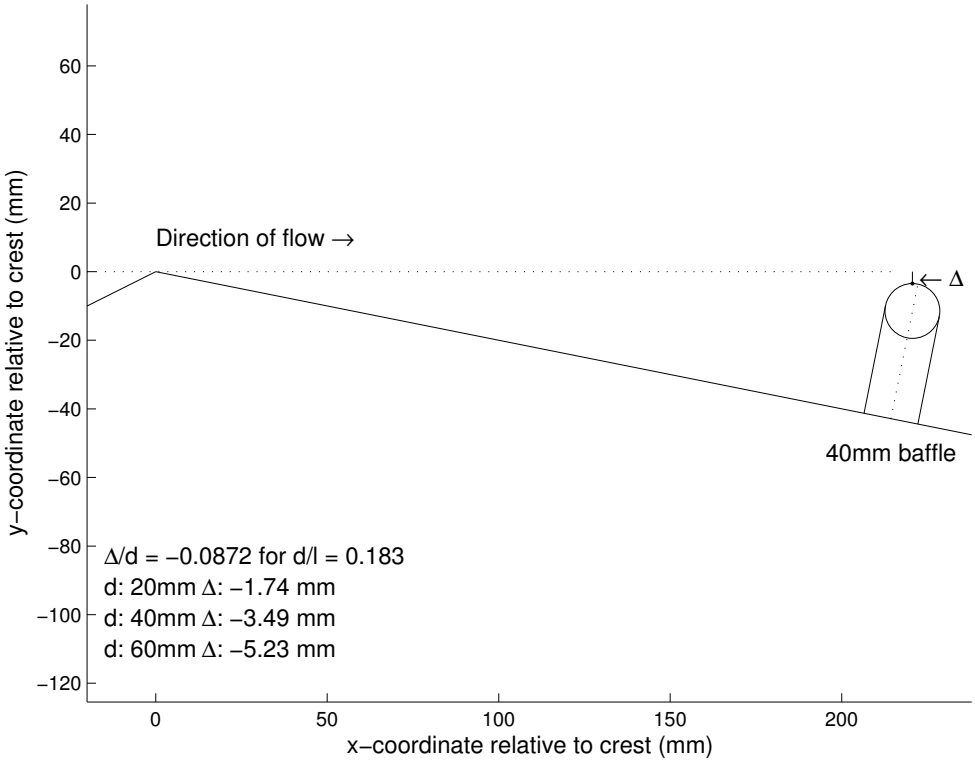

Figure 5–10: Placement of baffle for $d/l = 0.183$

Figure 5–11 shows the total head-discharge data for the three baffle heights tested. Note that for all of the d/l ratios, the quality of the data was evaluated on the basis of the non-dimensional graphs (i.e. Figure 5–12 in this case). Two orifice plate sizes were used, namely 109.91 mm and 61.95 mm. Where data overlapped in the non-dimensional graph (i.e. Figure 5–12 in this case), precedence was given to the smaller orifice plate which was more accurate for the lower heads, and the data from the larger orifice plate was generally disregarded. This has had the effect of causing a gap in the normal total head-discharge plot, which is perhaps best observed for the 40 mm data sets for $d/l = 0.183$ (i.e. Figure 5–11).

The curve plotted in the non-dimensional Figure 5–12 does not show the peak in the data as observed for $d/l = 0.24$ and 0.2. The maximum of $C_d/C_{d_{BS}} = 0.98$ occurs

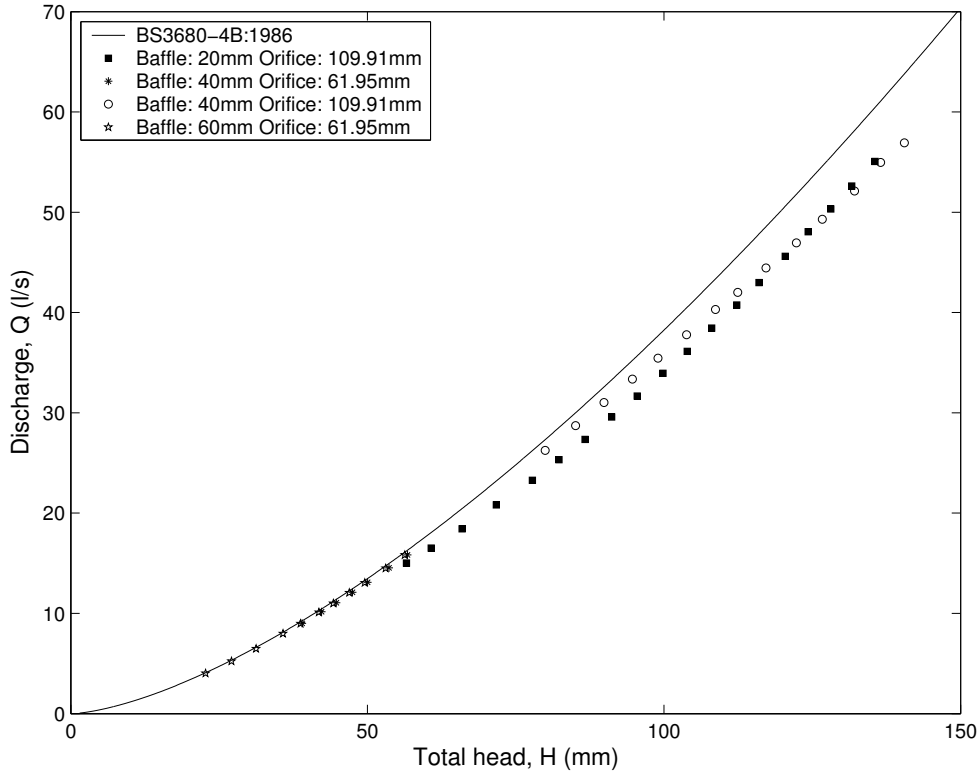

Figure 5–11: Total head-discharge curves with single baffle, $d/l = 0.183$

at the lower value of $H_1/d = 0.78$. The 20 mm and 40 mm data sets measured for the small orifice diameter appear to be shifted somewhat from each other. In addition, there is a gap of approximately $H_1/d = 0.5$ between the 40 mm data sets when testing was done using the small orifice and large orifice plates respectively. Retrospectively it might have been useful to complete the set by including the 30 mm baffle. As this was an unexpected result, this omission was not identified at the time when the single baffle experiments were conducted, and time constraints prevented this oversight from being rectified. Nevertheless, the trend seems well established and does not prevent analysis of the complete d/l data set.

Past the maximum point, the data falls to a local minimum factor of approximately 0.88, whereupon a gentle rise occurs to the limit of the data.

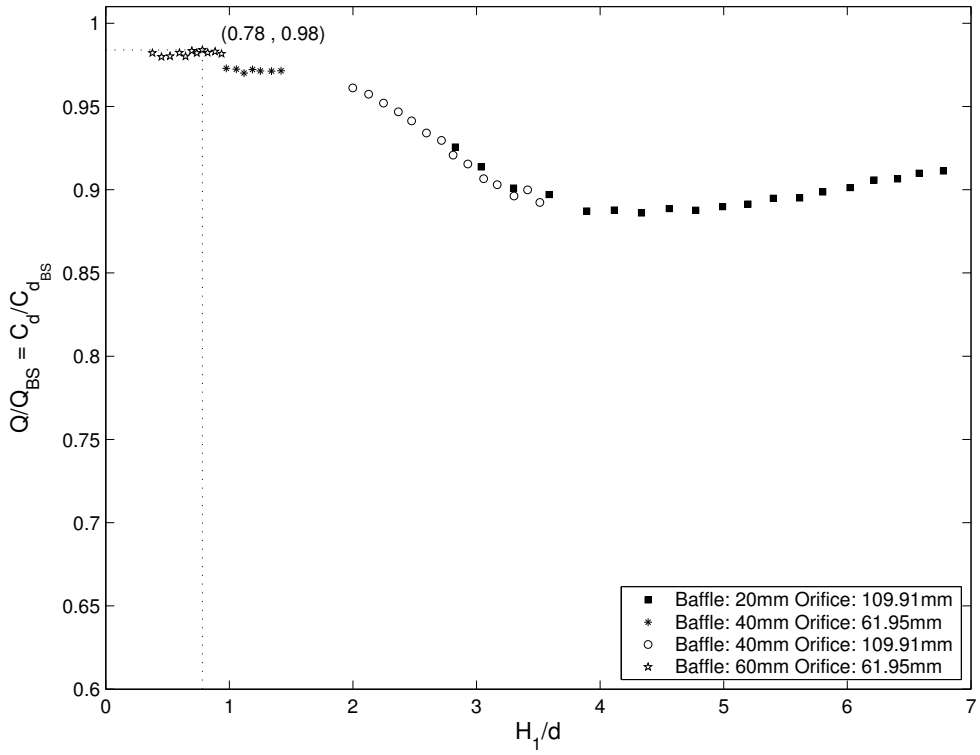

Figure 5–12: Non-dimensional total head-discharge relationships with single baffle, $d/l = 0.183$

d/l = 0.167

Figure 5–13 illustrates that for $d/l = 0.167$, the highest point of the baffle is below the weir crest for all of the baffle sizes. For example, $\Delta = -11.4$ mm for the 60 mm baffle resulting in the relationship of $\Delta/d = -0.19$.

Figure 5–14 shows the total head-discharge data for the three baffle heights tested.

The non-dimensional data set depicted in Figure 5–15 shows a very slight rise up until a maximum of $H_1/d = 0.94$ and $C_d/C_{d_{BS}} = 0.98$. The resolution of the peak in each non-dimensional curve depended on the number of the data points, and increments of discharge were deliberately kept small for that reason. The estimated location of each peak varied with d/l. Once again, there is a slight gap between the two 40 mm data sets for the two different orifice plate sizes, and the conclusions drawn from the $d/l = 0.183$ results are considered to be valid here also.

From the maximum point, the non-dimensional curve falls gently at first and then slightly more steeply until a local minimum factor of 0.89 is reached, whereupon the curve rises to the limit of the data.

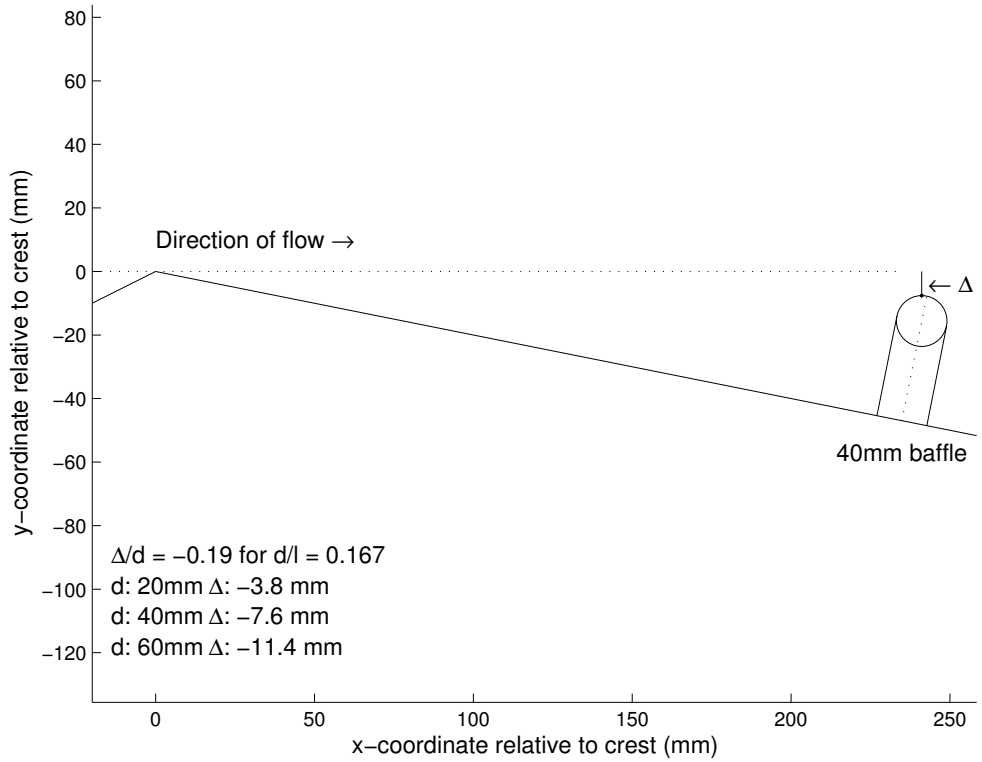

Figure 5–13: Placement of baffle for $d/l = 0.167$

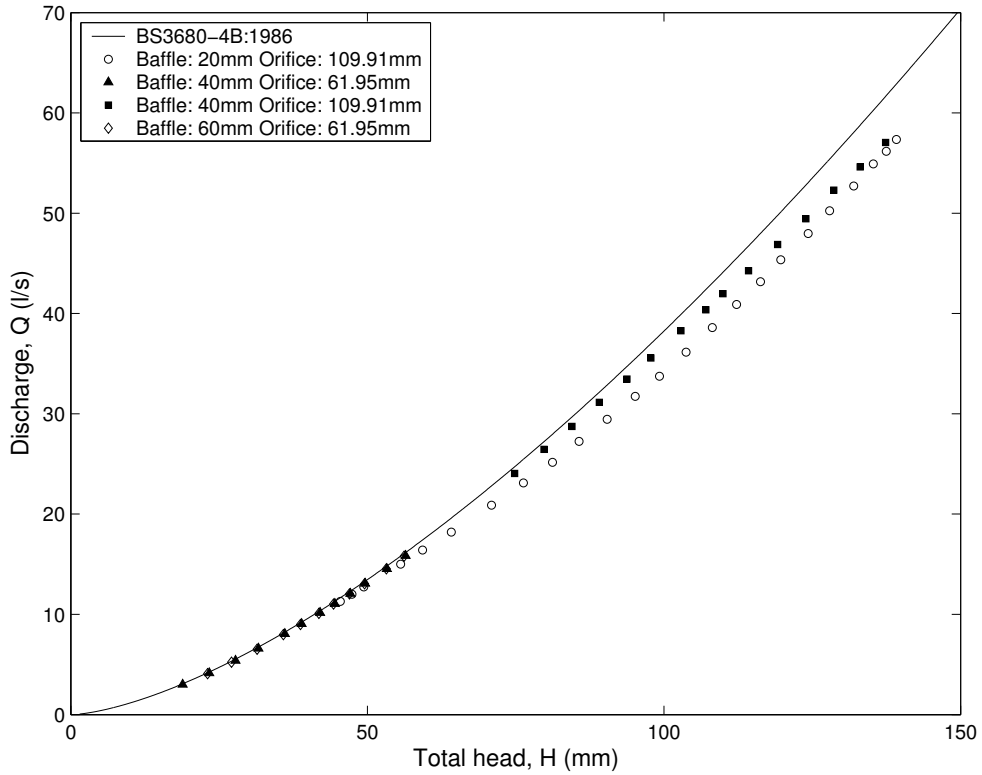

Figure 5–14: Total head-discharge curves with single baffle, $d/l = 0.167$

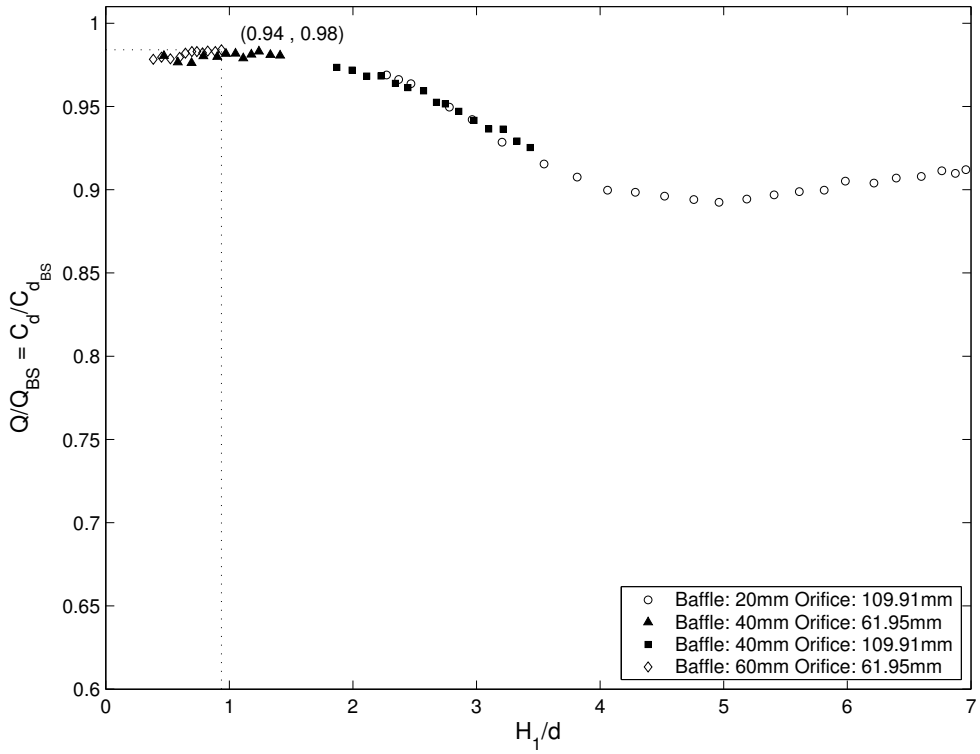

Figure 5–15: Non-dimensional total head-discharge relationships, $d/l = 0.167$

d/l = 0.133

Figure 5–16 illustrates that for $d/l = 0.133$, the highest point of the baffle is below the weir crest for all of the baffle sizes. For example, $\Delta = -29.4$ mm for the 60 mm baffle resulting in the relationship of $\Delta/d = -0.49$.

Figure 5–17 shows the total head-discharge data for the three baffle heights tested.

The 60 mm data set on the non-dimensional Figure 5–18 is slightly discontinuous with the rest of the data. After a slight rise in the 60 mm section of the curve, the data joins with the 40 mm data set, which contains the maximum H_1/d value of 0.97 and $C_d/C_{d(BS)} = 0.99$. A steady fall in the curve continues to the limit of the data, where a factor of approximately 0.92 is noted, as determined by the minimum baffle height and the maximum head on the weir. It is postulated that for $d/l = 0.133$, no local minimum was observed on the non-dimensional total-head discharge graph as it was not possible to achieve a large enough H_1/d.

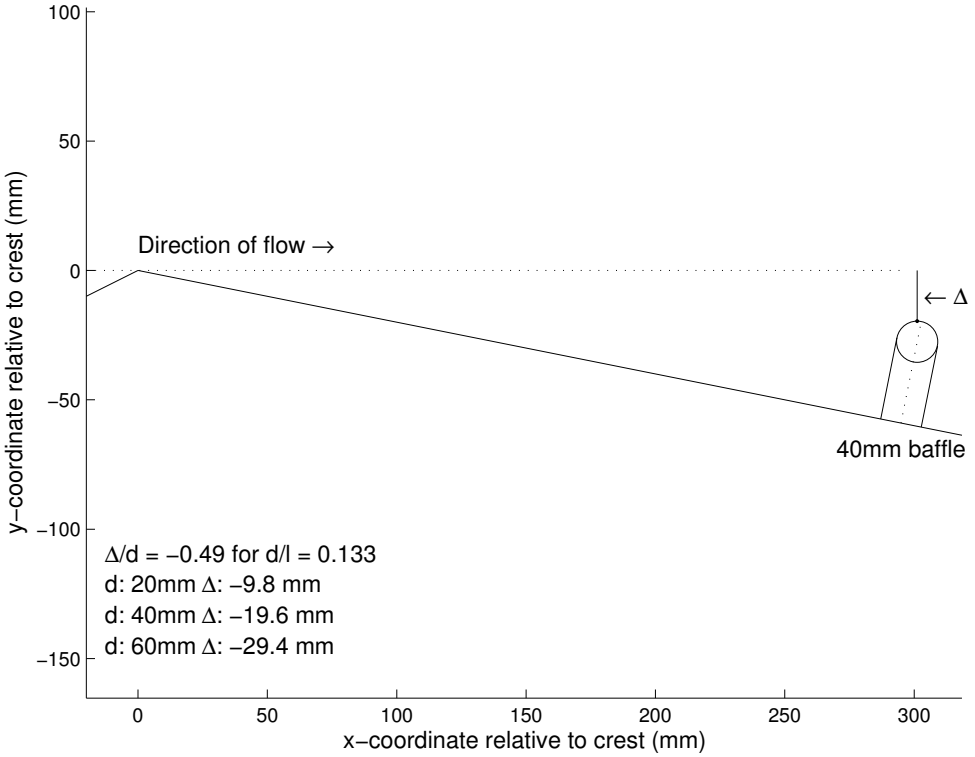

Figure 5–16: Placement of baffle for $d/l = 0.133$

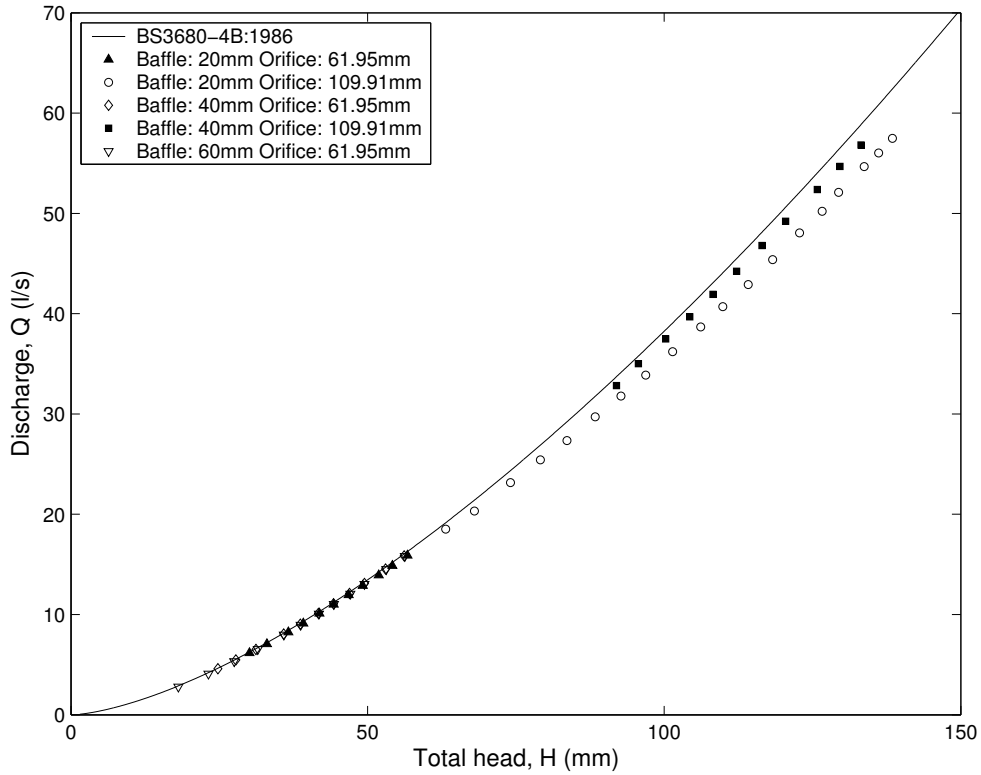

Figure 5–17: Total head-discharge curves with single baffle, $d/l = 0.133$

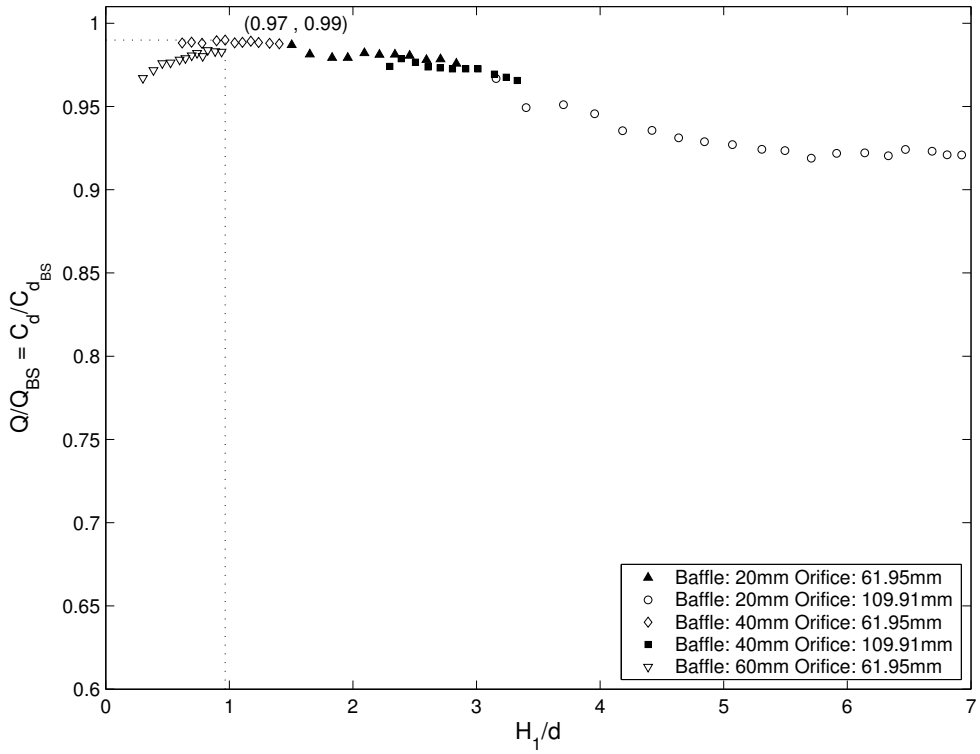

Figure 5–18: Non-dimensional total head-discharge relationships with single baffle, $d/l = 0.133$

d/l = 0.1

Figure 5–19 illustrates that for $d/l = 0.1$, the highest point of the baffle is below the weir crest for all the baffle sizes. For example, $\Delta = -58.6$ mm for the 60 mm baffle resulting in the relationship of $\Delta/d = -0.977$.

Figure 5–20 shows the total head-discharge data for the three baffle heights tested.

$C_d/C_{d_{BS}}$ in Figure 5–21 shows a slight rise for increasing values of H_1/d less than 1, whereupon the data levels out until $H_1/d \approx 3.25$. From $H_1/d \approx 3.5$ there is a slight decrease in $C_d/C_{d_{BS}}$ to approximately 0.95 where the limit of the data is reached. It is postulated that for $d/l = 0.1$, no local minimum was observed on the non-dimensional total-head discharge graph as it was not possible to achieve a large enough H_1/d.

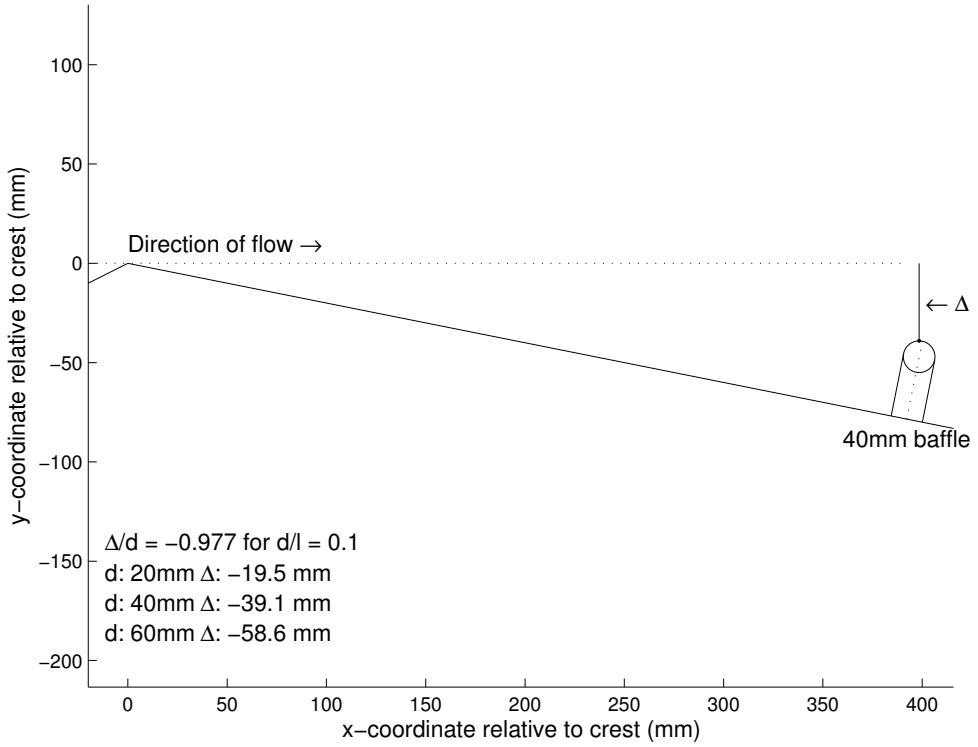

Figure 5–19: Placement of baffle for $d/l = 0.1$

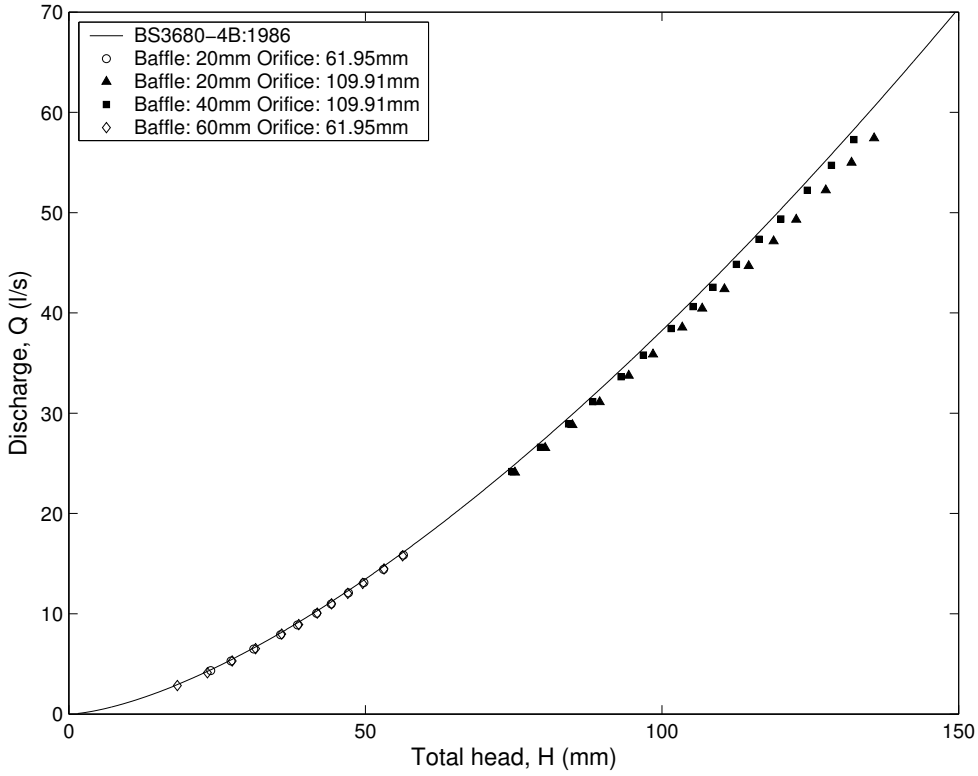

Figure 5–20: Total head-discharge curves with single baffle, $d/l = 0.1$

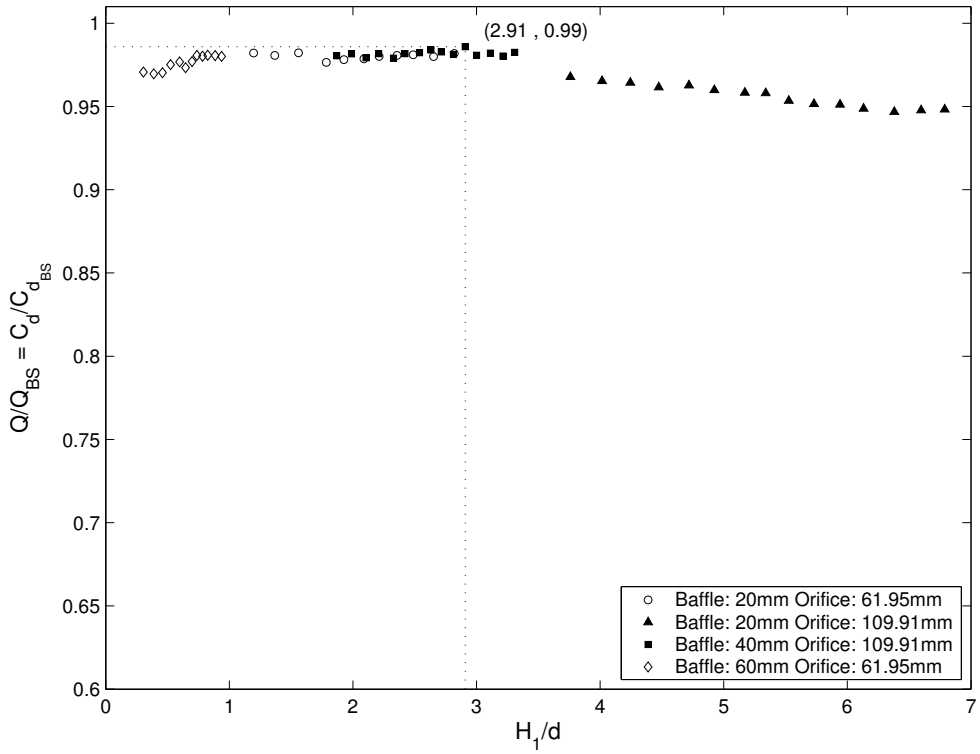

Figure 5–21: Non-dimensional total head-discharge relationships with single baffle, $d/l = 0.1$

d/l = 0.067

Figure 5–22 illustrates that for $d/l = 0.067$, the highest point of the baffle is below the weir crest for all baffle sizes. For example, $\Delta = -117$ mm for the 60 mm baffle resulting in the relationship of $\Delta/d = -1.94$. Note that Δ is approximately twice the height of the baffle.

Figure 5–23 shows the total head-discharge data for the three baffle heights tested.

As can been seen in Figure 5–24, there is a fair amount of scatter within this data set which is especially noticeable for values of H_1/d less than 2. For values of $H_1/d < 1$, $C_d/C_{d_{BS}}$ decreases from approximately 1 to roughly 0.96. The shape of the curve presented in Figure 5–24 is convex downwards, with a minimum $C_d/C_{d_{BS}} \approx 0.96$ observed for approximately $1 < H_1/d < 4$. When $H_1/d > 4$, $C_d/C_{d_{BS}}$ begins to increase until the limit of the data is reached. The maximum value for $C_d/C_{d_{BS}}$ is 1, at a value of $H_1/d = 6.54$.

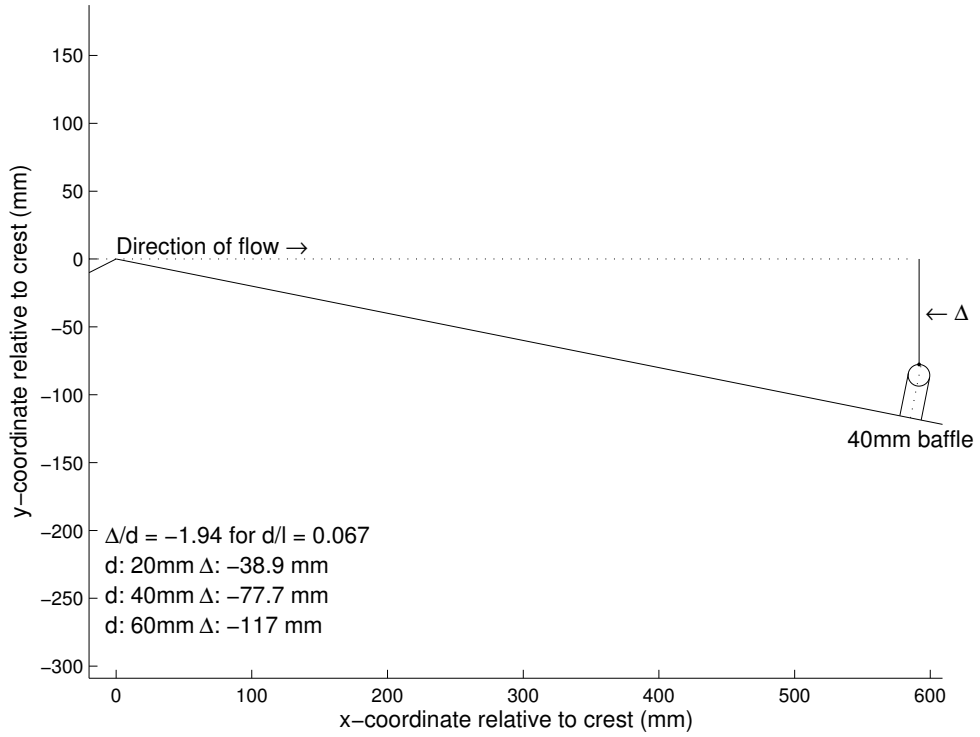

Figure 5–22: Placement of baffle for $d/l = 0.067$

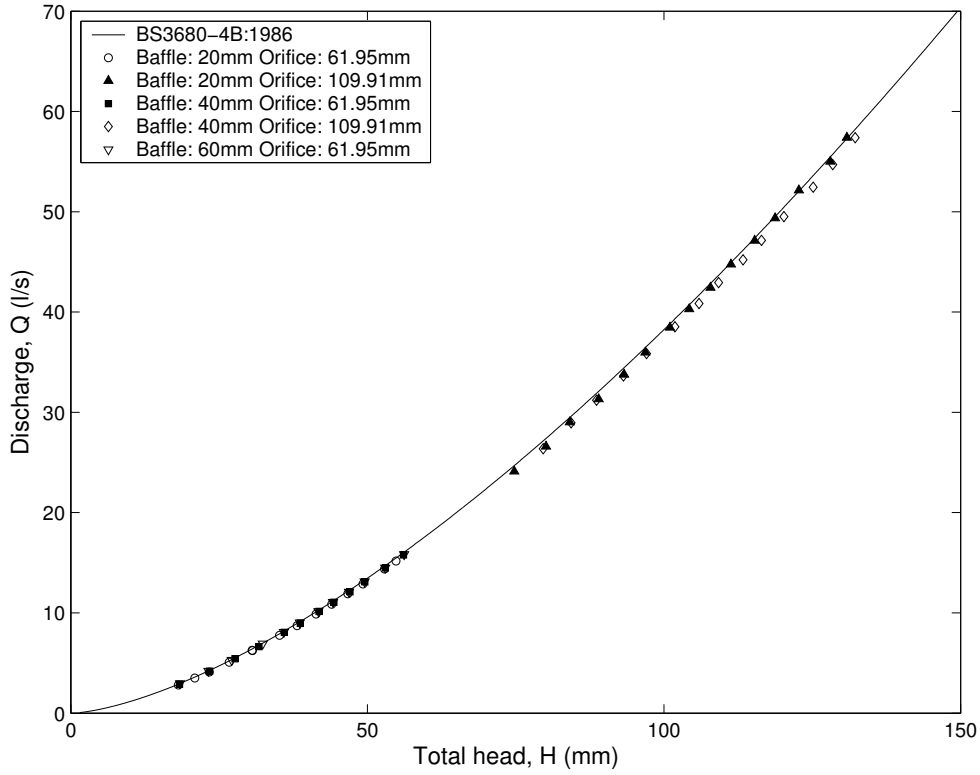

Figure 5–23: Total head-discharge curves with single baffle, $d/l = 0.067$

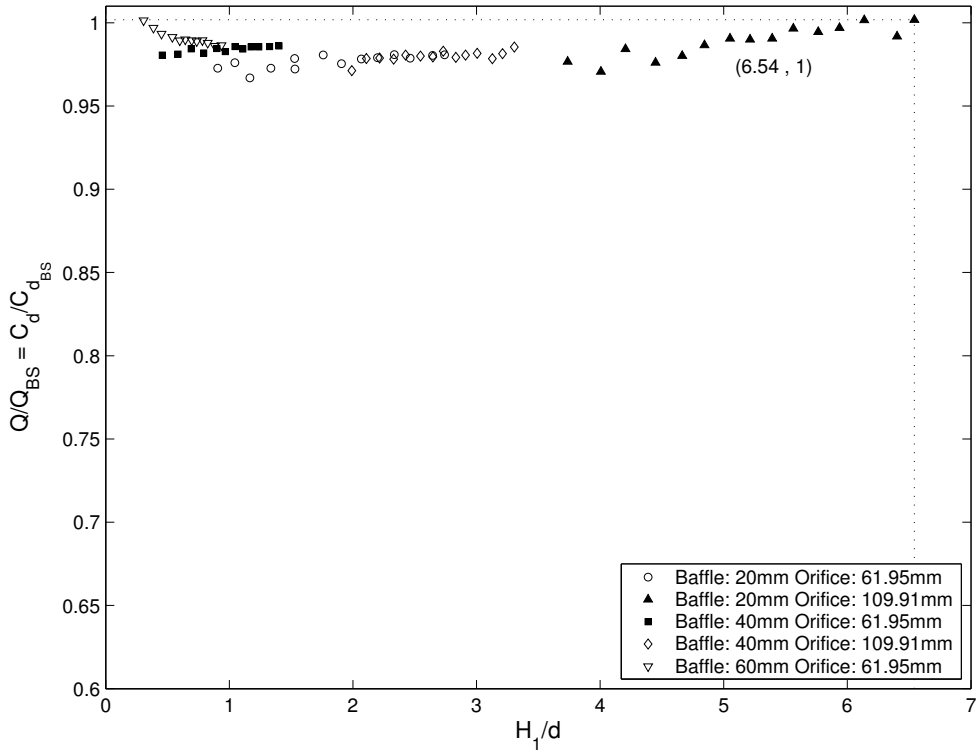

Figure 5–24: Non-dimensional total head-discharge relationships with single baffle, $d/l = 0.067$

Comparison of all the single baffle data

For comparison, the results from all of the single baffle experiments are plotted on the same set of axes, and once again both the normal and the non-dimensional total head-discharge curves are presented in Figures 5–25 and 5–26 respectively. The results represent data from the seven d/l configurations investigated, and include data for the various baffle sizes (summarised in Table 5–1) and the two orifice plates used.

Figure 5–25 demonstrates that departure from the British Standard curve varies according to the baffle size used as well as the d/l configuration. For $d/l = 0.24$, where the baffle is higher than the weir crest, the difference between the actual flow and the British Standard theoretical flow is apparent over the whole flow range. The rest of the d/l ratios represent those baffles where the baffle height is either equal to or less than the weir crest.

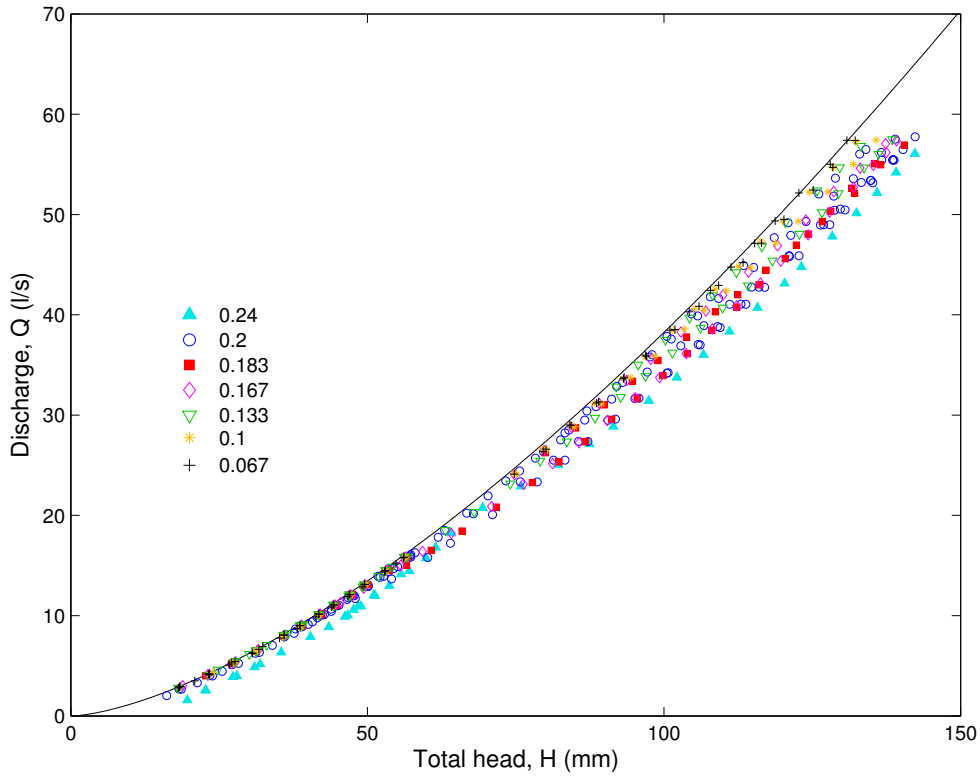

Figure 5–25: Total head-discharge curves with single baffle, all d/l data sets

The same measurements are represented in the non-dimensional graph (Figure 5–26), and demonstrate that there is an unique curve for each d/l ratio.

The situation where the single baffle no longer causes the observed discharge to deviate from the calculated British Standard discharge can be represented by $Cd/Cd_{BS} = 1$, and this is appears to be reached for $d/l = 0.067$ where $H_1/d \geq 6$. Figures 2–19 and 2–20 illustrate the separation bubble mechanism for the unmodified Crump weir, and the weir with a single baffle respectively.

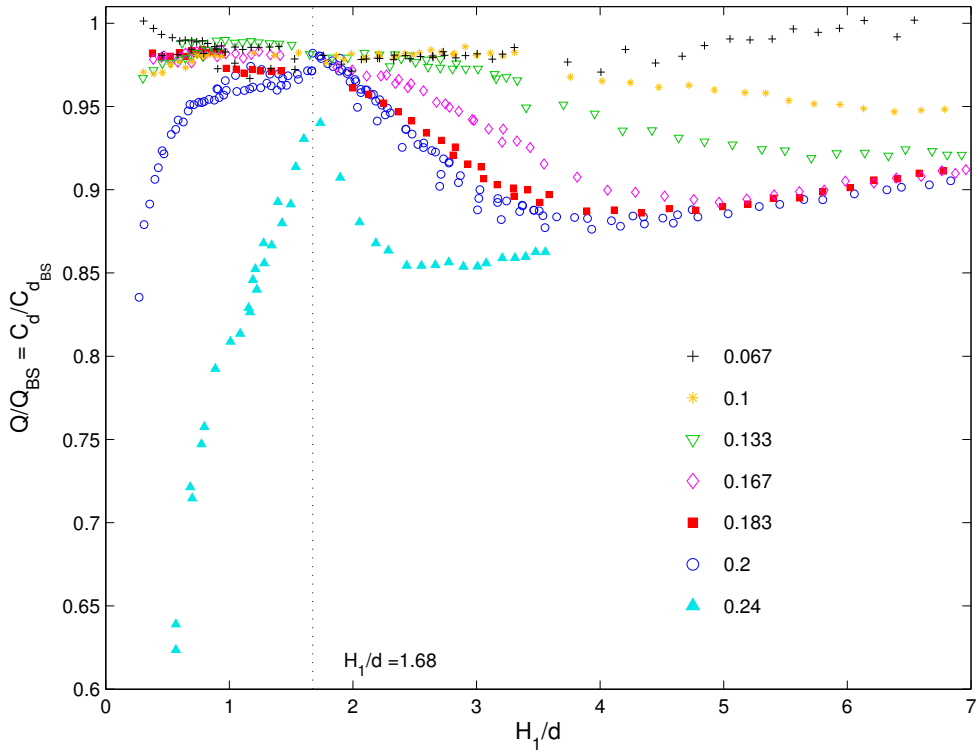

Figure 5–26: Non-dimensional total head-discharge relationships with single baffle, all d/l data sets

The maximum factor of 0.98 corresponding to $H_1/d = 1.68$ is plotted as the dotted line on Figure 5–26. Although this point is also the peak for $d/l = 0.2$ data set, it also appears to be a significant point for the entire d/l range investigated. To the left of this dividing line the data can be separated into two different categories:

Baffle equal to or higher than the crest: Both the $d/l = 0.24$ and $d/l = 0.2$ show similar trends. As a result of the fact that the baffle is higher than the crest, for very low heads $C_d/C_{d_{BS}}$ departs significantly from the British Standard. The curves then rise to a peak. For $d/l = 0.24$, Q would be over-estimated at best by 6% and at worst by 51.5%[6].

Baffle lower than the crest: For the rest of the d/l ratios, the data to the left of the dotted line either rises slightly for the higher d/l values or falls slightly for the lower d/l values around $C_d/C_{d_{BS}}$ approximately equal to 0.98. Thus up until the dotted line the minimum deviation of C_d from the British Standard is approximately 1% and the maximum is approximately 4%, corresponding with an over-estimate of Q of less than 4%.

To the right of the dotted line, for $H_1/d = 1.68$, it is postulated that the influence of the baffle on the separation bubble causes the variation in the deviation from the British Standard. It could be inferred from this data set that for $H_1/d > 1.68$, the

[6]See Figure 5–5 as this data point is not plotted on the standardised range used for comparative purposes for the range under consideration

presence of the baffle increasingly interferes with the separated flow region until a minimum value is reached whereupon the separation bubble has become large enough to encompass the baffle (as shown in Figure 2–20), and this effect diminishes at the higher values of H_1/d. For the largest d/l ratios, this deviation is far more marked; for decreasing d/l ratios the local minimum factor is reached at a higher value of H_1/d, while for the smallest d/l values it appears not to have been reached within the data range.

The outcome of this set of results is that a generalised rule may be drawn up for the prediction of the overestimation of discharge in the presence of a single baffle. For $H_1/d < 1.68$ and $0.067 \leq d/l \leq 0.183$, the discharge will be over-estimated by between 1% and 4%. For $d/l = 0.2$, the discharge will be overestimated by up to 16.5% for very low H_1/d values, or assuming a $H_1/d \geq 1.68$, a maximum overestimation would be 13% for $H_1/d \approx 3.5$. By raising the baffle above the crest this overestimation in discharge can exceed 50% when $d/l = 0.241$. For $H_1/d \geq 1.68$ and the smaller the d/l ratio (i.e. the further the baffle from the crest), the less the deviation from the British Standard. Thus for a maximum overestimation of 6%, a $d/l \leq 0.1$ is required. However, in order to reduce the velocity and increase the flow depth on the downstream face of the Crump weir for realistic fish passage improvement, it has already been shown that the optimal placement of the first baffle is for a $d/l = 0.2$. If these single baffle experiments were used for guidance, the maximum overestimation in discharge predicted would be 13%.

5.1.3. Comparison of the single baffle experiments with the HR Wallingford results

Recent research conducted at HR Wallingford by White *et al.* (2005e) has been introduced in sections 2.3.4 and 2.3.5. This data set is referred to as the HR Wallingford data in this section.

The baffles used by Cranfield and HR Wallingford are geometrically dissimilar. The Cranfield single baffle dimensions ($w = d/2.5$) were based on the preferred perspex baffle layout under investigation whereas HR Wallingford based the baffle dimensions ($w = d/1.5$) on those used at the Hurn Weir (see section 2.3.4).

The HR Wallingford data[7] is presented in Figure 5–27. Note that the axes definition is identical to that used for all of the Cranfield non-dimensionalised total head-discharge figures. In addition and for ease of reference, the data was adjusted such that the baffle parameter definitions l, d and w were in line with the Cranfield definitions shown in Figure 3–30.

The HR Wallingford design approach for this experiment data set was to test for conditions where flow control was required to be maintained at crest level and did not encroach upon the baffle in any way. In order to achieve this, the configurations used were set such that the minimum value of $H_1/d = 2.5$. For the scenarios tested, a maximum of 7% deviation to the basic Crump weir coefficient of discharge was

[7]The data was obtained by careful analysis of Figure 5.4: Hydrometric effect of near crest baffles, in White *et al.* (2005e).

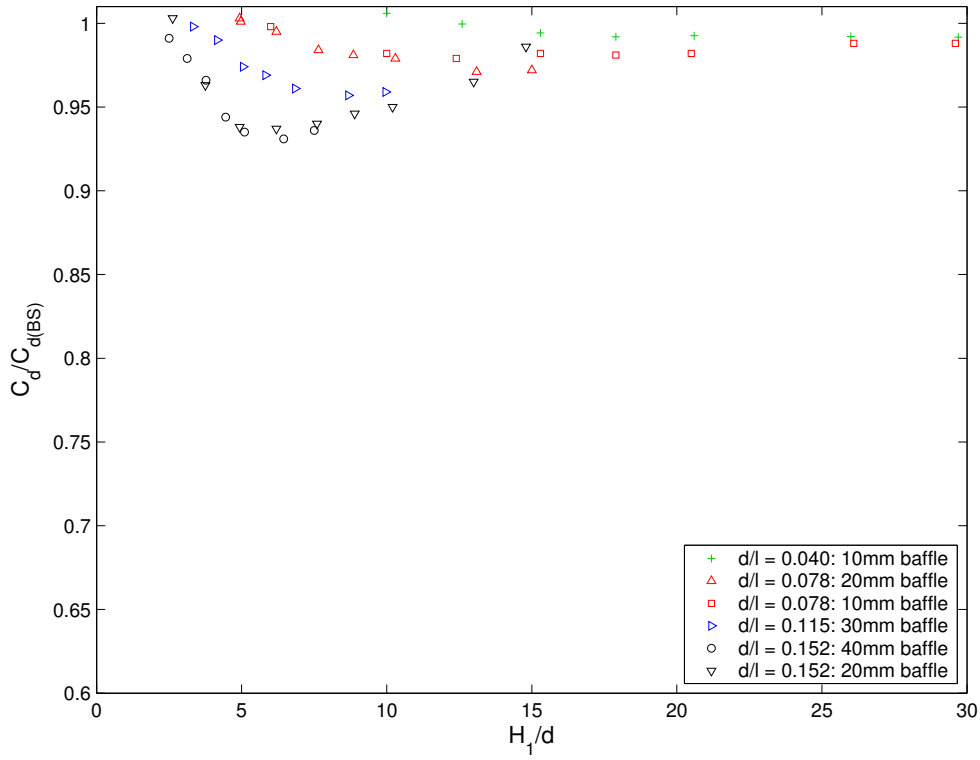

Figure 5–27: Non-dimensional total head-discharge relationships: HR Wallingford (White *et al.* 2005e)

recorded. The minimum design distance of the baffle closest to the crest was then recommended such that there would only be a 1% reduction in the coefficient of discharge for the basic Crump weir (i.e. a 'no-effect' criterion) (White *et al.* 2005e).

The non-dimensional curves show a similar shape to the Cranfield results, and the following graph, Figure 5–28, shows the two data sets plotted on the same set of axes. The Cranfield data set ranged from $0.25 \leq H_1/d \leq 7$ as limited by the maximum head achievable on the weir, compared to the HR Wallingford data set where the range was $2.5 \leq H_1/d \leq 30$. The minimum H_1/d Cranfield values were far smaller than those investigated by HR Wallingford[8].

Figure 5–29 represents the data in Figure 5–28 over that portion of the H_1/d axis where overlap between the data sets was observed, i.e. $1.75 \leq H_1/d \leq 7$. As the experiments were carried out independently, not only were the baffles geometrically dissimilar, but the d/l ratios used were different.

Although the shapes of the d/l curves are similar, the curves from the different data sets do not interleave as was initially anticipated. For example, the HR Wallingford $d/l = 0.152$ curve lies between the $d/l = 0.1$ and $d/l = 0.133$ curves rather than between the $d/l = 0.133$ and $d/l = 0.167$ curves. Although no conclusive reason was reached, it is thought that this shift between the data sets is probably as a result of the geometric dissimilarity. Thus although it was hoped that the combination of

[8]The main reason for this was the Cranfield approach to the height of the baffle relative to the crest (see section 5.1.2).

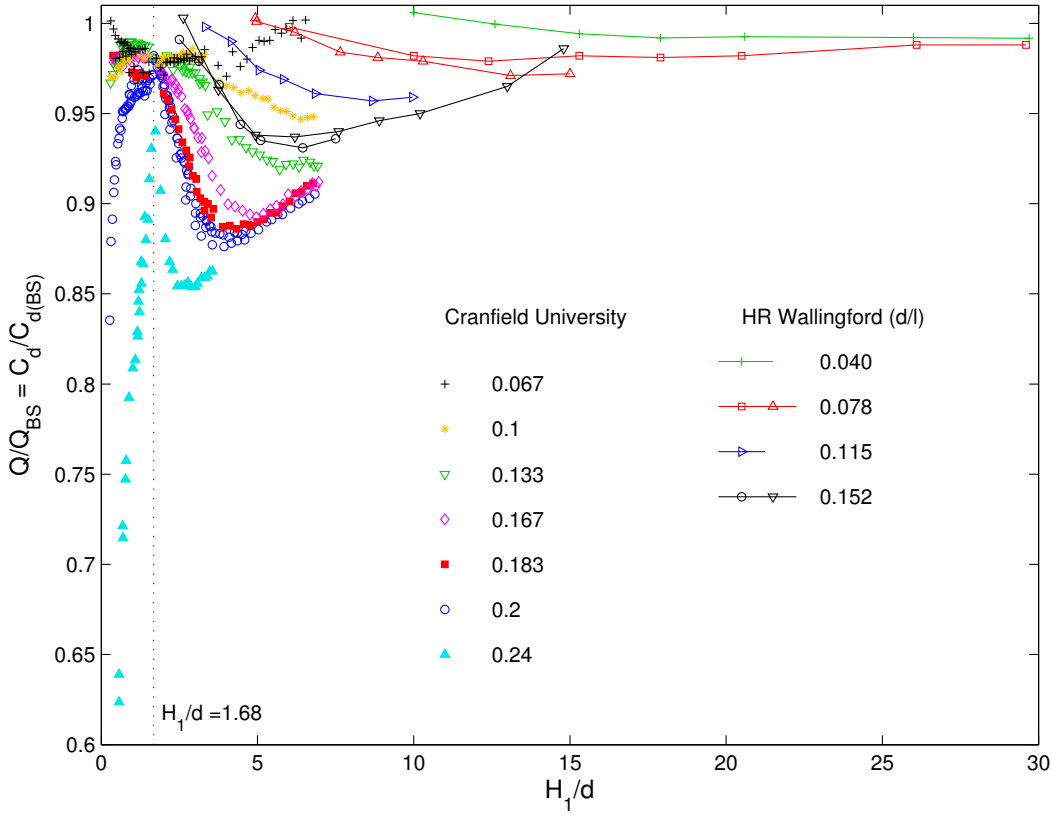

Figure 5–28: Non-dimensional total head-discharge relationships: Combined Cranfield and HR Wallingford results

the data sets would enable the provision of general guidelines for the use of single baffles over the total range, this has not been possible. However, as the premise that the single baffle results would be useful in predicting the discharge coefficient of the baffled weir has been shown to be limited when using the rotated-V fish pass arrangement (see section 5.1.5), the cause in the difference between the HR Wallingford and Cranfield data sets has not been established.

5.1.4. Double baffle experiments

Three ratios, namely d_1/d_2, d_1/l_1 and d_2/l_2 (see Figure 5–30), have been identified as useful parameters for analysing the double baffle experiment results. The experimental data, as presented in Table 5–2, has been sorted using these parameters as well as baffle width (all of which are described in more detail below the table).

Ratio d_1/d_2***:*** This column presents the ratio of baffle height between the first and second baffles.

Ratio d_1/l_1***:*** This column indicates the ratio of the height of the first baffle and the distance to the crest (to the centre of the baffle). For all double baffle experiments this ratio was set at 0.2.

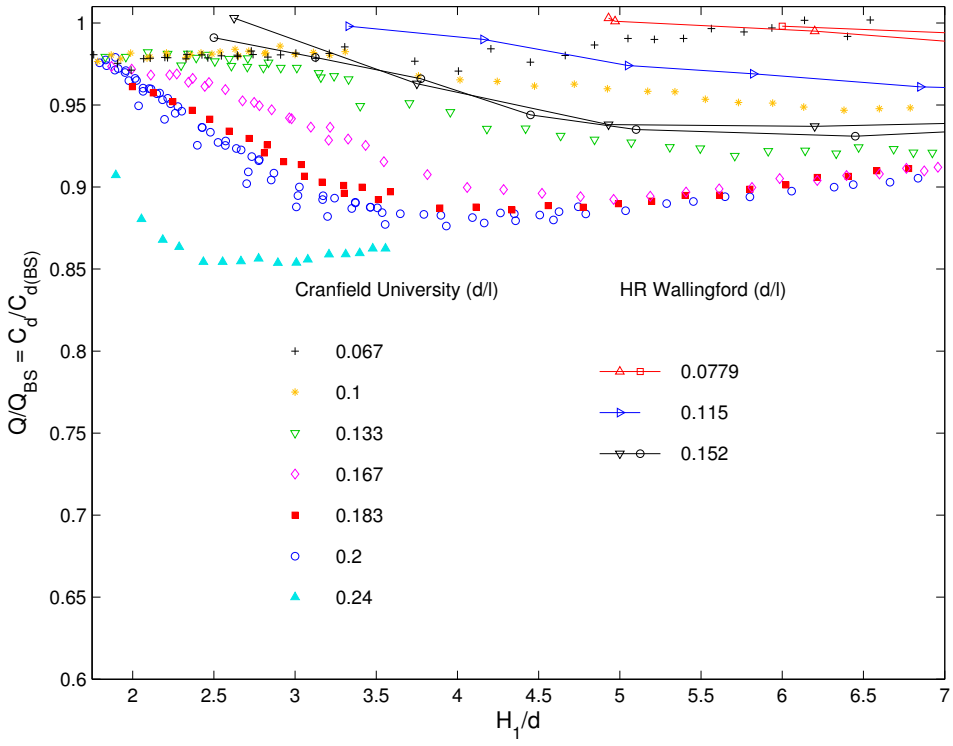

Figure 5–29: Non-dimensional total head-discharge relationships: Overlapping Cranfield and HR Wallingford results

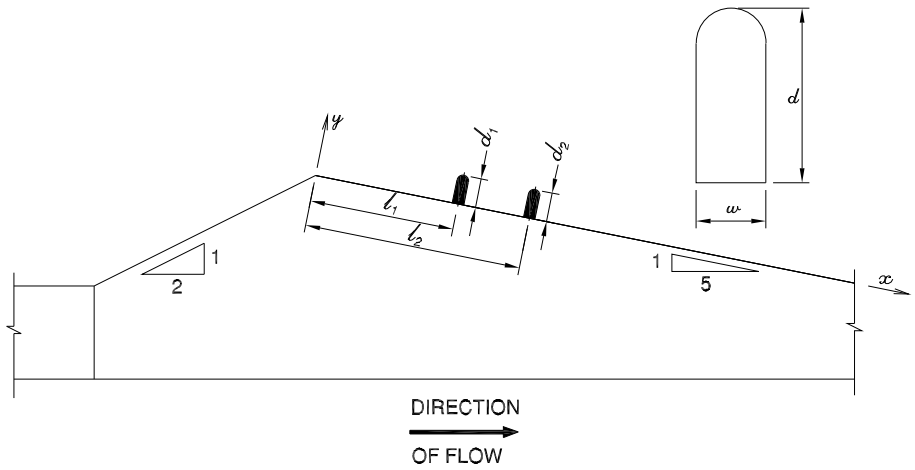

Figure 5–30: Parameters used in the double baffle experiments

Ratio d_2/l_2***:*** This column indicates the ratio of the height of the second baffle and the distance to the crest (to the centre of the baffle).

- N/A: Not applicable (i.e. single baffle experiment)
- 0.143: The first baffle was set to weir crest level. The second baffle was identical in size to the first baffle and thus the crest level of the second baffle was below the crest of the weir and the first baffle.

Table 5–2: List of double baffle experiments (in the modular flow range)

Ratio	**Baffle sizes** (mm)		**Baffle 1**				**Baffle 2**			
d_1/d_2	109.91 mm orifice	61.95 mm orifice	d_1	w_1	l_1	d_1/l_1	d_2	w_2	l_2	d_2/l_2
N/A	20	20	20	$d_1/2.5$	100	0.2	N/A	N/A	N/A	N/A
N/A	40	40	40	$d_1/2.5$	200	0.2	N/A	N/A	N/A	N/A
1	20 + 20	20 + 20	20	$d_1/2.5$	100	0.2	20	$d_2/2.5$	140	0.143
1	40 + 40	40 + 40	40	$d_1/2.61$	200	0.2	40	$d_2/2.5$	280	0.143
0.5	20 + 40	not done	20	$d_1/2.5$	100	0.2	40	$d_2/2.5$	200	0.2
0.571	20 + 35	20 + 35	20	$d_1/2.5$	100	0.2	35	$d_2/2.5$	175	0.2
0.6	24 + 40	24 + 40	24	$d_1/1.57$	120	0.2	40	$d_2/2.61$	200	0.2

- 0.200: The first and second baffle crests were set level with the crest of the weir. By implication, these baffles were of different sizes.

Baffle width Although the baffles used for the single baffle experiments had a fixed ratio of width to height (i.e. $w = d/2.5$), the baffles used on the perspex fish pass were of a fixed width (15.3 mm) resulting in a width ratio of either $w = d/1.57$ or $w = d/2.61$.

By using these parameter descriptions, the double baffle experiments have been divided into two distinct groups:

- First and second baffle heights are identical ($d_1/d_2 = 1$ and $d_2/l_2 = 0.143$)
- First and second baffle heights are different ($d_1/d_2 =$ various and $d_2/l_2 = 0.2$)

Experiment procedure was similar to that used for the single baffle experiments in terms of equipment setup and methodology. In order to reduce systematic error, the 20 mm single baffle experiment was repeated before the second baffle was added for the double baffle experiments. Time constraints prevented such repetition for the rest of the double baffle experiments.

Identical first and second baffle heights ($d_1/d_2 = 1$ and $d_2/l_2 = 0.143$)**:**

Although two baffles sizes were used, the results have not been plotted on the same set of axes as the first baffle in the 20 mm double baffle experiment was similar to the second baffle (i.e. $w_1 = w_2$), whereas the first and second baffle in the 40 mm double baffle experiment were dissimilar[9] (i.e. $w_1 \neq w_2$).

20mm single baffle vs 20mm + 20mm double baffles The total head-discharge data is plotted on Figure 5–31.

[9]These experiments were conducted approximately six months apart, and this oversight was not recognised until the writing-up period of this thesis.

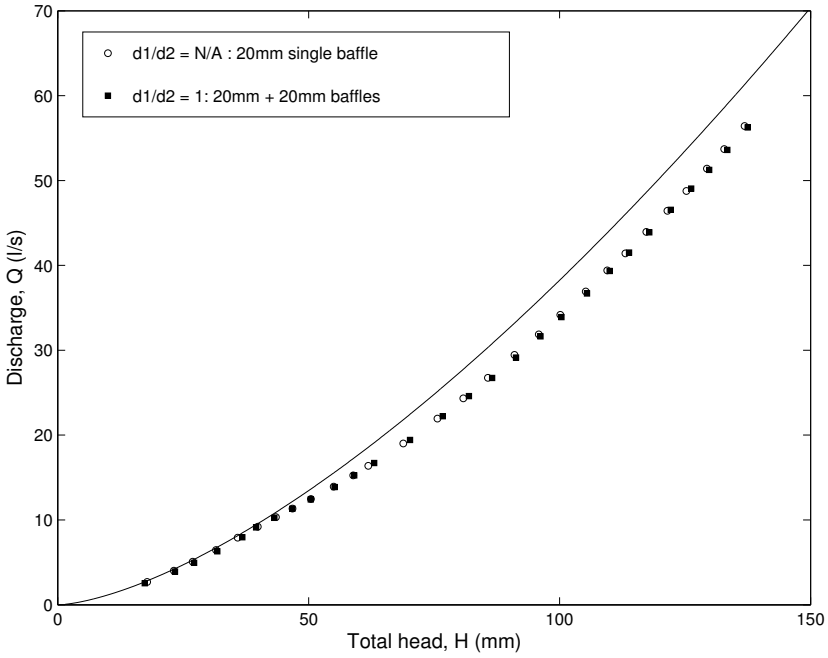

Figure 5–31: Total head-discharge curves with single baffle 20 mm & double 20 + 20 mm

The single baffle non-dimensional data curve plotted in Figure 5–32 is similar to that in Figure 5–9 showing all of the $d/l = 0.2$ single baffle experiment data, with the exception that the peak occurs at $C_d/C_{d_{BS}} = 1.793$ (compared to $C_d/C_{d_{BS}} = 1.68$)[10]) and $H_1/d_1 = 0.972$ (compared to $H_1/d_1 = 0.98$). These differences can probably be attributed to the reinstallation of the 20 mm baffle, possible distortion of the weir crest and the fact that only one baffle size is being used to obtain this peak value.

For the double baffle experiment, the peak occurs at a higher H_1/d_1 and a lower $C_d/C_{d_{BS}}$ than the peak for the single baffle experiment. There is approximately a maximum of 4% difference between the two different data sets. In addition, the shape of the double baffle curve to the left of the peak is also markedly different from that of the single baffle data. Instead of a general increase, the double baffle curve is convex downwards[11], to a local minimum of approximately $H_1/d_1 \approx 1.17$ and $C_d/C_{d_{BS}} \approx 0.92$. As with the single baffle, the presence of the double baffle interferes with the formation of the separation bubble immediately downstream of the weir crest (see Figure 5–33). It would appear that the interference mechanism results in the difference in shape for the double baffle.

To the right of $H_1/d_1 \approx 1.98$, the two sets of data fall on the same curve, gradually diverging towards a local minimum associated with each curve,

[10]Although two decimal places were sufficient for the single baffle experiments, three decimal places are required for the double baffle experiments in order to make useful comparisons between the peaks.

[11]A similar convex shape was observed for the double baffle 40 mm + 40 mm experiment, shown on Figure 5–35

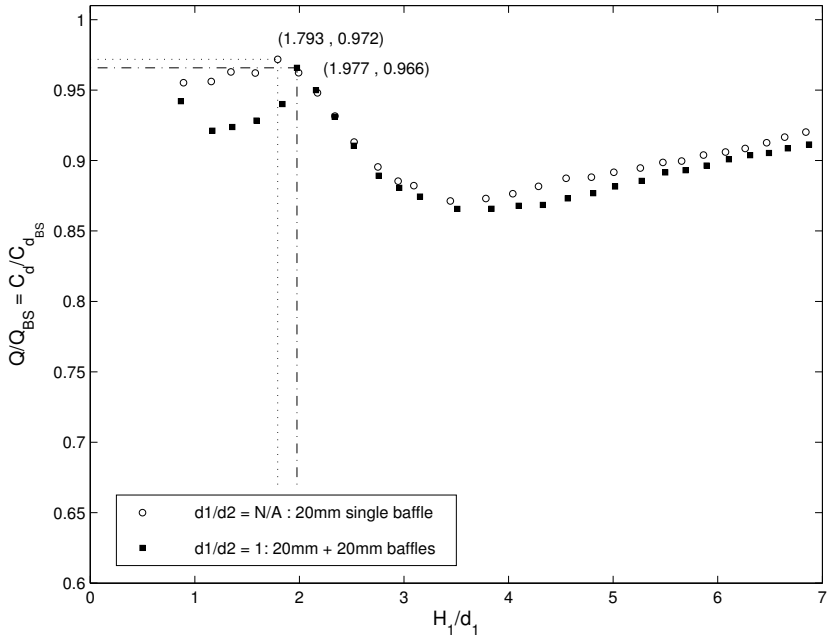

Figure 5–32: Non-dimensional total head-discharge relationships: Single baffle 20 mm & double 20 mm + 20 mm

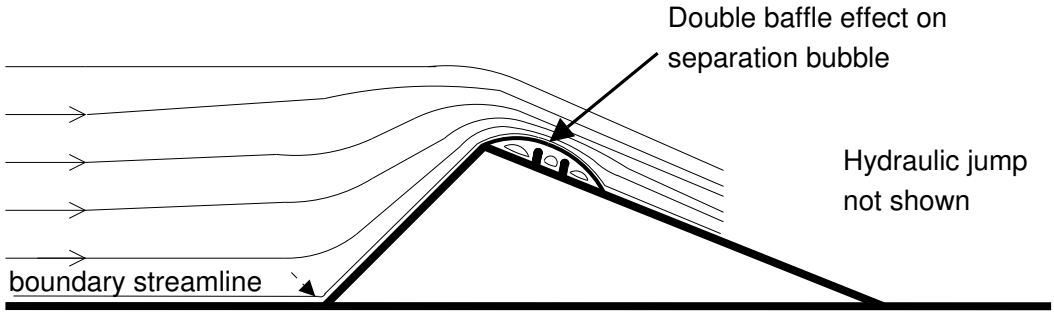

Figure 5–33: Theoretical diagram showing the possible effect of a double baffle on streamlines at the crest of the Crump weir

and then diverge further as the curves start to rise. If the single baffle data is used to represent the double baffle data for values of $H_1/d_1 > 1.98$, the maximum error would be an overestimation in $C_d/C_{d_{BS}}$ of approximately 1.6%.

40mm single baffle vs 40 + 40mm double baffles Owing to time and fabrication constraints, two dissimilar 40 mm baffles (i.e. $w_1 \neq w_2$) were used in the double baffle experiments. An oversight in the installation of the 40 mm baffle led to the baffle fabricated to the perspex width specifications being used as the first baffle (see Table 5–2). Therefore although the single and double baffle experiments are plotted on the same set of axes (in Figures 5–34 and 5–35) so that trends can be identified, the data sets are not directly comparable.

The single and double baffle curves represented in the non-dimensionalised Figure 5–35 are similar to that described for the 20 mm comparison de-

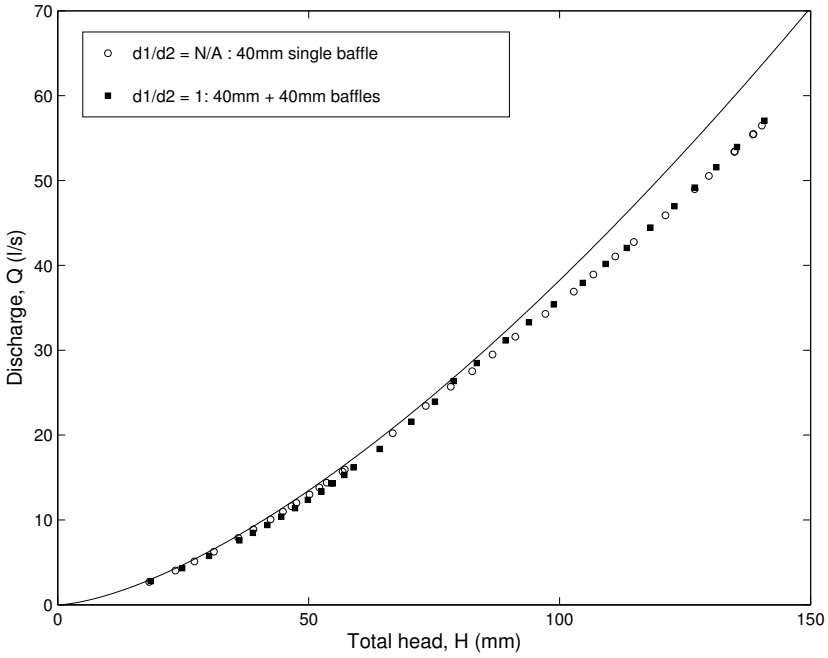

Figure 5–34: Total head-discharge curves with single baffle 40 mm & double 40 mm+ 40 mm

scribed previously. Both curves peak at slightly different points, and the data to the right of the peak ($H_1/d_1 = 1.972$, $C_d/C_{d_{BS}} = 0.985$) does not fall on the same curve immediately to the right of the peak. This is probably as a result of the fact that the original 40 mm single baffle data has been used for comparison, even though the first baffle of the double baffle set was narrower. Convergence of the data seems to occur for increasing H_1/d_1. If the single baffle data is used to represent the double baffle data for values of $H_1/d_1 > 1.97$, the maximum error would be an overestimation in $C_d/C_{d_{BS}}$ of approximately 2%.

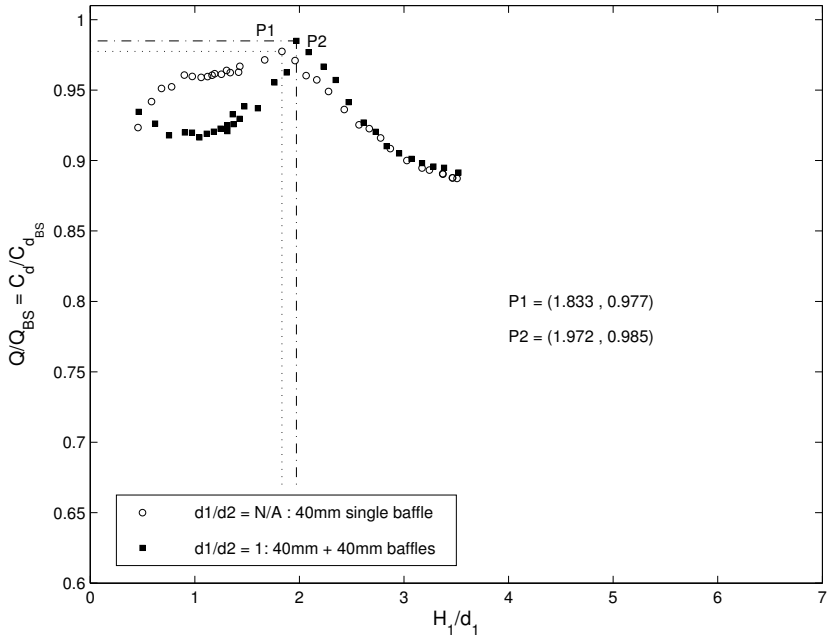

Figure 5–35: Non-dimensional total head-discharge relationships: Single baffle 40 mm & double 40 mm + 40 mm

Different first and second baffle heights (d_1/d_2 = various and $d_2/l_2 = 0.2$) **:**

For these experiments, $d_1/l_1 = d_2/l_2 = 0.2$, with the implication that each baffle height was different. Regarding baffle widths, the 20 mm + 40 mm and 20 mm + 35 mm double baffle combinations used the same baffles as were used in the single baffle experiments (i.e. baffle width = $d/2.5$). The 24 mm+40 mm combination[12] baffles were based on the perspex dimensions (i.e. baffle width = $d/1.57$ and $d/2.61$ respectively).

Figure 5–36 shows the total head-discharge curve for the 20 mm single baffle experiment plotted for comparison with the three double baffle experiments.

The non-dimensional total head-discharge curves are plotted on Figure 5–37. As with the double baffle experiments of equal height, these experiments with different baffle heights and a constant d/l ratio once again show a departure from the single baffle results. The deviation from both the British Standard $C_d/C_{d_{BS}}$ and the 20 mm single baffle, increases with a decreasing d_1/d_2 ratio. Thus the premise that the first baffle located downstream of the crest would dominate the hydrometric effect and could therefore be used as a direct indicator for design in the placement of a baffle system on the downstream face of a Crump weir has been proved to be incorrect for unequal first and second baffles. The main reason for this deviation is likely to be the effect that the second baffle has on the separation bubble (see Figure 5–33).

P1 ($H_1/d_1 = 1.793, C_d/C_{d_{BS}} = 0.972$) on Figure 5–37 represents the coordinates of the single peak occurring for the 20 mm single baffle data, whereas

[12]The 24 mm + 40 mm combination should have been compared to a 24 mm first baffle, but time constraints prevented this from being carried out.

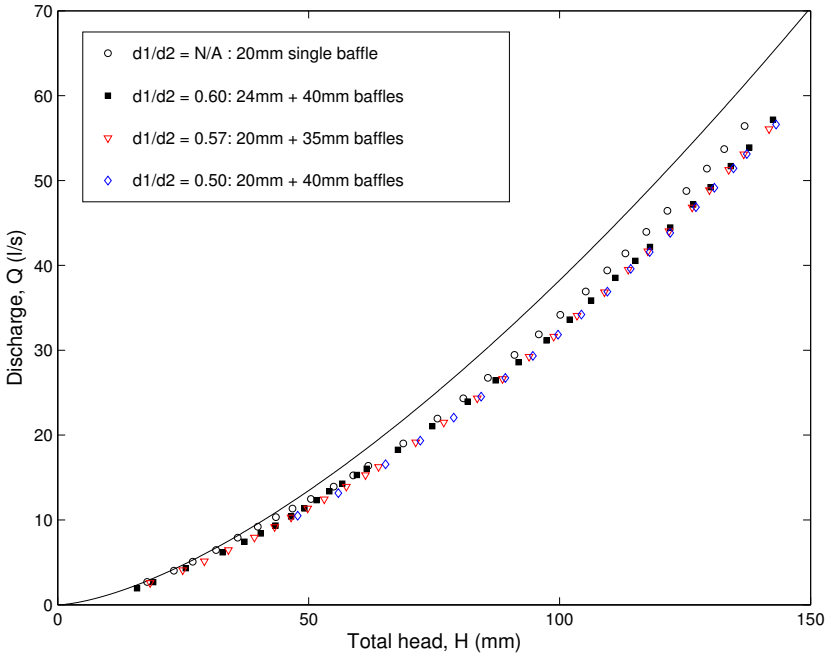

Figure 5–36: Total head-discharge curves with single baffle 20 mm, and double baffle combinations (i.e. $d_1/l_1 = d_2/l_2 = 0.2$)

P2 ($H_1/d_1 = 1.064, C_d/C_{d_{BS}} = 0.888$) and P3 ($H_1/d_1 = 2.255, C_d/C_{d_{BS}} = 0.882$) are those coordinates associated with the double peak caused by the 24 mm + 40 mm double baffle combination. There is a less distinct second peak (P4 where $H_1/d_1 = 2.326, C_d/C_{d_{BS}} = 0.853$) for the 20 mm + 35 mm data, whereas the 20 mm + 40 mm data set combination was not completed for $H_1/d_1 < 2.4$.

The data set of most interest is the 24 mm + 40 mm double baffle combination as being a measure to compare the double baffle data set with the perspex fish pass baffles, and further analysis for this combination is thus provided in the next section.

5.1.5. Fish pass experiments

One of the main aims of this research project was to identify the effect of baffled modifications on the hydrometric functioning of the Crump weir. Although useful as an initial estimation the deviation from the British Standard, the single baffle non-dimensional graphs providing the relationship between H_1/d_1 and $C_d/C_{d_{BS}}$ do not adequately model the deviation from this relationship for a fully baffled fish pass on the downstream slope of the weir.

Although the preferred fish pass solution selected in this research project is the layout with a 24 mm first baffle, the total head-discharge relationship for the 40 mm first baffle has also been studied and these additional graphs are presented in Appendix G.

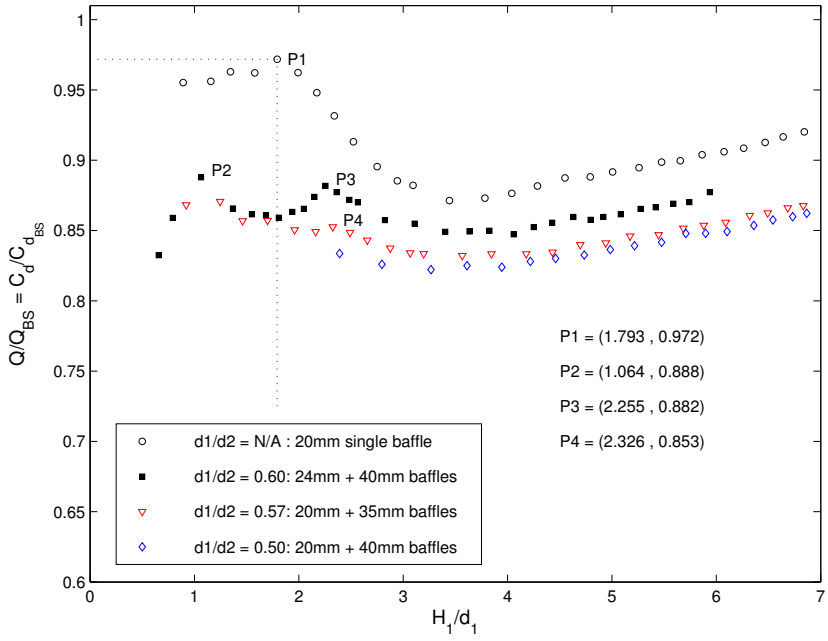

Figure 5–37: Non-dimensional total head-discharge relationships: Single baffle 20 mm, and double baffle combinations (i.e. $d_1/l_1 = d_2/l_2 = 0.2$)

Table 5–3 provides an overview of the fish pass experiments [13] (see below Table 5–2 for an explanation on the columns).

Table 5–3: List of fish pass experiments (in the modular flow range)

Ratio	**Baffle sizes** (mm)		**Baffle 1**				**Baffle 2**			
d_1/d_2	109.91 mm orifice	61.95 mm orifice	d_1	w_1	l_1	d_1/l_1	d_2	w_2	l_2	d_2/l_2
1	40 + 40	40 + 40	40	$d_1/2.61$	200	0.2	40	$d_2/2.61$	280	0.143
0.6	24 + 40	24 + 40	24	$d_1/1.57$	120	0.2	40	$d_2/2.61$	200	0.2

Figure 5–38 shows the total head-discharge data comparing the double baffle 24 mm+ 40 mm combination with the preferred fish pass with the first baffle set to 24 mm (referred to as 'fish pass 24 mm + 40 mm + 40 mm+ . . . '). As a reference, the 20 mm single baffle data is also included in this graph although as a baseline it is not directly comparable being geometrically dissimilar. From this graph it is apparent that the deviation from the British Standard increases with increasing number of baffles.

The non-dimensional total head-discharge curves plotted in Figure 5–39 show that there is a single peak (P1) for the single baffle data, whilst a double peak occurs in the double baffle (P2 and P3) and fish pass (P4 and P5) data sets[14]. As has

[13]The total head-discharge experiments for the fish pass took four laboratory testing days, excluding installation time, to complete.

[14]As the single baffle and double baffle data sets were used in the double baffle analysis in section 5.1.4, P1, P2 and P3 are repeated from Figure 5–36.

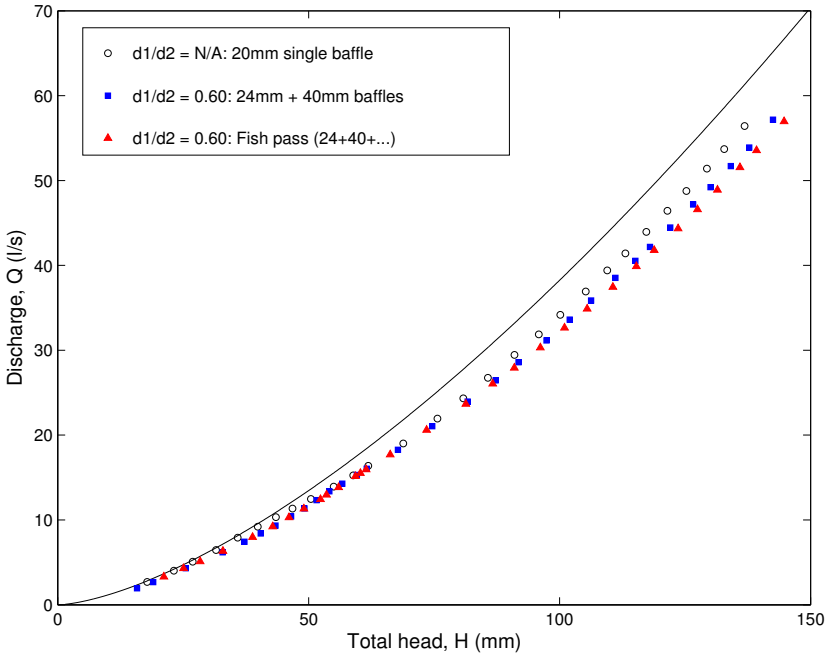

Figure 5–38: Total head-discharge curves with single baffle 20 mm, double baffle 24 mm + 40 mm and fish pass (24 mm + 40 mm + 40 mm+...)

already been noted in the previous section, the double baffle data deviates from the single baffle data set (although not directly comparable as the baffle sizes were geometrically dissimilar). The double baffle and fish pass data show similar trends.

The separation bubble causes a significant effect on the relationship between H_1/d_1 and $C_d/C_{d_{BS}}$ to the left of the second peak (i.e. P3 and P5) for both double baffle and fish pass data sets. Although these curves are not identical, they are similar in shape and position. For increasing H_1/d_1, the curves initially rise to a peak (P2 and P4), then convex downwards to a local minima before rising again to the second peak (P3 and P5). In general, to the left of this second peak, for smaller values of H_1/d_1, the fish pass curve is a little closer to the British Standard than the double baffle curve, an overlap occurs at $H_1/d_1 = 2.05$ after which the double baffle curve is closest to the British Standard. If the double baffle is used as an estimation of the effect of the fish pass on the modular flow for values of $H_1/d_1 \leq 2.47$ (i.e. P5), the fish pass will either be underestimated or overestimated by a maximum of approximately 2.5% or 1.5% respectively.

To the right of the second peak (P3 and P5), the fish pass data and double baffle data coincide briefly and then as H_1/d_1 increases, the deviation in the fish pass curve from the double baffle data increases. Thus if the double baffle curve is used to estimate the effect of the fish pass layout, discharge will be overestimated by a 2.5%. Use of the British Standard equation to estimate discharge over this fish passage layout would lead to a minimum overestimation of discharge of 10% and a maximum overestimation of approximately 16%.

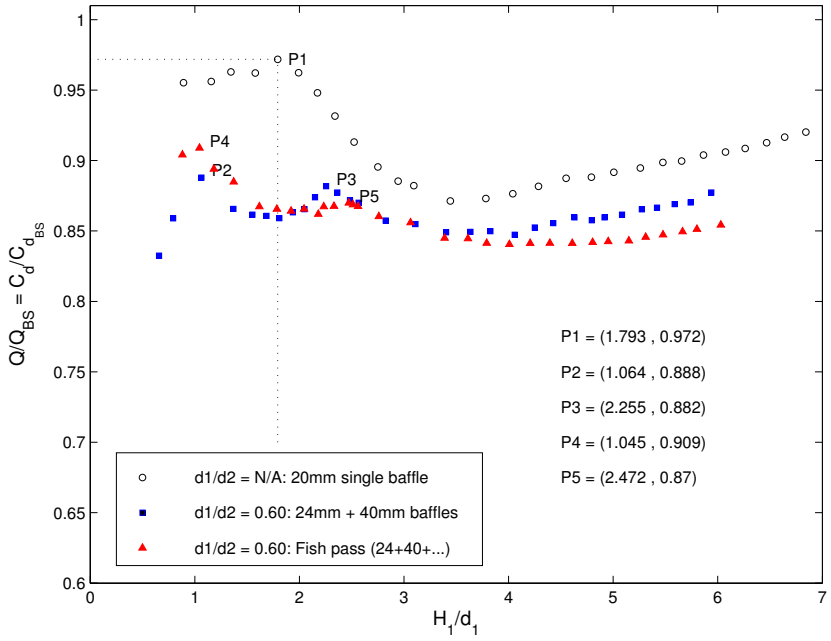

Figure 5–39: Non-dimensional total head-discharge relationships: single baffle 20 mm, double baffle 24 mm + 40 mm and fish pass (24 mm + 40 mm + 40 mm+...)

5.2. Non-modular flow experiments

One of the project objectives was to ascertain the effect of fish pass modifications upon the hydrometric function over the whole flow range, both for modular and non-modular flow. As discussed earlier the modular flow experiments were conducted on the standard weir, weir with a single baffle, weir with double baffles and on the optimum fish pass arrangement (including two different upstream baffle sizes). This section looks at the experimental procedure and analysis for non-modular flow.

5.2.1. Presentation and analysis of results

Four sets of experiments[15] were conducted under non-modular flow conditions and the corresponding modular experiments were then plotted on total head-discharge diagrams. The presentation of these results have been divided into three sections: unmodified Crump, single baffle and the perspex fish pass. In the case of the Perspex fish pass, the results for two different flow rates have been plotted on the same set of graphs: The 39.5 ls^{-1} flow rate was chosen as it closely represented the 10 percentile low-flow rate for Brimpton weir (see Table 3–9), whilst the 47 ls^{-1} was an arbitrary higher flow rate within the pump range, and chosen for comparative purposes. Table 5–4 lists the non-modular flow experiments.

For the case of the unmodified Crump and single baffle experiments, it was possible to obtain measurements from all three pressure tappings indicated in Figure 3–32. However, for the perspex fish pass arrangements, the installation of the brass plate

[15]The non-modular experiments represent three laboratory testing days excluding setup time.

Table 5–4: List of non-modular flow experiments (using 109.91 mm orifice plate)

Description	**Flow rate** [$l.s^{-1}$]
Unmodified Crump (no baffles)	39.5
Single baffle (40 mm)	39.5
Perspex fish pass (24 mm 1st baffle)	39.5
Perspex fish pass (24 mm 1st baffle)	47

and perspex sheeting was on top of the existing wooden apron and covered the crest pressure tappings. Time and funding constraints did not allow for the installation of appropriate crest tappings at that late stage. Thus for every case it was only possible to plot the non-modular flow reduction factor f against the ratio of the downstream total head and the upstream total head (H_2/H_1) (as shown in Figures 5–41(a), 5–43(a) and 5–45). The theoretical curve is described by the following three equations 5–1, 5–2 and 5–3 (Herschy *et al.* 1977).

$$f = 1.035(0.817 - (H_2/H_1)^4)^{0.0647} \qquad \text{if} \qquad 0.75 < H_2/H_1 < 0.93 \tag{5–1}$$

$$f = 8.686 - 8.403(H_2/H_1) \qquad \text{if} \qquad H_2/H_1 > 0.93 \tag{5–2}$$

$$f = 1 \qquad \text{if} \qquad 0.25 < H_2/H_1 < 0.75 \tag{5–3}$$

For the standard crest and single baffle experiments, an additional graph showing the relationship between f and the ratio of the crest static head to the upstream total head (h_p/H_1) has also been plotted (see Figures 5–41 and 5–43). The theoretical curve is described by the following equation 5–4 (Herschy *et al.* 1977):

$$f = 1.04 * (0.945 - (h_p/H_1)^{1.5})^{0.256} \tag{5–4}$$

It is important to note that for the laboratory data, the value of the flow reduction factor f has been calculated as follows:

$$f = Q_{measured}/Q_{modular} \tag{5–5}$$

where $Q_{modular}$ is determined as follows:

Unmodified Crump weir $Q_{modular}$ is the interpolated Q value on the British Standard curve for each measured total head data point in the non-modular experiment (Figure 5–40).

Single baffle and Perspex fish pass $Q_{modular}$ is the interpolated Q value on the modular range, which was limited by the maximum flow rate of $Q \approx 60\ ls^{-1}$ resulting in data only being available for values of $f > 0.7$ (Figures 5–42 and 5–44).

5.2.2. Unmodified Crump weir (no baffles)

Figure 5–40 represents the total head-discharge results for the unmodified Crump weir.

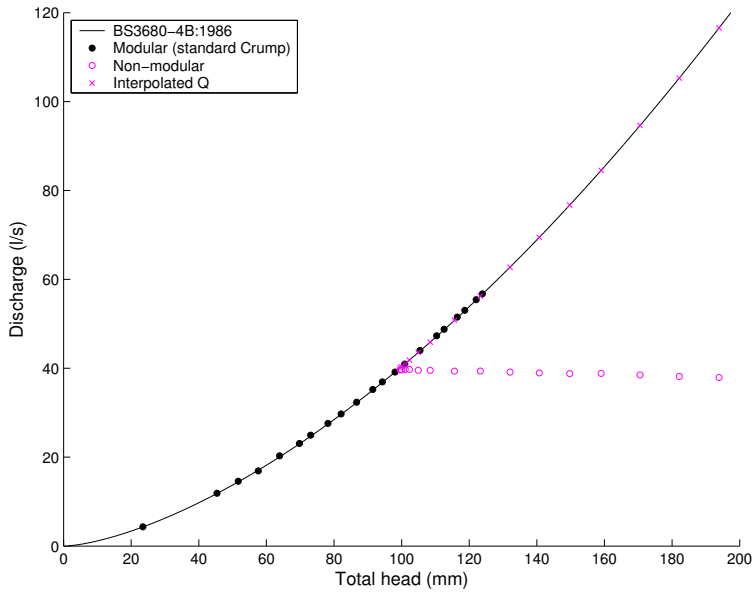

Figure 5–40: Unmodified Crump weir: Total head-discharge curves

The value of f in Figure 5–41(a) was calculated using the ratio of the laboratory non-modular data to the British Standard theoretical curve for modular flow. There is a slight deviation from the theoretical f vs H_2/H_1 curve which is probably accounted for by some small systematic error introduced into the non-modular data during the experimental process[16]. It will also be noted that the theoretical curve has been divided into two parts. This break has been included as it is caused by the direct use of Equations 5–1 and 5–3.

A similar deviation from the theoretical curve is observed in Figure 5–41(b), and this is presumably as a result of the same small systematic error in the non-modular data.

5.2.3. Single baffle

A 40 mm single baffle located 200 mm on the downstream slope from the crest to the centre of the baffle was used in this experiment. This particular arrangement maintained the d/l ratio of 0.2 investigated in the modular analysis (section 5.1), while being at the same scale as the majority of the fish pass baffles.

As has been discussed previously, the presence of the single baffle causes the modular flow curve on Figure 5–42 to deviate significantly from the British Standard curve.

[16]See section 5.1.1 for further details on systematic error introduced during modular flow measurement. It is postulated that a similar mechanism is the error source for non-modular flow measurement.

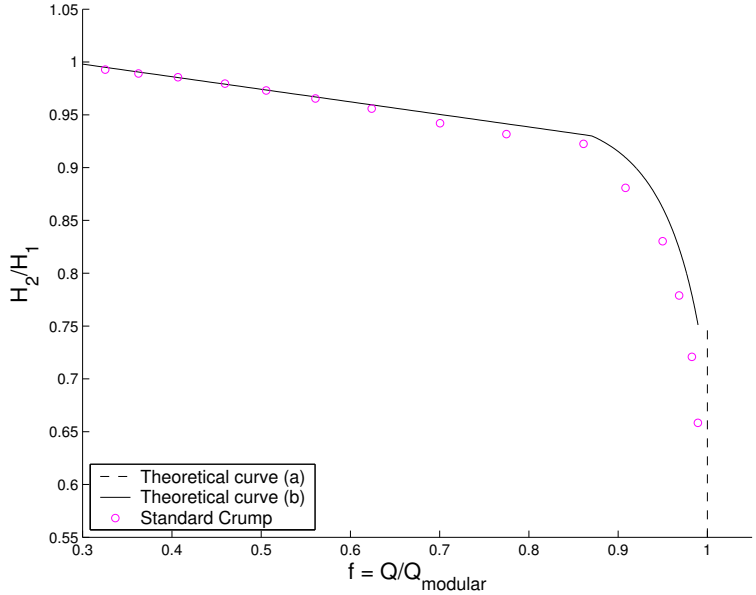

(a) f vs H_2/H_1

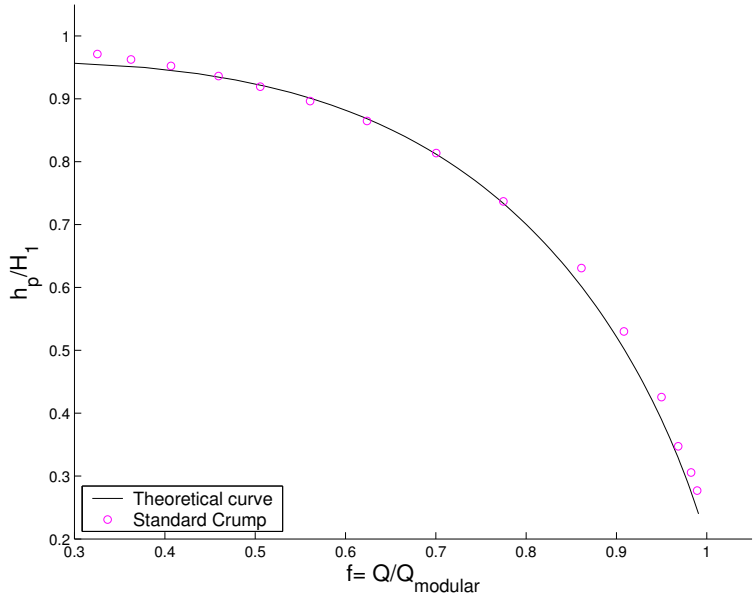

(b) f vs h_p/H_1

Figure 5–41: Unmodified Crump weir: Non-dimensional curves where the flow reduction factor f is plotted against H_2/H_1 and h_p/H_1 respectively

Once again the non-modular and associated modular discharge for the measured total head values have been plotted on the same set of axes. The average discharge for the non-modular flow experiment was set to the same flow rate as that used for the non-modular unmodified Crump experiment described earlier.

The effect of the single baffle on f, at the same value of H_2/H_1 or at the same value of h_p/H_1, is significant. For the former the non-dimensional curve has been left-shifted, while in the latter relationship, the curve is right-shifted. During observation of the modular part of the experiment, it was noted that as the head increased on the

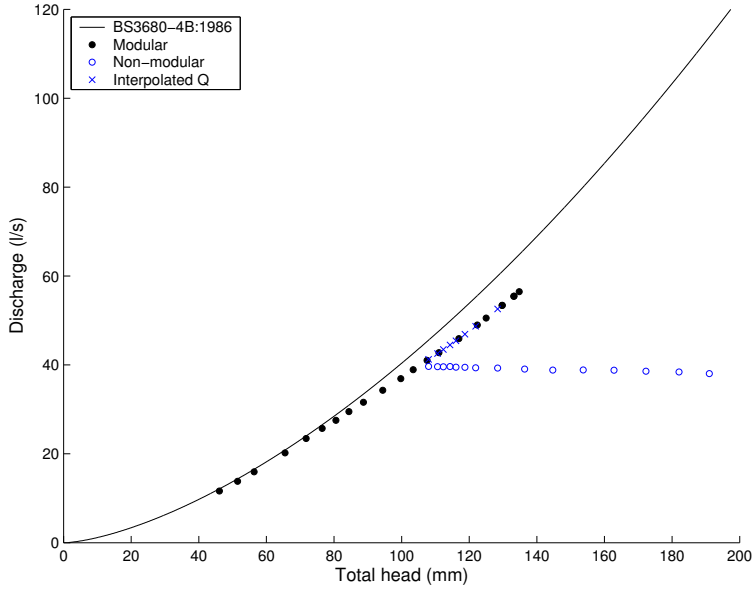

Figure 5–42: Single baffle experiment: Total head-discharge curves

weir, the point where flow changes from subcritical to supercritical as exerted by the position of the crest appeared to move downstream to the location of the single baffle and consequently, flow just downstream of the baffle became super-critical in nature. Therefore h_p was influenced by presence of the baffle.

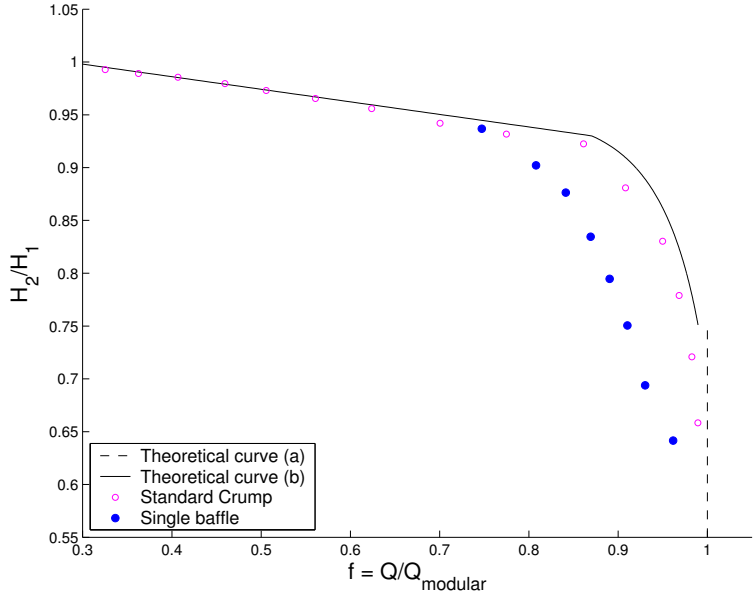

(a) f vs H_2/H_1

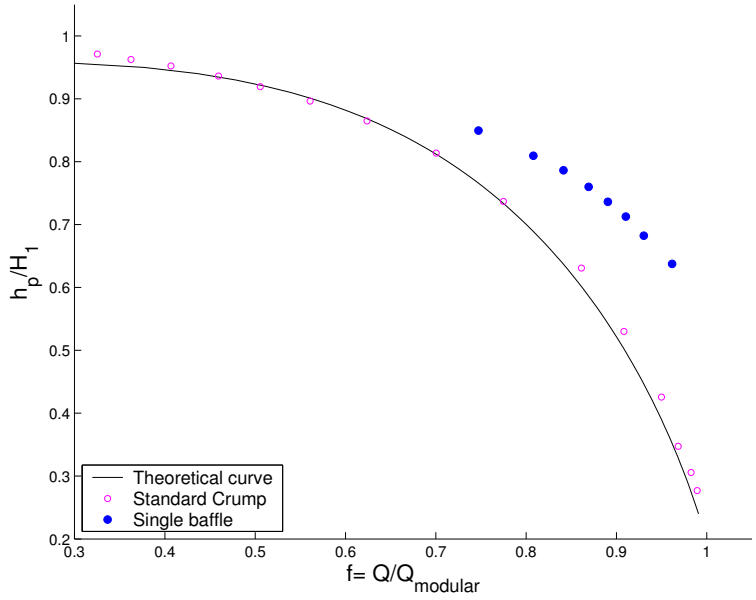

(b) f vs h_p/H_1

Figure 5–43: Single baffle experiment: Non-dimensional curves where the flow reduction factor f is plotted against H_2/H_1 and h_p/H_1 respectively

5.2.4. Perspex fish pass

The two experiments on the perspex fish pass differed only in the flow rate. For ease of reference, the flow rates have been identified as $Q1$ and $Q2$, which correspond to values of approximately 47 ls^{-1} and 39.5 ls^{-1} respectively. $Q2$ was set to approximately the same flow rate as used for the unmodified Crump and single baffle experiments described above, which in turn relates to the 10 percentile low-flow (at model scale) for the Brimpton weir.

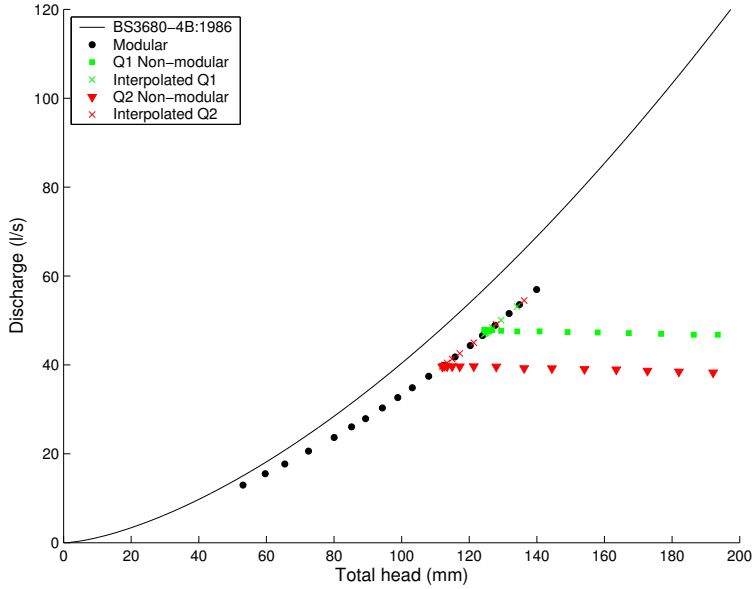

Figure 5–44: Perspex fish pass experiment: Total head-discharge curves

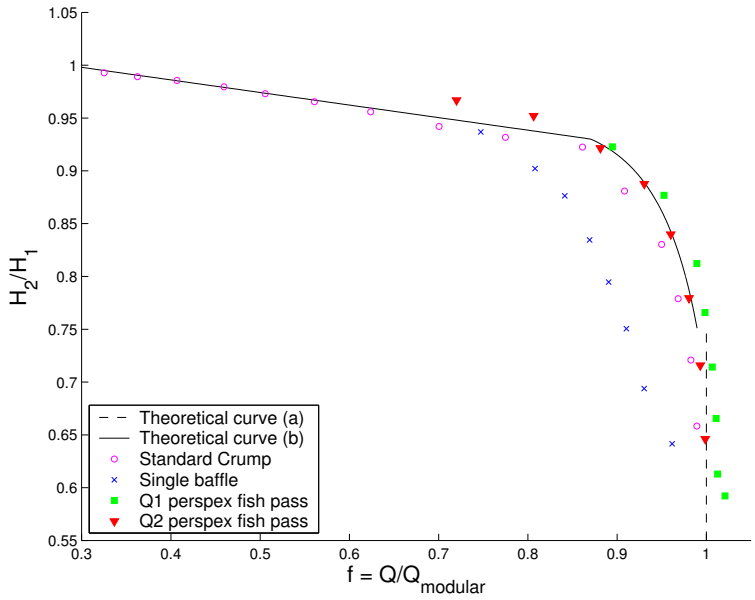

(a) f vs H_2/H_1

Figure 5–45: Perspex fish pass experiment: Non-dimensional flow reduction factor f plotted against H_2/H_1

Similarly to Figure 5–42 and as discussed previously, Figure 5–44 shows that the presence of the fish pass causes the modular flow to deviate from the British Standard.

Figure 5–45 presents the relationship between the non-dimensional flow reduction factor f and the ratio of the downstream to the upstream total head H_2/H_1. Both the unmodified Crump and the single baffle results have also been plotted in on the same axes so that the effects are can be compared. The measured data from

both flow rates Q1 and Q2 fall approximately onto the theoretical line for this non-dimensional plot, which is at least as close to the theoretical curve as the unmodified Crump data used as control.

5.3. Conclusions and recommendations

The overall purpose of these experiments has been to consider the effect of a single baffle, a double baffle and ultimately the effect of the preferred fish pass arrangement on the hydrometric functioning of a typical Crump weir for both modular and non-modular flow conditions.

5.3.1. Modular flow

The results from the single baffle experiments were plotted non-dimensionally, showing that there is a unique curve for each d/l ratio and a generalised rule for predicting the estimation error of the discharge was drawn up. In order to allow velocities on the downstream slope of the Crump weir to be reduced, the optimal placement of the first baffle is effectively where the top of the baffle is equal to the crest level of the Crump weir, or where $d/l = 0.2$. For $d/l = 0.2$, the discharge will be overestimated by up to 16.5% for very low H_1/d values, or assuming $H_1/d \geq 1.68$, a maximum overestimation would be 13%.

HR Wallingford conducted a similar trial in the same time period, using the baffles based on the Hurn-type baffle parameters (White *et al.* 2005e). Their initial assumption was that a baffle needed to be located far enough down the slope of the weir such that the coefficient of discharge would only deviate by 1%. The Cranfield approach had been to find a fish pass which would accommodate the fish under review, and then to determine the effect of that fish pass upon the hydrometric functioning of the weir. The two result sets are considered to be complementary because the Cranfield data set ranged from $0.25 \leq H_1/d \leq 7$ as limited by the maximum head achievable on the weir, compared to the HR Wallingford data set where the range was $2.5 \leq H_1/d \leq 30$. Unfortunately the two data sets do not interleave as neatly as anticipated. Although this is possibly due to the height:width ratio when comparing the two baffle sets, this was not proved.

A series of double baffle experiments was also completed since initial comparisons of the single baffle data with the LEGO arrangements indicated that the single baffle data might not provide a good enough estimation of the baffled pass. Two sets of double baffle experiments were conducted. The first considered the case for baffles equal in height and the second looked at unequal or different first and second baffle heights.

For the equal double baffles, two experiments were conducted using pairs of 20 mm and 40 mm baffles. In both cases the non-dimensional curves were similar in shape to the single baffle curves of the same height, with both curves showing a single peak. For values of $H_1/d_1 > 2$, the maximum error which would be incurred when

using the single baffle as opposed to the double baffle coefficients of discharge would be in the order of 2%.

For the unequal double baffles, three different combinations were tested. In all cases the curves were substantially different from the single baffle curve. Firstly the shape of the curve was different. For the two cases where the first baffle was either half or approximately half the height of the second baffle (i.e. $d_1/d_2 \simeq 0.5$), a slightly flatter curve was produced, which on average deviated approximately 6 - 8% from the single baffle data. The third case represented the unequal fish pass arrangement (i.e. $d_1/d_2 \simeq 0.6$) and showed the most significant deviation from the single baffle arrangement in terms of the shape of the curve. For this combination a double peak was observed. For values of $H_1/d_1 > 2.26$, the maximum error was slightly less than for the scenarios where $d_1/d_2 \simeq 0.5$, at approximately 5% from the single baffle data.

As previously explained, the preferred fish pass arrangement was tested using two different first baffle heights, both with $d/l = 0.2$, resulting in equal and unequal baffle pairing arrangements. Comparing the measured discharge to the calculated British Standard discharge provided an indication as to the percentage overestimation which would be incurred if the British Standard coefficient of discharge was used directly. The results were non-dimensionalised, with H_1/d_1 plotted on the x-axis versus $Q/Q_{BS} = C_d/Cd_{BS}$ plotted on the y-axis. For the unequal baffle pairing, the discharge would be overestimated by a minimum of 10% and a maximum of 16% dependent on head. For the equal baffle pairing the maximum difference was in the order of 4.5% over the range, although for $H_1/d_1 > 2.2$, the maximum difference was in the order of 3%. The purpose of the single baffle experiments was to have generated a revised standard which would be generally applicable for a baffled pass. It was found that for the scenario $d/l = 0.2$ this approach would not be acceptable because the new draft guidelines for fish passes at flow gauging stations state that an uncertainty of less than 2% at the 95% confidence interval would be typically expected for the determined coefficient of discharge White *et al.* (2005a).

The percentage deviations for the coefficient of discharge from the British Standard vary depending on whether one is considering a single, double or fish pass arrangement. However, in terms of the significance, this is a function of what would be acceptable to the hydrometric practitioner. Other considerations could include the strategic importance of a particular weir and what level of accuracy is required.

In conclusion therefore, in terms of the proposed fish pass arrangement for a Crump weir, additional calibration using volumetric flow measurement techniques (or similar) which are accepted and approved by the hydrometric community would need to be performed. Although the unequal baffle pairing arrangement (i.e. first baffle smaller than the second baffle) was favoured in the laboratory trials, both arrangements would benefit from being calibrated according to the accepted British Standard.

5.3.2. Non-modular flow

Because of time constraints, only a limited number of experiments could be conducted under non-modular flow conditions. Therefore, in contrast to the detailed

investigation conducted for modular flow, the non-modular experiments were designed to give an indication of non-modular flow effects and to direct further work in this area. The unmodified Crump (no baffle) condition was conducted as a control to determine how well the laboratory model functioned and to enable comparison with the theoretical relationships between the non-modular flow reduction factor and H_2/H_1 or, where possible, h_p/H_1.

Because all these experiments have been carried out during the tail-end of the project, the weir itself had been subject to much wear and tear. The crest of the weir had warped slightly, and the surface of the wood is not as smooth as it was three years previously.

The results from the unmodified Crump weir (i.e. no baffles) show that there is some systematic error within the system resulting in an observed deviation of the measured non-dimensionalised data points when compared to the theoretical relationships. However, the results still provide a control in the non-modular experiments for comparing the single and perspex fish pass layouts. Although the presence of a single baffle caused significant deviation from the theoretical curves, the perspex fish pass layout did not cause the drowned flow characteristics to be significantly affected at the two flow rates considered.

In conclusion, from the laboratory experiments conducted thus far, the downstream modification of the Crump weir using the diagonal-V baffle arrangements appears not to affect the non-modular flow relationship of the flow reduction factor f and H_2/H_1. The effect on the crest static head, used at some weirs as a means to record non-modular flow, has not been established. Thus further testing, both at laboratory and field scale would be necessary to validate these results and enable a complete analysis and calibration for non-modular flow conditions at existing weirs, were this type of baffled fish pass to be installed.

6. Conclusions and recommendations

The research reported in this dissertation focussed on two main aspects, namely modifications to the Crump weir to improve fish passage, and the effect of the preferred modifications on the hydrometric functioning of the weir. In this chapter, the key findings are presented, the preceding chapters are reviewed and ideas for future work are explored.

6.1. Key findings

This section provides an overview of the key findings from this research project.

6.1.1. Developing baffle arrangements

- In developing low cost modifications to improve fish passage on the downstream slope of the Crump weir, the preferred arrangement (termed a 'rotated-V' layout) was found to be a series of baffles located on the downstream slope.
- The baffles effectively act as weirs at low flows and roughness elements at high flows. Each baffle has a slot which helps form the path of ascent for fish. In plan view the slots form a 'rotated-V' pattern.
- Although based on Brimpton weir (on the river Enborne), the results have been generalised by calculating flow rate as 'flow rate per unit width'. The results in this thesis are Brimpton-specific, while the guidelines written for the Environment Agency (Rhodes and Servais 2006) use the flow rate per unit width. For general application in the field, all designs would need to be made with site-specific details taken into consideration.
- Two options for the 'rotated-V' arrangement were tested: Scenario A: first baffle height equivalent to the rest of the baffles ('equal baffle pairing') and Scenario B: first and second baffle heights set level to the crest ('unequal baffle pairing'). In both cases the ratio of the height of the baffle (d) and distance (i.e. parallel to the downstream slope) of the centre of the baffle to the weir crest (l) were set equal such that $d/l = 0.2$.
- The slot sizes, baffle heights, baffle spacing and slot overlaps have been designed using the physical properties of coarse fish as a guideline. Thus scaling of this layout is not recommended.

- The theoretical effectiveness of the fish pass has been determined by developing and using a 'fish pass efficiency matrix'. Measured model water velocities for four different flow rates were scaled up to full-scale and compared to the Swimit fish swimming speeds database (Environment Agency 2001b, 2003). The burst swimming speeds data for eight fish species as well as eel/elver of varying lengths has been used in the compilation of the efficiency matrix. The matrix provides a means of assessing the pass/fail of each fish at each slot and over the whole fish pass.

- The rotated-V arrangement could be used on a single Crump weir or on the low-flow section of a compound Crump. For weirs of substantially different heights and/or widths, a modular approach is suggested. For higher weirs, additional baffles could be added to the downstream slope (the slots would need to maintain the rotated-V pattern). Wider weirs could include the installation of identical passes placed side-to-side.

6.1.2. Investigating the hydrometric effects

- Although the proposed solution results in a change in a weir's hydrometric characteristics, the deviation in the coefficient of discharge is predictable. Both modular and non-modular flow scenarios were considered.

- Modular flow scenarios: In the single baffle trials of varying sizes and distances from the crest a unique, non-dimensional curve for each d/l ratio was obtained which allowed for a generalised rule to predict the estimation error of the discharge to be drawn up. For the optimal baffle placement set level to the crest (i.e. $d/l = 0.2$), the resultant estimation curve was found to lead to an overestimation of the discharge. Similar curves were obtained from a series of double baffle experiments. Further trials were performed with the preferred solution in place, demonstrating the predicability of the coefficient of discharge. If the coefficient of discharge using the British Standard method, the single baffle results or the double baffle results is used instead of a standardised calibration using volumetric flow measurement techniques of the preferred fish pass, the discharge would be overestimated to some degree (generally greater than 5%) in each case.

- Non-modular flow scenarios: A single baffle and the preferred fish pass arrangement were compared to an unmodified Crump weir (used as a control). The single baffle data showed a marked deviation from the control whereas the data from the fish passage arrangement was at least as close to the theoretical curve as the control data.

6.2. Summary

The Environment Agency is responsible for a number of Crump weirs, used primarily for gauging, which are known to provide difficulty in terms of fish passage. In line

with an increased environmental sensitivity, reduction in water pollution and a wider knowledge base of fish physical and behavioural attributes, this functionality now needs to be extended to encompass a biological operating range. This research project was aimed at finding low-cost solution(s) so as to provide a mechanism for modifying such weirs whilst still maintaining a gauging function. Therefore, the purposes of this project were two-fold:

- To develop favourable swimming conditions for fish passage improvement at a Crump weir, and
- To investigate the effect of the modifications on the hydrometric functioning.

The literature review introduced relevant fish-related research, including the latest data on coarse fish swimming speeds, reviewed existing Crump design and specifications, and finally linked these two fields with fish passage approaches.

Brimpton weir on the river Enborne, which had been identified as one of the Crump weirs where fish passage was known to be a problem (Pinniger 1998), was chosen as a suitable reference on which to base laboratory model tests. Although results in the thesis are generally referred to in terms of Brimpton weir, they have also been generalised for the guidelines required by the Environment Agency (Rhodes and Servais 2006) by calculating the flow rate as a 'flow rate per unit width'. As physical modelling lent itself to a multiplicity of layouts being tested in a short period of time, numerical modelling (and the associated time-consuming calibration requirements) was not considered to be the best approach for this research project.

The 1:5 scale model of the Brimpton low-flow section was set up in a flume equipped with a 3-axis computer controlled traverse gear system. Data acquisition, including the instrumentation installed in the traverse gear, provided for accurate and repeatable experimentation methods.

Initially, LEGO bricks were used to test a multiplicity of layouts for the 90 percentile low-flow range (i.e. corresponding to a flow rate per unit width of 0.34 m^2s^{-1}). Five categories were tested, and using the criterion that a layout was to be capable of passing the majority of five species of fish greater than 10cm in length (identified in the first Swimit trial, Environment Agency 2001b), a rotated-V with narrow channel layout was chosen for further refinement over a larger flow range. Final adjustments to this layout included the removal of the narrow channel, an increase in baffle height, and ensuring that slots were unaligned about the x-axis (i.e. before and after the point of inflection).

This preferred arrangement was then prefabricated in perspex. While keeping the first baffle level with the crest, provision was made for testing two different first baffle heights. These were referred to as the 'equal baffle pairing' (i.e. first baffle equal in height to the rest) and the 'unequal baffle pairing' (i.e. first baffle smaller than the rest of the baffles). A detailed analysis of the flow conditions on the downstream slope of the weir was thus carried out for both scenarios. These included using a wave probe to locate free surface profiles and a Pitot tube - static tube (PT-ST)

combination to perform a slot-based, contour-plot velocity distribution analysis accompanied by a fish pass efficiency matrix over a range of flows. The equipment initially intended for three-dimensional flow analysis, particle tracking using DigImage, was not suitable for the high velocity scenarios encountered. However, the video footage proved useful for flow visualisation and the camera installation was also used to record a debris trial.

In terms of depth of flow, fish swimming conditions benefitted from the use of baffles on the downstream slope of the weir. Assuming that an hydraulic jump is designed to occur on the downstream face of the weir, water depth is thickened at all flow rates from the position of the first baffle to the hydraulic jump. Together with the velocity results, the most challenging section of the weir would thus be between the crest and the first baffle. Although the fish pass arrangement has been designed with the maximum burst speeds in mind, fish are considered to be able to attain instantaneous speeds that are higher than burst speed velocities for very short periods of time (Armstrong 2003a, 2006). It is expected that fish would be able to exploit these speeds enabling them to surmount the final stretch between the first baffle and the crest. The slots were staggered so that the jet from each slot would impinge directly on the baffle below. Slot size and baffle spacing were both chosen using the coarse fish guidelines provided by Armstrong (2002b). Baffle spacing was further selected to ensure that velocities downstream of each baffle slot were kept less than the velocities within the slots, and the baffle height was increased to cause the baffles to act as roughness elements for the higher flow rates.

Contour-plot velocity distributions were presented for a range of flow rates (i.e. corresponding to generalised flow rates per unit width of 0.067 m^2s^{-1},0.236 m^2s^{-1}, 0.392 m^2s^{-1} and 0.680 m^2s^{-1}), both for the equal and unequal baffle pairing arrangements. In addition, the effects of a steeper downstream slope were investigated for the unequal baffle pairing. As part of a novel approach to determining the effectiveness of the fish pass, a fish pass efficiency matrix method was developed and applied to each slot individually and to the pass as a whole. This matrix provided an indication as to the predicted pass / fail rate of each fish species and length, using an area-based comparison between fish burst swimming speed and the water velocity. The overall results of the fish pass prediction matrices for the four flow rates tested showed that the use the low-cost modifications to create a fish pass (using both the equal and unequal baffle pairings) at either the 1:5 or 1:4.55 gradient prove effective to varying degrees. Field tests are needed to verify the validity of these predictions.

Crump weirs as gauging structures are well understood, and if designed and constructed within the British Standard specifications (BS3680 1986), measured flow deviations will fall within the limits acceptable to the hydrometric community. Because a fish pass on the downstream slope of the Crump weir would affect gauging capacity, the hydrometric effect of the chosen fish pass solution needed to be determined for both modular and non-modular flow.

The modular flow conditions were considered first. As a starting point and because two different first baffle heights had been tested, a series of single baffle experiments were initiated. The results were plotted non-dimensionally showing that there is a unique curve for each d/l ratio (where d equals baffle height and l is the distance from

the crest to the centre of the baffle, parallel to the bed slope). A generalised rule for predicting the estimation error of the discharge was drawn up. In order to allow velocities on the downstream slope of the Crump weir to be reduced, the optimal placement of the first baffle is effectively where the top of the baffle is equal to the crest level of the Crump weir, or where $d/l = 0.2$. For $d/l = 0.2$, the discharge will be overestimated by up to 16.5% for very low H_1/d values, or assuming $H_1/d \geq 1.68$, a maximum overestimation would be 13%.

HR Wallingford conducted a similar trial in the same time period, using the baffles based on the Hurn-type baffle parameters (White *et al.* 2005e). Their initial assumption was that a baffle needed to be located far enough down the slope of the weir such that the coefficient of discharge would only deviate by 1%. The Cranfield approach had been to find a fish pass which would accommodate the fish under review, and then to determine the effect of that fish pass upon the hydrometric functioning of the weir. The two result sets are considered to be complementary because the Cranfield data set ranged from $0.25 \leq H_1/d \leq 7$ as limited by the maximum head achievable on the weir, compared to the HR Wallingford data set where the range was $2.5 \leq H_1/d \leq 30$.

A series of double baffle experiments was also completed since initial comparisons of the single baffle data with the perspex arrangements indicated that the single baffle data might not provide a good enough estimation of the baffled pass.

As previously explained, the preferred fish pass arrangement was tested using two different first baffle heights, both with $d/l = 0.2$, resulting in equal and unequal baffle pairing arrangements. Comparing the measured discharge to the calculated British Standard discharge provided an indication as to the percentage overestimation which would be incurred if the British Standard coefficient of discharge was used directly. The results were non-dimensionalised, with H_1/d_1 plotted on the x-axis versus $Q/Q_{BS} = C_d/C_{dBS}$ plotted on the y-axis. For the unequal baffle pairing, the discharge would be overestimated by a minimum of 10% and a maximum of 16% dependent on head. For the equal baffle pairing the maximum difference was in the order of 4.5% over the range, although for $H_1/d_1 > 2.2$, the maximum difference was in the order of 3%. The purpose of the single baffle experiments was to have generated a revised standard which would be generally applicable for a baffled pass. It was found that for the scenario $d/l = 0.2$ this approach would not be acceptable because the new draft guidelines for fish passes at flow gauging stations state that an uncertainty of less than 2% at the 95% confidence interval would be typically expected for the determined coefficient of discharge White *et al.* (2005a).

In conclusion therefore, in terms of the proposed fish pass arrangement for a Crump weir, additional calibration using volumetric flow measurement techniques (or similar) which are accepted and approved by the hydrometric community would need to be performed. Although the unequal baffle pairing arrangement (i.e. first baffle smaller than the second baffle) was favoured in the laboratory trials, both arrangements would benefit from being calibrated according to the accepted British Standard.

Only a limited number of non-modular flow experiments were completed within the research project time-frame. The unmodified Crump weir experiment was used

as a control and compared to a single baffle and the fish pass (i.e. unequal first baffle arrangement), all at a single flow rate. For comparative purposes, the fish pass arrangement was tested at a second, higher flow rate. For the single baffle experiment as compared to the unmodified Crump weir, non-dimensional curves were plotted where the flow reduction factor f was plotted against H_2/H_1 and h_p/H_1 respectively. The single baffle data showed a marked deviation from the standard curve in both cases. However, in the case of the fish passage arrangement, the data points lie at least as close to the theoretical curve as the unmodified Crump data used as control. Since no crest pressure tappings were available for the fish passage experiment, only f versus H_2/H_1 was plotted.

These results show that future research into the non-modular aspects of baffled fish passes would not be best represented by experiments using a single baffle.

6.3. General comments and recommendations

In this section a number of general comments are made and implications are discussed with regard to the findings from this research project. Where relevant and drawing upon the experience gained and results achieved, a number of recommendations are made relating to future work in this subject area. For ease of reference, such comments and recommendations have been divided into various themes.

6.3.1. Drawing up general guidelines

Based on the findings of this research project, general guidelines relating to the use of the rotated-V arrangement and the resultant hydrometric effect are being drawn up for the Environment Agency as part of the original remit and are still in press at the time of completion of this thesis.[1]

6.3.2. Scaling the results

A proposal for scaling the Hurn-type baffles has been made (Armstrong *et al.* 2004) such that that arrangement may be used on different weir sizes and flow rates. A wider research project incorporating fish migration needs within the design of flow measurement structures, with the stated intention of maintaining existing levels of accuracy, also included a near-crest baffle study (White *et al.* 2005b,e). This research into the effect of the first baffle was designed to determine the position of the baffle, such that the coefficient of discharge on a Crump or Flat-V weir would not be altered by more the 1%. With this existing scaling approach at a similar low-cost scheme to that proposed for Brimpton and similar weirs as background, the following comments are made:

[1]Owing to maternity related time-constraints, the primary author of that document is Dr David Rhodes (Rhodes and Servais 2006).

An important aspect of the Brimpton-inspired fish pass design is that the slot sizes, baffle heights, baffle spacing and slot overlaps were designed at field scale using fish characteristics as guidelines (suggested by Armstrong 2002b). The implications of this are that it is intended that this fish pass design be used as it is, without further scaling taking place.

It is expected that the rotated-V arrangement would be constructed on either a single Crump weir, or on the low-flow section of a compound Crump weir. In order to accommodate weirs of substantially different heights and widths to that of Brimpton (on which this design was based and tested), a modular approach is suggested. For a higher weir, more baffles would need to be added to the downstream end of the apron until the last baffle height is below the level of the hydraulic jump. A change in the path of ascent would need to be added at every seventh baffle[2], and it would also be important to ensure that slots above and below this change-over baffle were not aligned. For very wide weirs, a number of identical passes could be installed. Such designs would be site-specific, but it would be useful, in terms of location and attraction concepts, to site the uppermost slot in the baffle nearest to the crest close to a side wall, and if possible a similar arrangement for the slots near the bottom of the weir. Such measures should help to guide fish to the entrance and direct them away from exit position.

6.3.3. Laboratory trials

Aspects relating to future laboratory work are discussed below:

Hydrometric testing One of the limitations of the laboratory arrangement at Shrivenham was the lack of a constant head tank in the water supply pipework. Flow rate delivery was thus dependent on the pump rate. The results from this research project were never intended as a definitive hydrometric standard, and consequently detailed weir calibration with the installed fish passage would need to be quantified in a laboratory with volumetric flow measurement facilities acceptable to the hydrometric community.

It would be desirable, from a hydrometric point of view, to place the first baffle far enough down the slope from the crest such that there was little or no impact on the stage-discharge curve. However, analysis during this research project has shown that in order to accommodate the species-dependent fish burst speed velocities from the Swimit data base (Environment Agency 2001b, 2003), having the first baffle at the same height as the crest was beneficial in keeping slot velocities manageable between the first baffle and foot of the weir. In addition, even with the first baffle height located level with the crest, fish would still need to exploit instantaneous speeds (i.e. higher than burst

[2]Changing the direction of the path of ascent was a constraint of the Brimpton geometry and consequently the effect of increasing the path of ascent has not been model-tested. If a longer path of ascent is used for a wider weir, it would be expedient to test this in a laboratory situation. It might also be possible to enable simple changes to be made to an in-situ fish pass if velocities downstream of the seventh baffle are found to be too challenging for the fish under consideration.

swimming speeds) in order to surmount that portion of the pass between the first baffle and the crest.

Modular flow testing showed that, for both the equal baffle pairing and unequal baffle pairing[3] fish passage arrangements, the calculated coefficients of discharge all deviated from the British Standard, single baffle and double baffle coefficients by some degree.

Because of time constraints, only a limited number of experiments could be conducted under non-modular flow conditions. The experimental results were used to calculate the flow reduction factor f, which was plotted against H_2/H_1 for all the experiments and h_p/H_1 for the control and single baffle experiments. Initial results comparing a control (i.e. unmodified Crump weir), single baffle and the unequal fish passage arrangement showed that the fish passage arrangement and control were within a similar range when compared to the theoretical curve, while the single baffle results were worse. These findings have implications for future research where baffled fish passes are represented by a single baffle for hydrometric calibration purposes.

An investigation into the effect of the crest static head with the presence of the fish pass also needs to be carried out. As it is anticipated that the rotated-V baffle arrangement would be used in a modular fashion to accommodate weirs of different heights and widths, trials would need to be carried out to confirm that the head-discharge relationships are independent of weir width.

Changing the downstream slope As not all triangular profile weirs have a 1:2 upstream slope and a 1:5 downstream slope, it would be useful to quantify the effect of the preferred fish passage arrangement on a wider range of downstream slopes. Such weirs are not likely to be calibrated, so low-cost modifications would need to be assessed according to fish species, flow rate per unit width and any adverse affects associated with increasing upstream water levels to some degree.

Within the time constraints and available resources governing this project, it was not feasible to replace the existing Crump weir within the flume so that the effect of the preferred fish pass could be tested for steeper and/or shallower triangular profile weirs. An alternative was to adjust the downstream angle of the flume using in-situ jacks under one end. Tilting the flume in this way had the effect of rotating the wooden weir installation in its entirety while allowing all the available testing facilities and coordinate systems to be used as is. Thus the fish pass was tested at the steepest available slope manageable with the existing arrangements, which resulted in an effective downstream slope of 1:4.55. Results showed that although the velocities were generally higher, fish passage would still be likely. Further research over a wider flow range and for both steeper and gentler slopes would be useful.

[3]In this context, the equal and unequal baffle pairings refer to the size of the first baffle in relation to the rest of the baffles in the fish pass with $d/l = 0.2$.

6.3.4. Field scale trials

Various constraints prevented the rotated-V arrangement from being trialled at field scale during the project time-period. These included, *inter alia*, the available time, budget (not included in the original costs) and effect of the trials on the hydrometry.

Figure 6–1 shows the proposed field scale baffle arrangement using Brimpton as an example, and is based on the preferred fish pass using the unequal baffle pairing. However, using Brimpton for field scale trials at this stage is hampered by the likely restriction that gauging would not be permitted to be compromised in any way (Armstrong 2004). Therefore either an alternative weir would need to be identified, or laboratory trials, suitable as a hydrometric standard, would need to be conducted first. Such trials would need to quantify the effect of the baffle solution on the coefficient of discharge (which has been shown to be affected).

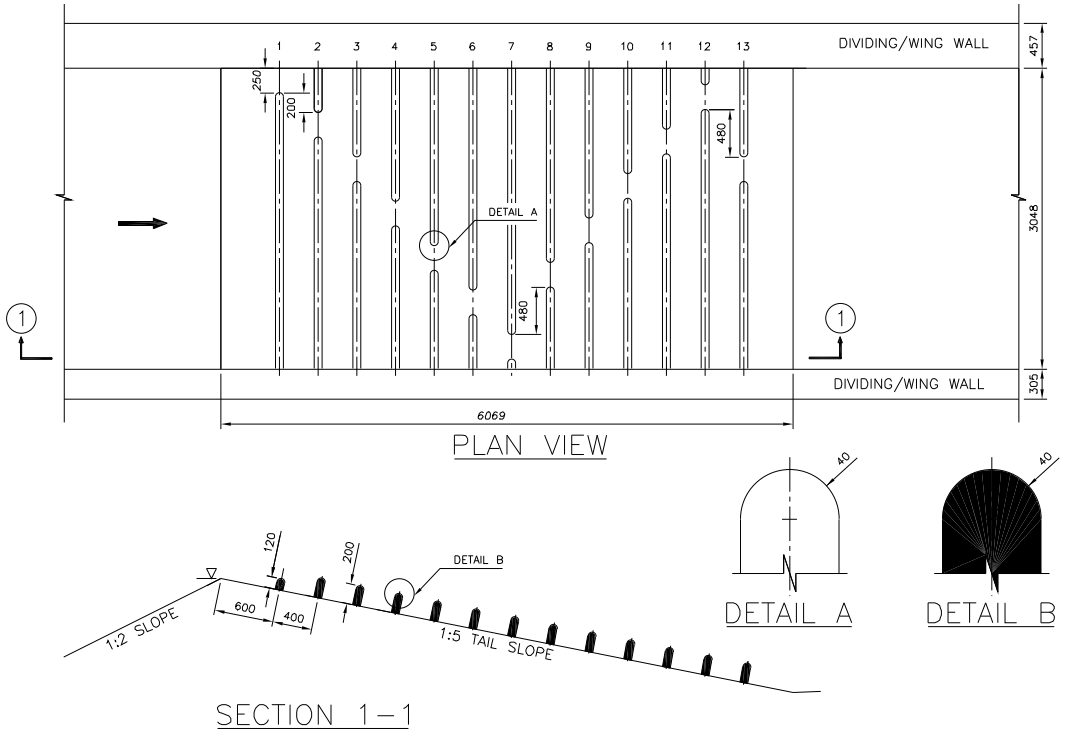

Figure 6–1: Brimpton weir: Proposed field scale layout of preferred fish pass using a 120 mm first baffle and 200 mm baffles for the rest of the pass (i.e. unequal baffle pairing)

Normally a field trial would also need to include fish monitoring aspects, preferably over more than one season, so as to determine success/failure rates associated with the fish passage installation. A comprehensive field scale trial would therefore be in order and would need to follow the normal design and legislative procedures as outlined in the Environment Agency's Fish Pass Manual (Armstrong *et al.* 2004). This would ensure that the full range of biological and hydrometric issues are considered, and managed as appropriate.

Although not an exhaustive list, the following items have been identified as aspects relating to this research project may need attention:

Air entrainment The issue of air entrainment was discussed during a site visit to see the use of baffles on the Hurn weir (Armstrong 2002a). It was revealed that air entrainment was not considered or predicted during the 1:13 Hurn scale model study, but was proving to be relevant at field scale.

Since model scale aeration is not indicative of field scale aeration, the 1:5 scale Brimpton model was not the intended vehicle to demonstrate this effect. Although at one stage during the research period it was hoped that a number of baffles, either at half or at full scale, might be modelled in the laboratory, this was not realised. Therefore the effect of air entrainment would need to be critically evaluated during a field scale investigation. Since the baffles have been designed according to fish, a single detailed investigation into air entrainment over a large range of flows should be sufficient to determine the effects thereof for most operating conditions.

Velocity trials using ADV At the outset of the project it was the intention to perform a detailed three-dimensional flow investigation using the DigImage particle tracking system. The velocities to be measured proved to be too high for this type of system, and a Pitot tube - static tube combination was used instead (to determine slot-based two-dimensional velocity distributions). Towards the end of the project, a downward-looking three-dimensional acoustic-Doppler velocimeter (ADV) became available and between-baffle velocity investigations were attempted. However, insufficient water depth and air entrainment caused by the presence of the available probe prevented useful information from being recorded at the 1:5 model scale. One of the conclusions from this trial was that for future investigations of a similar nature and scale (i.e. in the laboratory) a side-looking two-dimensional MicroADV would be useful.

Field-scale trials would provide the necessary water depth required to use the more widely available down-looking 3D instrumentation. Guiny *et al.* (2005) used a Sonteck ADV in full-scale trials as part of a recent research project into fish pass trials for Atlantic salmon. This type of instrumentation was reported to be suitable for submerged jets or vertical slot flow. However, where flow was both aerated and highly three-dimensional, as for a plunging weir jet, effective data sampling was not possible as a result of signal problems. Because the flow between the rotated-V baffle arrangement has been shown to be highly three dimensional, this type of experience needs to be taken into consideration if using a similar ADV at field scale.

Fish passage efficiency matrices The fish pass efficiency matrices have been developed using the predicted mean burst speeds for each of the fish species under consideration. As water temperature is seasonal and site-specific, as are fish species, generic fish pass efficiency matrices have not been plotted in this thesis.

The fish passage efficiency matrix as a method for determining pass/ failure at specific slot or over the fish passage also needs to be verified at field scale against the fish it is intended to represent.

Once the method has been proved in a field-trial, generic fish matrices could be extended for a range of water temperatures (e.g. 5 °C to 25 °C). It might also be useful to plot each fish species on its own fish pass efficiency matrix. In this manner, the 90 percentile confidence interval burst swimming speeds available from the Environment Agency (2001b, 2003) Swimit studies could also be accommodated.

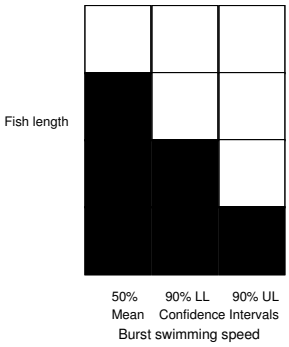

Figure 6–2: Example of a typical extended fish pass efficiency matrix (where black = pass, white = fail)

Upstream water level As is apparent from the impact of the baffled solution on the coefficient of discharge, retrofitting an existing Crump weir with a rotated-V fish pass will have an effect on the upstream water level. This site-specific effect would need to be determined so that any changes to existing floodlines can be taken into consideration. If the baffled solution is applied to the low-flow section of a compound Crump weir this is unlikely to have a serious impact, but this would need to be quantified.

This laboratory model would need to be tested and proved in the field from both the biological and hydraulic perspectives. This would then inspire confidence in the solution so that it might be used by engineers and fish pass practitioners and would not merely remain as 'blue sky research'.

6.4. Closing remarks

Based on substantial laboratory trials, the 'rotated-V' fish pass arrangement shows considerable promise in providing low cost modifications to the Crump weir, which are aimed at improving fish passage. By comparing burst swimming speeds and measured water velocities, a novel 'fish pass efficiency matrix' has been produced which is used to determine both the most challenging slots as well as the ultimate success rate of a fish pass over a range of flows. The visual presentation of this matrix provides a quick method for determining the suitability of this type of fish pass for

a range of fish species and sizes, dependent on the flow rate. From a hydrometric perspective, as the deviation in the coefficient of discharge is predictable, reliable flow measurement can be achieved (subject to a standardised calibration trial). It is therefore expected that application of this 'rotated-V' layout to existing Crump weirs would produce both favourable swimming conditions for fish, while continuing to provide for accurate and reliable flow measurement function.

References

Advantech (1994). *User's Manual: PCL818HG High Performance, High Gain Data Aquisition Card*. Advantech Co.,Ltd., Taiwan, 2nd edition.

Andrew, F. (1990). The use of vertical-slot fishways in British Columbia, Canada. In Publications Committee of the International Symposium of Fishways, editor, *Proceedings of the International Symposium of Fishways '90*, Gifu, Japan.

Armstrong, G. (2000). National Fish Pass Officer, Environment Agency. Personal Communication with Dr. D.G. Rhodes.

Armstrong, G. (2002a). Low Cost Solutions for Crump Weirs Board: Meeting held at St Leonards Hotel/Hurn GS, 21 February 2002. unpublished. SA Servais: personal meeting notes.

Armstrong, G. (2002b). Some principle guidelines/criteria for improving fish movement at Crump weirs using low-cost baffle solutions or other methods. Unpublished, private communication.

Armstrong, G. (2003a). Low Cost Solutions Board Meeting: 3 April 2003. unpublished. SA Servais: personal meeting notes.

Armstrong, G. (2003b). Table 3: Mean water temperature Lower River Kennet. personal communication from G.S. Armstrong, National Fish Pass Officer.

Armstrong, G. (2004). Low Cost Solutions for Crump Weirs Board R&D Board Meeting: 20 May 2004. unpublished. minutes.

Armstrong, G. (2006). Emails regarding use of fish cross-sectional area. personal communications.

Armstrong, G., Power, P., Fewings, A., Brown, H., Ayers, S., and Rhodes, D. (2002). Low Cost Solutions Board Meeting. Unpublished meeting notes.

Armstrong, G., Aprahamian, M., Fewings, A., Gough, P., Reader, N., and Varallo, P. (2004). *Guidance Notes on the Legislation, Selection and Approval of Fish Passes in England and Wales*. Environment Agency: National Fish Pass Manual, Version 1.1 on cd edition.

Ayers, S. (2002). Low cost solutions for improving fish passage at Crump-type weirs. Poster at 3rd IWA UK Young Researchers Conference.

Bates, K. (2000). Fish ways guidelines for Washington State. Washington Department of Fish and Wildlife, draft edition. Edited by T Whiley.

Beach, M. (1984). Fish pass design criteria for the design and approval of fish passes and other structures to facilitate the passage of migratory fish in rivers. Fisheries Research Technical Report No. 78, Ministry of Agriculture, Fisheries and Food, Lowestoft.

Beaumont, W., Mills, C., and Williams, G. (1986). Use of a microcomputer as an aid to identifying objects passing through a resistivity fish counter. *Aquaculture and Fisheries Management*, **17**, pp. 213–226.

Brown, H. (2001). Memorandum of Understanding between The Environment Agency and Cranfield University.

BS1042 (1992). *Measurement of fluid flow in closed channels - Part 1: Pressure differential devices - Section 4: Guide to the use of devices specified in Sections 1.1 and 1.2.* British Standard Institution. Incorporating Amendment No. 1.

BS3680 (1986). *Measurement of liquid flow in open channels - Part 4: Weirs and flumes - Part 4B:Triangular Profile Weirs.* British Standard Institution.

Carling, P. and Dobson, J. (1992). Fish Pass Design and Evaluation: Phase 1 Initial Review. Research and Development 110.

Chadwick, A. and Morfett, J. (1994). *Hydraulics in Civil and Environmental engineering.* E & FN Spon, London, 2nd edition.

Christensen, P. (1993). Cost-effective solutions to fishway design. In *Proceedings of the International Conference on Hydropower*, volume 1, New York. ASCE.

Clay, C. (1995). *Design of Fishways and Other Fish Facilities.* Lewis Publishers, Boca Raton, Florida, 2nd edition.

Clifton-Dey, D. (2006). Environment Agency Project Manager. Personal email regarding Swimit version 3.2 which supersedes the previous versions.

Clough, S. and Turnpenny, A. (2001). Swimming Speeds in Fish: Phase 1. Research and Development W2-026/TR1, Environment Agency, Bristol.

Crump, E. (1952). A new method of gauging stream flow with little afflux by means of a submerged weir of triangular profile. volume 1, pages 223–242. Institution of Civil Engineers.

Deitel, H. and Deitel, P. (2001). *C How to Program.* Prentice Hall, Upper Saddle River, New Jersey, 3rd edition.

Egonjic, D. (2000). Turbulent Flow Structure of Compound Channel Flows. MPhil/PhD Transfer Report, RMCS, Cranfield University, Shrivenham.

Environment Agency (1966). Drawing No. HYD 126/2 for the gauging weir at River Enbourne, Brimpton, England.

Environment Agency (1997b). Strategic Overview of Impounding Structures. Internal discussion paper, Environment Agency Thames Region. (Restricted).

Environment Agency (2001a). Problem Gauging Sites. Excel spreadsheet.

Environment Agency (2001b). Swimming Speeds in Fish: Phase 1. Environment Agency R&D Project W2-026. Swimit version 1.11 is an Excel spreadsheet produced by 'Fawley Aquatic Research' (now known as 'Jacobs Babtie Aquatic') for the Environment Agency.

Environment Agency (2003). Swimming Speeds in Fish: Phase 2. Environment Agency R&D Project W2-029. Swimit version 2.0 is an Excel spreadsheet produced by 'Fawley Aquatic Research' (now known as 'Jacobs Babtie Aquatic') for the Environment Agency.

Environment Agency (2005). Swimming Speeds in Fish: Phase 2. Environment Agency R&D Project W2-029. The Excel spreadsheet Swimit version 3.2 supercedes all previous versions.

Environment Agency (Undated, approximately 1997a). Hurn Weir Fish Pass. Pamphlet published by Environment Agency.

Environment Agency hydrology section (2002). Flow-duration data for Brimpton weir. personal communications.

Everard, N. (2002). Environment Agency Officer. Email communication with Dr. D.G. Rhodes.

Fort, R. and Brayshaw, J. (1961). *Fishery Management*. Faber and Faber, London.

Guiny, E., Ervine, D. A., and Armstrong, J. (2005). Hydraulic and Biological Aspects of Fish Passes for Atlantic Salmon. *ASCE Journal of Hydraulic Engineering*, pages 542 – 553.

Hamill, L. (2001). *Understanding Hydraulics*. Palgrave, Basingstoke, 2nd edition.

Herschy, R., White, W., and Whitehead, E. (1977). The Design of Crump Weirs. Technical Memorandum 8, Department of the Environment: Water Data Unit, Reading.

Hertel, H. (1969). Hydrodynamics of swimming and wave-riding dolphins. In Anderson H.T., editor, *Biology of marine mammals*, pages 31–63. Academic Press, London.

HMSO (1963). *Water Resources Act*. Her Majesty's Stationery Office, London.

Horton, G. (2002). Water Words Dictionary: Nevada Division of Water Planning, Department of Conservation and Natural Resources. Internet: http://state.nv.us/cnr/ndwp/dict-1/waterwds.htm.

HR Wallingford (undated, approximately 2002). *Wave Probe Monitor: Operating Instructions - Issue 15*. HR Wallingford Ltd., Wallingford.

ICOLD (1999). Dams and Fishes: Review and Recommendations. Bulletin 116, Commission Internationale des Grands Barrages (i.e. International Commission on Large Dams or 'ICOLD'), Paris.

Katopodis, C. (2005). Developing a toolkit for fish passage, ecological flow management and fish habitat works. *Journal of Hydrauic Research*, **43**(5), 451–467. International Association of Hydraulic Engineering and Research.

Larinier, M. (2002a). Baffle Fishways. In Bunch F. and Fournier M.S., editors, *Fishways: biological basis, design criteria and monitoring*, volume Bulletin Francais de la Peche et de la Pisciculture, No 364 supplement., pages 83–101. Food and Agriculture Organization of the United Nations.

Larinier, M. (2002b). Fishways - Biological factors to be taken into account in the design of fishways, the concept of obstruction to upstream migration. In Bunch F. and Fournier M.S., editors, *Fishways: biological basis, design criteria and monitoring*, volume Bulletin Francais de la Peche et de la Pisciculture, No 364 supplement., pages 28–38. Food and Agriculture Organization of the United Nations.

Larinier, M. (2002c). Fishways - General Considerations. In Bunch F. and Fournier M.S., editors, *Fishways: biological basis, design criteria and monitoring*, volume Bulletin Francais de la Peche et de la Pisciculture, No 364 supplement., pages 21–27. Food and Agriculture Organization of the United Nations.

Larinier, M., Travade, F., and Porcher, J. (2002). Pool fishways, pre-barrages and natural bypass channels. In Bunch F. and Fournier M.S., editors, *Fishways: biological basis, design criteria and monitoring*, volume Bulletin Francais de la Peche et de la Pisciculture, No 364 supplement., pages 54–82. Food and Agriculture Organization of the United Nations.

LEGO company (2006). Company Profile 2005. Internet: http://www.lego.com/info/pdf/LEGO_company_profile_UK.pdf. Accessed May 2006.

Lomax, W. and Saul, A. (1979). *Laboratory work in hydraulics*. Crosby Lockwood Staples. Granada Publishing Limited.

Lucas, M. and Baras, E. (2001). *Migration of Freshwater Fishes*. Blackwell Science, Malden, M.A.

Lucas, M. and Frear, P. (1995). Effects of a flow-gauging weir on the migratory behaviour of adult barbel, Barbus barbus, a river cyprinid. *Journal of Fish Biology*, (50), pp. 382–396.

Masters, J., Beaumont, W., Hodder, K., Pinder, A., Gozlan, R., and Ladle, M. (2002). Habitat utilisation by pike Esox lucius L. during winter floods in a southern English chalk river. *Hydrobiologia*, **483**(1-3), pp. 185–191.

Oxford University Press (2003). *Colour Oxford Dictionary Thesaurus and Wordpower Guide*. Oxford University Press, Oxford.

Pinniger, J. (1998). A study of the impact of gauging weir structures on coarse fish and their spawning migrations. Professional training report presented in part fulfilment of B.Sc Hons. Degree of Zoology, University of Wales, College of Cardiff.

Porcher, J. and Travade, F. (2002). Fishways: Biological Basis, Limits and Legal Considerations. In Bunch F. and Fournier M.S., editors, *Fishways: biological basis, design criteria and monitoring*, volume Bulletin Francais de la Peche et de la Pisciculture, No 364 supplement., pages 9–20. Food and Agriculture Organization of the United Nations.

Power, P. (2002). Thames Hydrometry Team Leader. Series of email communications with Dr. D.G. Rhodes.

Rhodes, D. (2001). Low Cost Modifications to the Crump Weir in Order to Facilitate Fish Passage. Case for Support to EPSRC.

Rhodes, D. (2002). Low-Cost Solutions for Improving Fish Passage at Crump-type Weirs. Notes presented at Low Cost Solutions Board Meeting.

Rhodes, D. and Servais, S. (2003). Methods for measuring the free surface position in laboratory flows. In Ganoulis J. , editor, *XXX IAHR Congress*, volume I, pages 441–448, Thessaloniki, Greece. IAHR. Theme C. Inland waters: Research, Engineering and Management.

Rhodes, D. and Servais, S. (2004). Hydrometric effect of fish pass modifications to the Crump weir. In Garcia J.L and Martinez P.V., editors, *Fifth International Symposium on Ecohydraulics. Aquatic Habitats: Analysis and Restoration*, volume II, pages 969–972, Madrid, Spain. IAHR. Fish passes and migration facilities.

Rhodes, D. and Servais, S. (2006). Guidelines: Low cost modifications to the Crump weir to improve fish passage. Technical report, Draft Document to be presented to the Environment Agency.

Rickard, C., Day, R., and Purseglove, J. (2003). *River Weirs Good Practice Guide*. Environment Agency, Bristol, R&D Publication W5B-023/HQP edition. Research Contractor: Mott MacDonald Ltd and University of Hertfordshire.

Salmon Advisory Committee (1997). Notes for Guidance on the Provision of Fish Passes and Screens for the safe passage of salmon. Report of the Salmon Advisory Committee, Ministry of Agriculture, Fisheries and Food: The Scottish Office Agriculture, Environment and Fisheries Department, Edinburgh.

Sarker, M. (2000). *Application of CFD to modelling local features in a river: free surface flow over broad-crested weir and modification of Crump weir for fish passage*. PhD Thesis, Cranfield University [RMCS], Shrivenham, U.K.

Sarker, M., Rhodes, D., and Armstrong, G. (2001). Modification of Crump weir to facilitate fish passage. In Guifen Li, editor, *Proceedings of the XXXIX IAHR Congress*, Beijing, China. IAHR, Tsinghua University Press. Theme B: Environmental Hydraulics and Eco-Hydraulics.

Servais, S. (2003). *Low cost modifications of the Crump weir to facilitate fish passage*. Transfer Report, Cranfield University [R.M.C.S.].

Servais, S. (2006). Susan Servais: Personal website. Internet: http://www.susan.googlepages.com.

Servais, S., Rhodes, D., and Armstrong, G. (2003). Development of low-cost modifications to the Crump weir to improve fish passage. In Ganoulis J. , editor, *XXX IAHR Congress*, volume I, pages 203–210, Thessaloniki, Greece. IAHR. Theme C. Inland waters: Research, Engineering and Management.

Servais, S., Rhodes, D., and Armstrong, G. (2004). Low-cost modifications to the Crump weir for fish passage: trial solutions. In Garcia J.L and Martinez P.V., editors, *Fifth International Symposium on Ecohydraulics. Aquatic Habitats: Analysis and Restoration*, volume II of *964-968*, Madrid, Spain. IAHR. Fish passes and migration facilities.

Smith, P. (2002). Fluid Mechanics and Hydraulics: E232C Section 1 (Similitude and modelling). Unpublished E232C lecture notes.

Solomon, D. J. (1992). Diversion and entrapment of fish at water intakes and outfalls. Technical report, National Rivers Authority, Bristol.

Stone and Webster Engineering Corp. (1996). *Assessment of Downstream Migrant Fish Protection Technologies for Hydroelectric Application. Final Report to Electric Power Research Institute.* EPRI AP-4711, Palo Alto, CA, Project 2694-1 edition.

Travade, F. and Larinier, M. (2002). Fish locks and fish lifts. In Bunch F. and Fournier M.S., editors, *Fishways: biological basis, design criteria and monitoring*, volume Bulletin Francais de la Peche et de la Pisciculture, No 364 supplement., pages 102–118. Food and Agriculture Organization of the United Nations.

Travade, M. L. F. (2002). Pool fishways, pre-barrages and natural bypass channels. In Bunch F. and Fournier M.S., editors, *Downstream migration: problems and facilities*, volume Bulletin Francais de la Peche et de la Pisciculture, No 364 supplement., pages 181 – 207. Food and Agriculture Organization of the United Nations.

Turnpenny, A. (1981). An analysis of mesh size required for screening fishes at water intakes. In *Estuaries*, volume 4(4), pages 363–368.

Turnpenny, A. (1989). Impoundment and abstraction - exclusion of fish from intakes. In J. Gregory, editor, *Proceedings of a workshop on the safeguarding of fisheries, University of Lancaster, April 1988*, pages 87–114, Pitlochry. Atlantic Salmon Trust.

Turnpenny, A. (2003). Fish swimming: personal email to DG Rhodes. unpublished. email sent by AWH Turnpenny, including comment from S Clough.

Turnpenny, A., Lawton, K., Clough, S., Hanson, K., and Ramsay, R. (1999). Fish passage of flow gauging stations in England and Wales. Phase 1: Literature Review and Regional Survey, Environment Agency. Draft.

Turnpenny, A., Blay, S., Carron, J., and Clough, S. (2001). Literature Review Swimming Speeds in Fish. Research and Development W2-026/TR2, Environment Agency, Bristol.

Walters, G. (1996a). Hydraulic model tests on the proposed fish pass structure for Hurn Gauging Weir, Dorset. Technical report, Exeter Enterprises, Exeter.

Walters, G. (1996b). Hydraulic model tests on the proposed fish pass structure for Hurn Gauging weir, Dorset: Supplementary Report. Technical report, Exeter Enterprises, Exeter.

Wardle, C. (1977). Effects of size on the swimming speeds of fish. In Pedley T.J., editor, *Scale effects in Animal Location*, pages 299–313. Academic Press, London.

Wardle, C. (1980). Effects of temperature on the maximum swimming speed of fishes. In Ali M.A., editor, *Environmental Physiology of Fishes*, pages 519–531. Plenum Publishing Corporation, New York.

White, R., Bowker, P., and McGahey, C. (2005a). Appendix M: Draft standard - Fishpasses at flow gauging stations. In *Flow measurement structure design to aid fish migration without compromising flow data accuracy.* Environment Agency, Science Report SC020053/SR2 edition.

White, R., Bowker, P., and McGahey, C. (2005b). Flow measurement structure design to aid fish migration without compromising flow data accuracy. Technical report, Research Contractor (HR Wallingford) for the Environment Agency. Science Report SC020053/SR2.

White, R., Bowker, P., and McGahey, C. (2005c). Study B Review of the problems of trash at fish passes and ways to minimise accumulations. In *Flow measurement structure design to aid fish migration without compromising flow data accuracy.* Environment Agency. Science Report SC020053/SR2.

White, R., Bowker, P., and McGahey, C. (2005d). Study C Laboratory tests to provide an accurate hydrometric calibration of a Larinier fish pass. In *Flow measurement structure design to aid fish migration without compromising flow data accuracy.* Environment Agency. Science Report SC020053/SR2.

White, R., Bowker, P., and McGahey, C. (2005e). Study D Fundamental requirments for the near-crest arrangements of baffles on the downstream face of a measuring weir . In *Flow measurement structure design to aid fish migration without compromising flow data accuracy.* Environment Agency. Science Report SC020053/SR2.

White, R., Bowker, P., and McGahey, C. (2005f). Study E Laboratory testing of a Larinier fish pass with a submerged orifice upstream intake set alongside a non-specific flow measurement structure. In *Flow measurement structure design to aid fish migration without compromising flow data accuracy.* Environment Agency. Science Report SC020053/SR2.

White, W. and Hartley, W. (undated, approximately 1970?). Experiments to compare the passage of fish over two triangular profile flat-vee weirs. Technical Report INT 67, Hydraulics Research Station: Wallingford, Wallingford.

Williams, R., Rhodes, D., and Servais, S. (2005). Meeting held at Shrivenham for demonstration of the 16MHz MicroADV. Attended by R.Williams (OSIL), D.Rhodes and S.Servais. unpublished notes.

A. Fish Swimming Speeds

A.1. Fish swimming speed data

Most texts on fish passes point out that fish are not machines, and it is worth reminding that like humans, the 'average' fish needs to be accommodated as opposed to only the 'athletes'. The Environment Agency (2003) Excel spreadsheet provides the data for nine species, although a distinction is made between eels and elver. As the user needs to input variables based on the output data, different options were available as required:

Swimming speeds For a given fish length and water temperature sustainable and burst swimming speeds were available from the database. The median and 90 percentile values were calculated for the maximum sustainable swimming speed (i.e. sustainable for 200 minutes), and the median and 90 percent confidence intervals were calculated for the burst swimming speed (i.e. sustainable for 20 seconds).

Endurance times The maximum endurance time was calculated for a given fish length, water velocity and water temperature.

It is assumed that fish would swim up the downstream slope of a Crump weir without resting, probably require fish to swim at the burst speed. Although the database (Environment Agency 2001b, 2003) includes both median and 90 percentile values,only the median burst data values have been used so as to represent an 'average' fish. Another aspect is that fish are considered to be able to attain instantaneous speeds that are higher than burst speed velocities for very short periods of time (Armstrong 2003a, 2006). It is expected that fish would be able to exploit these speeds in order to surmount the final distance between the first baffle and the crest for a Crump weir adapted with the rotated-V baffle arrangement.

Note that in this thesis, the mean burst speeds for each of the fish species has been used. The Swimit (Environment Agency 2001b, 2003) provide the 90 percentile confidence interval values associated with each of these mean burst speeds, and if desired, this information could be worked into the approach used.

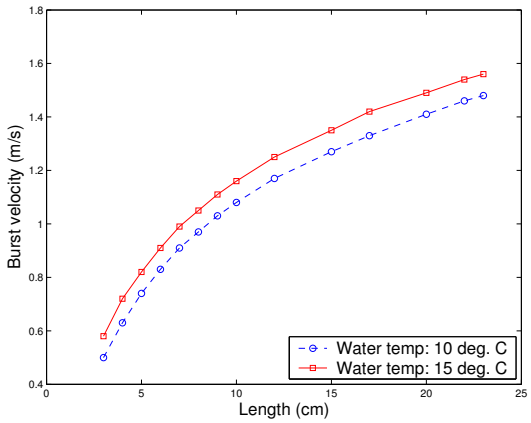

(a) Roach

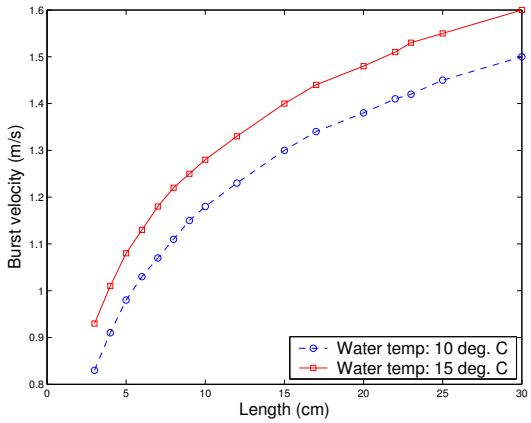

(b) Chub

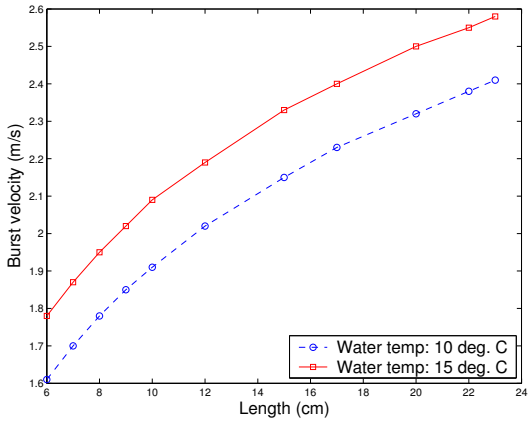

(c) Barbel

Figure A–1: Burst swimming speeds increasing with fish size and increasing water temperature

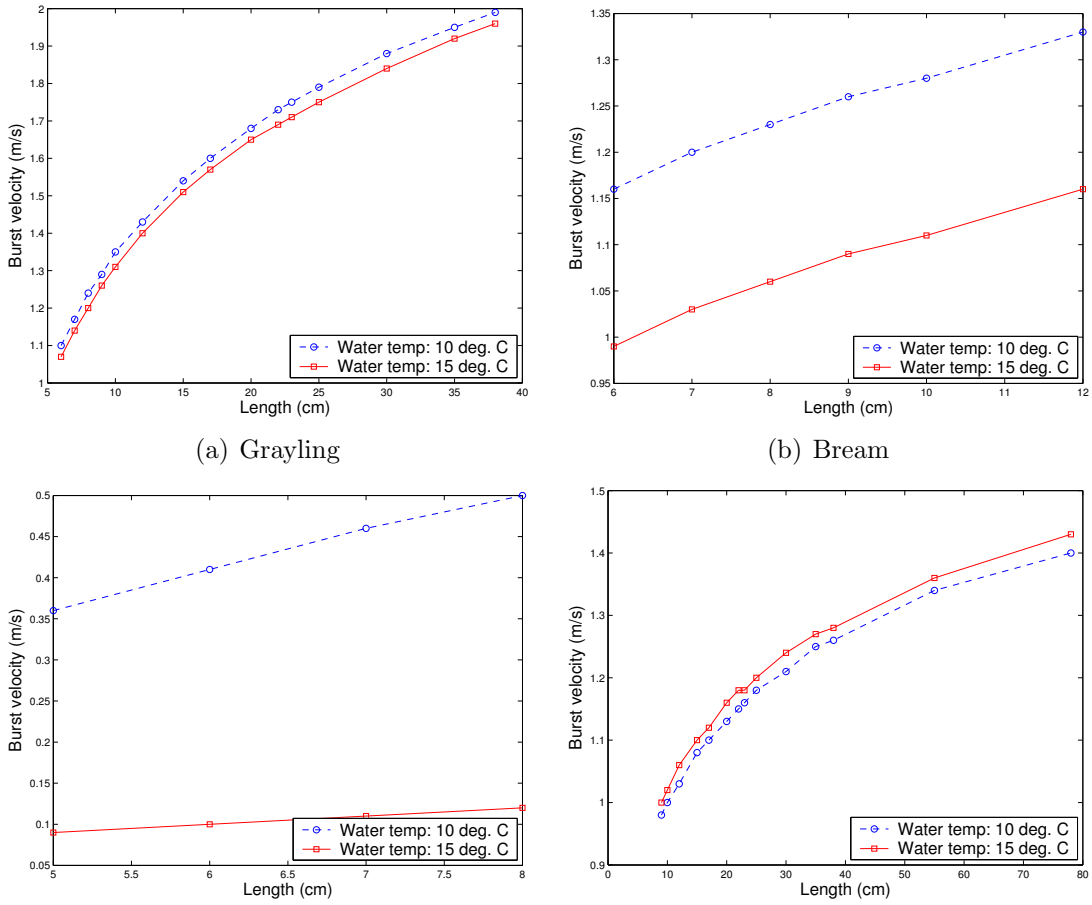

(a) Grayling (b) Bream

(c) Elvers (d) Eels

Figure A–2: Burst swimming speeds increasing with fish size but decreasing with increasing water temperature

B. C PROGRAMS

This appendix provides an overview of the C programs created during the course of this research project as used in the laboratory. Over the duration of the project approximately six months in total was spent developing and then making additional changes during their application. These C programs have not been attached to this thesis as they were lengthy and are not specifically useful outside of their specific context.

B.0.1. Development of the programs

The approach to the programming was that of modular development. A series of source (.c) files with the accompanying header (.h) files were created, each with a basic remit. A summary of the main programs created is given in Table B–1. The user was then able use these functions to drive the traverse gear and/or trigger the A/D conversion to the LabCard as required.

Table B–1: List of main programs, associated Make and Batch files and the program functions

Program	**Make file**	**Batch file**	**Function of Program**
f_mainLC.c	fmakeLC.mak	fbatLC.bat	A/D converter verification
f_mainPT.c	fmakePT.mak	fbatPT.bat	Pressure Transducer Calibration
f_mainSD.c	fmakeSD.mak	fbatSD.bat	Stage-discharge
f_mainTG.c	fmakeTG.mak	fbatTG.bat	Traverse gear - general move and log, or just move
f_mainVT.c	fmakeVT.mak	fbatVT.bat	Velocity traverse of flume using Pitot tube
f_mainWP.c	fmakeWP.mak	fbatWP.bat	Wave Probe Calibration and Use

The LabCard was used in a DOS-mode environment. Because the programs included more than one .c and .h file, the normal Borland Turbo C++ environment was not able to link all of the programs together with the outside library resources, as required by the LabCard. Consequently it was necessary to create a *makefile*. Running *make* together with the executable programs for the traverse gear and the LabCard creates a single executable file for each project. As there were different objectives for the use of the traverse gear and LabCard, a suite of executable C programs was written (as listed in Table B–1).

In addition, a batch file was created for each of these executable C programs. Each specific batch file first deleted the existing object files created from previous makefile use, then loaded the LabCard software, ran the correct makefile, ran the new .exe file, and upon completion of the program, unloaded the LabCard software. Table B–1 lists the main executable programs together with the associated 'make' and 'bat' files, Table B–2 lists the input and output files associated with each main .c program, and Table B–3 lists the files which also need to be in the 'bin' directory.

Table B–2: Comments on the files used and generated by the programs

Program	Function/Use of Program and Associated Input and Output Files
f_mainLC.c	A/D converter verification (modified 'ADTRIG.exe') *Input:* FCountLC.txt *Output:* Fx_LCxx.out ('xx' represents the incremental number allocated to the file each time the program is run.)
f_mainPT.c	Pressure Transducer Calibration *Input:* FcountPT.txt *Output:* Fx_PTxx.out Fx_PTtbl.out
f_mainSD.c	Stage-discharge *Input:* FCountEA.txt *Output:* Fx_EAxx.out Fx_SD.out
f_mainTG.c	Traverse gear - general move and log, or just move *Input:* FCountAA.txt *Output:* Fx_AAxx.out
f_mainVT.c	Pressure traverse of flume using Pitot tube (> velocity) *Input:* FCountDA.txt *Output:* Fx_DAxx.out Fx_VDat.out
f_mainWP.c	Wave Probe Calibration and Use **Calibration:** *Input:* FCountBA.txt *Output:* Fx_BAxx.out Fx_WPD.out **Use:** *Input:* FCountBB.txt *Output:* Fx_BB.out Fx_WLog.out

The user could specify in the hardware.h file whether to define the traverse gear specific functions and/or the LabCard specific functions as the need arose. This decision was made to aid debugging, as well as prioritising resources.

B.0.2. Pseudocode

Pseudocode is a method for presenting the logic as used in the C code in a flow diagram without presenting the code itself. In this section, part of one of the programs

Table B–3: List of all additional files required to run the Fish Suite of programs

Library Files	**.c Files**	**.h Files**	**Object File**	**.exe File**
graphics.lib	fishcomm.c	fishcomm.h	c0l.obj	wait.exe
emu.lib	fish_wpd.c	fish_wpd.h		
cl.lib	fishdefn.c	fishdefn.h		
mathl.lib	fishminc.c	fishminc.h		
818hgcl.lib	fishmove.c	fishmove.h		
	fishprob.c	fishprob.h		
	tc20lib.c	tc20lib.h		
	fishrho.c	fishrho.h		
		hardware.h		

developed during the research project is given. This example shows the level of programming learned during the course of this research as it was one of the tools needed to expand, create and update the suite of in-house laboratory testing programs.

The following pseudocode was developed using the guidelines provided by Deitel and Deitel (2001). As is the standard practice (for this type of coding), the *diamond symbol* represents a **decision**; the *rectangle* represents an **action**; a large *oval* represents the beginning and end of the program, and a small *circle* represents connection symbols for various items of code. A small part of the C programs written for this research project are represented by this pseudocode (i.e. C code presented in a flow diagram format).

Figure B–1 illustrates a typical main program - f_mainWP.c, as well as a key to the rest of the pseudocode. Figure B–2 illustrates the pseudocode for the action: *AT_6400address()* (This was a function supplied with the traverse gear controller.).

The following figures do not attempt to provide all the pseudocode for the suite of C programs. However, **Option 1** has been fully displayed in Figure B–3 in pseudocode in order to best explain the typical structure and flexibility of modular program design. Most of the functions found in Figure B–3:*Option 1* are defined in the Figures B–4, B–5, B–6 and B–7.

As can be seen from the bottom of Figure B–3, the file in which this code is found is *fishdefn.c*. Alongside, some of the functions are indicated as having come from other .c files. By way of example, the contents of *fishdefn.h* are represented in Table B–4.

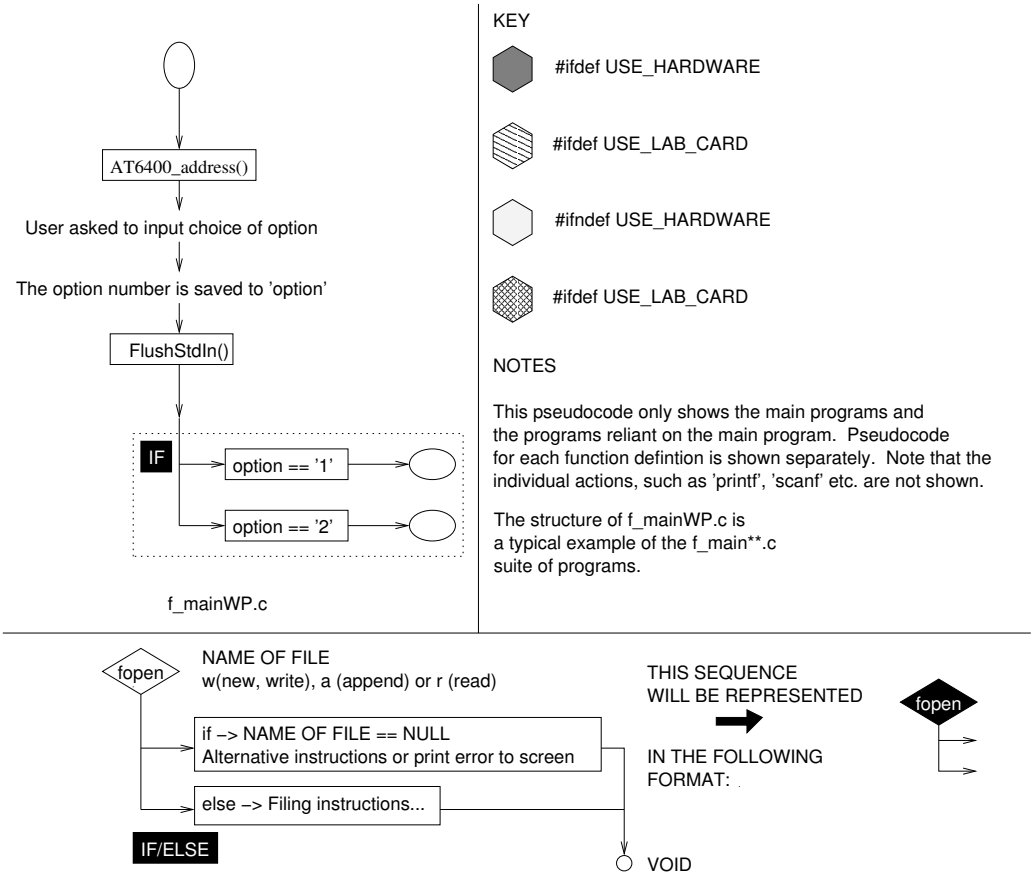

Figure B–1: Typical main program (f_mainWP.c) and key

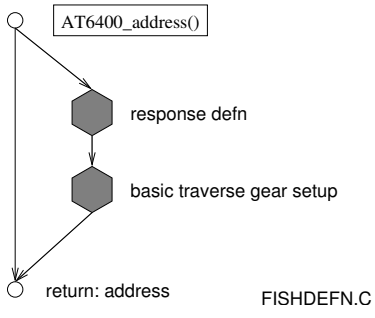

Figure B–2: Pseudocode for function: AT_6400address()

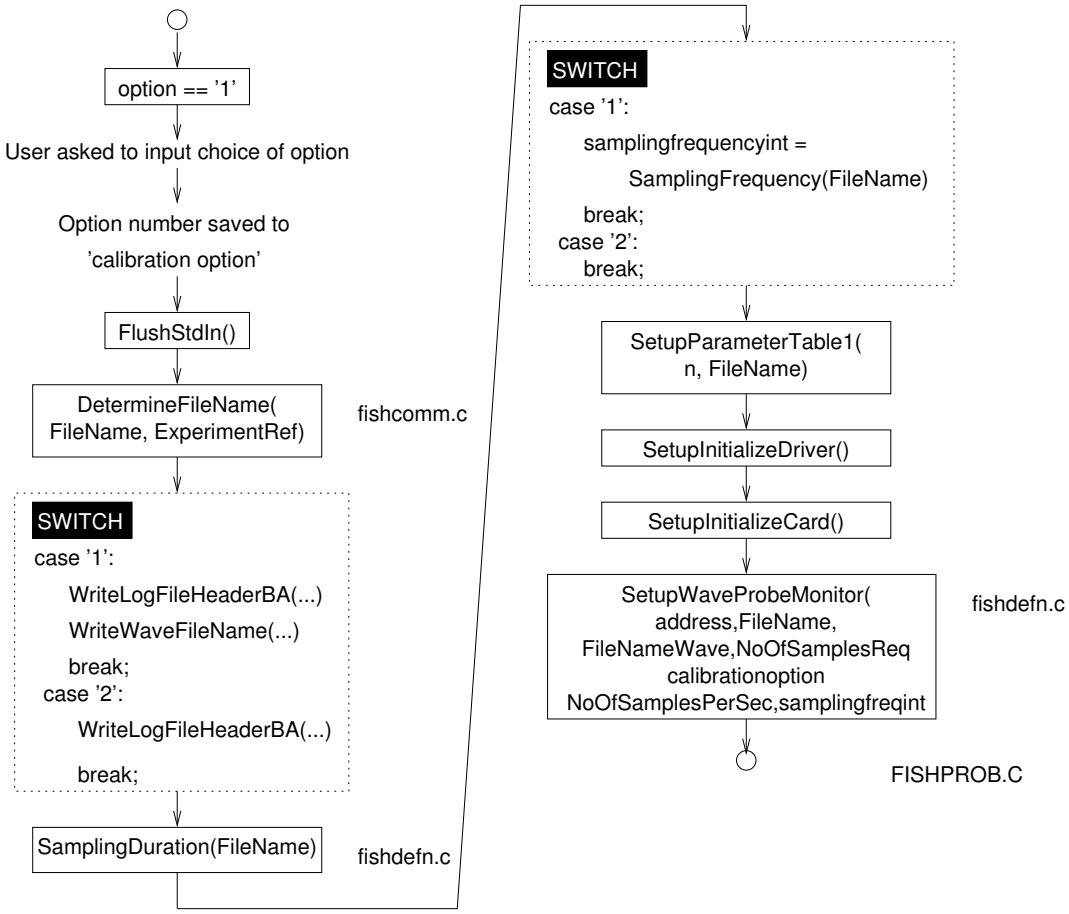

Figure B–3: Option 1 Algorithm

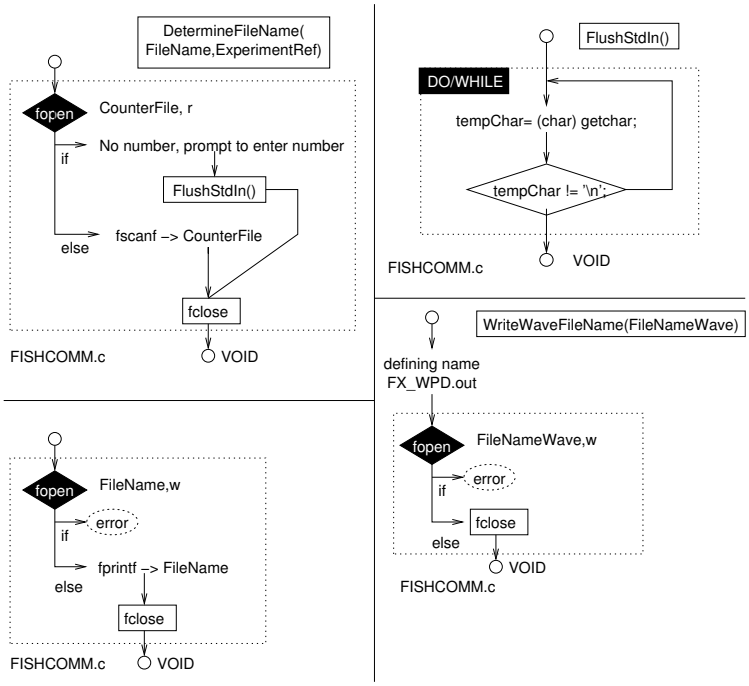

Figure B–4: Functions: DetermineFileName, FlushStdIn, WriteLogHeaderBA and WriteWaveFileName [from Fishcomm.c]

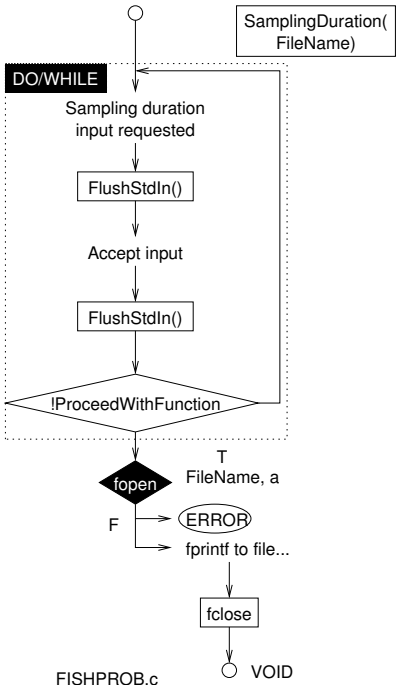

Figure B–5: Function: Sampling duration [from Fishprob.c]

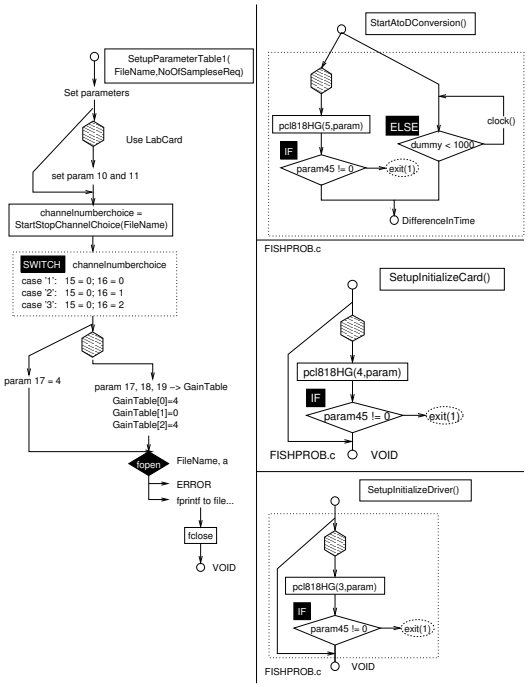

Figure B–6: Functions: SetupParameterTable1, StartAtoDConversion, SetupInitializeCard and SetupInitializeDriver [from Fishprob.c]

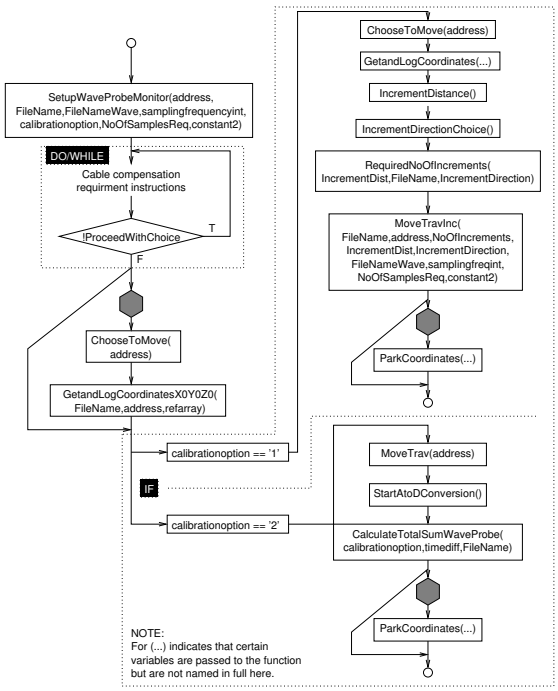

Figure B–7: Function: SetupWaveProbeMonitor [from Fishdefn.c]

Table B–4: Fishdefn.h

```
#ifndef __FISHDEFN_H
#define __FISHDEFN_H
//VOID FUNCTIONS
void LineReturnInFile (char *WhateverTheFile);
void MaxSamplingDuration(int NoOfSamplesPerSec);
void SetupStageDischarge();
void SetupWaveProbeMonitor(unsigned int address,
char *FileName, char *FileNameWave, int NoOfSamplesReqd,
int constant2, char calibrationoption,int samplingfreqencyint);
void StageDischarge(char *FileName, char *FileNameStageDischarge,
int NoOfSamplesReq, float MaxPressure,float VoltageDatum);
//FUNCTIONS RETURNING A CHAR
char AtoDChoiceFunction (char *FileName);
char IncrementDirectionChoice();
char OptionChoice ();
char SelectSizeOfWaveProbe(char* FileName);
//FUNCTIONS RETURNING A DOUBLE
double CalibrationSwitchShort(char NotchUsed);
double CalibrationSwitchLong(char NotchUsed);
double SettingUpManometer(char* FileNamePT);
double OrificePlate(char* FileName);
//FUNCTIONS RETURNING A FLOAT
float CalculatedDiff(char *FileName,float manlevelleft,float manlevelright);
float FlowRateQuery(char* FileName);
float IncrementDistance();
float LoggingNoOfIncrements(char *FileNameLego);
float ManometerLevelLeft(char* FileName);
float ManometerLevelRight(char* FileName);
float PressureTransducer(char* FileNamePT);
float ReadTotalPressureHead(char* FileName);
float ManualManometerLevel(char* FileName);
//FUNCTIONS RETURNING AN INT
int ChoiceDefaultSamplingPeriod (char *FileName);
int PauseTime (char *FileName);
int RequiredNoOfIncrements(float, char *, char);
int SamplingDuration(char *);
int SamplingFrequency (char *FileName);
#endif
```

C. Calibration Data and Equipment Layout

C.1. Experiment set-up requirements

The following process was applied at the start of each experiment:

1. Ensure that the flume was ready before the pump was started (bleed screws in the weir had to be opened, manometer valves closed,tailgate raised to required position).
2. Start the pump - ensure that full flow was not directed on the glass floor until tailwater level was deep enough to dissipate the energy - and to prevent the glass floor from being damaged.
3. Set a flow rate (use orifice plate formula) as required.
4. Record the water temperature and atmospheric pressure at the beginning and end of the experiment.

C.1.1. Priming the pressure tappings and the reservoir tubing

The use of the pressure tappings and reservoir have been described in section 3.1.5. Depending on which pressure tappings were to be primed, identify the high pressure and low pressure lines for connection to the transducer. A similar method (using syphoning) was applied when priming the reservoir. The following process needed to be followed for each set of pressure tappings to be primed:

1. Take an unprimed tube out of the manifold.
2. Prime the syphon, and replace tube in the manifold.
3. Ensure that air bubbles had finished bleeding out of the tubing.
4. Repeat 1-3 for each of the six tubes. The manifold needed to be held at an angle to prevent the ingress of air.
5. It was very important that the air bubbles were all bled out of the system. The larger the tube, the slower this was done.

C.1.2. Retaining crest water level

The following procedure was derived in order to ensure that identical crest water levels are attained for each experiment:

1 Raise the tail gate above the crest level,
submerge the weir and allow water to settle.
(Flow from the pump must be switched off.)
2 Ensure that the cap on the reservoir (Section 3.1.5) is screwed off.
3 The water level is slowly lowered by lowering the downstream tail gate.
The pin which has been sited upstream and is level with the crest, is used to eye in the water level. This ensures that the crest water level can be eyed into as similar a level as is possible between experiments.
4 Looking below water level, the pin is observed in the reflection.
When the *pin* touches the *reflection of the pin*, crest water level is considered to have been achieved.
5 Close the ball valve on the reservoir - this will maintain crest water level within the reservoir. This must be done as quickly as possible.
6 Replace the cap on the reservoir (minimise evaporation).
7 As an extra precaution, lower the pointer gauge to water level and record this level as datum. (The pointer gauge should be in line with the upstream static pressure tappings.)

C.1.3. Priming a pressure transducer (with water)

The following directions need to be followed when setting up the pressure transducer for use:

1 Ensure that the pressure transducer is unplugged.
2 Ensure that there are no air bubbles present in the system.
3 Insert the low pressure line into the low pressure port (top),
and the high pressure into the high pressure port (bottom).
4 Loosely screw in bleed screws.
5 Observe the water flow through the bleed screws.
6 Tighten bleed screws.
7 Switch on the pressure transducer.
8 Ensure that the LabCard is correctly wired.
9 Make use of the C program ‘adcread’ to check that the transducer is working, and is within the correct ballpark.
10 NB: Allow pressure transducer to warm up for 60 minutes.
11 Use ‘adcread’ and record the pressure transducer datum for the current session.

C.2. Calibrating and using the wave probe

At the beginning and end of testing on any different day, the datum adjustment setting on the probe monitor had to be set to zero for a user-specified depth of immersion of the probe. Each of the different wave probes had a suitable maximum immersion depth, and this initial immersion depth was set to a mid-range value.

The test results confirmed that the relationship between water depth and voltage was linear. The following conclusions were drawn from the tests:

Calibration Process Initial tests were carried out in a beaker of water sampled from the flume. However as this water was then outside of the flume itself, it was considered that the temperature[1] and possibly the chemical composition of the water would have influenced the wave probe measurements. As a result, it was necessary to perform the calibration procedures using in-situ flume water. The pump was started and the water was allowed to circulate for approximately half an hour in order to ensure adequate mixing of the water to get homogeneity. At the end of the allocated time, the tail gate was raised above crest level, pumping was terminated and the free surface was allowed to settle.

The wave probe was then driven into contact with the free surface, where great care was required in 'eyeing-in' the probe. One of the C program functions allowed the user to set the datum adjust position on the wave probe monitor and then the probe was driven to a new position to commence voltage sampling. Alternatively, the probe could be set at an arbitrary datum below the free surface and then driven up to the free surface. Once calibration commenced, incremental movements accompanied by voltage sampling were automatically controlled. The results were presented in Figure 3–11.

Response time Initial tests revealed that a period of time was required to reach a steady state when moving the wave probe to a new depth and reading a steady voltage reading. This period, referred to subsequently as *pause time*, was estimated by driving the probe to a new position in a beaker of water, immediately starting data acquisition and noting the time required to reach a steady voltage output. A pause time of 15 seconds was found to be conservative. One of the traverse gear controller (AT6400) functions, which returned control back to the main C program only when the probe had stopped moving was used to ensure error proofing before data sampling commenced.

Voltage Range The wave probe output ranged from -5V to +5V. Using the equipment beyond that range resulted in a shift of the initial datum adjust position (observed when returning the probe back to the datum position at the end of the test). However, provided that measurements were kept within the range, the datum was undisturbed.

[1] A simple thermometer test during the half an hour required for calibration purposes showed that the water in the beaker approached room temperature which was different to the water temperature.

Datum Adjustment Because the wave probe output was dependent on water temperature, the calibration procedure was carried out at the beginning and end of each set of measurements. The resulting calibration data was compared, and the appropriate adjustments were made to sampled data when necessary.

The conductivity of water is also dependent on temperature and the presence of dissolved salts. For example, an increase in temperature of 1°C, increases the conductivity of the water by approximately 2% (HR Wallingford 2002). Consequently, calibration procedures were carried out at both the beginning and end of each test sequence. Using two such calibration stages helped to provide a more reliable estimate of probe immersion depth (based on the measured voltage values).

C.3. Total head - discharge measurement procedure

The total head - discharge measurements were conducted over the range of the flow rate. The maximum flow rate was dependent on the size of the orifice plate used. Before total head - discharge measurements commenced, the relevant procedures as described in section C.1 were performed. The following procedure (as captured in the C program f_mainSD.c) describes the steps taken at a specific flow rate:

1. Once the flow rate had been established, a period of five minutes was allowed to elapse so as to ensure that water levels had reached an equilibrium.

2. The head on the orifice plate was measured using the 400 mb pressure transducer. These results were cross-checked using readings from the 4 m manometer.

3. The upstream static head relative to weir crest level was determined by simultaneously logging the pressure difference between the upstream reservoir and the upstream pressure tappings. An independent check was carried out using a pointer gauge and vernier scale method to measure the water level directly above the upstream pressure tappings. The head could then be calculated by subtracting this value from the initial water level captured before an experiment session commenced.

C.4. Pressure transducer calibration

This section describes the procedure used to calibrate the pressure transducers.

1. The DC output voltage of the transducer to be calibrated was connected to channel 0 of the LabCard. The transducer pressure ports were initially left open to the atmosphere thus applying zero differential pressure. Figure C–1 shows the schematic layout.

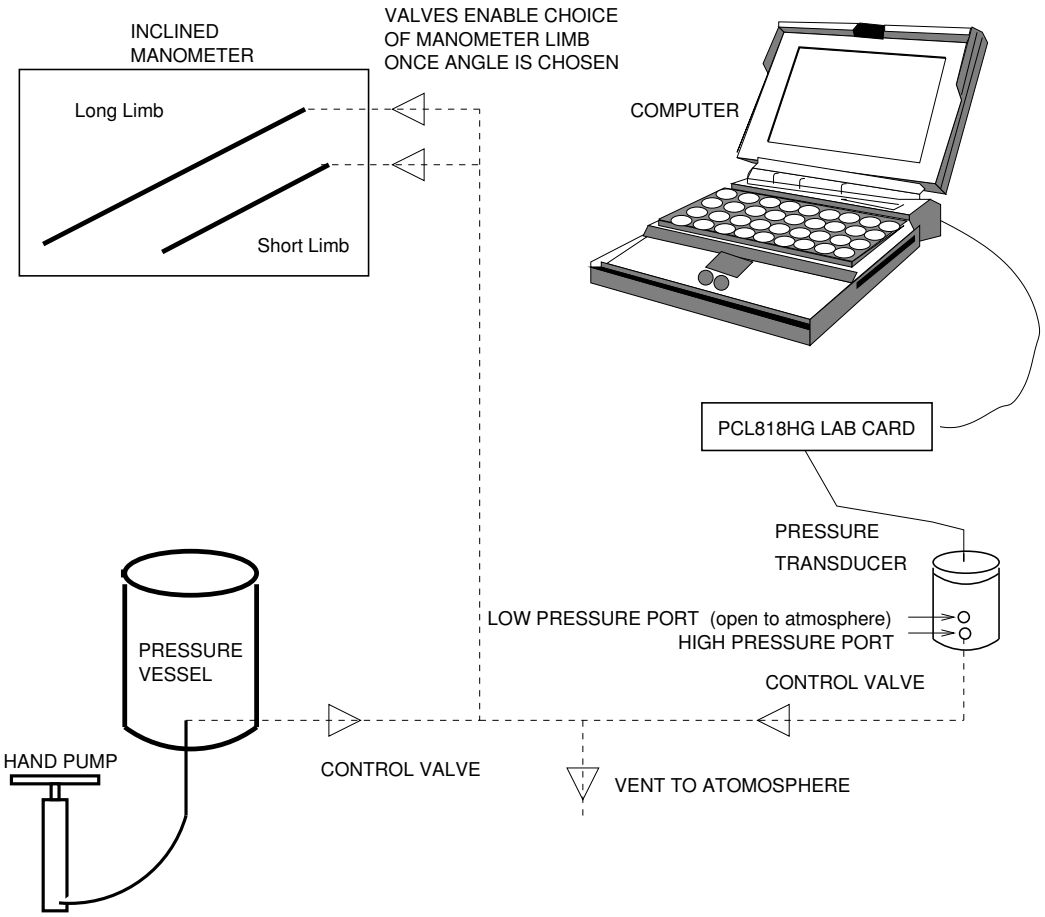

Figure C–1: Schematic layout of pressure transducer calibration

2. The inclined manometer (Airflow: Mk4 Man.Port kPa) was placed on a level, stable surface and the spirit levels were adjusted to ensure that the apparatus was horizontal. Either the long or the short limb of the manometer was adjusted to the position appropriate to the required range of pressure. The inclined manometer had been serviced and recalibrated by Airflow Developments Ltd. on 17 July 2002. An adjusted multiplication factor (see Table C–1 given on the calibration certificate was then used for the relevant limb and notch position.

3. A hand pump and a pressure reservoir were connected to the appropriate limb using a system of tubing, Legris push-fit pneumatic connections and valves (see Figure C–1).

4. The calibration of the pressure transducer proceeded by carefully incrementing the pressure in the system with the hand pump. The pressure was increased to the required level, the valves were shut-off to maintain pressure and equilibrium was re-established. The manometer reading and the corresponding pressure transducer voltage were recorded for each increment.

5. Two output files were produced: the first provided a simple lookup table

Table C–1: Manometer multiplier table

Limb Position	Range	Multiplier
Short limb - Bottom	0 to 125 Pa	0.05
Short limb - Middle	0 to 250 Pa	0.101
Short limb - Top	0 to 500 Pa	0.201
Short limb - Vertical	0 to 2500 Pa	1.004
Long limb - Bottom	0 to 500 Pa	0.1005
Long limb - Top	0 to 1000 Pa	0.201
Long limb - Vertical	0 to 5000 Pa	1.001

relating pressure to voltage, and the second recorded more details of the experiment.

6. Linear regression analysis was performed and the relationship between voltage and pressure for the 20 mb transducer is represented graphically in Figure 3–10. It should be noted that the 20 mb pressure transducer required recalibration (after a hard knock) on 22 April 2004. The regression equations for all of the pressure transducers are given in Table 3–4. The regression equations were then coded into the software used for pressure measurement. The C programs requested user input regarding which pressure transducer was in use, and consequently the appropriate equation was used to directly calculate the pressure before saving results to an output file.

A sample MATLAB program is shown in Table C–2. Figures C–2, C–3 and 3–10 show the resultant calibration graphs for the 0.5 mb, 5 mb and 20 mb pressure transducers.

Table C–2: Matlab program for linear regression of 0.5mb pressure transducer

A program to fit a straight line to the 0 to 0.5 mb **pressure transducer calibration data and to plot the data**
dat05mb Read in data (3 columns) from 5mb.m
n=length(data(:,1)); Length of first column vector, ie number of rows
pressure = data(:,2)*1000; Change from kN/m2 to N/m2
voltage = data(:,3);
coef=polyfit(voltage,pressure,1); Fit straight line
Plot line and data points
x2=0:.1:10;
y2=polyval(coef,x2);
plot(voltage,pressure,'ko',x2,y2,'k-','MarkerSize',4)
h3=get(gca,'XLabel');
set(h3,'String','fontname(times) Voltage (V)','Fontsize',12)
h4=get(gca,'YLabel');
set(h4,'String','fontname(times) Pressure (N/m2)','Fontsize',12)
coef(2)=coef(2)/coef(1);
Print equation of line
text(4,10,['Pressure = ', num2str(coef(1)),' (Voltage ',num2str(coef(2)),')'])
text(4,7,['(Manometer calibrated on 17 July 2002)'])
Print title
h5=get(gca,'Title');
set(h5,'String','fontname(times) 0-0.5 mb Pressure Transducer','Fontsize',12)

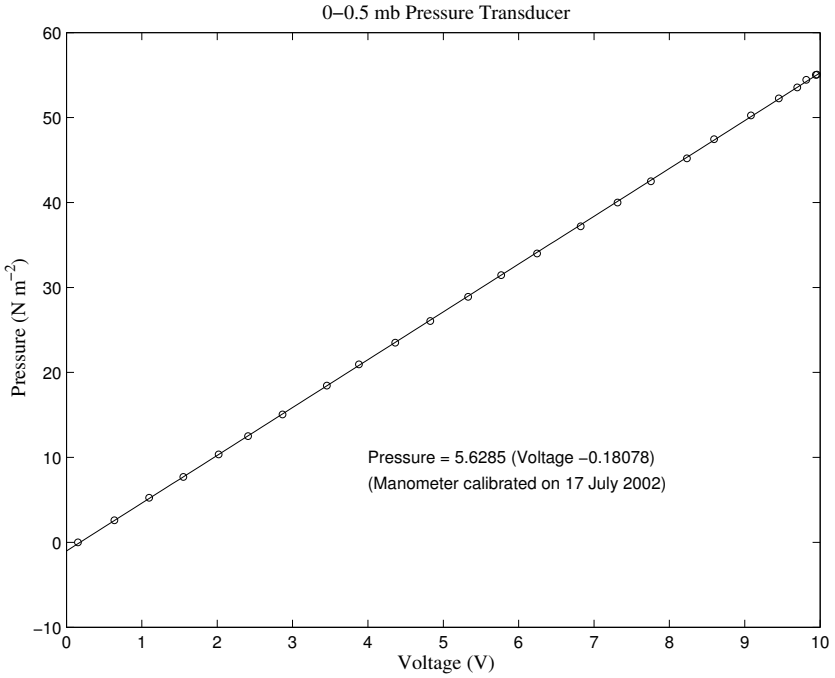

Figure C–2: 0.5 mb pressure transducer

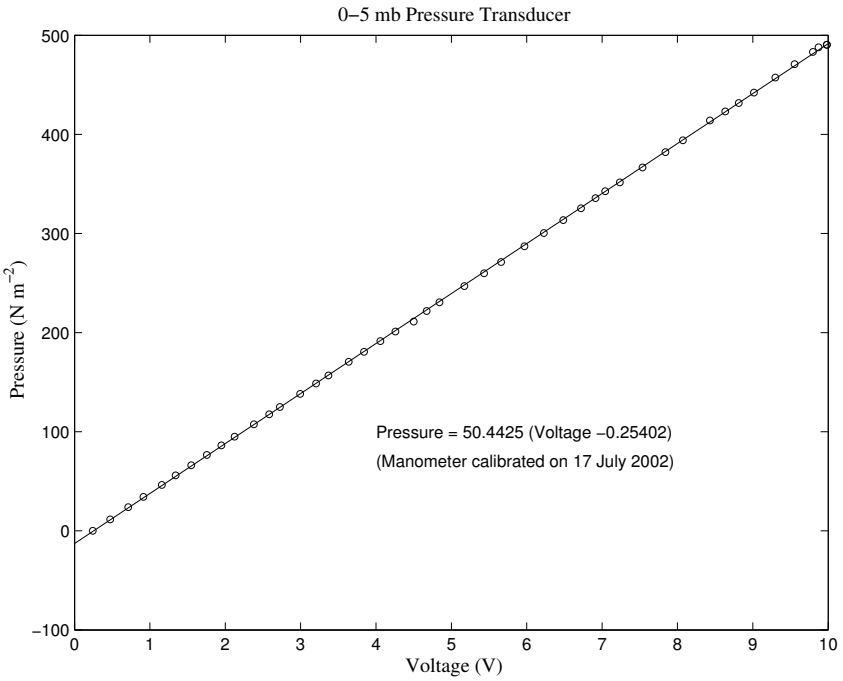

Figure C–3: 5 mb pressure transducer

D. Trial baffle arrangements using LEGO bricks

The trial baffle arrangements using LEGO bricks were divided into two sections. Firstly, trials were conducted on a multiplicity of arrangements at one specific flow rate. The most promising arrangement (and variation thereof) was then tested and fine-tuned over a range of flow rates.

D.1. Experiments conducted at the 90 percentile low-flow

These experiments were designed to a rapid assessment of the efficacy of each of the many baffle arrangements tested. Only spot measurements of velocity were taken,one at each baffle slot. Each velocity distribution is displayed on the weir cross-section in part a) of each of Figures D–2 to D–29. Water depths were not measured, but were inspected visually[1] to check that they were adequate for fish passage: a water level higher than the baffle crest was generally deemed to be sufficient, except in the region between the weir crest and the first baffle where a shallower depth was tolerated.

The spot measurements of velocity were taken using the velocity propeller meter (VPM). The VPM was much quicker to use than the Pitot tube-static tube combination. This had to be connected to the pressure transducer via a siphon, had to be primed and was difficult to relocate without breaking the siphon. At the start of each experiment, the coordinate system was determined by eying-in the VPM into contact with the panel pin located at the centre of the weir crest. This position was designated the coordinate (0,0,0) in the position control software controlling the traverse gear system. The part of the VPM in contact with the pin was the lowest point of the protective ring surrounding the propeller, with the effect that the y-coordinate of the velocity sampling point (on the axis of the propeller) was about 7 mm higher.

Table D–1 lists the categories of baffle arrangement and, within each category, the corresponding figure numbers in which the trial results are displayed. The figures, drawn in Excel, are each divided in parts a) and b), both of which show the spot velocity distributions. Part a) shows the graphical representation (i.e. cross-sectional velocities) and part b) shows the numerical values (both at model and, boxed, at field scale).

[1] Tracings, an example of which is shown in Figure 4–22, were also made. However they were an awkward shape, and were not generally of sufficient quality to warrant inclusion in this thesis.

As the cross-sectional diagrams in part a) in these figures were originally used as a method for comparing velocities from one baffle arrangement to the next, the notation that was used is not ideal. The outline of the crest was drawn in using two equations (referred to as 'crest' and 'extrapolated y') and the burst speed criterion was referred to as 'Most fish will succeed'. As these diagrams are presented primarily for record-keeping purposes, they have not been relabelled.

As the primary purpose of part b) was to keep a record of the LEGO layout, the numerical record keeping was dispensed with from Figure D–18 onwards.

Table D–1: Trial arrangements at the 90 percentile low-flow rate for the fish pass modifications

Category	**Figure Numbers**
Category 1: Centre Channel	D–2
Category 2: Baulk	D–3
Category 3: Diagonal	D–4 to D–14
Category 4: Rotated-V	D–15 to D–17
Category 4: Rotated-V with Narrow channel	D–18 to D–28
Category 5: Side gaps	D–29 to D–33

In the plan view of each baffle arrangement, the size of each Excel square represents a specific LEGO brick size. For Figures D–2 to D–6, each Excel square represents a 2×2 LEGO brick (i.e. 2 LEGO studs square). Later during the trials, a smaller brick size was required for finer adjustments in the geometry, and therefore in Figures D–7 to D–29 each Excel square represents a 1×2 LEGO brick.

For the 90 percentile low-flow range, the distance from the crest to the upstream face of the first baffle was kept constant. In practical terms, the position of the upstream face was a summation of the distance (76 mm) from the crest to the edge of the LEGO base and the distance (96 mm or 12 studs) from the edge of the LEGO base to the upstream face of the baffle, giving 172 mm in total. This distance from the crest to the upstream baffle face was used for all of the LEGO layout sections reported in section 4.1.3.

The most promising solutions identified during this trial period were LEGO layout 1.16 and LEGO layout 2.5 as shown in Figures D–20 and D–26 respectively.

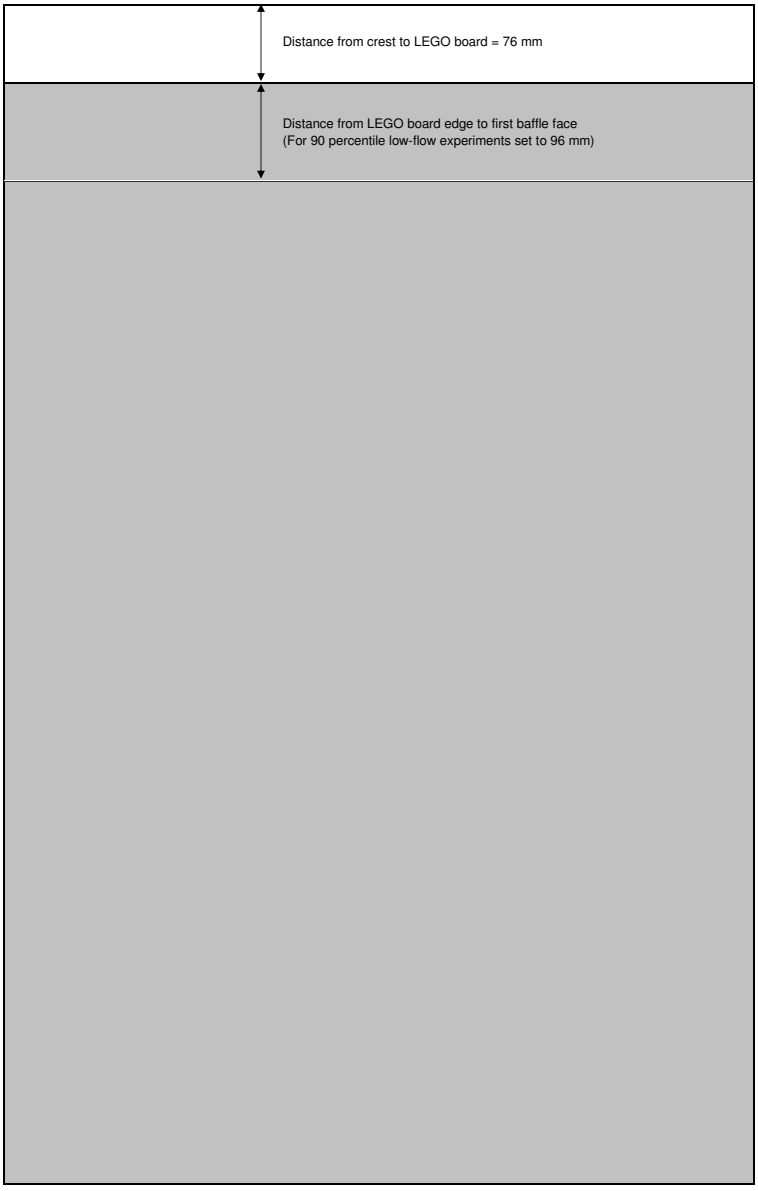

Figure D–1: Schematic layout of LEGO board

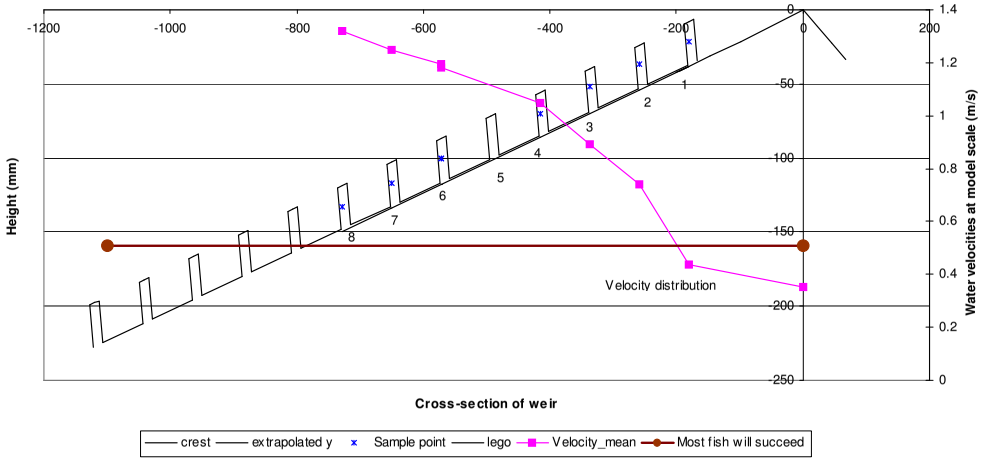

(a) Cross-section

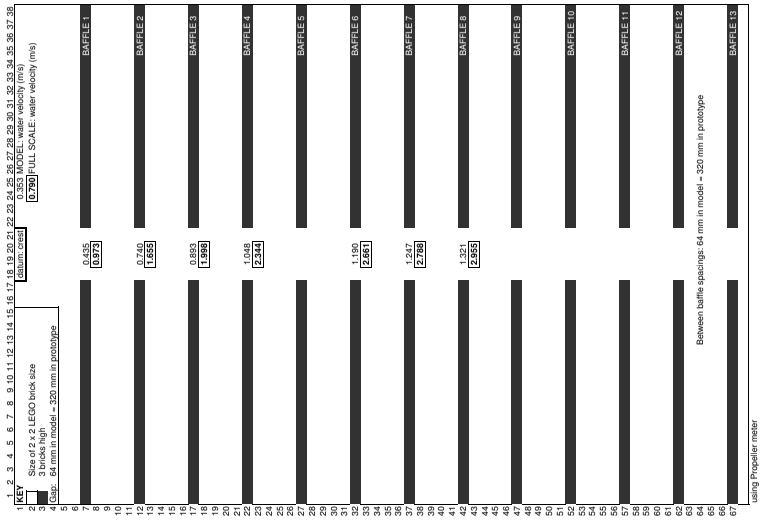

(b) Plan

Figure D–2: Centre Channel: Baffle Layout 1

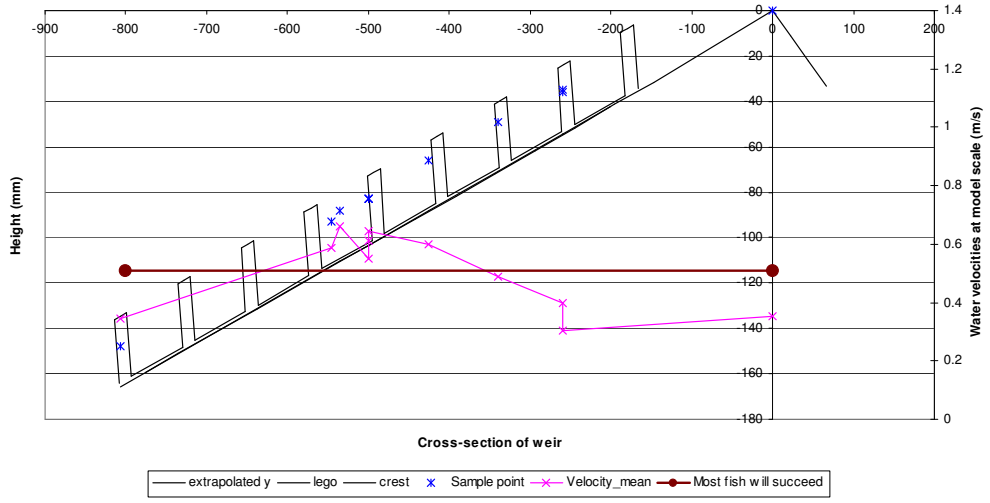

(a) Cross-section

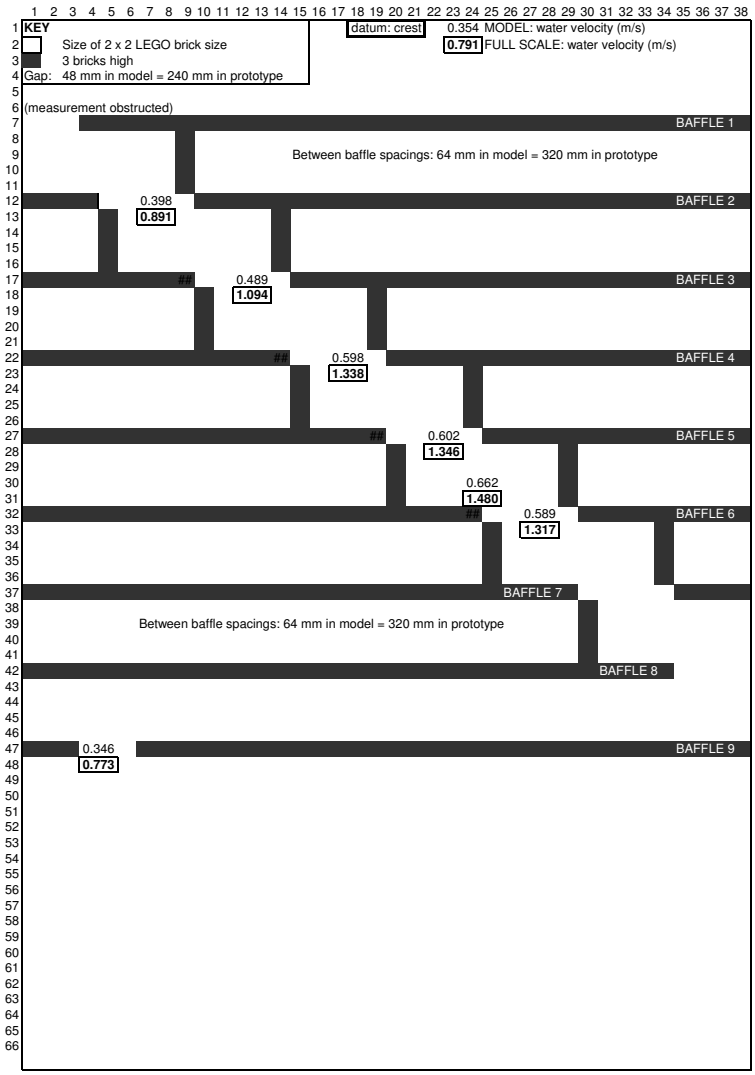

(b) Plan

Figure D–3: Baulk: Baffle layout 3

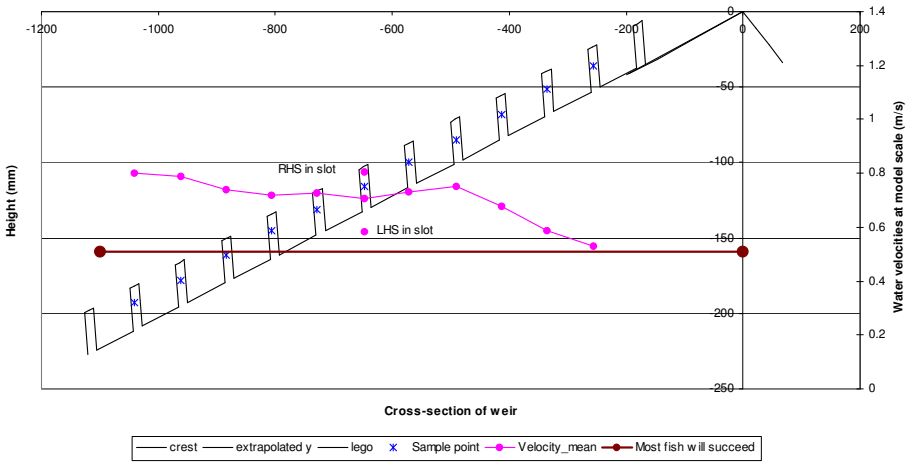

(a) Cross-section

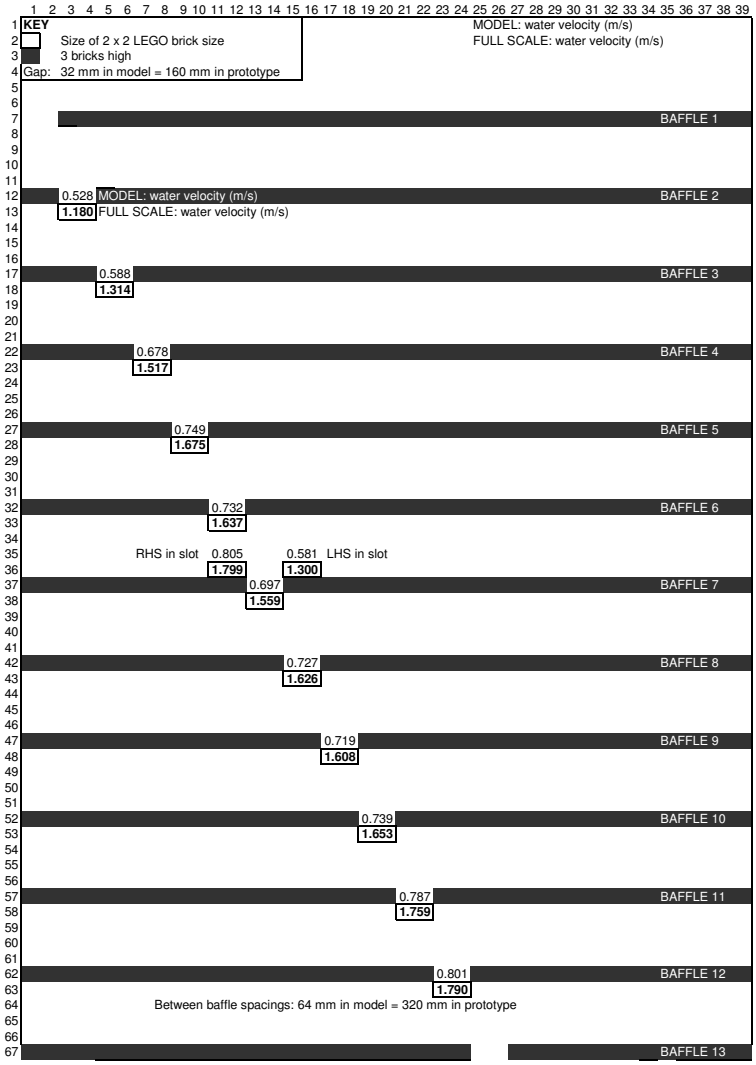

(b) Plan

Figure D–4: Diagonal: Baffle Layout 5

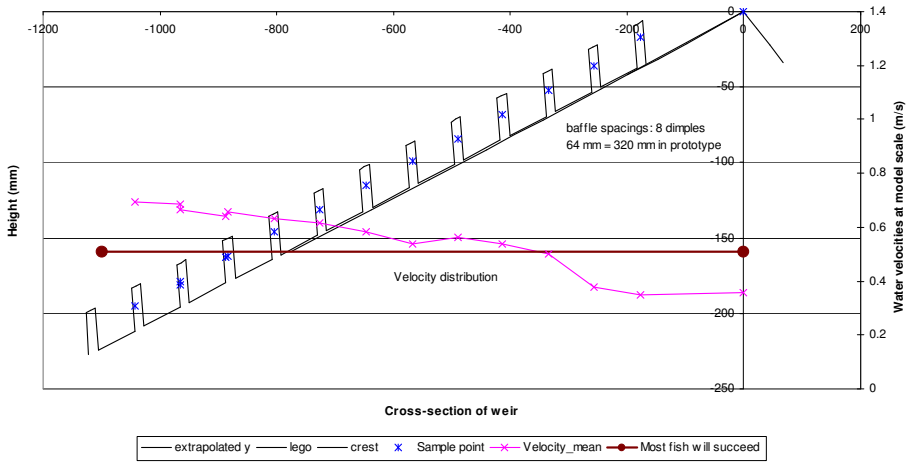

(a) Cross-section

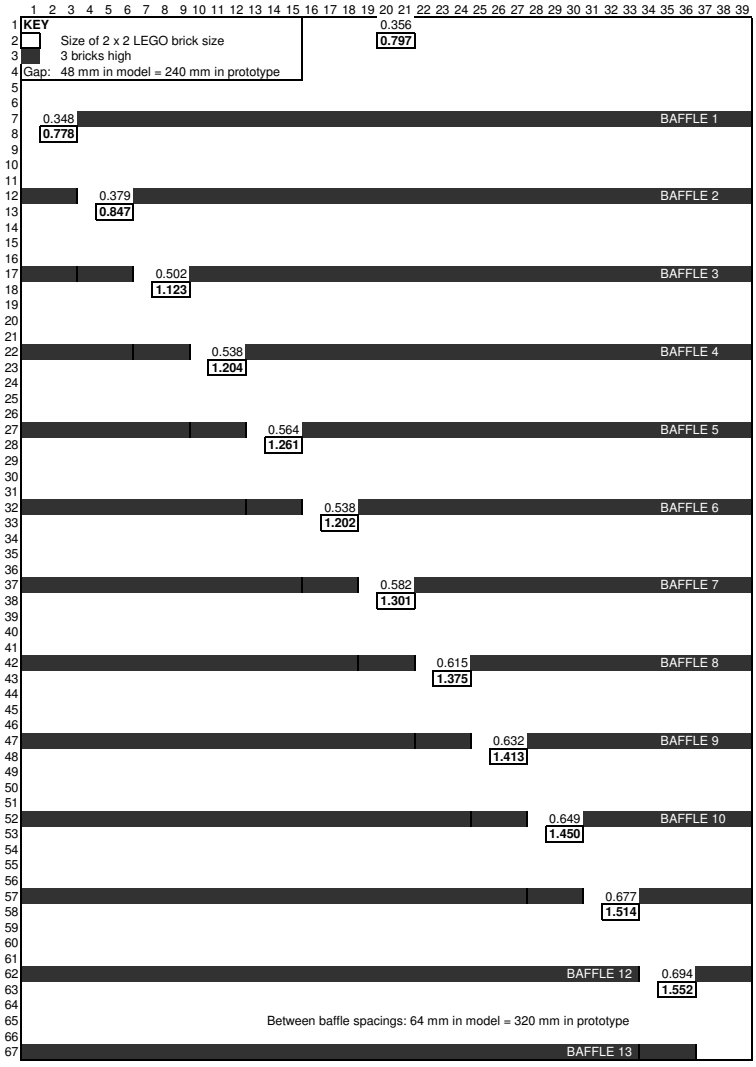

(b) Plan

Figure D–5: Diagonal: LEGO Layout 1.1

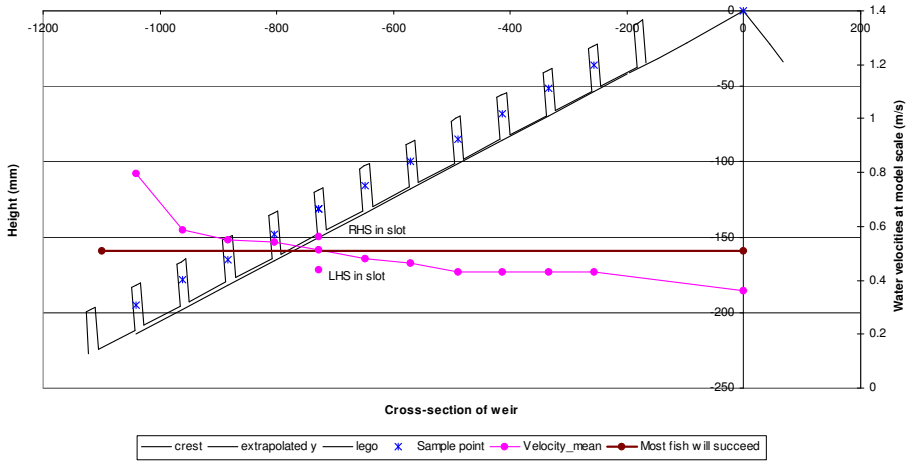

(a) Cross-section

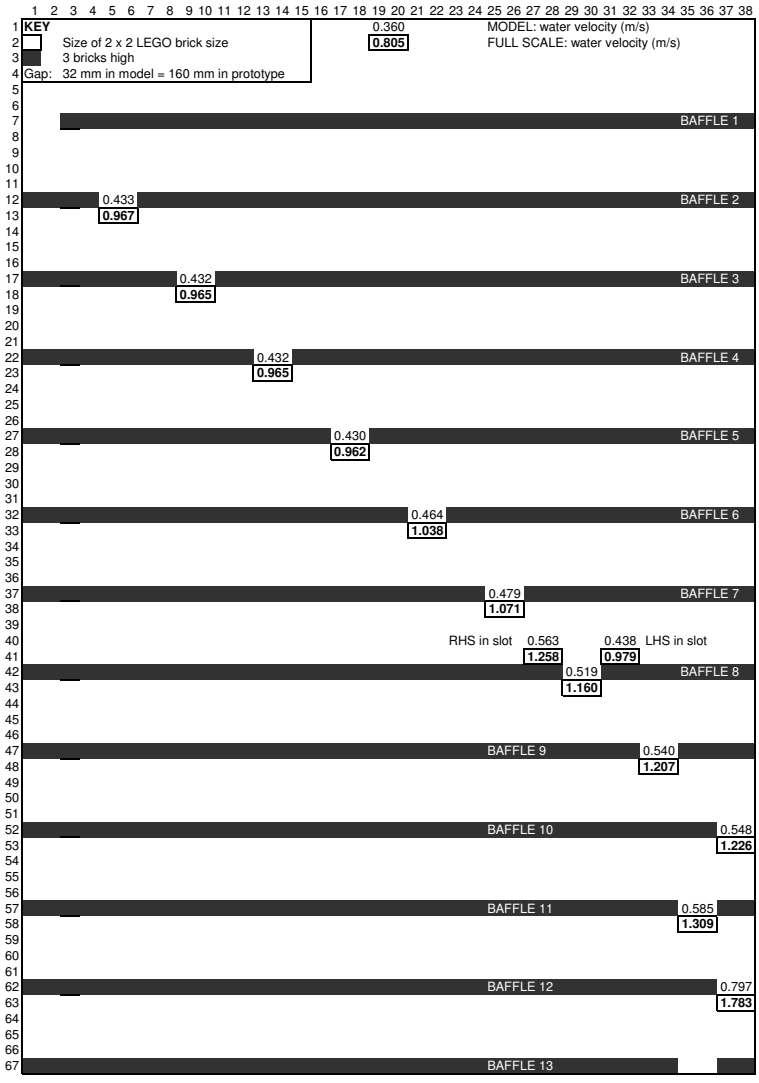

(b) Plan

Figure D–6: Diagonal: Baffle Layout 6

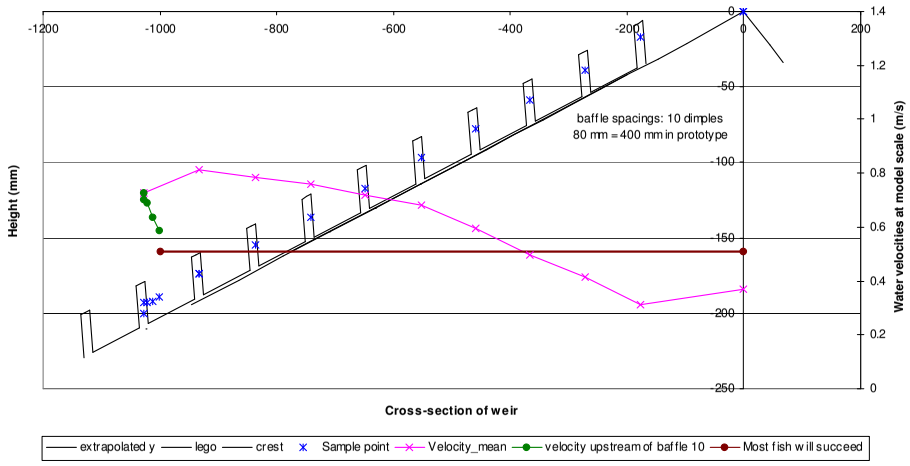

(a) Cross-section

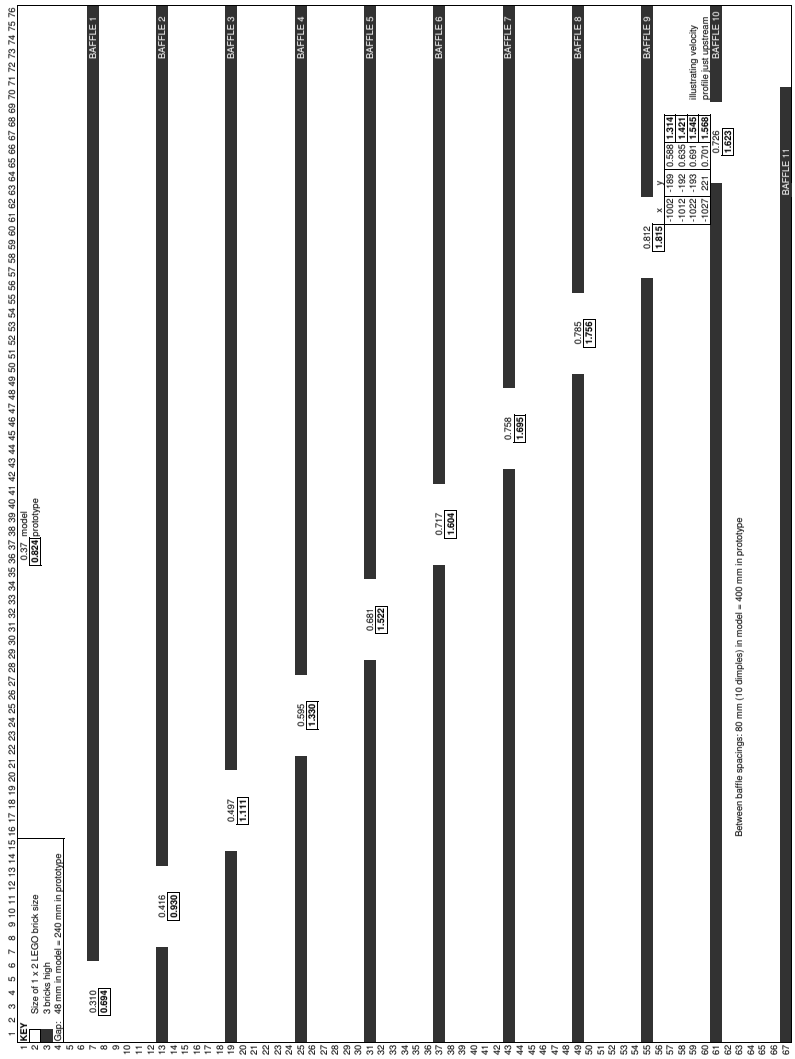

(b) Plan (i.e. rotated)

Figure D–7: Diagonal: LEGO Layout 1.5

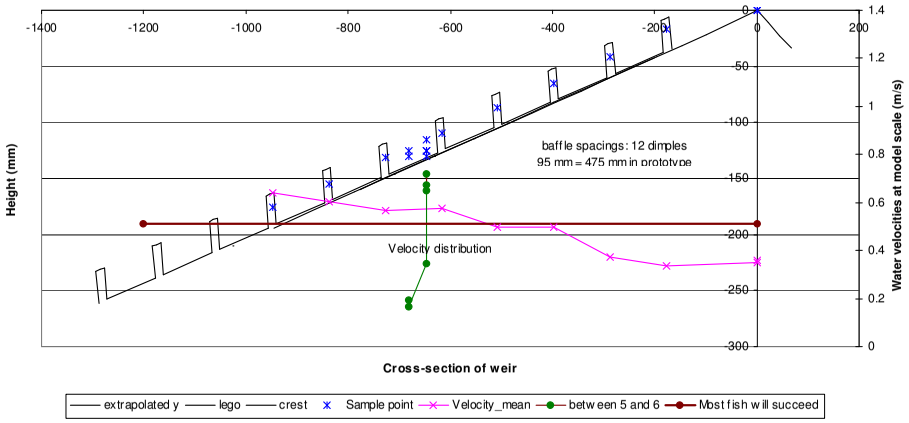

(a) Cross-section

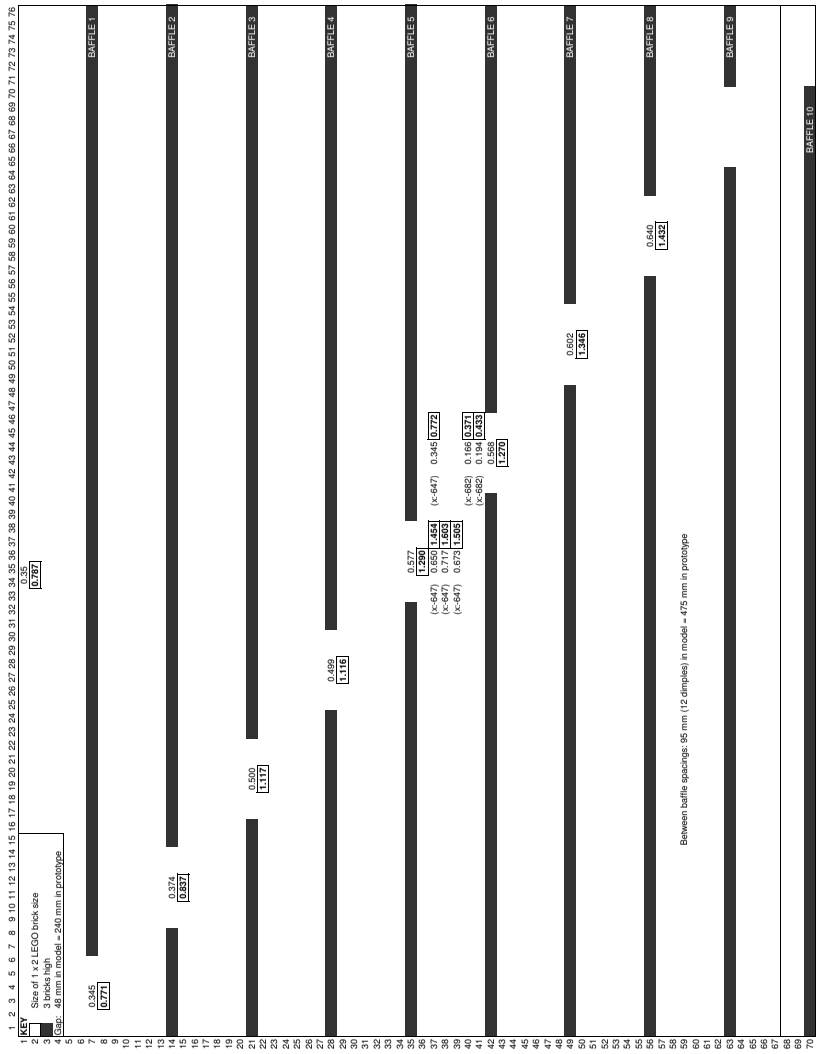

(b) Plan

Figure D–8: Diagonal: LEGO Layout 1.7

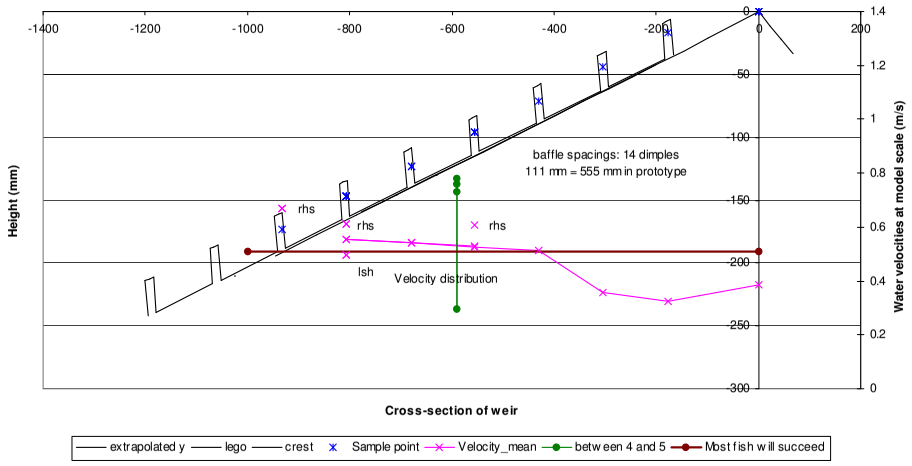

(a) Cross-section

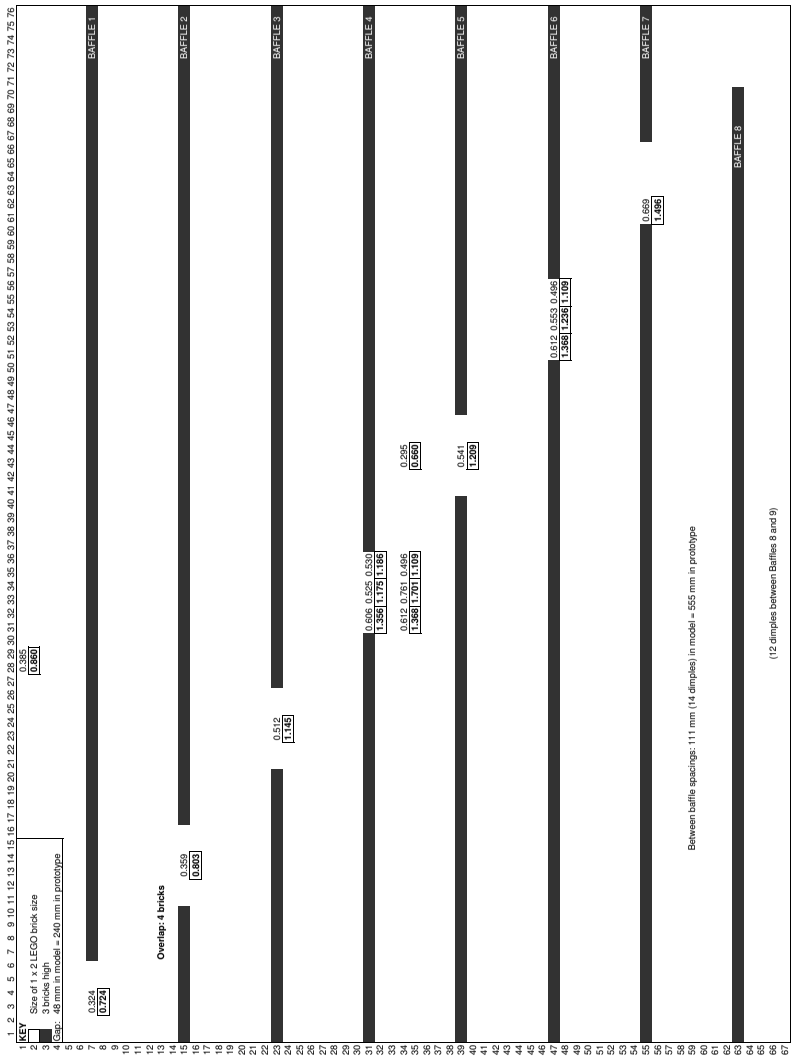

(b) Plan

Figure D–9: Diagonal: LEGO Layout 1.8

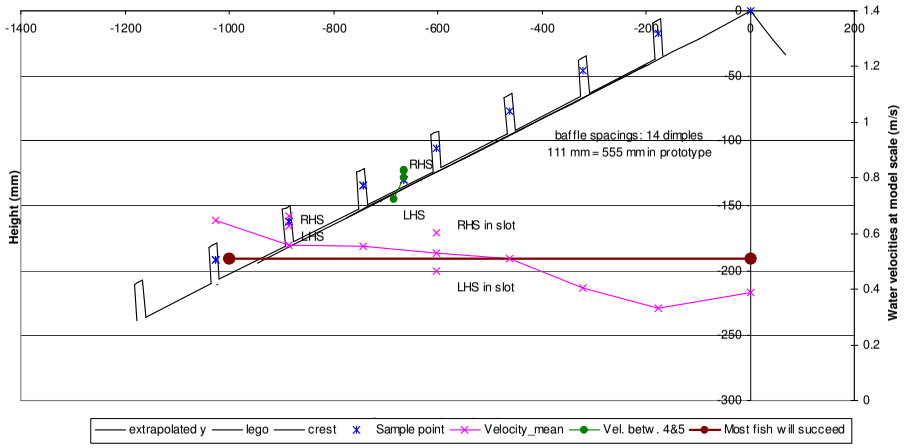

(a) Cross-section

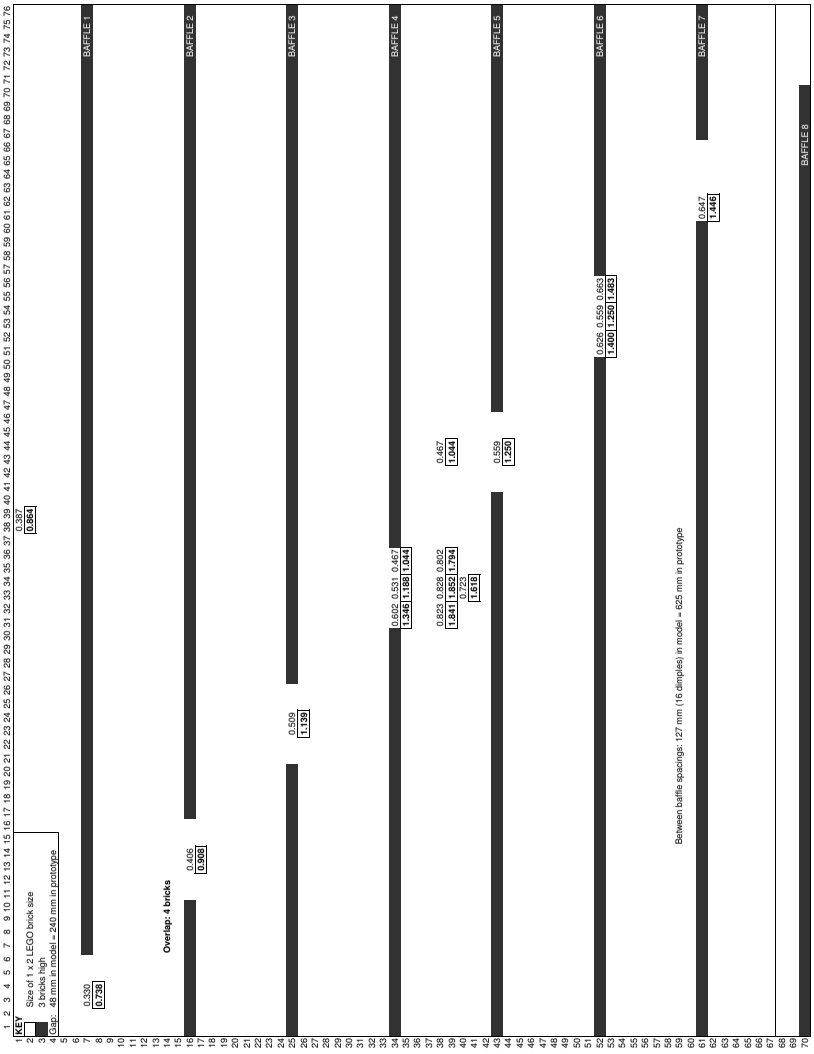

(b) Plan (i.e. rotated)

Figure D–10: Diagonal: LEGO Layout 1.9

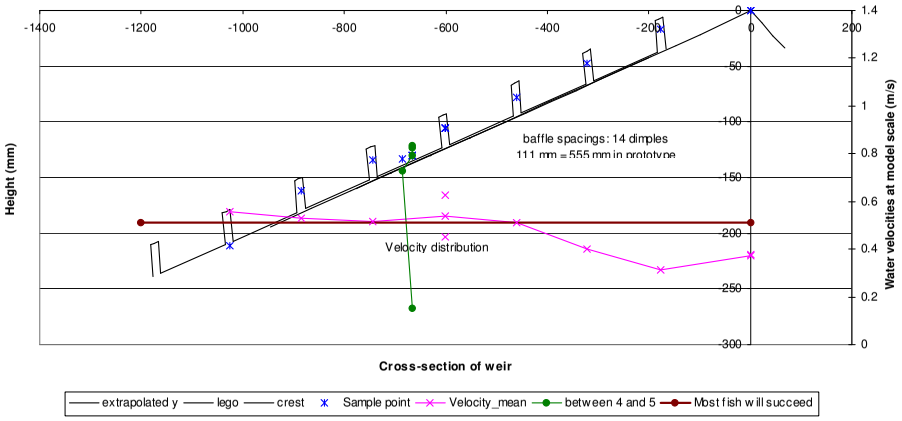

(a) Cross-section

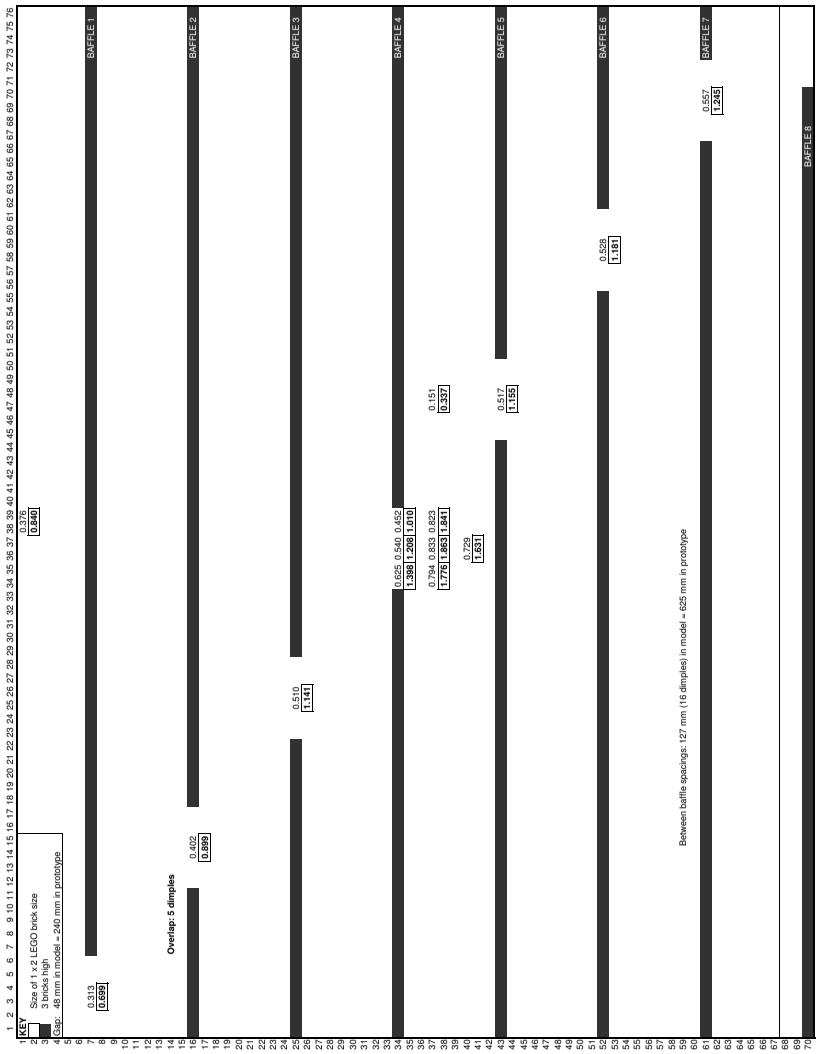

(b) Plan (i.e. rotated)

Figure D–11: Diagonal: LEGO Layout 1.9(2)

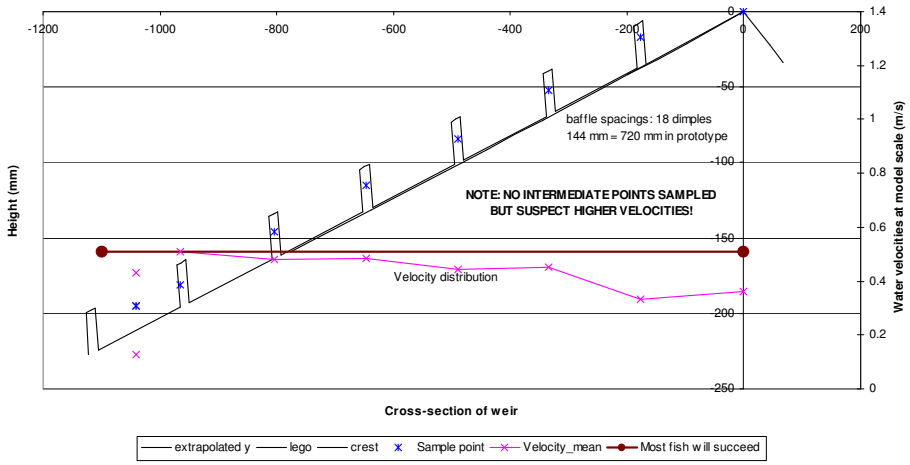

(a) Cross-section

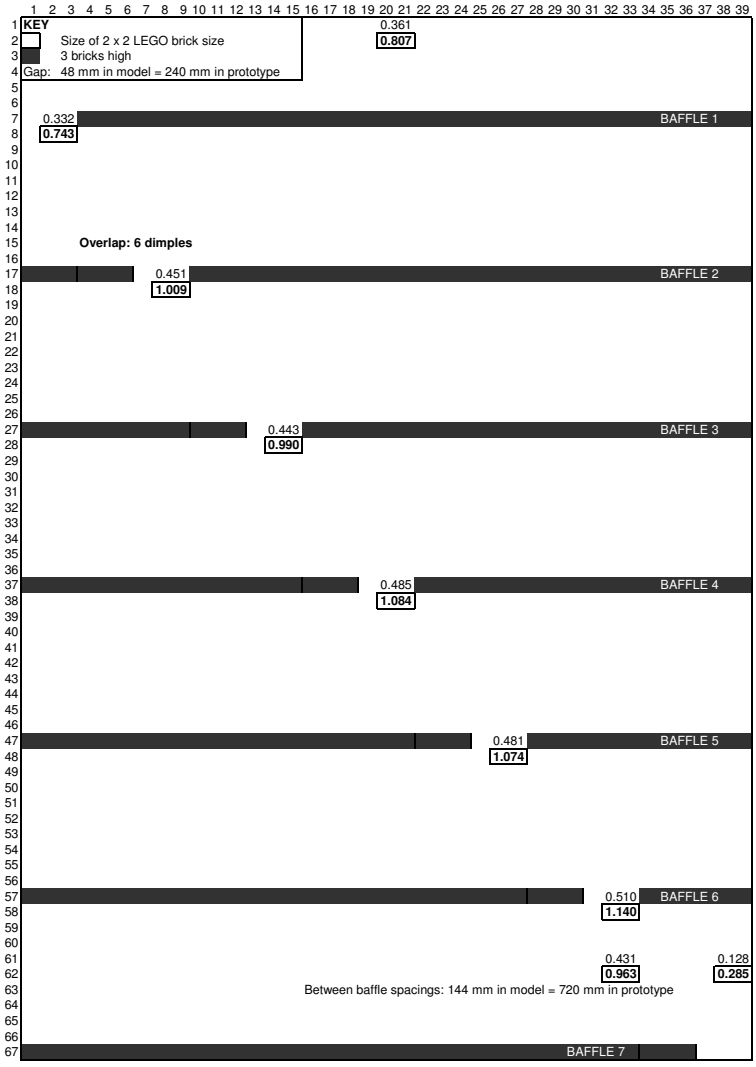

(b) Plan

Figure D–12: Diagonal: LEGO Layout 1.4

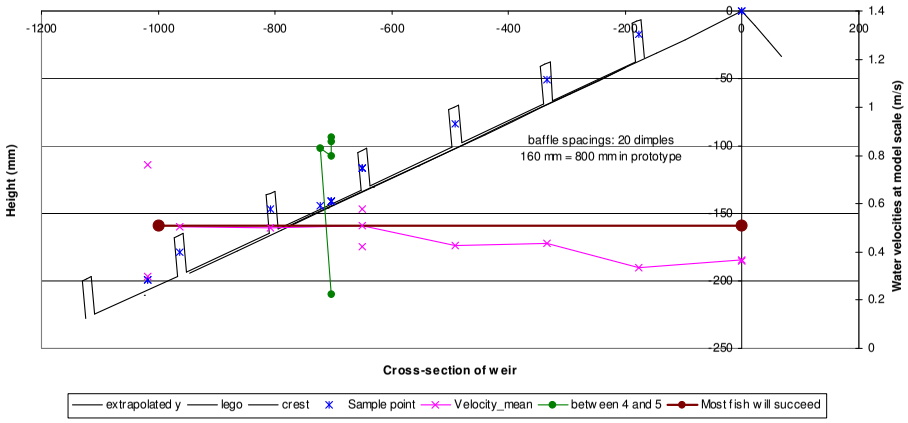

(a) Cross-section

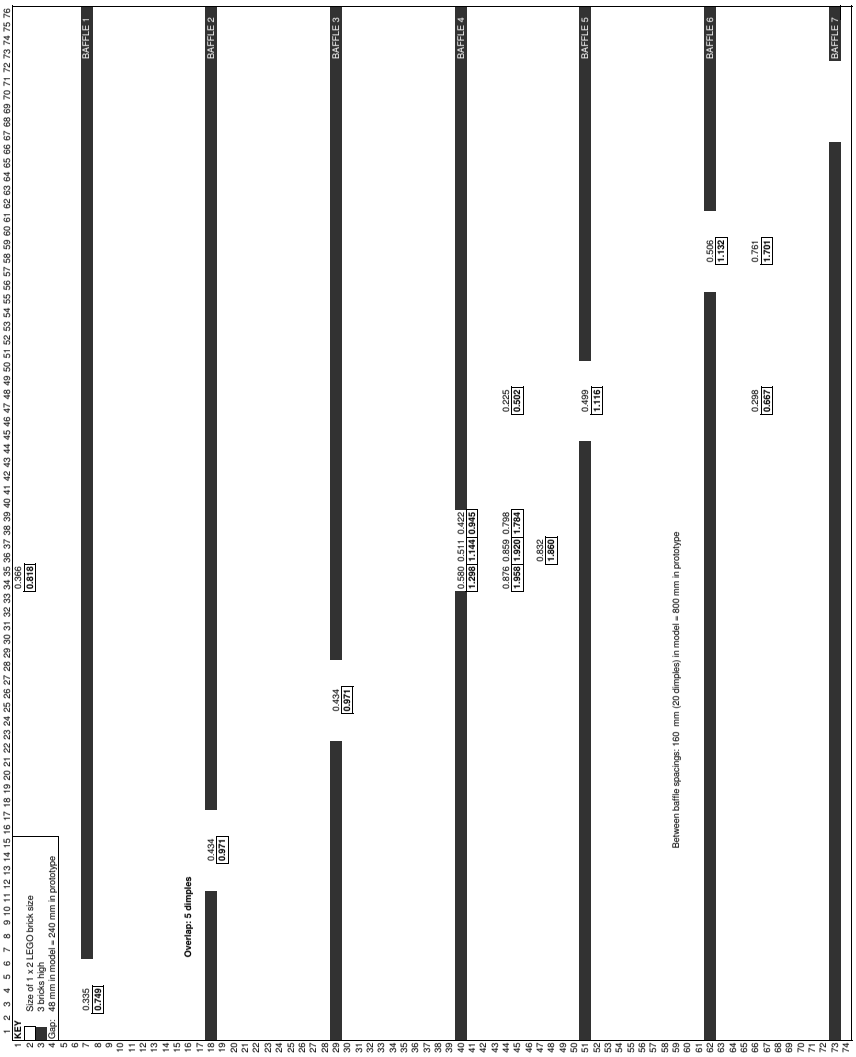

(b) Plan (i.e. rotated)

Figure D–13: Diagonal: LEGO Layout 1.10

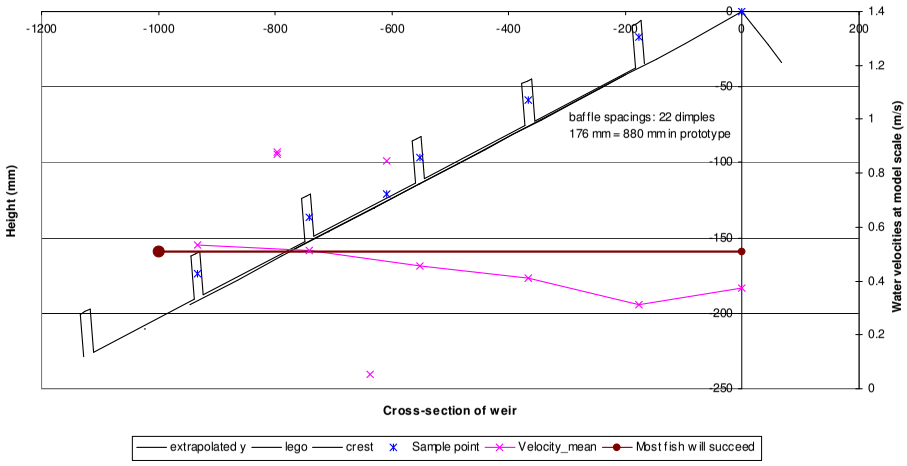

(a) Cross-section

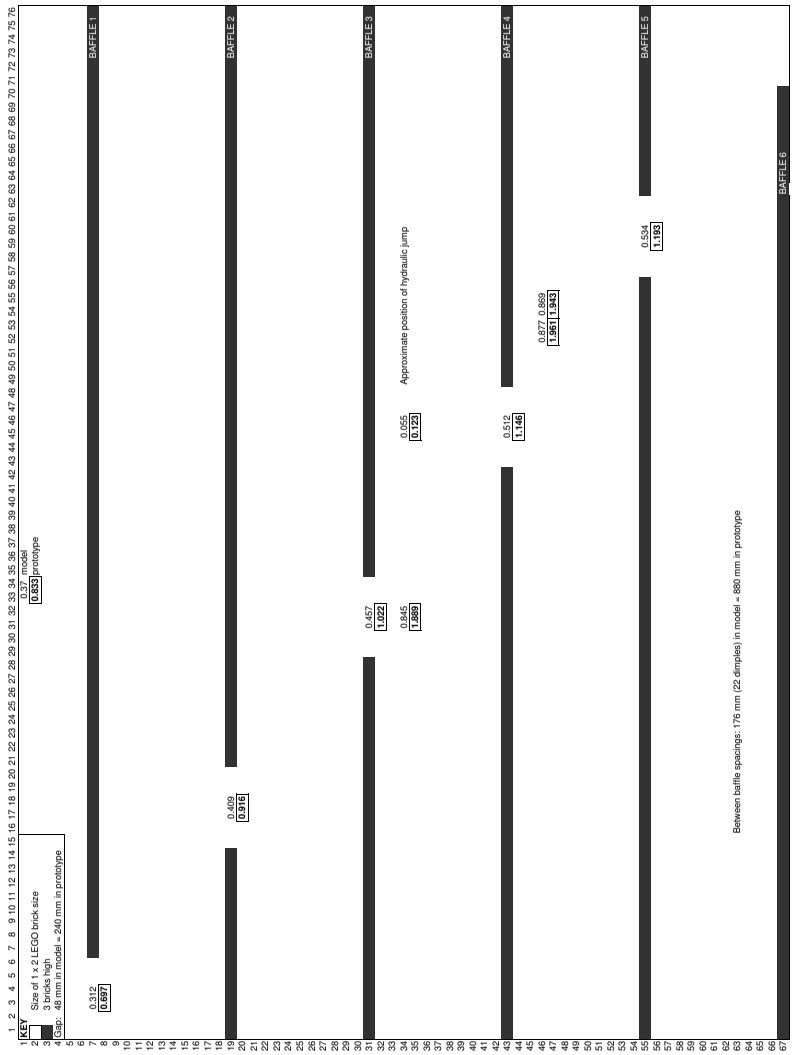

(b) Plan (i.e. rotated)

Figure D–14: Diagonal: LEGO Layout 1.6

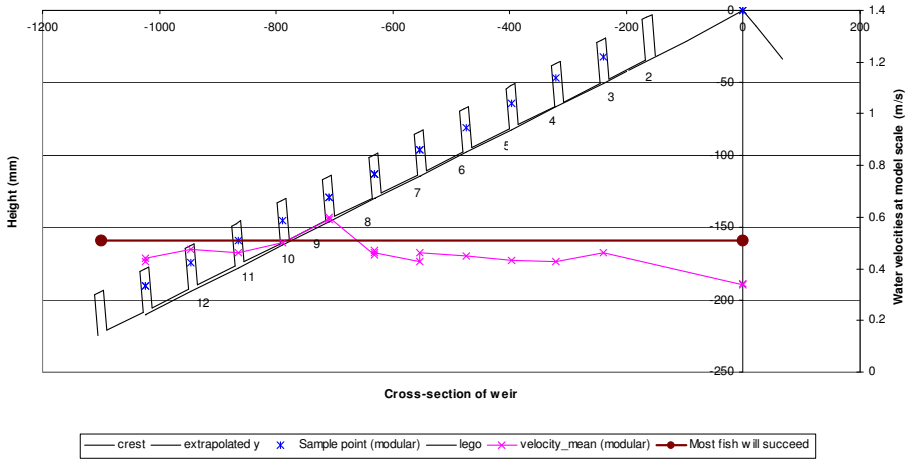

(a) Cross-section

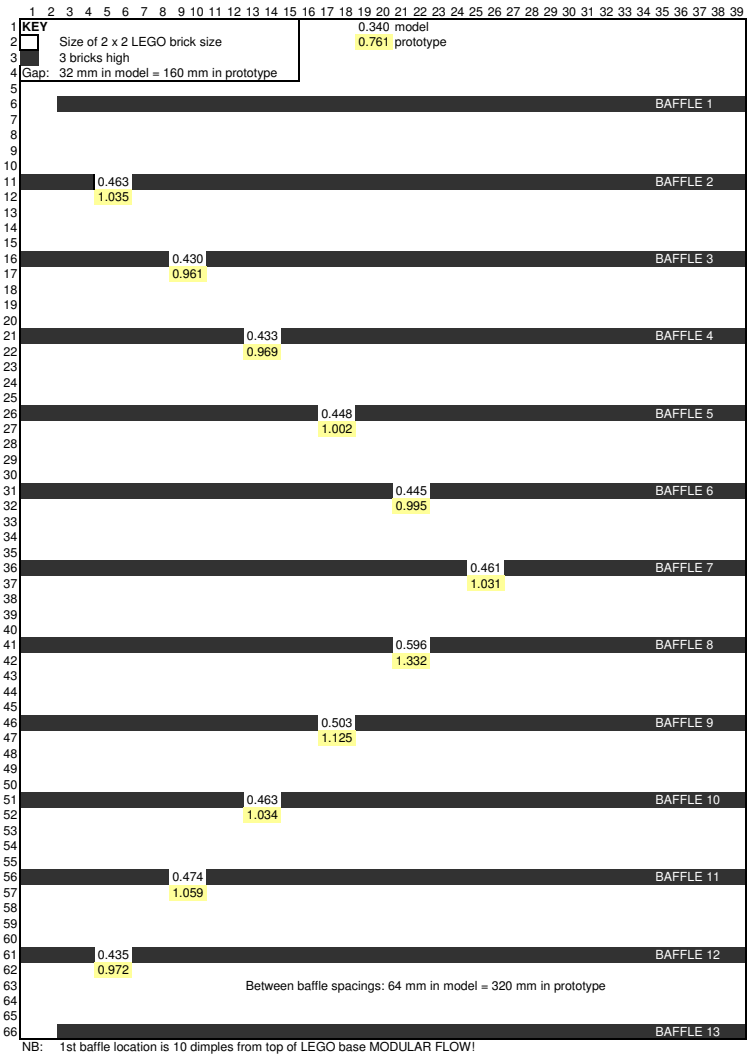

(b) Plan

Figure D–15: Rotated-V: Baffle layout 2

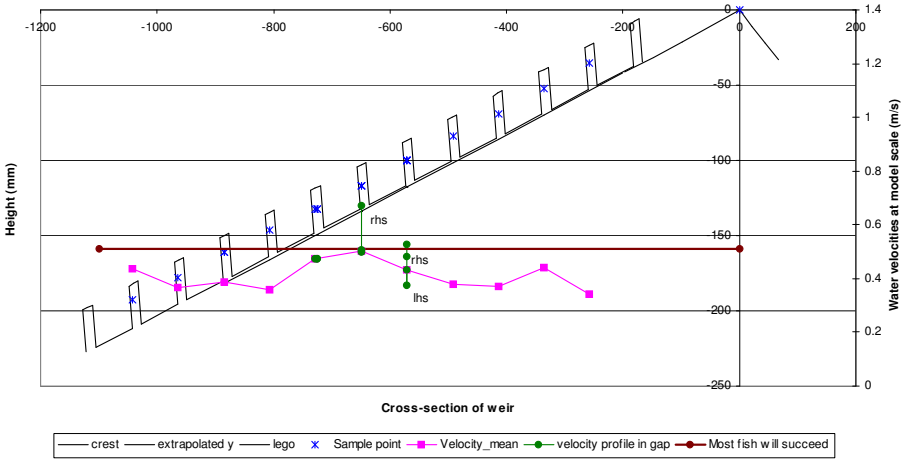

(a) Cross-section

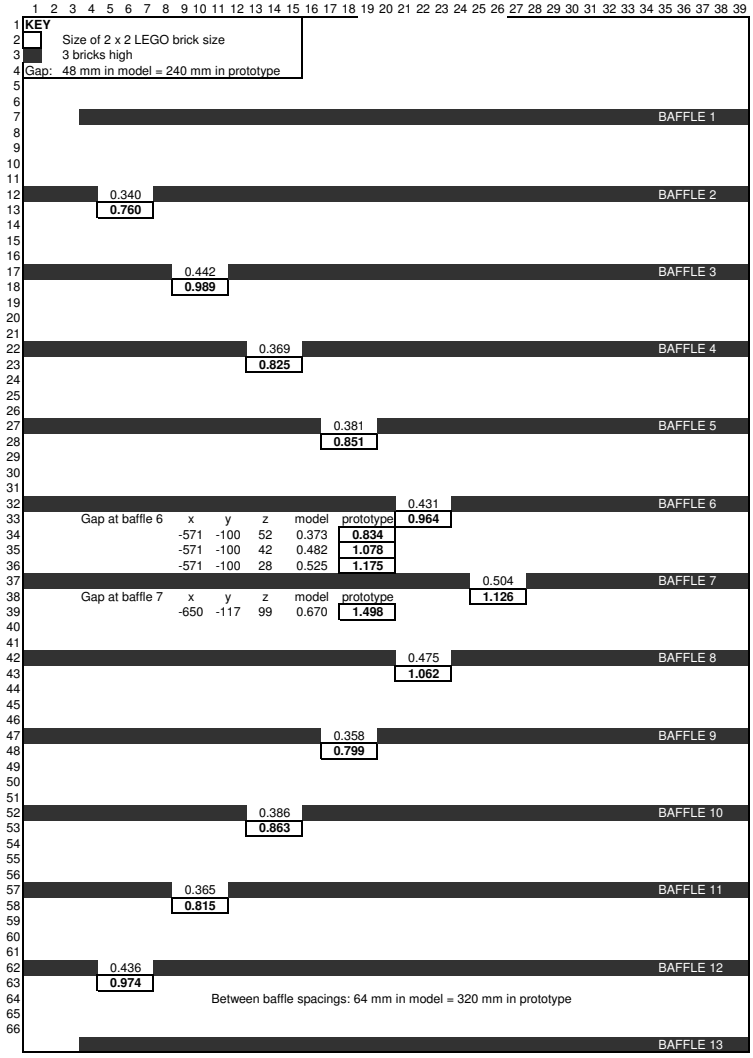

(b) Plan

Figure D–16: Rotated-V: Baffle layout 4

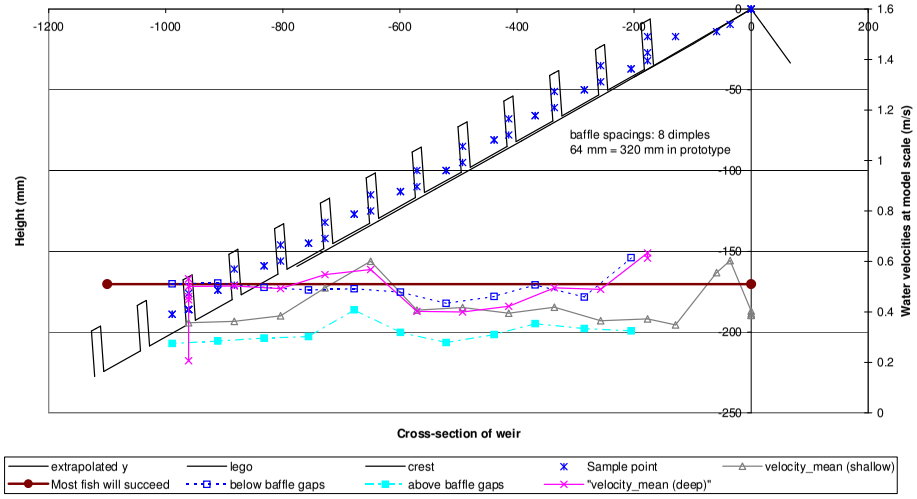

(a) Cross-section

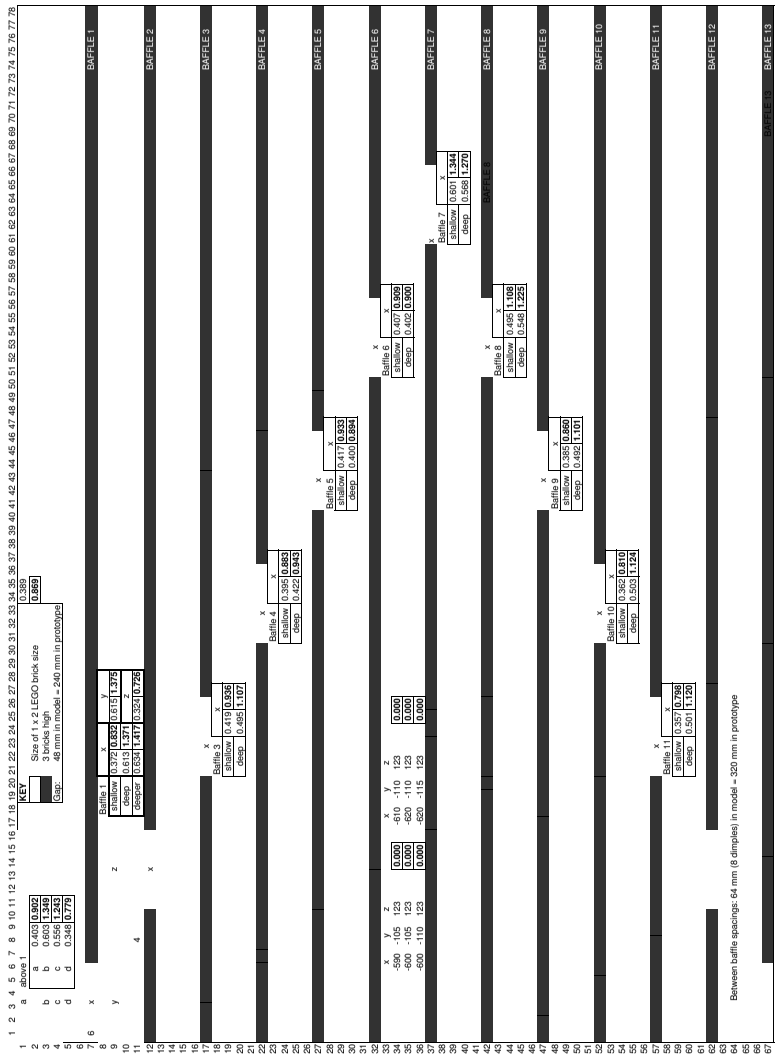

(b) Plan (i.e. rotated)

Figure D–17: Rotated-V: LEGO layout 1.14

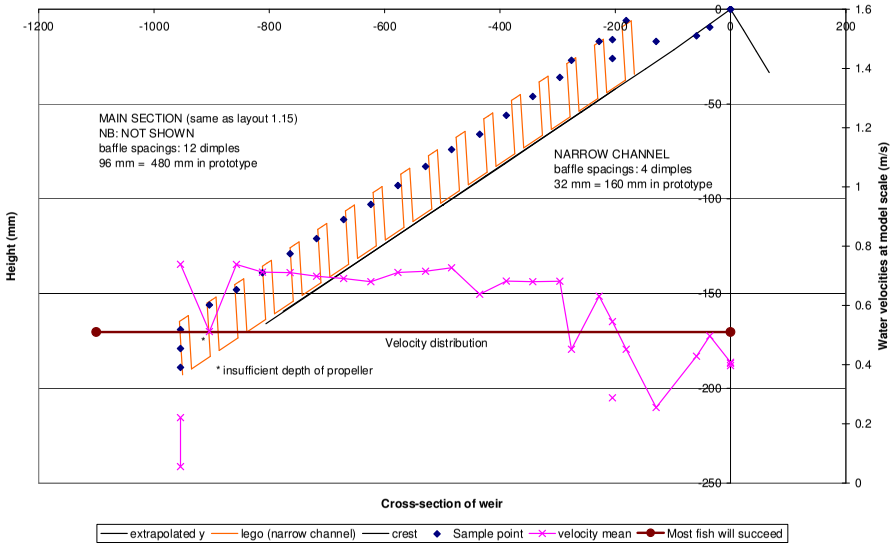

(a) Cross-section

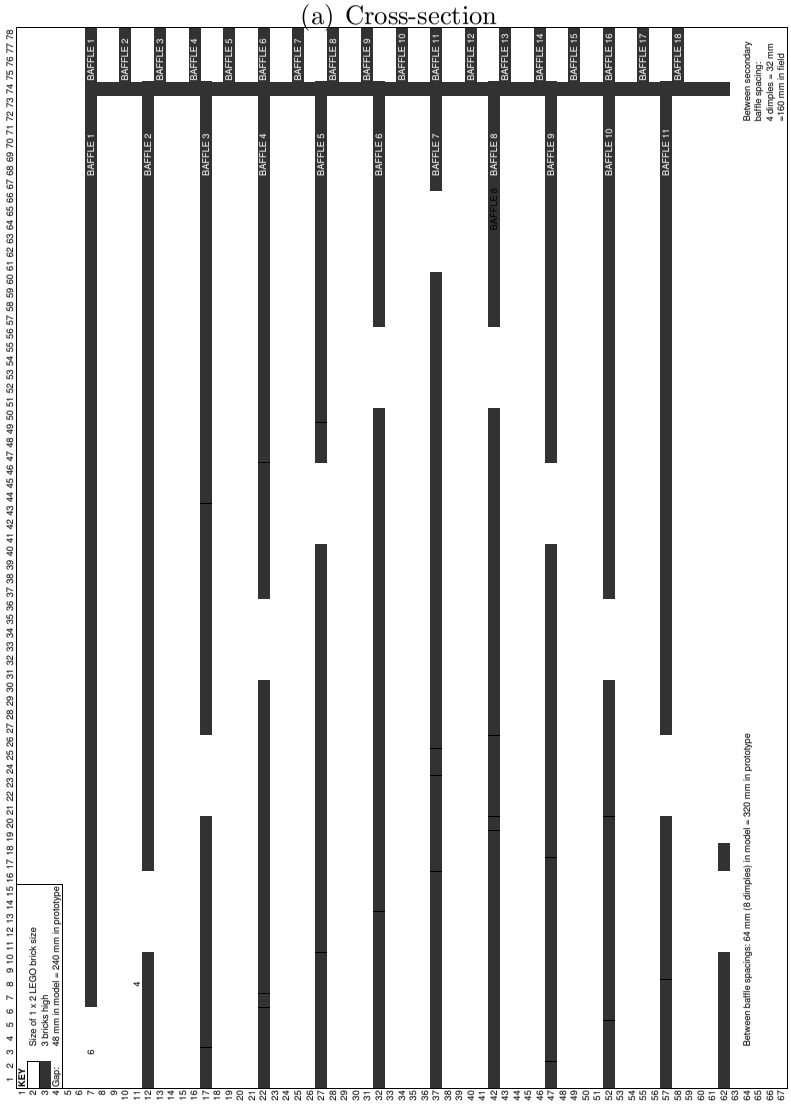

(b) Plan

Figure D–18: Rotated-V and Narrow Channel: LEGO layout 2.1

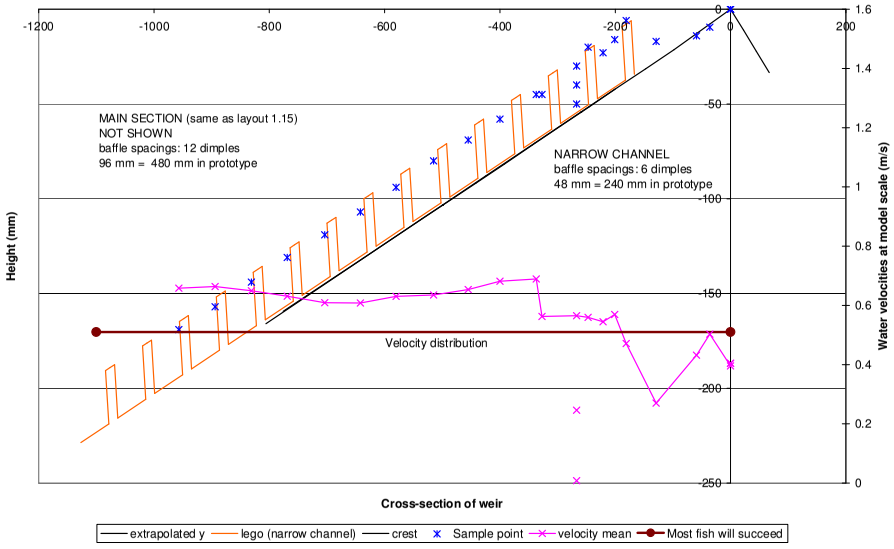

(a) Cross-section

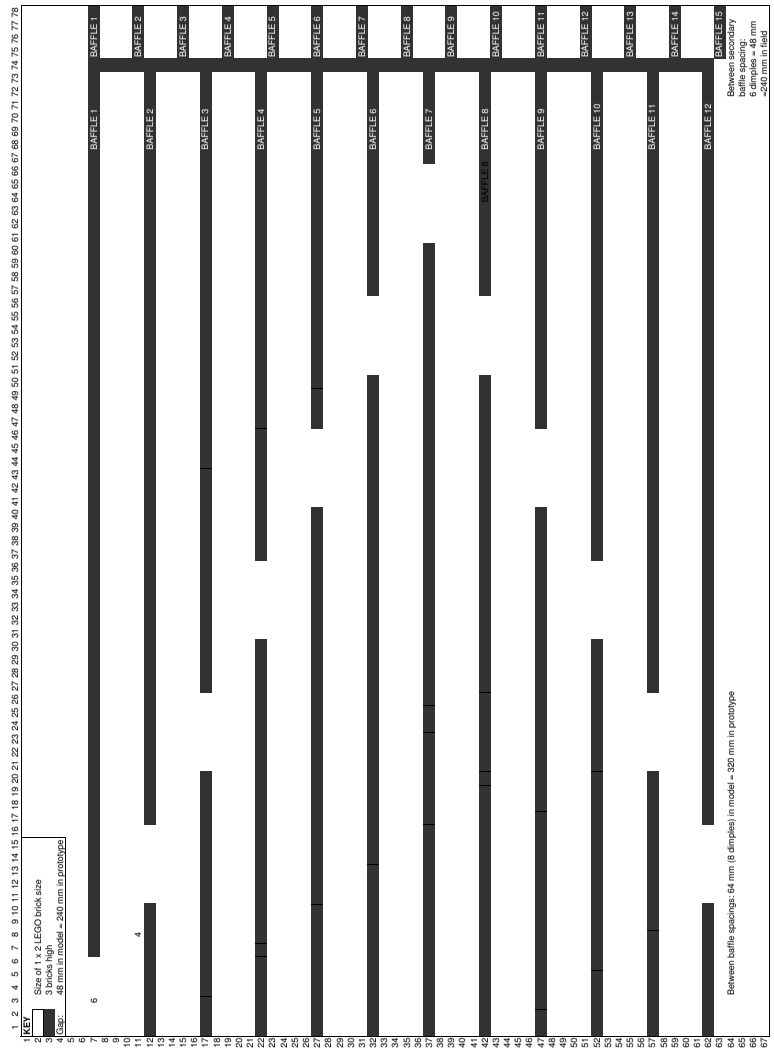

(b) Plan (i.e. rotated)

Figure D–19: Rotated-V and Narrow Channel: LEGO layout 2.2

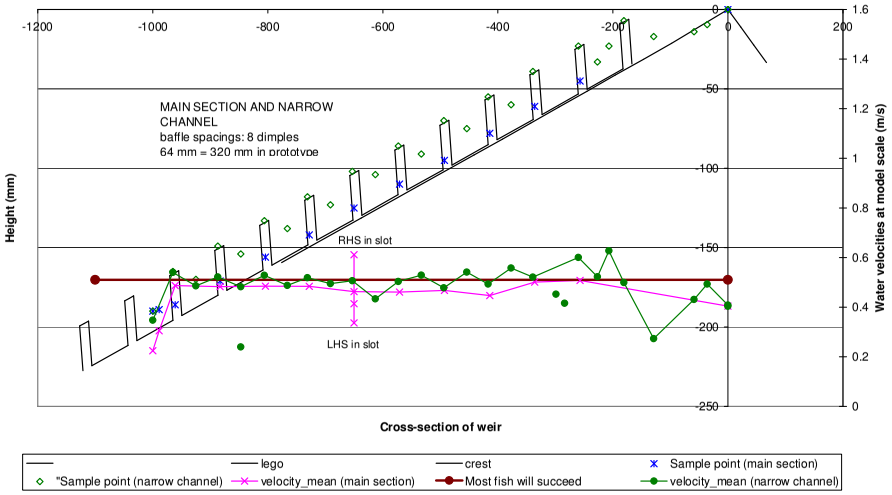

(a) Cross-section

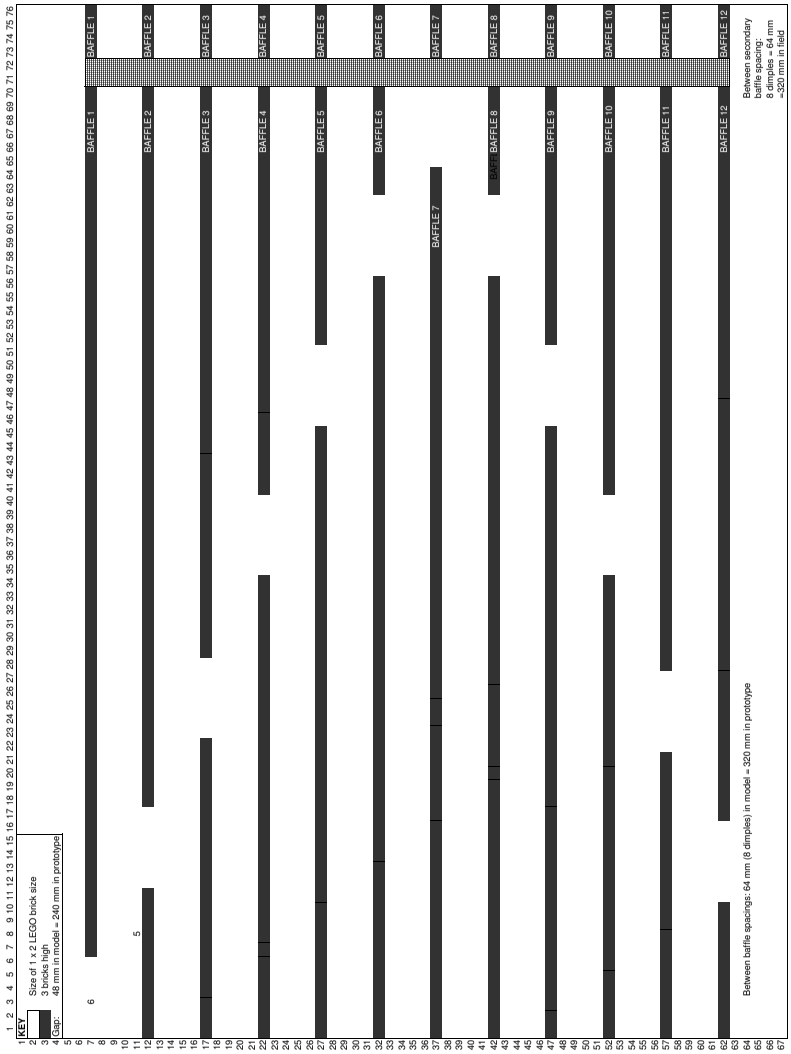

(b) Plan (i.e. rotated)

Figure D–20: Rotated-V and Narrow Channel: LEGO layout 1.16

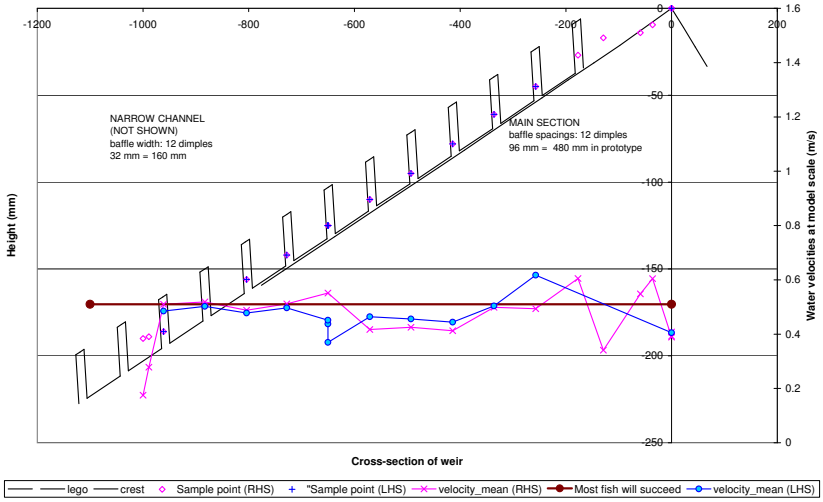

(a) Cross-section: Main channel

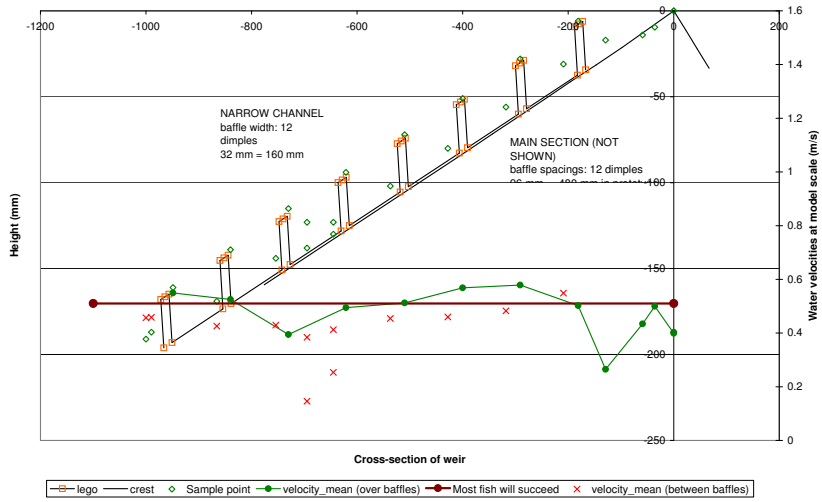

(b) Cross-section: Narrow channel

Figure D–21: Cross-sections of Rotated-V and Narrow Channel: LEGO layout 1.15

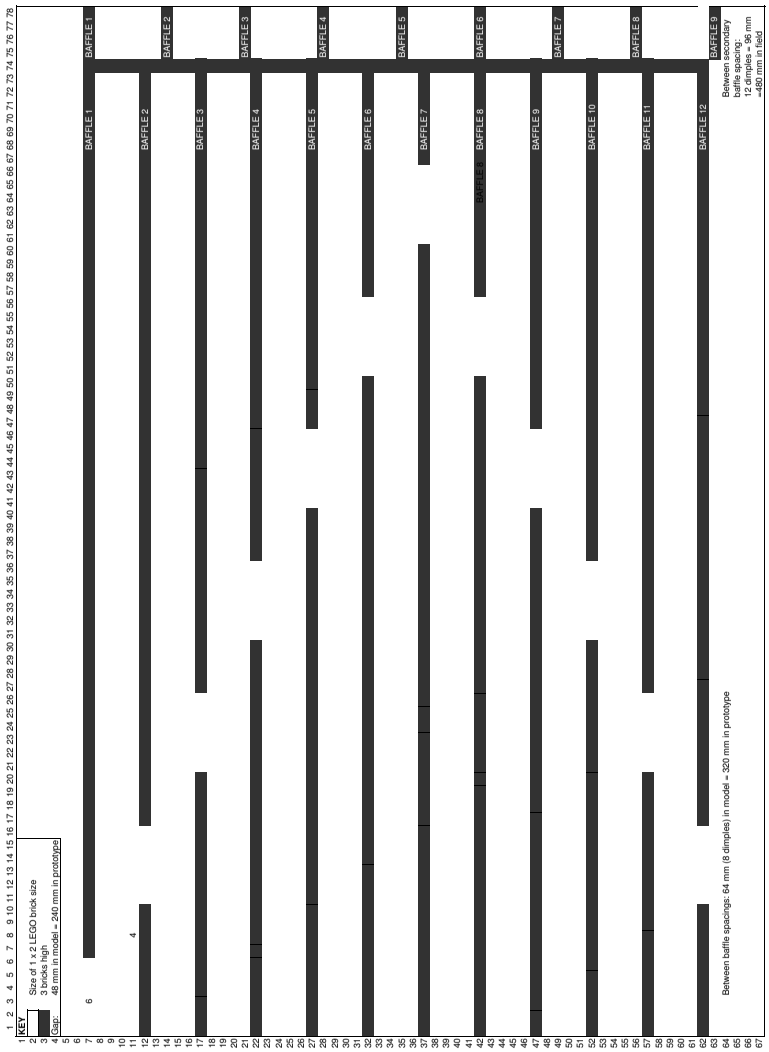

(a) Plan (i.e. rotated)

Figure D–22: Plan view of Rotated-V and Narrow Channel: LEGO layout 1.15

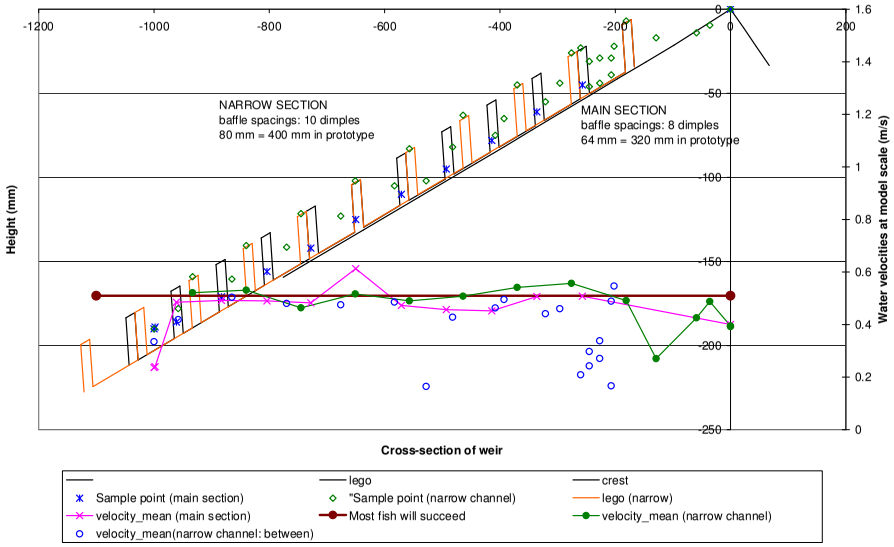

(a) Cross-section

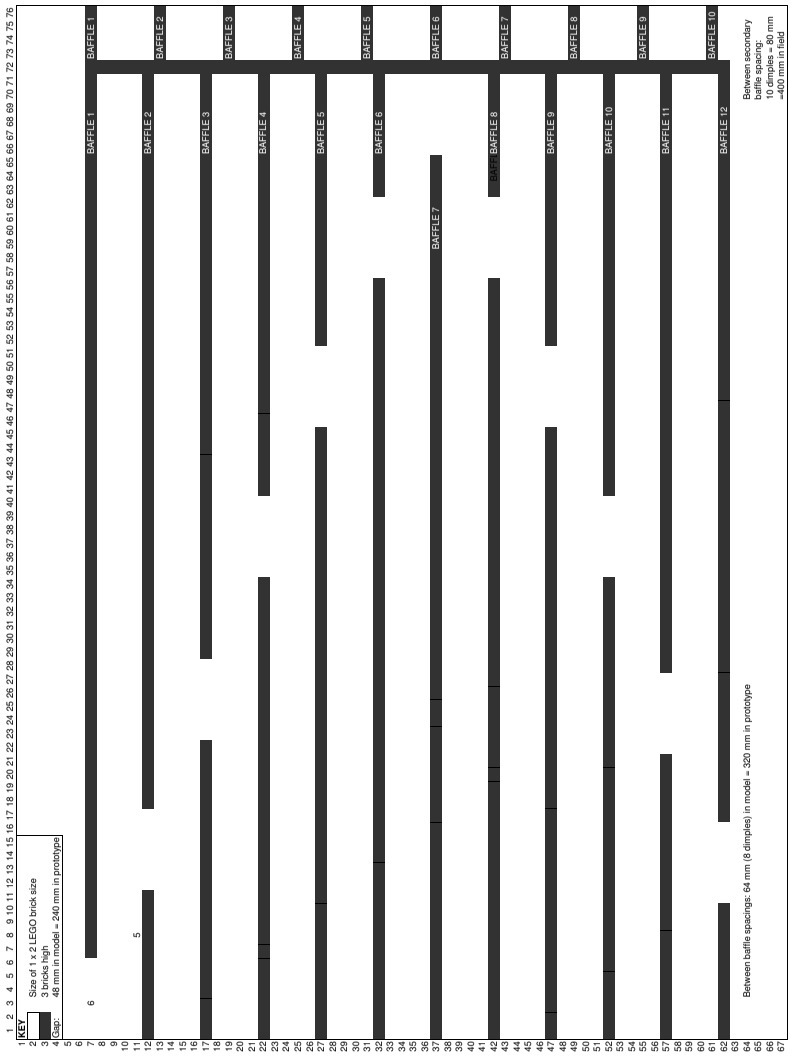

(b) Plan (i.e. rotated)

Figure D–23: Rotated-V and Narrow Channel: LEGO layout 1.17

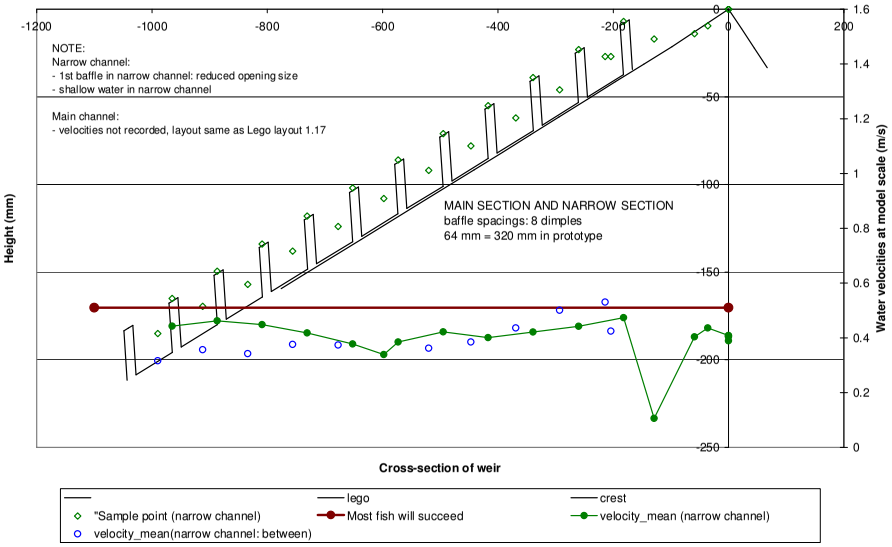

(a) Cross-section

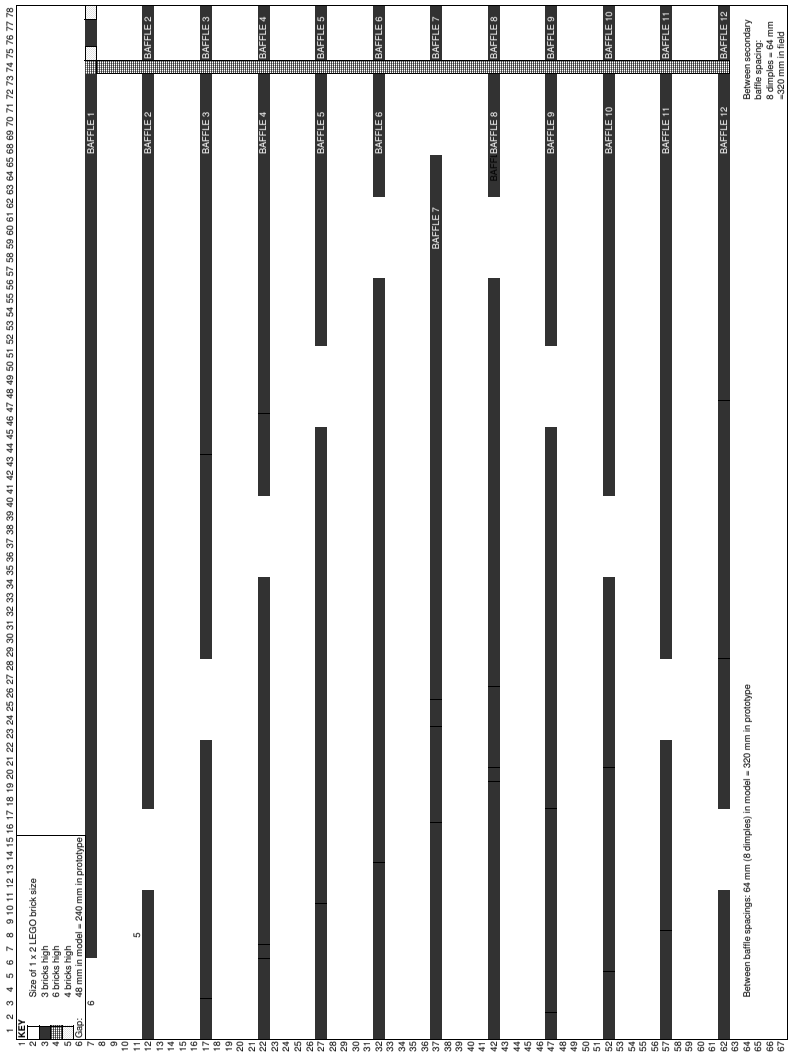

(b) Plan (i.e. rotated)

Figure D–24: Rotated-V and Narrow Channel: LEGO layout 1.19

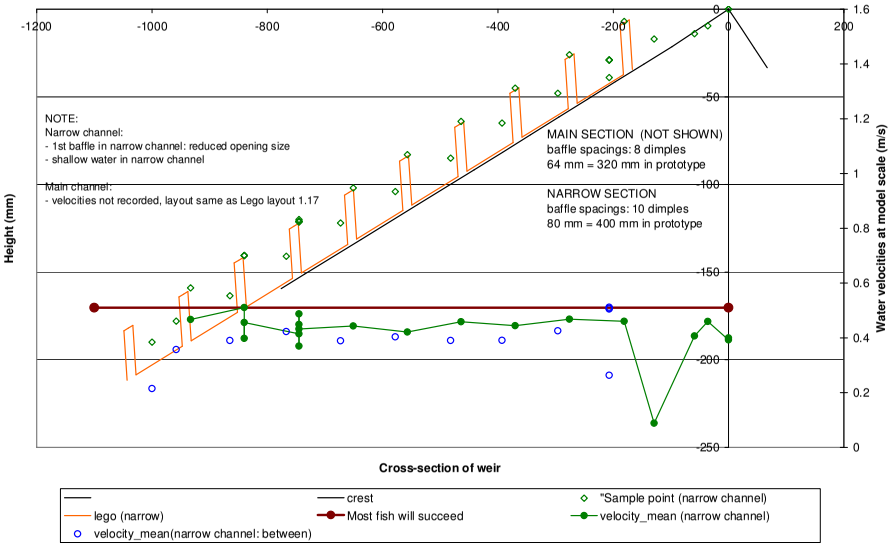

(a) Cross-section

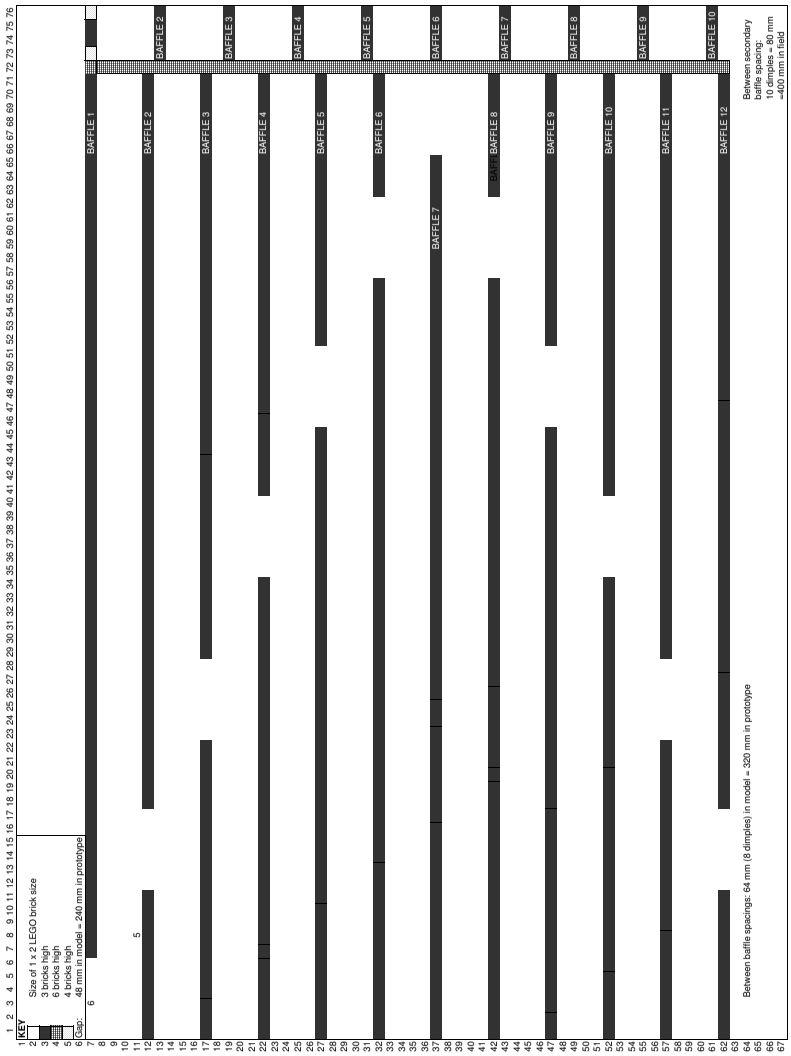

(b) Plan (i.e. rotated)

Figure D–25: Rotated-V and Narrow Channel: LEGO layout 1.18

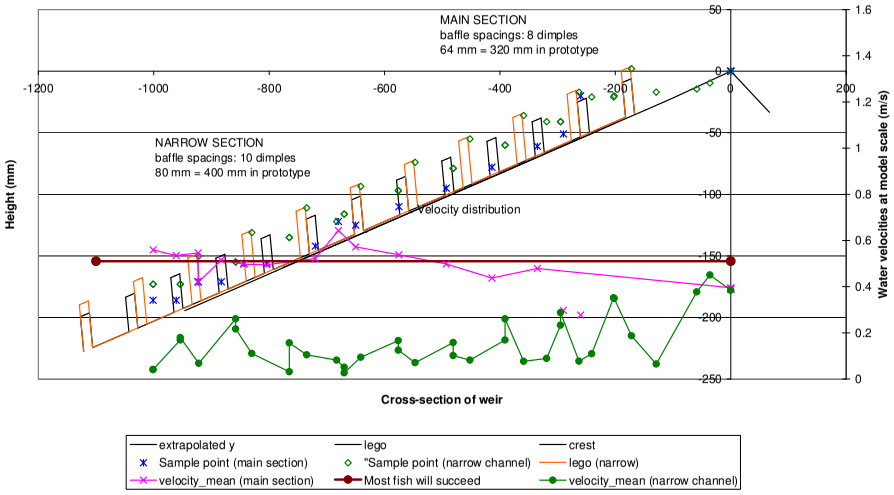

(a) Cross-section

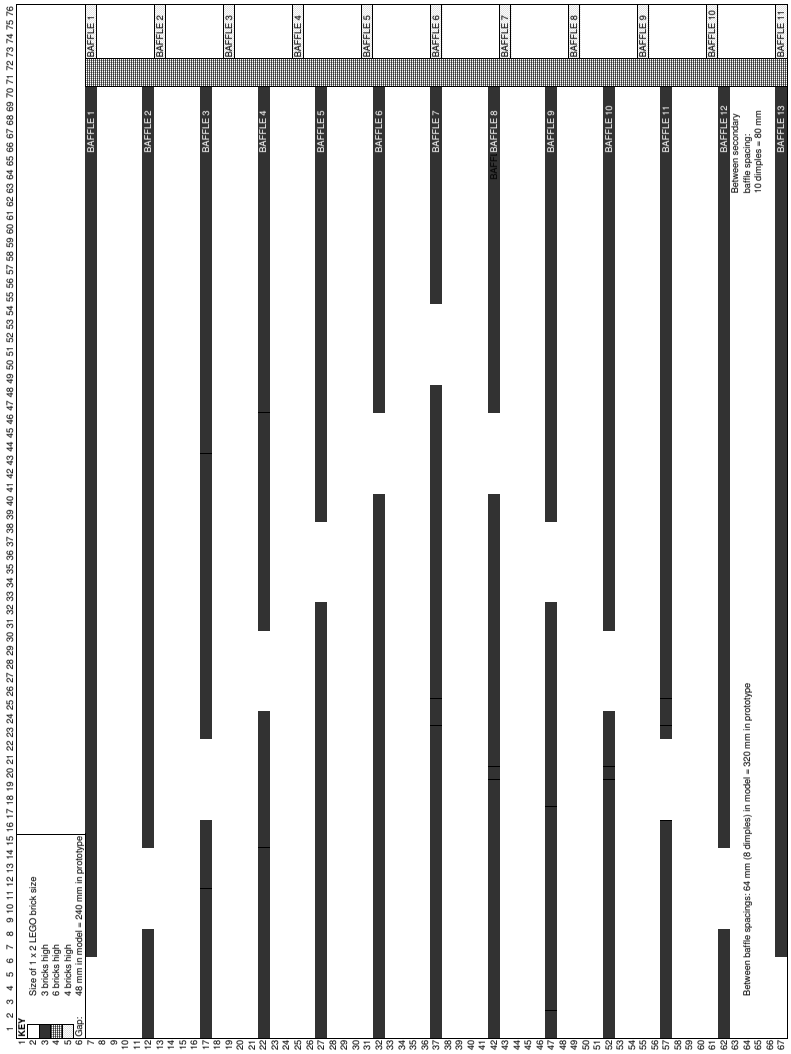

(b) Plan (i.e. rotated)

Figure D–26: Rotated-V and Narrow Channel: LEGO layout 2.5

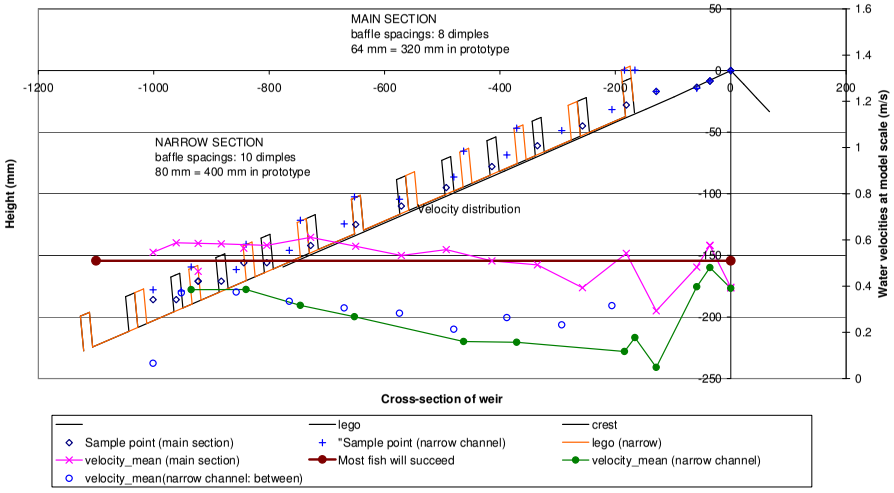

(a) Cross-section

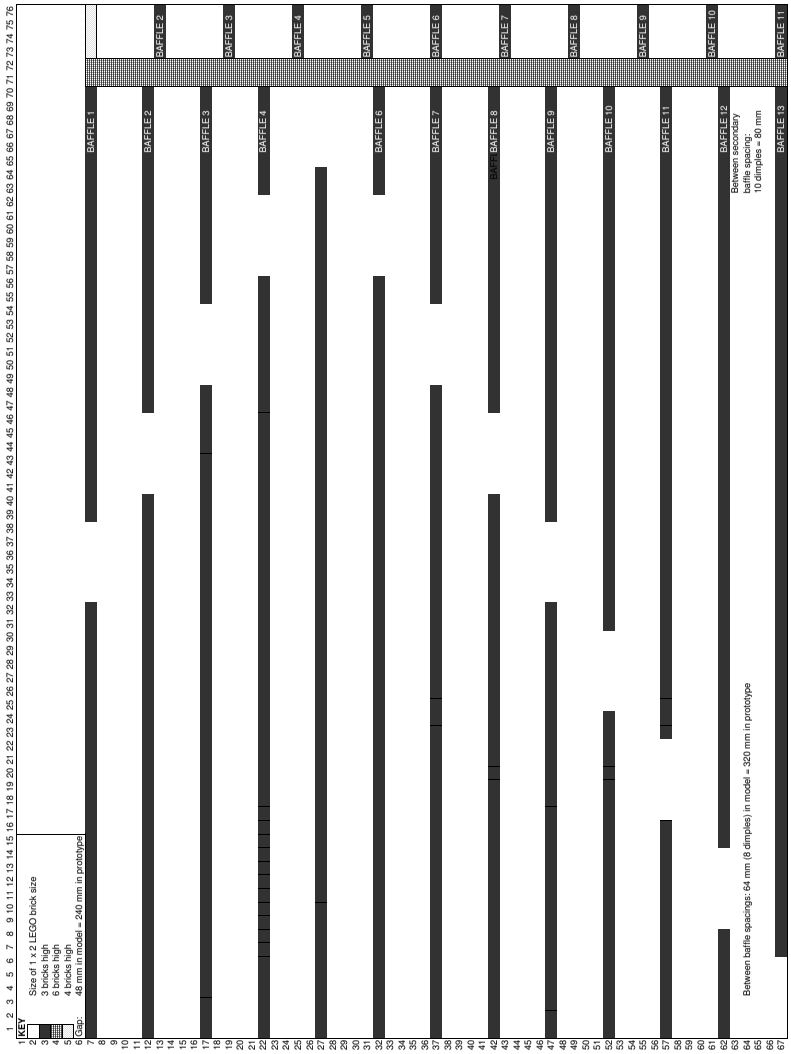

(b) Plan (i.e. rotated)

Figure D–27: Rotated-V and Narrow Channel: LEGO layout 2.6

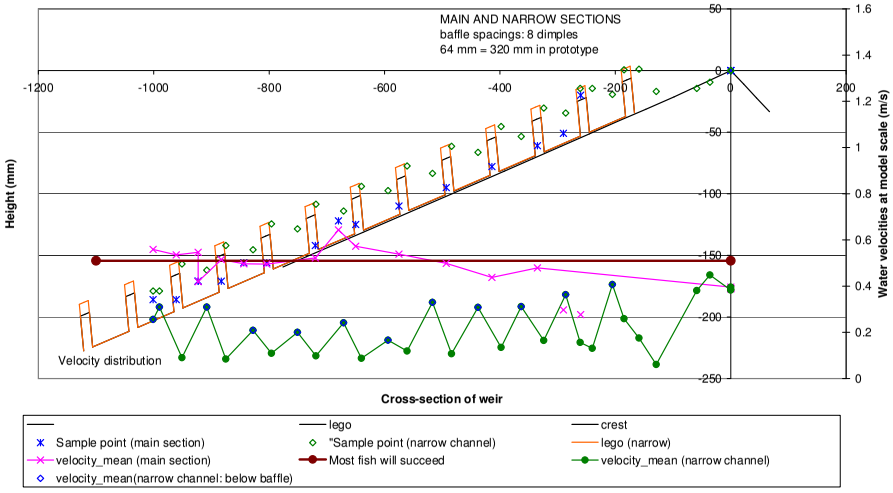

(a) Cross-section

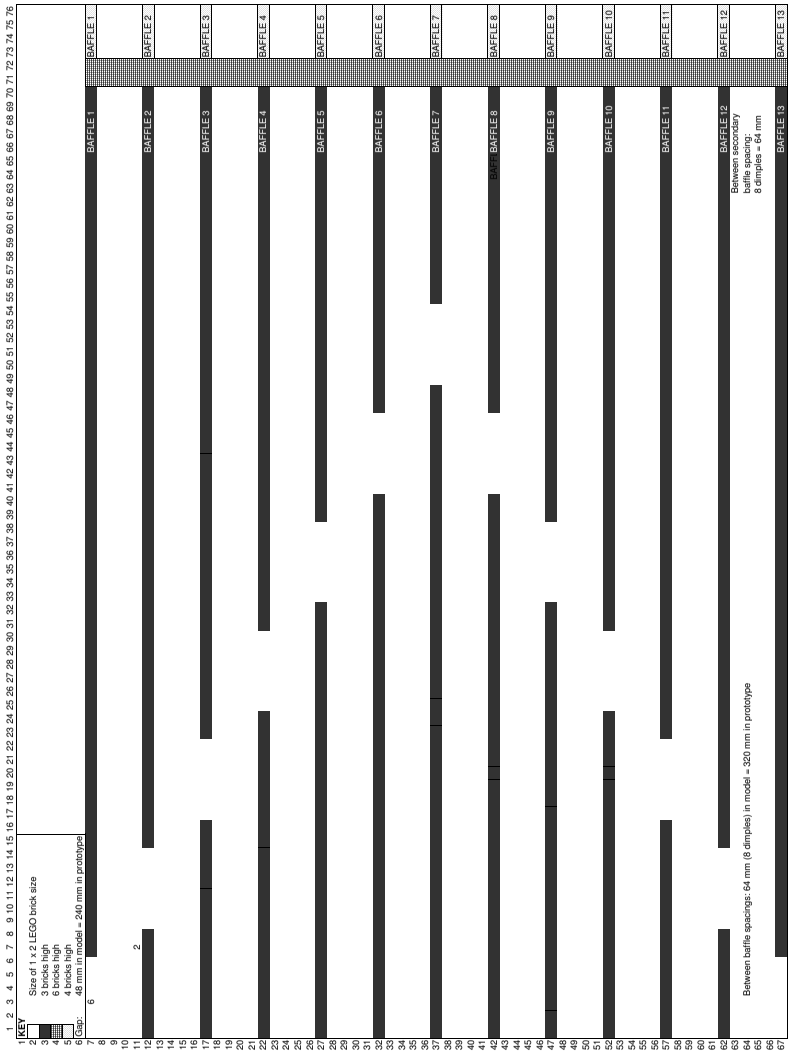

(b) Plan (i.e. rotated)

Figure D–28: Rotated-V and Narrow Channel: LEGO layout 2.7

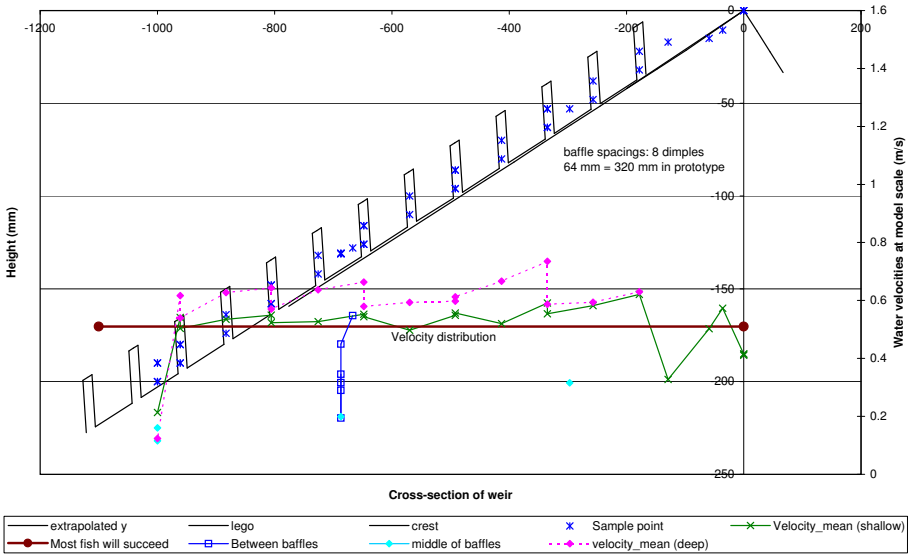

(a) Cross-section

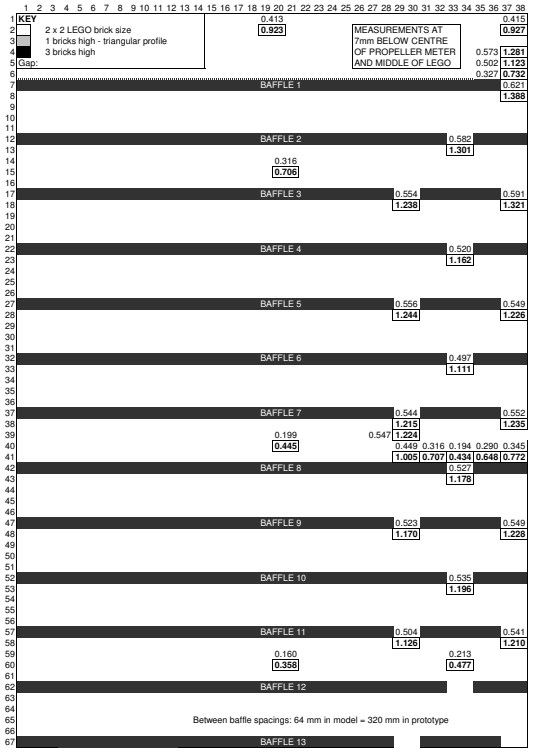

(b) Plan (shallow)

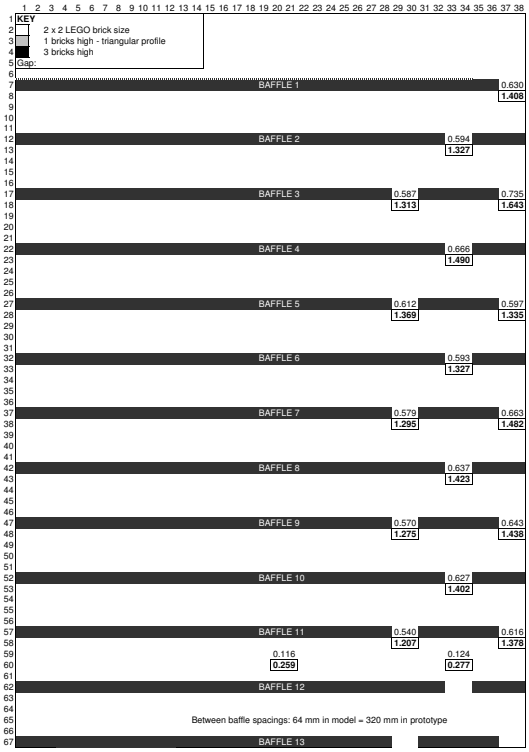

(c) Plan (deep)

Figure D–29: Side-gaps: LEGO layout 2.3

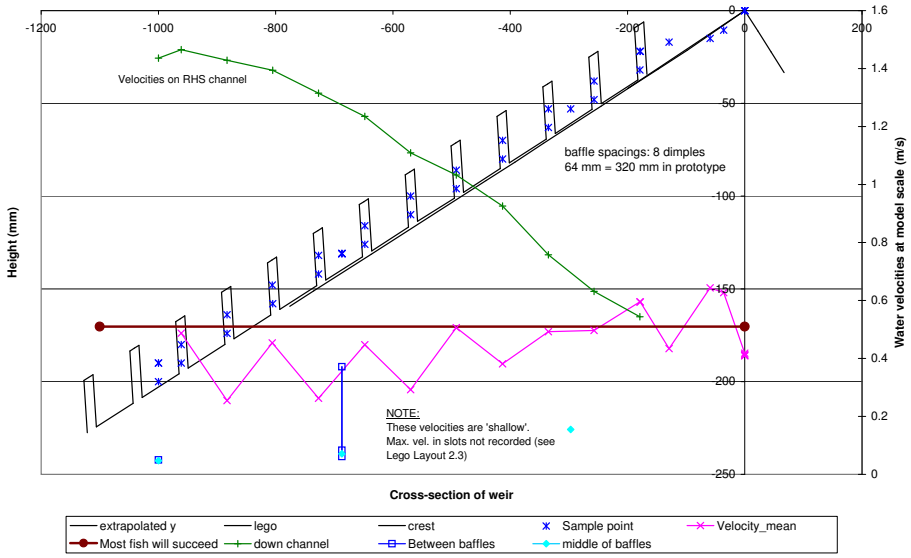

(a) Cross-section

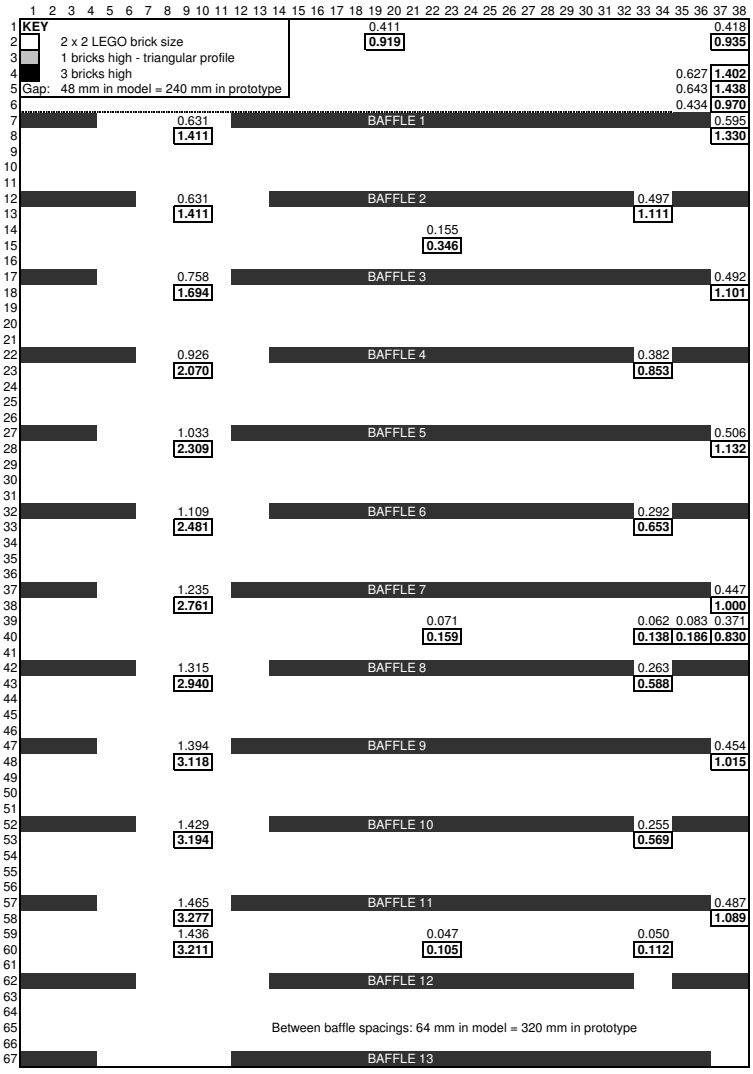

(b) Plan

Figure D–30: Side-gaps: LEGO layout 5.1

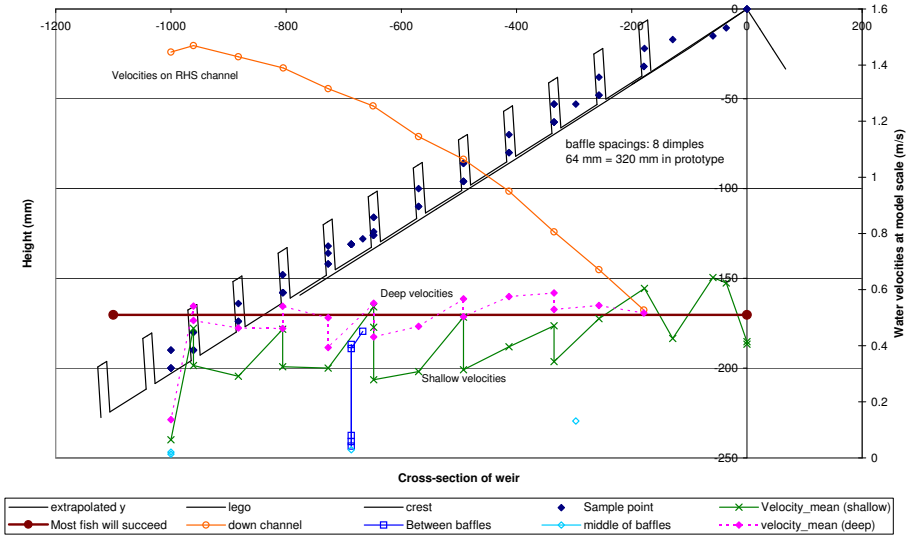

(a) Cross-section

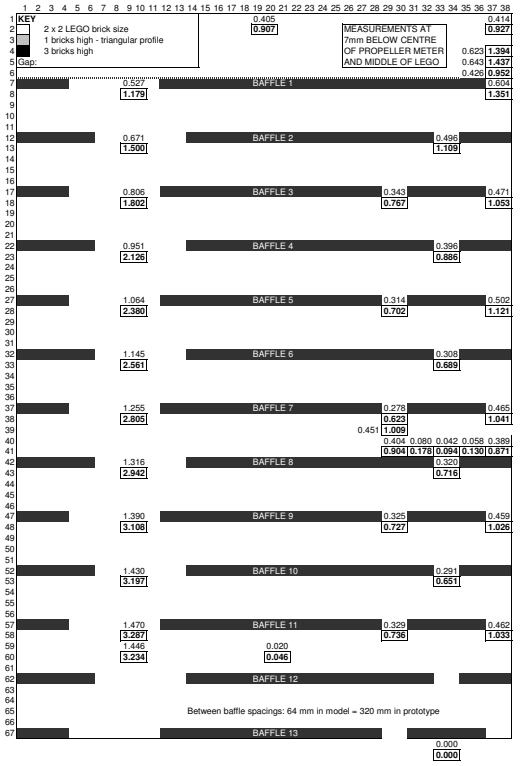

(b) Plan (shallow)

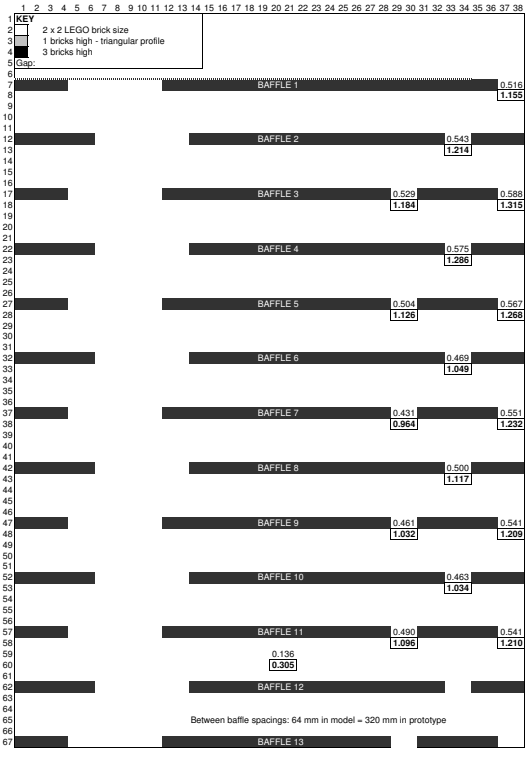

(c) Plan (deep)

Figure D–31: Side-gaps: LEGO layout 5.2

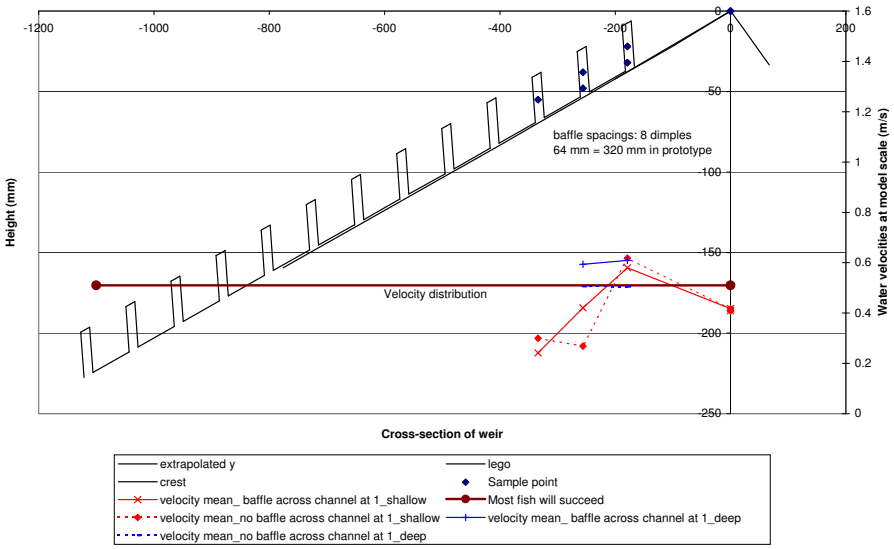

(a) Cross-section

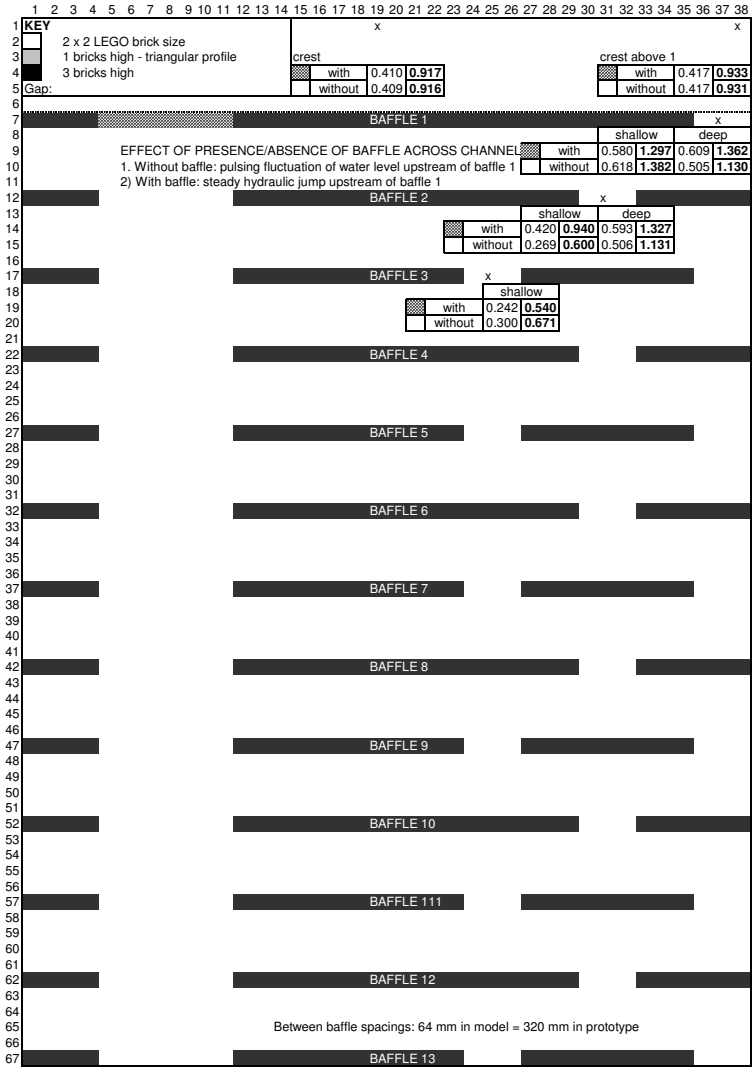

(b) Plan

Figure D–32: Side-gaps: LEGO layout 5.3

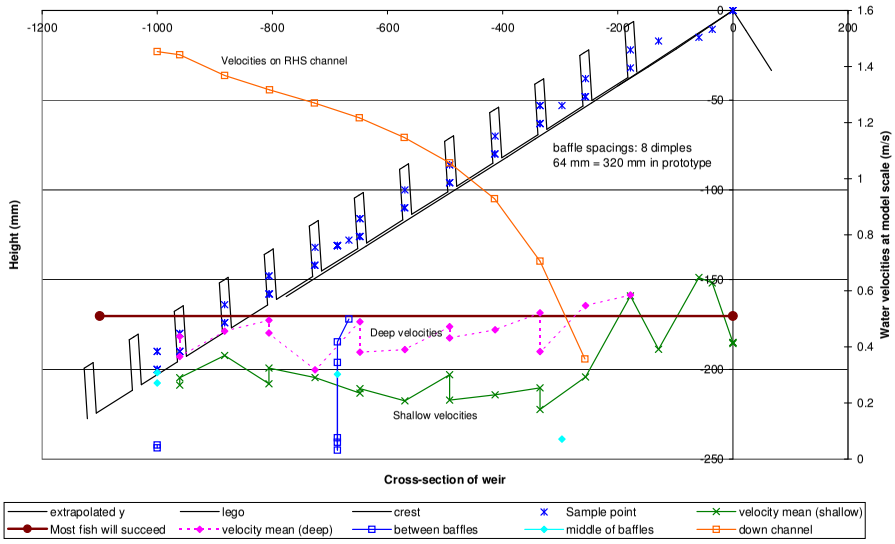

(a) Cross-section

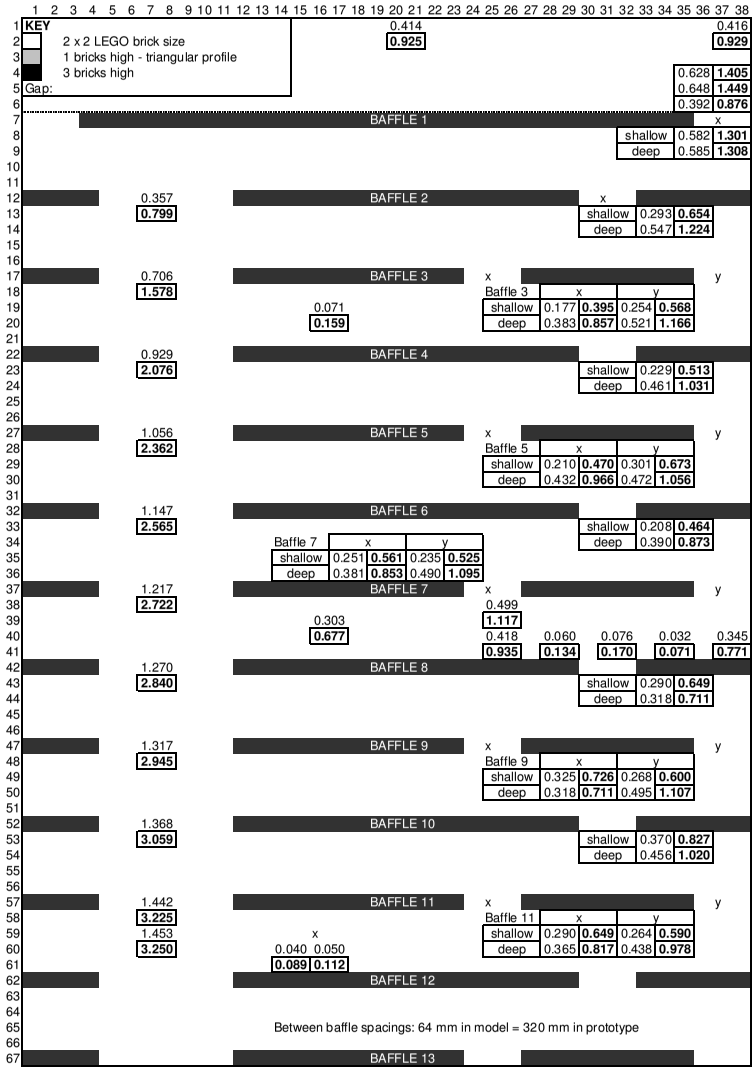

(b) Plan

Figure D–33: Side-gaps: LEGO layout 5.4

D.2. Experiments conducted over flow range

LEGO layouts 1.16 and 2.5 were the most promising LEGO layouts identified in the 90 percentile low-flow trials. In this section, the results from each experiment are presented for each specific layout. Table D–2 presents the experiment name and the flow rates for which it was tested.

Table D–2: LEGO layouts tested over the wider flow range

LEGO layout	**Flow rate**	**Figure no.**
6.1	Q25, Q30, Q50	Figures D–34 and D–35
6.2	Q30, Q50	Figure D–36
6.3	Q25, Q30	Figure D–37
6.4	Q30, Q50, Q60, Q70, Q90	Figures D–38 and D–39
6.4(2)	Q30, Q50, Q60, Q70, Q90	Figure D–40
6.5	Q30, Q50	Figure D–41

During the refinement process, the narrow channel was removed, and the baffle heights were increased (as described in section 4.1.4). The preferred layout based on the range of flow experiments was that of LEGO layout 6.4.

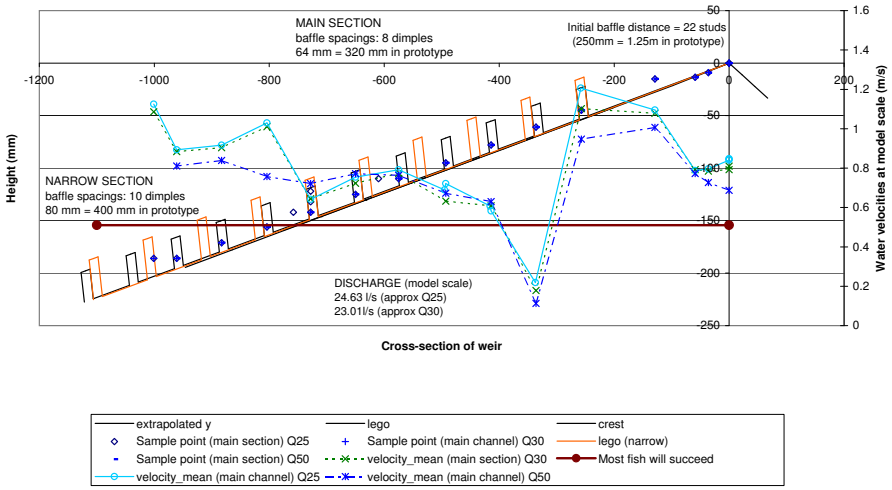

(a) Comparison of flow rates

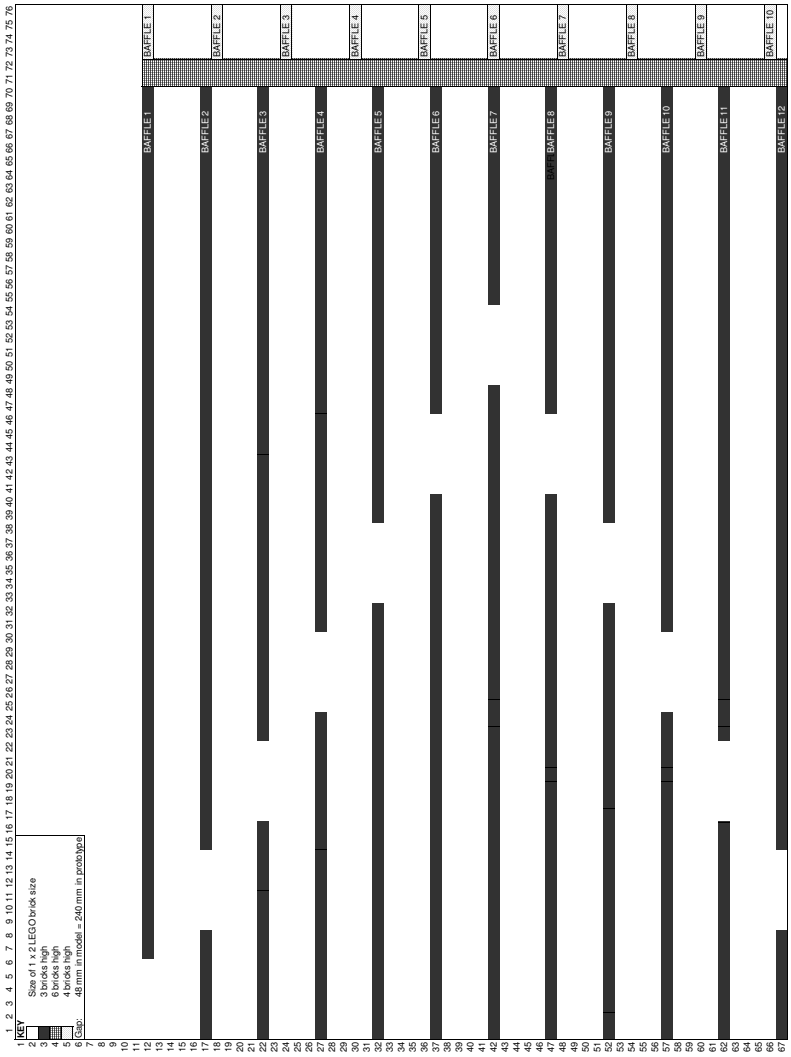

(b) Plan (i.e. rotated)

Figure D–34: Rotated-V and Narrow Channel: LEGO layout 6.1

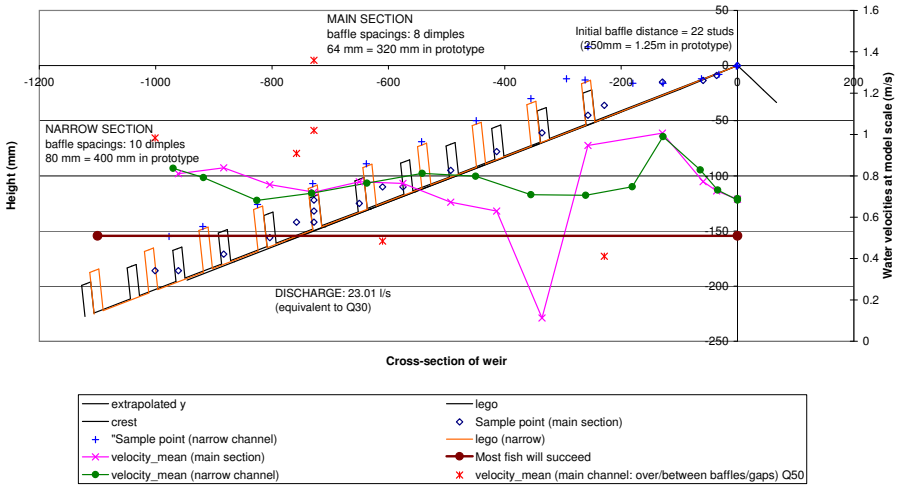

(a) Q50

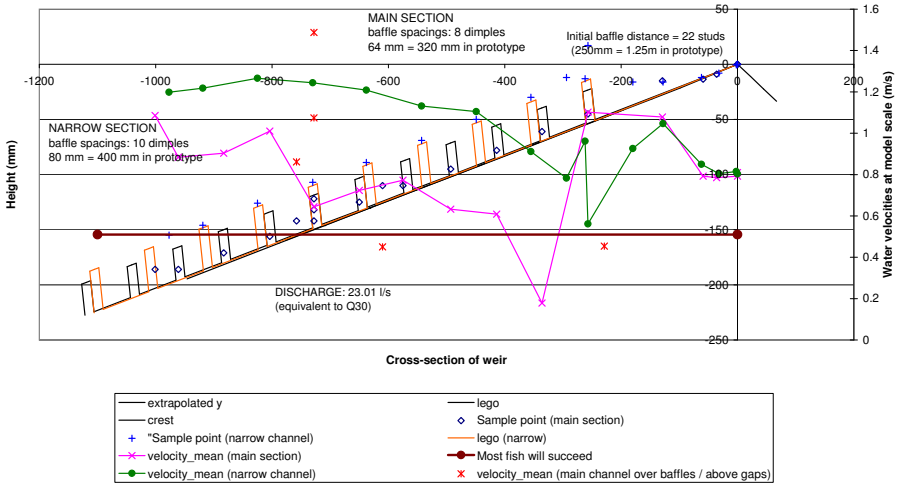

(b) Q30

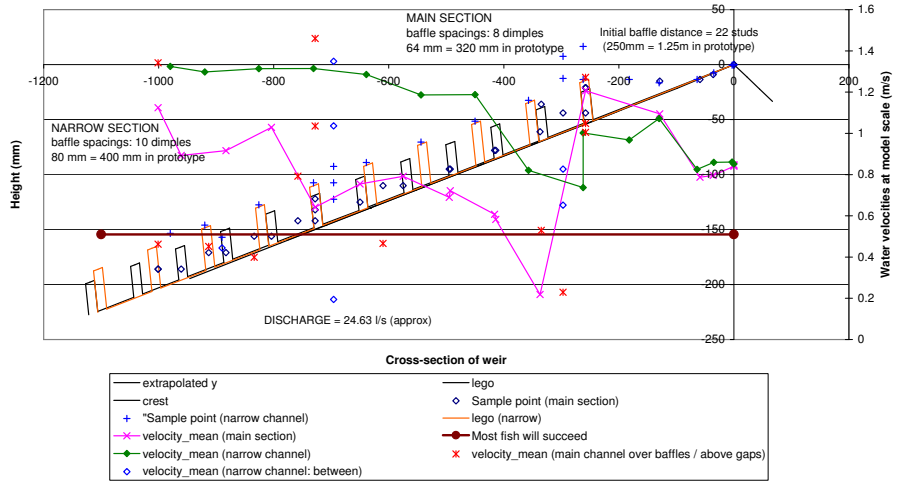

(c) Q25

Figure D–35: Rotated-V and Narrow Channel: Cross-sections of LEGO layout 6.1

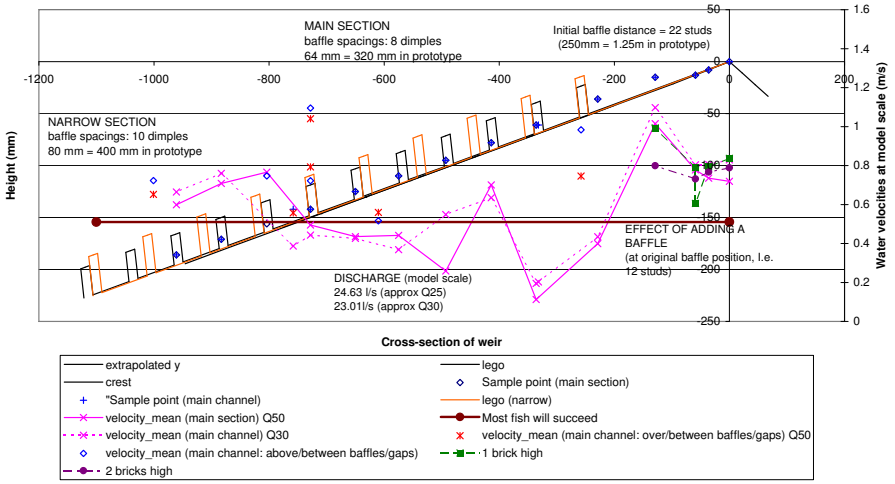

(a) Comparison of flow rates

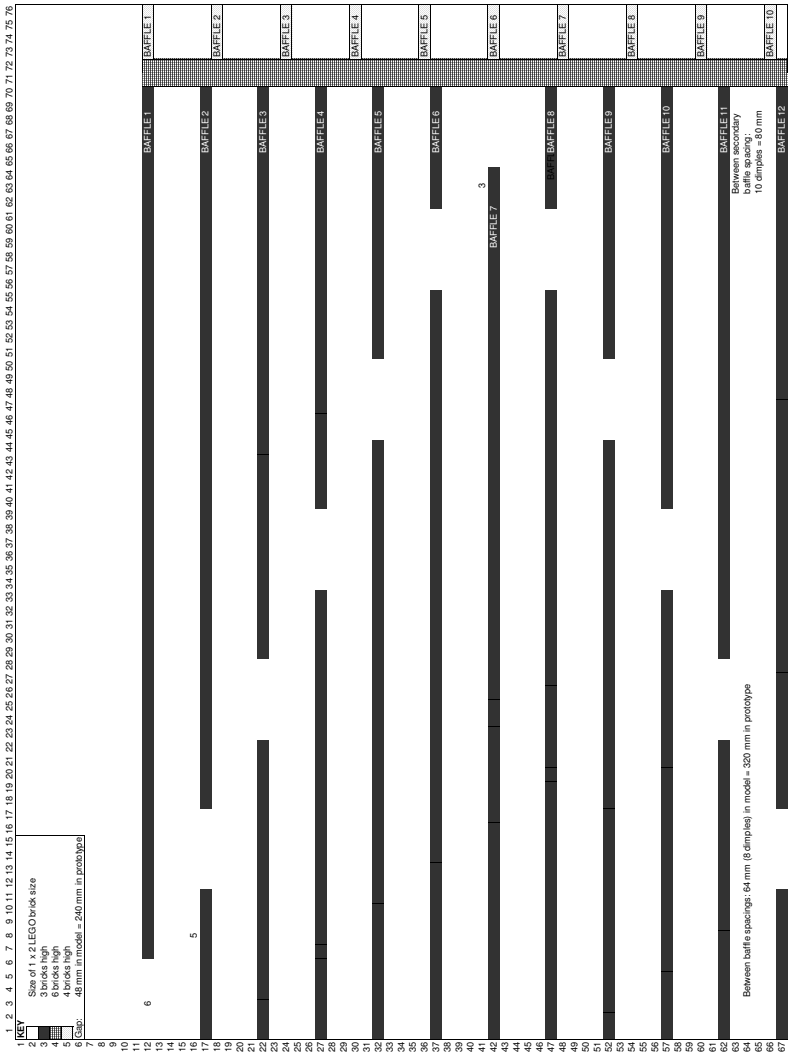

(b) Plan (i.e. rotated)

Figure D–36: Rotated-V and Narrow Channel: LEGO layout 6.2

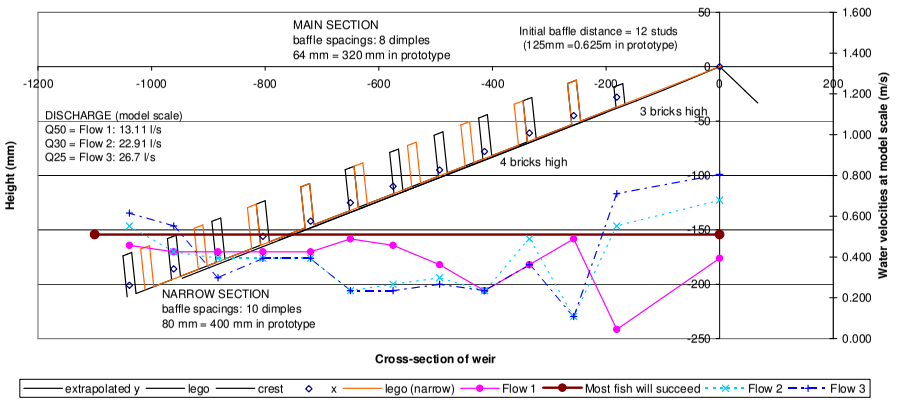

(a) Comparison of flow rates

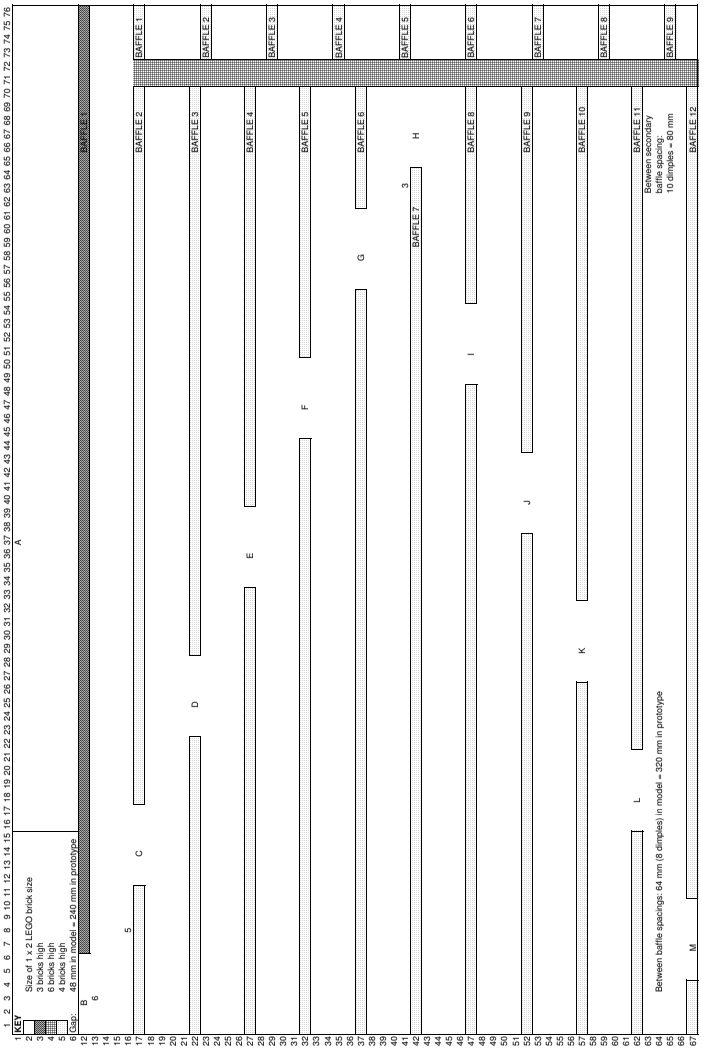

(b) Plan (i.e. rotated)

Figure D–37: Rotated-V and Narrow Channel: LEGO layout 6.3

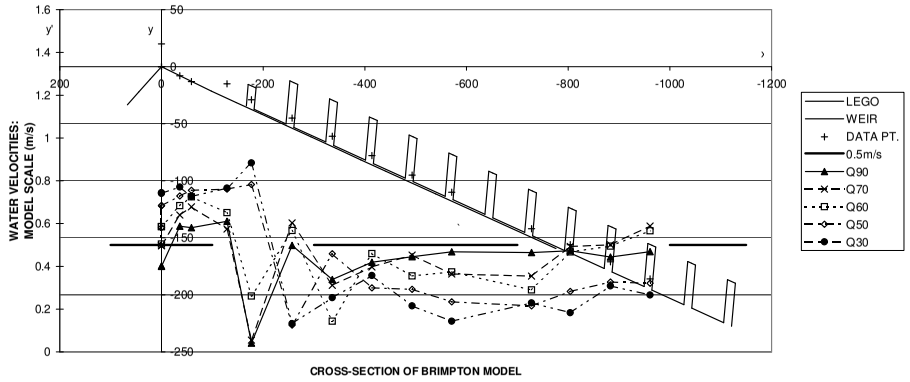

(a) Comparison of flow rates

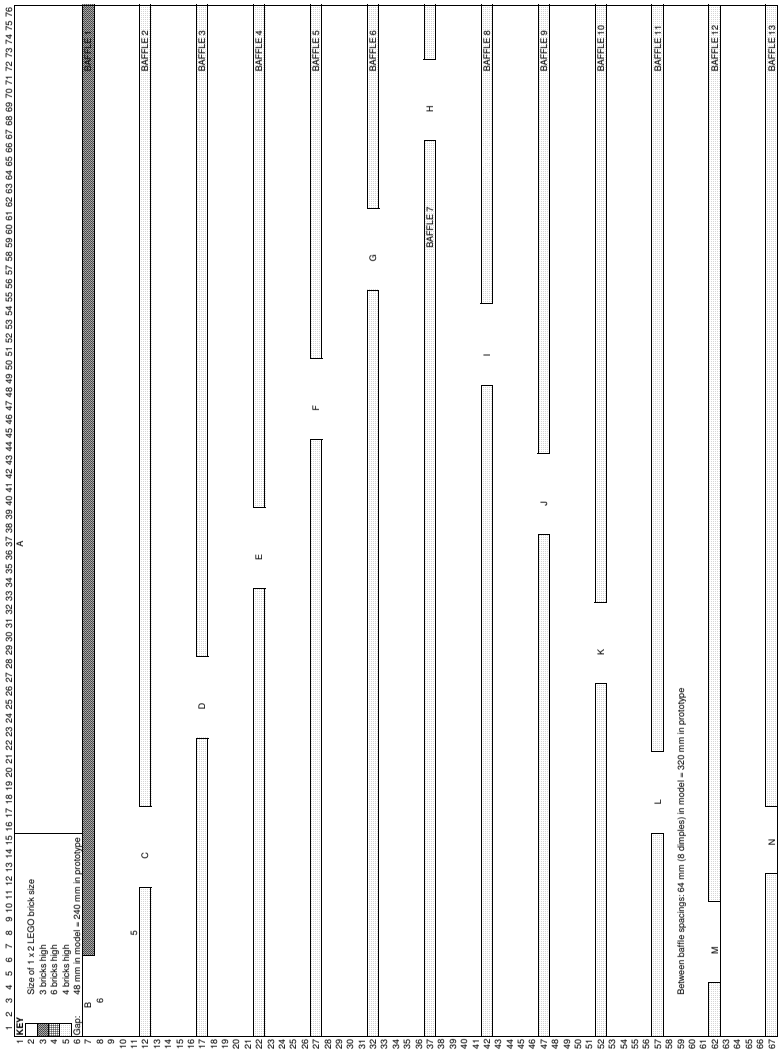

(b) Plan (i.e. rotated)

Figure D–38: Rotated-V: LEGO layout 6.4

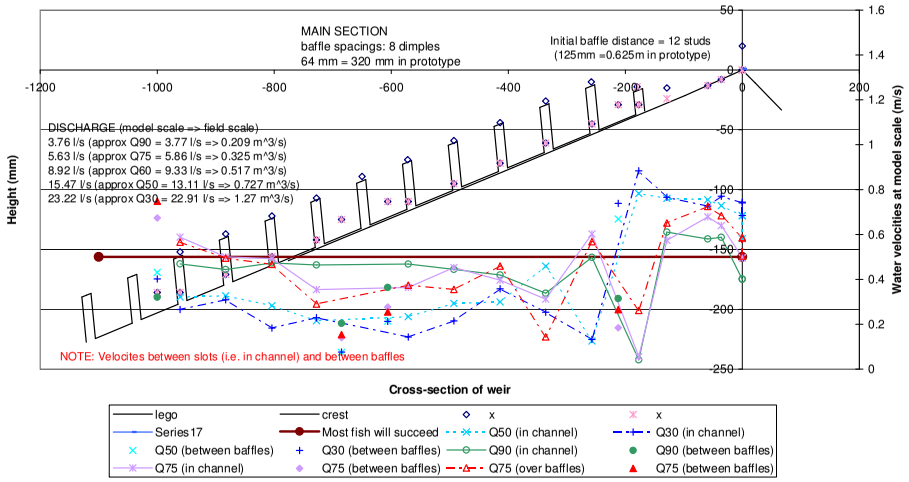

(a) Flows through slots and between baffles

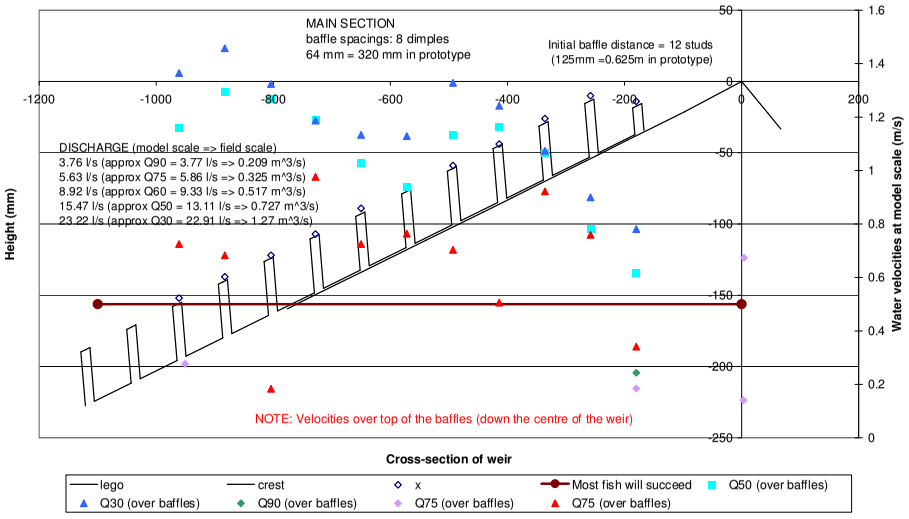

(b) Flows over the top of baffles

Figure D–39: Rotated-V: LEGO layout 6.4

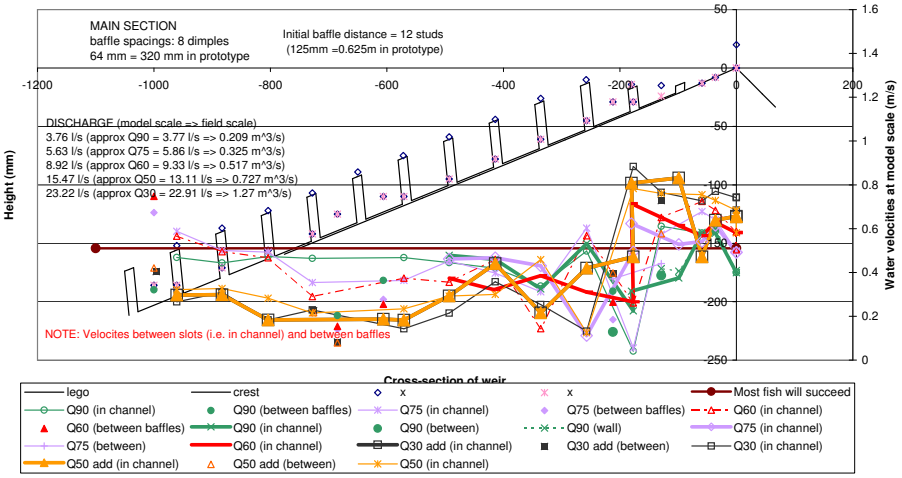

(a) Comparison of flow rates

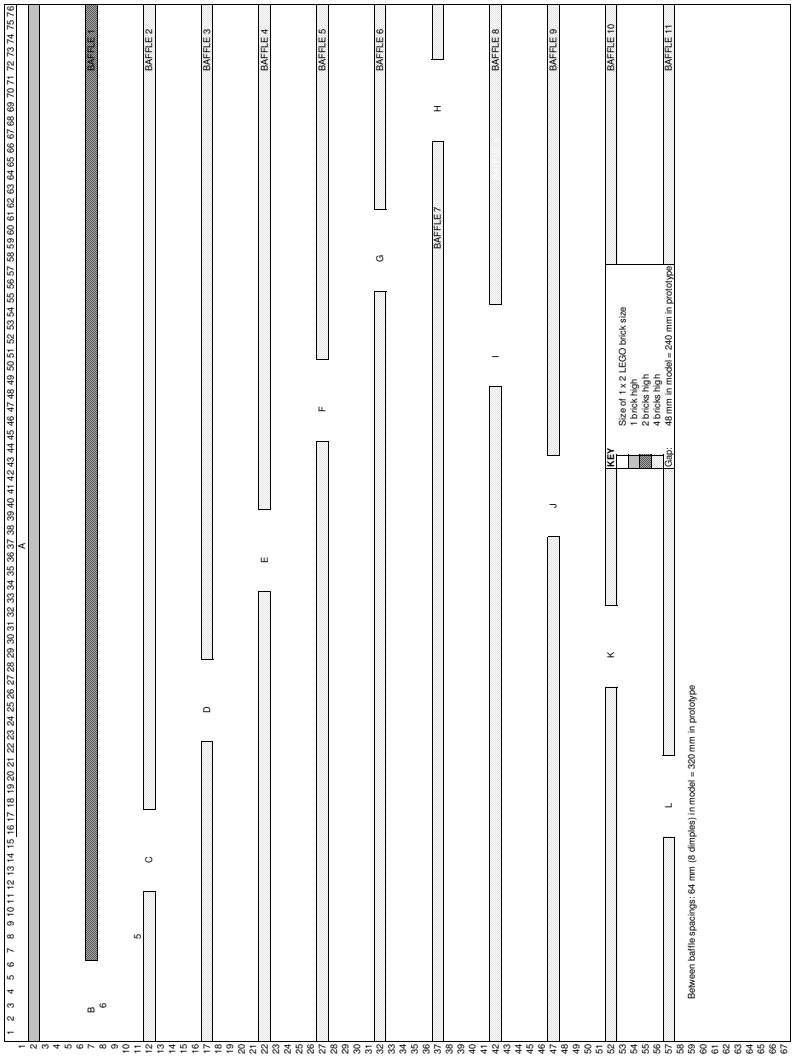

(b) Plan (i.e. rotated)

Figure D–40: Rotated-V: LEGO layout 6.4(2)

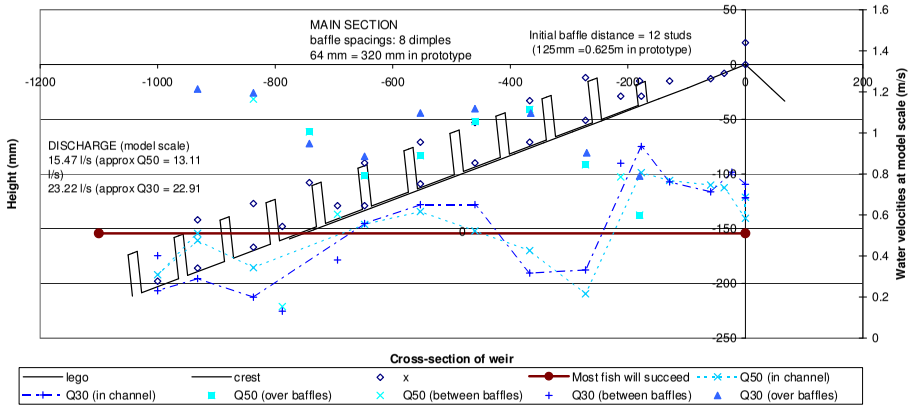

(a) Comparison of flow rates

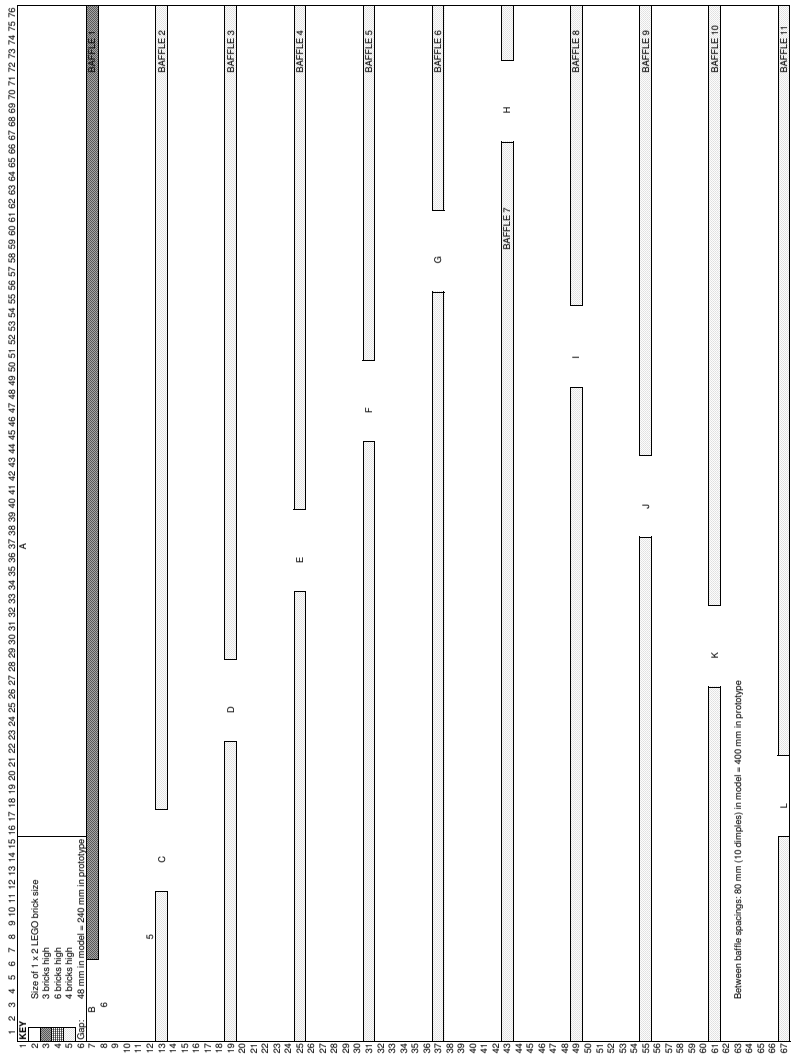

(b) Plan (i.e. rotated)

Figure D–41: Rotated-V: LEGO layout 6.5

E. Perspex fish pass: velocity distributions

Table E–1: Significant field flow rates and generalised flow rates per unit width

Percentile low flow	Flow rate/ unit width ($m^3s^{-1}/m = m^2s^{-1}$)
Q90	0.067
Q50	0.236
Q30	0.392
Q10	0.680

Note that although Swimit versions 1.11 and 2.0 (on which the burst swimming speeds are based) have been used throughout this thesis, the latest version, Swimit version 3.2 (Environment Agency 2005) supercedes all previous versions (Clifton-Dey 2006). Details of any analysis using subsequent version(s) of Swimit will be made available at the author's website Servais (2006).

E.1. Equal baffle pairing (1:5, gradient)

E.1.1. Equal baffle pairing: Q50, gradient 1:5

Table E–2: Equal baffle pairing, Q50, Reynolds number, normal

	Model scale					Field scale
Slot No.	Water depth mm	Sample depth mm	Hydraulic radius mm	Mean velocity ms^{-1}	Reynolds No.	Mean velocity ms^{-1}
1	71.03	41.31	12.68	0.71	9007	1.58
2	57.34	36.41	14.46	0.69	9964	1.53
3	53.30	36.41	14.46	0.78	11518	1.75
4	52.17	36.41	14.46	0.86	12719	1.93
5	54.72	36.41	14.46	0.88	12184	1.97
6	60.69	36.41	14.46	0.77	10592	1.71
7	59.13	36.41	14.46	0.71	9891	1.60
8	53.51	36.41	14.46	0.74	10275	1.66
9	50.98	36.41	14.46	0.69	10200	1.55
10	53.96	31.51	13.61	0.75	10073	1.68
11	NaN	31.51	13.61	0.78	10458	1.74

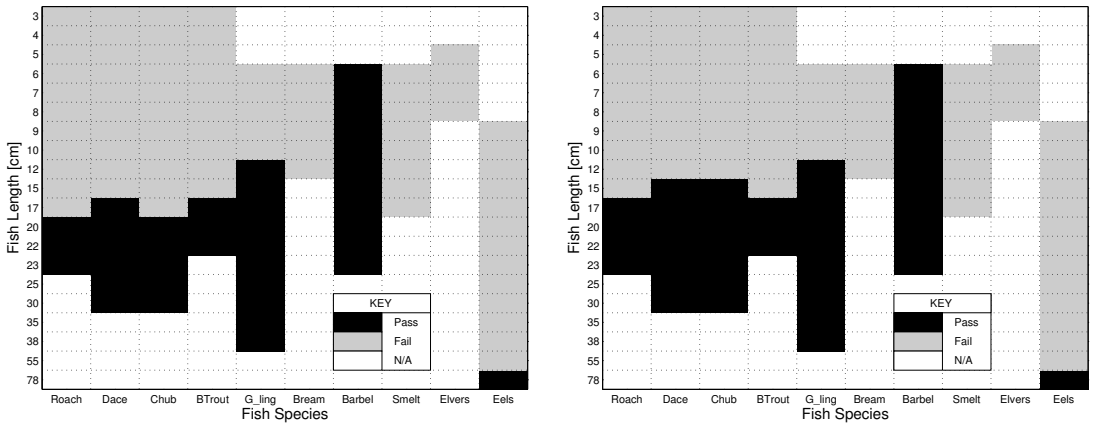

(a) 10 °C (b) 15 °C

Figure E–1: Equal baffle pairing: Q50, gradient 1:5, 10 °C and 15 °C, Slot 1 to 11

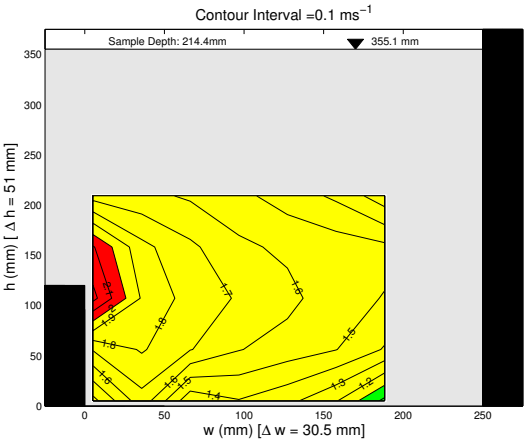

(a) Slot 1

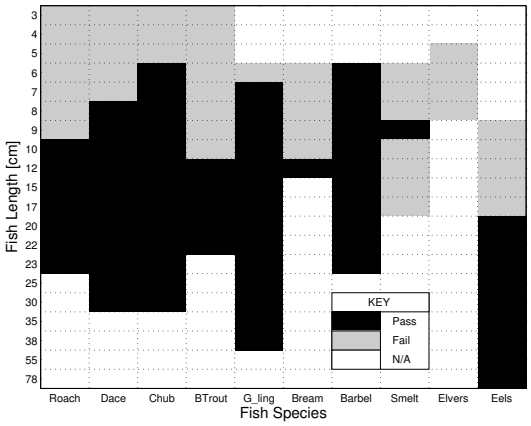

(b) Slot 1

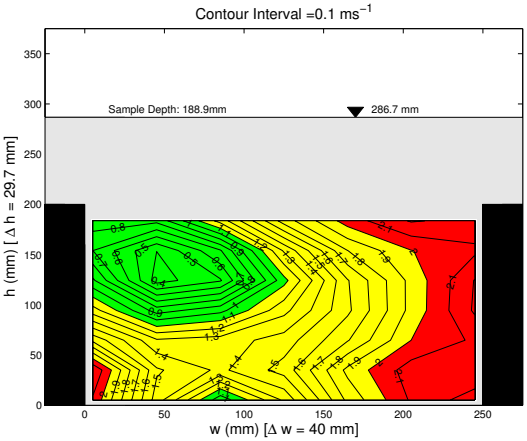

(c) Slot 2

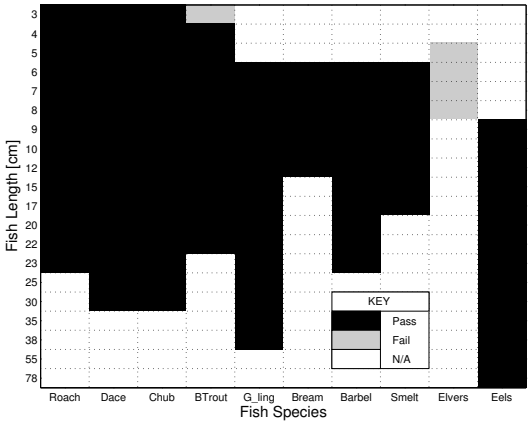

(d) Slot 2

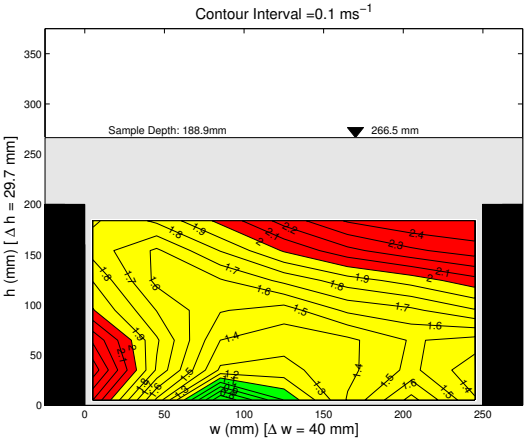

(e) Slot 3

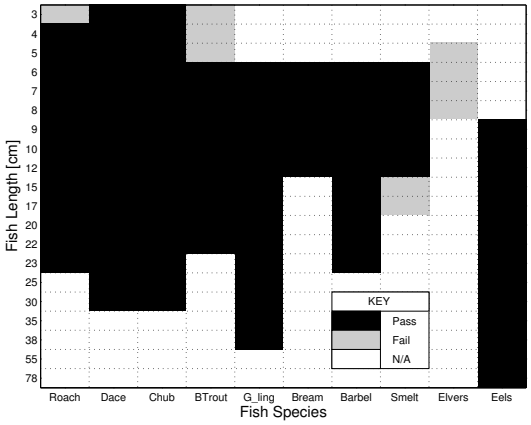

(f) Slot 3

Figure E–2: Equal baffle pairing: Q50, gradient 1:5, 15 °C, Slot 1 to 3

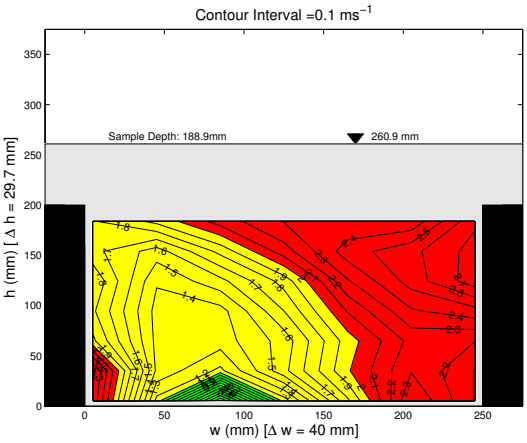

(a) Slot 4

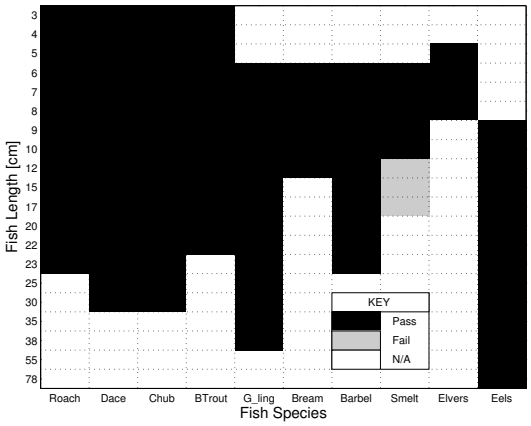

(b) Slot 4

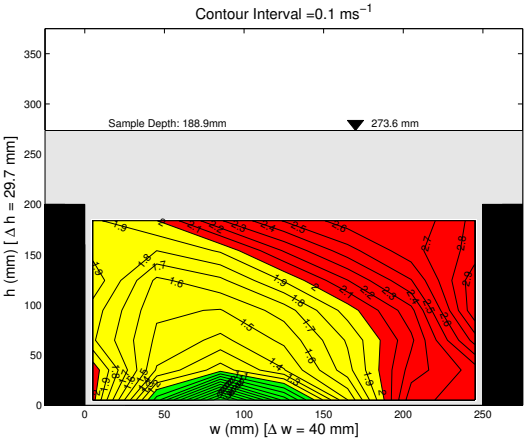

(c) Slot 5

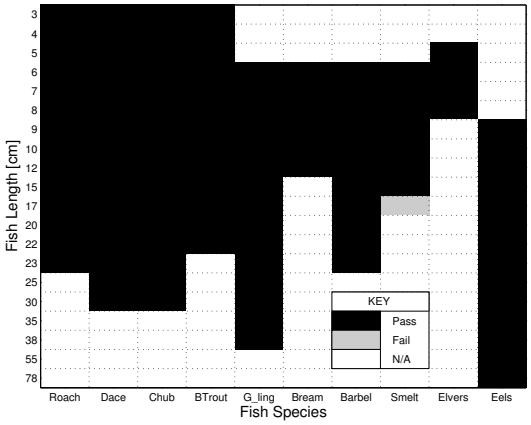

(d) Slot 5

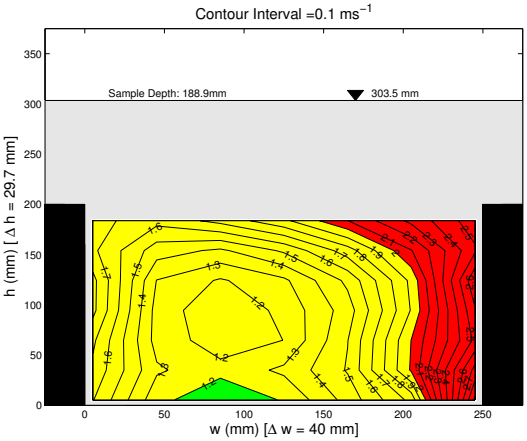

(e) Slot 6

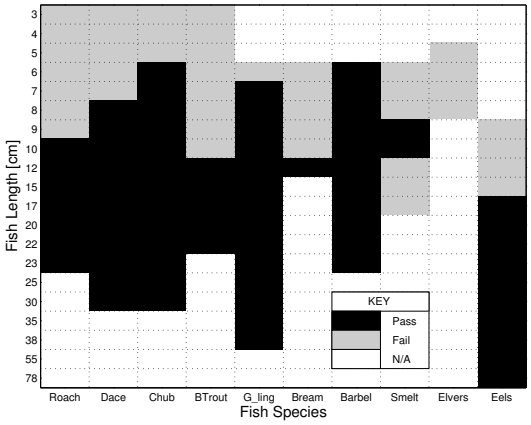

(f) Slot 6

Figure E–3: Equal baffle pairing: Q50, gradient 1:5, 15 °C, Slot 4 to 6

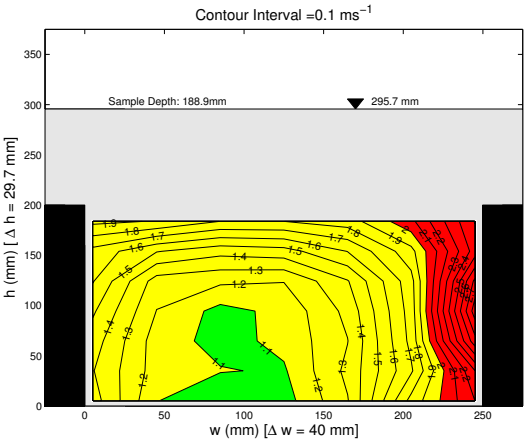

(a) Slot 7

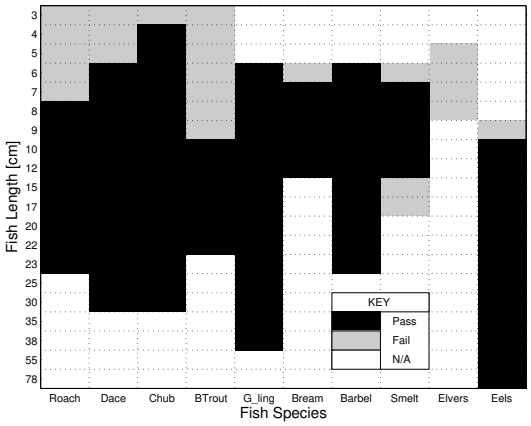

(b) Slot 7

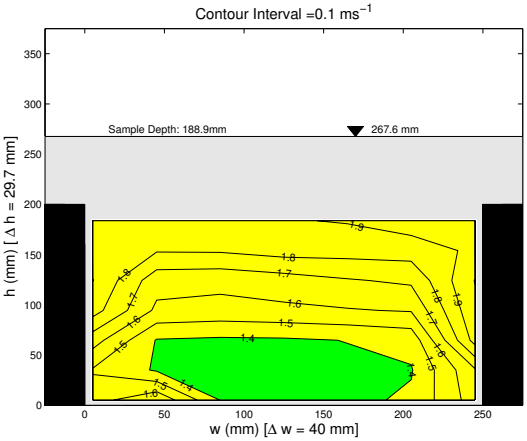

(c) Slot 8

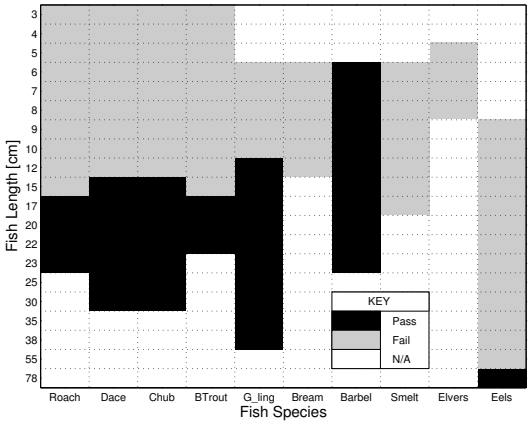

(d) Slot 8

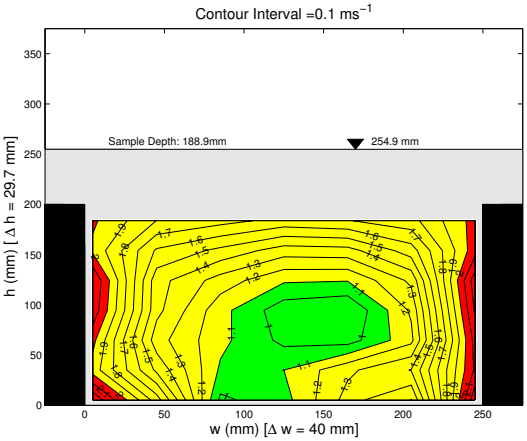

(e) Slot 9

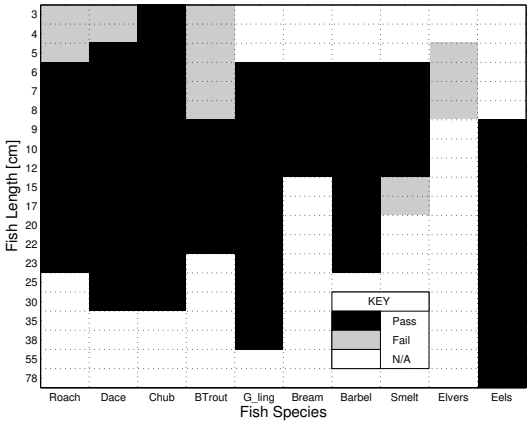

(f) Slot 9

Figure E–4: Equal baffle pairing: Q50, gradient 1:5, 15 °C, Slot 7 to 9

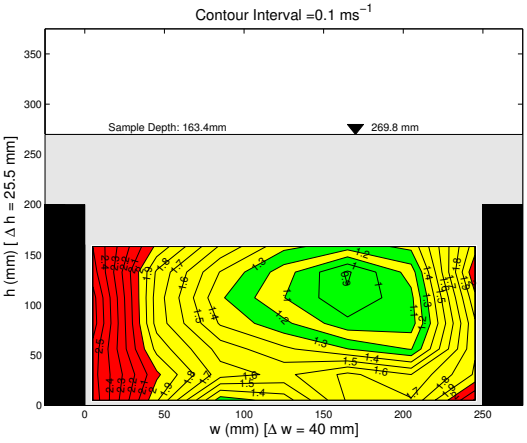

(a) Slot 10

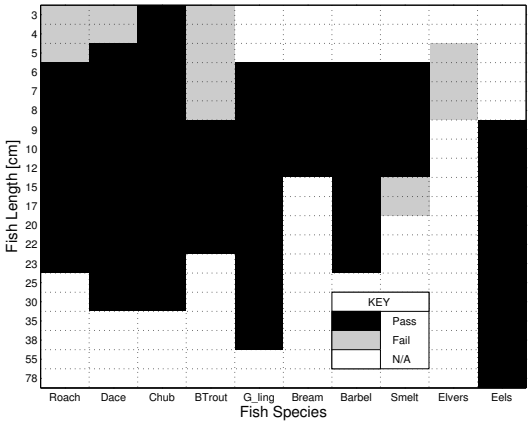

(b) Slot 10

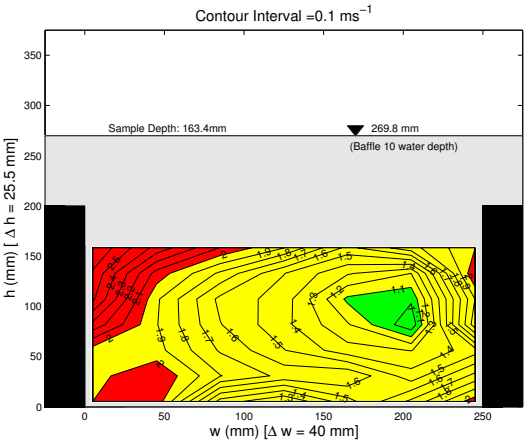

(c) Slot 11

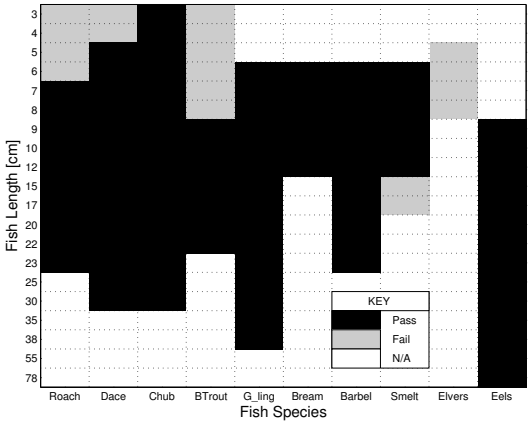

(d) Slot 11

Figure E–5: Equal baffle pairing: Q50, gradient 1:5, 15 °C, Slot 10 to 11

E.1.2. Equal baffle pairing: Q90, gradient 1:5

Table E–3: Equal baffle pairing, Q90, Reynolds number, normal

	Model scale					Field scale
Slot No.	Water depth mm	Sample depth mm	Hydraulic radius mm	Mean velocity ms^{-1}	Reynolds No.	Mean velocity ms^{-1}
1	43.33	26.60	10.00	0.59	5356	1.32
2	46.38	31.51	12.23	0.51	5711	1.14
3	46.35	31.51	12.23	0.54	6072	1.21
4	47.49	31.51	13.61	0.45	5661	1.01
5	45.14	31.51	13.61	0.54	6990	1.22
6	45.69	31.51	13.61	0.52	6704	1.17
7	47.48	31.51	13.61	0.52	6674	1.16
8	39.17	31.51	13.61	0.51	6502	1.13
9	40.20	31.51	13.61	0.37	4749	0.84
10	40.92	31.51	13.61	0.38	4807	0.85
11	NaN	31.51	13.61	0.39	4978	0.88

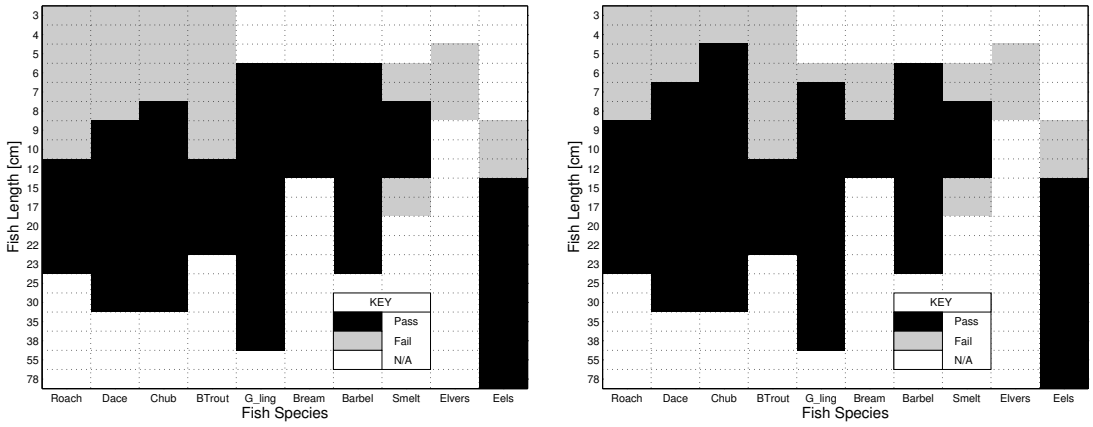

(a) 10 °C (b) 15 °C

Figure E–6: Equal baffle pairing: Q90, gradient 1:5, 10 °C and 15 °C, Slot 1 to 11

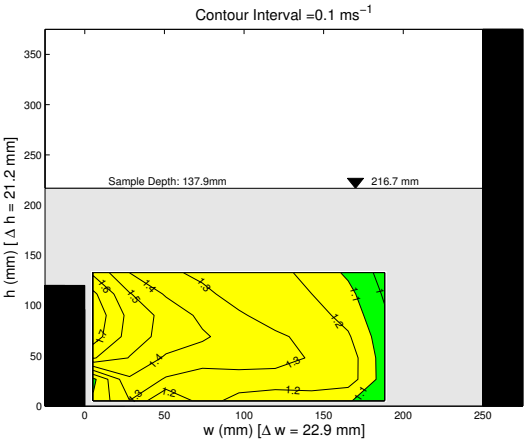

(a) Slot 1

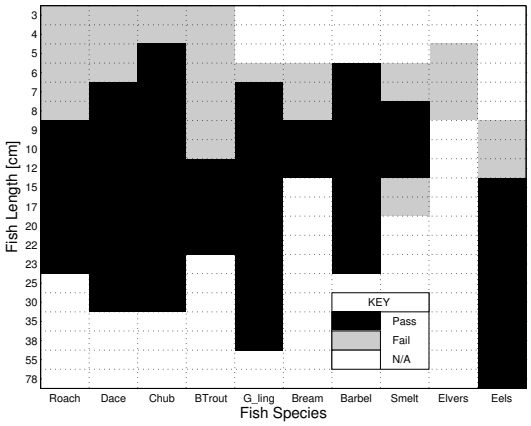

(b) Slot 1

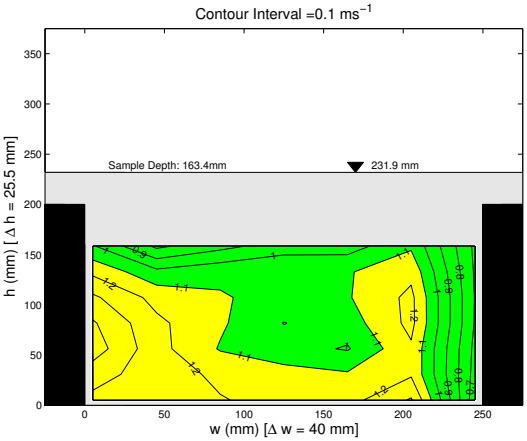

(c) Slot 2

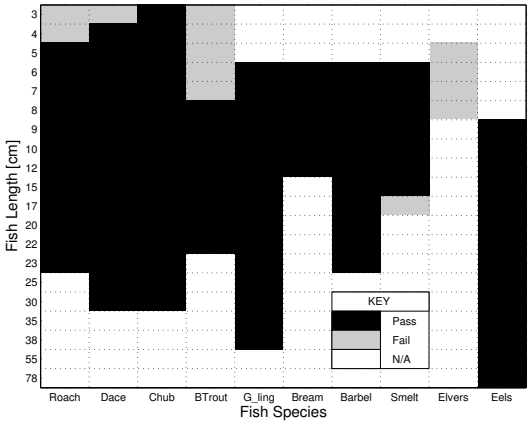

(d) Slot 2

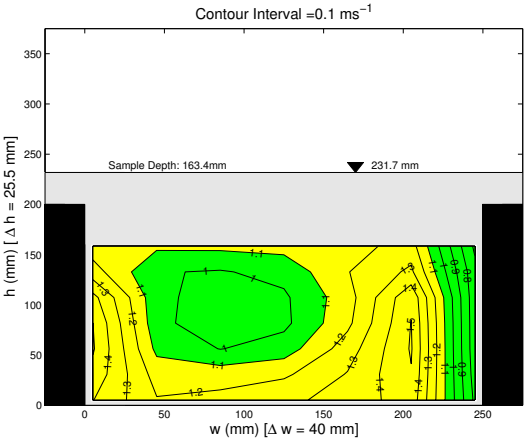

(e) Slot 3

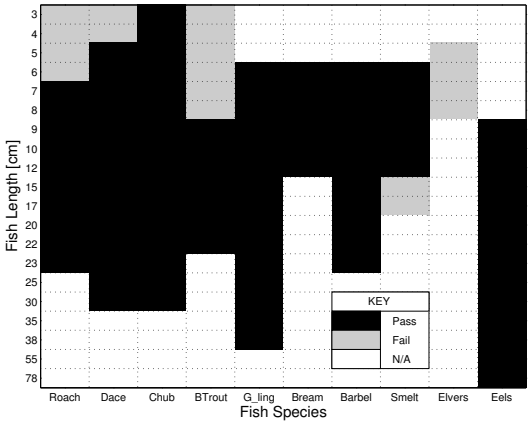

(f) Slot 3

Figure E–7: Equal baffle pairing: Q90, gradient 1:5, 15 °C, Slot 1 to 3

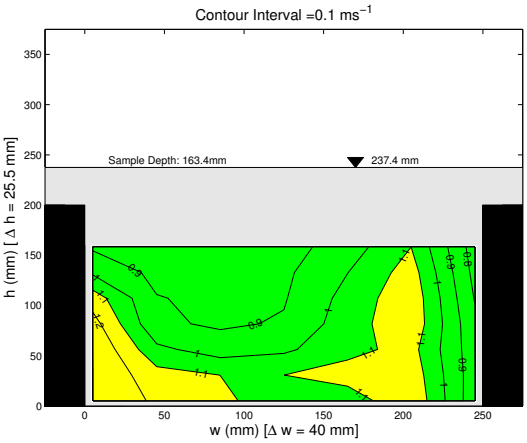

(a) Slot 4

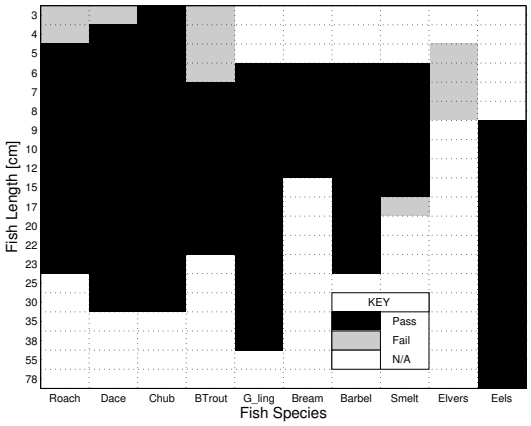

(b) Slot 4

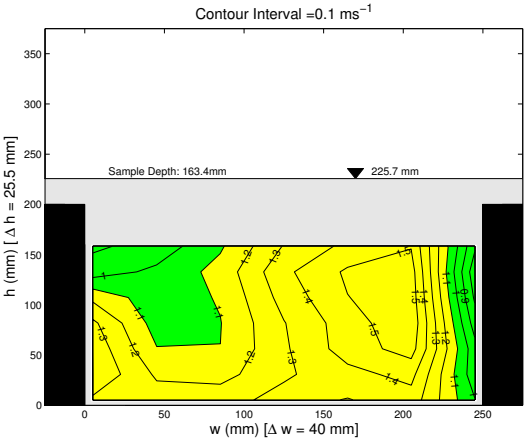

(c) Slot 5

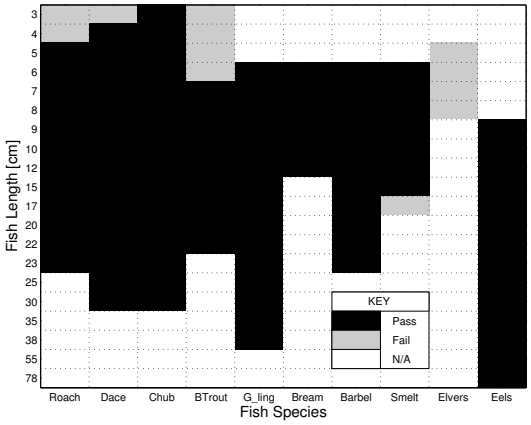

(d) Slot 5

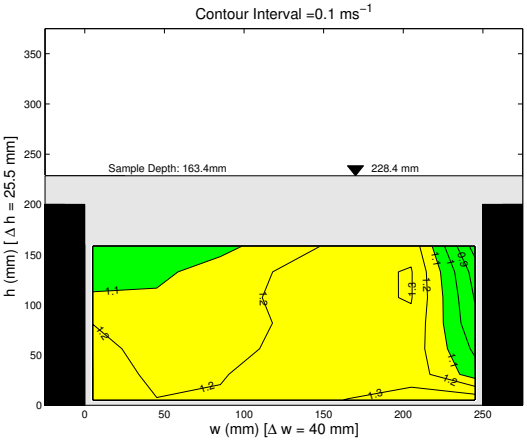

(e) Slot 6

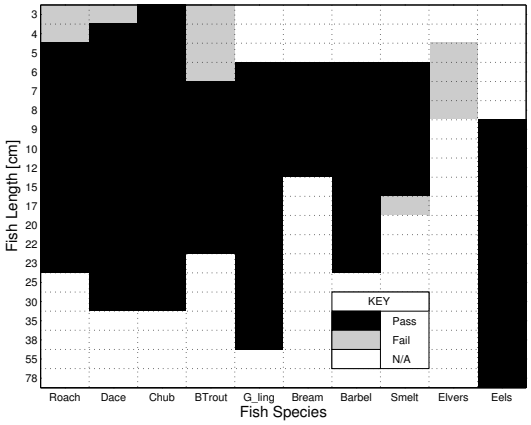

(f) Slot 6

Figure E–8: Equal baffle pairing: Q90, gradient 1:5, 15 °C, Slot 4 to 6

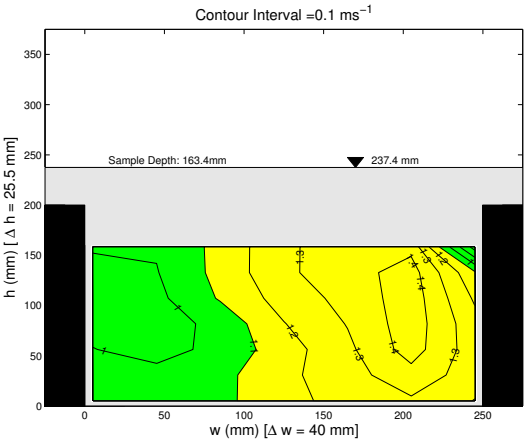

(a) Slot 7

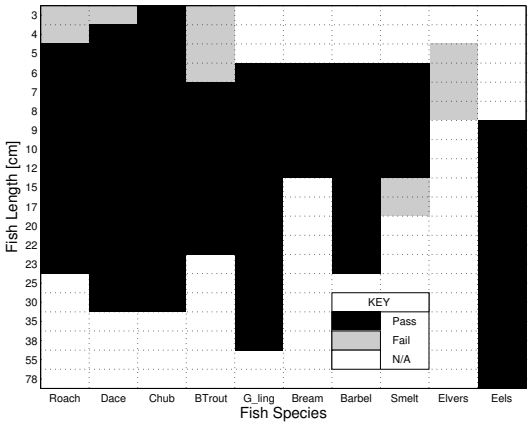

(b) Slot 7

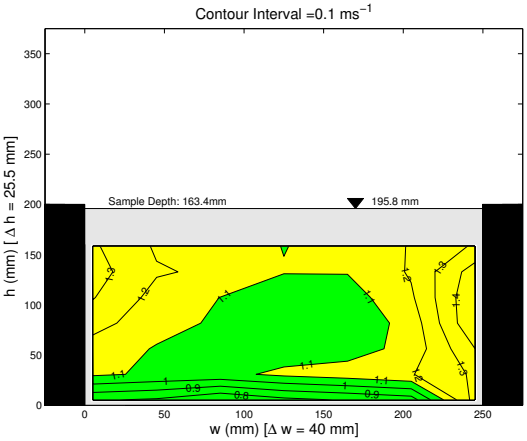

(c) Slot 8

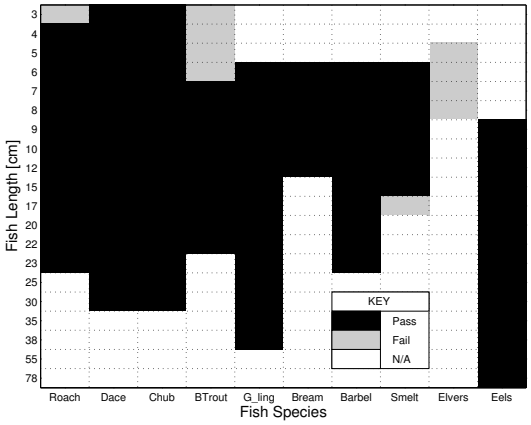

(d) Slot 8

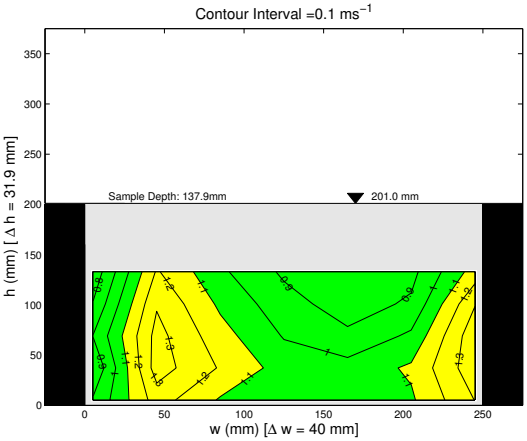

(e) Slot 9

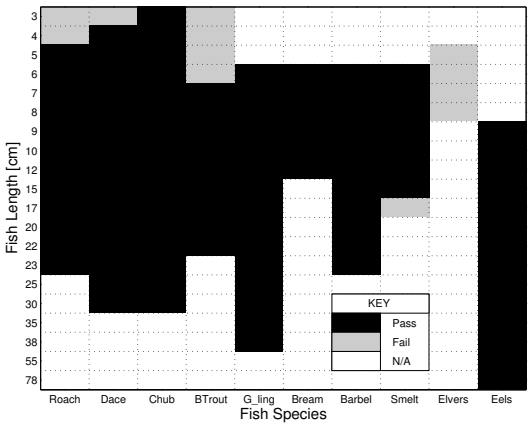

(f) Slot 9

Figure E–9: Equal baffle pairing: Q90, gradient 1:5, 15 °C, Slot 7 to 9

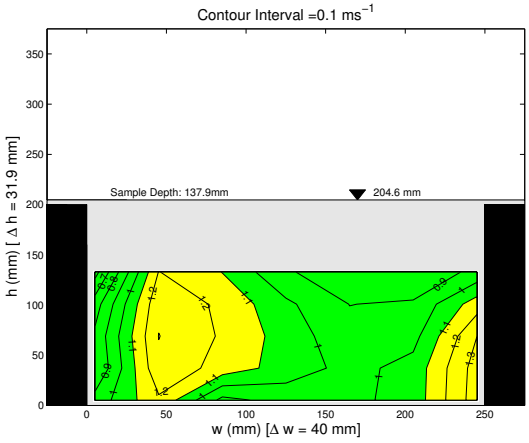

(a) Slot 10

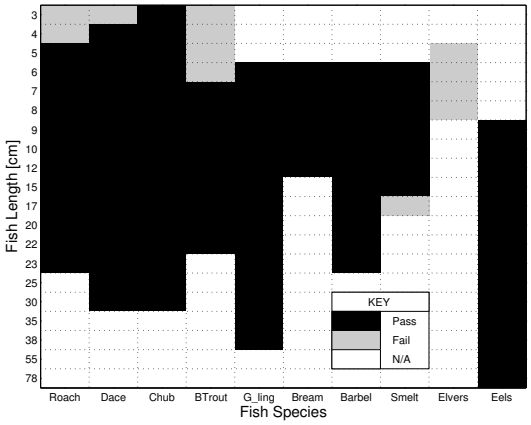

(b) Slot 10

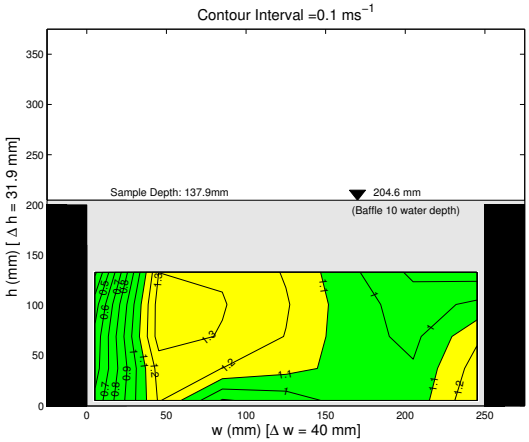

(c) Slot 11

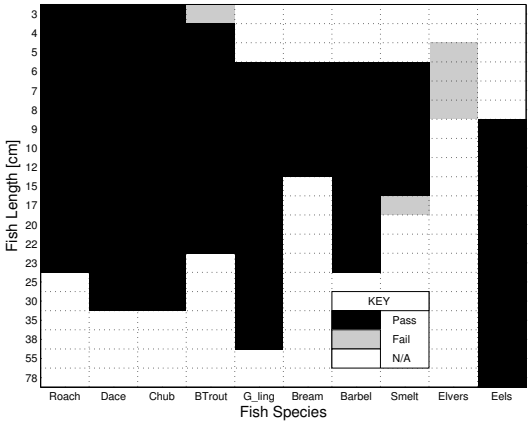

(d) Slot 11

Figure E–10: Equal baffle pairing: Q90, gradient 1:5, 15 °C, Slot 10 to 11

E.2. Unequal baffle pairing (1:5, gradient)

E.2.1. Unequal baffle pairing: Q10, gradient 1:5

Table E–4: Unequal baffle pairing, Q10, Reynolds number, normal

	Model scale					Field scale
Slot No.	Water depth mm	Sample depth mm	Hydraulic radius mm	Mean velocity ms^{-1}	Reynolds No.	Mean velocity ms^{-1}
1	90.91	68.72	16.79	0.83	13532	1.86
2	90.71	68.72	17.77	0.98	17080	2.19
3	85.41	58.91	17.04	0.92	15475	2.06
4	82.02	54.01	16.60	0.97	15826	2.17
5	84.00	49.11	16.11	0.87	13551	1.94
6	83.82	49.11	16.11	0.79	12639	1.77
7	80.98	49.11	16.11	0.80	13026	1.78
8	68.48	49.11	16.11	1.01	16726	2.26
9	89.25	49.11	16.11	0.76	12824	1.70
10	78.29	54.01	16.60	1.13	19440	2.54
11	76.60	51.12	16.32	0.88	14775	1.96
12	NaN	49.11	16.11	0.83	13828	1.86

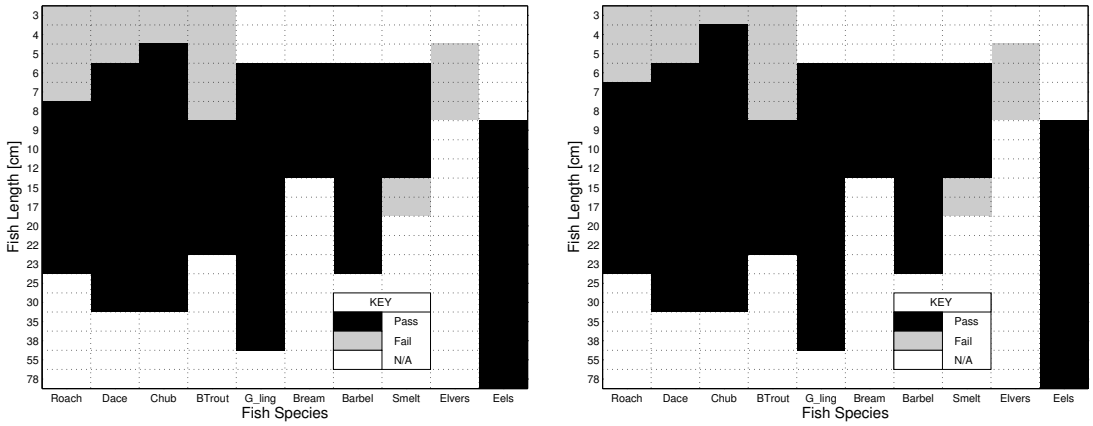

(a) 10 °C (b) 15 °C

Figure E–11: Unequal baffle pairing: Q10, gradient 1:5, 10 °C and 15 °C, Slot 1 to 12

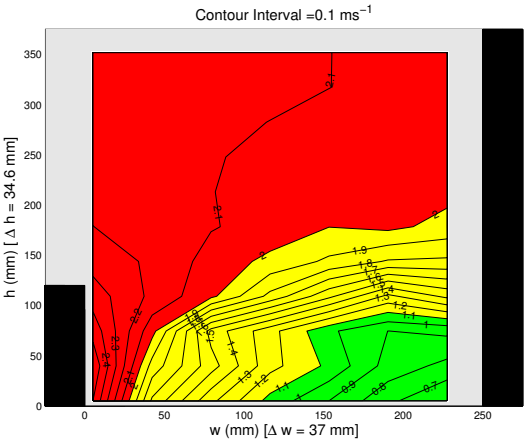

(a) Slot 1

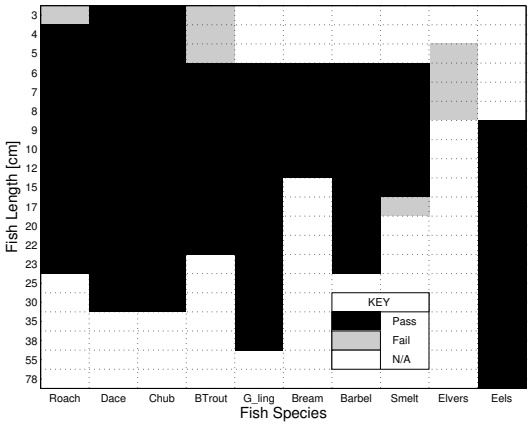

(b) Slot 1

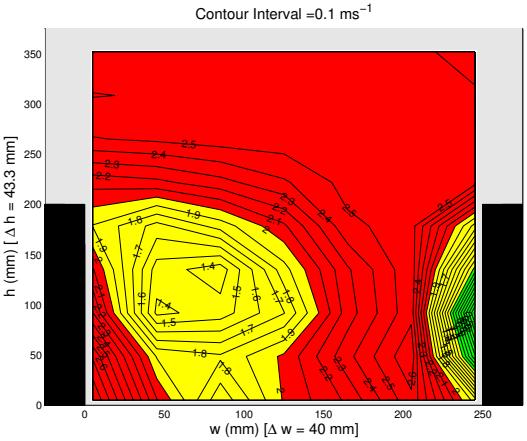

(c) Slot 2

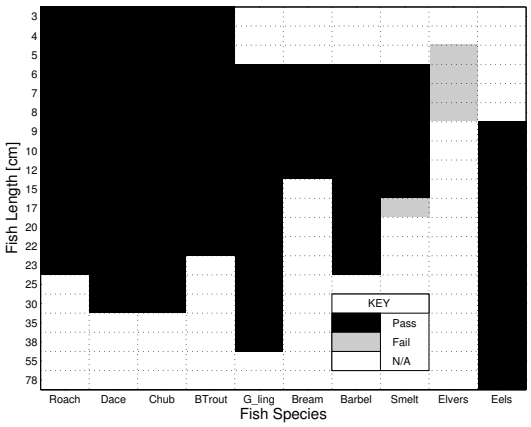

(d) Slot 2

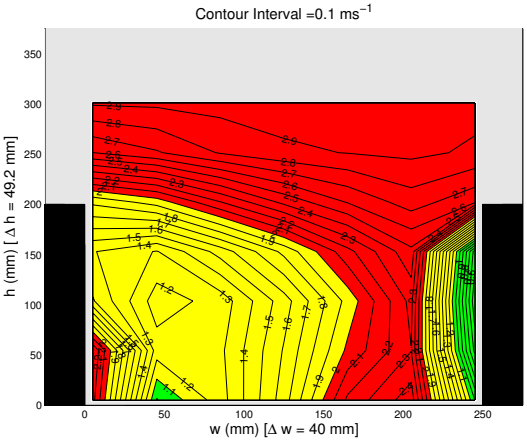

(e) Slot 3

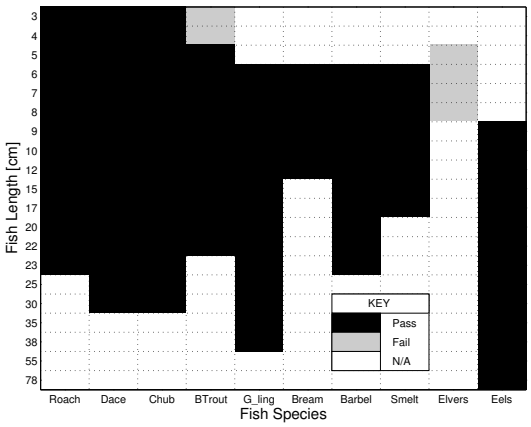

(f) Slot 3

Figure E–12: Unequal baffle pairing: Q10, gradient 1:5, 15 °C, Slot 1 to 3

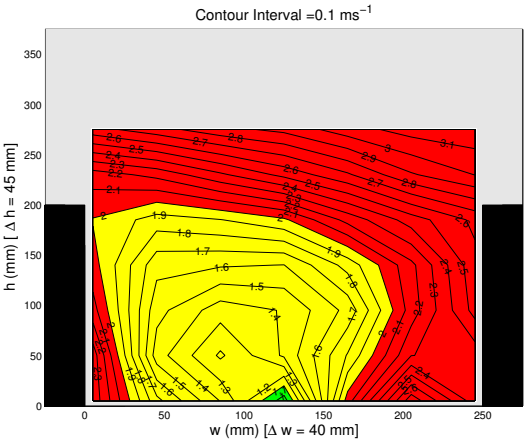

(a) Slot 4

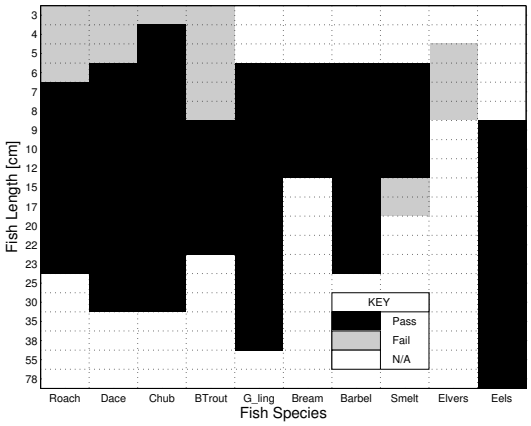

(b) Slot 4

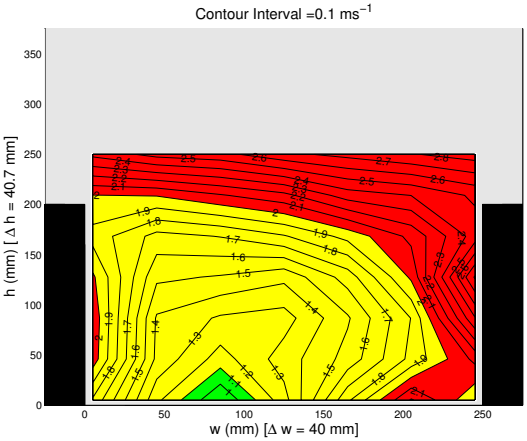

(c) Slot 5

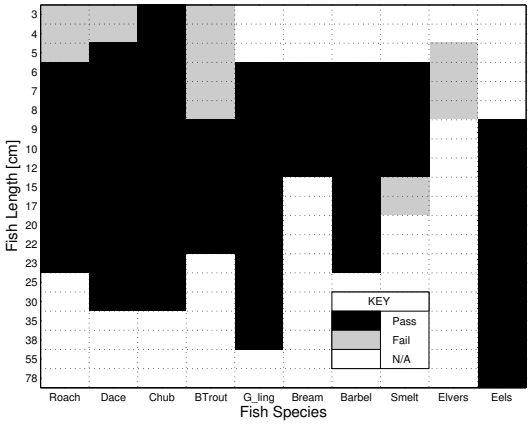

(d) Slot 5

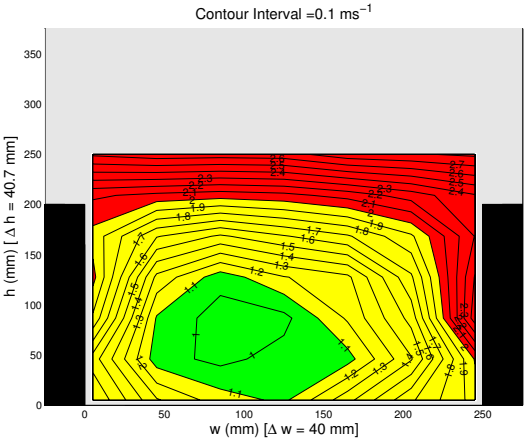

(e) Slot 6

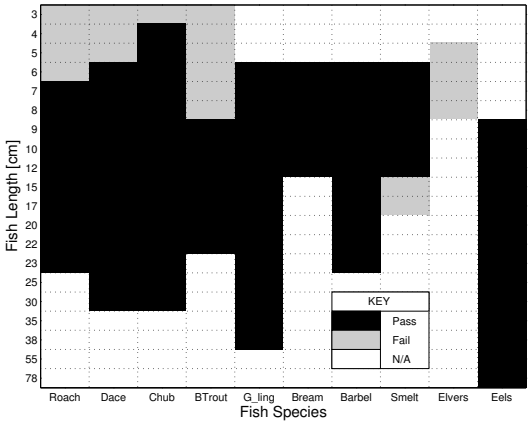

(f) Slot 6

Figure E–13: Unequal baffle pairing: Q10, gradient 1:5, 15 °C, Slot 4 to 6

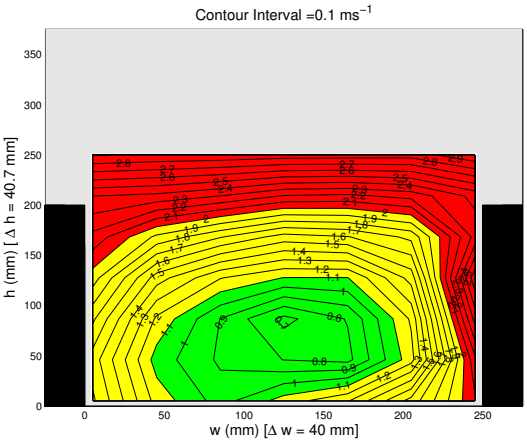

(a) Slot 7

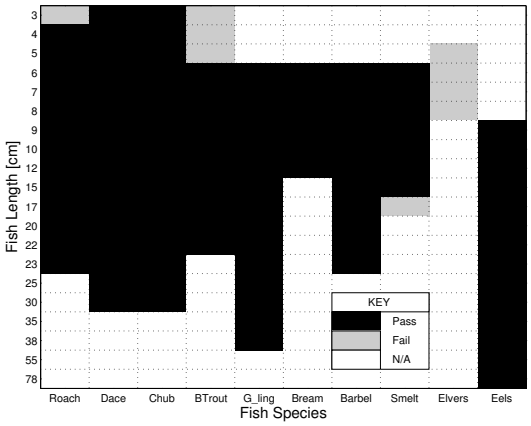

(b) Slot 7

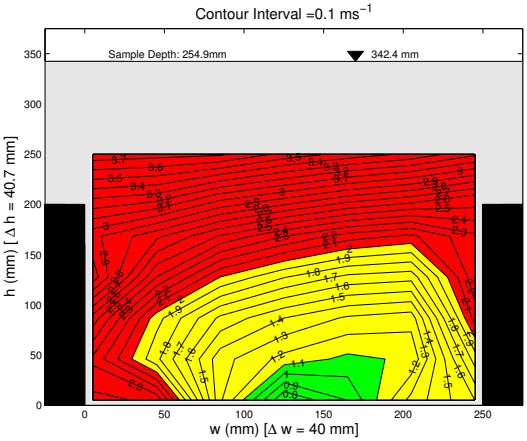

(c) Slot 8

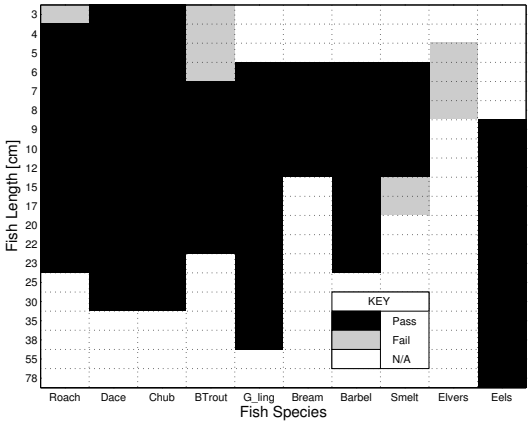

(d) Slot 8

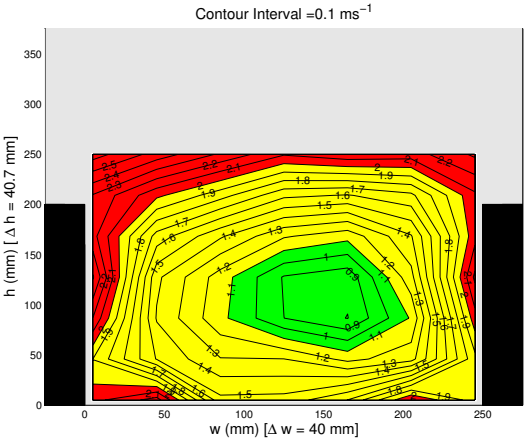

(e) Slot 9

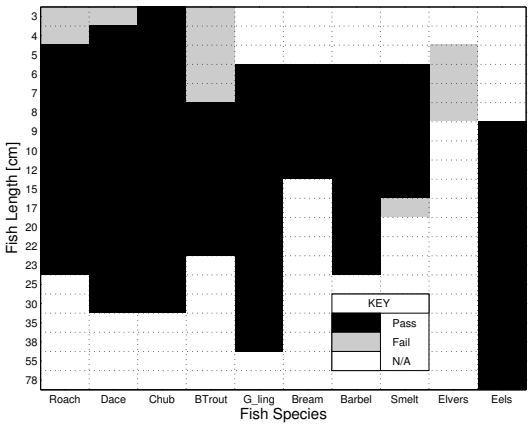

(f) Slot 9

Figure E–14: Unequal baffle pairing: Q10, gradient 1:5, 15 °C, Slot 7 to 9

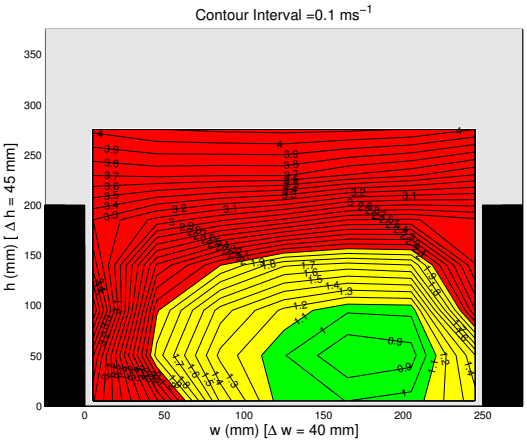

(a) Slot 10

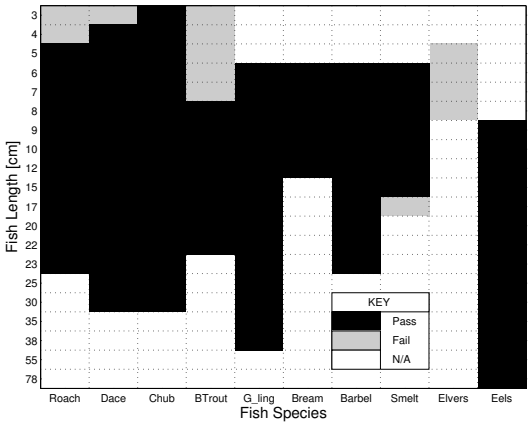

(b) Slot 10

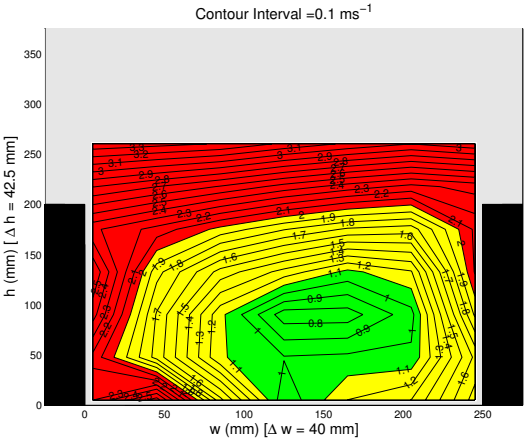

(c) Slot 11

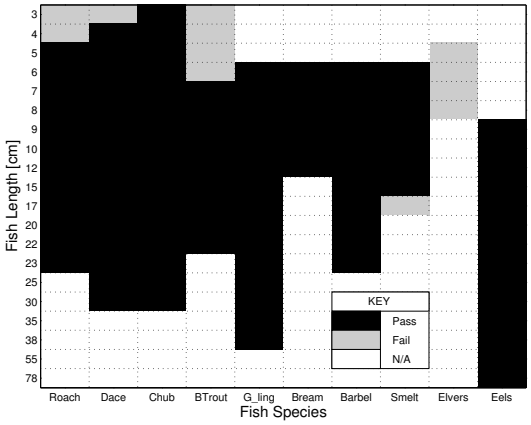

(d) Slot 11

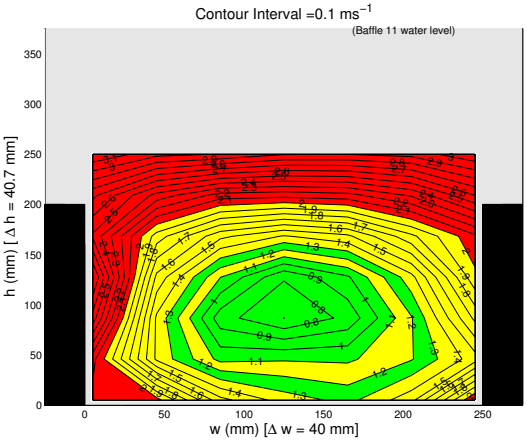

(e) Slot 12

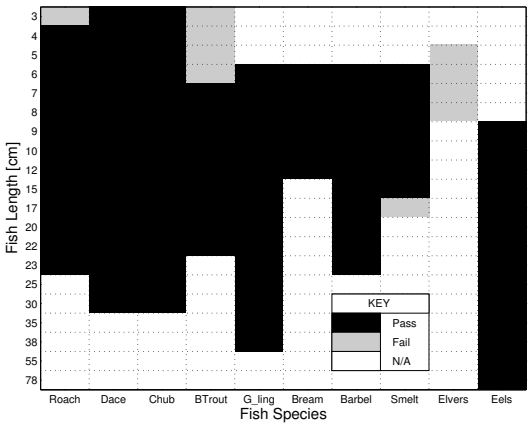

(f) Slot 12

Figure E–15: Unequal baffle pairing: Q10, gradient 1:5, 15 °, Slot 10 to 12

E.2.2. Unequal baffle pairing: Q30, gradient 1:5

Table E–5: Unequal baffle pairing, Q30, Reynolds number, normal

	Model scale					Field scale
Slot No.	Water depth mm	Sample depth mm	Hydraulic radius mm	Mean velocity ms^{-1}	Reynolds No.	Mean velocity ms^{-1}
1	64.76	41.31	14.45	0.77	11101	1.71
2	70.28	49.11	16.11	0.72	11793	1.60
3	66.24	41.31	15.17	0.82	12834	1.83
4	64.56	41.31	15.17	0.89	13995	2.00
5	65.08	41.31	15.17	0.84	12980	1.89
6	65.29	41.31	15.17	0.70	10845	1.56
7	63.54	41.31	15.17	0.71	11147	1.59
8	64.46	41.31	15.17	0.69	10756	1.54
9	61.38	41.31	15.17	0.75	11733	1.67
10	61.71	41.31	15.17	0.81	12731	1.82
11	59.08	49.11	16.11	0.90	14560	2.02
12	NaN	39.30	14.89	0.76	11702	1.70

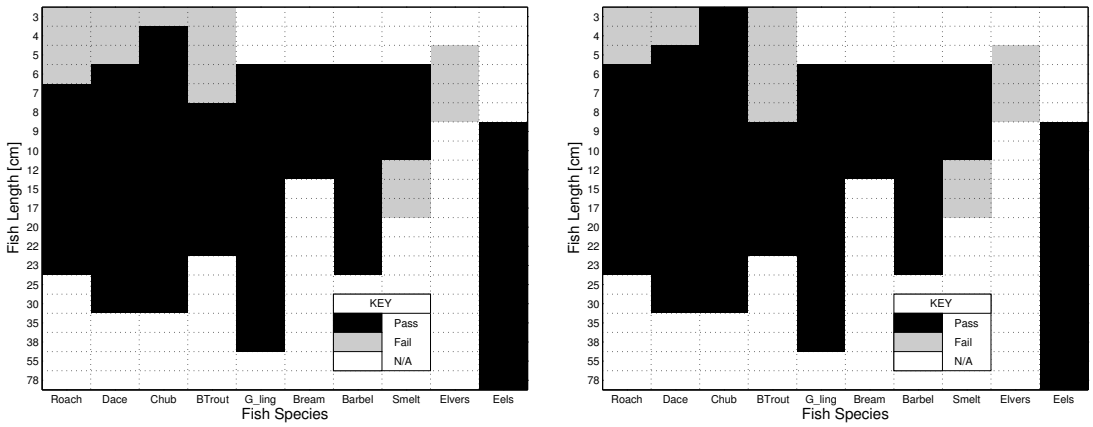

(a) 10 °C (b) 15 °C

Figure E–16: Unequal baffle pairing: Q30, gradient 1:5, 10 °C and 15 °C, Slot 1 to 12

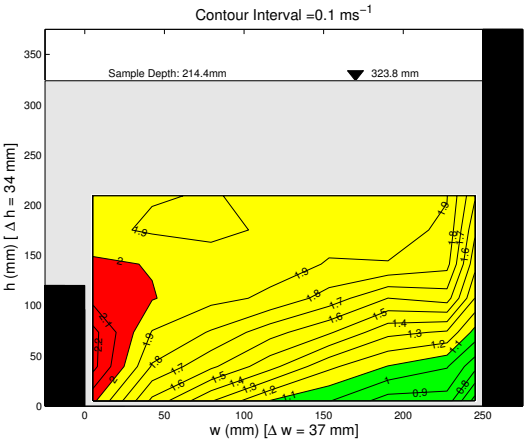

(a) Slot 1

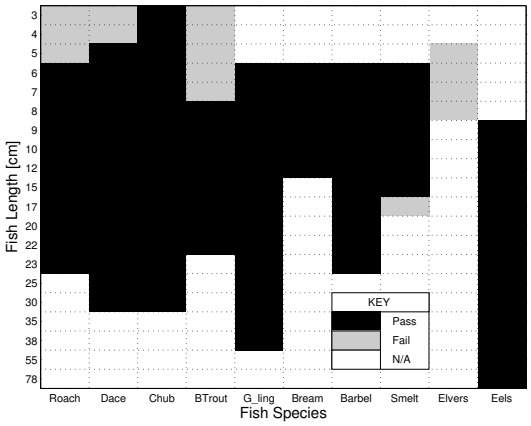

(b) Slot 1

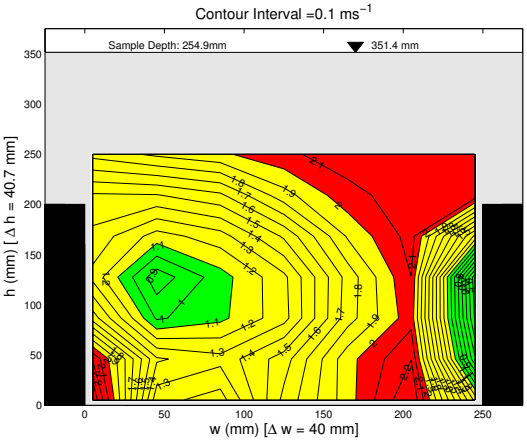

(c) Slot 2

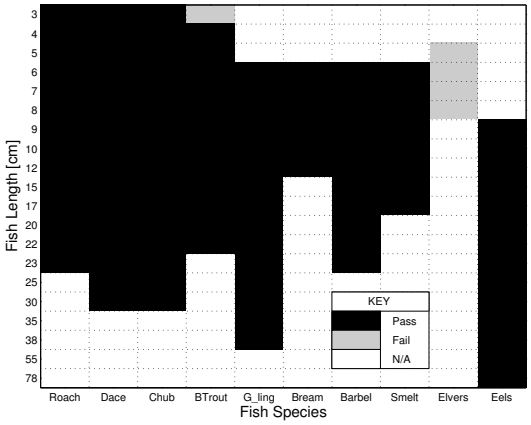

(d) Slot 2

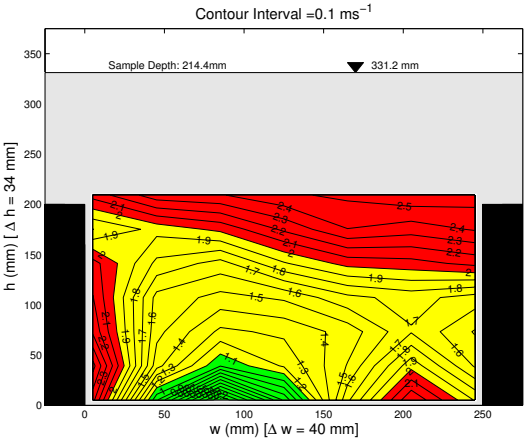

(e) Slot 3

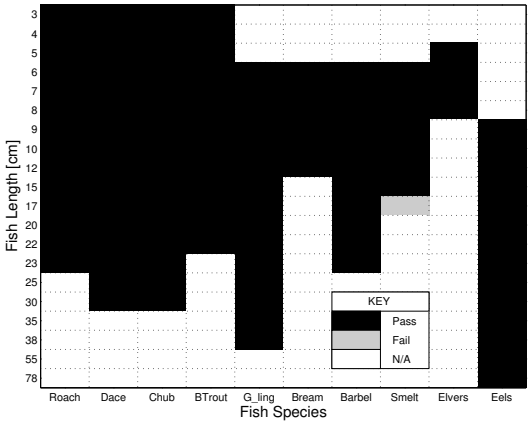

(f) Slot 3

Figure E–17: Unequal baffle pairing: Q30, gradient 1:5, 15 °C, Slot 1 to 3

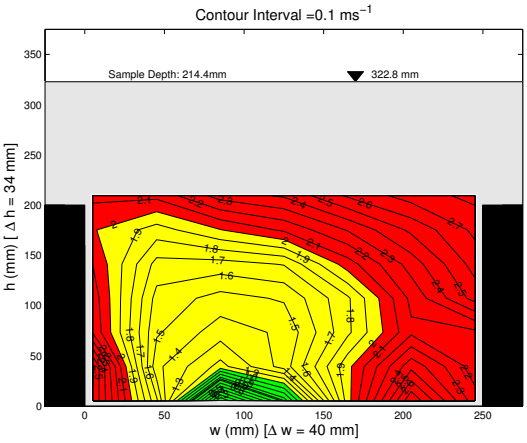

(a) Slot 4

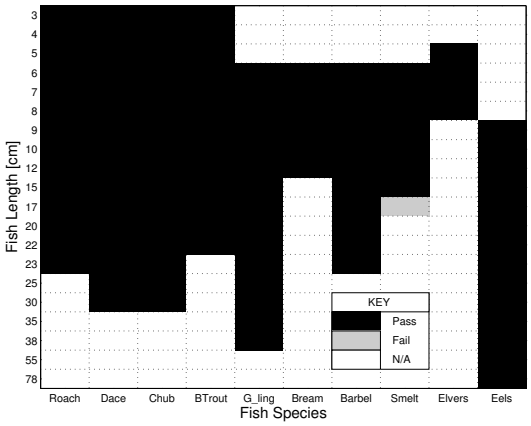

(b) Slot 4

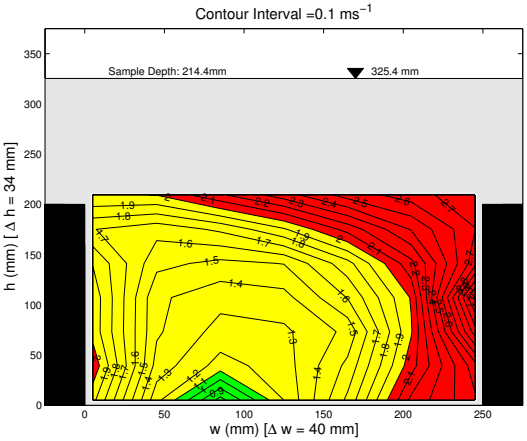

(c) Slot 5

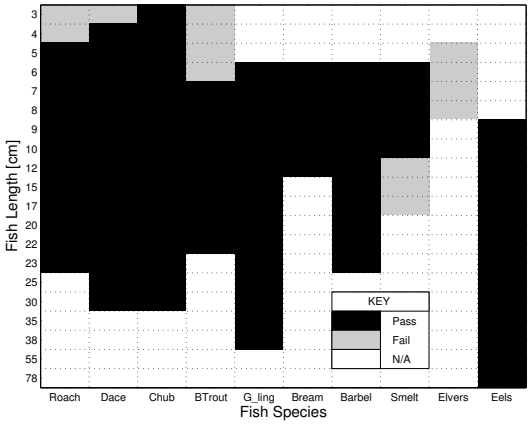

(d) Slot 5

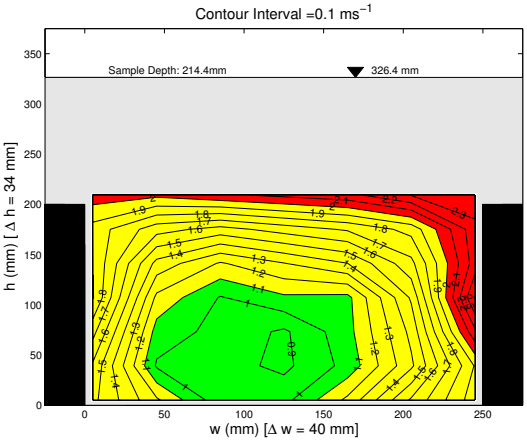

(e) Slot 6

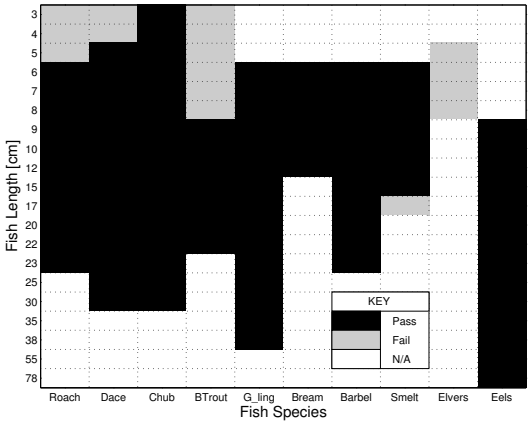

(f) Slot 6

Figure E–18: Unequal baffle pairing: Q30, gradient 1:5, 15 °C, Slot 4 to 6

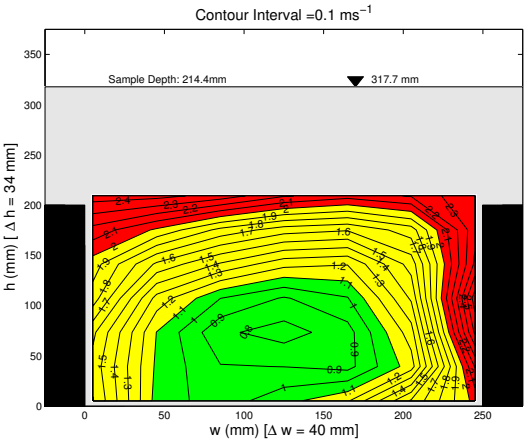

(a) Slot 7

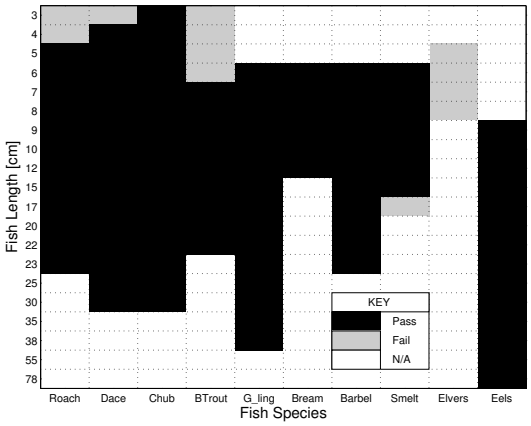

(b) Slot 7

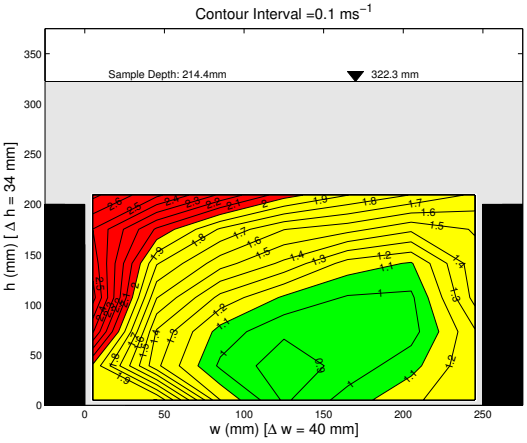

(c) Slot 8

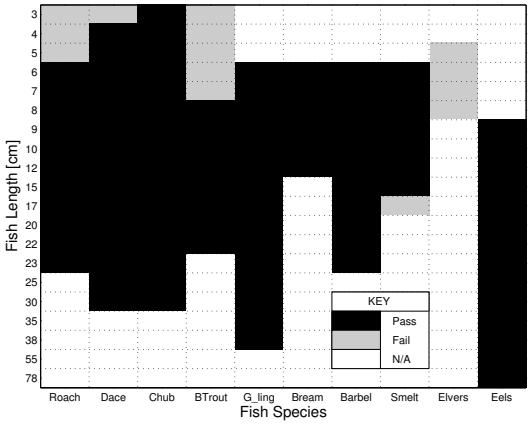

(d) Slot 8

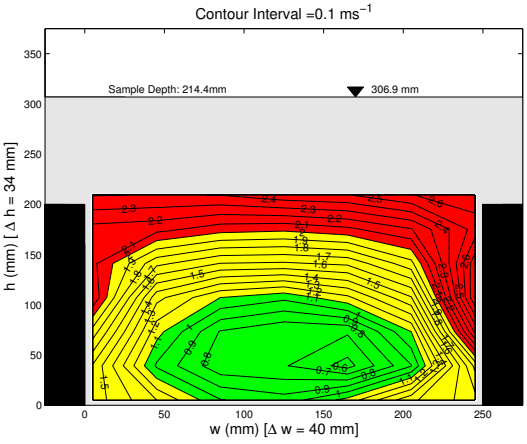

(e) Slot 9

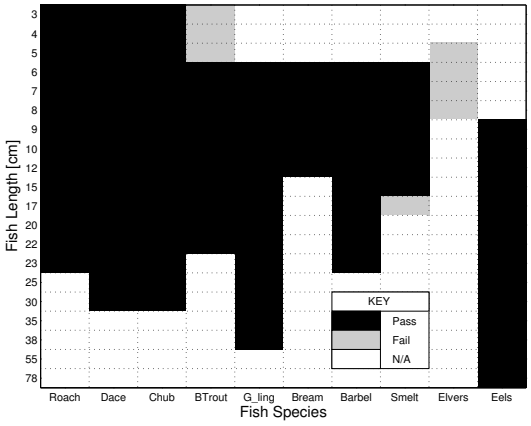

(f) Slot 9

Figure E–19: Unequal baffle pairing: Q30, gradient 1:5, 15 °C, Slot 7 to 9

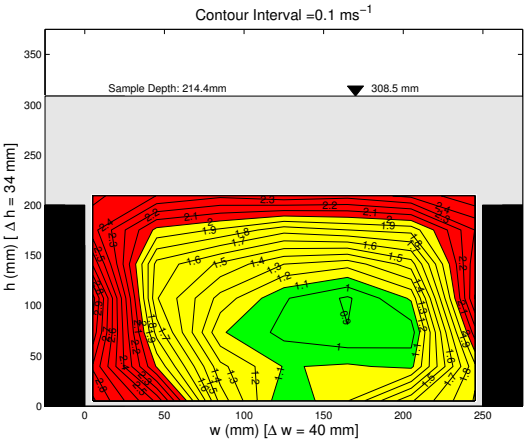

(a) Slot 10

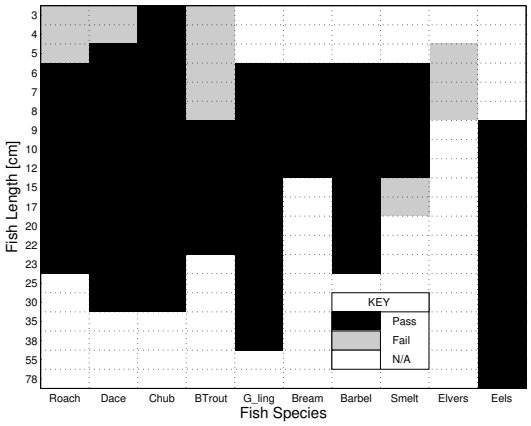

(b) Slot 10

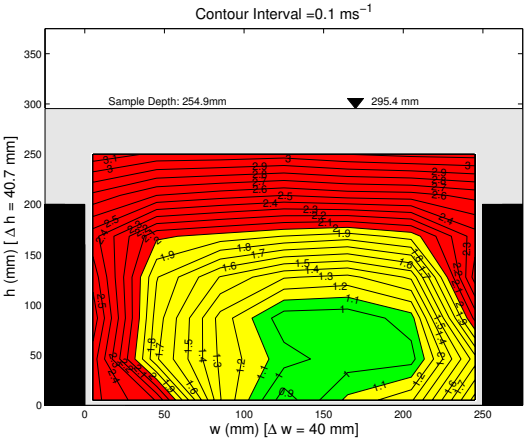

(c) Slot 11

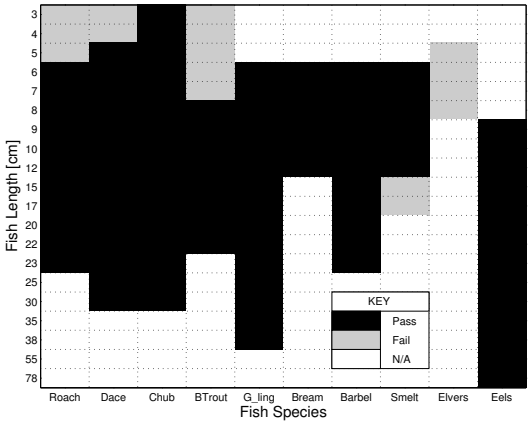

(d) Slot 11

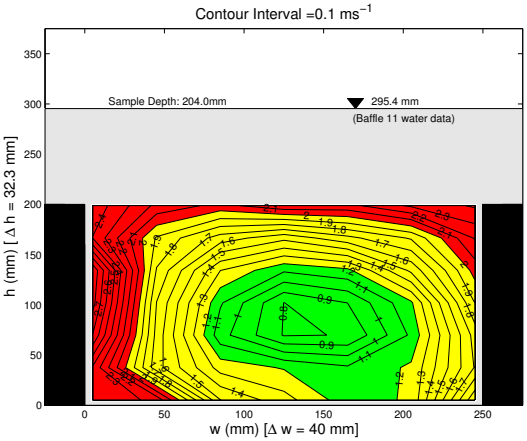

(e) Slot 12

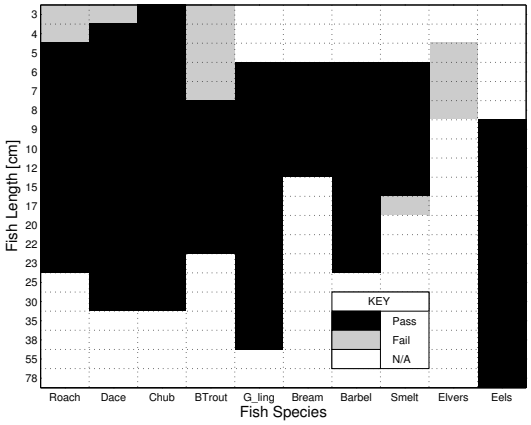

(f) Slot 12

Figure E–20: Unequal baffle pairing: Q30, gradient 1:5, 15 °C, Slot 10 to 12

E.2.3. Unequal baffle pairing: Q50, gradient 1:5

Table 4–7 was included in section 4.2.4, Case Study A.

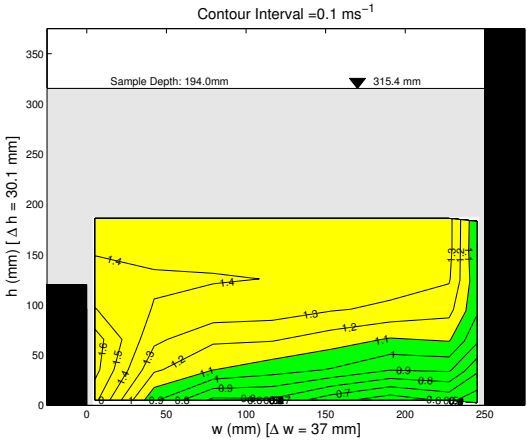

(a) Velocity Distribution: Slot 1

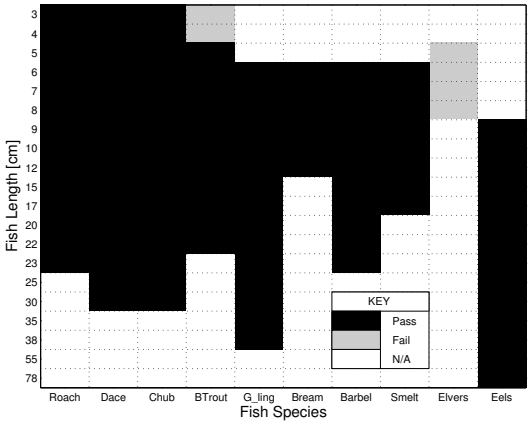

(b) Fish pass efficiency matrix: Slot 1

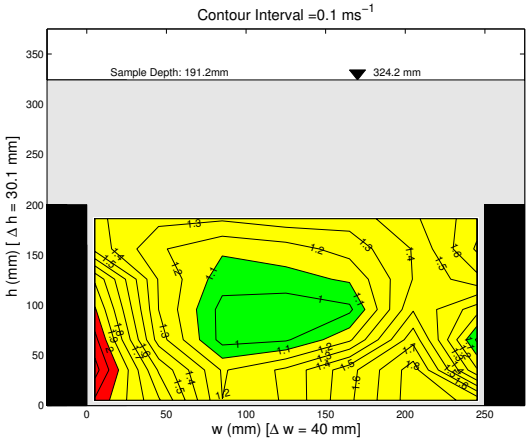

(c) Velocity Distribution: Slot 2

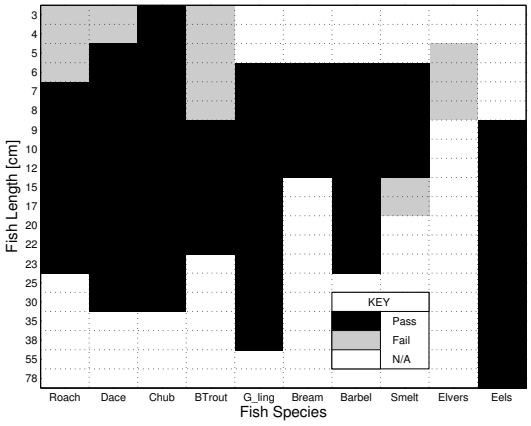

(d) Fish pass efficiency matrix: Slot 2

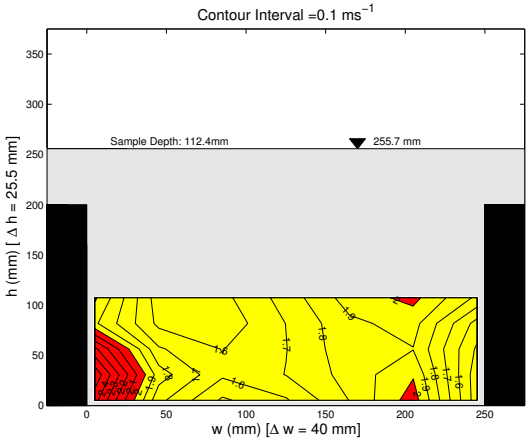

(e) Velocity Distribution: Slot 3

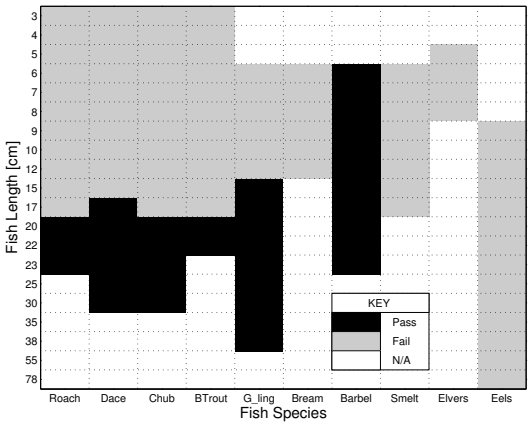

(f) Fish pass efficiency matrix: Slot 3

Figure E–21: Unequal baffle pairing: Q50, gradient 1:5, 15 °C, Slot 1 to 3

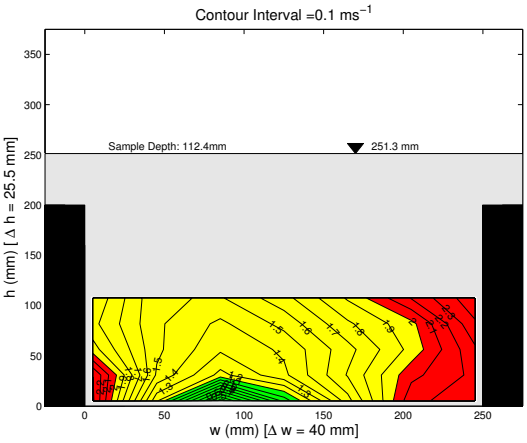

(a) Velocity Distribution: Slot 4

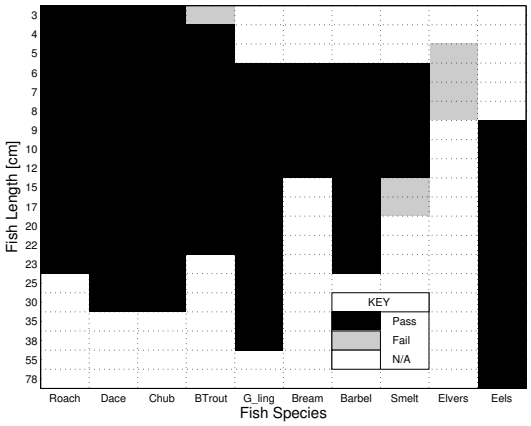

(b) Fish pass efficiency matrix: Slot 4

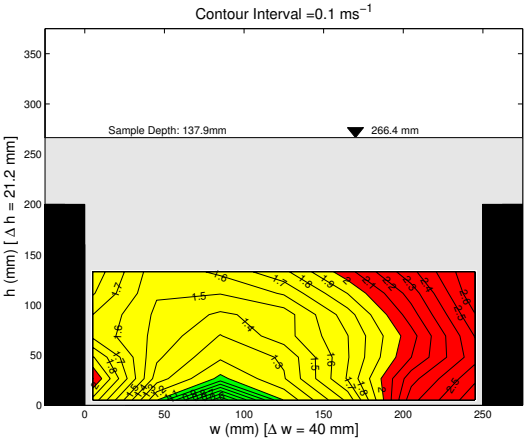

(c) Velocity Distribution: Slot 5

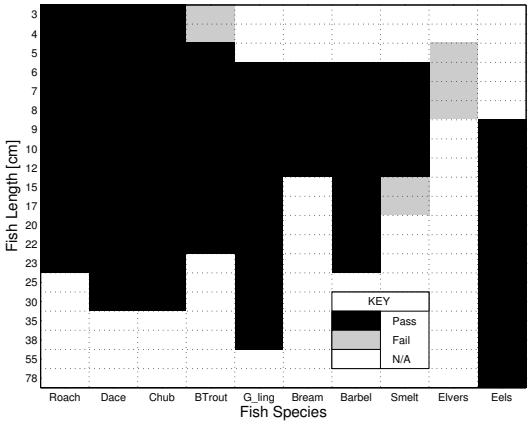

(d) Fish pass efficiency matrix: Slot 5

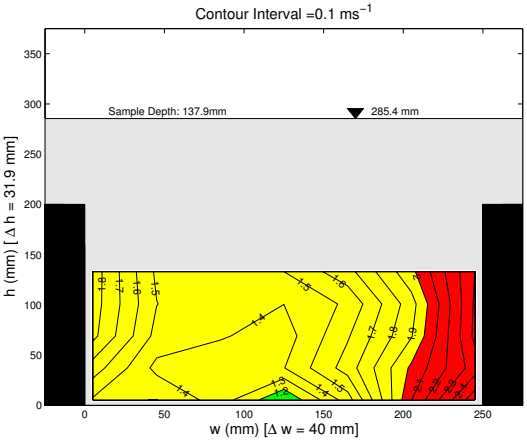

(e) Velocity Distribution: Slot 6

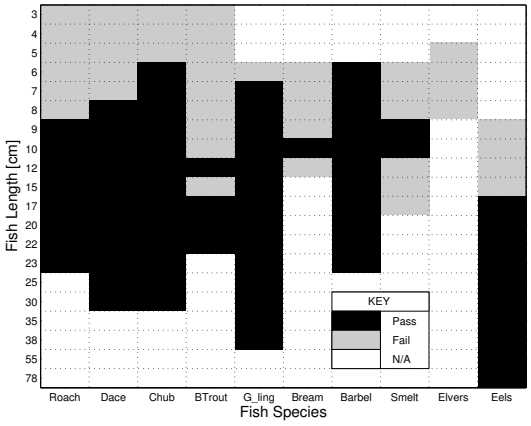

(f) Fish pass efficiency matrix: Slot 6

Figure E–22: Unequal baffle pairing: Q50, gradient 1:5, 15 °C, Slot 4 to 6

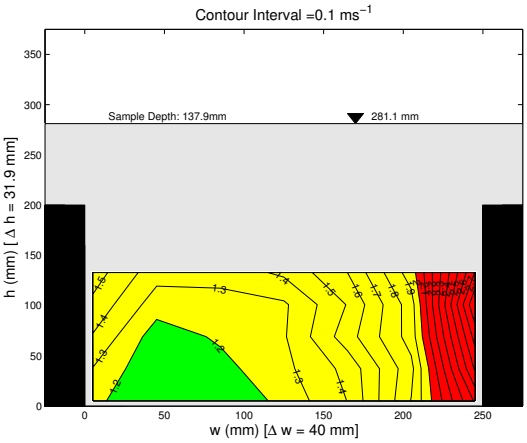

(a) Velocity Distribution: Slot 7

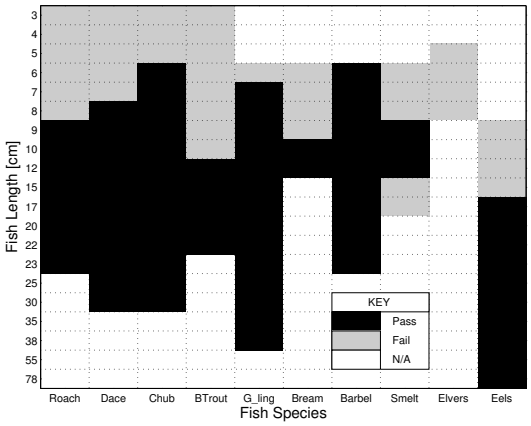

(b) Fish pass efficiency matrix: Slot 7

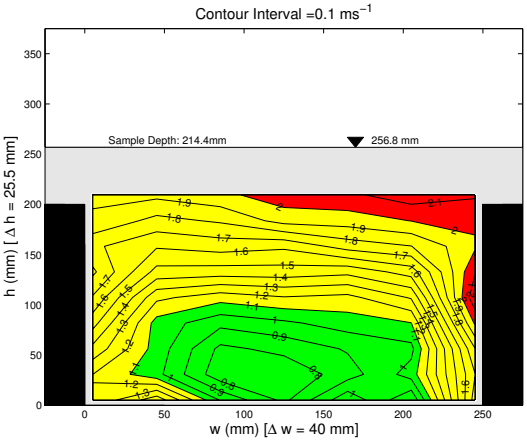

(c) Velocity Distribution: Slot 8

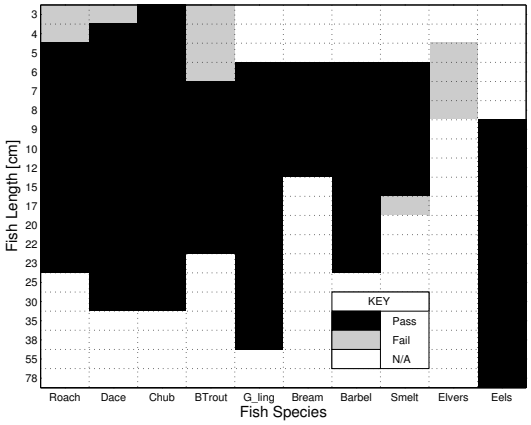

(d) Fish pass efficiency matrix: Slot 8

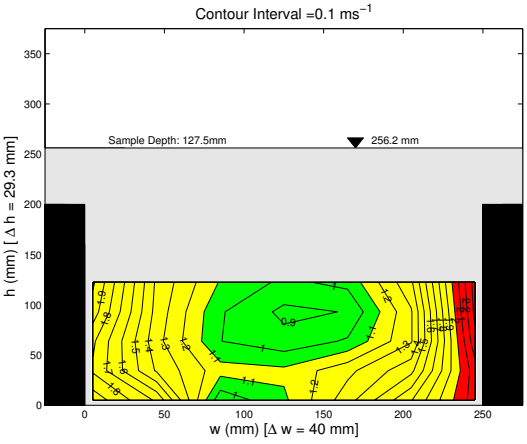

(e) Velocity Distribution: Slot 9

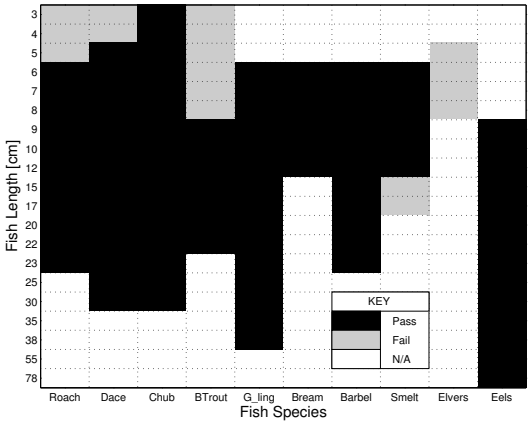

(f) Fish pass efficiency matrix: Slot 9

Figure E–23: Unequal baffle pairing: Q50, gradient 1:5, 15 °C, Slot 7 to 9

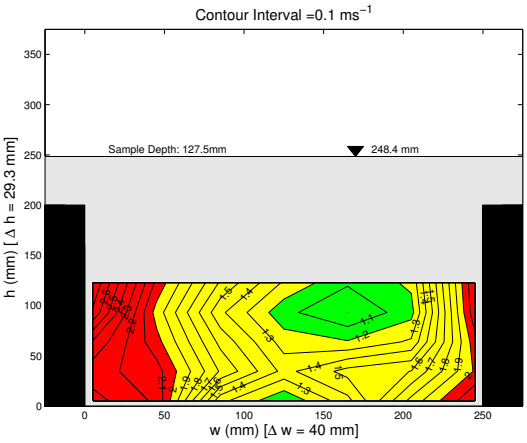

(a) Velocity Distribution: Slot 10

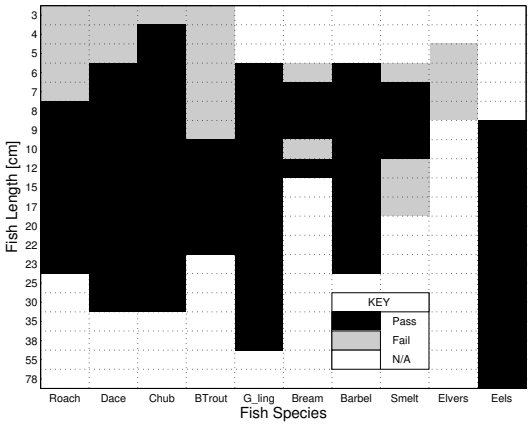

(b) Fish pass efficiency matrix: Slot 10

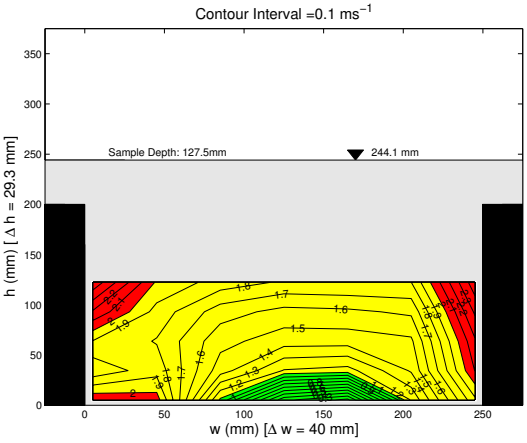

(c) Velocity Distribution: Slot 11

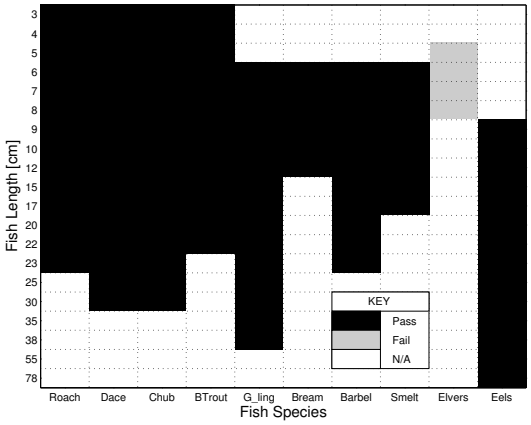

(d) Fish pass efficiency matrix: Slot 11

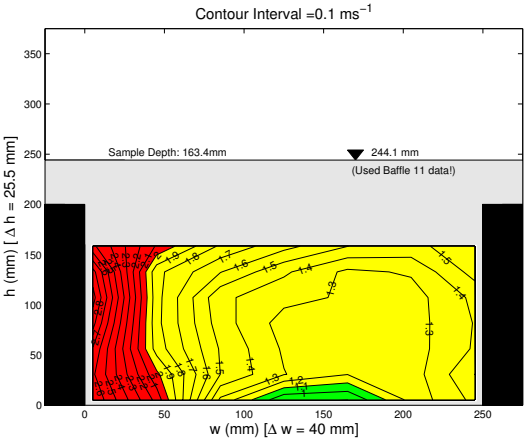

(e) Velocity Distribution: Slot 12

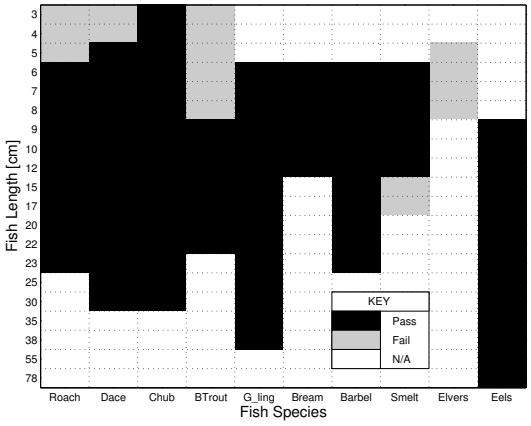

(f) Fish pass efficiency matrix: Slot 12

Figure E–24: Unequal baffle pairing: Q50, gradient 1:5, 15 °C, Slot 10 to 12

E.2.4. Unequal baffle pairing: Q90, gradient 1:5

Table E–6: Unequal baffle pairing, Q90, Reynolds number, normal

	Model scale					Field scale
Slot No.	Water depth mm	Sample depth mm	Hydraulic radius mm	Mean velocity ms^{-1}	Reynolds No.	Mean velocity ms^{-1}
1	34.14	18.22	10.01	0.43	4160	0.97
2	43.91	25.60	12.38	0.42	5069	0.94
3	44.82	28.51	13.02	0.51	6488	1.15
4	45.33	28.51	13.02	0.45	5734	1.01
5	46.07	25.60	12.38	0.48	5916	1.07
6	46.04	25.60	12.38	0.52	6407	1.16
7	46.06	25.60	12.38	0.51	6385	1.15
8	39.89	25.60	12.38	0.48	5968	1.07
9	43.37	25.60	12.38	0.46	5811	1.03
10	45.23	25.60	12.38	0.43	5368	0.97
11	47.77	25.60	12.38	0.45	5577	1.00
12	NaN	25.60	12.38	0.46	5846	1.03

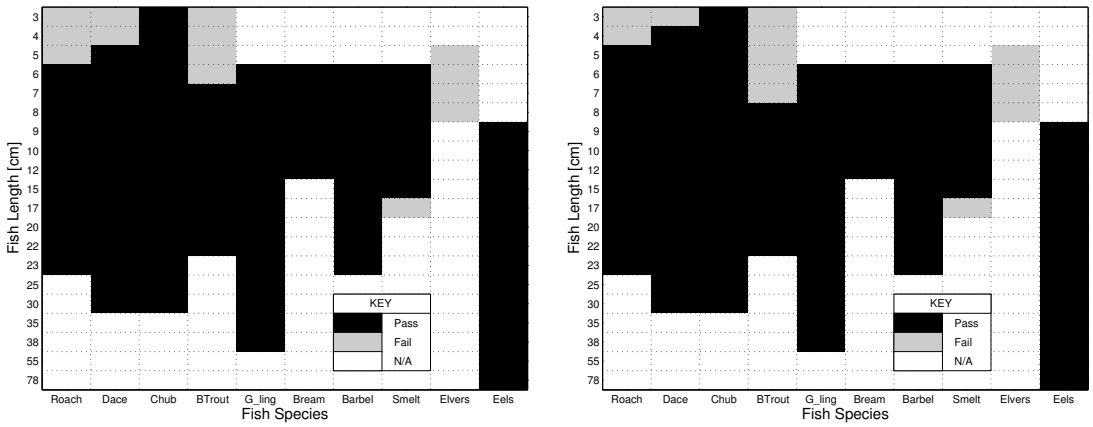

(a) 10 °C (b) 15 °C

Figure E–25: Unequal baffle pairing: Q90, gradient 1:5, 10 °C and 15 °C, Slot 1 to 12

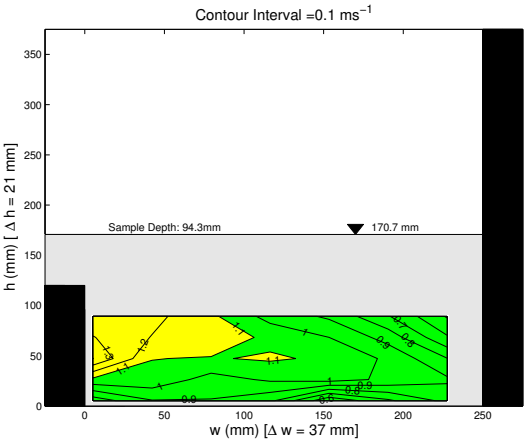

(a) Slot 1

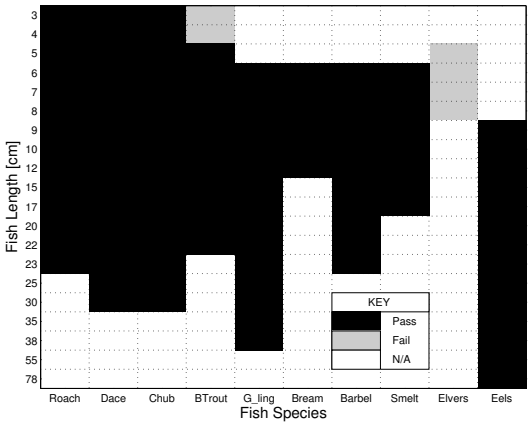

(b) Slot 1

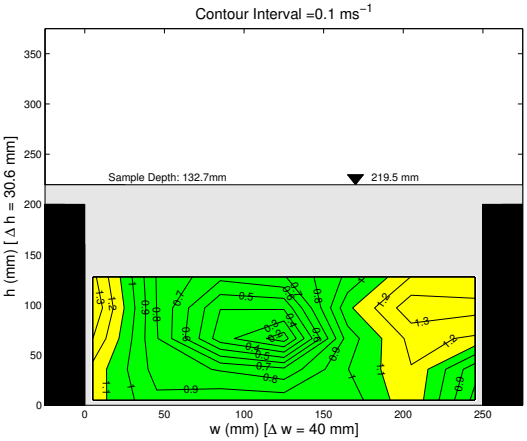

(c) Slot 2

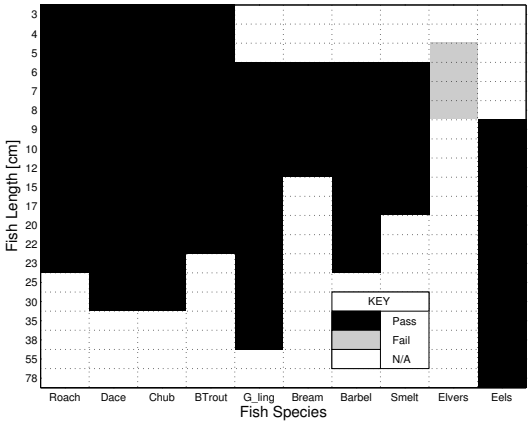

(d) Slot 2

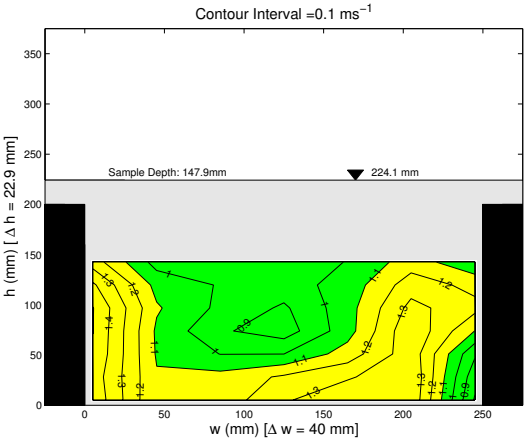

(e) Slot 3

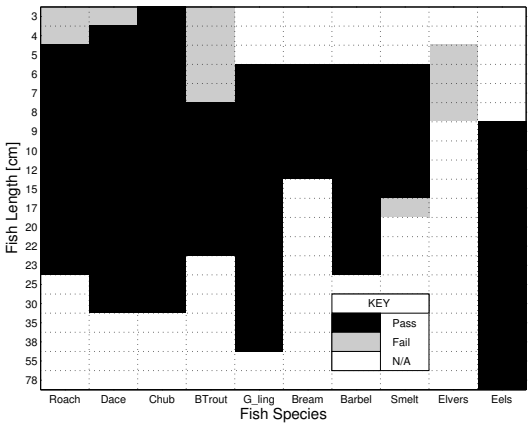

(f) Slot 3

Figure E–26: Unequal baffle pairing: Q90, gradient 1:5, 15 °C, Slot 1 to 3

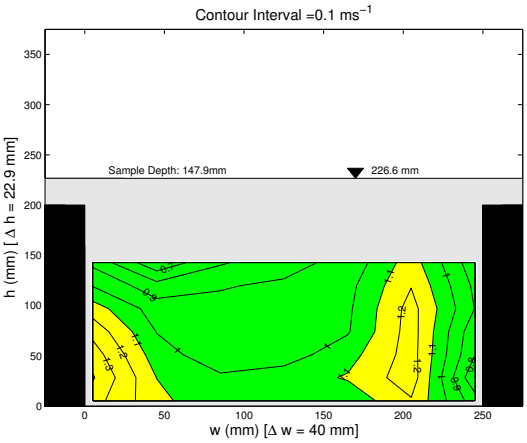

(a) Slot 4

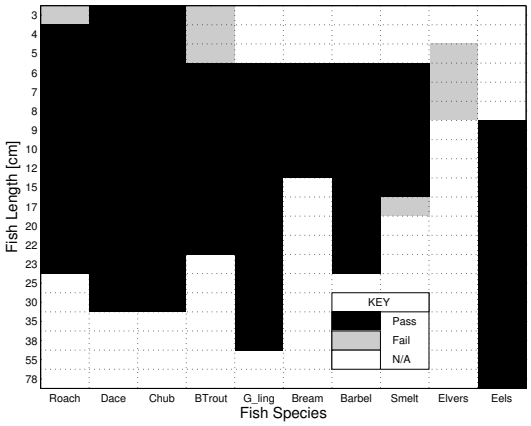

(b) Slot 4

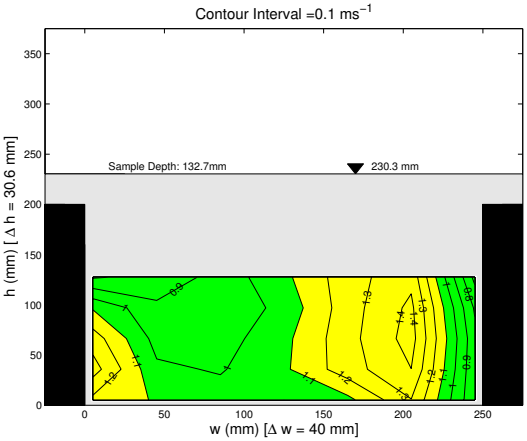

(c) Slot 5

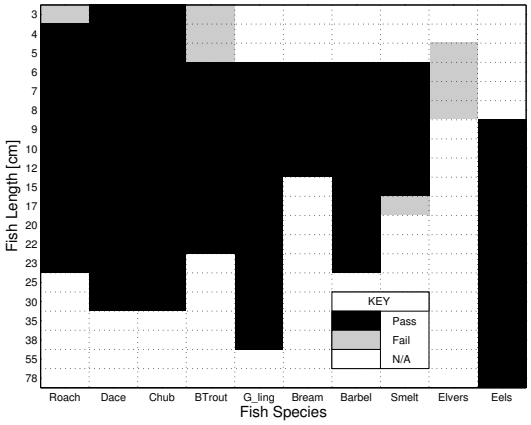

(d) Slot 5

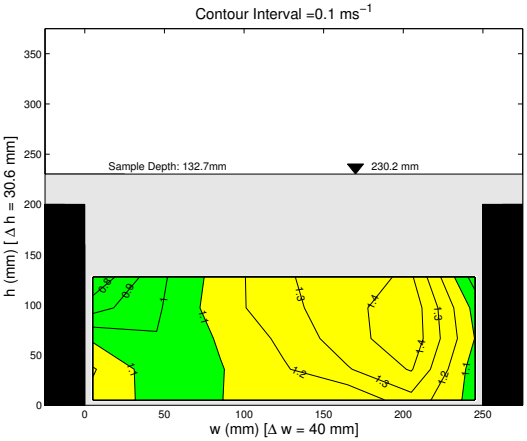

(e) Slot 6

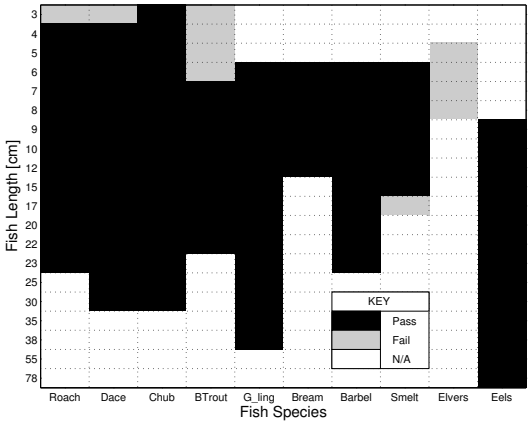

(f) Slot 6

Figure E–27: Unequal baffle pairing: Q90, gradient 1:5, 15 °C, Slot 4 to 6

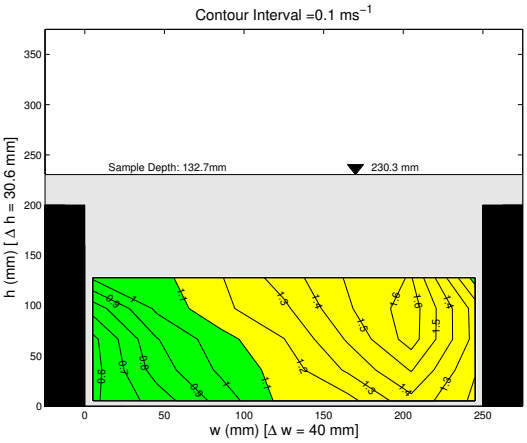

(a) Slot 7

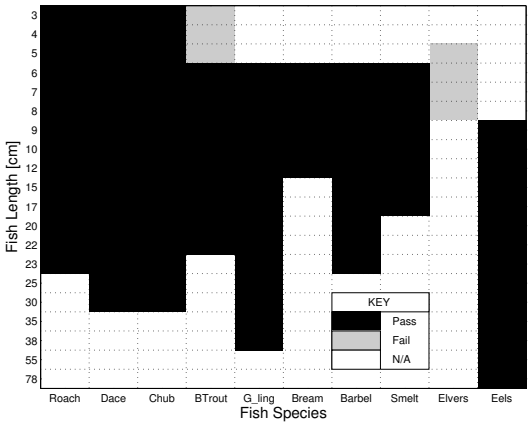

(b) Slot 7

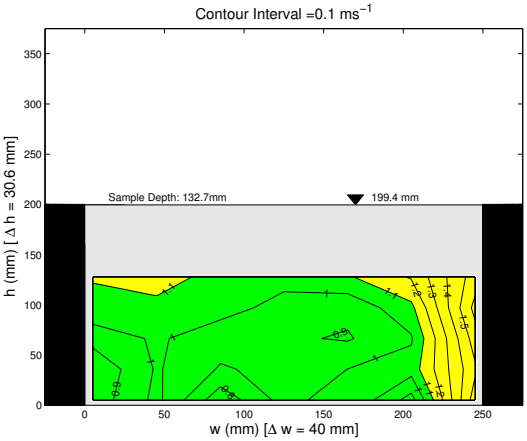

(c) Slot 8

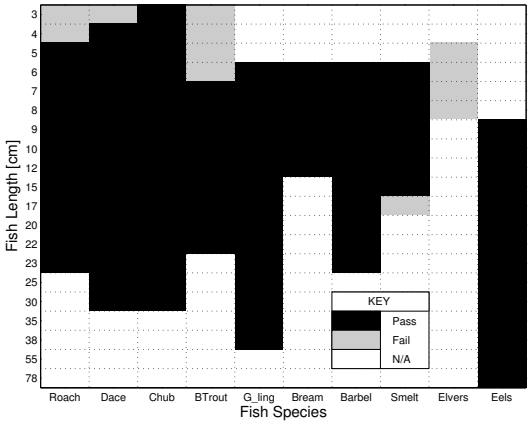

(d) Slot 8

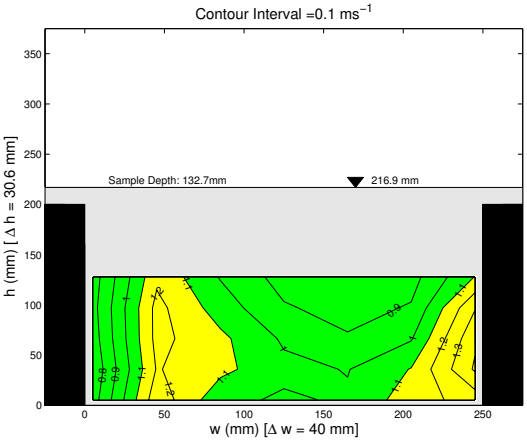

(e) Slot 9

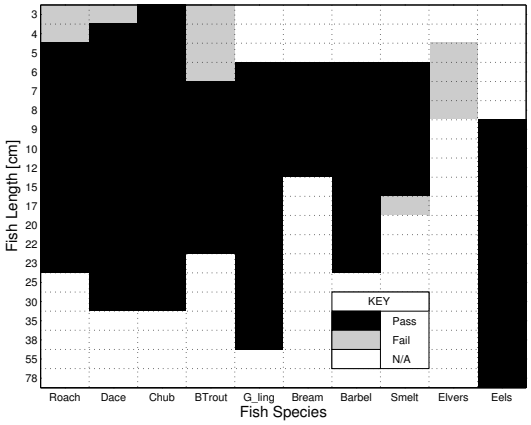

(f) Slot 9

Figure E–28: Unequal baffle pairing: Q90, gradient 1:5, 15 °C, Slot 7 to 9

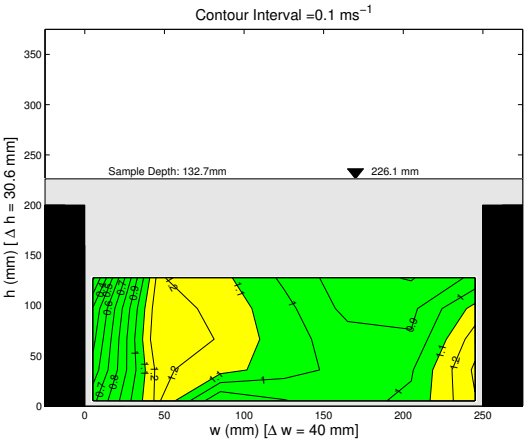

(a) Slot 10

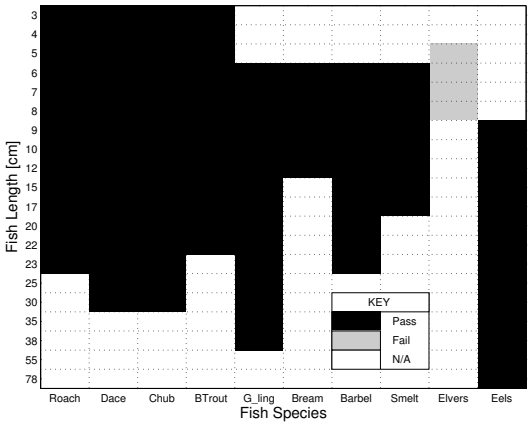

(b) Slot 10

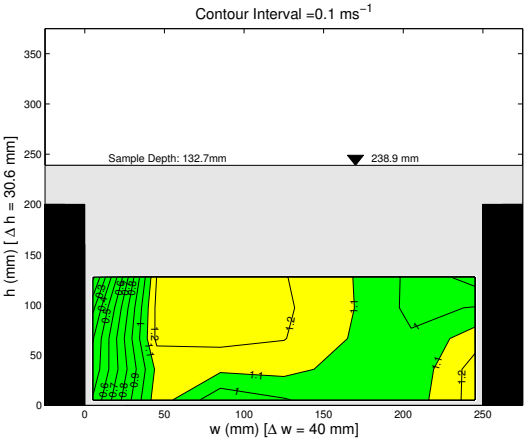

(c) Slot 11

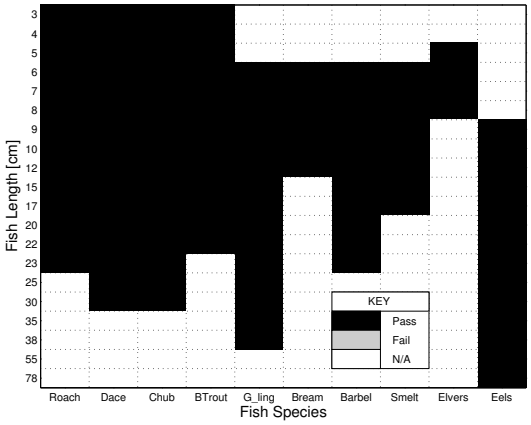

(d) Slot 11

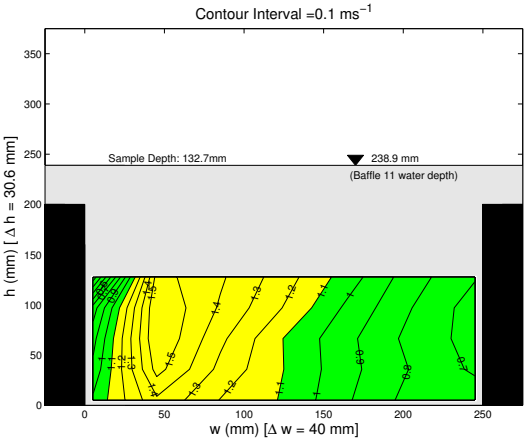

(e) Slot 12

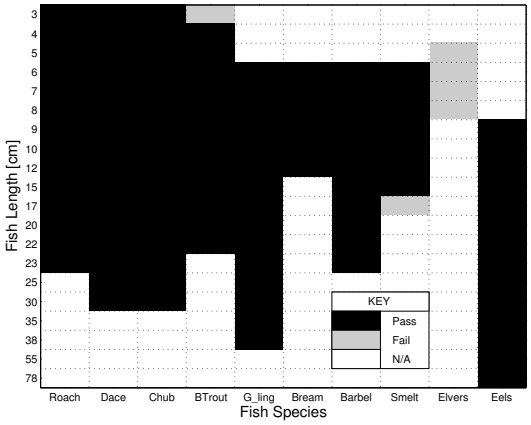

(f) Slot 12

Figure E–29: Unequal baffle pairing: Q90, gradient 1:5, 15 °C, Slot 10 to 12

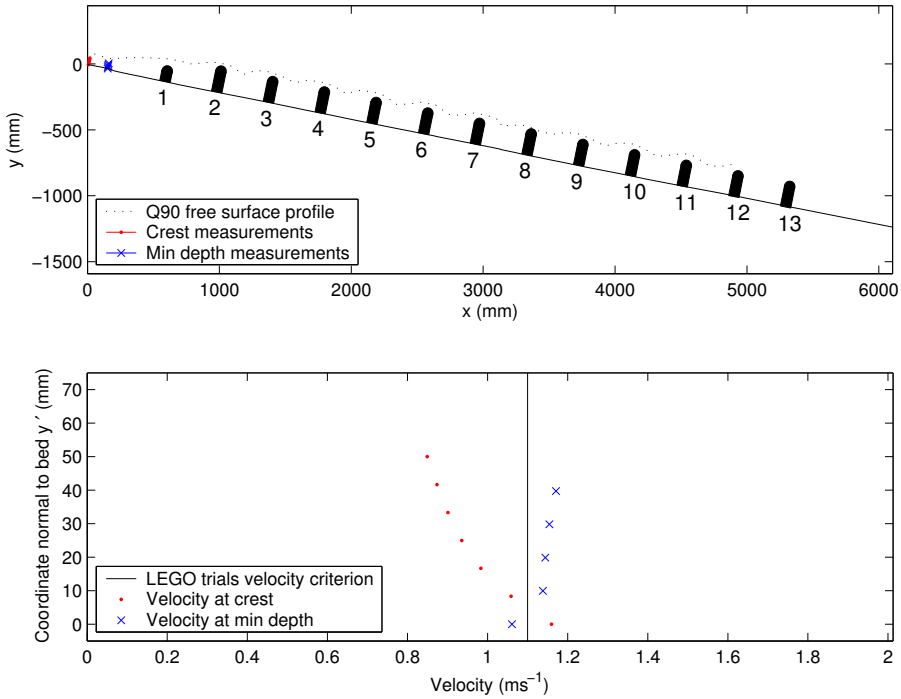

Figure E–30: Velocities upstream of first baffle for the equal baffle pairing at a 50 percentile low-flow, normal flume

E.3. Unequal baffle pairing (1:4.55, gradient)

E.3.1. Unequal baffle pairing: Q10, gradient 1:4.55

As described in section 4.2, for the tilted flume arrangements, only one slot was tested for the 10 percentile, 30 percentile and 90 percentile low flows.

Table E–7: Unequal baffle pairing, Q10, Reynolds number, tilted

	Model scale					Field scale
Slot No.	Water depth mm	Sample depth mm	Hydraulic radius mm	Mean velocity ms^{-1}	Reynolds No.	Mean velocity ms^{-1}
11	75.55	49.11	16.11	0.90	14441	2.02

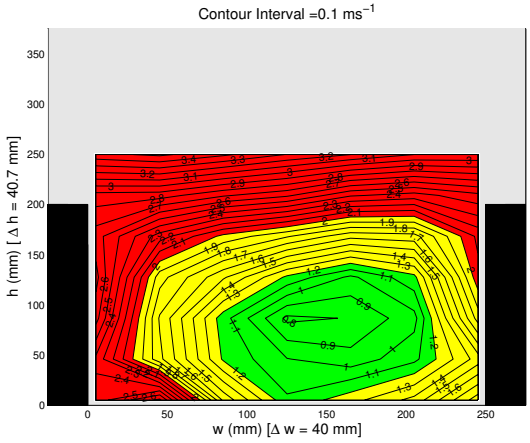

(a) Velocity Distribution

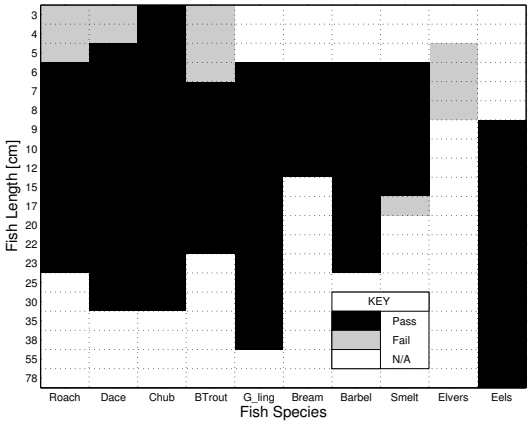

(b) Fish pass efficiency matrix: 10 °C

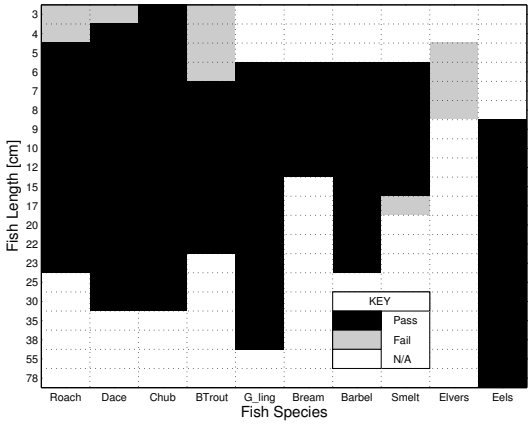

(c) Fish pass efficiency matrix: 15 °C

Figure E–31: Unequal baffle pairing: Q10, gradient 1:4.55, 10 °C and 15 °C, Slot 11

E.3.2. Unequal baffle pairing: Q30, gradient 1:4.55

Table E–8: Unequal baffle pairing, Q30, Reynolds number, tilted

	Model scale					Field scale
Slot No.	Water depth mm	Sample depth mm	Hydraulic radius mm	Mean velocity ms^{-1}	Reynolds No.	Mean velocity ms^{-1}
11	59.67	39.30	14.89	0.82	12053	1.82

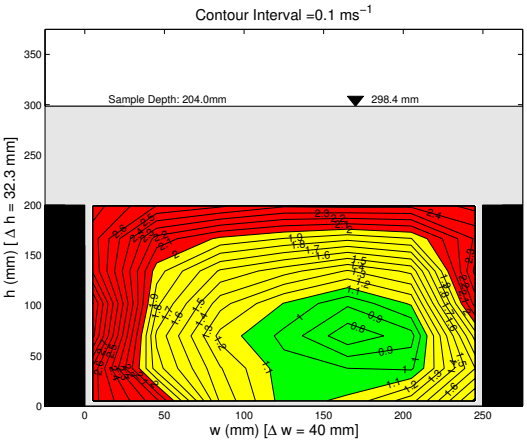

(a) Velocity Distribution

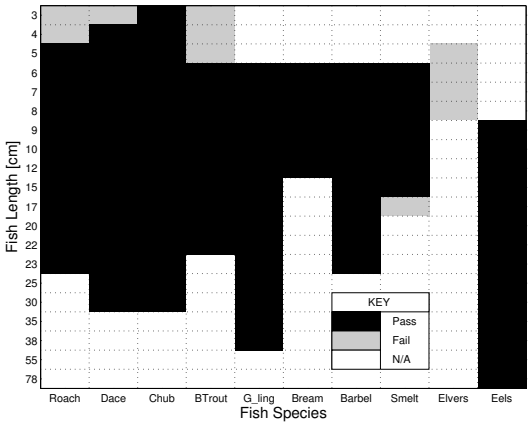

(b) Fish pass efficiency matrix: 10 °C

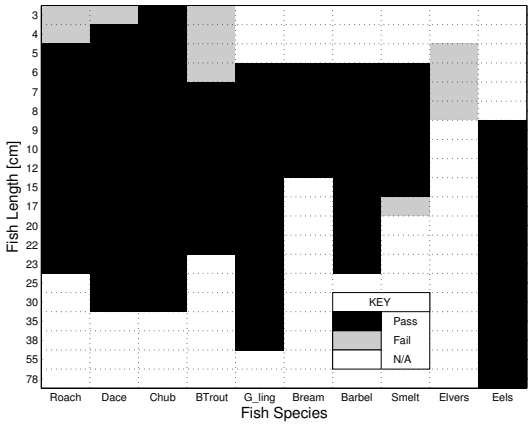

(c) Fish pass efficiency matrix: 15 °C

Figure E–32: Unequal baffle pairing: Q30, gradient 1:4.55, 10 °C and 15 °C, Slot 11

E.3.3. Unequal baffle pairing: Q50 gradient 1:4.55

Table E–9: Unequal baffle pairing, Q50, Reynolds number, tilted

	Model scale					Field scale
Slot No.	Water depth mm	Sample depth mm	Hydraulic radius mm	Mean velocity ms^{-1}	Reynolds No.	Mean velocity ms^{-1}
1	57.48	36.85	13.86	0.79	9864	1.76
2	63.90	36.85	14.52	0.77	10118	1.71
3	51.68	26.61	12.61	0.93	10779	2.08
4	50.36	36.85	14.52	0.88	11955	1.97
5	54.03	39.30	14.89	0.92	12306	2.05
6	57.97	39.30	14.89	0.89	12149	1.98
7	58.98	36.85	14.52	0.83	11237	1.85
8	53.04	36.85	14.52	0.69	9505	1.54
9	52.45	29.50	13.22	0.65	8040	1.46
10	50.31	29.50	13.22	0.81	10013	1.82
11	48.56	29.50	13.22	0.82	10054	1.83
12	NaN	29.50	13.22	0.74	9184	1.66

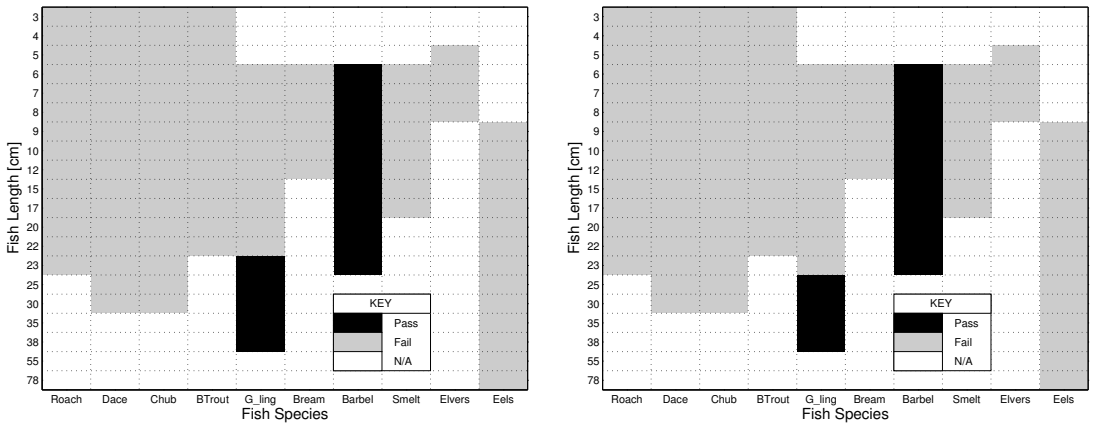

(a) 10 °C (b) 15 °C

Figure E–33: Unequal baffle pairing: Q15 gradient 1:4.55, 10 °C and 15 °C, Slot 1 to 12

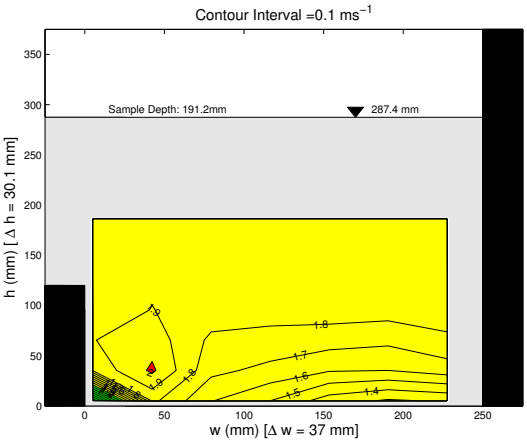

(a) Slot 1

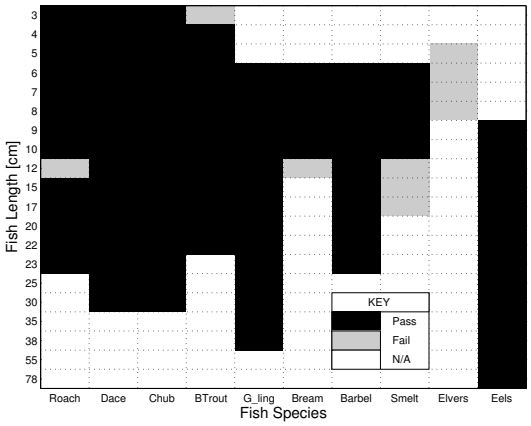

(b) Slot 1

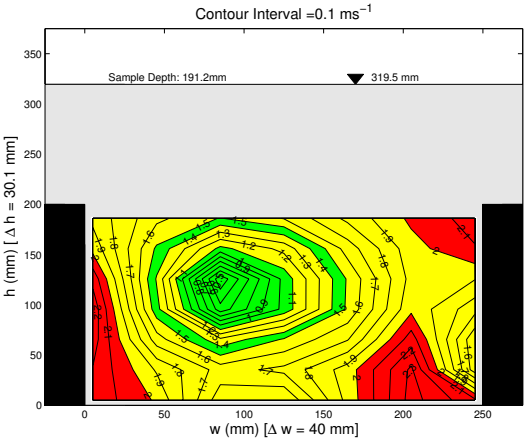

(c) Slot 2

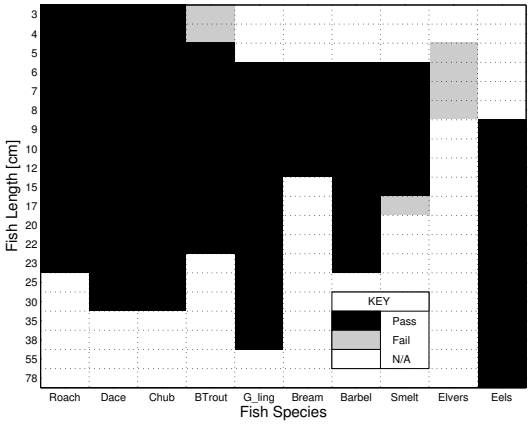

(d) Slot 2

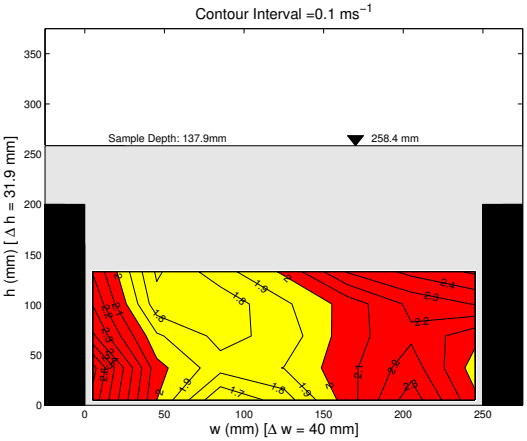

(e) Slot 3

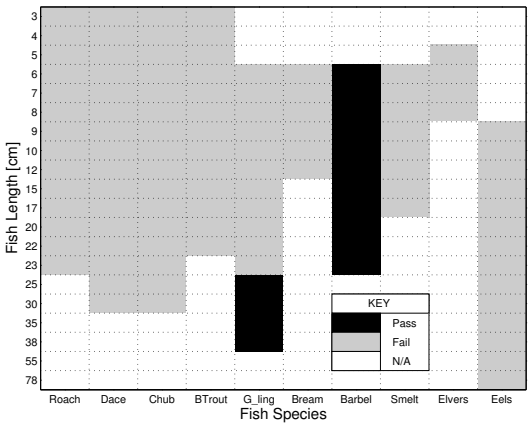

(f) Slot 3

Figure E–34: Q50 Baffles 1 to 3

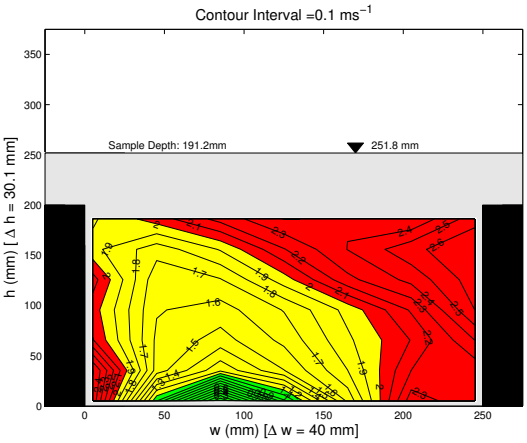

(a) Slot 4

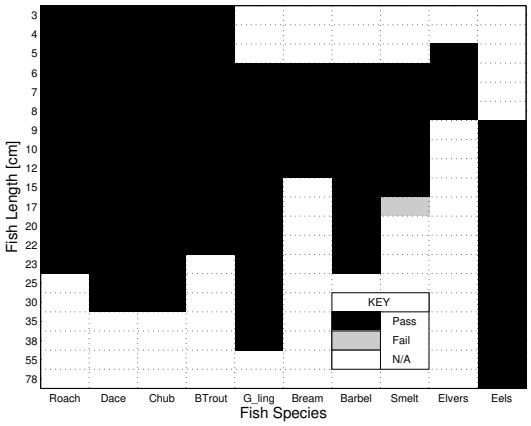

(b) Slot 4

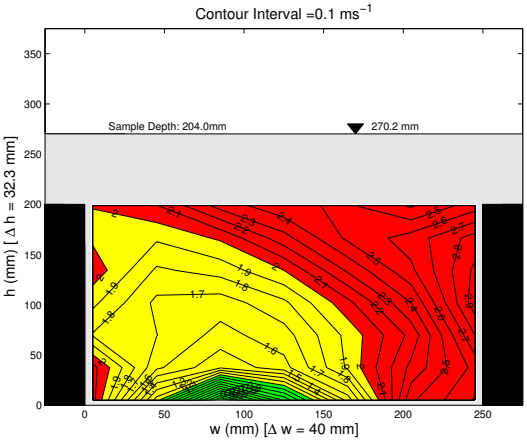

(c) Slot 5

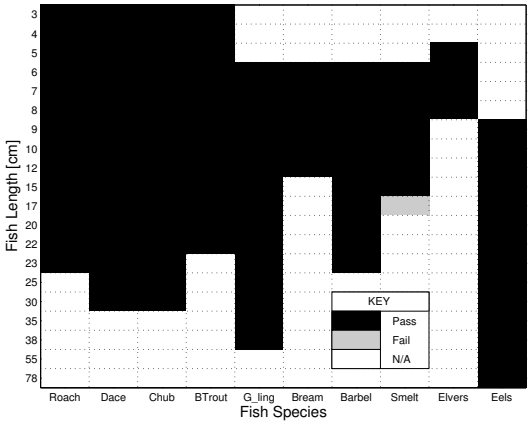

(d) Slot 5

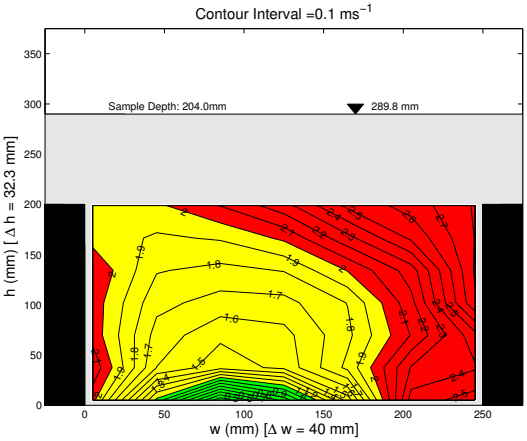

(e) Slot 6

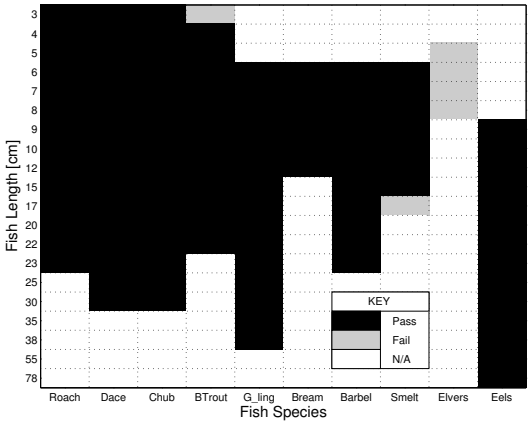

(f) Slot 6

Figure E–35: Q50 Baffles 4 to 6

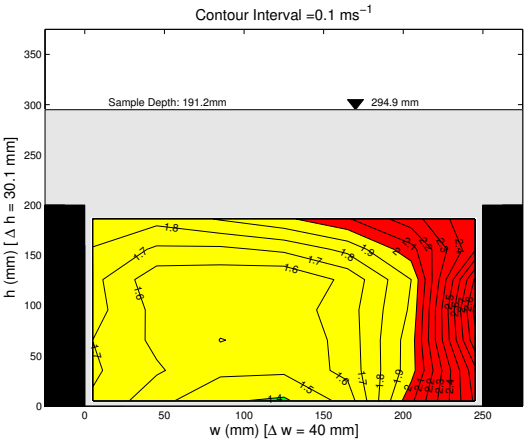

(a) Slot 7

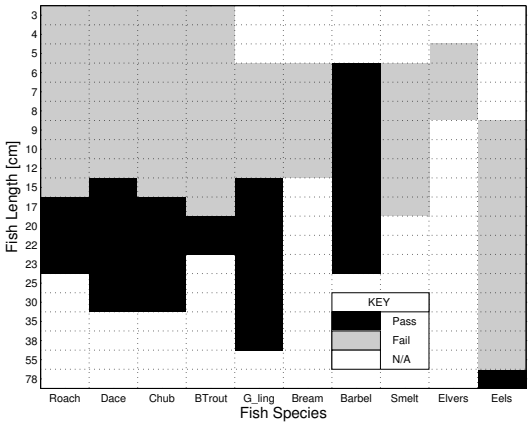

(b) Slot 7

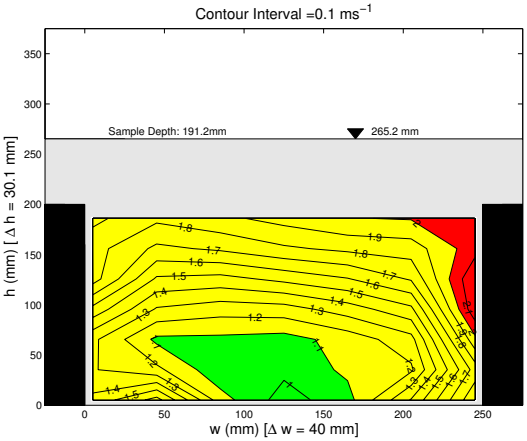

(c) Slot 8

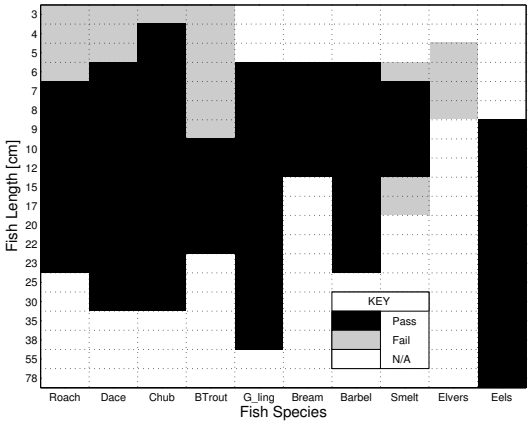

(d) Slot 8

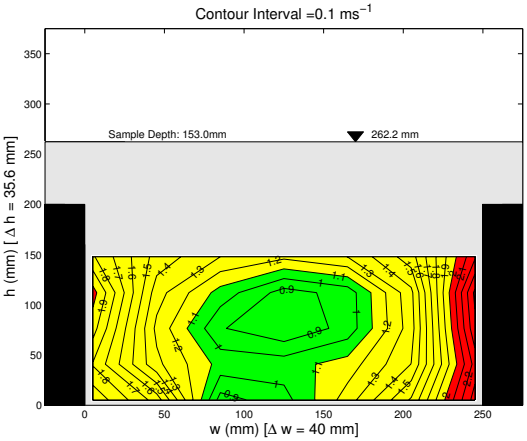

(e) Slot 9

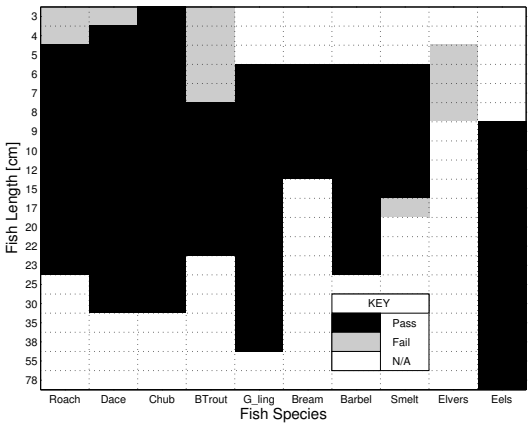

(f) Slot 9

Figure E–36: Q50 Baffles 7 to 9

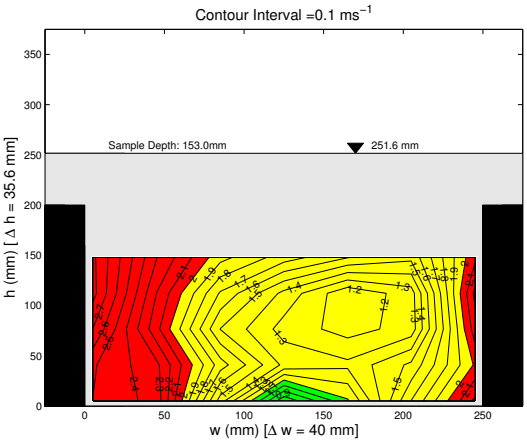

(a) Slot 10

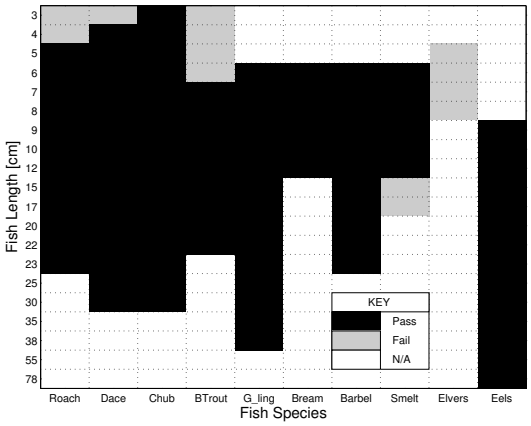

(b) Slot 10

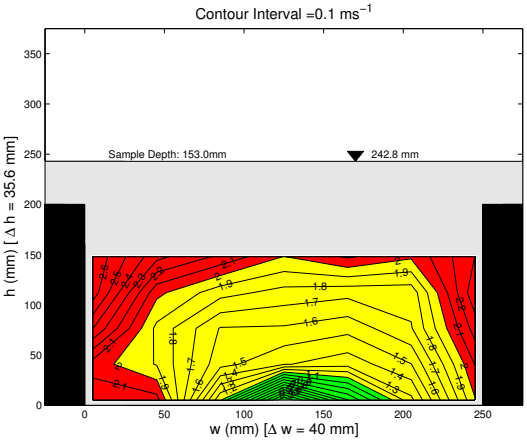

(c) Slot 11

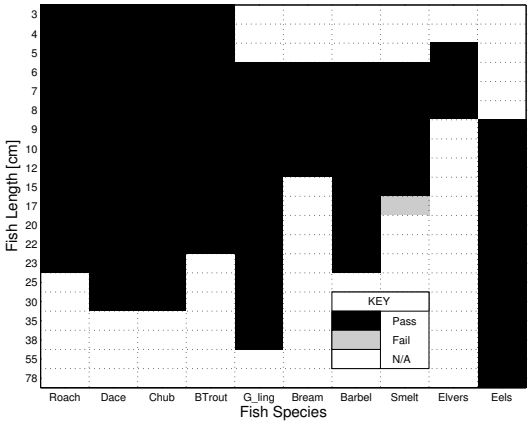

(d) Slot 11

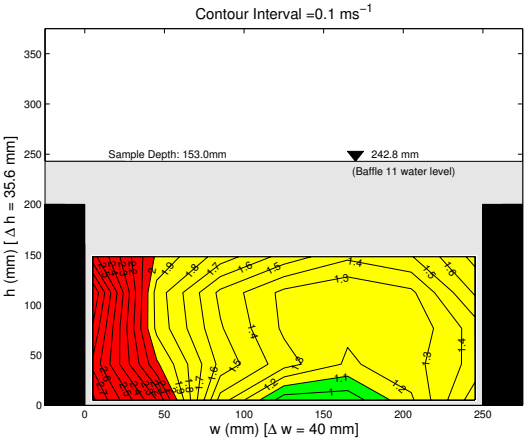

(e) Slot 12

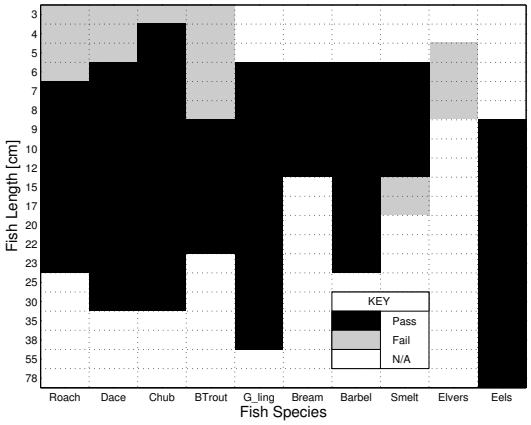

(f) Slot 12

Figure E–37: Unequal baffle pairing: Q50 gradient 1:4.55, 15 °C, Baffles 10 to 12

E.3.4. Unequal baffle pairing: Q90, gradient 1:4.55

Table E–10: Unequal baffle pairing, Q90, Reynolds number, tilted

	Model scale					Field scale
Slot No.	Water depth mm	Sample depth mm	Hydraulic radius mm	Mean velocity ms^{-1}	Reynolds No.	Mean velocity ms^{-1}
11	47.97	25.60	12.38	0.49	5630	1.09

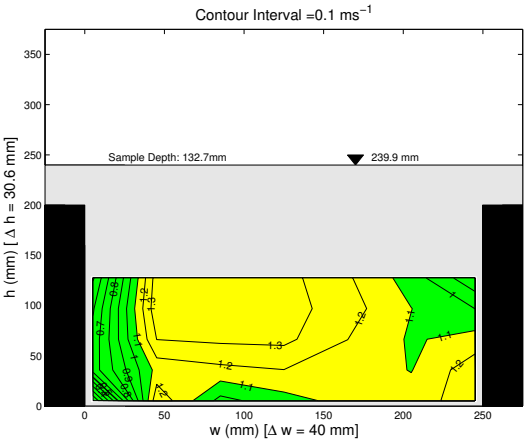

(a) Velocity Distribution

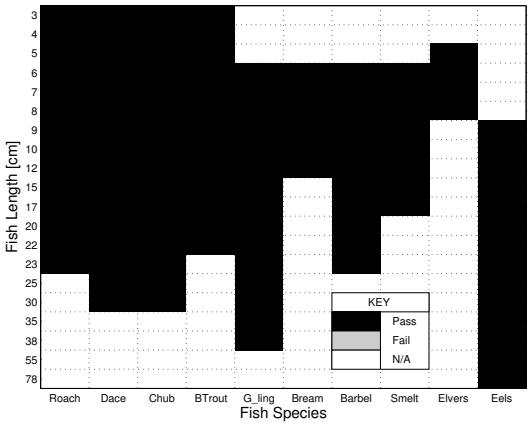

(b) Fish pass efficiency matrix: 10 °C

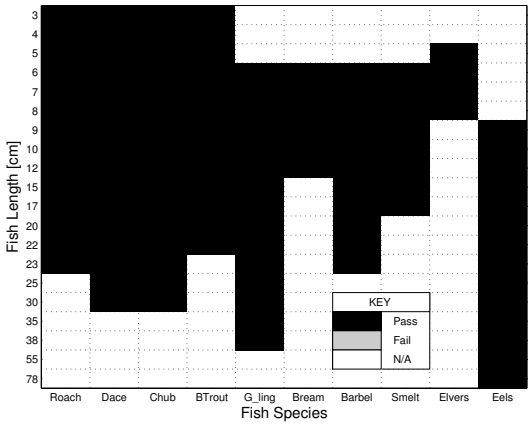

(c) Fish pass efficiency matrix: 15 °C

Figure E–38: Unequal baffle pairing: Q90, gradient 1:4.55, 10 °C and 15 °C,Slot 11

F. Video footage from the perspex fish pass trials

The CCTV camera that was used to capture the DigImage footage was also used to video the debris trials.

As part of the experiment record, all of the available footage has been written to a DVD which is appended to this PhD.

To view the footage, the file named 'VIDEO_TS.IFO' needs to be run on a suitable platform, for example WinDVD version 5.

F.1. Flow visualisation: footage filmed during the DigImage experiments

Five different sets of footage were captured. For each case the following procedure was followed. Firstly, a background information sheet was videoed giving the experiment parameters. This was followed by the reference grid required by the DigImage program and finally flow footage was filmed.

F.1.1. SET A: 26 May 2004 Plan view (50 percentile low-flow)

Information **(Time: 0:0:00 - 0:05:15)** Q50 = 13.11 ls^{-1}, Position: between Baffle 1-2 and 2-3, OP (i.e. orifice plate): 61.95 mm, head on orifice plate: 2.6 m.

Reference grid **(Time: 0:05:16 - 0:10:16)**

Flow footage Provides a description of the footage

Time: 0:10:17 - 0:13:09 Not useful

Time: 0:13:09 - 0:16:10 Slightly better, but has surface reflection off free surface. Some speckles, difficult to make out.

Time: 0:16:11 - 0:19:56 Useable. Used to make sketch in Figure 4–43.

F.1.2. SET B: 1 July 2004 Plan view (50 percentile low-flow)

Information **(Time: 0:20:30 - 0:25:30)** Q50 = 13.11 ls^{-1}, Position: between Baffle 1-2 and 2-3, OP (i.e. orifice plate): 61.95 mm,Slot height: 20 mm, Slot size: 10 mm.

Reference grid **(Time: 0:25:30 - 0:30:35)**

Flow footage Provides a description of the footage

Time: 0:30:36 - 0:34:40 No good, not enough light or particles

Time: 0:34:41 - 0:40:30 Much better, but not as good as Set A. Some surface water reflection, wider frame of reference. *Comment: Video footage also saved as a media file (36-38.wmf)*

F.1.3. SET C: 2 July 2004 Plan view (70 percentile low-flow)

Information **(Time: 0:40:30 - 0:45:30)** Q70, Position: between Baffle 1-2 and 2-3, Approximately 696 mm on manometer.

Reference grid **(Time: 0:45:30 - 0:50:30)**

Flow footage Provides a description of the footage

Time: 0:50:30 - 0:55:55 No good, not enough light or particles

Time: 0:55:56 - 0:57:57 OK. But still surface reflection downstream.

Time: 0:57:57 - 1:00:30 Too few particles.

F.1.4. SET D: 12 July 2004 Cross-sectional view (90 percentile low-flow)

Information Q50 = 13.11 ls^{-1}, Position: Baffle 1- Slot 2- Baffle 3, OP (i.e. orifice plate): 61.95 mm,Camera positioned at 2nd baffle

(Time: 1:00:32 - 1:05:31) Q50, Position: between Baffle 1-2 and 2-3, Approximately 696 mm on manometer.

Reference grid **(Time: 1:05:32 - 1:10:31)**

Flow footage Provides a description of the footage

Time: 1:10:32 - 1:14:15 Fuzzy image, not useful

Time: 1:14:15 - 1:15:21 Bit better, during this period focus was adjusted.

Time: 1:15:21 - 1:16:57 Much better. *Comment: Video footage also saved as a media file (76-78.wmf)*

Time: 1:17:04 - 1:18:45 Not quite as good.

Time: 1:18:45 - 1:20:30 Good for flow visualisation. Combined with Set E and used to make sketch in Figure 4–44.

F.1.5. SET E: 13 July 2004 Cross-sectional view (90 percentile low-flow)

Information Q50 = 13.11 ls^{-1}, Position: Crest - Slot 1 - Baffle 2, OP (i.e. orifice plate): 61.95 mm,Head : 2.6 m Camera positioned at Slot 1

Reference grid **(Time: 1:25:45 - 1:30:30)**

Flow footage Provides a description of the footage

Time: 1:30:30 - 1:34:05 Fuzzy image, not useful

Time: 1:34:06 - 1:36:30 Ok

Time: 1:36:30 - 1:38:00 Footage gets too dark

Time: 1:38:00 - 1:39:00 Good footage. Combined with Set E and used to make sketch in Figure 4–44.

Time: 1:39:00 - 1:41:10 Gets darker

F.2. Debris Analysis

The footage runs for the period 1:41:10 to 2:32:00 and was taken over a period of two days.

F.2.1. Comments on the debris analysis footage

The paper documentation for the debris analysis footage were included in the laboratory book which was stolen in January 2005. This documentation included the detailed notes correlating experiment times to flow rates as well as the pass/failure tables. Therefore the debris analysis experiments had to be re-run and the results shown and analysed in section 4.2.5, Tables 4–8 to 4–11 are consequently not based on the video footage data, but on these repeats.

The original methodology for debris analysis was revised and the number of experiments was increased when these experiments were rerun. It was not possible to re-video the revised experiments, but the footage is useful from a flow visualisation and debris entrapment point of view and for this reason is still included in this thesis.

The footage was filmed over a two day period, and it was possible to link the approximate flow rates with the data sets taken from Day 1. The actual flow rates from Day 2 were not taken in the same order and therefore the specific flow rates are not stated directly.

F.2.2. Day 1

During Day 1 only one set of dowels and/or three sandwich bags (at the same time) and/or five twigs (at the same time) were tested for each flow rate.

90 percentile low-flow
- Dowels (Time: 1:41:10 - 1:41:45)
- Plastic bags (Time: 1:41:45 - 1:42:40)

50 percentile low-flow
- Dowels (Time: 1:32:40 - 1:42:55)
- Plastic bags (Time: 1:42:55 - 1:43:25)

30 percentile low-flow
- Dowels (Time: 1:43:25 - 1:44:11)
- Plastic bags (Time: 1:44:11 - 1:44:30)
- Twigs (Time: 1:44:30 - 1:44:55)

10 percentile low-flow
- Dowels (Time: 1:44:55 - 1:45:55)
- Twigs (Time: 1:45:45 - 1:46:37)

F.2.3. Day 2

During Day 2 three sets of dowels and/or three sandwich bags tested individually and/or five twigs tested individually were tested for each flow rate. Some of the flow rates were repeated. The footage was filmed for the period 1:46:37 - 2:32:00. As it is not easy to determine which flow rate was which no further information is given here.

G. Experiments on the hydrometric effect

G.1. Modular flow: Additional graphs from the fish pass experiments

Single baffle, double baffle combination, and fish pass Single baffle 40mm, double baffle combination: 40mm + 40mm, and fish pass 40mm + 40mm+40...

a) **left** of peak - fish pass more or less falls between the single and the double baffle experiments.

b) **right** of peak - fish pass deviates further away from British Standard then either the single or the double baffle experiments.

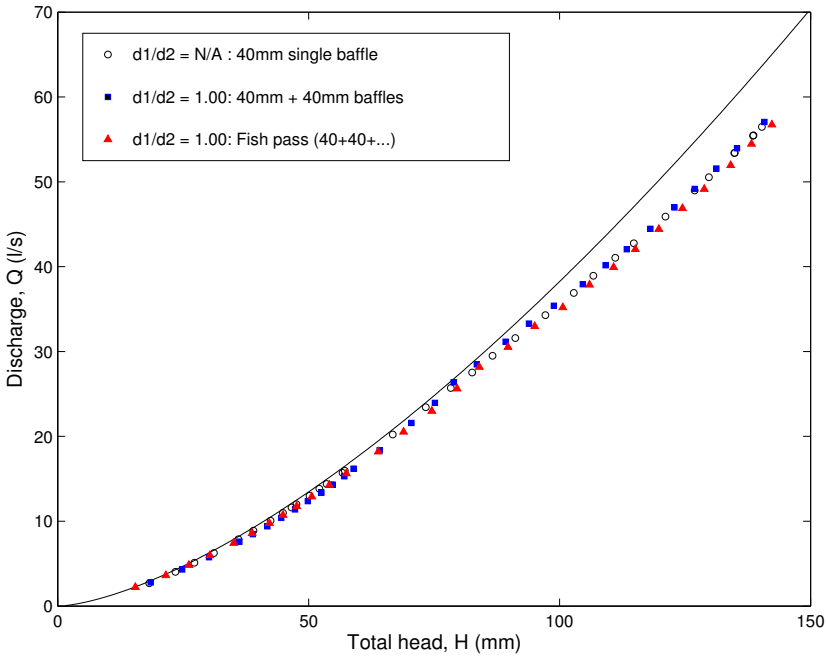

Figure G–1: Total head-discharge curves with single baffle 40mm, double baffle 40mm + 40mm and fish pass (40mm + 40mm + 40mm+...)

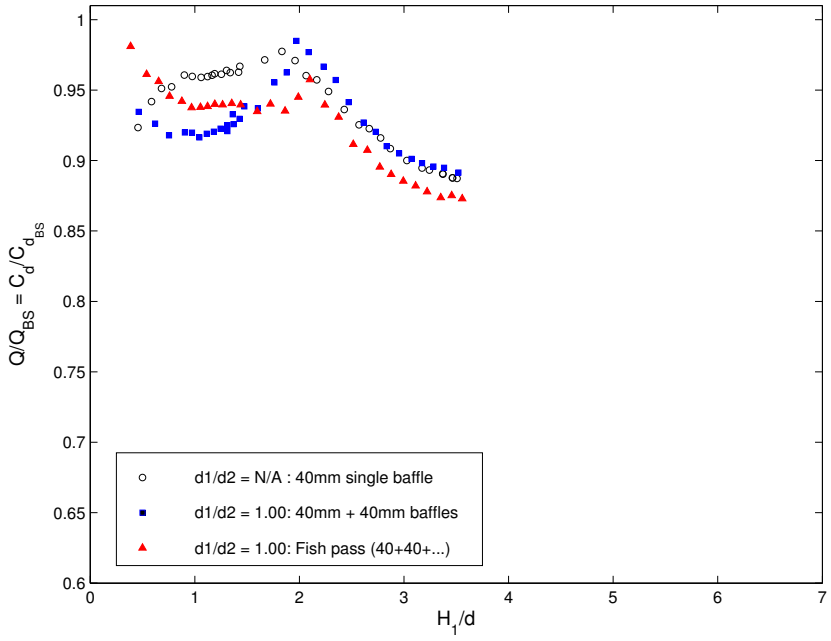

Figure G–2: Non-dimensional total head-discharge relationships: single baffle 40mm, double baffle 40mm + 40mm and fish pass (40mm + 40mm + 40mm+. . .)

G.2. Validation of measurements

Three examples of the validation of the experimental results from the single baffle investigation are given in this appendix in graphical format. Similar graphs were produced for each total head-discharge experiment in order to identify any problems with a particular data set.

In order to ensure accurate measurements as far as possible, pressure transducer readings were supplemented with a physical reading. In practical terms, the 20mb pressure transducer was cross-checked with the pointer gauge, and the 400 mb pressure transducer was cross-checked with the 4 m wall manometer (within keeping of health and safety requirements regarding the climbing of the ladder).

Figures G–3 to G–5 show the non-dimensional graphs for the given experiments, with the validation curves plotted alongside. For the hydrometric experiments, the static heads from both the 20 mm and 400 mm were compared to the pointer gauge and 4 m wall manometer respectively, and the resulting first order equation plotted.

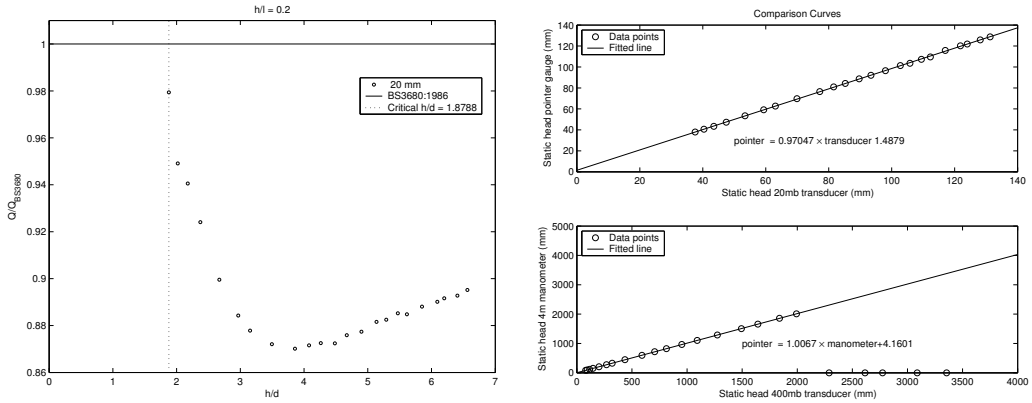

(a) Non-dimensional static head-discharge curve

(b) Accuracy of measurements 031203

Figure G–3: $d/l = 0.2$ using 20 mm baffle

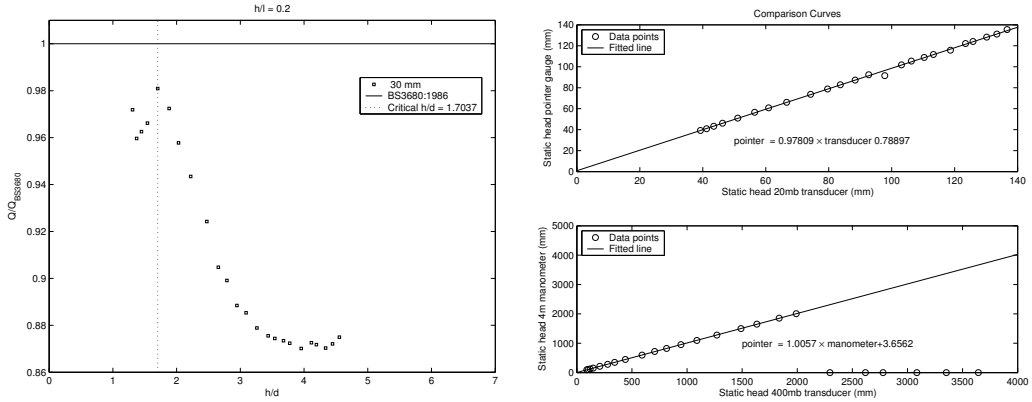

(a) Non-dimensional static head-discharge curve

(b) Accuracy of measurements 041203

Figure G–4: $d/l = 0.2$ using 30 mm baffle

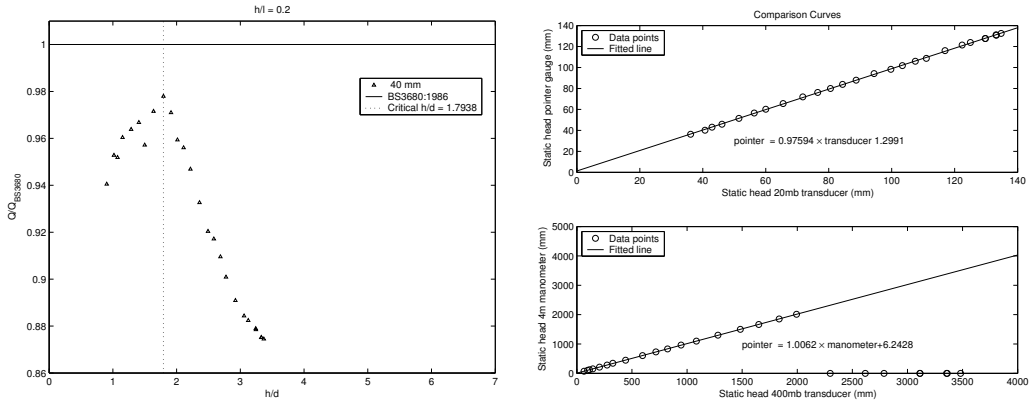

(a) Non-dimensional static head-discharge curve

(b) Accuracy of measurements 021203

Figure G–5: $d/l = 0.2$ using 40 mm baffle

H. List of Publications

The following is a list of publications produced during the duration of this project:

- Poster presentation at the 3rd IWA UK Young Researchers Conference: 'Low cost solutions for improving fish passage at Crump-type weirs' (Ayers 2002)
- Presentation at the XXX IAHR Congress: 'Methods for measuring the free surface position in laboratory flows' (Rhodes and Servais 2003)
- Presentation at the XXX IAHR Congress: 'Development of low-cost modifications to the Crump weir to improve fish passage' (Servais *et al.* 2003)
- Presentation at the Fifth International Symposium on Ecohydraulics. Aquatic Habitats: Analysis and Restoration: 'Hydrometric effect of fish pass modifications to the Crump weir' (Rhodes and Servais 2004)
- Presentation at the Fifth International Symposium on Ecohydraulics. Aquatic Habitats: Analysis and Restoration: 'Low-cost modifications to the Crump weir for fish passage: trial solutions' (Servais *et al.* 2004)

Any further publications and/or associated research will be made available on the author's personal website (http://www.susan.googlepages.com).